Identification and characterisation of novel components of the Pmk1 MAP kinase pathway during plant infection by the rice blast fungus *Magnaporthe oryzae*

Neftaly de Jesús Cruz Mireles

A thesis submitted to the University of East Anglia for the degree of Doctor of Philosophy

The Sainsbury Laboratory

Norwich, UK

March 2022

A Reyna, Santos y Celeste

Abstract

The fungus *Magnaporthe oryzae* causes rice blast disease which requires a series of morphogenetic transitions to develop specialised infection structures called appressoria and transpressoria. The Pmk1 MAP kinase (MAPK) signalling pathway has been reported to control appressorium development, plant penetration and host colonisation. However, the mechanisms by which the Pmk1 MAPK regulates these complex growth changes are poorly understood. In this thesis, I report two phosphoproteomic pipelines to identify direct downstream targets of the Pmk1 MAPK during plant infection. Using discovery phosphoproteomics followed by Parallel Reaction Monitoring (PRM) from a time series study of appressorium samples, I identified 55 putative direct downstream targets of Pmk1. These putative phosphorylated targets include proteins related to cellular processes such as autophagy, cytoskeleton remodelling, vesicle trafficking, and cell cycle control. One of the targets, named Vts1, is a SAM domain-containing protein of unknown function. Using *in vitro* and *in vivo* assays, I have demonstrated that Vts1 interacts with Pmk1 and contains two phosphorylation sites within a MAPK motif that depend on Pmk1 function and its kinase activity. Targeted gene replacement showed that Vts1 is necessary for efficient growth, sporulation, appressorium development and pathogenicity. Additionally, Vts1 phosphorylation-directed mutants demonstrated the importance of its phosphorylation in virulence. To understand the role of Pmk1 during rice tissue invasion, I carried out discovery phosphoproteomics analysis using a *M. oryzae pmk1*^{AS} analogue sensitive mutant. I obtained 39 phosphorylated candidate proteins, most of which are non-characterised in the blast fungus. Interestingly, I identified a subset of 3 phosphorylated effector proteins and components of the secretory pathway such as Sec31. Pmk1-regulated effectors (PREs) and Sec31 functions are potentially regulated by Pmk1 during Pmk1-dependent invasive growth. When considered together, this work demonstrates the utility of quantitative phosphoproteomics to identify novel Pmk1-dependent regulators, such as Vts1, that are essential for rice blast disease.

Statement

The work submitted within this thesis is entirely my own, except where due reference has been paid, and has not been submitted to this or any other university as part of any degree.

Access Condition and Agreement

Contents

List of Figures

List of Tables

Acknowledgements

bachata), football, running, badminton, trips, darts, etc; and made life out of the lab (and quarantines) a great experience along these years. Especially, I want to thank my "camaradas": Pablo, Juan Carlos, Lola, Abraham, and Roger for making this journey less stressful and full of positive vibes. Muchas gracias por todo gente, los quiero un chingo y que vengan muchos buenos momentos más por compartir. Uff! Uff! Uff!

THANK YOU TO MY PARENTS AND SISTER, gracias por apoyarme absolutamente en todo. Estar lejos de ustedes no es fácil, pero con su alegría y motivación siempre logran que pueda seguir echándole los kilos! Todo lo que hago se los debo a ustedes, los quiero mucho.

Finally, I would like to acknowledge Dr. Isabel Diez. Thanks for doing my PhD an amazing experience. Thanks for your patience, advice, "por la caña" and fun. You made me improve as a scientist and as a person. I just hope to have the opportunity to give all this back to you one day. Te quiero!

List of abbreviations

AIM	Autoinduction media
BASTA	BAR gene to confer bialophos
BIC	Biotrophic interfacial complex
cAMP-PKA	Cyclic AMP-protein kinase A
CBB	Coomassie blue
CE	Crude extract
CIA	Chloroform iso-amyl alcohol
CK2	Casein kinase II
CM	Complete medium
Co-IP	Co-immunoprecipitation
CTAB	Hexadecyltrimethylammonium bromide
CWDE	Cell wall-degrading enzymes
DIC	Differential interference contrast
EIHM	Extra-invasive hyphal membrane
ER	Endoplasmic reticulum
ERKs	Extracellular signal-related kinases
GFP	Green fluorescence protein
GO	Gene ontology
GST	Glutathione S-transferase
HPH	Hygromycin B gene
hpi	hours post inoculation
HRP	Horseradish peroxidase
IMAC	Immobilised metal affinity chromatography
IP-MS	Immunoprecipitation coupled to mass-spectrometry
JNK	Jun amino-terminal kinases
Las17	the Wiskott-Aldrich syndrome protein
MAPK	Mitogen-activated protein kinases
MAPKK	MAP kinase kinase
MAPKKK	MAP kinase kinase kinase
MS	Mass-spectrometry
NaOAc	Sodium acetate
PAS	Pre-autophagosomal structure
PCR	Polymerase chain reaction
PH	Pleckstrin-homology
PI4,5P2	Phosphatidylinositol-4,5-biphosphate
PI4P	Phosphatidylinositol-4-phosphate
PIC	Pmk1-interacting clone
PKD	Protein kinase d

Pmk1	Pathogenicity MAP kinase 1
PREs	Pmk1 regulated effectors
PRM	Parallel reaction monitoring
PTM	Post-translational modification
PVDF	Polyvinylidene diflouride
SAM	Sterile-alpha motif
SDW	Sterile distilled water
SEM	Scanning electron microscopy
SF	Soluble fraction
TCEP	Tris (2-carboxyethyl) phosphine
Tea1	Ezrin, Radixin and Moesin protein (ERM) 1
TF	Transcription factor
TFA	Trifluoroacetic acid
TiO_2	Titanium dioxide
TMT	Tandem mass tag
Y2H	Yeast-two hybrid

Chapter 1:

1 General Introduction

1.1 Plant diseases are a threat to global food security

Plant diseases are responsible for devastating economic, social, and ecological problems worldwide. They have been an obstacle for centuries and are considered one of the most serious threats to global food security in the context of the rising human population (Savary et al., 2019). Pests and pathogens cause enormous loses in food quality and quantity annually. Indeed, it is estimated that they generate significant yield losses to a variety of commercially and socially valuable crops, such as wheat (21.5%), rice (30%), maize (22.5%), potato (17.2%) and soybean (21.4%) at a global scale (Savary et al., 2019). Despite different efforts to thwart crop diseases, plant pathogens continue to pose a major threat to food security (van Esse et al., 2019). This problem is becoming more difficult considering global environmental changes and the rapid emergence of new diseases that negatively affects agro-ecosystems (Bartoli et al., 2015; Fisher et al., 2012; Velásquez et al., 2018).

Pathogenic fungi are also increasingly contributing to the global emerging disease burden. Fungal pathogens, for example, are constantly threating biodiversity and imposing more cost on agro-ecosystem health (Fisher et al., 2012). Although most fungal infections can be mitigated by modern methods of crop management, massive epidemics with catastrophic effects still occur (Fausto et al., 2019). Therefore, work on biosecurity is required worldwide to reduce the rate of fungal disease emergence in a durable and sustainable manner (Valent, 2021). Moreover, it is important to emphasise the need to use rapid and high throughput diagnosis to respond quickly to disease epidemic scenarios (Ghosh et al., 2018).

1.2 Blast disease is caused by the filamentous fungus *Magnaporthe oryzae*

Blast disease remains one of the most serious threats to global food security (Valent, 2021). This destructive plant fungal disease is caused by the filamentous ascomycete *Magnaporthe oryzae* (synonym of *Pyricularia oryzae*) (Zhang et al., 2016). The blast fungus is a multi-host pathogen that is able to infect more than 50 different grass species, including staple crops such as wheat, rice and barley (Langner et al., 2018; Wilson & Talbot, 2009). For rice production alone, it is estimated that blast disease causes losses of up to 30% of the global annual harvest (Savary et al., 2019; Talbot, 2003). This rice lost represents

enough grain to feed 60 million people (Talbot, 2003). Therefore, blast disease threatens more than 50% of the world's population that depend on rice as a main source of calories (Khush, 2005), and it is a severe problem in at least 85 countries where rice is grown (Skamnioti & Gurr, 2009; Talbot, 2003; Wilson & Talbot, 2009). Moreover, the blast fungus is a pathogen that can also spread through seed, providing opportunities for global disease transmission (Cruz & Valent, 2017).

M. oryzae is able to rapidly adapt to different host plants due to its diverse evolutionary mechanisms (Huang et al., 2014). The propensity to jump from one host to another, together with global trade and climate change, has resulted in an increased incidence of blast disease (Langner et al., 2018; Singh et al., 2021). For instance, in 2016 an outbreak of wheat blast in Bangladesh threatened wheat production in South Asia (Islam et al., 2016) and the neighbouring regions including India, the world's second largest wheat producer (Islam et al., 2019). In 2017, the blast fungus was first observed in Zambia and it is predicted that it can impact other vulnerable areas across the world (Singh et al., 2021; Tembo et al., 2020). In sub-Saharan Africa, the blast fungus evolvability also represents a significant constraint to small-scale farming systems (Mutiga et al., 2021). When considered together, *M. oryzae* is a significant threat to food security worldwide. Therefore, developing durable disease resistance and a robust international surveillance system is crucial to manage this devastating pathogen.

The blast pathogen has been extensively studied over the past three decades (Valent, 2021). *M. oryzae* has developed into a very tractable experimental model system to illustrate most of the important concepts governing fungal-plant interactions (Dean et al., 2012). Rice-*M. oryzae* pathosystem has become a significant starting point to understand issues in plant pathology more broadly (Ebbole, 2007). However, many aspects about the biology of the fungus at the cellular and molecular level remain poorly understood. In this Chapter, I will describe pre- and post-penetration strategies that the blast fungus employs to cause disease. I will emphasise the morphogenetic transitions that the fungus undergoes for successful host colonisation. I will focus on what we know about the Pmk1 mitogen-activated protein (MAPK) kinase signalling pathway which is a master regulator of pathogenicity in *M. oryzae* infection (Wilson & Talbot, 2009). I will also provide information regarding the morphogenetic transitions involved in appressorium formation and cell-to-cell movement during invasive growth, highlighting major questions that remain to be elucidated and which have driven the ideas presented in this thesis.

1.3 The infection cycle of *M. oryzae*

M. oryzae is a hemibiotrophic pathogen (Koeck et al., 2011). This means that the blast fungus has an initial biotrophic phase followed by a necrotrophic phase to complete its infection cycle. During biotrophy, the host immune system is suppressed which allows invasive hyphae to spread within living tissue from which nutrients are taken up (Mendgen & Hahn, 2002) enabling the fungus to proliferate. However, during necrotrophy, the pathogen secretes toxins to induce host cell death and then takes up nutrients from dead tissue (Horbach et al., 2011). Based on the time of primary host cell rupture, the *M. oryzae* life cycle of the can be divided into events that occur *before* (pre-penetration) and *after* (post-penetration) host penetration (Figure 1.1).
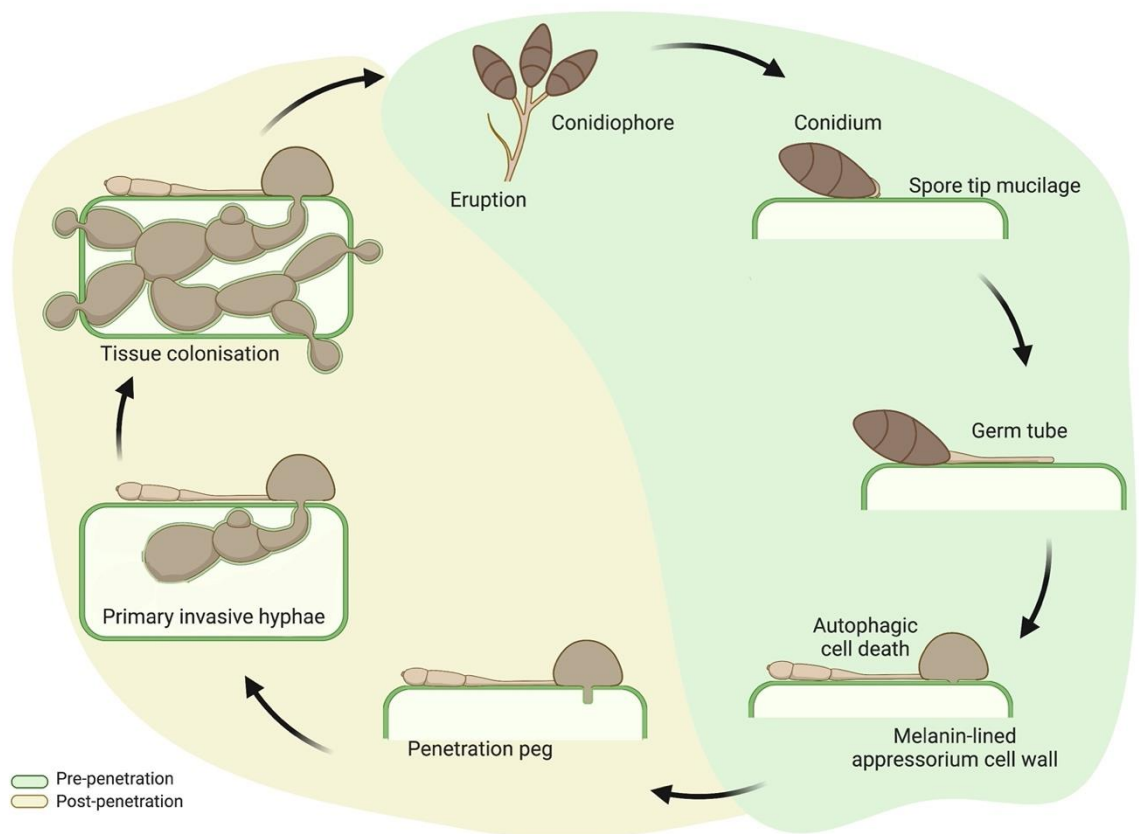
Figure 1.1. The infection cycle of *Magnaporthe oryzae*. Schematic representation to show pre-penetration and post-penetration events during *M. oryzae* infection (modified from Eseola et al., 2021).

Pre-penetration events are initiated when a three-celled pyriform asexual spore, known as a conidium, lands on the waxy cuticle of the leaf surface of the host plant and sticks itself by secretion of spore tip mucilage (Hamer et al., 1988). Once attached, the conidium quickly germinates to generate a polarised germ tube that stops growing apically within 4 hours

(Wilson & Talbot, 2009). At this point, the germ tube flattens and adheres to the leaf surface. Subsequently, the fungus undergoes the first morphogenetic transition changing from polarised to isotropic growth in a process known as "hooking". This is a critical step of the infection because hooking constitutes a recognition phase in which surface features are sensed and assessed prior to commitment to the formation of an appressorium (Whiteford & Spanu, 2002). The fungus secretes hydrophobin proteins, such as Mpg1 and Mhp1 (Kim, et al., 2005; Talbot et al., 1993). Hydrophobins are implicated in conidium spore adhesion, surface perception and the action of cutinases; which are necessary pre-requisites to initiate appressorium formation (Kim et al., 2005; Pham et al., 2016; Talbot et al., 1993; Whiteford & Spanu, 2002).
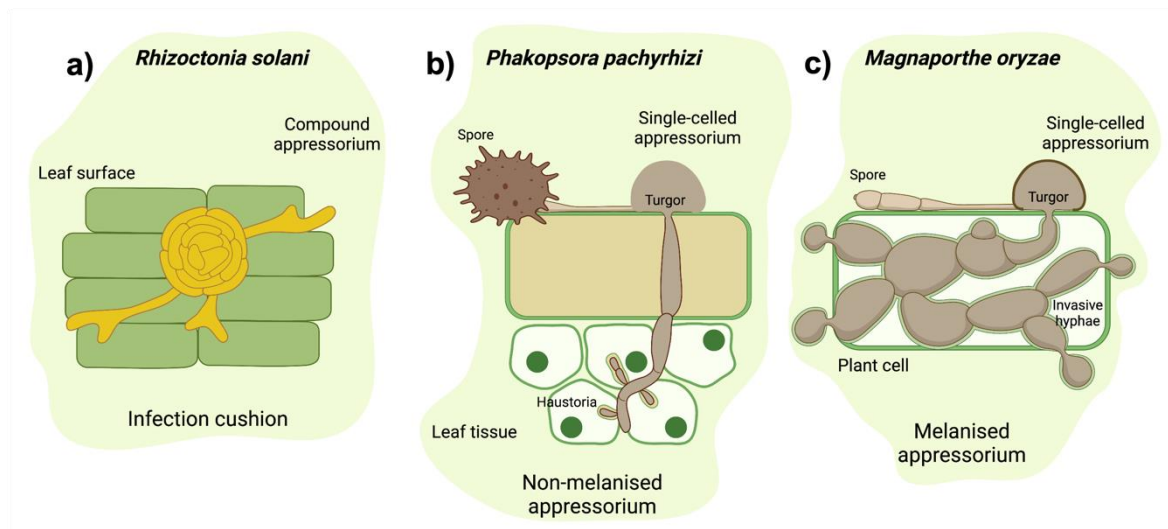
Figure 1.2. Different types of appressorium. Scheme to show compound and single-celled appressoria. To penetrate their hosts, a) *Rhizoctonia solani* uses a compound appressorium. Whereas single-celled appressoria can be non-melanised as in b) *Phakopsora pachyrhizi* or melanised as in c) *M. oryzae* (Ryder et al., 2022).

Appressoria are specialised dome-shaped structures required to break through the tough outer layer of the host plant (Cruz-Mireles et al., 2021; Eseola et al., 2021; Talbot, 2019). In fact, appressorium-related structures are commonly used by diverse fungal pathogens to gain access to the host (Ryder et al., 2022) (Figure 1.2). In the blast fungus, the appressorium constitutes an important morphogenetic stage in infection-related development (Veneault-Fourrey et al., 2006). After hooking, the germ tube ceases elongation and swells to form an incipient appressorium (Dean, 1997). To cause plant

disease, the appressorium develops enormous turgor of up to 8.0 MPa, by accumulating high concentrations of glycerol and other polyols (de Jong et al., 1997). In *M. oryzae*, the single-celled appressorium has a differentiated cell wall rich in melanin, which is essential for turgor generation (Ryder & Talbot, 2015). Turgor is rapidly translated into mechanical force allowing a narrow penetration hypha to emerge from the base of the appressorium, rupturing the rice leaf cuticle and allowing the fungus to invade host tissue and cause disease (de Jong et al., 1997; Foster, 2017).
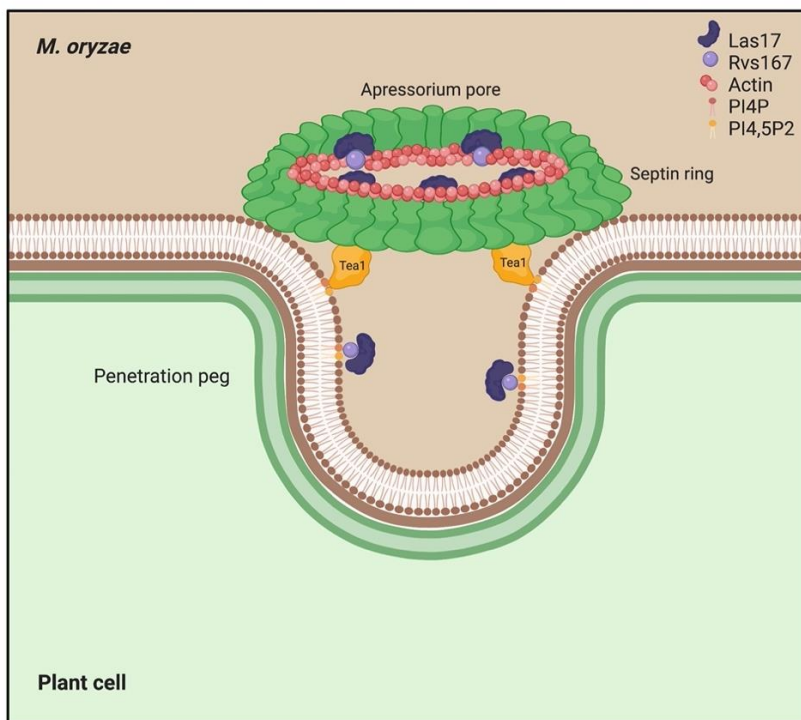
Figure 1.3. Septin-mediated host penetration during early *M. oryzae* infection. Schematic representation of septin ring assembly at the appressorium pore with its polarity determinants. Tea1 = Ezrin, Radixin and Moesin protein (ERM) 1, Las17 = the Wiskott-Aldrich syndrome protein, PI4P = phosphatidylinositol-4-phosphate, PI4,5P2 = phosphatidylinositol-4,5-biphosphate. Septin assembly is shown in green, functioning as an actin scaffold and diffusion barrier.

Prior to host penetration, cytoskeletal reorientation occurs at the base of the appressorium (Dagdas et al., 2012; Osés-Ruiz & Talbot, 2017). This requires the action of septins, a family of small GTPases specifically recruited to a region at the base of the appressorium that lacks melanin, called the appressorium pore (Dagdas et al., 2012; Gupta et al., 2015).

These septins organise a hetero-oligomeric F-actin ring, providing cortical rigidity and acting as a diffusion barrier for organisation of polarity and secretion proteins (Dagdas et al., 2012; Gupta et al., 2015; Ryder et al., 2013) (Figure 1.3). Septins associate with polarity determinants such as Las17, Rvs167 and Tea1, that are hypothesised to facilitate membrane curvature making a direct link to phosphoinositide-enriched membrane domains containing phosphatidylinositol-4-phosphate (PI4P) and phosphatidylinositol-4,5-biphosphate (PI4,5P) (Dagdas et al., 2012; Dulal et al., 2020; Mattila et al., 2007; Van Ngo & Mostowy, 2019) (Figure 1.3). After septin ring assembly, a specialised rigid hypha called a penetration peg, emerges to break through the cuticle of the leaf to gain entry to the host (Bourett & Howard, 1992). This represents the first morphogenetic transition inside the host, involving a switch from anisotropic to polarised expansion (isotropy) towards the appressorium pore (Bourett & Howard, 1990) (Figure 1.3).

Post-penetration events start once the pathogen is inside the host primary plant cell. Here, the penetration peg differentiates into primary invasive hyphae (Kankanala et al., 2007). These aggressive hyphae proliferate inside host cells for a prolonged period in a symptomless, biotrophic manner (Kankanala et al., 2007). During this stage, the plant responds to infection by employing its multi-layered immune system (Jones & Dangl, 2006). In turn, *M. oryzae* induces formation of a lobed compartment termed the *Biotrophic Interfacial Complex* (BIC) within each occupied cell. At this stage, the blast fungus produces and secretes effector proteins to manipulate and suppress plant immunity, facilitating its growth and development (Kankanala et al., 2007; Mosquera et al., 2009). Accumulating evidence suggests that effectors in the blast fungus can be secreted at the BIC (cytoplasmic effectors) or at the hyphal tip (apoplastic effectors), following different secretory mechanisms to disrupt host defences (Giraldo et al., 2013). Remarkably, *M. oryzae* effectors play a critical role in host adaptation (Latorre et al., 2020). Therefore, effector biology of the blast fungus is an exciting topic with considerable explanation including structure-function studies of effector recognition by immune receptors (Bentham et al., 2020; Concepcioni et al., 2021; De La Concepcion et al., 2019). How the fungus controls effector gene expression during invasive growth, which molecular mechanisms are required for translocation and how effectors function to cause disease are some of the relevant questions that remain unanswered (Valent, 2021).

Later in infection, the primary penetration hyphae differentiates into bulbous invasive hyphae that fill completely the primary host cell (Yi & Valent, 2013). Once at cell wall crossing points, the hyphal tip expands into an appressorium-like structure, termed the transpressorium (Cruz-Mireles et al., 2021). Transpressorium formation requires the morphogenetic transition of a swollen bulbous hyphae to a narrow invasive that grows

through pit fields, where plasmodesmata cluster (Cruz-Mireles et al., 2021; Kankanala et al., 2007; Yi & Valent, 2013). After 32-36 hours post-infection, *M. oryzae* develops filamentous invasive hyphae that move to adjacent cells where they differentiate again into bulbous hyphae to continue colonisation (Fernandez & Wilson, 2014). The fungus promptly colonises host tissue during this biotrophic stage until necrotrophy occurs. Disease lesions become apparent on the leaf surface within 4 to 5 days of initial infection (Shi et al., 2003). During its life cycle, the blast fungus therefore undergoes different morphogenetic transitions as a response to the local environment which are essential for progression of the disease (Fernandez & Wilson, 2014). Determining how the fungus senses signals to change growth direction is a major question than remains to be elucidated.

1.4 Mitogen-activated protein kinases (MAPK) are important regulators in Eukaryotes

Mitogens are external molecules that induce mitosis or enhance cell division rate, their use led to the discovery of the mitogen-activated protein kinase (MAPK) family in Eukaryotes (Rossomando et al., 1989). The first MAPKs reported were Kss1 and Fus3 from the pheromone response pathway of *Saccharomyces cerevisiae* (Courchesne et al., 1989; Elion et al., 1991; Elion et al., 1990), and the mammalian MAPKs ERK1, ERK2 and ERK3 (Boulton et al., 1991). MAPKs are key regulators in the conversion of extracellular signals to intracellular responses (Z. Wei & Liu, 2002). They have been reported to control diverse processes including growth, development, stress response and pathogenicity (Bardwell, 2006).

MAPKs modules are conserved among Eukaryotes. In mammals, at least four separate families of MAPKs are present: the extracellular signal-related kinases (ERK1/2), the Jun amino-terminal kinases (JNK1/2/3), the p38 proteins (p38α/β/γ/δ) and ERK5 (Chang & Karin, 2001). Although they are all activated by a specific MAPKK, the upstream MAPKKK can activate more than one MAPKK; presumably, to confer responsiveness to different stimuli (Kyriakis & Avruch, 2012). In plants, MAPK family can be classified into 6 different groups based on phylogeny (Taj et al., 2010). Interestingly, plant MAPKs have evolved unique roles in Eukaryotes such as signalling in cytokinesis and phytohormones (Zhang et al., 2001). Other very diversified role of plant MAPKs is in processes related to immunity (Asai et al., 2002; Menke et al., 2004; Zhang & Klessig, 2001). Most of the knowledge on MAPK signalling comes from fungal model system *S. cerevisiae* (Gustin et al., 1998). The budding yeast contains five MAPK modules that have been also studied in other fungi.

Because of the diversity of the physiological processes that control in Eukaryotes, MAPK signalling is an exciting and intensive research field in modern biology (Zhang et al., 2016).

The study of MAPK pathways in *S. cerevisiae* has contributed to the understanding of this signalling in other organisms (Chen & Thorner, 2007). In yeast, five MAPK pathways have been identified: Hog1, Mpk1, Smk1, Fus3 and Kss1. The Hog1 pathway is activated in response to osmotic stress to promote adaptation upon increased osmolarity (Alepuz et al., 2001). The Mpk1 pathway has been shown to be essential for cell wall integrity (Kim et al., 2008). The Smk1 cascade meanwhile has been linked to coordinate spore wall assembly (Krisak et al., 1994), whereas Fus3 and Kss1 are functional homologues of the pheromone module responsible for regulating pheromone responses and invasive growth (Chen & Thorner, 2007; Gartner et al., 1992). The Fus3/Kss1 and its functional homologues in mammals ERK1/2 are probably the most studied MAPK modules because they were the first identified in Eukaryotes (Pearson et al., 2001). The Fus3/Kss1 MAPK core complex is formed by Ste11 (MAPKKK), Ste7 (MAPKK), Fus3/Kss1 (MAPK) and the MAPK scaffold protein Ste5 (Elion, 2015). In diverse fungi, orthologues of this pathway have been discovered to regulate a wide range of physiological responses, including cell proliferation, asexual and sexual development, secondary metabolite production and pathogenicity (Frawley & Bayram, 2020; Rispail et al., 2009).

From yeast to humans, MAPKs are arranged in a three-component module that is activated in response to a broad range of stimuli (Widmann et al., 1999). A typical MAPK phosphorylation cascade involves sequential action of three serine/threonine kinases: a MAP kinase kinase kinase (MAPKKK), a MAP kinase kinase (MAPKK) and the MAP kinase (MAPK) itself (Jiang et al., 2018). This three-tiered kinase system is evolutionary conserved and functions in response to extracellular stimuli. MAPKKK activation causes the MAPKK to be phosphorylated and activated, which then promotes MAPK activity via dual phosphorylation of threonine and tyrosine residues within a conserved Thr-X-Tyr motif present in the phospho-acceptor loop of the kinase domain (Cargnello & Roux, 2011).

To execute their functions, MAPKs phosphorylate downstream target proteins. MAPK cascades modulate diverse responses through phosphorylation of substrates, including other kinases, enzymes, cytoskeletal proteins or transcription factors (TFs) (Jagodzik et al., 2018). TFs are among the most studied MAPK targets. It is well-known that MAPKs can shape the transcriptional cellular landscape via TF phosphorylation (Nadal-Ribelles et al., 2018). In fungal pathogens, it has been reported that MAPKs transmit plant-derived signals to the nucleus, leading the initiation of a virulence program that will allow to gain entry into the host and fungal colonisation (Hamel et al., 2012; Li et al., 2012; Zhao et al., 2007).

1.5 The conserved Pmk1 MAP kinase signalling pathway is important in many fungal plant pathogen species

MAPKs have been also studied in plant pathogenic fungi, where they are central regulators of virulence (Zhao et al., 2007). To cause infection, fungal pathogens require the coordination of diverse cellular processes that allow infection-related morphogenetic switches (Zhao et al., 2007). In this context, fungal MAPKs are important because they play a key role in development (Jiang et al., 2018). The role of MAPKs in pathogenesis has also been related to the control of mechanical and/or enzymatic activities for successful host infection (Hamel et al., 2012). The most investigated MAPKs in plant fungal pathogens are the functional orthologues of Fus3/Kss1 in yeast (Frawley & Bayram, 2020).

The first MAPK characterised in plant fungal pathogens was the Pathogenicity MAP kinase 1 (Pmk1) from *M. oryzae* (Xu & Hamer, 1996). Since then, other Fus3/Kss1 orthologues have been characterised and reported to be crucial for plant infection in more than 30 fungal pathogens (Jiang et al., 2018; Turrà et al., 2014) (Table 1.1). This MAPK is critical to cause disease in appressorium and non- appressorium forming fungal species, including pathogens considered a serious threat to food security such as *Botrytis cinerea* (Zhao et al., 2007)*, Blumeria graminis* (Zhang & Gurr, 2001)*, Colletotrichum spp* (Fu et al., 2022; He et al., 2017; Li et al., 2022; Liang et al., 2019; Takano et al., 2000; Wei et al., 2016)*. Fusarium graminearum* (Jenczmionka & Schäfer, 2005)*, Fusarium oxysporum* (Di Pietro et al., 2001)*, Puccinia graminis* (Panwar et al., 2013), *Ustilago maydis* (Brachmann et al., 2003; Müller et al., 1999) and *M. oryzae* (Xu & Hamer, 1996) (for more details see Table 1.1). Taken together, this shows that Pmk1 signalling cascade is widely conserved in taxonomically diverse pathogenic fungi.

The MAPK Pmk1 cascade is involved in different steps of fungal infection. In *M. oryzae*, it has been involved in sensing mechanisms of the host because the sensor proteins Msb2 and Sho1 activate Pmk1 pathway by recognizing surface hydrophobicity and plant-derived compounds such as cutin monomers and leaf waxes (Liu et al., 2011). Similarly, it has been demonstrated that Msb2 and Sho1 orthologues in *F. oxysporum* cooperate to regulate invasive growth and plant infection via Fmk1 (Perez-Nadales & Di Pietro, 2015; Pérez-Nadales & Di Pietro, 2011). The Pmk1 pathway has been also shown to be important in morphogenesis of infection structures such as appressoria, penetration pegs or invasive hyphae in diverse fungal pathogens (Pérez-Nadales & Di Pietro, 2011; Turrà et al., 2014). It has been hypothesised that this regulation happens via cytoskeletal reorganisation during host penetration and colonisation (Park et al., 2002; Sakulkoo et al., 2018). The Pmk1 cascade has been also reported as regulator of secreted cell wall-degrading enzymes

(CWDEs) in *Cochliobolus heterostrophus* (Lev & Horwitz, 2003) and *F. graminearum* (Jenczmionka & Schäfer, 2005).

Table 1.1. Reported pathogenicity MAPKs in plant pathogenic fungi. List of characterised Fus3/Kss1 orthologues in fungal pathogens.

Fungal species	Fus3/Kss1 orthologue	Reference
Alternaria alternata	Fus3	(Lin et al., 2010)
Alternaria brassicicola	Amk1	(Cho et al., 2007)
Aspergillus flavus	MpkB	(Jun et al., 2020)
Bipolaris oryzae	Bmk1	(Moriwaki et al., 2007)
Bipolaris sorokiniana (Cochliobolus sativus)	Fus3	(Leng & Zhong, 2015)
Blumeria graminis	Mpk1	(Zhang & Gurr, 2001)
Botrytis cinerea	Bmp1	(Zheng et al., 2000)
Claviceps purpurea	Cpmk1	(Mey et al., 2002)
Cochliobolus heterostrophus	Chk1	(Lev et al., 1999)
Colletotrichum fructicola	Cfmk1	(Li et al., 2022; Liang et al., 2019)
Colletotrichum gloeosporioides	CgMk1	(He et al., 2017)
Colletotrichum higginsianum	ChMK1	(Wei et al., 2016)
Colletotrichum lagenarium	Cmk1	(Takano et al., 2000)
Colletotrichum scovillei	CsPmk1	(Fu et al., 2022)
Cytospora chrysosperma	CcPmk1	(Xiong et al., 2021)
Fusarium graminearum	Gmpk1	(Jenczmionka & Schäfer, 2005)
Fusarium oxysporum	Fmk1	(Di Pietro et al., 2001)
Fusarium verticillioides	Mk1	(Zhang et al., 2011)
Magnaporthe oryzae	Pmk1	(Xu & Hamer, 1996)
Metarhizium robertsii	Fus3	(Meng et al., 2021)
Mycosphaerella graminicola	Fus3	(Cousin et al., 2006)
Penicillium oxalicum	PoxMk1	(Ma et al., 2021)
Puccinia striiformis	Mapk1	(Guo et al., 2011)
Pyrenophora teres	Ptk1	(Ruiz-Roldán et al., 2001)
Sclerotinia sclerotiorum	Smk1	(Chen et al., 2007)
Setosphaeria turcica	Stk2	(Gu et al., 2013)
Stagonospora nodorum	Mak2	(Solomon et al., 2005)
Ustilaginoidea virens	UvPmk1	(Tang et al., 2020)
Ustilago maydis	Kpp2 Kpp6	(Brachmann et al., 1999)
Valsa mali	VmPmk1	(Wu et al., 2017)
Verticillium dahliae	Vmk1	(Rauyaree et al., 2005)

Although it is known that the Pmk1 pathway has a central role in pathogenesis for various fungi, there have been less reports of the characterisation of other components of the cascade. However, genetic studies of orthologues of the pheromone module in yeast have started to dissect the signalling mechanisms of the MAPK Pmk1 cascade in fungal pathogens (Frawley & Bayram, 2020). In *Botrytis cinera*, null mutants of orthologues of Ste11, Ste7, Ste50 and Bmp1 (termed the homologue of Pmk1 in this pathogen), were unable to generate lesions on tomato leaves and penetrate onion epidermal layers (Doehlemann et al., 2006; Schamber et al., 2010; Zheng et al., 2000). Similarly, wounded apples infected with *Δbmp1* mutants showed considerably slower lesion growth when

compared to the wild type (Schamber et al., 2010). In *Ustilago maydis*, orthologues of yeast Fus3/Kss1 (called Kpp2/Ubc3 pathway) module are involved in the regulation of both development and virulence. Ubc4 (Ste11 homologue) and Kpp2 (Fus3/Pmk1 homologue) null mutants are impaired in conjugation tube formation and pathogenicity and regulate the hormone sensing pathway required for dikaryon formation and invasive growth (Brachmann et al., 2003; Müller et al., 1999; Müller et al., 2003). In *Fusarium graminearum*, null mutants of FgSte11, FgSte7 and FgGpmk1 have been demonstrated to be important for developmental programmes as well as pathogenicity (Wang et al., 2011). Finally, in the soilborne fungus *F. oxysporum*, *Δfmk1* (Fus3/Pmk1 homologue) and *Δste12* (Ste12 homologue) mutants are affected in invasive growth on tomato leaves and apple fruit tissue, as well as in cellophane membrane penetration, functions that are important to cause wilt disease (Di Pietro et al., 2001; Rispail & Di Pietro, 2009).

1.6 The Pmk1 MAP kinase signalling pathway is crucial for morphogenetic transitions in the *M. oryzae* infection cycle

In the pathosystem rice-*M. oryzae*, the Pmk1 MAPK pathway has been intensively studied (Xu, 2000). It is known that Pmk1 regulates different morphogenetic switches during *M. oryzae* infection. First Pmk1 regulates the transition from polar to isotropic growth during appressorium development (Xu & Hamer, 1996). Once the appressorium is mature, Pmk1 mediates the transition from isotropic to polarised (aniosotropic) growth during plant penetration acting via the transcription factor Mst12 (Osés-Ruiz et al., 2021; Park et al., 2002). Remarkably, it has been demonstrated that the morphogenetic switch from the bulbous growing hyphae to the thin invasive hyphae during transpressorium-dependent cell-to-cell movement is also mediated by this MAPK cascade (Sakulkoo et al., 2018).

1.6.1 Pmk1 regulates appressorium morphogenesis

In *M. oryzae*, it is more than 25 years since the Pmk1 MAPK was discovered and shown to be required for appressorium morphogenesis. Genetic studies have shown that the absence of Pmk1 (*Δpmk1* null mutant) or its inactive allele (*pmk1^{AS}* analogue sensitive allele) leads to failure to form an appressorium (Sakulkoo et al., 2018; Xu & Hamer, 1996). Therefore, blast fungus strains lacking Pmk1 activity are unable to cause disease in plants (Sakulkoo et al., 2018; Xu & Hamer, 1996). In fact, the Pmk1 null mutants are non-pathogenic even when spores are inoculated directly onto wounded leaves. However, *Δpmk1* still responds

to hydrophobic surfaces or exogenous cAMP by forming swollen germ tube tips (Xu & Hamer, 1996). In Pmk1 localisation experiments, it has been observed that a GFP-tagged Pmk1 (GFP, Green Fluorescence Protein) shows stronger GFP signal in developing conidia and appressoria compared to vegetative hyphae, conidiophores, conidia, and germ tubes (Bruno et al., 2004). During appressorium formation and maturation, GFP-Pmk1 is localised to the cytoplasm and appressorium nucleus, consistent with observations in different organisms that MAPKs are translocated into the nucleus in response to specific stimuli (Bruno et al., 2004).

During appressorium development, the Pmk1 MAP kinase is activated by its upstream MAPKK Mst7 and MAPKKK Mst11 (Zhao et al., 2005) (Figure 1.4). Similar to Δ*pmk1*, Mst7 and Mst11 deletion mutants fail to form an appressorium and are non-pathogenic (Zhao et al., 2005). Mst7 activates Pmk1 by phosphorylation at the threonine and tyrosine residues in the well-conserved MAP kinase TXY motif (Jiang et al., 2018; Zhao et al., 2005). It has been reported that the interaction between Mst7 and Pmk1 occurs via the Mst7 MAPK-docking domain (Li et al., 2012; Zhao et al., 2007). A recent study has shown that Mst7 also forms homodimers that involve the action of thioredoxins to activate Pmk1 pathway during ROS signalling (Zhang et al., 2016). Alternatively, the MAPKKK Mst11 can be regulated by self-inhibitory binding and through interaction with Ras proteins via the Ras association domain (Qi et al., 2015; Zhou et al., 2014) (Figure 1.4). Both Mst11 and Mst7, appear to form a complex with the scaffold protein Mst50 that works as an adaptor and has been shown to operate upstream signalling (Li et al., 2017; Park et al., 2006) (Figure 1.4). In the same way as the component kinases of the pathway, the Mst50 deletion mutants are defective in appressorium formation and are non-pathogenic (Park et al., 2006). The Mst50 interaction with Mst7 and Mst11 is direct, and the interaction of Mst50 with Mst11 occurs through its sterile alpha-motif (SAM) domain (Park et al., 2006). Therefore, the upstream components of the Pmk1 pathway are critical for the regulation of the MAPK cascade during appressorium formation.
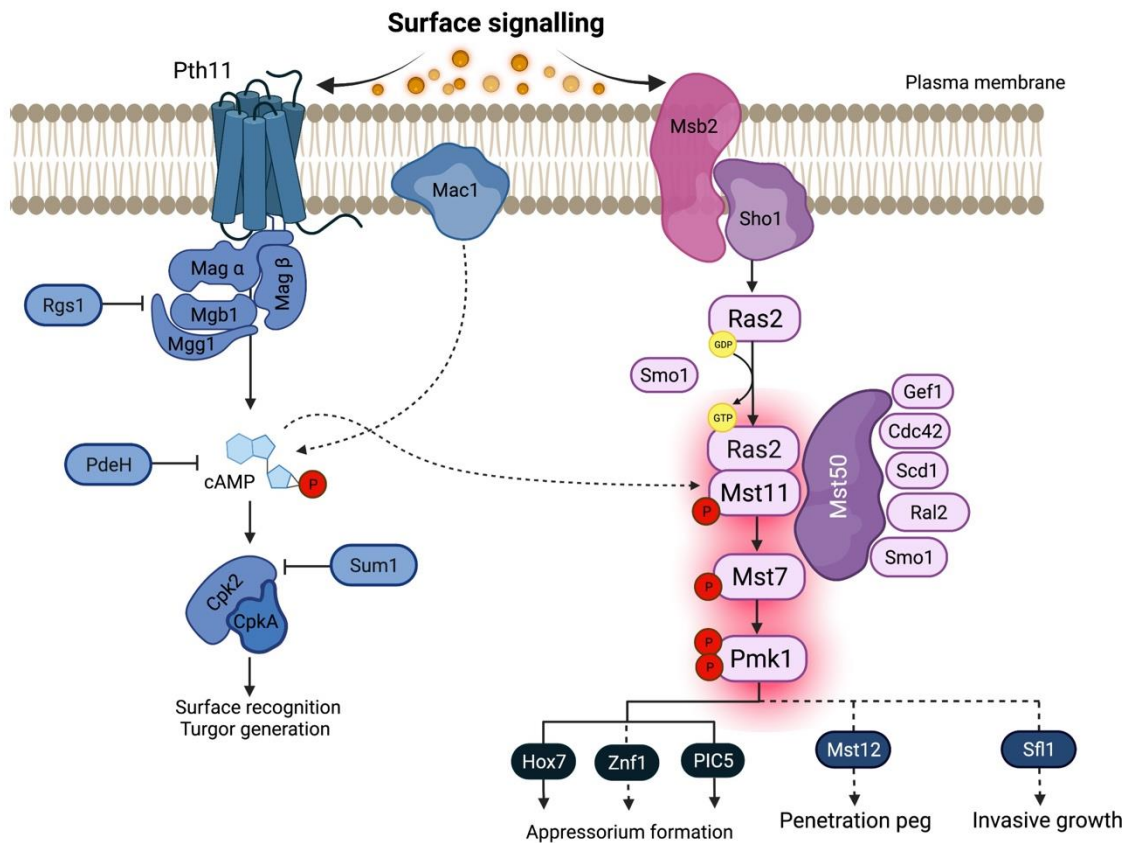
Figure 1.4. The Pmk1 MAPK signalling pathway during *M. oryzae* infection. Schematic diagram to show the Pmk1 MAPK cascade and its crosstalk with the cAMP-response pathway. The Pmk1 MAPK module is tethered by the Mst50 scaffold protein and constitutes a phosphorelay that culminates in movement of the phosphorylated Pmk1 MAPK to the nucleus to activate TFs, such as Mst12. Activation of the Pmk1 pathway involves Ras proteins, Cdc42 and the Gβ-subunit protein Mgb1 (Adapted from Wilson & Talbot, 2009). Dotted lines show hypothesised links (Without current experimental support).

Some novel components of the Pmk1 MAPK signalling pathway have been reported to act upstream of the Mst50-Mst11-Mst7 complex and are necessary for appressorium development. Among these are proteins such as the G-β subunit Mgb1 (Nishimura et al., 2003), the plasma membrane GPCR protein Pth11 (DeZwaan et al., 1999; Kou et al., 2017), and the sensing surface proteins Msb2 and Sho1 (Li et al., 2012) (Figure 1.4). Mgb1 interacts directly with Mst50, suggesting that Mst50 may integrate multiple upstream signals to activate the Pmk1 cascade (Park et al., 2006). Mgb1, Pth11, Msb2 and Sho1 also play a role in the surface recognition pathway requiring cyclic AMP-protein kinase A (cAMP-PKA)

(Li et al., 2012) (Figure 1.4). For this reason, it is thought that there is a link between cAMP-PKA and Pmk1 pathways, but this remains unclear (Ryder & Talbot, 2015).

Little is known about the Pmk1 downstream targets that regulate appressorium development. By yeast-two hybrid analysis (Y2H), two Pmk1-interacting clones (PICs) were identified to have roles in conidiation and appressorium differentiation (Zhang et al., 2011). The Pic5 mutants are defective in germ tube growth and appressorium formation (Zhang et al., 2011) (Figure 1.4). Transcription factors such as the homeobox protein Hox7 and the C2/H2 Zn finger-domain protein Znf1 operate downstream of Pmk1 cascade and are indispensable for appressorium formation (Cao et al., 2016; Kim et al., 2009; Osés-Ruiz et al., 2021; Yue et al., 2016) (Figure 1.4). Additionally, a comparative transcriptomics analysis of *Δpmk1* showed that 481 genes might be positively regulated by Pmk1 during germination, including known pathogenic components such as GAS proteins, Hox7 and Pth11 (Soanes et al., 2012). It is well recognized that Pmk1 regulates this change from polarised growth to isotropic expansion. However, how the pathway controls this significant step is not yet clear (Ryder & Talbot, 2015).

1.6.2 Pmk1 controls appressorium-mediated plant penetration

The Pmk1 MAPK pathway is also involved in the control of the morphogenetic transition occurring during host penetration. At this point, the blast fungus re-establishes polarity at the base of the appressorium enabling emergence of the narrow penetration peg hyphae (Dagdas et al., 2012; Gupta et al., 2015; Howard et al., 1991; Howard & Valent, 1996) (Figure 1.3). It has been demonstrated that the TFs Mst12 and Slf1, direct interactors of Pmk1, mediate early plant invasion events during host colonisation (Li et al., 2011; Park et al., 2002). Mst12 is important for penetration and invasive growth but dispensable for appressorium formation (Park et al., 2002). Null mutants of Mst12 (*Δmst12*) are non-pathogenic on rice and barley leaves but they are able to produce typical dome-shaped melanised appressoria (Park et al., 2002). A recent study, however, has shown that Pmk1 can directly phosphorylate Mst12 at serine 133 to control genes expressed late during appressorium formation, such as those related to septin-mediated appressorium pore formation, exocytosis and effectors (Osés-Ruiz et al., 2021). In a large-scale *in vitro* phosphorylation experiment, it was discovered that Slf1 is a target of Pmk1. Sfl1 null mutants (*Δsfl1*) can form appressoria but they show reduced virulence on rice and barley (Li et al., 2011). Altogether, it is hypothesised that Pmk1 pathway controls F-actin re-organisation and polarity determinants at the appressorium pore through TFs such as Mst12

and Slf1 (Figure 1.4). However, how Pmk1 controls primary cell host penetration has been poorly investigated in the blast fungus.

1.6.3 Pmk1 mediates cell-to-cell invasion during tissue colonisation

Recently, it has been reported that the Pmk1 cascade regulates invasive growth during hyphal constriction which allows movement from one plant cell to the next (Sakulkoo et al., 2018). It has been demonstrated that Pmk1 controls the septin-dependent mechanism by which narrow invasive hyphae constrict at the cell wall crossing points (Sakulkoo et al., 2018). This suggests that the Pmk1 pathway is also involved in differentiation of bulbous hyphae into the thin invasive hypha peg by the transpressorium, which is one of the most important morphogenetic switches of *M. oryzae* during plant colonisation (Cruz-Mireles et al., 2021). Interestingly, it has been also revealed that Pmk1 regulates expression of a subset of fungal effector genes to manipulate plasmodesmata conductance when the fungus crosses to neighbouring cells, providing a direct link between this pathway and the manipulation of the host immune response (Sakulkoo et al., 2018). Appressorium and transpressorium morphogenesis are, therefore, Pmk1-regulated processes. It is hypothesised that, similar to the appressorium, transpressorium formation is also a septin-mediated mechanism (Figure 1.5). The biology of the transpressorium is a poorly explored topic. Its parallels with the appressorium might, however, help to define how this specialised infection structure is regulated (Cruz-Mireles et al., 2021).
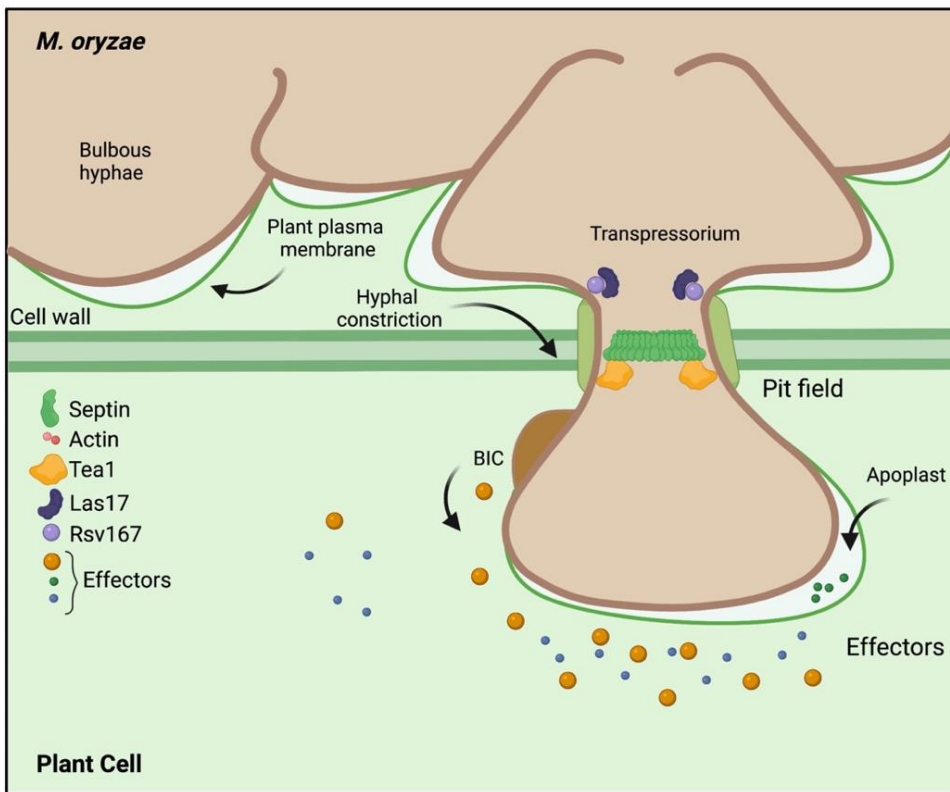
Figure 1.5. Septin-mediated transpressorium formation during *M. oryzae* invasive growth. Scheme to show the hypothesised septin ring assembly at the transpressorium pore with its polarity determinants.

1.7 Introduction to the current study

In this study, I set out to explore the operation of the Pmk1 MAPK pathway on the rice blast fungus using a quantitative phosphoproteomic approach. The rationale for this study was that by defining the phosphorylation events that are dependent on Pmk1, it would be possible to identify the proteins directly targeted by the MAPK. In this way, we sought to identify new components of the signalling pathway, such as the transcriptional regulators necessary for entry of the large changes in gene expression required for appressorium and transpressorium morphogenesis. We also reasoned that, using this approach, it would be possible to define the cellular functions dependent on Pmk1.

In Chapter 3, I describe how we generated a pipeline to investigate *M. oryzae* early appressorium development using novel quantitative proteomic methods. In collaboration with the TSL proteomics team, I show how we employ Parallel Reaction Monitoring (PRM),

that have not been applied to plant pathogenic fungi previously, to identify putative direct targets of Pmk1. This analysis allowed the identification of 55 potential interactors of Pmk1.

In Chapter 4, I illustrate how I functionally validated one of the Pmk1 putative targets, the phosphoprotein Vts1. Using *in vivo* and *in vitro* strategies, I confirmed that Vts1 is a direct target of Pmk1. I present evidence that this regulating protein is directly phosphorylated by Pmk1 and demonstrate that it has a role in the rice blast disease using gene functional analysis. I then demonstrate that the role of Vts1 in virulence is dependent on its Pmk1 phosphorylation.

Finally, in Chapter 5, I report the analysis of Pmk1-dependant phosphorylation of proteins during invasive growth and transpressorium formation by *M. oryzae*. Interestingly, a distinct set of Pmk1 targets can be observed during *in planta* growth including proteins involved in vesicle trafficking, cytoskeleton reorganisation and a group of putative effector proteins. The potential functions of these Pmk1 targets are discussed.

This thesis demonstrates the utility of phosphoproteomics to the study of cell signalling in fungi. I report the identification of a range of phosphoproteins associated with appressorium and transpressorium morphogenesis. This study allowed a comparative analysis of the distinct appressorium and transpressorium phosphoproteins, which are discussed in Chapter 6.

Chapter 2:

2 General materials and methods

2.1 *Magnaporthe oryzae* growth conditions

Magnaporthe oryzae strains used in this study were routinely grown on agar plates with solid complete medium (CM) incubated at 24°C with a 12 h light and dark cycle (Talbot et al., 1993). CM contains 10 g/L glucose, 2 g/L peptone, 1 g /L yeast extract (BD Biosciences), 1 g/L casamino acids, 0.1 % (v/v) trace elements (22 mg/L zinc sulphate heptahydrate, 11 mg/L boric acid, 5 mg/L manganese (II) chloride tetrahydrate, 5 mg/L iron (II) sulphate heptahydrate, 1.7 mg/L cobalt (II) chloride hexahydrate, 1.6 mg/L copper (II) sulphate pentahydrate, 1.5 mg/L sodium molybdate dehydrate, 50 mg/L ethylenediaminetra-acetic acid), 0.1 % (v/v) vitamin supplement (0.001 g/L biotin, 0.001 g/L pyridoxine, 0.001 g/L thiamine, 0.001 g/L riboflavin, 0.001 g/L, 0.001 g/L nicotinic acid), 6 g/L $NaNO_3$, 0.5 g/L KCl, 0.5 g/L $MgSO_4$, 1.5 g/L KH_2PO_4, [adjust pH to 6.5 with NaOH]), and 15 g/L agar. Agar was not used for liquid cultures. For long-term storage, *M. oryzae* strains were grown over sterile filter paper discs (Whatman International) placed on CM agar plates. The paper discs were then dehydrated and stored at -20°C. Unless otherwise noted, all chemicals were supplied from Sigma-Aldrich.

2.2 Pathogenicity and infection-related development assays

2.2.1 Virulence analysis of fungal strains on rice and barley

Conidia were harvested from a Petri dish culture using a sterile disposable plastic spreader in 3 mL sterile distilled water from 8–12 days old cultures grown on CM agar. The conidial suspension was filtered through sterile Miracloth (Calbiochem, UK) and fractionated by centrifugation at 5000 x g (Beckman, JA-17) for 15 min at room temperature. The pellet of conidia was re-suspended in 0.2 % (w/v) gelatin (BDH) and the spore concentration determined using a haemocytometer (Improved Neubauer, UK). Spores were diluted to a final concentration of 5 x10^4 conidia mL^{-1}. For spray infection assays, the spore suspension was used to infect rice using an airbrush (Badger. USA). After spray inoculation, the plants were covered in polythene bags and incubated in a controlled plant growth chamber (Conviron, UK) at 24°C for 48 h with a 12 h light and dark cycle, and 85% relative humidity. The inoculated plants were incubated for 5-6 days before scoring the lesions (Valent et al.,

1991). For leaf drop assays, the spore suspension was drop-inoculated on detached rice or barley leaves using a micropipette. Rice plants CO-39 and barley plants were grown for 3 weeks and 8-10 days, respectively, in 9 cm diameter plastic plant pots.

2.2.2 Fungal invasive hyphae proliferation assay on rice

To observe the intracellular growth of fungal invasive hyphae, leaf sheath inoculation assays were performed as previously reported (Kankanala et al., 2007). Rice of cultivar CO-39 leaf sheaths were cut into approximate 5 cm length from 3-4 weeks old plants. A conidial suspension at 5×10^4 conidia mL^{-1} concentration was used to inoculated leaf sheaths by pipetting the hollow space enclosed by the sides of the leaf sheath. Inoculated sheaths were then placed horizontally flat with the mid-vein faces downward in a moist chamber for the spores to settle on the mid-vein region. Inoculated leaf sheaths were incubated at 24°C for 26 h, 32 h or 48 h according to the experiment. For microscopic observations, leaf sheaths were hand-trimmed to remove the sides and expose the epidermis above the mid-vein. Lower mid-vein cells were cut to produce a thin section of three to four cell layers. The section was then mounted on a glass slide and examined by differential interference contrast (DIC) microscopy. For protein extraction, infected leaf sheath samples were collected by blotting with dry paper and were immediately frozen in liquid nitrogen to be stored at −80 °C.

2.2.3 Conidial germination and appressorium development

Conidial suspensions were prepared as previously described in section 2.2.2. Conidia were quantified and then diluted in sterile water to 7.5×10^5 conidia/mL in the presence of 50 ng/µL 1,16-Hexadecanediol (Sigma SA). For microscopic observations, a 50 µL aliquot of conidial suspension was inoculated onto a borosilicate glass coverslip (Menzel-Gläser, Fisher Scientific UK Ltd.) and placed on a moist paper towel. Conidia were incubated at 24 °C and observed as indicated. For large-scale conidial germination assays, conidial suspensions were poured into square petri plates (12 cm X 12 cm X 1.7 cm) (Greiner Bio One) to which 10 glass cover slips (Menzel-Gläser, Fisher Scientific UK Ltd.) were attached by adhesive. Appressorium formation was monitored under a Will-Wetzlar light inverted microscope (Wilovert®, Hund Wetzlar, Germany) for ensuring homogeneous and synchronized infection structure formation. Samples were collected as indicated by scraping the surface of the coverslips with a sterile razor blade (Fisher Scientific, UK). Harvested samples were immediately frozen in liquid nitrogen and stored at −80 °C for subsequent protein extraction. The appressorium *in vitro* development assay was adapted from Hamer et al., 1988.

19

2.3   Microscopy

2.3.1   Epifluorescence microscopy

Conventional epifluorescence and differential interference contrast (DIC) microscopy were performed on an IX81 motorized inverted microscope (Olympus, Hamburg, Germany) with X100/1.4 or X60/1.35 oil objectives. Images from the microscope were captured using a Photometrics CoolSNAP HQ2 camera system (Roper Scientific, Germany) under the control of MetaMorph software package (MDS Analytical Technologies, Winnersh, UK).

2.3.2   Confocal laser scanning microscopy

Confocal laser scanning fluorescence microscopy was performed on a Leica TCS SP8 microscope using 40x or 63x/1.4 oil immersion objective lens. Images were acquired using Leica LAS AF software (Leica Macrosystems Inc., Buffalo Grove, IL, USA). Fluorescence was observed using HyD detectors and white laser. The filter sets used for GFP were excitation wavelength 488 nm and emission collected at 495–550 nm. For RFP probes, the excitation wavelength was 543 nm and emission collected at 584 nm.

2.3.3   Image processing and data analysis

Confocal microscopy images were processed with the Leica LAS AF software and ImageJ (2.0) programs.

2.4   Molecular biology

All DNA manipulation and cloning techniques, including the isolation of plasmid DNA from bacteria, were carried out according to the manufacturer's instructions. Sanger sequencing was used to confirm all DNA constructs at Genewiz Azenta Life Scienes.

2.4.1   DNA restriction digestion

Restriction endonucleases used in this study were obtained from New England Biolabs (Hitchin, UK). DNA digestion reaction mix was composed of 1-15 µg DNA, 5-10 units of enzyme, 5 µL of manufacturer supplied buffer with a final volume of 50 µL nuclease-free water. The mixture was incubated at 37°C overnight for genomic DNA and at least 4 h for plasmid DNA. Agarose gel electrophoresis was used to fractionate digested DNA fragments.

2.4.2 Polymerase chain reaction (PCR)

Amplification of DNA fragments was performed using Phusion™ high-fidelity DNA polymerase (Thermo Scientific™) according to the manufacturer's protocol, allowing 30 s per kb. PCR annealing temperatures were calculated using T_m Calculator v1.12.0 (New England Biolabs). Colony PCR was performed with GoTaq® G2 DNA polymerase (Promega UK) or SapphireAmp® Fast PCR Master Mix (Takara Bio, USA) using pre-mixed buffer containing dNTPs, $MgCl_2$, and a gel loading dye according to the manufacturer's protocol, with 30 s or 10 s of amplification per kb, respectively. Single isolated colonies were added to the mixture using a sterile micropipette tip.

2.4.3 In-Fusion™ cloning

Genes of interest were cloned into pScBar-GFP for localisation experiments, into yeast-2-hybrid (Y2H) vectors (pGADT7 or pGBKT7) for protein-protein interaction experiments, and pOPIN vectors (Berrow et al., 2007) for protein production in *E. coli* by the In-Fusion™ cloning system (Takara Bio, USA). Sequences were amplified with primers containing homologous overhang sequences matching the cloning plasmid. Cloning reactions were performed using 1 µL 5x In-Fusion® HD enzyme premix combined with 100 ng of linearized vector and 50-100 ng of purified PCR fragment in a total reaction volume of 5 µL. After incubation at 42 °C for 30 min, the reaction was transformed into *E. coli* Stellar™ (Takara Bio, USA) competent cells.

2.4.4 DNA gel electrophoresis

Gel electrophoresis was used to separate PCR amplification products and restriction enzyme digestion products. DNA samples were fractionated through a 0.8 - 1.0 % (w/v) agarose gel in 1X Tris-borate EDTA (TBE) buffer (0.09 M Tris-borate and 2 mM EDTA). Ethidium bromide was added to molten agarose gel to 0.5 µg/mL final concentration to enable DNA visualisation under UV-light. To estimate the size of DNA fragments in the agarose gel, 1 Kb plus size marker (Invitrogen) was loaded alongside the samples. A UV transilluminator (Image Master VDS) and gel documentation system (Fujifilm Thermal Imaging) were used to visualise and record the separated DNA fragments in the gel.

2.4.5 DNA fragments purification

DNA fragments were purified from agarose gels using a commercial Wizard® Plus SV Gel and PCR Clean-up System kit (Promega, UK) following the manufacturer's instructions.

Agarose containing the desired size of DNA fragment was removed using a sterile razor blade and weighed in a sterile 1.5 mL microcentrifuge tube. Membrane binding solution (4.5 M Guanidine isothiocyanate and 0.5 M Potassium acetate, pH 5.0) was added to the tube containing the cut gel at the ratio of 10 µL per 10mg gel. The sample was incubated in a 65°C water bath until the gel was completely dissolved in membrane binding solution. An 800 µL aliquot of the DNA in molten agarose and membrane binding solution was transferred onto the Wizard® SV Minicolumn placed on a supplied 2 mL collection tube and incubated at room temperature for 1 min. The sample was centrifuged at 13,000 x *g* for 1 min to allow dissolved DNA to bind onto the Wizard® SV Minicolumn and the flow through waste to be discarded. An amount of 700 µL of membrane wash buffer (with 100% ethanol added) was added straight onto the column and centrifuged for 1 min. This step was repeated by adding 500 µL of membrane wash buffer and centrifugation for 5 min. The column bound DNA was eluted by directly pipetting 25-50 µL of Nuclease-Free water onto the column and incubating at room temperature for 1 min before centrifuging at 13,000 x *g* for 1 min. DNA solution was stored at -20°C for long term storage.

2.4.6 *Escherichia coli* transformation

For DNA plasmid production, Stellar™ Competent Cells were placed on ice to thaw before use. An aliquot of 50 µL of competent cells was placed into a 14 mL round bottom tube and 5 ng of DNA added for each transformation. The tubes were placed on ice for 30 min. The cells suffer a heat shock at 42ºC for exactly 45 seconds. Then, the tubes were incubated on ice for 2 min. SOC medium was added to bring the final volume to 500 µL. LB medium was first warmed to 37ºC. The tubes were incubated with shaking for 1 h at 37ºC. Finally, the 500 µL was divided and cultured on LB containing appropriate antibiotic for resistance screening. Plates were incubated overnight at 37ºC. Positive colonies were then screened by colony PCR using GoTaq® G2 DNA polymerase (Promega UK) or SapphireAmp® Fast PCR Master Mix (Takara Bio, USA) PCR master mix. The same protocol was used to transform Rosetta™ (DE3) Competent cells (Sigma-Aldich, UK) with pOPIN plasmids containing the gene of interest into for recombinant protein production. LB agar plates for Rosetta™ (DE3) transformants were supplemented with chloramphenicol.

2.4.7 DNA plasmid purification

After Sanger DNA sequence analysis, a colony harbouring the desired plasmid was chosen for further investigation. To obtain higher yields of plasmid DNA, the PureYield™ Plasmid Midi-Prep System (Promega, UK) was used. A positive colony was grown in 100 mL LB liquid medium for 18-20 h at 37ºC with vigorous aeration (225 rpm) in an Innova 4000 rotary

incubator (New Brunswick Scientific). Bacteria culture was pelleted by centrifugation at 10,000 x g for 10 min. The pellet was resuspended in 3 mL of Cell Resuspension Solution (50 mM Tris (pH 7.5), 10mM EDTA and 100 µg mL-1 of RNAse) and 3 mL of Cell Lysis Solution (0.2 M NaOH, 1% SDS). The samples were then inverted 5 times and left to incubate for 3 min at room temperature. After that, 5 mL of Neutralization solution (4.09 M guanidine hydrochloride, 0.759 M potassium acetate, 2.12 M glacial acetic acid (pH 4.2)) was added, and samples inverted to mix. Then, a centrifugation step was performed at 14,000 x g for 15 min. The supernatant was poured into a clearing column using a vacuum manifold. Plasmid DNA bound to the column was treated with 5 mL of Endotoxin Removal solution and washed with 20 mL of the Column Wash Solution (60mM potassium acetate, 8.3 mM Tris-HCl (pH 7.5), 0.04 mM EDTA, 60% ethanol). A vacuum was applied until the solution passed through, and the membrane was dried. Binding column was placed into a new 50 mL falcon tube and 600 µL of Nuclease-Free Water were added. After 1 min, the column was subjected to centrifugation at 1,500 x g for 5 min. Plasmid DNA was stored at 20ºC. For storage, 500 µL of the bacterial culture was incubated with 300 µL glycerol at -80ºC.

2.4.8 Co-transformation of yeast cells for Y2H

Desired constructs in pGBKT7 and pGADT7 were co-transformed into chemically competent *Saccharomyces cerevisiae* Y2HGold cells (Takara Bio, USA) using the commercial kit Frozen-EZ Yeast Transformation II™ (Zymo Research, UK). The cells were streaked onto YPDA (10 g/L yeast extract, 20 g/L Bactopeptone, 20 g/L Glucose monohydrate, 40 mg/L Adenine hemisulfate) agar and incubated for 72 h at 30 °C. Isolated colonies were then inoculated into 10 mL of liquid YPDA media and incubated overnight with vigorous aeration (225 rpm) in an Innova 4000 rotary incubator (New Brunswick Scientific). Saturated cultures were then diluted in fresh YPDA and grown for 3–4 h until mid-log phase (OD$_{600}$ of 0.0-1.0). Cells were pelleted by centrifugation at 500 x g. Cells were subsequently washed with 10 mL of Frozen-EZ Yeast Solution 1 (containing Tris, EDTA) and resuspended in Frozen-EZ Yeast Solution 2 (containing DMSO $\leq$ 10 %). An amount of 25 µL of resuspended competent cells were mixed with 100–200 ng of appropriate bait and prey plasmids (resuspended in less than 5 µl volume). Then, 500 µl of Frozen-EZ Yeast Solution 3 (containing PEG $\leq$ 45 %) was added to mixture and incubated for 90 min at 30 °C. Yeast cells were then pelleted by centrifugation at 1000 x g and plated on SD media -Leu -Trp. Co-transformed colonies containing both pGBKT7 and pGADT7 -based constructs were typically isolated after 72 h of incubation at 30 °C.

2.4.9 *M. oryzae* genomic DNA purification

For large-scale DNA extraction, fungal mycelium was generated by growing fungal culture on either cellophane discs or liquid. Using a mortar and pestle, 7-12 days old mycelium was ground into powder. Mycelial powder was decanted to a 1.5 mL microcentrifuge tube and mixed with 500 µL of pre-warmed CTAB (2% (w/v) Hexadecyltrimethylammonium Bromide (CTAB), 100 mM Tris base, 10 mM EDTA and 0.7 M NaCl) and incubated at 65°C with gentle mixing every 10 min. An equal volume of chloroform iso-amyl alcohol (CIA) was added, mixed thoroughly, and incubated with shaking for 30 min at room temperature. This was followed by centrifugation at 17000 x g for 10 min. This step was repeated twice by adding equal volumes of CIA and mixing vigorously on a shaker before centrifugation. The final supernatant was transferred into a clean sterile microcentrifuge tube and of isopropanol (2 x vol) added before incubating at -20°C overnight. The samples were centrifuged at 17000 x g for 10 min and the supernatant (isopropanol) was gently removed and the resulting pellet re-suspended in 500 µL sterile distilled water (SDW) and left to dissolve at room temperature with gentle tapping to mix. Sodium acetate (NaOAc) (0.1 vol) and 100% ethanol (2 vol) were added to re-precipitate nucleic acids. The mixture was incubated at -20°C for 2 h and pelleted by centrifugation at maximum speed, before washing with 400 µL of 70% (v/v) ethanol. The DNA was re-suspended in nuclease-free water. RNase (2 µL) was added and incubated at 37°C for 1 h to digest contaminating RNA.

2.4.10 Southern blotting

In this study, Southern blot analysis was used to determine positive *M. oryzae* null mutants for the *VTS1* gene. DNA digestion of *M. oryzae* transformants was performed overnight using *Hind*III endonuclease and subsequently fractionated by electrophoresis in an agarose gel at 100V. Fragments of genomic DNA were separated in agarose gels were transferred to Hybond-NX (Amersham Biosciences). Prior to blotting, partial depurination of DNA molecules was performed to enhance DNA transfer by submerging the agarose gel in 0.25 M with gentle rocking. Gels were then neutralised by replacing HCl with 0.4 M NaOH. For transfer of DNA from the agarose gel to the positively charged membrane, blots were carried out using a 0.4M NaOH transfer buffer that was drawn through a wet paper wick (Whatman /international) supported by a Perspex panel onto which the agarose gel was placed. A sheet of Hybond-NX membrane was then laid on the gel and positions of the wells were pencil marked. Three layers of Whatman 3MM paper and a stack of paper towels (Kimberley Clark Corporation) were laid over the membrane followed by a glass plate and a 500 g weight were placed on the stack as a weight. The transfer was left at room temperature

overnight. Then, the nucleic acid was fixed to the membrane by UV crosslinking to the membrane with 120 milijoules.cm^{-2} using a BLX crosslinker (Bio-Link).

2.4.10.1 Membrane hybridisation conditions and chemiluminescent detection of DIG-labelled DNA

The Hybond-NX membrane was pre-hybridised with Southern hybridization buffer (0.5M sodium phosphate buffer (pH7), 7% (w/v) SDS) using a hybridisation bottle (Hybaid Ltd) in the hybridization oven (Hybaid Ltd) at 62ºC with rotation for at least 30 min. Then, buffer was removed and replaced with the probe for overnight incubation at 62 ºC. The digoxigenin-(DIG) labelled probes were generated by PCR using Phusion® High-Fidelity DNA polymerase and DIG DNA labelling mix (Roche Applied Science) (5 µL per 50 µL reaction). The amplified fragment was fractionated by gel electrophoresis, purified, and added to 50mL of Southern hybridization buffer. Before the hybridisation step of the Hybond-NX membranes, the probe was boiled in a water bath at 100ºC for at least 10 min to denature the DNA. After hybridisation, the membrane was washed twice with Southern wash buffer (0.1M of sodium phosphate buffer (pH7), 1% (w/v) SDS) in the hybridisation tube at 62ºC for 15 min. The membrane was equilibrated in DIG wash buffer (150mM NaCl, 01.M maleic acid, pH to 7.5 with NaOH, 0.3% (v/v) Tween 20) at room temperature for 5 min, then to quench background signal DIG buffer was replaced with DIG-blocking solution (150mM NaCl, 01.M maleic acid, pH to 7.5 with NaOH, 1% milk powder). After this the membrane was incubated with 40 mL antibody solution (0.0001% (v/v) Anti-Digoxigenin-AP, Fab fragments (Roche) and subjected to centrifugation for 20 min at 16000 x g prior to addition to prevent inclusion of small antibody aggregated, 150 mM NaCl, 0.1 maleic acid, pH to 7.5 with NaOH, 1% (w/v) milk powder) for 30 min. The membrane was then washed twice with DIG wash buffer for 15 min, followed by being equilibrated in 20mL DIG buffer (0.1Tris/HCl (pH9.5), 0.1M NaCl, 50mM magnesium chloride) for 5 min. For the chemiluminescent reaction, 2 mL of the CDP-Star Solution (Roche) was pipetted onto the membrane and incubated for 5 min at room temperature. The membrane was further incubated at 37ºC for 15 min. DIG-labelled nucleic acids were detected through a chemiluminescent reaction with a chemiluminescent Substrate CDP-star® (Sigma). This reaction was performed by transferring the membrane onto a polypropylene sheet with 1mL CDP-Star® and covered by another polypropylene sheet and incubating for 30 min at 37 ºC. The membrane was developed using an ImageQuant LAS 4010 system (Amersham, UK).

2.4.11 *M. oryzae* whole genome sequencing

Purified DNA was obtained using the CTAB procedure, as explained earlier in Section 2.4.9. A NanoDrop spectrophotometer (Thermo Scientific, UK) and a Qubit BR assay (Thermo Fischer, USA) were used to analyse template quality and determine the concentration of double-stranded DNA. Sequencing was carried out using Novogene Sequencing services (Cambridge, UK). Whole genome sequencing was performed on NovaSeq 6000 system (Illumina), with two lanes per sample. Sequencing results were analysed by Dr. Vincent Were at The Sainsbury Laboratory.

2.5   RNA extraction

Total RNA was isolated from mycelia tissue after 48 h growth on CM liquid culture using a commercial kit (QIAGEN RNeasy Plant Mini Kit) according to then manufacturer's instructions. The procedure is based on guanidine-isothiocyanate lysis and silica-membrane purification. Briefly, 100 mg of dried mycelia was ground thoroughly in liquid nitrogen using a sterile mortar and pestle. The ground material was immediately transferred into a liquid-nitrogen-cooled 2 mL microcentrifuge tube, to which was added 450 µL buffer RLT previously mixed with 10 µL β-mercaptoethenol for every 1 mL of the RLT buffer, and vortexed vigorously. The lysate was transferred to a QIAshredder spin column placed in a 2 mL collection tube and was centrifuged for 2 min at 13,000 rpm. Supernatant of the flow-through was transferred to a microcentrifuge tube and mixed with 0.5 volumes of absolute ethanol by pipetting. The mixture was transferred to a RNeasy mini pin column placed in a 2 mL collection tube, and centrifuged at 13,000 rpm for 15 sec. The flow-through was discarded. 700 µL Buffer RW1 and 500 µL Buffer RPE were sequentially added to the RNeasy spin column with centrifugation at 13,000 rpm for 15 sec. Flow-through was removed between the steps. Next, a further 500 µL buffer RPE was added and centrifuged for 2 min at 13,000 rpm to dry the membrane. The RNeasy spin column was placed in a new 1.5 mL collection tube. RNA bound to the membrane of the RNeasy spin column was eluted in 30-50 µL RNase-free water and stored at –80 °C. Extracted RNA was used for cDNA synthesis.

2.6   Protoplast-mediated transformation of *M. oryzae*

A section of 2.5 cm^2 mycelium from a *M. oryzae* plate culture (8-10 days-old) was blended in 150 mL CM liquid and incubated at 25ºC, shaking (125 rpm) in an orbital incubator for 48h. Fresh ST (sucrose, 0.6M, Tris-HCl 0.1 M (pH 7), STC (sucrose, 1.2 M, Tris-HCl, 10 mM (pH 7.5)) and PTC (PRG 4000, 60%, Tris-HCl, 10 mM (pH 7.5), calcium chloride)

buffers were prepared and stored at 4°C. The culture was harvested by filtration through sterile Miracloth and the mycelium washed with sterile deionized water (SDW). The mycelium was transferred to a 50 mL falcon tube with 40 mL OM buffer (1.2 M magnesium sulfate, 10 mM sodium phosphate (pH5.8), Glucanex 5% (Novo Industries, Copenhagen)). Mycelium in the falcon tube with OM buffer was shaken gently to disperse hyphal clumps. Then, it was incubated at 30°C with gentle (75 rpm) shaking, for 3 h. The digested mycelium was transferred to two sterile polycarbonate Oakridge tubes (Nalgene) and overlaid with an equal volume of cold ST buffer. Resulting protoplasts were recovered at the OM/ST interface by centrifugation at 5000 x g, for 15 min at 4°C in a swinging bucket rotor (Beckman JS-13.1) in a Beckman J2.MC centrifuge. Protoplasts were recovered and transferred to a sterile Oakridge tube, which was then filled with cold STC buffer. The protoplasts were pelleted at 3,000 x g for 10 min (Beckman JS-13.1 rotor). This wash was carried out twice more with STC, with complete re-suspension of the pellet After the last wash, protoplasts were resuspended in 1 mL of STC and checked by microscopy. In an Eppendorf tube, an aliquot of protoplasts was combined with 6 µg DNA. The mixture was incubated at room temperature for 30 min. After incubation, 1 mL of PTC was added in 2 aliquots, mixed gently by inversion, and incubated at room temperature for 20 min. The transformation mixture was added to 150 mL of molten agar medium and poured into 5 sterile Petri dishes. For selection of transformants on hygromycin B (Calbiochem), plate cultures were incubated in the dark for at least 16 h at 24°C and then overlaid with approximately 15 mL of OCM/1% agar (CM osmotically stabilised with sucrose, 0.8M) containing 600µg mL^{-1} hygromycin B. For selection of bialophos (Basta) resistant transformants, OCM was replaced with BDCM (yeast nitrogen base without amino acids and ammonium sulfate, 1.7 g L^{-1} (Difco), ammonium nitrate, 2 g L^{-1} asparagine, 1 g L^{-1} glucose, 10 g L^{-1} sucrose, 0.8 (pH 6)). In the overlay, CM was replaced by BDCM without sucrose and hygromycin B was replaced by glufosinate (30 µg mL^{-1}) from a stock at 100 mg mL^{-1} in DSW. For selection of sulfonylurea resistant transformants, OCM was replaced with BDCM and in the overlay, hygromycin B was replaced with chlorimuron ethyl, at 30 µg mL-1 freshly diluted from a stock solution, at 100 mg mL^{-1}.

2.7   SDS-PAGE and Western blot

Western blot analysis was performed on recombinant proteins and *M. oryzae* total protein. Recombinant proteins were purified as indicated in Section 2.8. *M. oryzae* total protein samples were collected at indicated time point and snap-frozen in liquid-nitrogen. Lyophilised samples were lysed, and proteins were extracted with GTEN buffer (10 % glycerol, 25 mM Tris pH 7.5, 1 mM EDTA, 150 mM NaCl) with 10 mM DTT, 1% NP-40 and

protease inhibitor cocktail (cOmplete™, EDTA-free; Merck), phosphatase inhibitor cocktail 2 (SigmaAldrich; P5726) and phosphatase inhibitor cocktail 3 (Sigma-Aldrich; P0044). After centrifugation at 13,000 rpm for 10 mins, protein concentration was measured and normalised with the Bradford assay (Protein Assay Dye Reagent Concentrate; Bio-Rad). After normalization, extracts were heated in 2× TruPAGE™ LDS Sample Buffer (SigmaAldrich) at 70 °C for at least 5 mins. Different percentage SDS-PAGE gels were used to run samples of difference sizes. Proteins were separated by SDS-PAGE and transferred onto a polyvinylidene diflouride (PVDF) membrane using a Trans-Blot turbo transfer system (Bio-Rad, Germany). The membrane was blocked with 3% BSA in Tris-buffered saline and Tween 20. Membranes were immunoblotted with antibodies specified in Table 2.1. Membrane imaging was carried out with an ImageQuant LAS 4000 luminescent imager (GE Healthcare Life Sciences, Piscataway, NJ, U.S.A.).

Table 2.1. Antibodies used in this study.

Antibody	Target	Working concentration	Source
pTEpY (p44/42 MAPK)	Phosphorylated Pmk1	1:4000	Cell Signalling Technology (4370S)
pS/pT-P	Phosphorylated Vts1	1:3000	Abcam (ab934)4
GFP	GFP epitope tag	1:3000	Santa Cruz Biotechnology (sc-9996)
FLAG	FLAG epitope tag	1:4000	Sigma, UK (F3165)
Actin	Actin	1:4000	Agrisera com AS13 2640
6xHis	His epitope tag	1:4000	Abcam (ab1187)
Rabbit	HRP antibody raised for rabbit	1:2000	Cell Signalling Technology (7074S)

2.8   Recombinant proteins production and purification

Recombinant pOPIN plasmids encoding 6xHisGST-Pmk1 and 6xHis-Vts1 were transformed into *E. coli* RosettaTM (DE3) cells. The bacteria were pre- inoculated in 100 mL of LB medium with carbenicillin and chloramphenicol overnight. An amount of 25 mL culture was then diluted into 1 L of autoinduction media (AIM) (10 g/L tryptone, 5 g/L yeast extract, 3.3 g/L $(NH_4)_2SO_4$, 6.8 g/L KH_2PO_4, 7.1 g/L Na_2HPO_4, 0.5 g/L glucose, 2 g/L α-lactose, 0.15 g/L $MgSO_4$ magnesium sulphate and 0.03 g/L trace elements) (Studier, 2005) with appropriate antibiotics and grown in at 37 °C (30 °C for Shuffle cells) for 6 h and then 16 °C overnight. Cells were harvested and resuspended in ice-cold lysis buffer (50 mM Tris-HCl pH 8.0, 50 mM glycine, 5% glycerol, 500 mM NaCl and 20 mM imidazole, supplemented

with cOmpleteTM EDTA-free Protease Inhibitor Cocktail). The cells were then disrupted by sonication using a Vibra-CellTM sonicator (SONICS) with a single 13 mm probe, with the cells chilled on ice. The sonicator was set at 40 % amplitude, with a 1 s pulse followed by a 3 s pause, for 16 min. After the first sonication cell lysate was stirred and followed by another sonication of 8 min. The soluble fraction of the cell lysate was obtained by centrifuging for 30 min at 36,250 g at 4 °C. The supernatant was transferred to an ÄKTAxpress to carry out immobilised metal affinity chromatography (IMAC) in tandem with gel filtration. IMAC was carried out using 5 mL HisTrapTM HP NTA columns (GE Healthcare). After washing with 100 mL of washing buffer (50 mM Tris-HCl pH 8.0, 50 mM glycine, 5% glycerol, 500 mM NaCl and 20 mM imidazole), proteins were then eluted with 25 mL of elution buffer (50 mM Tris- HCl pH 8.0, 50 mM glycine, 500 mM NaCl, 500 mM imidazole, 5% (v/v) glycerol). This elution was then loaded onto a gel filtration SuperdexTM 200 HiLoadTM 26/600 column (GE Healthcare) equilibrated with gel filtration buffer (20 mM HEPES pH 7.5 and 150 mM NaCl). The gel filtration buffer for 6xHisGST-Pmk1 proteins was supplemented with 1 mM TCEP. Protein samples were separated by size and fractionated in 2 mL fractions that were analysed by SDS-PAGE to assess the presence of proteins. Fractions containing the proteins of interest where pooled and concentrated to 1 mL using VivaSpin® concentrators (Sartorius) with an appropriate molecular weight cut-off. Recombinant proteins were aliquoted and frozen in liquid nitrogen for storage at -80 °C. Heterologous production and purification of MEK2[DD] was performed, as previously described (Menke et al., 2005).

2.9 Protein-protein interactions assays

2.9.1 Yeast-Two-Hybrid (Y2H) analysis

The Matchmaker® Gold Yeast Two-Hybrid System (Takara Bio USA) was used to detect protein–protein interactions between Pmk1 and its putative targets. The Pmk1 coding sequence was cloned intopGBKT7 and co-transformed with each of its putative interactors in pGADT7, into chemically competent *Saccharomyces cerevisiae* Y2HGold (Takara Bio USA) cells as described in section 2. 4.8. Single colonies grown on selection plates were inoculated in 5mL of SD[-Leu-Trp] and grown overnight at 30˚C. Saturated culture was then used to make serial dilutions of OD$_{600}$ 1, 1^{-1}, 1^{-2}, 1^{-3}, respectively. An aliquot of 5µl of each dilution was then spotted on a SD[-Leu-Trp] plate as a growth control, SD[-Leu-Trp-His] (low stringency media) and SD[-Leu-Trp-Ade-His] (high stringency media) plate containing X-α-gal and aureobasidine A, as detailed in the user manual. Plates were imaged after incubation for 60 - 72 hr at 30˚C.

2.9.2 Co-immunoprecipitation (Co-IP)

Co-IP experiments were performed to validate Pmk1 - Vts1 interactions during appressorium development. *M. oryzae* appressorium samples of 4 h development transformed were generated as explained in section 2.2.3 for *ToxA*:GFP and *VTS1-GFP*. Total protein was extracted from each frozen sample using mortar and pestle to ground into fine powder. Appressorium powder was mixed with 2x w/v ice-cold extraction buffer (10% glycerol, 25 mM Tris pH 7.5, 1 mM EDTA, 150 mM NaCl, 2% w/v PVPP, 10 mM DTT, 1x protease inhibitor cocktail (Sigma), 0.1% Tween 20 (Sigma)) and vortexed vigorously. After centrifugation at 4,200 x *g*/4 °C for 20-30 min, the supernatant was used to determine the protein concentration by the Bradford assay. The presence of each protein in the input was determined by SDS-PAGE/Western blot. *ToxA*:GFP and VTS1-GFP proteins were detected by probing the membrane with anti-GFP horseradish peroxidase (HRP)-conjugated antibody (Santa Cruz Biotechnology, USA), Pmk1 with a Phospho-p44/42 MAPK (Erk1/2) (Thr202/Tyr204) (D13.14.4E) antibody (Santa Cruz Biotechnology, Santa Cruz, CA, U.S.A.) and a HRP-conjugated anti-rabbit antibody (Abcam, UK). *M. oryzae* actin protein was used as loading control and detected with an anti-actin primary antibody (Agrisera com, Sweden) and the anti-rabbit HRP conjugated antibody.

For immunoprecipitation, 1 ug of total protein was incubated with 30 µL of GFP beads (ChromoTek, Germany) in a rotatory mixer at 4 °C. After 3 h, the beads were pelleted (800 x *g*, 1 min) and the supernatant removed. The pellet was washed and resuspended in 1 mL of IP buffer (10% glycerol, 25 mM Tris pH 7.5, 1 mM EDTA, 150 mM NaCl, 0.1% Tween 20 (Sigma)) and pelleted again by centrifugation as before. Washing steps were repeated five times. Finally, 30 µL of 1:1 dilution of SDS buffer and water supplemented with 100 mM DTT was added to the beads and incubated for 10 min at 70 °C. The beads were pelleted again, and the supernatant loaded onto SDS-PAGE gels prior to Western blotting. Membranes were probed with anti-GFP and a Phospho-p44/42 MAPK (Erk1/2) (Thr202/Tyr204) (D13.14.4E) antibody as described before. Blots membrane imaging was carried out with an ImageQuant LAS 4000 luminescent imager (GE Healthcare Life Sciences, Piscataway, NJ, U.S.A.).

2.9.3 *In vitro* phosphorylation assay

For *in vitro* phosphorylation assays, 6xHis-GST tagged Pmk1 (250ng) was activated by incubation with recombinant MEK2^{DD} (250ng). Recombinant 6xHis tagged Vts1 (500ng) (500ng) was incubated with active Pmk1 in kinase buffer (25mM Tris pH 7.5, 10mM MnCl$_2$,

1mM EGTA and 1mM DTT) in the presence of 1 mM ATP at 30 °C for 30 min. Proteins were separated by SDS-PAGE and transferred to a polyvinylidene difluoride (PVDF) membrane using a Trans-Blot turbo transfer system (Bio-Rad). PVDF membrane was blocked with 2% bovine serum albumin (BSA) in Tris-buffered saline and 1% Tween 20. His tag detection was carried using polyclonal anti-6xHis horseradish peroxidase (HRP) -conjugated antibody (Abcam). Pmk1 activated was detected using Phospho-p44/42 MAPK (Erk1/2) (Thr202/Tyr204) (Santa Cruz Biotechnology) and anti-rabbit HRP-conjugated antibodies. Pierce ECL Western Blotting Substrate (Thermo Fisher Scientific) was used for detection. Membranes were imaged using ImageQuant LAS 4000 luminescent imager (GE Life Sciences). Phosphorylation assays were analysed by mass spectrometry.

2.10 Computational analysis

2.10.1 Functional categorization of Pmk1 targets

To further understand the putative direct Pmk1 targets obtained from the MS approach, selected phosphoproteins containing a MAPK phosphorylation motif (Pxx[S/T] P or [S/T] P) were categorized based on functional annotations from Blast2GO (Conesa & Götz, 2008) and Pfam (Finn et al., 2014).

2.10.2 Phylogenetic analysis

Multiple sequence alignment of fungal Vts1 sequences was performed in Clustal Omega (Sievers & Higgins, 2014). The phylogenetic tree of Vts1 was constructed using the maximum likelihood method and neighbour-joining method in MEGA X (Kumar et al., 2018) with bootstrap values based on 1000 iterations.

2.11 Phosphoproteomic analysis

2.11.1 Protein extraction and phosphoproteins enrichment

Frozen tissue was ground to a powder in liquid nitrogen, resuspended in extraction buffer (Urea 8M, NaCl 150 mM, Tris pH 8 100 mM, EDTA 5 Mm, aprotinin 1 µg/mL, leupeptin 2 µg/mL) and mechanically broken in a 30 mL Potter-Elvehjem homogenizer on ice (8 min at 1000 rpm). The homogenate was centrifuged for 30 min at 10,000 × g (Sorvall SW34 rotor). The supernatant was centrifuged for 60 min at 100,000 x g (Sorvall T-647.5 rotor) to obtain cytosolic fraction (supernatant) and microsomal fraction (pellet). The microsomal pellet was resuspended in extraction buffer. For phosphopeptide enrichment sample preparation

started from 1-3 mg of cytosolic or microsomal protein extract (determined using the Bradford assay) dissolved in ammonium bicarbonate buffer containing 8 M urea. First, the protein extracts were reduced with 5 mM Tris (2-carboxyethyl) phosphine (TCEP) for 30 min at 30°C with gentle shaking, followed by alkylation of cysteine residues with 40mM iodoacetamide at room temperature for 1 hour. Subsequently, the samples were diluted to a final concentration of 1.6 M urea with 50mM ammonium bicarbonate and digested overnight with trypsin (Promega; 1:100 enzyme to substrate ratio). Peptide digests were purified using C18 SepPak columns as described before (Mithoe et al., 2016). Phosphopeptides were enriched using titanium dioxide (TiO_2, GL Science) with phthalic acid as a modifier as described previously (Mithoe et al., 2016). Phosphopeptides were eluted by a pH-shift to pH 10.5 and immediately purified using C18 microspin columns (The Nest Group Inc., 5 – 60 µg loading capacity). After purification, all samples were dried in a Speedvac, stored at -80°C and re-suspended in 2% Acetonitril (AcN) with 0.1% trifluoroacetic acid (TFA) just before the mass spectrometric measurement.

2.11.2 Mass-Spectrometry analysis

LC-MS/MS analysis was performed using a Orbitrap Fusion trihybrid mass spectrometer (Thermo Scientific) and a nanoflow-UHPLC system (Dionex Ultimate3000, Thermo Scientific) Peptides were trapped to a reverse phase trap column (Acclaim PepMap, C18 5 µm, 100 µm x 2 c§m, Thermo Scientific) connected to an analytical column (Acclaim PepMap 100, C18 3 µm, 75 µm x 50 cm, Thermo Scientific). Peptides were eluted in a gradient of 3-40 % acetonitrile in 0.1 % formic (solvent B) acid over 120 min followed by gradient of 40-80 % B over 6 min at a flow rate of 200 nL/min at 40°C. The mass spectrometer was operated in positive ion mode with nano-electrospray ion source with ID 0.02mm fused silica emitter (New Objective). Voltage +2200 V was applied via platinum wire held in PEEK T-shaped coupling union with transfer capillary temperature set to 275 ºC. The Orbitrap, MS scan resolution of 120,000 at 400 m/z, range 300 to 1800 m/z was used, and automatic gain control (AGC) was set at 2e5 and maximum inject time to 50 ms. In the linear ion trap, MS/MS spectra were triggered with data dependent acquisition method using 'top speed' and 'most intense ion' settings. The selected precursor ions were fragmented sequentially in both the ion trap using CID and in the HCD cell. Dynamic exclusion was set to 15 sec. Charge state allowed between 2+ and 7+ charge states to be selected for MS/MS fragmentation.

Peak lists in the format of Mascot generic files (.mgf files) were prepared from raw data using MSConvert package (Matrix Science). Peak lists were searched on Mascot server v.2.4.1 (Matrix Science) against either *Magnaporthe oryzae* (isolate 70-15, version 8)

database, an in-house contaminants database, or *Magnaporthe oryzae* (isolate 70-15 version 8) database, Uniprot Rice database (UP000007015; *Oryza sativa subspecies indica*, strain: cv. 93-11) and an in-house contaminants database. Tryptic peptides with up to 2 possible mis-cleavages and charge states +2, +3, +4, were allowed in the search. The following modifications were included in the search: oxidized methionine, phosphorylation on Serine, Threonine, Tyrosine as variable modification and carbamidomethylated cysteine as static modification. Data were searched with a monoisotopic precursor and fragment ions mass tolerance 10ppm and 0.6 Da respectively. Mascot results were combined in Scaffold v. 4 (Proteome Software) and exported in Excel (Microsoft Office).

2.11.3 Parallel Reaction Monitoring (PRM)

Peptide quantitation was performed using Parallel Reaction Monitoring (PRM) as described previously (Guo et al., 2020). Briefly, mass to charge ratios (m/z) corresponding to selected phospho-peptides were monitored and filtered by the first quadrupole and fragment ions were scanned out in the orbitrap mass analyser over the duration of the elution profile. The PRM assay also included a selection of control peptides having similar relative intensities in each sample and used to measure relative phospho-peptide content. Raw data were peak picked and searched against the data bases on the Mascot server as described above and combined with chromatographic profiles in Skyline (MacLean et al., 2010) to determine individual peptide intensities. Extracted phospho-peptides intensity were normalised against the summed control peptide intensities to correct for differences in phospho-peptide yield. The assay was performed once for each of three biological replicates and results averaged ± SE.

Chapter 3:

3 A quantitative phosphoproteomic approach to discover novel components of the MAPK Pmk1 signalling pathway during appressorium development

3.1 Introduction

Phosphorylation is the most studied post-translational modification (PTM) (Ramazi & Zahiri, 2021). Out of more than 400 PTMs, the occurrence of phosphoserine, phosphothreonine and phosphotyrosine residues on proteins and their impact on protein behaviour are explored in most detail (Khoury et al., 2011). These PTMs are important because they represent a reversible regulatory mechanism that controls multiple cellular processes in all organisms (Khoury et al., 2011). Phosphorylation occurs in the cytoplasm or nucleus where the target protein receives a phosphate group (PO_4) to the lateral chain of a polar residue such as serine, threonine and tyrosine (Ardito et al., 2017). As a result, protein phosphorylation introduces a negative charge for each modified residue (Blazek et al., 2015). Such charge modification in the protein, can leads to changes in conformation, interaction, localisation and stability (Ardito et al., 2017; Olsen & Mann, 2013). Therefore, phosphorylation can impact protein function which can be translated into modulation of signal transduction (Nishi et al., 2014).

The identification and characterisation of phosphorylation sites in proteins is a critical step in the understanding of signalling networks (Dephoure et al., 2013). Recent advances in Mass-Spectrometry (MS) and computational pipelines have allowed the analysis of phosphorylation at the level of individual proteins and on the proteome scale (Strumillo et al., 2019). In fact, the study of the first entire proteome occurred just over a decade ago (De Godoy et al., 2008; Gruhler et al., 2005). Since then, MS has become a powerful tool in the identification and characterisation of PTMs, such as protein phosphorylation (Strumillo et al., 2019). Modern proteomics is changing quickly by implementing novel hight-throughput methods to study phosphoprotome profiling with improved sensitivity and accuracy (Bekker-Jensen et al., 2020).

The study of phosphoproteomes requires elaborated pipelines that combine MS and computational technologies (Bensimon et al., 2012). To carry out a MS experiment, the sample needs to be digested into peptides that will provide information such as peptide mass, ion intensity and a list of fragments which is required for the analysis (Choudhary &

Mann, 2010). In a general discovery phosphoproteomic pipeline, using a data dependent acquisition (DDA) method , the workflow can be divided into 4 steps (Choudhary & Mann, 2010). Firstly, the purified protein sample is digested with a protease that produces small peptides by cutting at specific sites. In this step, phosphopeptides are also enriched using either Fe^{3+} based Immobilized Metal Affinity Chromatography (IMAC), TiO_2 enrichment, a combination of IMAC and TiO_2 enrichment or phospho-residue-specific antibodies. Secondly, peptides are separated by chromatography using an organic solvent and then ionized by electrospray in the mass-spectrometer. Then, the mass spectra of individual peptides and their fragments are obtained. And, finally, the mass and list of fragment masses for each peptide are compared to protein databases, resulting in a list of identified peptides from which the proteins are inferred.

In the absence any form of quantification, the acquired phosphopeptide dataset can provide only limited biological insight (Mithoe & Menke, 2011). Therefore, discovery phosphoproteomics data can be coupled to quantitative methods, such as Parallel Reaction Monitoring (PRM), to accurately quantify phosphopeptides at the MS_2 level. By combining data from multiple biological replicates, data acquired by PRM provides confident quantitation with statistical robustness that can drive biological discoveries (Lilley & Dupree, 2006). In PRM, peptides to be measured are first selected from a phosphopeptide library, usually generated by a DDA method. The corresponding mass to charge ratios (m/z) are selectively scanned out and several MS/MS data points are acquired over the course of the elution profile. Finally, raw data is searched against a protein database and chromatograms interpreted in dedicated software, such as Skyline (MacLean et al., 2010) to calculate peptide level abundance (Rauniyar, 2015). Identification and quantification of phosphorylation sites constitute the first step to understand signalling mechanisms (Mithoe & Menke, 2011).

The use of MS-based phosphoprotemic approaches is quickly becoming a standard tool to study global cellular signalling (Savage & Zhang, 2020). In particular, the understanding of MAPK signalling has substantially benefited from applying phosphoproteomics methods (Takáč & Šamaj, 2015). In mammals, for instance, the use of phosphoproteomics has helped to decipher phosphorylation networks in cancer research (Gnad et al., 2016). In plants, phosphoproteomic studies employing genetically modified kinase expression systems have identified downstream targets on MEK2 and MPK3/6 signalling (Hoehenwarter et al., 2013; Lassowskat et al., 2014). In yeast, a quantitative phosphoproteomics analysis of the pheromone response pathway identified determinants of polarised growth and cell-cycle (Gruhler et al., 2005). When considered together, the use

A quantitative phosphoproteomic approach to discover novel components of the MAPK Pmk1 signalling pathway during appressorium development

of phosphoproteomics methods has contributed to dissect MAPK signalling in a wide range of organisms.

In the blast fungus *M. oryzae*, the Pmk1 MAPK is a central regulator of appressorium morphogenesis. The importance of Pmk1 is illustrated by the fact that its absence (*Δpmk1*) or through chemical inhibition of the kinase (*pmk1^AS* treated with 1-Na-PP1) leads to a failure to develop and appressorium (Sakulkoo et al., 2018; Xu & Hamer, 1996). Indeed, a recent analysis has revealed that Pmk1 regulates approximately 49% of *M. oryzae* transcriptome during appressorium development, highlighting its importance as a master regulator of infection-related morphogenesis (Osés-Ruiz et al., 2021). Despite its significance, there is as lack of understanding regarding the molecular mechanisms that underpin Pmk1 cascade.

Most of the identified components of the Pmk1 cascade have been validated genetically based on homology to their counterparts in the yeast Fus3/Kss1 pathway (Elion et al., 1991, Elion et al., 1990). The upstream Pmk1 kinases Mst11 and Mst7 were functionally characterised because they are homologues of the yeast MAPKKK Ste11 and the MAPKK Ste7, respectively (Zhao et al., 2005). Similarly, the adaptor protein Mst50 was identified due to its homology to the yeast protein Ste50 (Park et al., 2006). It has been demonstrated that Mst11-Mst7-Pmk1 form the three-tiered MAP kinase module regulating appressorium formation during blast disease whose activity is controlled by the adaptor protein Mst50. Also, the transcription factor Mst12 was initially described as a potential target of Pmk1 because it is a homologue of Ste12, another previously reported component of the Fus3/Kss1 pathway in yeast (Park et al., 2002). Mst12 was recently validated as a Pmk1 target using an *in vitro* MAPK assay where it was shown to be phosphorylated by Pmk1 in S133 (Osés-Ruiz et al., 2021). The individual null mutants of all these components are non-pathogenic, demonstrating that the Pmk1 MAPK cascade is critical for infection by *M. oryzae*.

Some efforts have been devoted to characterising Pmk1 downstream interactors in the blast fungus. A large-scale *in vitro* phosphorylation assay coupled to a protein microarray containing 573 transcription factors identified Slf1 as a Pmk1 target (Li et al., 2011). Slf1 has been reported to function in virulence and heat tolerance (Li et al., 2011). A yeast-two-hybrid screening from genes expressed in hyphae under nitrogen starvation and in mature appressoria (36 h) revealed two Pmk1-interacting clones (Pic), Pic1 and Pic5 (Zhang et al., 2011). *PIC1* was shown to have a role in conidiogenesis and *PIC5* in virulence (Zhang et al., 2011). More recently, a hierarchical transcriptional network study revealed that the transcription factor Hox7 is a direct target of Pmk1, controlling hyphal-like growth and

appressorium morphogenesis (Osés-Ruiz et al., 2021). Nevertheless, the molecular mechanisms of how these downstream Pmk1 signalling components control blast infection remain elusive.

In this Chapter, I describe a temporal quantitative phosphoproteomic approach to analyse early appressorium development and identify novel Pmk1 interactors. Collectively, these data provide the first comprehensive overview of phosphorylation events during early blast disease in the context of the Pmk1 MAPK signalling pathway.

3.2 Results

3.2.1 Pmk1 is required for appressorium development

As a starting point for this project, I studied the phenotype of Pmk1 mutants during appressorium development. To this end, I set up an *in vitro* appressorium assay at different timepoints from 0 to 24 h. To ensure a synchronised infection structure formation, I used 50 ng/μl^{-1} 1,6 hexadecanediol (Sigma), which is a powerful stimulator of appressorium development (Gilbert et at., 1996). Consistent with previous research, $\Delta pmk1$ mutants were unable to develop appressoria upon contact with a hydrophobic surface (Figure 3.1). Similarly, when the conditional mutant $pmk1^{AS}$ was used to abrogate Pmk1 function by using the ATP-analogue 1NA-PP1, appressorium formation is compromised (Figure 3.1). These results confirm that $\Delta pmk1$ and $pmk1^{AS}$ mutants have the same phenotype affecting appressorium morphogenesis.

To gain more details of appressorium morphogenesis in the Pmk1 null mutant, I sought to study its phenotype *in planta* using electron microscopy. Rice leaves of the blast-susceptible *indica* rice variety CO-39 were inoculated with conidia of Guy11 and $\Delta pmk1$ and visualised after 24h (in association with Dr. Lauren Ryder). Samples were then processed and visualised using Scanning Electron Microscopy (SEM), in collaboration with Dr. Kim Findlay. In rice leaves infected with Guy11, we observed that conidia produced a germ tube that differentiated into an appressorium (Figure 3.2). As previously observed, the conidium collapsed as a result of autophagy-mediated cell death (Figure 3.2) (Eseola et al., 2021; Veneault-Fourrey et al., 2006). By contrast, in leaves infected with the $\Delta pmk1$ mutant, conidia failed to form an appressoria. We observed long germ tubes growing over the leaf surface and no collapsed conidia (Figure 3.2). As suggested by previous studies, these data confirm that the Pmk1 null mutant has the same phenotype under *in vitro* and *in vivo* experimental conditions.

A quantitative phosphoproteomic approach to discover novel components of the MAPK Pmk1 signalling pathway during appressorium development
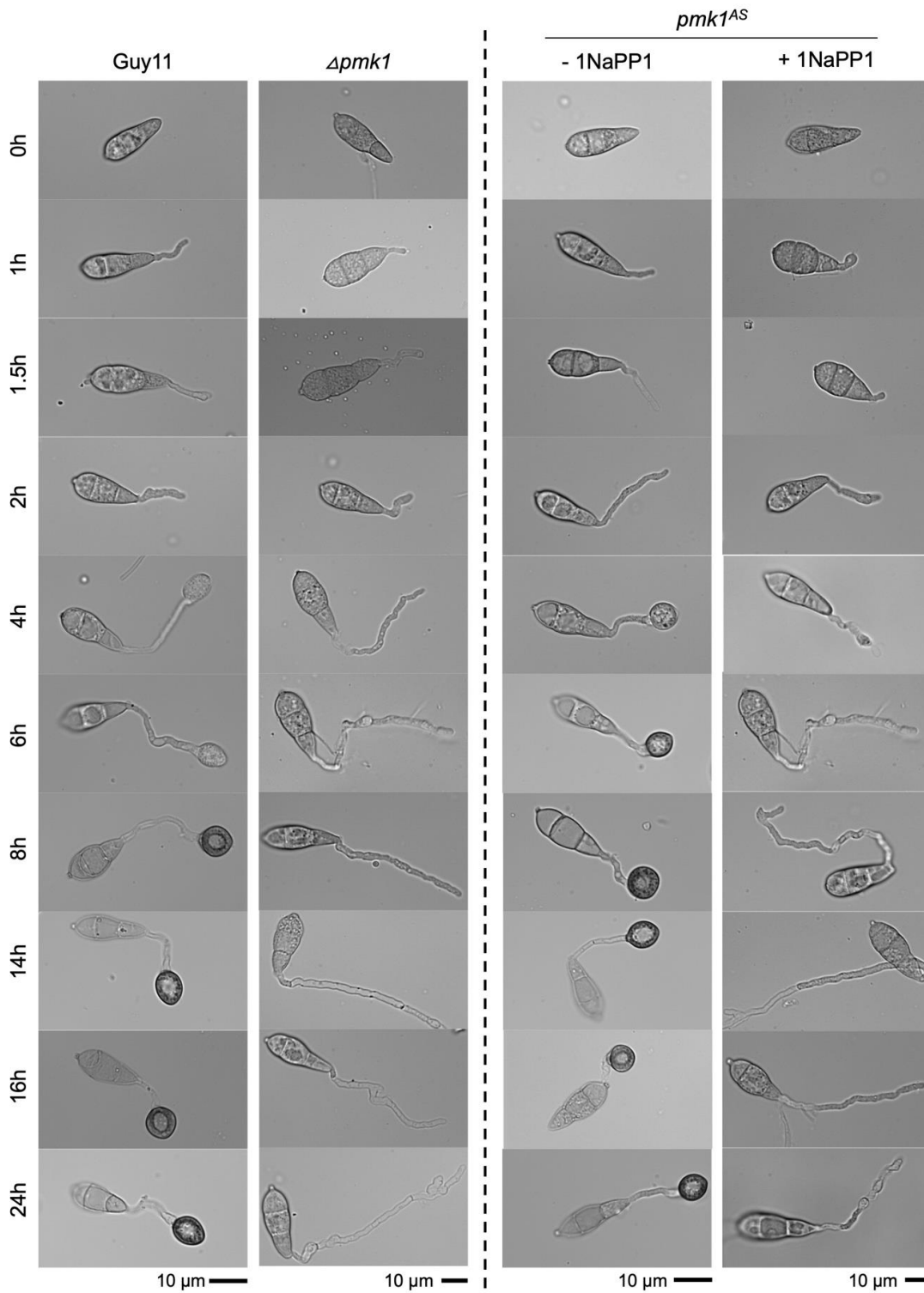
Figure 3.1. Phenotype of *Δpmk1* and *pmk1^AS* during appressorium development. Representative micrographs to show the requirement of Pmk1 activity during appressorium formation in the null mutant *Δpmk1* (on the left) and in the analogue-sensitive mutant *pmk1^AS* in the presence/absence of 1Na- PP1 (on the right) in a time course from 0h-24h. Appressorium formation of *M. oryzae* strains was evaluated at the indicated time at 24°C. All scale bars indicate 10 µm.

A quantitative phosphoproteomic approach to discover novel components of the MAPK Pmk1 signalling pathway during appressorium development
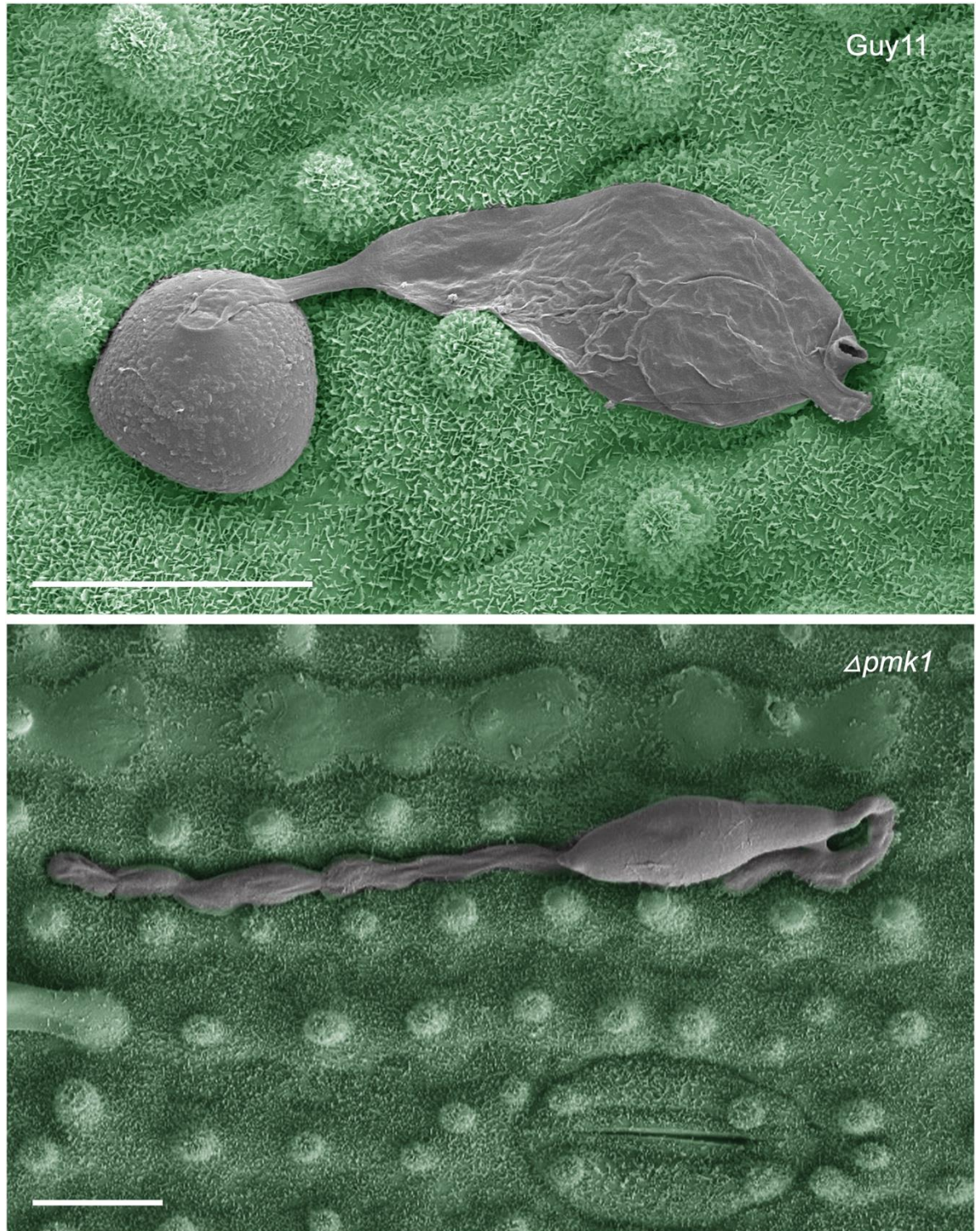
Figure 3.2. Scanning electron micrograph of appressorium morphogenesis on rice blast leaves. Scanning electron micrographs with false colouring to show appressorium germination of wild-type strain Guy11 (on top) and *Δpmk1* (at the bottom). The blast fungus is shown in grey, and rice leaf surface is false-colour imaged to green. Images were taken at 24 h. Scale bars indicate 10 μm.

3.2.2 Pmk1 is activated early during appressorium development

The initial hours of conidia germination are critical for appressorium formation. After contact with a hydrophobic surface, conidia attach using an adhesive called spore tip mucilage (Hamer et al., 1988). Within the first 2 hours, and in the presence of water, a polarised germ tube emerges from the apical cell. It then flattens against the substratum and swells minimally at its tip, in a process described as "hooking" (Bourett & Howard, 1990). At this point, the germ tube switches from polar to isotropic growth (Bourett & Howard, 1990; Cruz-Mireles et al., 2021). Because Pmk1 is required for appressorium formation, this signalling cascade must regulate the early events of the process.

The precise time at which Pmk1 starts to control the onset of appressorium morphogenesis is unknown. From my *in vitro* appressorium assay, I observed that an incipient appressorium is formed 4 h after conidial germination. Therefore, I reasoned that Pmk1 must be activated earlier than 4 h. In general, MAPKs are activated by dual phosphorylation of threonine and tyrosine within a TEY motif (pTEpY) in the activation loop of the kinase domain (Cargnello & Roux, 2011).

To investigate Pmk1 activation in the appressorium, I decided to use an antibody that recognises the pTEpY motif. For this purpose, I used the complemented strain *Δpmk1: PMK1-GFP* (Sakulkoo et al., 2018) and *Δpmk1* (Xu & Hamer, 1996) as a control. I generated synchronised samples from 0 h (spores), 1 h, 1.5 h, 2 h and 4 h of conidia germination for *Δpmk1: PMK1-GFP* and *Δpmk1.* I extracted total protein from each time point and detected Pmk1 activation by Western blot analysis. As expected, Pmk1 was only detected in the complemented strain *Δpmk1: PMK1-GFP* but not in the mutant. Interestingly, I detected total endogenous Pmk1 in all different timepoints (Figure 3.3). However, Pmk1 double phosphorylation in the activation motif (pTEpY) was only detected in samples from 1h - 4h (Figure 3.3). Although endogenous Pmk1 is present at all stages from spores to incipient appressorium (0-4 h), this experiment demonstrates that it only becomes pTEpY phosphorylated upon contact with a hydrophobic surface. Taken together, these results provide strong evidence that Pmk1 is activated prior to appressorium morphogenesis.

A quantitative phosphoproteomic approach to discover novel components of the MAPK Pmk1 signalling pathway during appressorium development
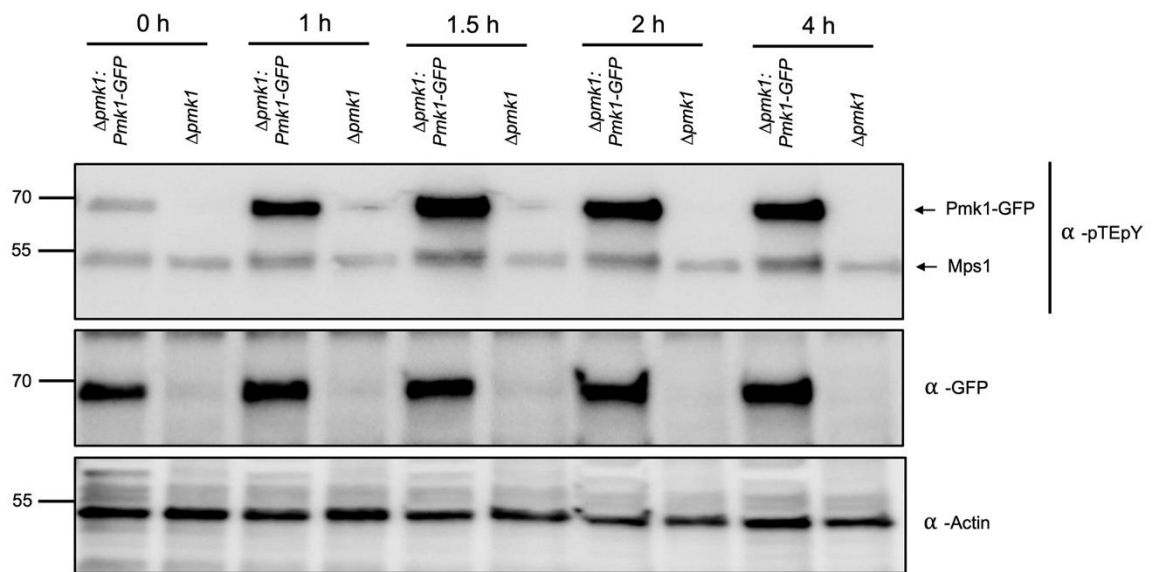
Figure 3.3. Detecting the activation of Pmk1 during the early stages of appressorium development by *M. oryzae*. Western blot analysis of total protein extracted from *in vitro* germinated spores at 0, 1, 1.5, 2 and 4 h from $\triangle pmk1$ complemented with *PMK1-GFP* and $\triangle pmk1$ using α-pTEpY (top panel), α-GFP (middle panel) and α-Actin (lower panel). α-pTEpY has been also reported to detect the MAPK Mps1 (Zhang et al., 2018). Proteins were immunoblotted with appropriate antisera (listed on the right). Arrows indicate expected band sizes.

3.2.3 Using discovery proteomics to identify protein phosphorylated in a MAPK motif during early appressorium formation

Large-scale phosphoproteomics analysis have been performed to identify potential MAPK substrate pairs (Zhang et al., 2016). Because the blast fungus forms an incipient appressorium within 4 h and Pmk1 is activated early in appressorium morphogenesis, I reasoned that Pmk1 targets required to control the development of this structure must be phosphorylated within 0-4 h of germination consistent with the activation of Pmk1 itself through dual phosphorylation on its activation loop. Therefore, I decided to carry out a comparative phosphoproteomic analysis in the appressorium in a time-course dependent manner. As described earlier, $\triangle pmk1$ and $pmk1^{AS}$ show the same mutant phenotype. Therefore, I decided to use Guy11 and $\triangle pmk1$ strains in this comparative phosphoproteomic study.

A quantitative phosphoproteomic approach to discover novel components of the MAPK Pmk1 signalling pathway during appressorium development

To investigate Guy11 and *Δpmk1* phosphoproteomes during early appressorium development, I first generated synchronised infection structures on a large-scale. To have an overview of the phosphoproteome during early appressorium morphogenesis, I studied 0 h, 1 h, 1.5 h, 2 h, 4 h and 6 h time points. For each time point, Dr. Miriam Osés-Ruiz and I germinated *in vitro* at least 200 mL of $5x10^4$ conidial suspension onto 40 - 50 hydrophobic coverslips (24 x 50 mm; Thermo Fisher Scientific, UK) per replicate and strain. In the case of 0 h timepoint, the conidial suspension was not exposed to an inductive surface. This enabled us to harvest sufficient biological material to obtain 1.5 mg of total protein for phosphopeptide enrichment. I extracted phosphorylated peptides according to the protocol described in Mithoe, et al., 2016. Dr. Frank Menke and Dr. Paul Derbyshire then examined 5% of phosphopeptides from at least 3 biological replicates per time point for each strain using a data-dependent method on an Orbitrap LC-MS/MS (Figure 3.4).

To identify potential Pmk1 targets, I searched for phosphorylated proteins in our dataset generated by mass-spectrometry. From this initial discovery phosphoproteomic analysis in Guy11 and *Δpmk1* samples, we identified 2722 phosphorylated proteins. Because I was interested in potential targets of Pmk1, I searched for proteins phosphorylated in a serine/threonine followed by a proline, in a so called proline-directed site that constitutes the MAPK motif (Bardwell, 2006). Using the proteomics software Scaffold 5, I found that a total of 1943 proteins were phosphorylated in the dipeptide motif S/T-P (Figure 3.4). Altogether, these results demonstrate that we can identify proteins that are phosphorylated in a MAPK motif from appressorium samples of *M. oryzae*.

A quantitative phosphoproteomic approach to discover novel components of the MAPK Pmk1 signalling pathway during appressorium development
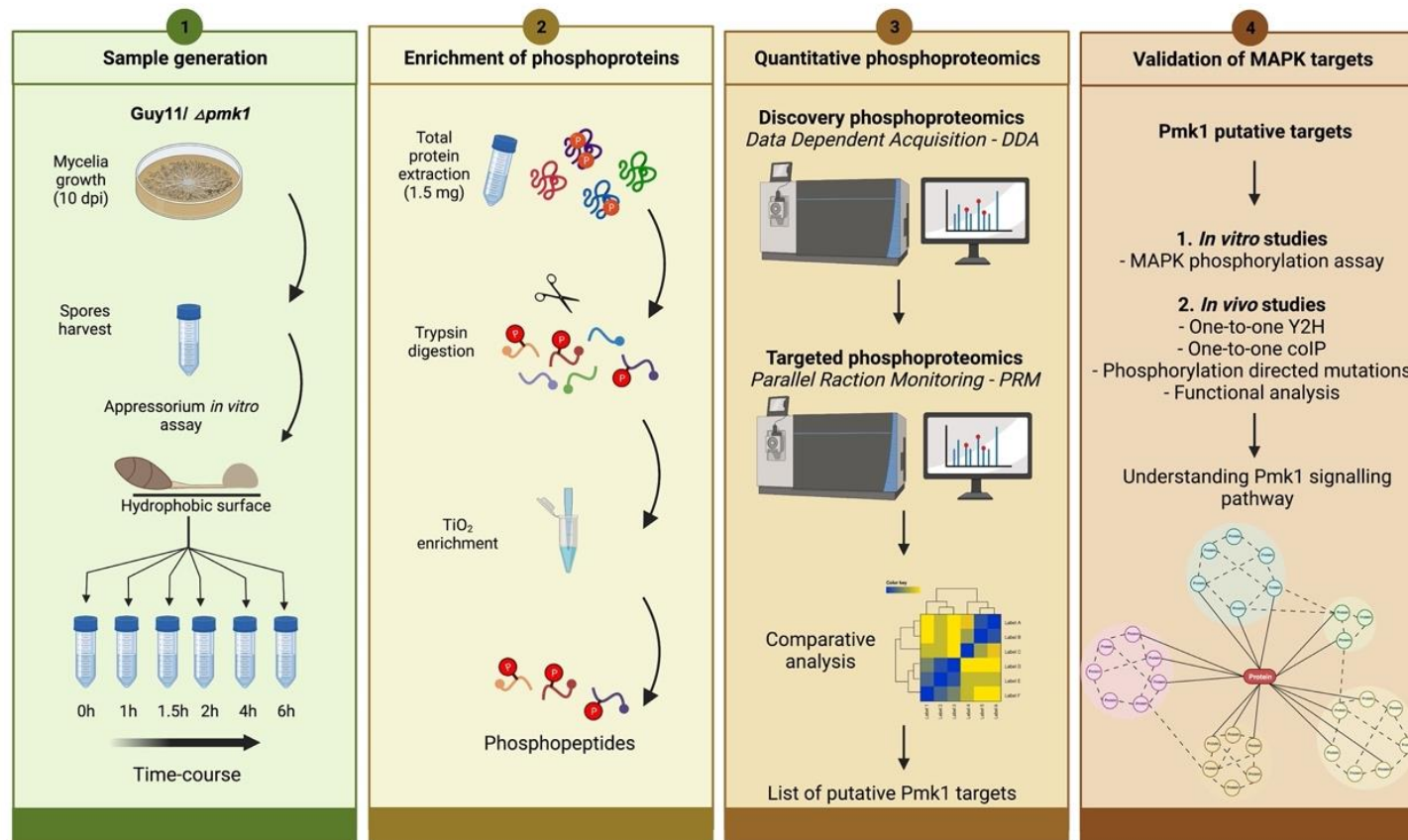
Figure 3.4. Phosphoproteomics experimental workflow and data analysis pipeline to identify Pmk1 targets in *M. oryzae.* Flowchart showing the experimental strategy to identify Pmk1 targets during appressorium development using phosphoproteomic

3.2.4 Using Parallel Reaction Monitoring to identify putative Pmk1 targets during appressorium formation

To identify components of the Pmk1 pathway, I next looked for differentially phosphorylated proteins in Guy11 and *Δpmk1*. I hypothesised that direct targets of Pmk1 would be phosphorylated only in the presence of Pmk1, and would therefore be specific, or differentially phosphorylated in the wild-type strain Guy11. By contrast, in *Δpmk1* mutants these putative targets would not be phosphorylated. Because discovery proteomics is a semi-quantitative approach (Fernández-Niño et al., 2015), we decided to opt for a quantitative strategy to discover differentially phosphorylated peptides. To this end, Dr. Paul Derbyshire used a Parallel Reaction Monitoring (PRM) approach to measure our samples. PRM is a high resolution method for targeted quantification of specific peptides (Peterson et al., 2012; Rauniyar, 2015). Therefore, before PRM analysis was initiated, we had to decide which peptides from our dataset to target.

From our list of proteins phosphorylated in a MAPK motif, we selected the peptides to target by PRM. For this purpose, I chose: a) potentially differentially phosphorylated peptides based on the discovery proteomics total spectral counts; b) peptides from proteins of previously reported Pmk1 targets; and, c) potential components of the Pmk1 pathway based on a hierarchical transcriptomic analysis (in collaboration with Dr. Paul Derbyshire and Dr. Miriam Osés-Ruiz) (Osés-Ruiz et al., 2021). With this information, we generated a list of 404 phosphopeptides belonging to 245 proteins.

To generate quantitative information of the phosphopeptides selected, Dr. Paul Derbyshire performed the PRM experiment and was able to confidently quantify 289 phosphopeptides. For this analysis, he used 5% from each of the samples generated in the early time-course appressorium experiment on Guy11 and *Δpmk1* to target the previously chosen peptides using the Orbitrap Fusion mass spectrometer. Dr. Paul Derbyshire analysed PRM results using Skyline software to determine the relative peptide abundance. Refined data from Skyline was exported to Excel where peptide abundances were normalised based on a collection of carefully selected non-differential phosphopeptides, present to equal measure in each sample irrespective of time point or genotype. Then, Dr. Dan MacLean calculated statistically significant difference of each sample compared to the spore sample (0 h) within each genotype. For this a boot-strap t-test was applied, with Bonferroni multiple testing correction. Statistically significant different peptides were plotted using ggplot on R package (Figure 3.6). This analysis revealed that 182 peptides from 89 proteins are differentially phosphorylated at one or more timepoints when we compared within the genotypes Guy11 and *Δpmk1.*

A quantitative phosphoproteomic approach to discover novel components of the MAPK Pmk1 signalling pathway during appressorium development

To dissect the PRM results, we decided to perform a cluster analysis. Dr. Dan MacLean first evaluated data complexity and categorised differentially phosphorylated peptides in 10 clusters based on minimal variance using a k-means approach (Figure 3.7). As shown in Figure 3.8, clusters 3, 4 and 5 represent peptides with the highest fold change when we compare peptide relative intensity from the two strains. These 101 peptides belonged to 55 proteins that we classified as putative Pmk1 targets. Therefore, using discovery proteomics followed by PRM analysis from a time series study of appressorium samples, we were able to identify a set of 55 putative targets of Pmk1 (Figure 3.5). Taken together, our quantitative phosphoproteomic approach therefore revealed an extensive set of potential downstream components of the Pmk1 MAPK cascade.
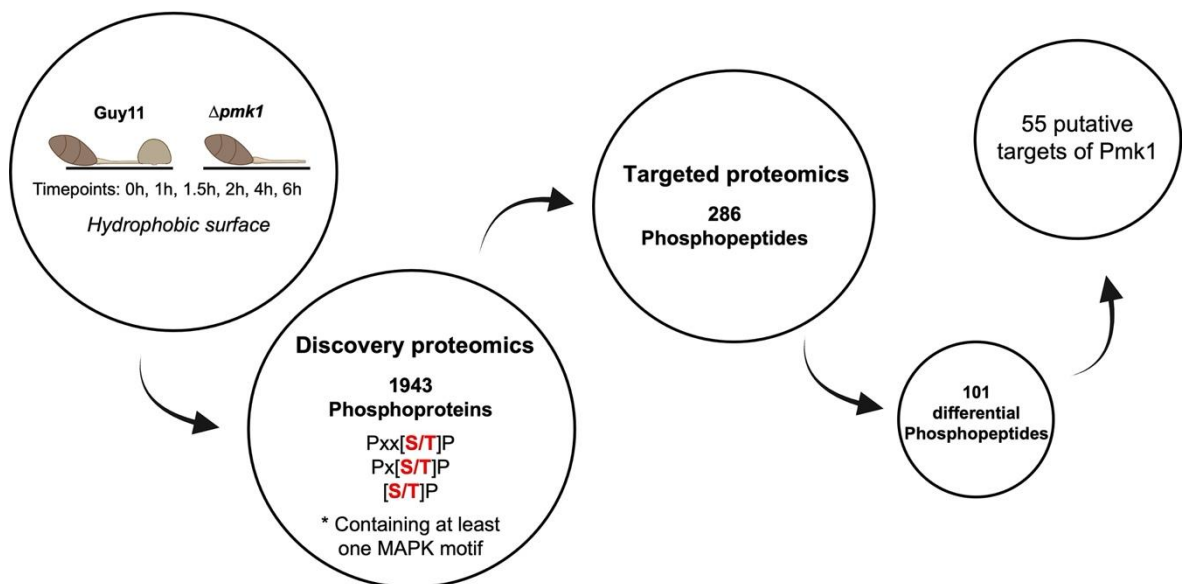
Figure 3.5. Identification of MAP kinase Pmk1 targets during appressorium formation by discovery and targeted phosphoproteomics. Flowchart showing the experimental strategy to identify Pmk1 targets during appressorium development using phosphoproteomics.

3.2.5 Putative Pmk1 targets play different cellular functions

To interpret proteomics data, it is necessary to perform functional categorisation analysis. This type of study allows the translation of -omics data into more valuable biological knowledge (Rydén et al., 2021). Using discovery proteomics followed by Parallel Reaction Monitoring, I identified 55 possible Pmk1 interactors. To understand the cellular processes that Pmk1 might be regulating through these potential targets, I performed functional categorisation using a Gene Ontology (GO) database generated in our lab (Osés-Ruiz et

A quantitative phosphoproteomic approach to discover novel components of the MAPK Pmk1 signalling pathway during appressorium development

al., 2021; Sakulkoo et al., 2018), where assignments were made using the Blast2GO suite (Conesa & Götz, 2008). I cross-referenced my analysis with "Magnagenes", a database of functionally characterised genes in *M. oryzae* (Foster et al., 2021). With this method, I classified the 55 Pmk1 putative interactors into different cellular functions and processes as well as identifying uncharacterised and non-described proteins in the blast fungus (Table 3.1).

Table 3.1. Pmk1 putative targets identified during appressorium formation by PRM.

Gene ID	Name	Function/ Process	Pmk1 dependent phosphorylation site
MGG_01311	Nuclear elongation protein	Uncharacterised	S216
MGG_02522	Dash complex protein	Uncharacterised	S113
MGG_01795	S/T protein kinase	Uncharacterised	S25
MGG_03064	Rho1	Uncharacterised	S20
MGG_03218	Calcipressin protein	Uncharacterised	T190, S193
MGG_03558	PH domain protein	Uncharacterised	S666, S688, S875
MGG_04421	PH finger and bah domain protein	Uncharacterised	T148
MGG_05220	S/T protein kinase	Uncharacterised	S267, S274, S320
MGG_05257	Ring finger protein	Uncharacterised	S667
MGG_05376	S/T protein kinase	Uncharacterised	T114
MGG_06334	Vts1	Uncharacterised	S175, S420
MGG_06403	PH domain protein	Uncharacterised	S272, S275
MGG_06413	Pitslre protein kinase	Uncharacterised	T67
MGG_06599	S/T protein kinase	Uncharacterised	S124
MGG_07714	Actin cytoskeleton organization protein	Uncharacterised	S258
MGG_09293	Cell division control protein	Uncharacterised	S97, S125, Y129, S133
MGG_09554	Anaphase-promoting complex subunit	Uncharacterised	S295
MGG_09697	PH domain protein	Uncharacterised	T798, T899
MGG_09866	Flagellar associated protein	Uncharacterised	S589
MGG_10538	RSC complex subunit	Uncharacterised	T512
MGG_12956	PH domain protein	Uncharacterised	T653
MGG_14329	S/T protein kinase	Uncharacterised	S218
XP_362522.2	Unknown function	Uncharacterised	S183
MGG_00345	RIM15	Kinases	S402, S625, S633
MGG_00803	SNF1	Kinases	S90
MGG_00883	BCK1/MCK1	Kinases	S854
MGG_01279	KIN1	Kinases	S914, T918, S920
MGG_04790	CDS1	Kinases	S1174
MGG_08097	YCK1	Kinases	S359
MGG_08689	PKC1	Kinases	S675
MGG_14773	SCH9	Kinases	T37
MGG_06393	Atg1	Autophagy	S476, S547
MGG_00454	Atg13	Autophagy	S517, S519, S920
MGG_07667	Atg17	Autophagy	S207, S209, S211, S214
MGG_03139	Atg18	Autophagy	S287, S295
MGG_08061	Atg28	Autophagy	S399
MGG_14847	Mst11	Pmk1 pathway	T551, S557

A quantitative phosphoproteomic approach to discover novel components of the MAPK Pmk1 signalling pathway during appressorium development

MGG_00800	Mst7	Pmk1 pathway	S351, S358, S370
XP_368444.2	Mst7	Pmk1 pathway	S318, T332, S358
MGG_05199	Mst50	Pmk1 pathway	S260
MGG_01836	FAR1	Transcription factor	S41
MGG_05306	ZIP12/MEAB	Transcription factor	S146
MGG_06258	FKH1	Transcription factor	S491, S641
MGG_06971	SFL1	Transcription factor	T90
MGG_08463	MOA2/APS2	Transcription factor	S450
MGG_12865	HOX7	Transcription factor	S126, S158, T161, S163
MGG_06726	Septin4	Cytoskeleton related	S313, S314, S318
MGG_04708	SOM1	cAMP pathway	S228, T588, T589, S591, S595
XP_365053.1	MAC1	cAMP pathway	S75
MGG_03196	RCM1	Transcriptional regulator	S645
MGG_01376	PTP2	Phosphatase	S288
MGG_02755	NUT1	Nitrogen metabolism	S129
MGG_09531	RGA4	Rho GTPase	S752, S763
MGG_09618	RGS6	G protein signalling	S33
MGG_09962	CHS4	Chitin synthase	S71

The potential Pmk1 targets have diverse functions and are broadly representative of cellular processes associated with early appressorium morphogenesis, based on previous studies (Osés-Ruiz et al., 2021). Based on the Magnagenes database, the function of 32 of the putative Pmk1 targets have already been studied in the blast fungus. However, 23 proteins of this subset have not yet been described (Table 3.1). Using information from GO, I assigned a function to each of these proteins, where possible. From the proteins that have been already studied in *M. oryzae*, I found 8 kinases, 6 transcription factors, 1 transcriptional regulator, 1 phosphatase, 1 Rho GTPase and 1 chitin synthase. Additionally, I also found 5 autophagy-related proteins, 4 components of the Pmk1 cascade, 2 components of the cAMP signalling pathway, 1 cytoskeleton related-protein, 1 protein involved in nitrogen metabolism and 1 member of a G-protein signalling pathway. As expected for a master regulator of appressorium formation, the downstream processes that might be regulated by Pmk1 are very varied.

Our quantitative phosphoproteomics method identified previously described targets of Pmk1. The transcription factors Hox7 and Slf1 have been shown to be phosphorylated by Pmk1 using *in vitro* phosphorylation assays (Li et al., 2011; Osés-Ruiz et al., 2021). Consistent with the Hox7 MAPK phosphorylation assay (Osés-Ruiz et al., 2021), we identified phosphosites S126 and S158. However, we also found novel phosphorylated residues in Hox7 such as T161 and S163. In the case of Slf1, there is no information about the residue (s) directly regulated by Pmk1, but we identified T90 as a potential candidate. When considered together, the analysis of Hox7 and Slf1 provide proof-of-concept evidence that our quantitative phosphoproteomic pipeline can be used to identify targets of Pmk1.

A quantitative phosphoproteomic approach to discover novel components of the MAPK Pmk1 signalling pathway during appressorium development

A quantitative phosphoproteomic approach to discover novel components of the MAPK Pmk1 signalling pathway during appressorium development

Figure 3.6. Heat map of differentially phosphorylated peptides in Guy11 and *Δpmk1* during appressorium formation. Heat map to show relative intensities of 181 differentially phosphorylated peptides in Guy11 and *Δpmk1.* MGG number, gene name and phosphosite detected are shown.
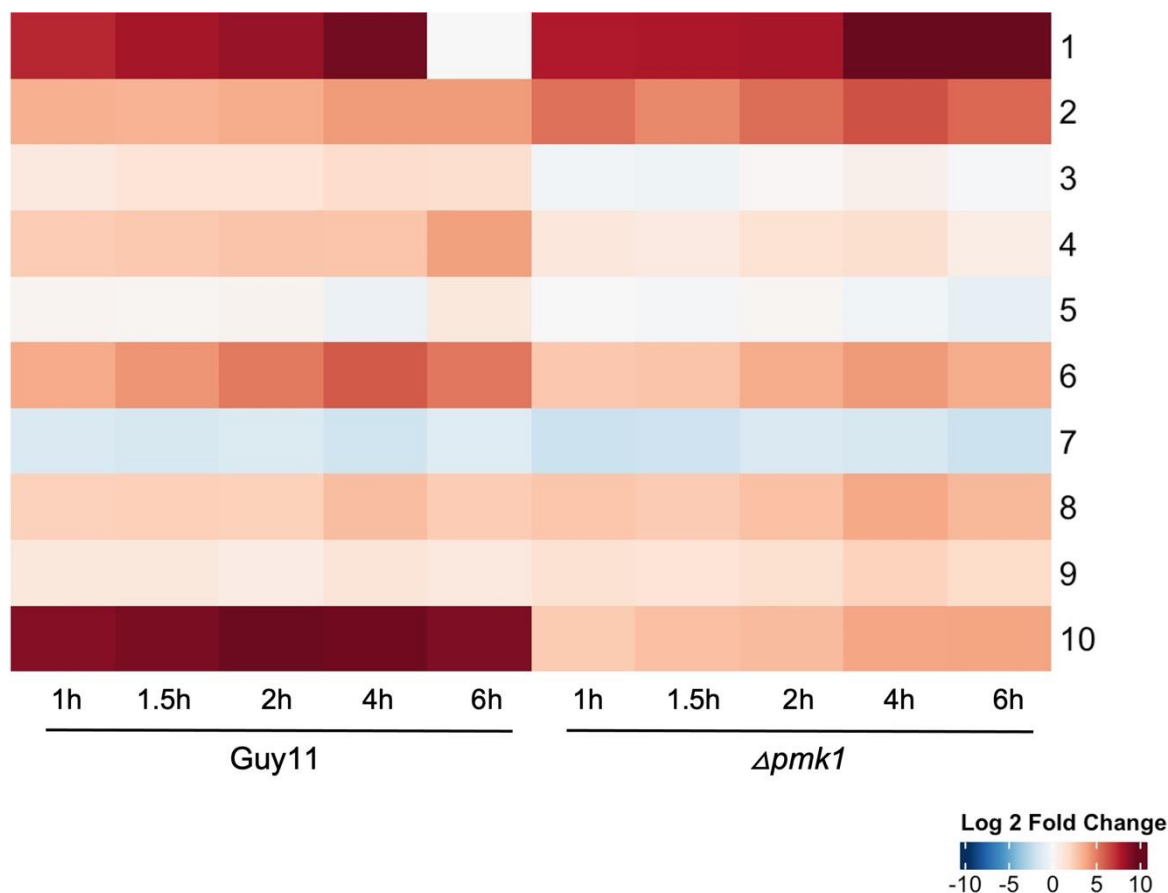
Figure 3.7. Representation of cluster analysis using K-mean approach. Heat map to show the 10 different intensity patterns found in the 181 differentially phosphorylated peptides using a K-means approach (Y. Li & Wu, 2012).
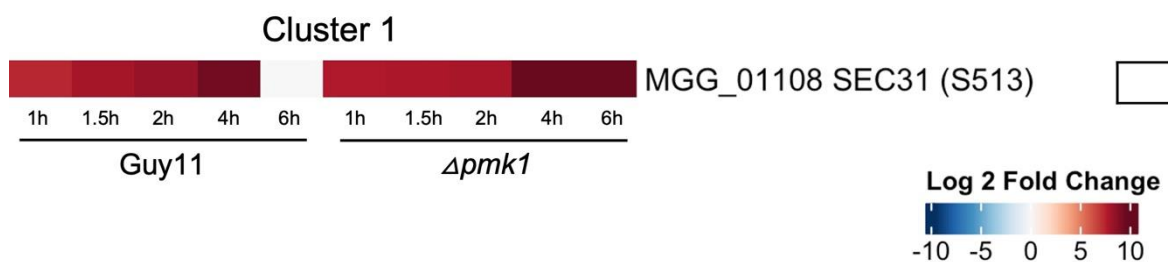
Figure 3.8. Heat map of differentially phosphorylated peptides in Guy11 and *Δpmk1* during appressorium formation by cluster. Ten different heat maps to show the clusters of intensity patterns found in the 181 differentially phosphorylated peptides using K-mean

A quantitative phosphoproteomic approach to discover novel components of the MAPK Pmk1 signalling pathway during appressorium development

approach. Phosphopeptides marked with (+) are considered as Pmk1 phosphorylation dependent.

A quantitative phosphoproteomic approach to discover novel components of the MAPK Pmk1 signalling pathway during appressorium development

Cluster 3

MGG_00800 MST7 (S351 & S358)
MGG_06334 VTS1 (S420)
MGG_07714 (S258)
MGG_04790 CDS1 (S1174)
MGG_04790 CDS1 (S1174)
MGG_00454 ATG13 (S517 & S519)
MGG_08061 (S399)
MGG_05306 ZIP12/MEAB (S146)
MGG_09293 (S97)
MGG_09697 (T798)
MGG_09697 (T798)
MGG_03139 ATG18 (S295)
MGG_09565 PMK1 (Y186)
MGG_06393 ATG1 (S476)
MGG_07667 ATG17 (S207 & S209)
MGG_07667 ATG17 (S207 & S211)
MGG_07667 ATG17 (S207 & S214)
MGG_14847 MST11 (T551)
MGG_01279 KIN1 (S920)
MGG_01279 KIN1 (T918)
MGG_03139 ATG18 (S287)
MGG_01279 KIN1 (S914)
MGG_01279 KIN1 (S914)

1h 1.5h 2h 4h 6h   1h 1.5h 2h 4h 6h

Guy11   Δpmk1

Log 2 Fold Change

-10 -5 0 5 10

A quantitative phosphoproteomic approach to discover novel components of the MAPK Pmk1 signalling pathway during appressorium development

Cluster 4

MGG_12865 HOX7 (S126)
gi|39964959|ref|XP_365053.1| MAC1 (S75)
MGG_00800 MST7 (S370)
MGG_03558 (S688)
MGG_00454 ATG13 (S920)
MGG_03064 (S20)
MGG_06726 SEP4p (S318)
MGG_06726 SEP4p (S318)
MGG_08689 PKC1 (S675)
MGG_06334 VTS1 (S175)
MGG_12865 HOX7 (S163)
MGG_00803 SNF1 (S90)
MGG_08097 YCK1 (S359)
MGG_03218 (T190)
MGG_03218 (S193)
MGG_05257 (S667)
MGG_00883 BCK1/MCK1 (S854)
MGG_03558 (S666)
MGG_05220 (S320)
gi|145610929|ref|XP_368444.2| MST7 (S358)
MGG_03196 RCM1 (S645)
MGG_04421 (T148)
MGG_06258 FKH1 (S491)
MGG_05199 MST50 (S260)
MGG_14847 MST11 (S557)
MGG_06403 (S272)
MGG_09565 PMK1 (T184)
MGG_09554 (S295)

1h 1.5h 2h 4h 6h   1h 1.5h 2h 4h 6h

Guy11   Δpmk1

Log 2 Fold Change
-10 -5 0 5 10

A quantitative phosphoproteomic approach to discover novel components of the MAPK Pmk1 signalling pathway during appressorium development

Cluster 5

Protein	
MGG_01836 FAR1 (S41)	+
MGG_06258 FKH1 (S641)	+
MGG_01311 (S216)	+
MGG_14773 SCH9 (T37)	+
MGG_03558 (S875)	+
MGG_06399 YAK1 (S937)	
MGG_06399 YAK1 (Y941)	
MGG_09697 (T899)	+
MGG_08463 MOA2/APS2 (S450)	+
MGG_04708 SOM1 (S228)	+
MGG_06971 SFL1 (T90)	+
MGG_02522 (S113)	+
MGG_05220 (S267)	+
MGG_05220 (S274)	+
MGG_00345 RIM15 (S402)	+
MGG_05376 (T114)	+
MGG_09554 (S295)	+
MGG_09293 (S133)	+
MGG_00345 RIM15 (S625 & S633)	+
MGG_10538 (T512)	+
MGG_06726 SEP4p (S313 & S318)	+
MGG_06726 SEP4p (S314 & S318)	+
MGG_09293 (S125 & Y129)	+
MGG_04708 SOM1 (T588 & S591)	+
MGG_04708 SOM1 (S591 & S595)	+
MGG_04708 SOM1 (T589 & S591)	+
MGG_01376 PTP2 (S288)	+
MGG_00454 ATG13 (S13)	
MGG_04708 SOM1 (S441)	
MGG_00883 BCK1/MCK1 (S457)	

1h 1.5h 2h 4h 6h   1h 1.5h 2h 4h 6h

Guy11   Δpmk1

Log 2 Fold Change

-10 -5 0 5 10

A quantitative phosphoproteomic approach to discover novel components of the MAPK Pmk1 signalling pathway during appressorium development

Cluster 6

	MGG_06393 ATG1 (S547)	+
	MGG_06599 (S124)	+
	MGG_02755 NUT1 (S129)	+
	MGG_00800 MST7 (S351)	+
	MGG_09618 RGS6 (S33)	+
	MGG_12865 HOX7 (S158)	+
	MGG_12865 HOX7 (S158)	+
	MGG_12865 HOX7 (T161)	+
	MGG_09962 CHS4 (S71)	+
	MGG_12865 HOX7 (S126)	+
	MGG_12865 HOX7 (S126)	+
	MGG_06403 (S275)	+
	MGG_12956 BUD4 (S158)	

1h 1.5h 2h 4h 6h   1h 1.5h 2h 4h 6h
Guy11   Δpmk1

Log 2 Fold Change
-10 -5 0 5 10

Cluster 7

	MGG_06726 SEP4p (S313 & S318)	+
	MGG_06726 SEP4p (S314 & S318)	+
	MGG_07063 GCC1 (S215 & S217)	
	MGG_09531 RGA4 (S735 & S739)	
	MGG_00354 HAPB (S293)	
	MGG_01376 PTP2 (T29)	
	MGG_14517 RGS1 (S696 & S700)	

1h 1.5h 2h 4h 6h   1h 1.5h 2h 4h 6h
Guy11   Δpmk1

A quantitative phosphoproteomic approach to discover novel components of the MAPK Pmk1 signalling pathway during appressorium development

Cluster 8

A quantitative phosphoproteomic approach to discover novel components of the MAPK Pmk1 signalling pathway during appressorium development

Cluster 9

MGG_01196 (S653)
MGG_10837 (S163)
MGG_14517 RGS1 (S510)
MGG_14517 RGS1 (T515)
MGG_08061 (T548)
MGG_00354 HAPB (S120)
MGG_05216 (T785)
MGG_01722 CAP1 (S358)
MGG_01258 (S50 & S56)
MGG_05664 PDEH (S883)
MGG_06334 VTS1 (T29)
MGG_06070 (S39)
MGG_04486 ATG11 (S1351)
MGG_01204 MIG1 (S674)
MGG_12821 MST20 (S104)
MGG_06971 SFL1 (S364)
MGG_09293 (S125)
MGG_05306 ZIP12/MEAB (S146)
MGG_09531 RGA4 (S739)
MGG_06393 ATG1 (S598)
MGG_01362 (Y15)
gi|145609287|ref|XP_367574.2| (S4)
MGG_00345 RIM15 (S633)
MGG_01641 (S71)
MGG_03459 ATG26/PTH8 (S714)
MGG_01258 (S56 & S59)
MGG_09293 (T94)
MGG_08547 (S32)
MGG_08463 MOA2/APS2 (S450)
MGG_12956 BUD4 (T653)   +
MGG_06070 (S259)
MGG_03163 (T57)
MGG_00454 ATG13 (S519)
MGG_06258 FKH1 (S528)
MGG_08061 (S399)   +

1h 1.5h 2h 4h 6h   1h 1.5h 2h 4h 6h
        Guy11   Δpmk1

Cluster 10

gi|145610929|ref|XP_368444.2| MST7 (S318)   +
gi|145610929|ref|XP_368444.2| MST7 (T332)   +

1h 1.5h 2h 4h 6h   1h 1.5h 2h 4h 6h
        Guy11   Δpmk1

Log 2 Fold Change

-10 -5 0 5 10

56

3.2.6 Pmk1 associates with autophagy-related proteins

From the functional categorisation of Pmk1 putative targets, the most represented cellular process observed is autophagy. Previous reports have shown that autophagy is an essential process for infection in the blast fungus (Veneault-Fourrey et al., 2006), leading to regulated cell death of the conidium, which is a key pre-requisite for development of a functional appressorium (Kershaw & Talbot, 2009). Additionally, it has been shown that the Pmk1 pathway is required for induction of autophagy during infection (Kershaw & Talbot, 2009) and this occurs early during appressorium formation facilitating recycling of the contents of the conidium and acting as a key developmental checkpoint for appressorium morphogenesis (Kershaw 2009; Liu et al., 2017). However, little is known about the mechanism by which Pmk1 controls autophagy during plant infection by *M. oryzae*.
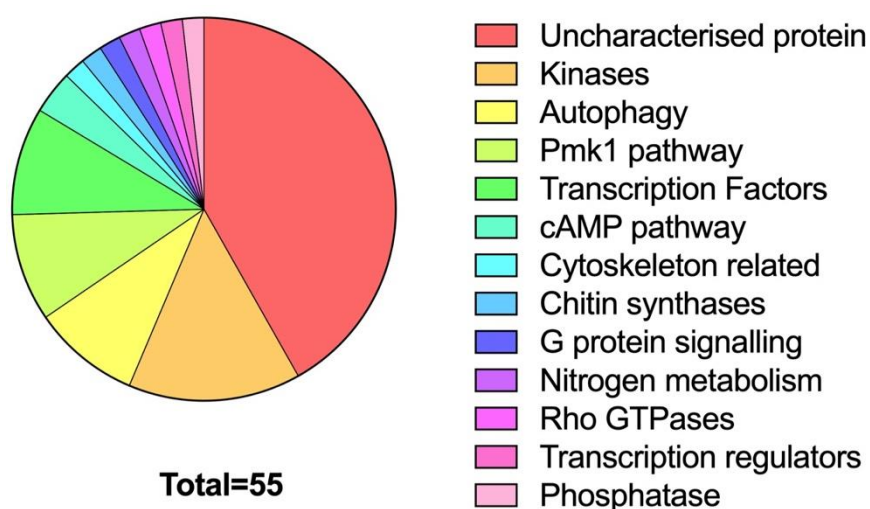
Figure 3.9. Functional analysis of putative Pmk1 targets identified by Parallel Reaction Monitoring (PRM). Pie chart to show functional analysis using Blast2GO and Magnagenes of the 55 proteins identified by PRM as putative interactors of Pmk1.
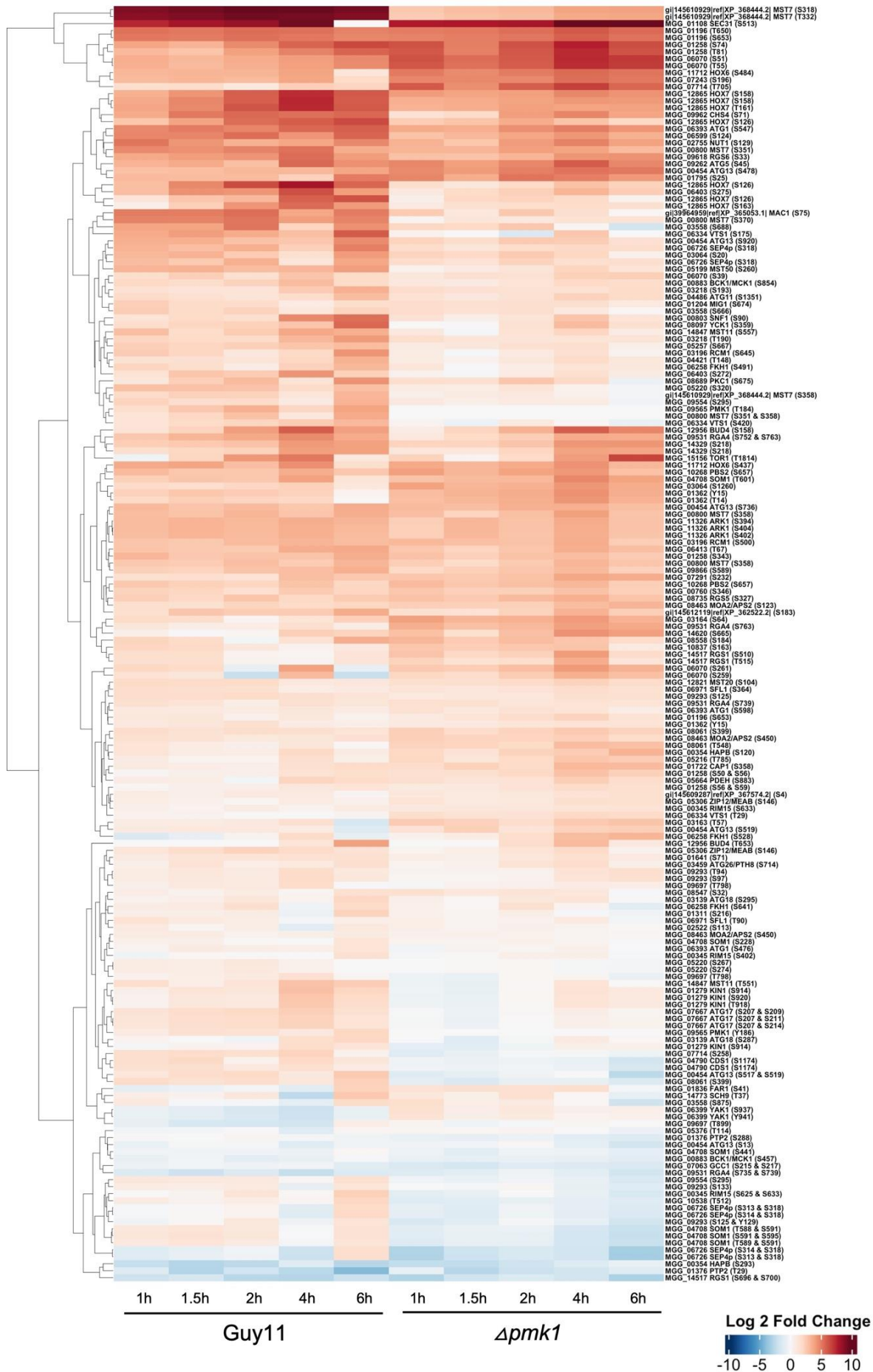
A quantitative phosphoproteomic approach to discover novel components of the MAPK Pmk1 signalling pathway during appressorium development
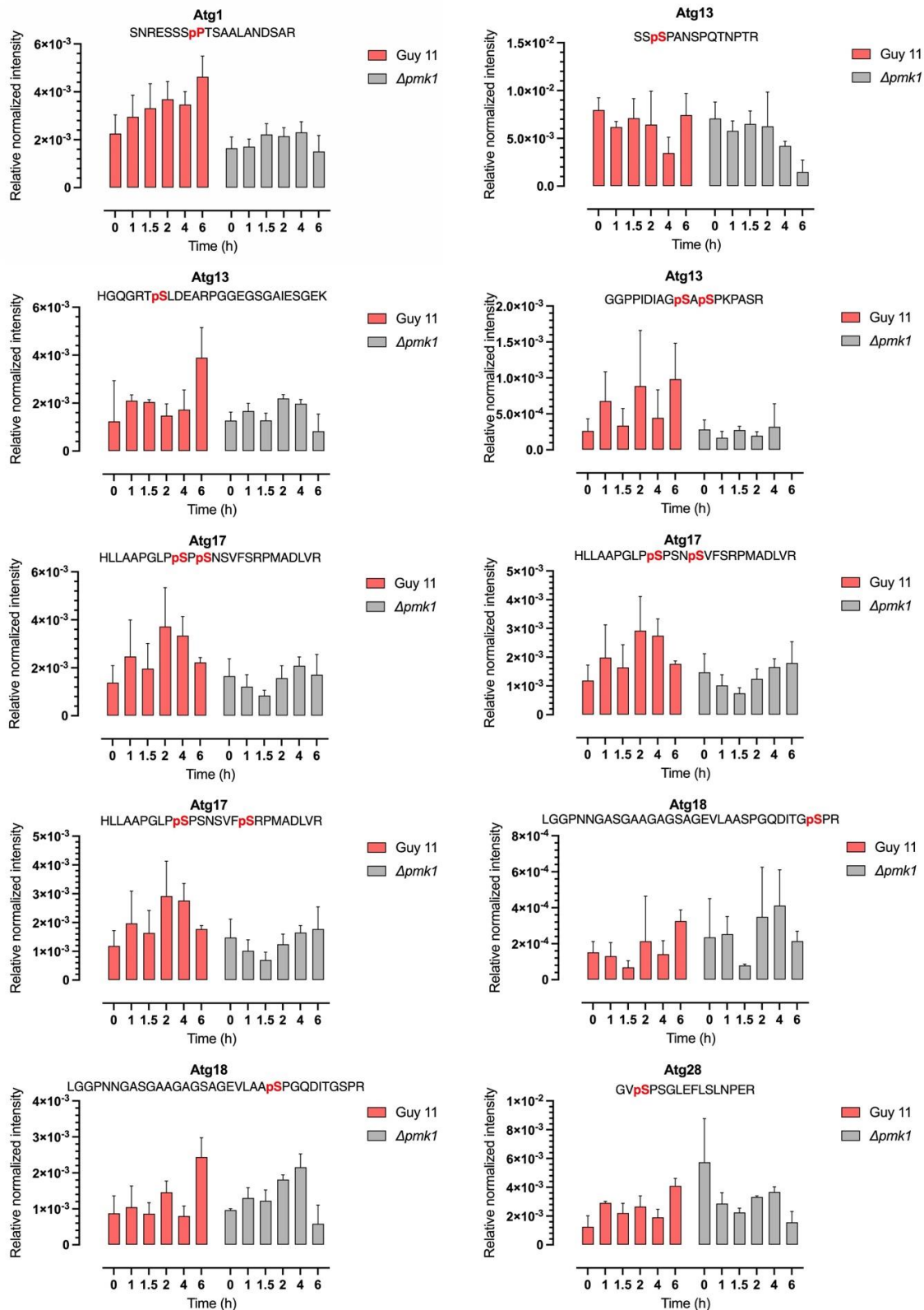
Figure 3.10. Atg-related proteins contain Pmk1 dependent phosphorylated peptides. Bar graphs to show relative normalised intensity determined by PRM of peptides associated to Atg1, Atg13, Atg17, Atg18 and Atg28 during appressorium development from 0-6h in Guy11 and $\Delta pmk1$.

A quantitative phosphoproteomic approach to discover novel components of the MAPK Pmk1 signalling pathway during appressorium development

In this study, I found that Atg1, Atg13, Atg17, Atg18 and Atg28 phosphorylation is clearly affected by the absence of Pmk1. Interestingly, these proteins are part of different complexes that control selective (cargo-dependent) and non-selective (cargo-independent) autophagy (Kershaw & Talbot, 2009). Among the non-selective autophagy components, all the proteins involved in the initiation step, such as Atg1, Atg13 and Atg17 (Yamamoto et al., 2016), were phosphorylated in a Pmk1-dependent manner. In addition, Atg18 which is part of the recycling step, is also differentially phosphorylated. In parallel, I found that the selective autophagy protein Atg28 is a putative target of Pmk1. It has previously been shown that Atg1 and Atg17 null mutants are non-pathogenic, whereas Atg13 and 18 are reduced in pathogenicity (Kershaw & Talbot, 2009). By contrast, Atg28 is not required for blast disease (Kershaw & Talbot, 2009). Because I have identified 5 autophagy proteins with 12 phosphorylated residues dependent on Pmk1 (Table 3.1), it is likely that Pmk1 regulates the initiation of conidial autophagy during appressorium morphogenesis.

To investigate this further, we quantified the abundance of peptides derived from Atg proteins (with Dr. Paul Derbyshire). Out of all Atg proteins that were identified as potential targets of Pmk1, the peptides containing the residues S517 and S519 of Atg13 and S399 of Atg28 showed the highest differential when we compared Guy11 and *Δpmk1* in (Figure 3.10). Interestingly, Atg1, Atg13 and Atg17 are the proteins involved in Pre-Autophagosomal Structure (PAS) formation, a critical step in autophagy initiation (Kawamata et al., 2008). The results indicate that Pmk1 may be regulating PAS formation required for autophagy-dependent appressorium development and infection. Validation of the specific phosphor-sites with each of these Atg proteins as Pmk1 targets will be necessary in order to understand how Pmk1 controls autophagy during plant infection.

3.2.7 Pmk1 associates with a SAM-domain containing protein.

To identify potentially new downstream processes elicited by Pmk1 phosphorylation during the initiation of appressorium development, I started the validation of putative Pmk1 interactors. A Yeast-Two-Hybrid (Y2H) experiment was therefore undertaken to identify potential interacting proteins from among the phosphoproteins characterised in the discovery proteomics screen. Y2H is a useful tool to validate protein interactions with MAPKs and has been used previously to identify potential substrates (Zhang et al., 2016). To this end, I extracted RNA from Guy11 mycelium to synthesise cDNA. I then used this cDNA as a template to amplify the CDS sequence of each gene product to be tested. I cloned each of the PCR products into the Y2H vectors pGBT7 (bait) and pGADT7 (prey). Dr. Miriam Osés-Ruiz kindly provided vectors pGBT7-Pmk1 and pGADT7-Pmk1 to test the potential Pmk1 interactors. Also, she provided pGBT7-Mst12 and pGADT7-Mst12 to use as

A quantitative phosphoproteomic approach to discover novel components of the MAPK Pmk1 signalling pathway during appressorium development
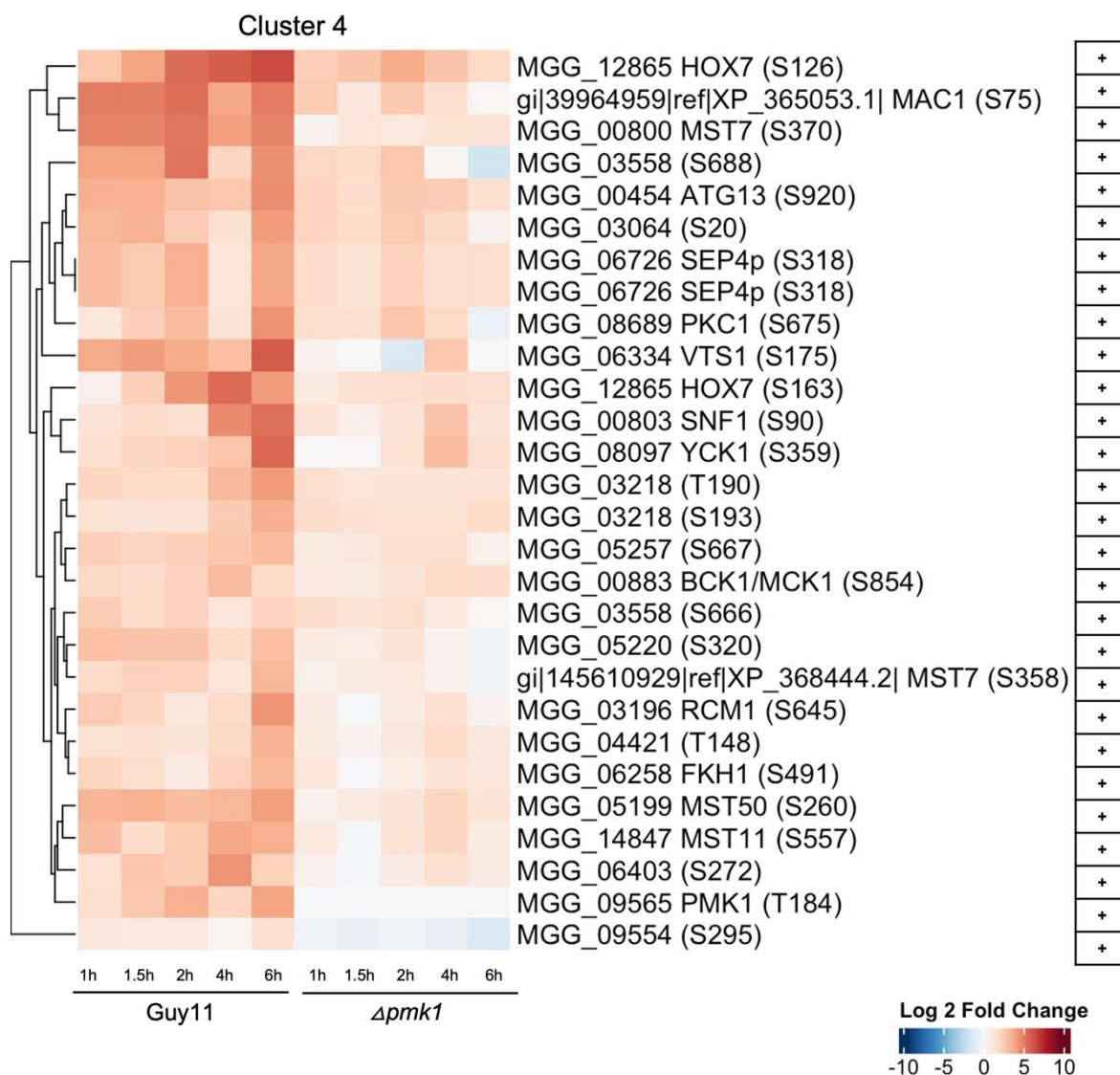
a control (Osés-Ruiz et al., 2021). Mst12 is a known interactor and transcriptional regulator that operates downstream of Pmk1 (Osés-Ruiz et al., 2021; Park et al., 2002). To perform the Y2H assays, I transformed both bait and prey vectors containing candidate CDS sequences with Pmk1 bait and prey vectors. This allowed me to test both possible interactor proteins as bait and prey. As expected, yeast co-transformed with Pmk1 and Mst12 showed significant growth in high stringency conditions. Similarly, one of the candidates, the Sterile Alpha Motif (SAM) domain containing protein Vts1 (MGG_06334), showed growth and blue coloration in the presence of X-α-gal in selective medium, both of which are readouts confirming protein-protein interaction (Figure 3.11). When considered together these results provide evidence that Pmk1 interacts with Vts1. The Vts1 protein was therefore selected as a potential, novel Pmk1 interactor for further analysis. In Chapter 4, I discuss the detailed analysis of Vts1 and try to define its biological function and the mechanism by which is regulated by Pmk1.
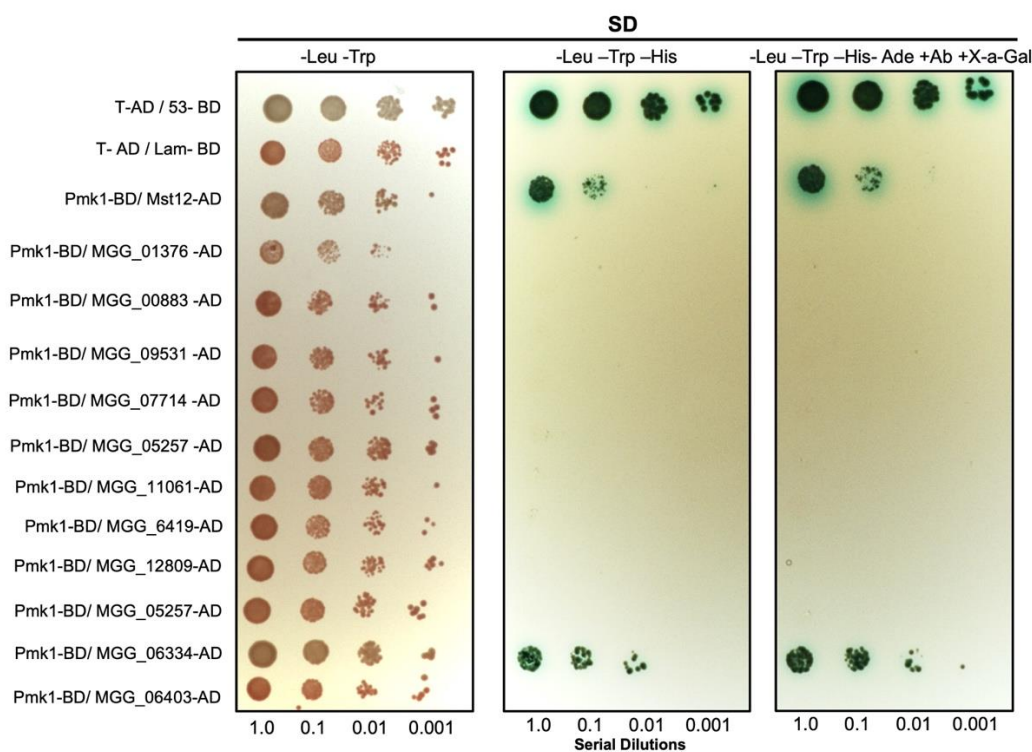
Figure 3.11. A SAM- domain containing protein, Vts1, interacts Pmk1 in a Y2H assay under stringent conditions. A yeast-two-hybrid (Y2H) assay was used to investigate the interaction of Pmk1 and Vts1. Protein interactions were tested in yeast grown on SD medium -Trp -Leu -Ade -His +X gal +Au (right panels). Viability of all transformed yeast cells was demonstrated by growth on SD medium -Trp -Leu (left panels). Yeast cells were inoculated onto media as a tenfold dilution series. Mst12 was used as the positive control.
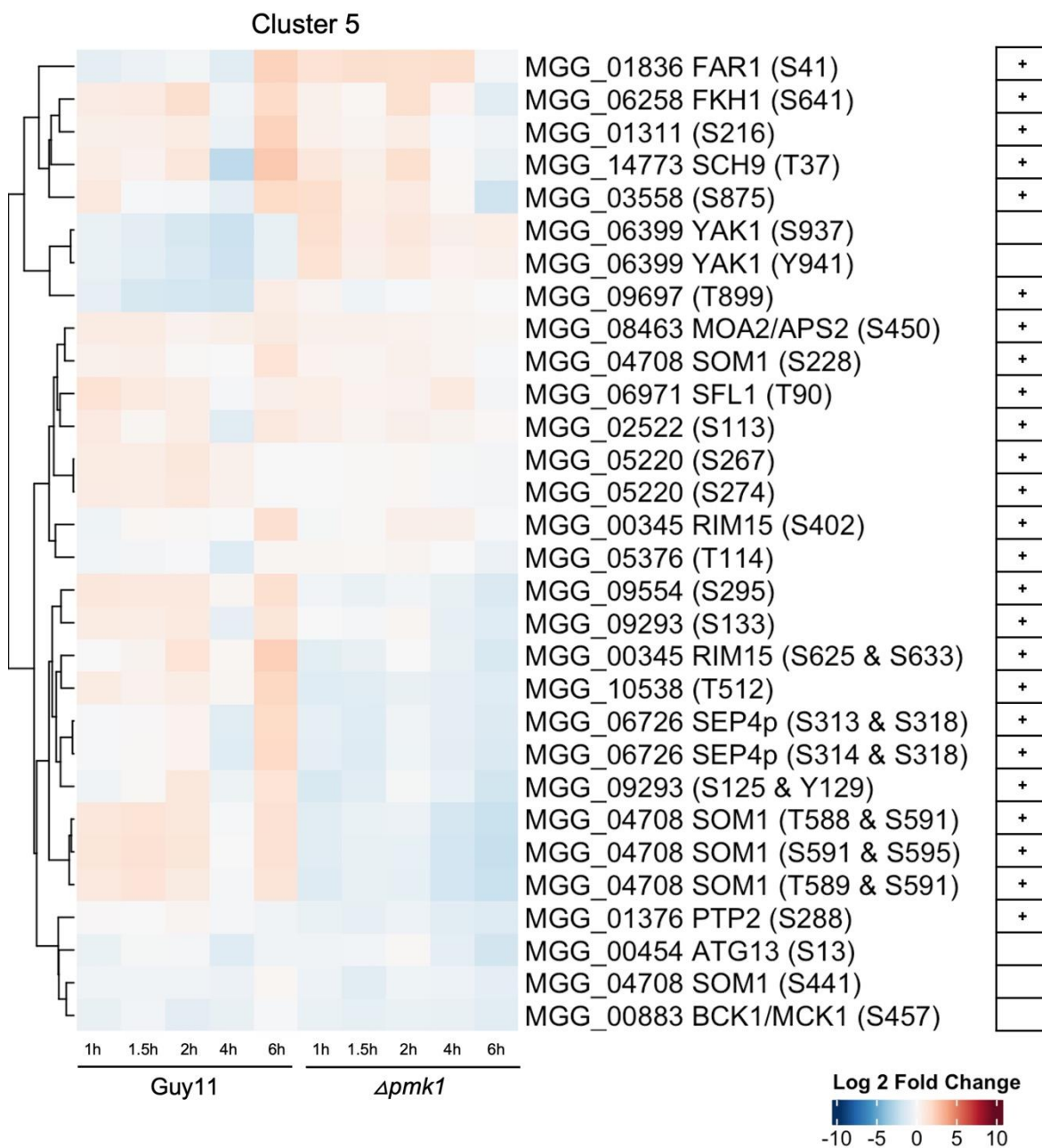
A quantitative phosphoproteomic approach to discover novel components of the MAPK Pmk1 signalling pathway during appressorium development
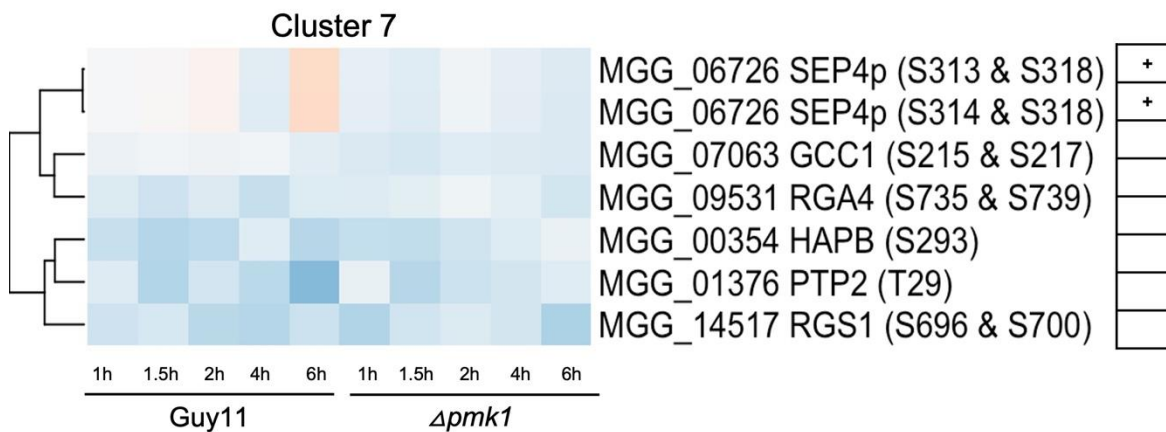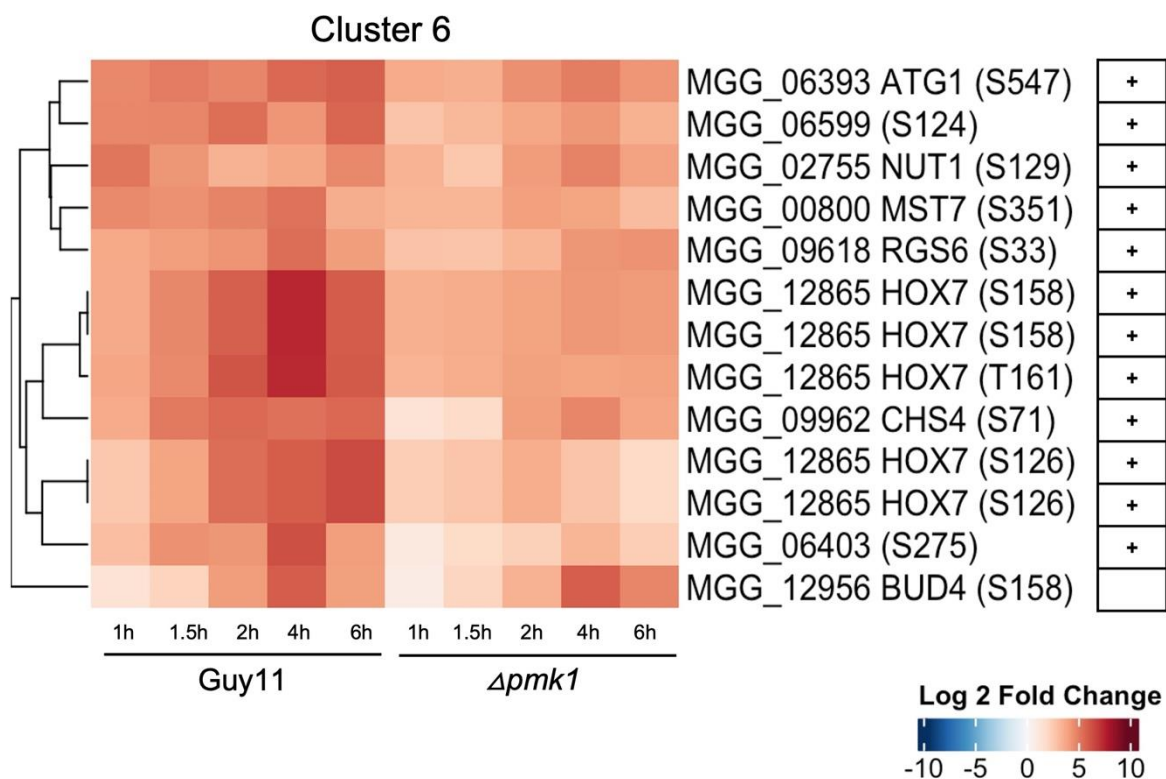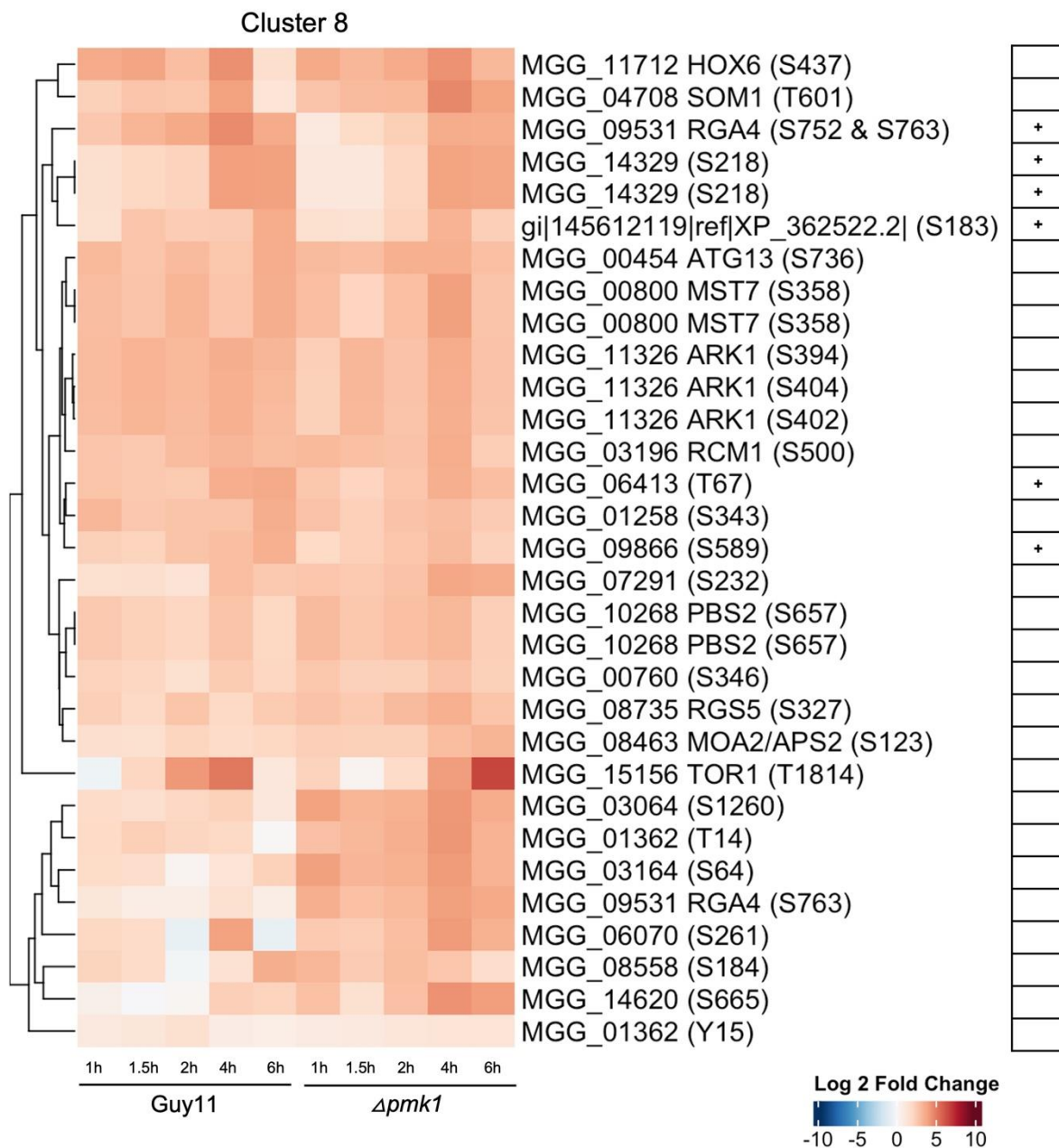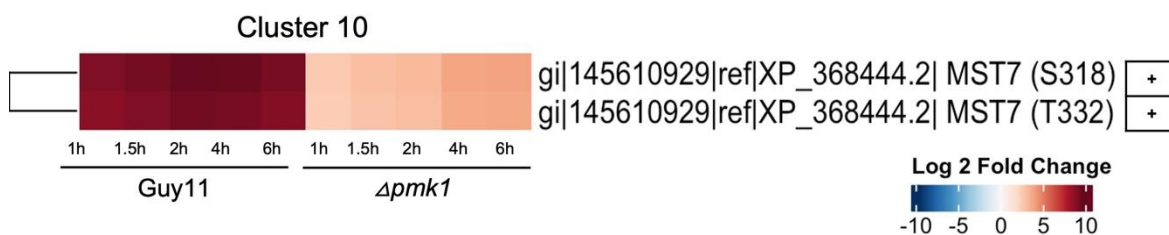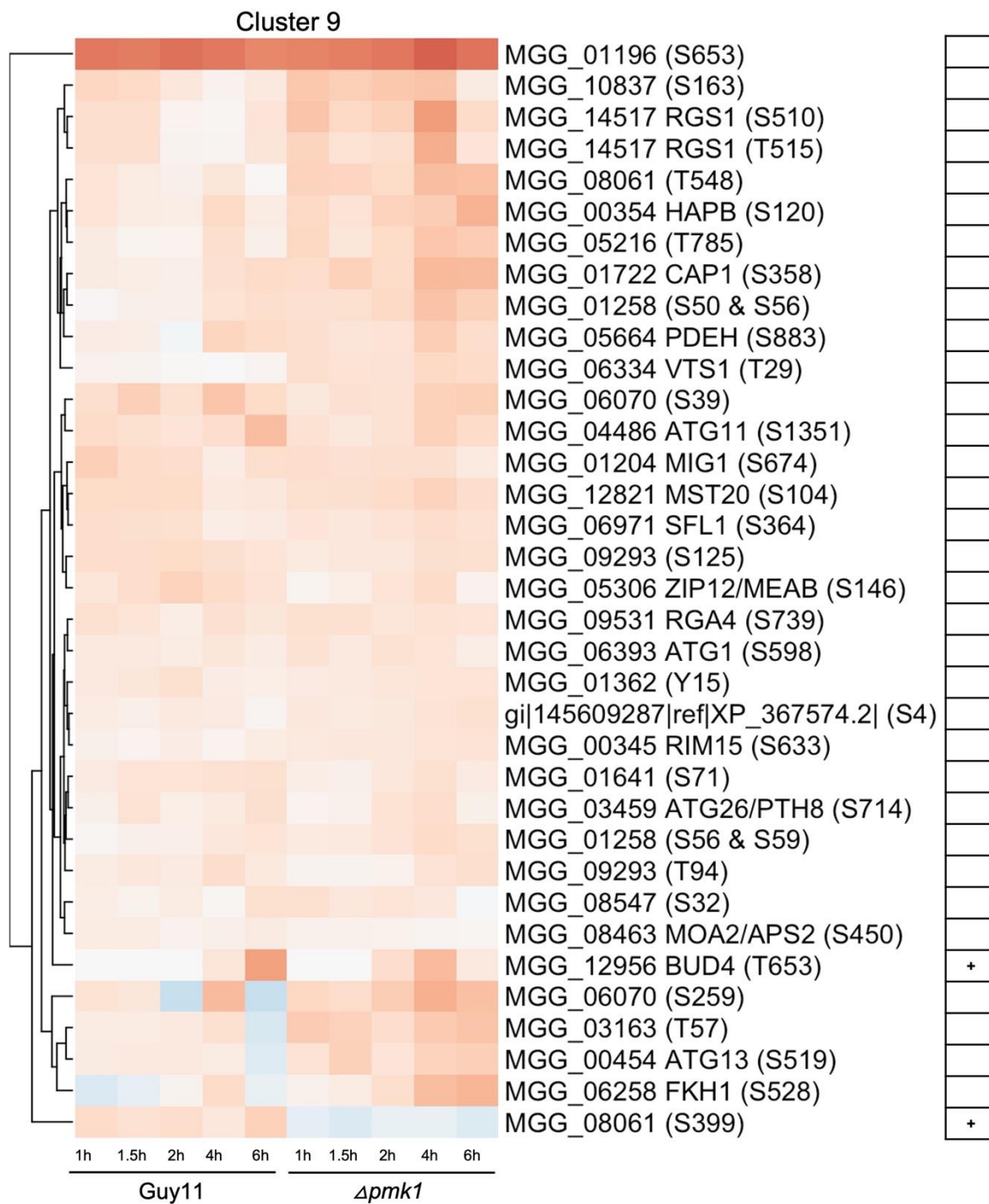
3.3 Discussion

In *M. oryzae*, there are many gaps in our understanding of how the Pmk1 MAPK regulates morphogenetic transitions during infection. Understanding the role of Pmk1 downstream targets will be key to deciphering how this cascade operates. This should include functionally analysing the contribution of the phosphorylation events on these targets during infection. Therefore, we need to characterise and quantify the phosphoproteome of developing appressoria using bottom-up phosphoproteomics methods (Cruz-Mireles et al., 2021). We reasoned that the use of advanced, quantitative phosphoproteomic methods might provide completely new insight into the biological processes regulated by Pmk1 and enable dissection of Pmk1 phosphorylation-dependent events that are necessary for appressorium development and function.

In this Chapter, I have shown how we have applied a quantitative phosphoproteomic approach to identify novel components of the Pmk1 cascade during early appressorium formation. Using this method, we identified 55 putative target proteins in which phosphorylation occurs when Pmk1 is active.

The first major finding of the discovery proteomics screen is that known components of the Pmk1 pathway appear to be phosphorylated in a Pmk1-dependent manner. The Mst11 MAPKKK, Mst7 MAPKK and Mst50 scaffold protein are part of the upstream complex regulating Pmk1 activity (Li et al., 2017; Liu et al., 2011; Park et al., 2006; Qi et al., 2015; Zhao et al., 2005; Zhao & Xu, 2007) and were all shown to be phosphorylated during appressorium development. MAPK regulatory feedback loops by downstream kinases have been previously reported to have regulatory roles other MAPK cascades (Gnad et al., 2016; Lake et al., 2016). Although they are poorly investigated in the Pmk1 cascade, it has been demonstrated that Mst11 phosphorylation on S453 and S458 are required for Pmk1 activation (Qi et al., 2015). In our analysis, we found that Mst11 Pmk1-dependent phosphorylated residues are T551 and S557. Because of the close proximity of the residues identified in Qi et al., 2015 study with the ones found in the current analysis, it might indicate that they are found in a regulatory phosphorylation hotspot (Strumillo et al., 2019). Validation experiments will be required to define whether Mst11 and Mst7 phosphosites identified with our approach are dependent on Pmk1 and whether these events are necessary for operation of the cascade. Perhaps, this regulation is important for maintenance of its activity– or potentiation of the signal– during appressorium morphogenesis, as other feedback loops have been reported to function (Lake et al., 2016; Qi et al., 2015). In addition, the data indicate that there are two orthologues (or isoforms) of Mst7 (MGG_00800 and XP_368444.2), with different Pmk1-dependent phosphorylation

A quantitative phosphoproteomic approach to discover novel components of the MAPK
Pmk1 signalling pathway during appressorium development

sites (see Table 3.1). A more detailed analysis of *M. oryzae* reported genome and proteome
will be required because the genomic database only consider one gene for Mst7
(MGG_00800), whereas the proteome database contains two proteins for Mst7
(MGG_00800 and XP_368444.2) with 99.8% identity. It will, therefore, be important to
validate whether Pmk1 can phosphorylate both orthologues (or isoforms) of its MAPKK by
distinct regulatory mechanisms. Taken together, these results are important in terms of
validating the approach, given that these proteins serve functions directly within the Pmk1
signalling pathway. Besides, this might help to explain whether Pmk1 exerts a regulatory
function on Mst11 and Mst7 that will be necessary to understand in order to unravel the
signalling mechanisms upstream of MAPK activation.

A second major finding of the discovery phosphoproteomics screen is that some putative
Pmk1 targets are components in the regulation of cellular processes previously linked to
action of the Pmk1 MAPK, such as autophagy, cell cycle control, cytoskeleton
reorganisation and the cAMP-dependent protein kinase A pathway. This is particularly
evident for autophagy, where our data suggest that the phosphorylation of the Atg1 kinase,
Atg13 and Atg17 is a Pmk1-dependent process. Interestingly, in *S. cerevisiae*, these
proteins are involved in the initiation of conidial autophagy via PAS formation (Yamamoto
et al., 2016). This provides the first evidence that Pmk1 acts directly on the regulation of
autophagy and very likely involves Pmk1-directed phosphorylation (either directly or
indirectly) of these key regulators. To validate this regulatory mechanism further it will be
necessary to generate appropriate phosphodead and phosphomimic alleles of Atg1, Atg13
and Atg17 and test their function. An analogue-sensitive mutant of Atg1 has also been
constructed (Kershaw & Talbot, unpublished) which provides a means by which the kinase
activity of Atg1 could be investigated directly in order to define whether it relies on Pmk1-
dependent phosphorylation. In this way, new insight into the onset of autophagy and its
regulatory mechanism can be generated in future.

The regulation of Pmk1 activity during appressorium formation is not very well understood.
As I mentioned earlier, Pmk1 is activated in a conserved pTEpY motif (Cargnello & Roux,
2011). We identified the presence of both phosphorylated residues in our proteomic
analysis in the wild-type strain Guy11– T184 in cluster 4 and Y186 in cluster 3 (Figure 3.3).
However, it is known that MAPK activation is not simple, and the duration and magnitude
of pTEpY phosphorylation is crucial for the physiological outcome (Theodosiou & Ashworth,
2002). Therefore, the role of phosphatases in dephosphorylation is vital for control of the
pathway (Theodosiou & Ashworth, 2002). In this study, I found the phosphatase Ptp2 as a
possible Pmk1 target. In the blast fungus, Ptp2 has been reported to dephosphorylate the
MAPK Osm1 and its null mutant or phosphatase dead mutant show reduced pathogenicity

A quantitative phosphoproteomic approach to discover novel components of the MAPK Pmk1 signalling pathway during appressorium development

(Liu et al., 2020). Because phosphatases are vital regulators of MAPK signalling pathways, Ptp2 might be a relevant target of Pmk1, which may reveal an additional level of control and modulation associated with activity of the MAPK pathway.

A series of uncharacterised proteins potentially involved in cell cycle control (MGG_01311, MGG_09293, MGG_09554) and proteins implicated in actin organisation (Septin4 and MGG_07714) were also revealed by the screen. Altogether, these findings might help to dissect how Pmk1 controls such processes in the phosphorylation cascade. Consistent with this observation, a recent transcriptomic analysis revealed that autophagy and cell cycle genes are regulated at the transcriptional level by the Pmk1 pathway via the TF Hox7. This approach also showed that Pmk1 controls cytoskeletal remodelling through the Mst12 TF which regulates a sub-set of the Pmk1-dependent genes, associated predominantly with the maturation of appressoria and their re-polarisation.

A third finding was the identification of a set of novel phosphoproteins that have the potential to reveal new biological roles not described previously as targets of the Pmk1 cascade. It is well-known that MAPKs can regulate signal transduction by altering transcription in response to changes in the cellular environment (Turjanski et al., 2007; Whitmarsh, 2007). Using our phosphoproteomic pipeline, I identified 4 transcription factors (TFs) which have previously been reported to play roles in virulence of *M. oryzae* (Hox7, Fkh1, Sfl1 and Moa2/Aps2) (Li et al., 2011; Osés-Ruiz et al., 2021; Park et al., 2014). In addition, Far1 has been reported to have a role in the regulation of genes controlling lipid metabolism although it is dispensable for virulence (Yusof & Talbot, 2014), and Zip12 has been linked with regulation of mycelium growth (Kong et al., 2015). The most studied of these TFs, however, is Hox7, which has been implicated in the regulation of autophagy and cell cycle control and is a key regulator of appressorium morphogenesis (Osés-Ruiz et al., 2021). Hox7 mutants generate aberrant germ tubes and incipient, non-melanised appressoria but these are unable to mature, generate turgor, or cause disease (Kim et al., 2009). Hox7 and Slf1 have been reported as downstream targets of Pmk1, validating the approach taken here. Our data also provide evidence that the TFs Fkh1, Moa2/Aps2, Far1 and Zip12 are potential targets of Pmk1. These widen the potential range of functions regulated by the MAPK cascade, including the control of lipid metabolism and fatty acid b-oxidation by the control of Far1, for example, as well as completely unknown functions that may be controlled by the other TFs. A combination of comparative RNA-seq analysis and CHIP-seq analysis would be used in future to define the genes regulated by these TFs and the wider hierarchical control exerted by Pmk1.

A quantitative phosphoproteomic approach to discover novel components of the MAPK Pmk1 signalling pathway during appressorium development

Most of the remaining putative Pmk1 targets identified were proteins with uncharacterised functions. Among them, there are proteins whose function has not yet been studied in other organisms. However, some have domains with essential functions in scaffold proteins of other MAPK pathways. For example, I found a subset of 5 proteins containing a pleckstrin-homology (PH) domain (MGG_03558, MGG_04421, MGG_06403, MGG_09697, MGG_12956). In *S. cereviseae*, it has been demonstrated that the scaffold protein Ste5 requires a PH domain for its stable membrane recruitment (Garrenton et al., 2006), which is necessary for its function as the scaffold in the Fus3 pheromone response MAPK pathway. Other interesting novel protein in *M. oryzae* is Vts1, a SAM domain containing protein. In *Drosophila*, proteins containing a SAM domain mediate a MAPK signalling (Rajakulendran et al., 2008). In Chapter 4, I describe more in detail the role of Vts1 as a component of the Pmk1 pathway. I conclude that a subset of uncharacterised proteins containing PH and SAM domains are potential targets of Pmk1.

Taken together, I identified 55 potential proteins that can be targets of Pmk1 using a quantitative phosphoprotoemic approach. This knowledge aims to pave the road in the understanding of the Pmk1 signalling during blast disease.

Chapter 4:

4 Vts1 is a novel component of the MAPK Pmk1 signalling pathway

4.1 Introduction

Protein phosphorylation is one of the most significant PTMs in Eukaryotes, governing a variety of biological processes such as signal transduction, cellular metabolism, and stress responses (Nakagami et al., 2010). In *M. oryzae,* little is known about the phosphorylation signalling that occurs during blast disease. However, the phosphorylation cascade operated by the MAPK Pmk1 it is well-known as a central regulator of this fungal infection (Osés-Ruiz et al., 2021; Sakulkoo et al., 2018; Xu & Hamer, 1996). The generation and annotation of *M. oryzae* genome has provided a unique opportunity for the use of large scale proteomic and transcriptomic approaches to be carried out to explore the biology of infection (Dean et al., 2005). To gain insight into the signal transduction processes regulated by the Pmk1 MAPK pathway, I set out to search for putative components of the cascade by using a comparative quantitative phosphoproteomic approach during early appressorium development. In Chapter 3, I explained how a phosphoproteomic pipeline was implemented to identify 55 putative components of the Pmk1 MAPK cascade.

One of the Pmk1 potential direct interactors, named Vts1, is a protein of unknown function in the rice blast fungus, which contains a sterile alpha motif (SAM) domain. SAM domain-containing proteins have been previously reported as important regulators of MAPK signalling cascades (Kim & Bowie, 2003). Proteins containing SAM domain are versatile because this domain has documented to take part in various interactions. They can, for example, show binding affinity to other SAM and non-SAM domain proteins, but can also show binding affinity to lipids and RNA (Knight et al, 2011). Importantly, SAM domains have been reported to mediate associations of MAPK modules in different fungi. In *Schizosaccharomyces pombe,* for instance, association between Ste4 and Byr2 occurs via a SAM motif (Ramachander et al., 2002). Similarly, in *S. cerevisiae*, the interaction between Ste11 and Ste50 is mediated by a SAM domain (Grimshaw et al., 2004). In *M. oryzae*, the MAPKK Mst11 and the putative scaffold protein Mst50 in the Pkm1 pathway both contain SAM domain (Zhao et al., 2005). Furthermore, it has been demonstrated that Mst50-Mst11 interaction occurs via their respective SAM domains and this is essential for appressorium development and plant infection (Park et al., 2006).

To determine putative MAPK-target associations, validation techniques involving protein-protein interaction experiments are necessary. Co-immunoprecipitation (co-IP) experiments allow the *in vivo* study of protein-protein interactions and have been used to provide evidence regarding multi-protein complex formation within cells (Zhang et al., 2016). Pmk1 interactors such as Mst7, Sfl1, Pic1 and Pic5 have, for example, been validated by co-IP analysis (Li et al., 2011; Zhang et al., 2011; Zhao & Xu, 2007). Another powerful tool which can be applied to determine the phosphorylation relationship between a MAPK and its putative substrate is to use an *in vitro* kinase assays that allows the mapping of phosphorylated residues using mass spectrometry (Zhang et al., 2016). A recent study using an *in vitro* kinase assay, for example, revealed that Pmk1 phosphorylates its target transcription factors Mst12 at S133 and Hox7 at S158 (Osés-Ruiz et al., 2021).

In this Chapter, I report the use of a combination of mass spectrometry, protein biochemistry, functional genetics, and cell biology-based approaches to validate and characterise the role of Vts1 in the context of the Pmk1 MAPK signalling pathway.

4.2 Results

4.2.1 Vts1 is a conserved SAM domain- containing protein

Among the putative Pmk1 target proteins identified in the discovery phosphoproteomic analysis was a hypothetical protein MGG_06334, which I selected as a candidate to characterise in order to test whether it acts as a novel component of the Pmk1 signalling pathway. MGG_06334 is a predicted orthologue of the Vts1 protein in *S. cerevisiae* (gene ID: YOR359W). However, analysis of an alignment of the predicted amino acid sequences of MGG_06334 and yeast Vts1 (Figure 4.1) shows that they only share 13% similarity, with 58.57% amino acid identity in the C-terminal region where the SAM domain is located (Figure 4.1). Although these two proteins present a low degree of similarity, I decided to name MGG_06334 hypothetical protein as *M. oryzae* Vts1.

M. oryzae Vts1 is a SAM domain containing protein and the domain comprises 62 amino acids between T550 and A611 (Figure 4.1). Vts1, Mst50 and Mst11 are the 3 proteins containing a SAM domain in *M. oryzae* proteome (Zhao et al., 2005). In Mst50 and Mst11, the SAM domain is located in the N-terminal region, whereas in Vts1 it is proximal to the C-terminus of the protein. *M. oryzae* Vts1 has 12 predicted MAPK motifs, with 9 serine and 3 threonine-directed sites. In addition, it has 1 predicted MAPK docking motif within the SAM domain (Figure 4.1).

Vts1 is a novel component of the MAPK Pmk1 signalling pathway
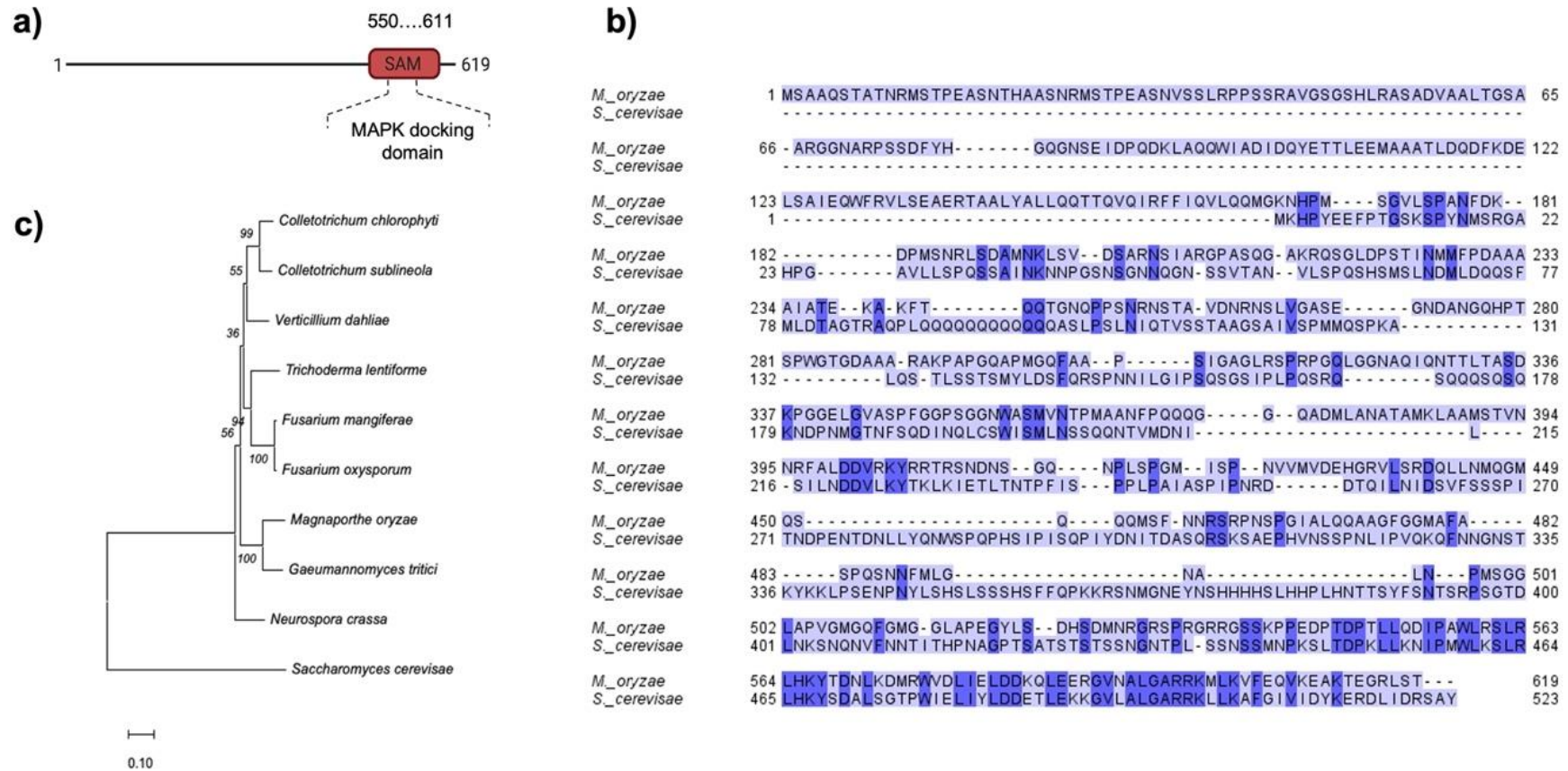
Figure 4.1. Vts1 is conserved across filamentous ascomycete fungi. a) Schematic diagram to show Vts1 domain structure and position of the predicted SAM domain. **b)** Phylogenetic neighbour-joining tree to show conservation across fungal species. Numbers show percentage support after 1000 bootstrap replications of the data set using MEGA X software (Kumar et al., 2018). **c)** Amino acid alignment of Vts1 proteins from *M. oryzae* and *S. cerevisiae*.

The Vts1 protein is encoded by a single copy gene and has no paralogues in the rice blast fungus genome. Understanding how Vts1 has evolved in other fungi can provide insight into its potential function. For that purpose, I aligned Vts1 orthologues from other fungal species and produced a phylogenetic tree using the neighbour-joining method. Consistent with previous studies, *M. oryzae* Vts1 clustered with other predicted Vts1 proteins from various filamentous fungal species including pathogens such as the take-all fungus *Gaeumannomyces tritici* and *Fusarium oxysporum*, as well as saprotrophic fungi such as *Neurospora crassa*. Interestingly, Vts1 is a highly conserved protein across many ascomycete filamentous fungal species (Figure 4.1).

4.2.2 Vts1 specifically associates with Pmk1

To investigate the Vts1-Pmk1 interaction in the context of appressorium development, I carried out a one-to-one co-immunoprecipitation (Co-IP) experiment. Because I did not find Vts1 in the Pmk1 IP- MS experiment in early appressorium samples, I decided to use Vts1 as the bait protein to perform this analysis. To carry out the experiment, I first cloned *VTS1* gene under control of its native promoter into the pScBAR vector as a C-terminal GFP fusion. I first amplified the *VTS1* gene including its 1.5 kb upstream region with a forward primer containing *Eco*RI and reverse primer containing *Hin*dIII restriction sites. I then cloned this amplicon into pScBAR containing the *GFP* gene to enable a C-terminal in-frame fusion with the *BAR* gene to allow selection in *M. oryzae,* to generate pScBar-Vts1-GFP plasmid. I then transformed Guy11 protoplasts with 8 μg of DNA of pScBar-Vts1-GFP plasmid. I selected transformants based on PCR and GFP signal screening. Additionally, I quantified copy number insertion by qPCR (Anglia iDNA). In this experiment, I used a Guy11 strain which expresses free GFP driven under the high level constitutive ToxA promoter (*ToxA:GFP*) as a control (Gupta et al., 2015) and two different transformants expressing a single copy of *VTS1* fused to GFP (pVts1:Vts1-GFP T6 and pVts1:Vts1-GFP T8). To generate the samples for co-IP analysis, I then carried out a large scale appressorium assay for each strain on hydrophobic coverslips (Figure 4.2). I harvested samples after 4h of germination and used 1 mg of total protein from each sample to carry out the experiment.
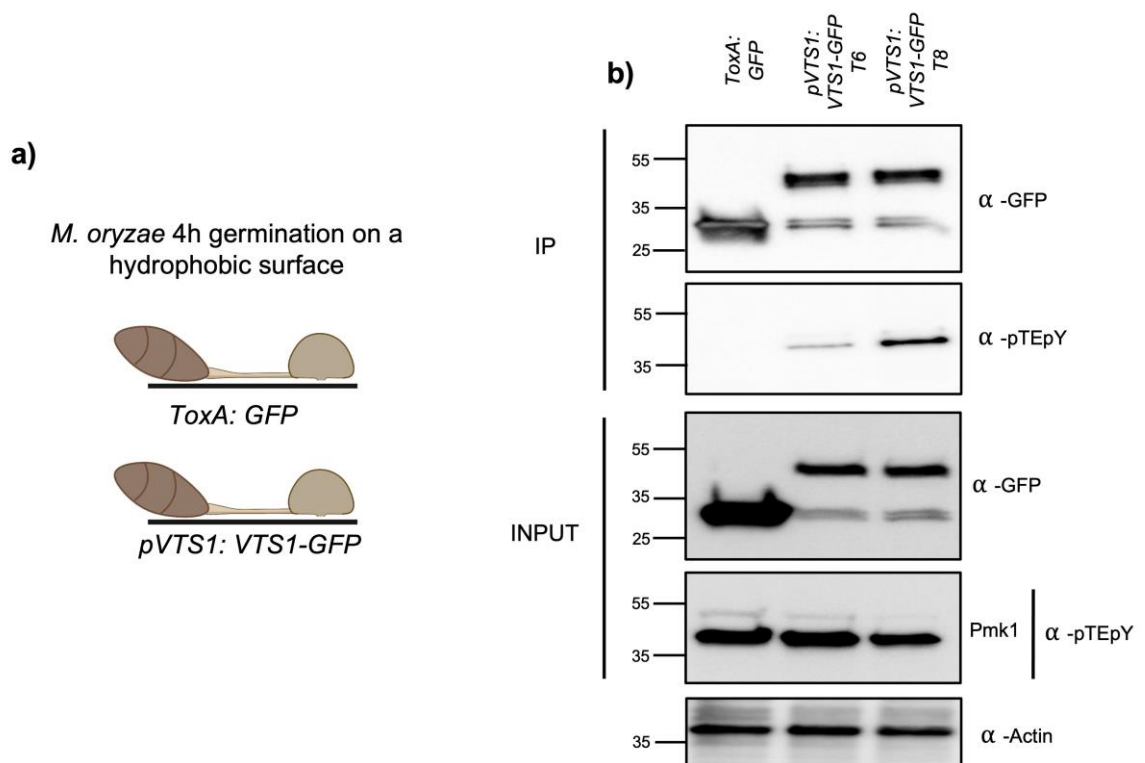
Figure 4.2. Vts1 interacts with Pmk1 during the early stages of appressorium formation in *M. oryzae*. a) Schematic representation of the experimental design for co-IP analysis. **b)** Co-immunoprecipitation of Vts1-GFP. C-terminal GFP tagged Vts1 was transformed into *M. oryzae* Guy11. Anti-pTEpY antiserum was used to detect double phosphorylated Pmk1. Immunoprecipitates obtained with anti-GFP antiserum, and total proteins extracts, were probed with appropriate antisera. The experiment was repeated three times with identical results.

Under these assay conditions, Pmk1 associates with Vts1 robustly (Figure 1.2). This experiment shows that Pmk1 is only present when immunoprecipitated by Vts1. Because Vts1-GFP fusion protein has a molecular weight of 92.97 kDa and I detected a protein band close to 50 kDa, I decided to analyse this sample by mass spectrometry. I confirmed that the immunoprecipitated protein was, indeed, Vts1-GFP. However, we only identified peptides corresponding the C-terminal part of the protein fused to GFP with a predicted size of 52.73 kDa (Vts1, from L387 to T619). Interestingly, this Vts1 truncated version contained the entire SAM domain where the MAPK docking motif is predicted. This data might suggest that Vts1 is cleaved *in vivo* and that its C-terminal part is sufficient for Pmk1 interaction. Experiments involving Vts1 truncations would, however, need to be carried out to test this hypothesis directly. Nevertheless, consistent with my initial Y2H screening, discussed in Chapter 3, these results provide evidence that Vts1 specifically associated with Pmk1 during the early stages of appressorium development.

4.2.3 Vts1 has two MAPK phosphorylated motifs dependent on Pmk1 activity

After a large-scale phosphoproteomic analysis, mapping the precise position of phosphorylation sites in a putative target is often the first step to understanding the MAPK-mediated mechanism (Zhang et al., 2016). Based on our quantitative phosphoproteomic analysis, I found that Vts1 is phosphorylated in the S/T of 4 different MAPK motifs during early appressorium development. In the wild-type *M. oryzae* strain Guy11, Vts1 is phosphorylated at positions T14, S175, S420 and S425. However, in the *Δpmk1* mutant, Vts1 is only phosphorylated at position T14 (Table 4.1).

Table 4.1. Quantitative phosphoproteomics analysis shows phosphorylation of Vts1 during early appressorium formation (0-6h time course)

Guy11						DeltaPmk1					
0h	1h	1.5h	2h	4h	6h	0h	1h	1.5h	2h	4h	6h
T14 S420 S425	T14 S175 S420	T14 S175 S420	T14 S175 S420 S425	T14 S175 S420 S425	T14 S17 S420 S425	T14	T14	T14	T14	T14	T14

Using Parallel Reaction Monitoring (PRM), we quantified the abundance of the peptides in which Vts1 phosphosites were present (with Dr. Paul Derbyshire). Vts1 residues T14 and S425 did not show significant differences between Guy11 and *Δpmk1* during early appressorium formation (Figure 4.3). However, S175 and S420 were differentially phosphorylated in Guy11 under these conditions. These results suggests that the absence of Pmk1 affects phosphorylation of two MAPK motifs of Vts1 during the early stages of appressorium development.
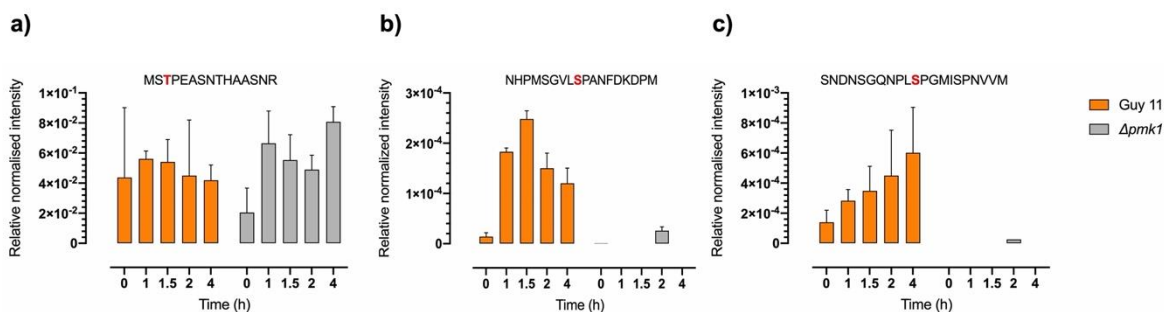
Figure 4.3. Vts1 has two MAPK phosphorylated motifs that require Pmk1. Relative normalised intensity determined by PRM of Vts1 phosphopeptides associated with **a)** T14, **b)** S175 and **c)** S420 during appressorium development from 0-6h in *M. oryzae* Guy11 and the *Δpmk1* mutant.

To test whether phosphorylation of S175 and S420 is dependent on Pmk1 activity, we investigated Vts1 phosphorylation in a Pmk1 analogue sensitive mutant (*pmk1^AS*). As previously reported, *pmk1^AS* is a conditional mutant which was created by introducing a point mutation in the gatekeeper residue of the ATP binding pocket of the kinase making it sensitive to an ATP-analogue named 1-(1,1-dimethylethyl)-3-(1-naphthalenyl)-1H-pyrazolo[3,4-d] pyrimidin-4-amine, in short 1NA-PP1 (Bishop et al., 2000). The mutant was then created by allelic replacement in *M. oryzae* and using this chemical genetic approach it was shown that Pmk1 could be specifically inhibited (Sakulkoo et al., 2018). The *M. oryzae* *pmk1^AS* conditional mutant was incubated on a hydrophobic surface for 1h (baseline), 2h, 3h and 4h in the presence or absence of 1NA-PP1 (Figure 4.4) (with Dr. Miriam Osés-Ruiz). I extracted phosphopeptides from these samples and analysed them by PRM (with Dr. Paul Derbyshire). Consistent with our PRM results from Guy11 and the *Δpmk1* mutant, we found that the abundance of phosphopeptides containing T14 and S425 do not show a significant difference in the presence or absence of 1NA-PP1. Conversely, S175 and S420 were differentially phosphorylated in the presence or absence of the inhibitor (Figure 4.5). We conclude that inhibition of Pmk1 activity impairs phosphorylation of the S175 and S420 residues of Vts1.
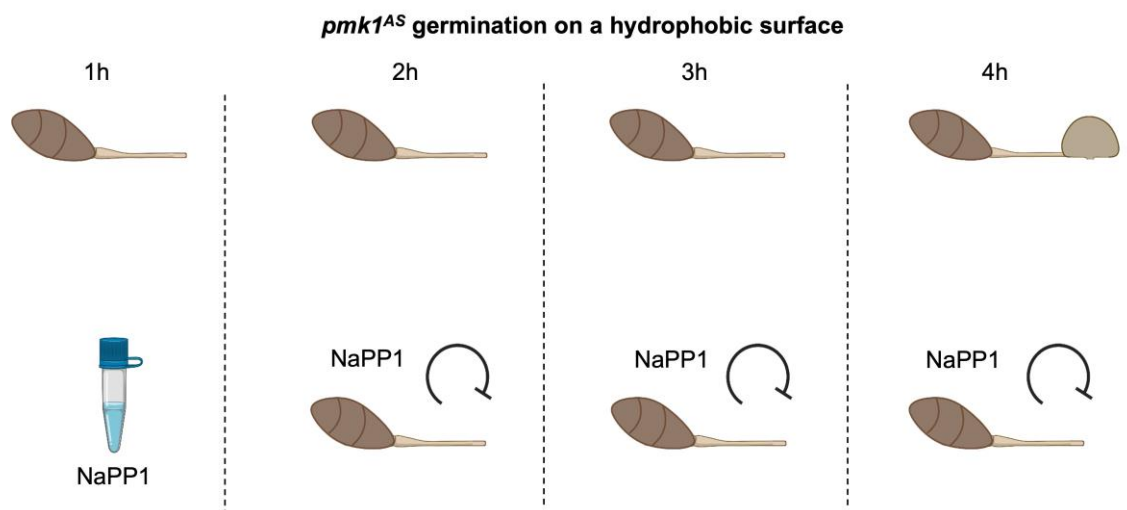
Figure 4.4. Experimental design for parallel reaction monitoring of the Pmk1 analogue-sensitive mutant of *M. oryzae* during the early stages of appressorium development. The *pmk1^AS* conditional mutant was incubated on a hydrophobic surface for 1, 2, 3 and 4 h in the presence or absence of the ATP analogue 1NaPP1 (Figure modified from Osés-Ruiz et al., 2021).
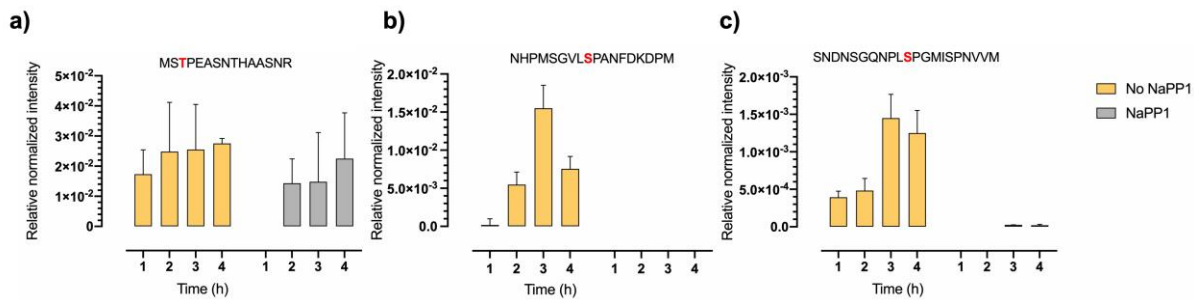
Figure 4.5. Inhibition of Pmk1 activity prevents phosphorylation of Vts1 at two MAPK motifs. Parallel reaction monitoring of the *pmk1*[AS] mutant. Bar charts show relative normalised intensity of Vts1 phosphopeptides associated with positions **a)** T14, **b)** S175 and **c)** S420 during appressorium development from 0-4h in the presence or absence of 1NaPP1 in *pmk1*[AS].

4.2.4 Pmk1 specifically phosphorylates Vts1 residues S175 and S420

To determine whether the interaction between Pmk1 and Vts1 leads to phosphorylation of Vts1, I therefore decided to perform an *in vitro* phosphorylation assay. To this end, I first aimed to produce stable recombinant proteins in *E. coli*. Previous reports have shown that when Pmk1 is fused to the 6xHis-glutathione S-transferase (GST) tag in the N-terminal region it has protein kinase activity *in vitro* (Li et al., 2011; Xu & Hamer, 1996). In the case of Vts1, the yeast orthologue has also been shown to be purified as an N-terminal 6xHis-tagged protein (Lee et al., 2010). Therefore, I sub-cloned Pmk1 and Vts1 coding sequences into pOPIN-J and pOPIN-F vectors, respectively (Berrow et al., 2007). For MAPK phosphorylation assays, apart from the MAPK and its putative target, a constitutively active MEK (MEK[DD]) is also required to activate MAPK function (Menke et al., 2005). For this assay, Dr. Frank Menke therefore purified a functional N-terminal 6x-His tagged MEK2[DD] from *Nicotiana tabacum* (6xHis-MEK2[DD]) (Menke et al., 2005). Because protein phosphorylation is a highly conserved mechanism in eukaryotes, I reasoned that MEK2[DD] could be used to activate Pmk1. I expressed recombinant proteins 6xHisGST-Pmk1 and 6xHis-Vts1 in *E. coli* Rosetta[TM] (DE3) pLysS strain (Novagen) and purified them using immobilised metal affinity chromatography (IMAC) coupled to gel filtration and size exclusion chromatography (Figure 4.6). I collected elution fractions which were evaluated by SDS-PAGE, revealing a band of 68 kDa for 6xHisGST-Pmk1 and 67 kDa for 6xHis-Vts1 (Figure 4.7). Purification of the correct recombinant proteins was then confirmed by LC-MS. Using this approach, I successfully purified Pmk1 and Vts1 at a sufficiently high concentration to facilitate an *in vitro* phosphorylation assay.
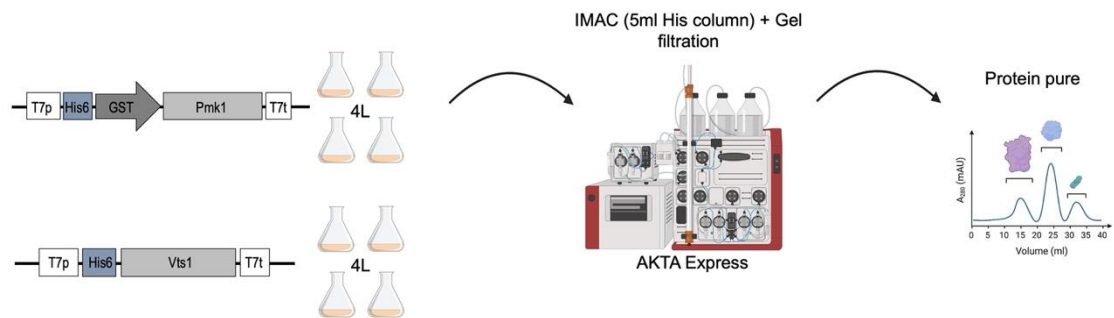
Figure 4.6. Pmk1 and Vts1 recombinant protein purification methodology. Four litres of *E. coli* Rosetta™ (DE3) pLysS strain harbouring either Pmk1 or Vts1 expression vector were purified by immobilised metal affinity chromatography (IMAC) coupled to gel filtration using an AKTA Express system. Purified protein was confirmed by SDS-PAGE and LC-MS.
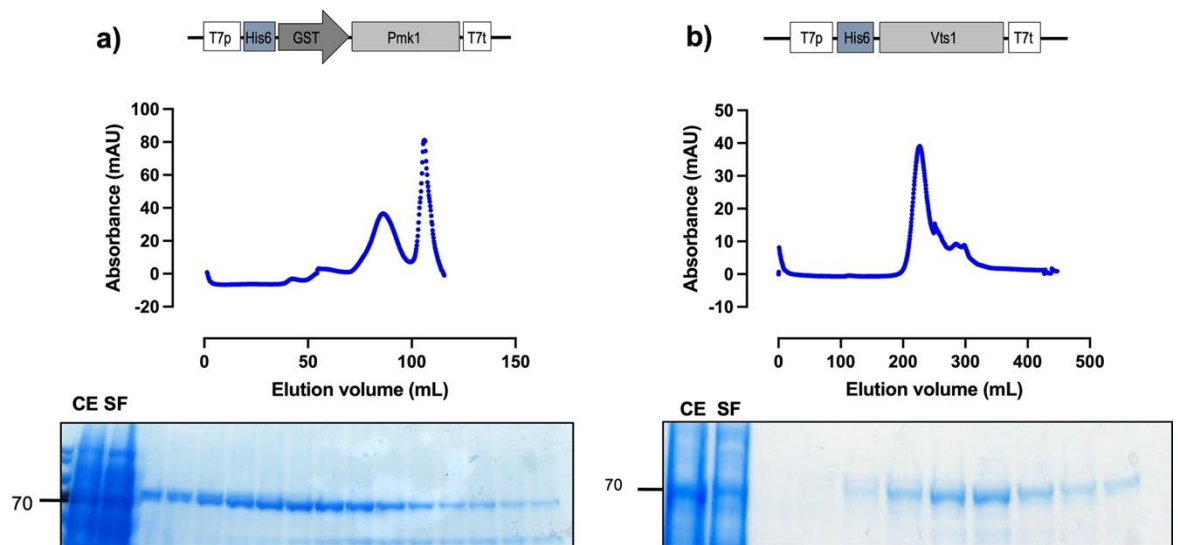
Figure 4.7. Pmk1 and Vts1 can be efficiently purified by IMAC and gel filtration. Elution trace of **a)** 6xHis-GST-Pmk1 and **b)** 6xHisVts1 after IMAC and gel filtration. Fractions were collected and analysed by SDS-PAGE, together with bacterial crude extract (CE) and the soluble fraction (SF) for comparison. A band of 68 kDa was observed for 6xHisGST-Pmk1 (a) and 67 kDa for 6xHis-Vts1.

Once purified, I investigated whether MEK2^{DD} was able to activate Pmk1. To do this, I incubated 250 ng of 6xHis-MEK2^{DD} with 250 ng of 6xHisGST-Pmk1 in kinase buffer. As a control, I used a previously reported MAPK activated by MEK2^{DD}, called MPK6 (provided by Dr. Frank Menke) (Menke et al., 2005; Menke et al., 2004). By western blot analysis, I detected that MEK2^{DD} was able to phosphorylate both MPK6 and Pmk1 using an antibody that specifically recognises phosphorylation at a pTEpY motif (Figure 4.8). These experimental samples were also analysed by LC-MS/MS to confirm the presence of the proteins and MAPK phosphorylation of threonine and tyrosine residues to indicate activation (Figure 4.8). With this *in vitro* phosphorylation assay, I therefore confirmed that Pmk1 can be double phosphorylated on residues T184 and Y186 (pTEpY motif) by MEK2^{DD} (Figure 4.8).

a)

b)

Total spectral counts for phosphopeptides

	1	2	3	4	5
MEK2^{DD}-His	88		110		65
MPK6-His		60	79		
Pmk1-GST				0	10

c)

Pmk1 phosphorylated peptide

Peptide	Position
SAASQEDNSGFMTEYVATR	184, 186
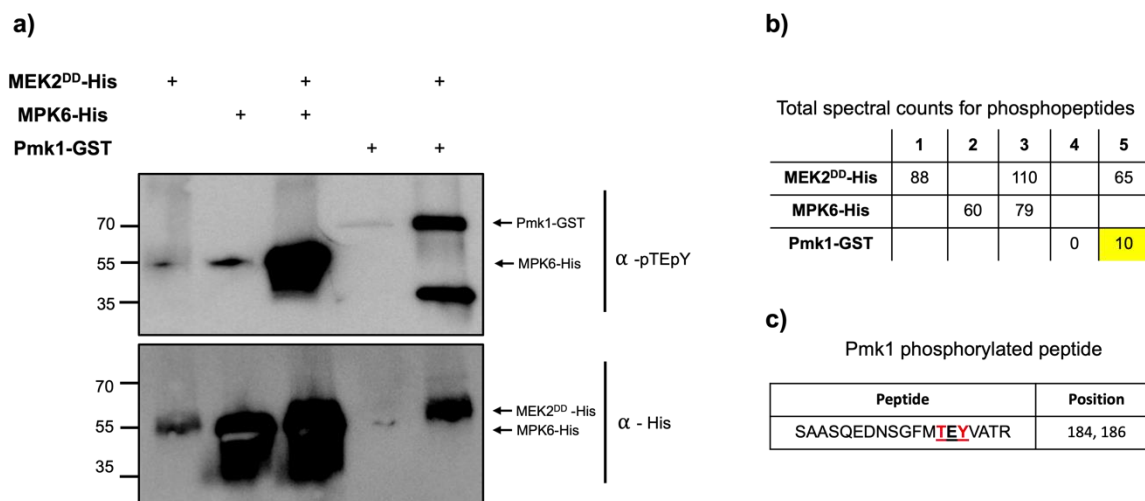
Figure 4.8. MEK2^{DD} phosphorylates Pmk1 *in vitro* on its TEY motif. a) Western blot analysis of *in vitro* phosphorylation experiment between MEK2^{DD} (N-terminally tagged with 6xHis) and Pmk1 (N-terminally tagged with GST). The previously reported MEK2^{DD} phosphorylation of MPK6 (N-terminally tagged with 6xHis) was used as a positive control. Proteins were immunoblotted with appropriate antisera (listed on the right). Arrows indicate expected band sizes. **b)** Phosphopeptides identified by LC-MS for the *in vitro* kinase assay. **c)** Phosphorylation sites (in red) identified by LC-MS on the Pmk1 MAPK.

Having confirmed that Pmk1 can be activated *in vitro*, I next determined whether Pmk1 can phosphorylate Vts1. For this purpose, I carried out an *in vitro* kinase assay in which I incubated 250 ng of Vts1 with activated Pmk1. By western blot analysis, I detected that when Pmk1 is activated in a pTEpY motif, Vts1 is phosphorylated at a MAPK motif [S/T]P (Figure 4.9). By LC-MS/MS, I confirmed that Vts1 is phosphorylated in S175 and S420 only

in the presence of active Pmk1 (Figure 4.9). These results are consistent with the observation made by discovery phosphoproteomics and PRM experiments. However, we also found phosphorylation at position S281 which occurs within a MAPK motif which was not detected in our PRM experiment (Figure 4.9). When considered together, the data indicate that Vts1 is phosphorylated in MAPK motifs in a Pmk1-dependent manner. Furthermore, consistent with our quantitative phosphoproteomic data, Vts1 phosphorylation in S175 and S420 residues depends on Pmk1 activity.
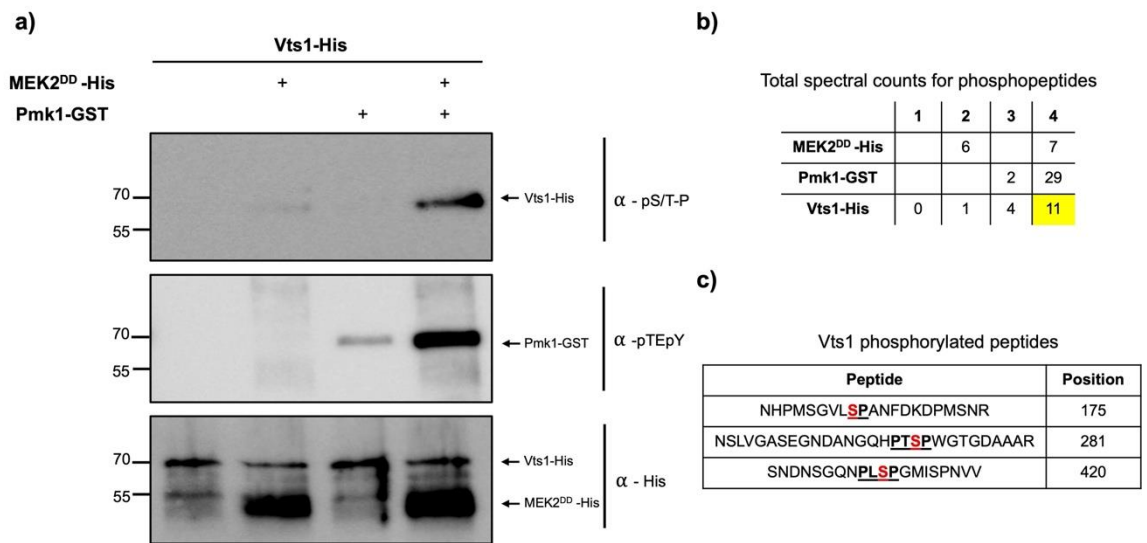
Figure 4.9. Pmk1 can phosphorylate Vts1 *in vitro* at three different MAPK motifs. a) Western blot analysis of *in vitro* phosphorylation experiment between Pmk1 and Vts1 (N-terminally tagged with 6xHis). Proteins were immunoblotted with appropriate antisera (listed on the right). Arrows indicate expected band sizes. **b)** Phosphopeptides identified by LC-MS for the *in vitro* kinase assay. **c)** Phosphorylation sites (in red) identified by LC-MS on Vts1.

4.2.5 Vts1 expression is independent of Pmk1 during appressorium formation and plant infection

Recently, a study from our research group was carried out to understand global gene regulation during blast fungus infection using transcriptomic analysis. This revealed a Pmk1-dependent transcriptional regulatory hierarchy that regulates key changes in gene expression during appressorium morphogenesis (Osés-Ruiz et al., 2021). In this study, we compared global transcriptional responses between Guy11 and a *Δpmk1* mutant. When I analysed Vts1 from this global transcriptional profile, I found that its transcript is present in

both Guy11 and *Δpmk1* mutants (Figure 4.10)*.* Furthermore, I observed that the abundance of the Vts1 mRNA fluctuates during appressorium development in both wild type and Pmk1 null mutant strains. This result suggests that *VTS1* gene is transcribed during appressorium formation, and that its transcription is independent of Pmk1.

Pmk1 mediated transcriptional regulation has also been investigated during rice tissue colonisation by *M. oryzae* (Sakulkoo et al., 2018). The study aimed to understand gene expression changes that are dependent on Pmk1 during plant colonisation. For this purpose, Sakulkoo, et al. used the analogue sensitive *pmk1^{AS}* mutant to inoculate detached rice leaf sheaths and then treated them with 1NA-PP1after 26 hpi, with untreated infected leaf sheaths used as a control for the experiment. My analysis of this data set also revealed that Vts1 is expressed during plant colonisation (Figure 4.10). However, Vts1 mRNA is not differentially accumulated in the presence of Pmk1 inhibitor. Taken together, these experiments demonstrate that *VTS1* expression is independent of Pmk1 activity during both appressorium formation and invasive growth.
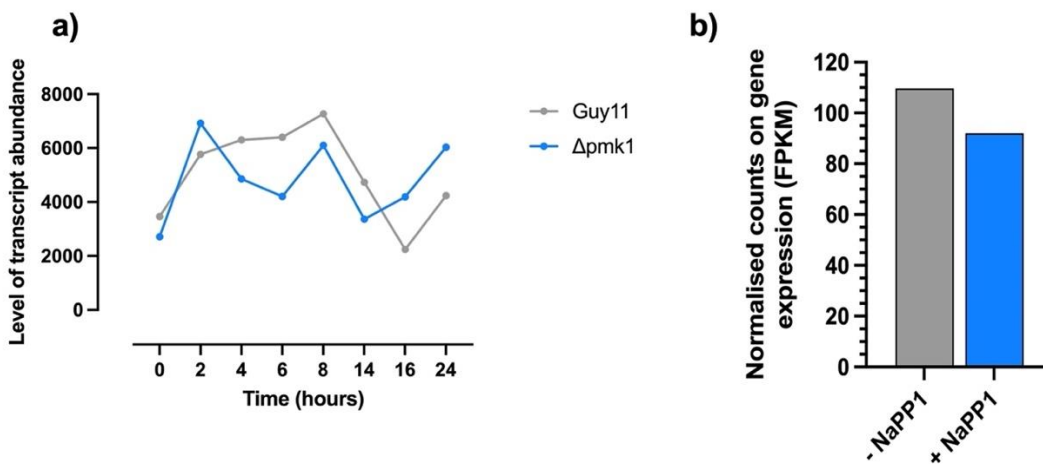
Figure 4.10. ***VTS1* gene is expressed during appressorium formation and plant infection. a)** Mean levels of relative transcript abundance of *VTS1* obtained from RNA-seq analysis during appressorium development of Guy11 and a *Δpmk1* mutant (Osés-Ruiz et al., 2021)**. b)** Bar chart comparing transcript abundance of *VTS1* during plant infection between the untreated and 1NaPP1 treated samples after 26 hpi (Sakulkoo et al., 2018).

4.2.6 Gene functional analysis of *VTS1* in *M. oryzae* using a split-marker targeted gene replacement

To investigate the role of *VTS1* in the Pmk1 MAPK signalling pathway during appressorium development in *M. oryzae*, I set out to characterise its function. Previous reports from *S. cerevisiae* showed that *VTS1* is a non-essential gene which can be mutated without loss of viability (Lee et al., 2010). The role of *VTS1* has not been studied previously in the blast fungus or in any other fungal pathogen. Therefore, I decided to generate a null mutant of *VTS1* in the wild-type strain Guy11.
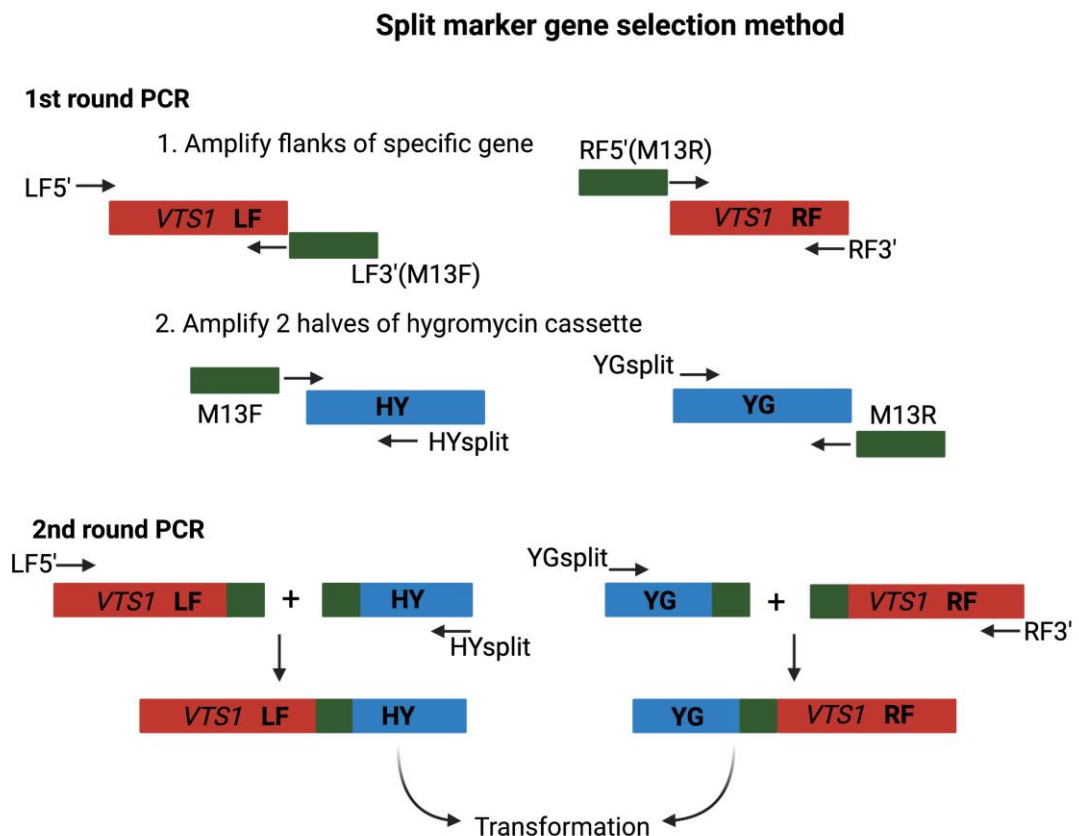
Figure 4.11. Split marker selection method. A first round of PCR is used to amplify flanking sequences on either side of the *VTS1*. At the same time overlapping fragments of the 5 and 3 end of the hygromycin resistance cassette are amplified. A fusion PCR results in 2 amplicons that are used to transform *M. oryzae*, resulting in homologous recombination and assembly of the selectable marker gene.
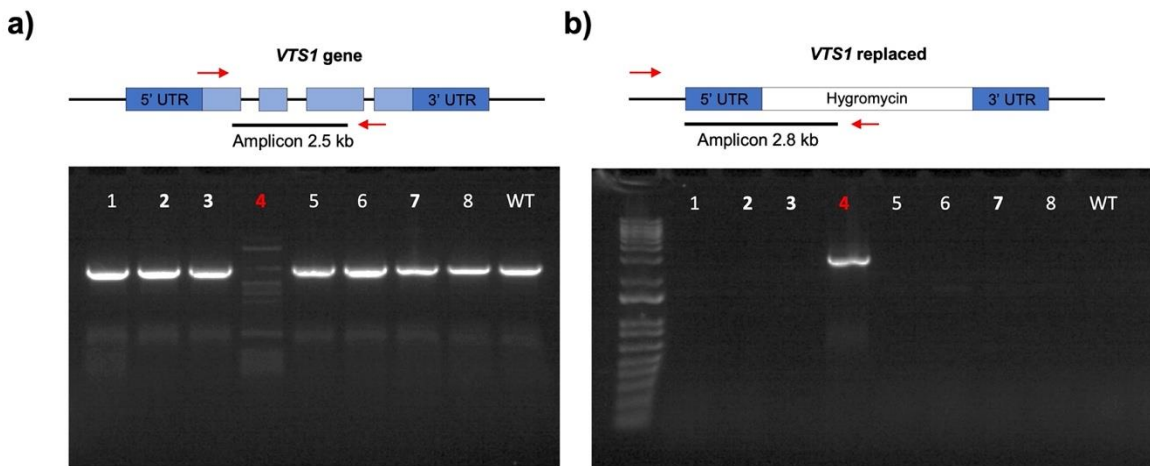
Figure 4.12. *VTS1* null mutant generation by targeted gene replacement. a) *VTS1* null mutant screening by PCR using internal specific primers for the *VTS1* gene. Gene deletion mutants were predicted not to produce an amplicon, whereas negative or ectopically integrated transformants would amplify a PCR product of 2.5 kb. **b**) *VTS1* null mutant screening by PCR using an internal specific primer for the *HPH* gene (bestowing hygromycin resistance) and one from the 5' flanking region of *VTS1*. Gene deletion transformants are predicted to amplify a PCR product of 2.5 kb, whereas negative or ectopic transformants do not amplify. In this example, strain number 4 (in red) was selected for downstream Southern blot analysis.
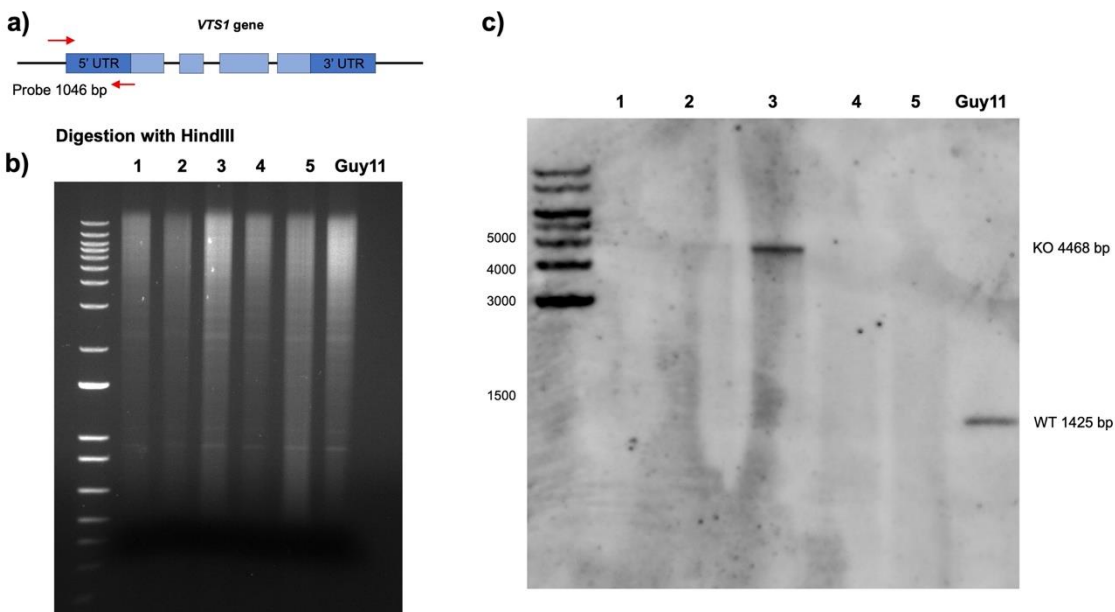
Figure 4.13. Southern blot analysis to confirm *VTS1* null mutant candidates. a) A probe of 1046 bp was generated to hybridise to the *VTS1* gene in its 5' UTR region. **b)**

Genomic DNA of the putative transformants was digested with *Hin*dIII, gel fractionated, and transferred to Hybond-NX. **c)** Southern blot analysis showing a single band of 4468 bp for positive null mutants (KO) and 1425 bp for wild-type strains (WT). The blot was probed with 1046 bp DNA fragment specific to *VTS1*.
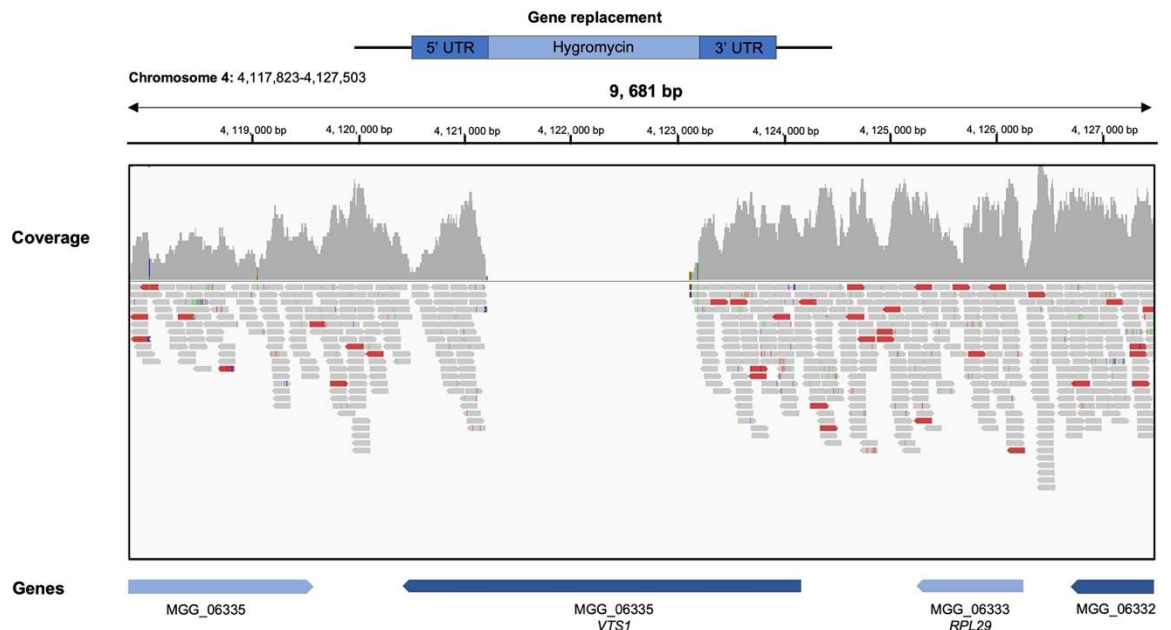
Figure 4.14. Whole genome sequencing of the *VTS1* null mutant. Bioinformatic analysis of one positive *Δvts1* null mutant showing the absence of coverage (reads) for the *VTS1* gene due to the presence of the *HPH* cassette inserted by the split marker strategy.

To generate a *Δvts1* null mutant, a targeted gene replacement method was carried out using the split marker strategy previously developed for *M. oryzae* (Catlett et al., 2003; Kershaw & Talbot, 2009). I amplified two halves of the hygromycin B (*HPH*) gene by PCR to use it as a selectable marker. To do this, I used the primers M13F with HY and M13R with YG to amplify the split *HPH* templates (Catlett et al., 2003). In parallel, I retrieved the *M. oryzae* *VTS1* genomic sequence from the Ensembl FungiDb database (https://fungi.ensembl.org/index.html) to design specific primers used to amplify regions of 1Kb flanking the gene. I then fused the *HPH* split fragments with *VTS1* flanking regions with a second PCR (Figure 4.11). Finally, I transformed Guy11 protoplasts with 4 μg of DNA of each flank to reconstitute the deletion cassette. I selected Guy11 transformants in the presence of hygromycin B (200 μg/mL). I analysed 30 of those transformants by PCR to verify the presence of *HPH* and the absence of *VTS1* (Figure 4.12).

Positive transformants were further confirmed by Southern blot analysis and whole genome sequencing. For 5 putative transformants, I isolated genomic DNA, which was digested with *Hind*III, fractionated by gel electrophoresis, and transferred onto HyBond-NX membrane (Amersham) to performed Southern blot analysis. I probed blots with a restriction fragment comprising the 5' UTR of *VTS1*. In contrast to 1.4 kb wild-type fragments, I validated successful allelic replacement for *Δvts1-T2* and *Δvts1-T3* transformants indicated by the presence of a 4.4 kb band due to insertion of the 1.7 kb *HPH* cassette at the *VTS1* locus (Figure 4.13.). To confirm that *VTS1* disruption was correct and there were no other disruptions in the genome, I sent *Δvts1-T3* DNA to Novogene for Illumina whole genome sequencing. With Dr. Vincent Were, I analysed the data and confirmed that a *Δvts1* mutant had been correctly generated (Figure 4.14). In summary, I was able to successfully delete *VTS1* in Guy11.

4.2.7 Vts1 plays roles in mycelial growth, conidiation and appressorium development, and is necessary for pathogenicity

Pmk1 pathway components have been functionally characterised by studying the phenotype of their respective mutants (Table 4.2). Gene deletion of each of the three key kinase-encoding genes, *MST11-MST7-PMK1,* for example, has a dramatic effect in the blast fungus. Each of the null mutants is affected in conidiation and, importantly, they do not differentiate into an appressorium (Xu & Hamer, 1996; Zhao et al., 2005). As a consequence, none of the Pmk1-associated mutants is pathogenic (Xu & Hamer, 1996; Zhao et al., 2005). A similar phenotype has, for instance, been observed for the adaptor protein-encoding gene *MST50* which is a key regulator of the kinases in the cascade (Li et al., 2017; Park et al., 2006). Null mutants of downstream targets of Pmk1 have been also characterised. Targeted gene deletion mutants of gene encoding the transcription factors Sfl1, Hox7, Znf1 and Mst12 are also defective in appressorium formation or function, and pathogenicity (Cao et al., 2016; Li et al., 2011; Osés-Ruiz et al., 2021; Park et al., 2002; Yue et al., 2016). All these individual mutants develop appressorium-like structures, but they are non-functional. There are other described components of the Pmk1 pathway (such as Pic1 and Pic5) whose null mutants have severe phenotypes in conidiation, appressorium formation, plant penetration and pathogenicity (Zhang et al., 2011). However, little is known about their mechanistic role in the cascade.
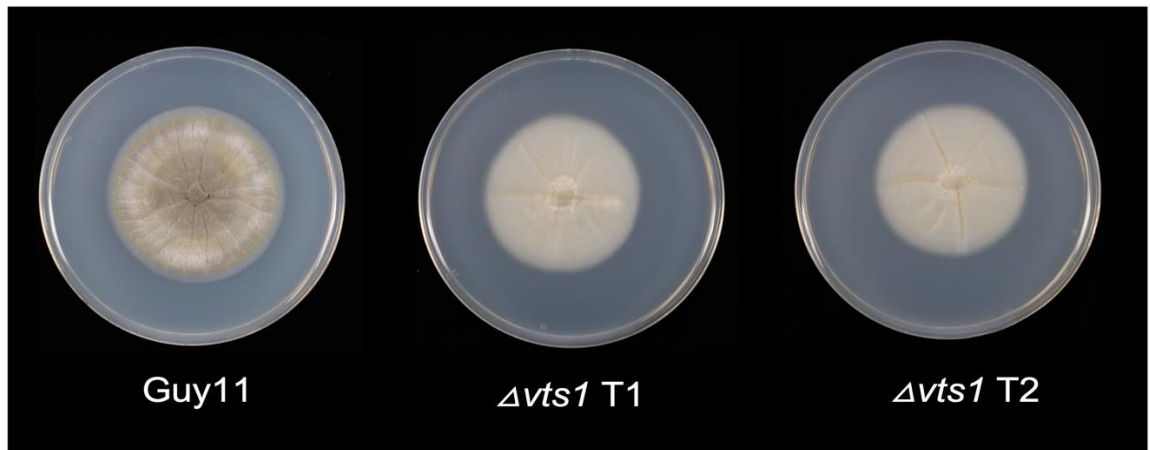
Figure 4.15. Vegetative growth phenotype of *Δvts1* null mutants in axenic culture. Photographs to show mycelial growth phenotype of colonies of the wild-type strain Guy11, and two independent *Δvts1* null mutants to show mycelial phenotype. Photographs were recorded after incubating on CM at 26 °C for 10 days.
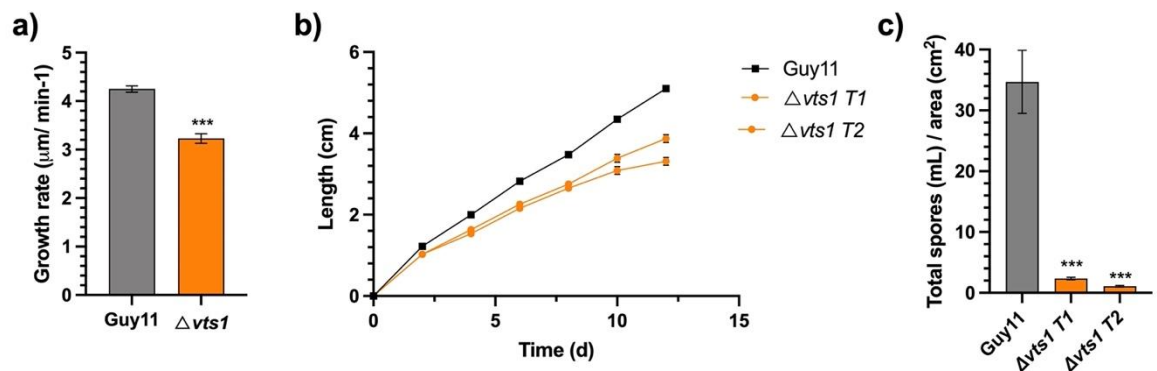
Figure 4.16. Phenotype of *Δvts1* mutants in vegetative growth and conidiogenesis. Charts to show **a)** growth rate and **b)** line graph to show growth of colonies measured at 2, 4, 6, 8, 10 and 12 dpi on CM plates. **c)** Bar chart to show conidiogenesis. For sporulation assays CM plates were flooded with 5 mL dH_2O to harvest conidia. Spores were harvested, pelleted by centrifugation, resuspended in 1 mL, and counted on a haemocytometer (Corning). Calculations were then carried out to determine the number of conidia generated *per* cm^2 of mycelium. CM plates were inoculated with 8mm plugs of mycelium from Guy11 and *Δvts1*. Plates were incubated at 26 °C for a period of 12 days (growth rate experiments) and 10 days (sporulation assay experiment). Three biological replicates were carried out with 50 appressoria recorded per replicate. *$P < 0.05$: **$P < 0.01$; ***$P < 0.001$ represent significance using an ANOVA test. Error bars represent the standard deviation of three independent biological replicates of the experiment.

The most evident phenotypes of *Δvts1* mutants were related to growth and conidiation. When vegetative hyphae of *Δvts1* were grown on solid complete medium (CM), they produced whitish colonies that were different from the typical grey colonies produced by Guy11 (Figure 4.15). I first performed a growth rate assay to compare mycelial growth between the wild-type strain Guy11 and *Δvts1*. After 12 days of growth in optimal conditions, *Δvts1* mycelium grew 3.23 mm/day whereas Guy11 mycelium grew 4.25 mm/day. The data shows that the *Δvts1* mutant has 24% slower growth rate than Guy11 (Figure 4.16). The difference in growth started to be significant after 4 days (Figure 4.16). For conidiation, *Δvts1* produced 2.3 spores/cm^2 whereas Guy11 strain 34.69 spores/cm^2. The *Δvts1* mutant therefore has a severe effect in sporulation, showing 94% less production than Guy11 (Figure 4.16). When considered together, these results show that *Δvts1* has a dramatic reduction of growth and conidiation.

I next decided to examine the frequency of appressorium formation in *Δvts1* mutants. I analysed appressorium development after 24 h of germination on hydrophobic coverslips. I found that *Δvts1* spores germinated equally as well as wild type (Figure 4.17). However, in Guy11 conidia, the apical cell germinated to form a single appressorium, whereas in *Δvts1* 58% of conidia generated one appressorium and, also, one aberrant appressorium-like structure. In wild-type conidia, the formation of two appressoria was rarely observed. By contrast, in *Δvts1*, the two appressorium emerged either from the same apical cell or from one of the other conidial cells (Figure 4.17). Based on this data, I conclude that *Δvts1* is impaired in the normal spatial pattering of appressorium development. A summary of mutant phenotypes of components of the Pmk1 signalling pathway and its downstream targets is shown in Table 4.2.

Table 4.2. Mutant phenotypes of the MAPK Pmk1 pathway components in *M. oryzae*.

Protein	Gene ID	Function	Mutant phenotype	Reference
Mst11	MGG_14847	MAPKKK (MEKK)	Defective in aerial hyphae and conidia growth, no appressorium formation and plant infection.	Zhao et al., 2005
Mst7	MGG_00800	MAPKK (MEK)	Defective in aerial hyphae and conidia growth, no appressorium formation and plant infection.	Zhao et al., 2005
Pmk1	MGG_09565	MAPK	Defective in conidiation, no appressorium formation and invasive growth.	Xu and Hamer, 1996
Mst50	MGG_05199	Scaffold protein	No appressorium formation and non-pathogenic.	Park et al., 2006
Hox7	MGG_12865	Transcription factor	Defective in appressorium formation and pathogenicity.	Sweigard et al., 1998; Osés-Ruiz et al., 2021
Znf1	MGG_14931	Transcription factor	Defective in appressorium formation and non-pathogenic	Yue et al., 2015; Cao et al., 2016
Mst12	MGG_12958	Transcription factor	Plant penetration.	Park et al., 2002
Sfl1	MGG_06971	Transcription factor	Defective in pathogenicity	Li et al., 2011
PIC1	MGG_11168	Unknown	Defective conidiation and abnormal germ tube differentiation.	Zhang et al., 2011
PIC5	MGG_08600	Unknown	Defective germ tube growth, appressorium differentiation, plant penetration and pathogenicity.	Zhang et al., 2011
Vts1	MGG_06334	Unknown	Defective in conidiation, growth rate, appressorium formation and pathogenicity	This study
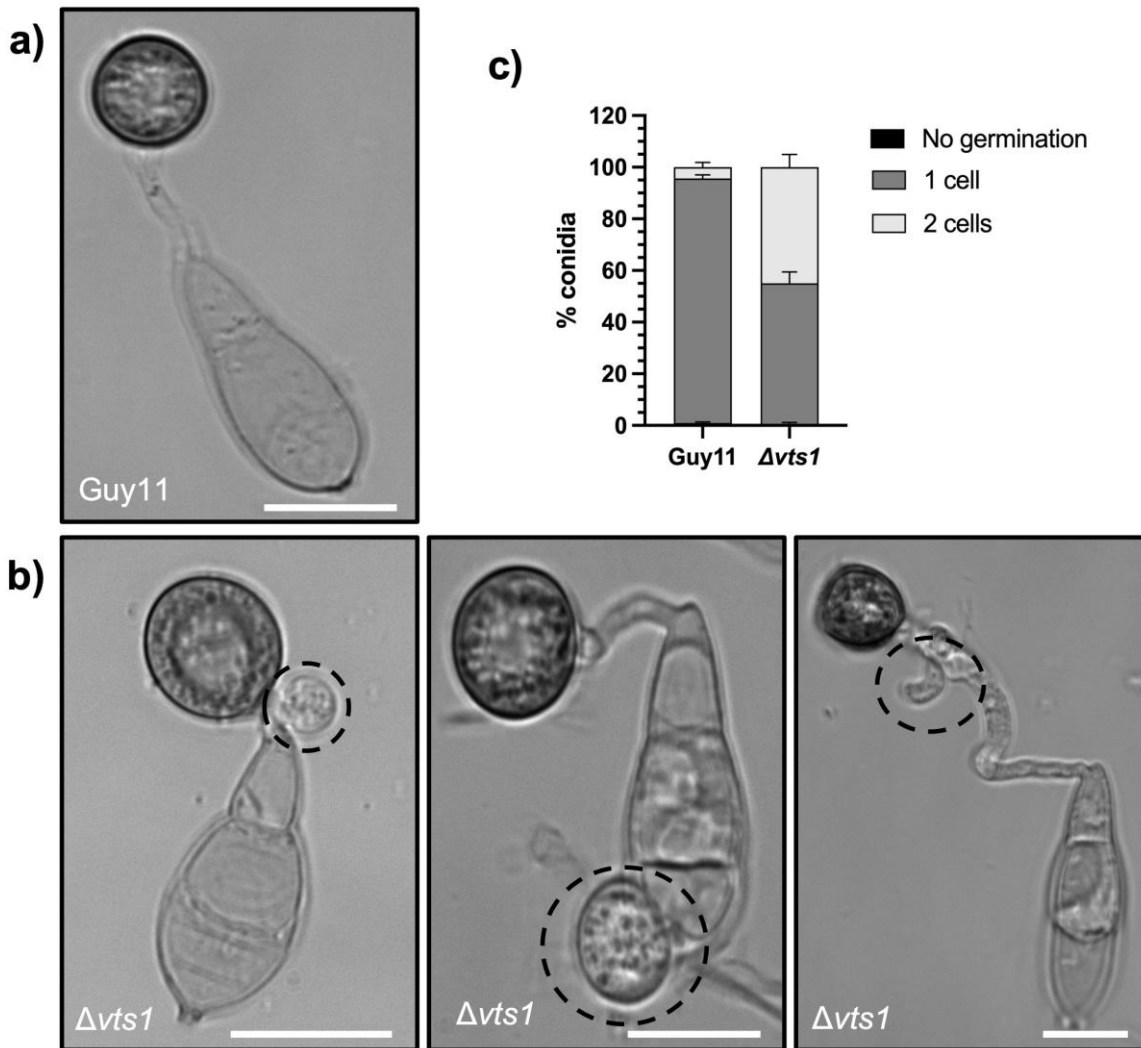
Figure 4.17. Vts1 is necessary for appressorium development. Micrographs to show appressorium development of **a)** Guy11 and **b)** *Δvts1* strains. Conidia were harvested from Guy11 and *Δvts1* mutants, inoculated onto glass coverslips, and observed at 24h. Scale bar= 10μm. **c)** Bar chart to show the frequency of conidial germination from one and two cells. Three biological replicates were carried out with 100 appressoria recorded per replicate. *$P < 0.05$: **$P < 0.01$; ***$P < 0.001$ represent significant differences using an unpaired two-tailed Student's *t*-test. Data are from three biological replicates.

All studied downstream targets of Pmk1 so far investigated in *M. oryzae* have been reported to have reduced or no pathogenicity. Therefore, I evaluated the ability of *Δvts1* mutants to cause rice blast disease. For this, I performed both a rice leaf sheath and spray infection assay using the blast-susceptible dwarf indica rice variety CO-39. For leaf sheath assays, after 48h, 91.78% of Guy11 conidia formed a functional appressorium, penetrated and invaded rice cells. A total of 82.1% of the invading fungal cells colonised up to the 3rd or more adjacent rice cells (Figure 4.18). Conversely, in *Δvts1*, only around 50% of conidia

formed a functional appressorium that was able to penetrate the plant. From these, only ~23% spread to the 3rd or more adjacent cells (Figure 4.18). These results suggest that appressorium-mediated plant infection is impaired in the *Δvts1* mutant. For spray infection assays, conidial suspensions of equal concentration were sprayed on to 21-day old seedlings of CO-39. I observed that *Δvts1* mutants produced only a small number of resistant-type or small lesions. The mutant showed around 85% reduced pathogenicity when compared to the isogenic wild-type strain Guy11 after 6 days post-inoculation (Figure 4.19). Both leaf sheath and spray infection assays were consistent with an affected virulence phenotype for *Δvts1* mutants during infection of rice tissue. I conclude that Vts1 is a pathogenicity determinant of the rice blast fungus.
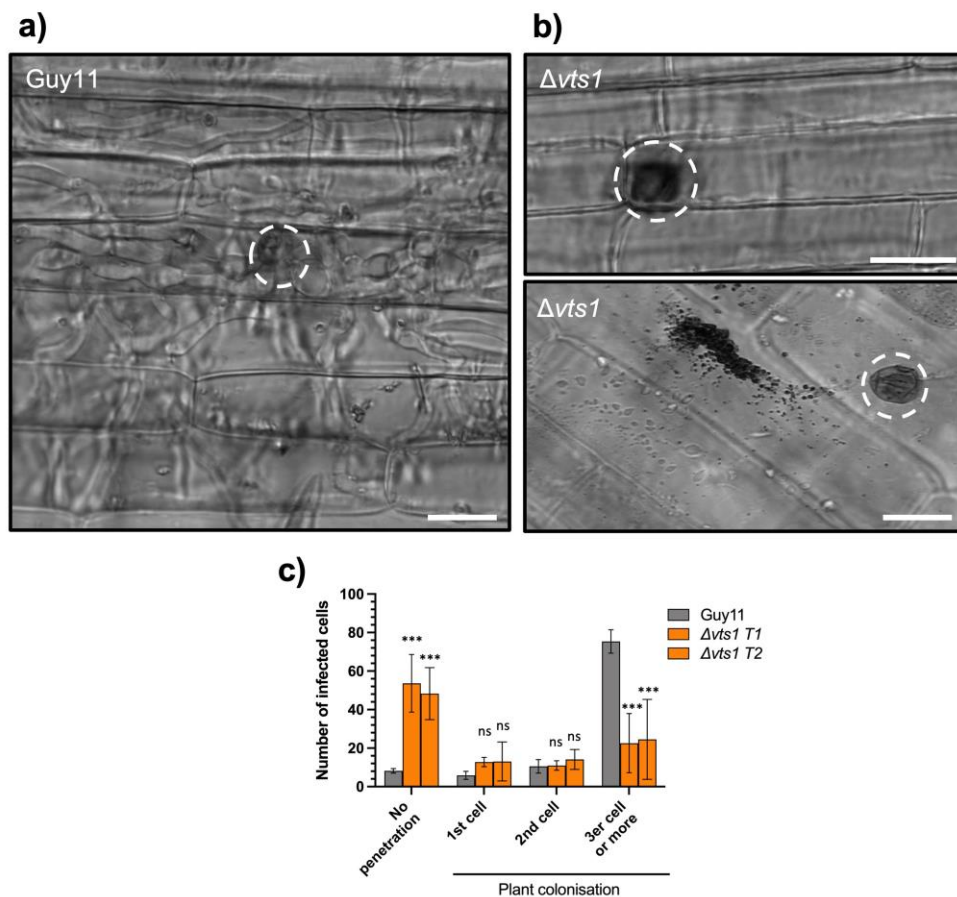
Figure 4.18. The *Δvts1* mutant of *M. oryzae* is impaired in plant tissue colonisation. Micrographs to show **a)** Guy11 and **b)** *Δvts1* phenotype during plant penetration. **c)** Bar chart to show the frequency and extent of plant penetration at 48 h. Detached rice leaf sheaths were incubated at 26°C. Scale bars = 10 μm. Three biological replicates were carried out with 50 appressoria recorded per replicate. *$P < 0.05$: **$P < 0.01$; ***$P < 0.001$ represent significant differences using an ANOVA test. Data are from three biological replicates.
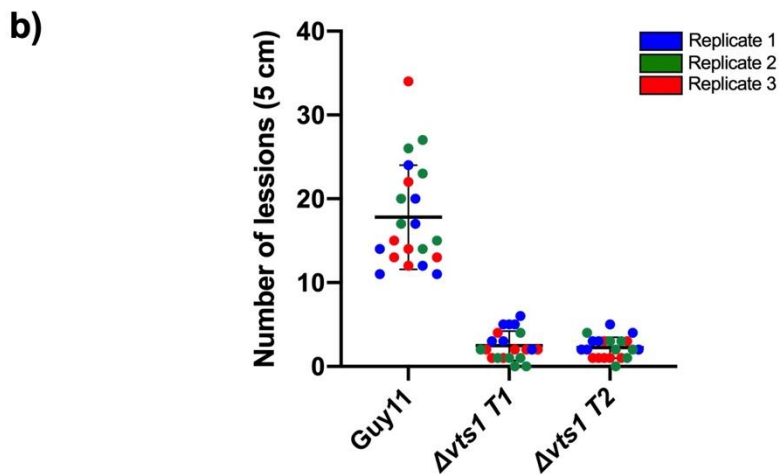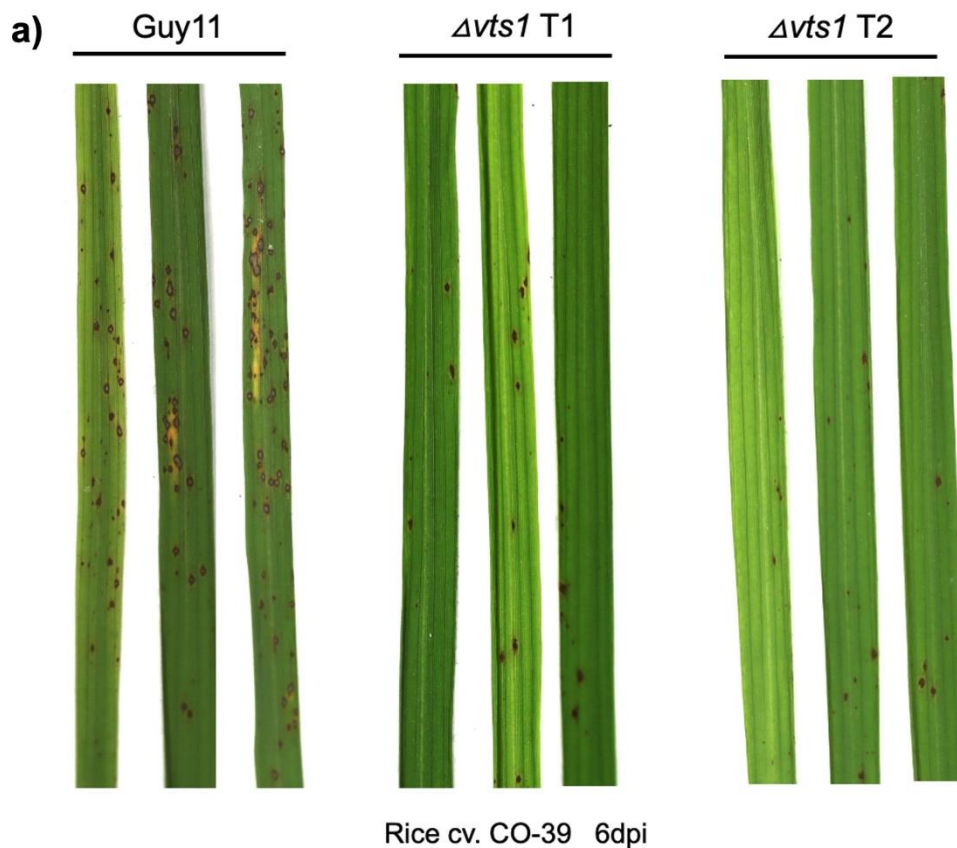
Figure 4.19. Vts1 is required for virulence by *M. oryzae*. a) Two-week-old seedlings of rice cultivar C0-39 were inoculated with equal amounts of conidial suspensions of Guy11 and *Δvts1* containing 10^5 conidia mL^{-1} in 0.2% gelatine. Seedlings were incubated for 6 days to develop blast disease at 26 °C and 90 % humidity. **b)** Scatter chart to show the number of disease lesions in Guy11 and two independent *Δvts1* mutants. Horizontal line represents the mean, and the error bar is the standard deviation. Data points are shown from three biological replicates in different colours (red, blue, green).

4.2.8 Cytoskeletal components are mis-localised in Vts1 null mutant

It is widely known that F-actin cytoskeletal re-organisation is essential for appressorium-mediated plant penetration by the blast fungus (Dagdas et al., 2012). Recently, it has been reported that the transcription factor Mst12, a downstream target of Pmk1, is required for septin-dependent re-polarization of the appressorium (Osés-Ruiz et al., 2021). To help define the function of Vts1 during plant infection, I decided to study cytoskeletal components in the *Δvts1* mutant during appressorium formation. I reasoned that because *Δvts1* was impaired in plant penetration, it might be because of the mis-regulation of septin ring formation. The use of the actin-binding protein Gelsolin-GFP and Septin5-GFP fluorescent markers has helped to visualise cytoskeleton dynamics during infection-related development (Ryder et al., 2013). I therefore decided to carry out live-cell imaging of the *Δvts1* mutant. To this end, I obtained Gelsolin-GFP and Septin5-GFP plasmids from Dr. Lauren Ryder to transform *Δvts1* mutants. Both plasmids have the *BAR* gene to confer bialophos (BASTA) resistance for selection in *M. oryzae*. Therefore, I selected positive transformants expressing GFP under the microscope and was able to grow them on selection media containing 200 μg/mL of BASTA.

I next investigated Gelsolin-GFP and Septin5-GFP localisation during appressorium formation in the *Δvts1* mutant compared to Guy11 (with Alice Eseola). For Gelsolin-GFP, I observed in Guy11 that it is organised into a ring structure in most appressoria. However, we found that 42% of *Δvts1* mutant appressoria had mis-localisation defects, forming a disorganised gelsolin patch at the base of the appressorium (Figure 4.20). Similarly, when we observed Septin5-GFP localisation in Guy11, we observed normal ring assembly in almost all appressoria. By contrast, in *Δvts1*, 55% of appressoria showed mis-localised aberrant rings (Figure 4.20). Given that gelsolin colocalises with F-actin at the appressorium pore (Ryder et al., 2013), the altered Gelsolin-GFP fluoresce pattern suggests that the toroidal F-actin ring in *Δvts1* is disorganised. Taken together, these results show that the disorganisation of the septin-dependent F-actin cytoskeleton occurs in the appressorium of *Δvts1* mutants. Therefore, I conclude that Vts1 is required for cytoskeleton reorganisation to enable plant penetration by *M. oryzae*.
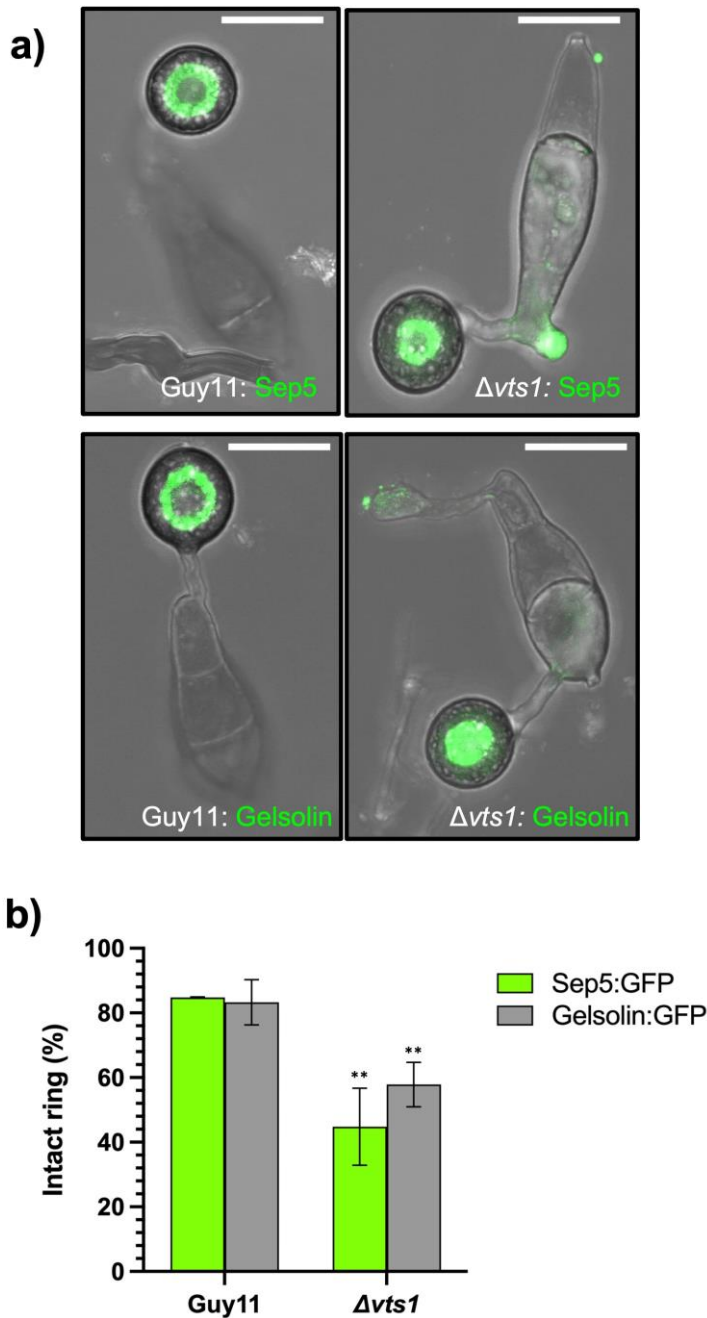
Figure 4.20. Vts1 is required for septin ring formation. a) Micrographs to show septin and F-actin ring organisation visualised by expression of Sep5-GFP and gelsolin-GFP in Guy11 and *Δvts1* strains. The *Δvts1* mutant produces aberrant septin and actin rings at the appressorium pore. **b)** Bar charts to show frequency of intact ring formation in Guy11 and *Δvts1*. Mis-localisation in Sep5-GFP and gelsolin-GFP was clear. Three biological replicates were carried out with 100 appressoria recorded for replicate. *$P < 0.05$: **$P < 0.01$; ***$P < 0.001$ represent significant differences using unpaired two-tailed Student's *t*-test. Data from three biological replicates.
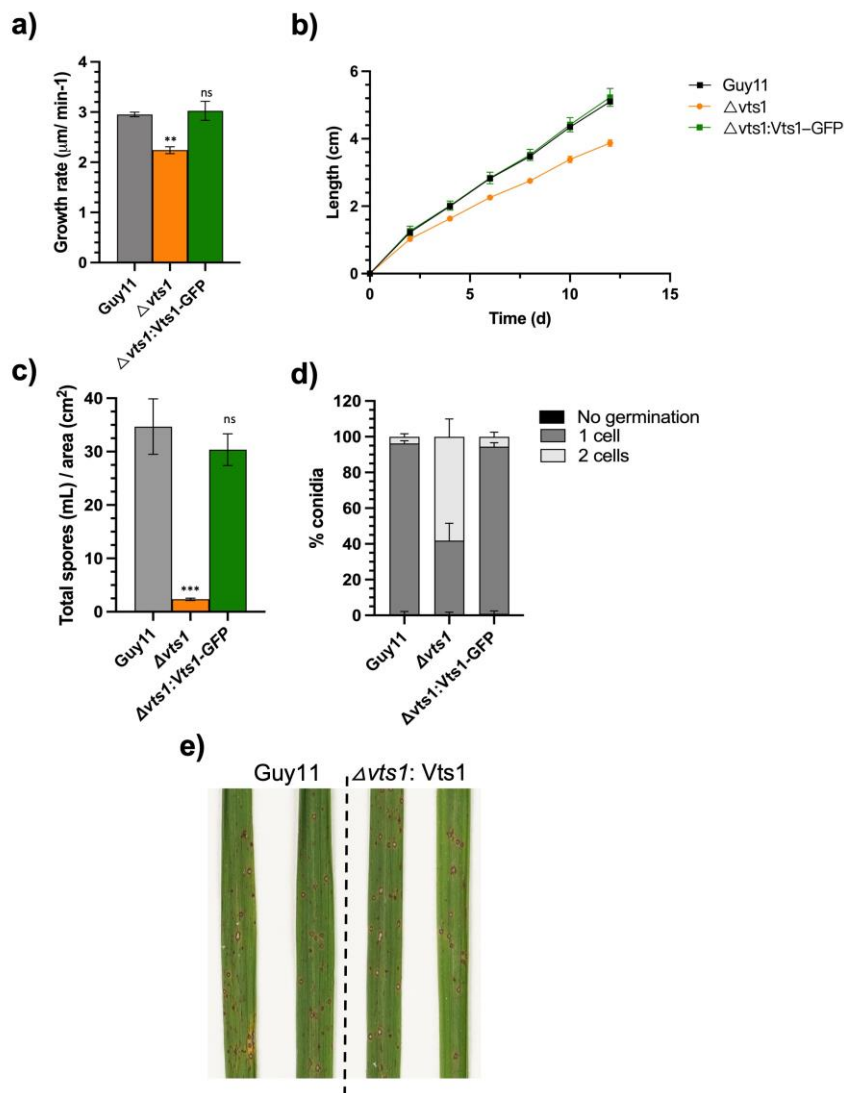
Figure 4.21. The *Δvts1* null mutant can be complemented by *VTS1-GFP*. a) Bar chart to show growth rate and **b)** line graph to show growth of colonies measured at 2, 4, 6, 8, 10 and 12 dpi on CM plates. **c)** Bar chart to show conidiogenesis. For sporulation assays CM plates were flooded with 5 mL dH_2O to harvest conidia. The number of conidia generated per cm^2 of mycelium was then calculated. CM plates were inoculated with $8mm^2$ plugs of mycelium from Guy11, *Δvts1* and *Δvts1*:*VTS1-GFP.* Plates were incubated at 26°C for a period of 12 days (growth rate experiments) and 10 days (sporulation assay experiment). **d)** Bar chart to show the frequency of conidia germination from one or two cells. Three biological replicates were carried out with 50 appressoria recorded for replicate. *$P < 0.05$: **$P < 0.01$; ***$P < 0.001$ represent significant differences using an ANOVA test. **e)** 2-week-old seedlings of rice cultivar C0-39 were inoculated with equal amounts of conidial suspensions of Guy11, *Δvts1* and *Δvts1*:*VTS1-GFP* (10^5 conidia mL^{-1}) in 0.2% gelatine. Seedlings were incubated for 6 days to develop blast disease at 26 °C and 90 % humidity. Data from three biological replicates.

4.2.9 Vts1 function can be complemented by re-introduction of *VTS1* into a *Δvts1* mutant

To confirm that phenotypes observed in the *vts1* mutant were all caused by deletion of the *VTS1* gene, I reintroduced the *VTS1* wild-type allele into *Δvts1*. I reasoned that if defects in growth, sporulation, appressorium development and pathogenicity were caused by the absence of this gene, they should be restored back to the wild-type phenotype by ectopic integration and expression of *VTS1*. I therefore decided to complement *Δvts1* with VTS1-GFP, which would also enable visualisation and localisation of a functional version of the protein.

To test whether I could complement a *Δvts1* mutant with a wild-type allele of *VTS1*, I transformed *M. oryzae* protoplasts with a translational gene fusion of the *VTS1* coding sequence and GFP (Vts1-GFP). To carry out this experiment, I used pScBar-Vts1-GFP plasmid that contains *VTS1* gene under control of its native promoter into pScBAR as a C-terminal GFP fusion. I transformed protoplasts of the *Δvts1* mutant with 8 μg of pScBar-Vts1-GFP plasmid. I then selected transformants based on PCR and GFP signal screening. To quantify the copy number of insertions, I sent genomic DNA of positive transformants to Anglia iDNA for qPCR analysis. For this experiment, I assessed two independent *Δvts1* transformants containing a single copy of Vts1-GFP.

For the complementation experiment, I tested the ability of the *Δvts1:VTS1-GFP* for growth, conidiation, appressorium formation and pathogenicity. When I tested growth rate and conidiation for the *Δvts1:VTS1-GFP* complemented strain compared to Guy11, there was no significant difference (Figure 4.21). Similarly, more than 95% of the conidia from both *Δvts1:VTS1-GFP* and Guy11 germinated to produced melanised appressorium (Figure 4.21). Finally, when I tested pathogenicity in both strains, I observed a similar number of typical rice blast disease lesions (Figure 4.21). These findings suggest that the Vts1-GFP fusion construct encodes a functional protein that complements the defects of a *Δvts1* mutant. I conclude that deletion of the *VTS1* gene is responsible for defects in growth rate, conidiation, appressorium development and pathogenicity of *M. oryzae*.
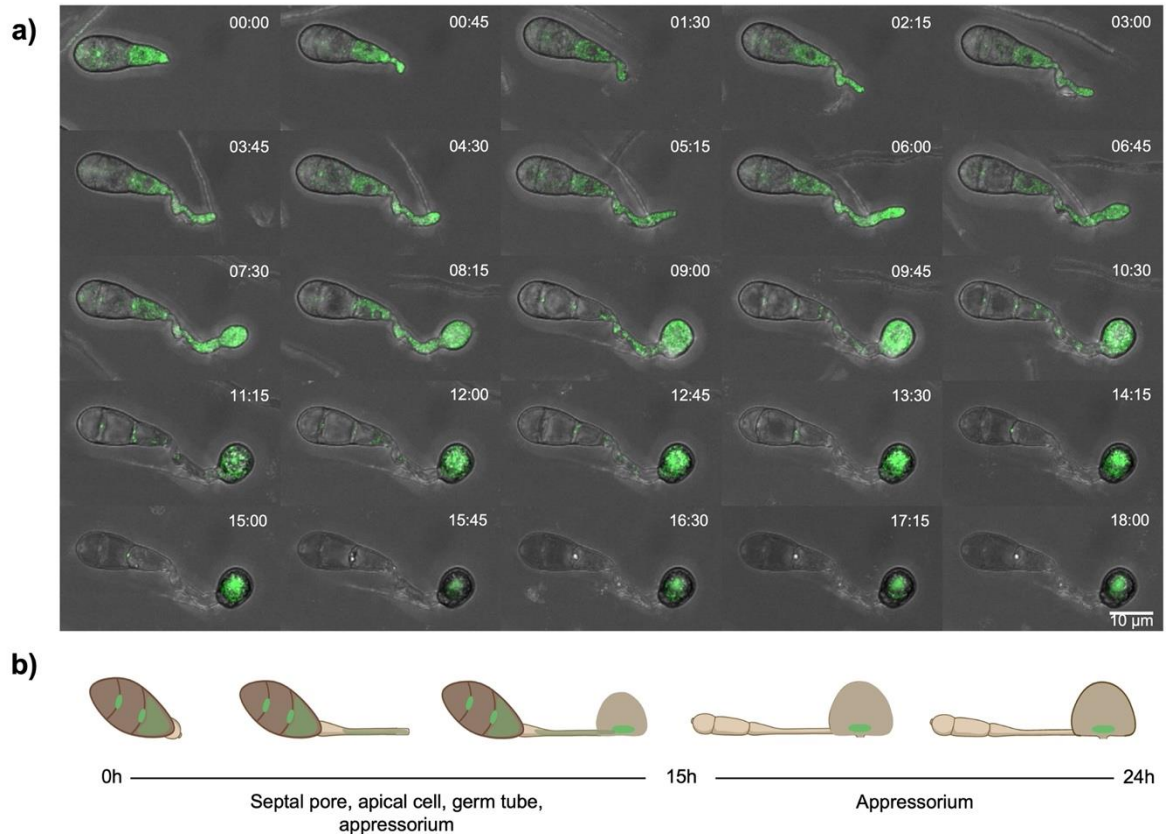
Figure 4.22. Vts1 localisation during appressorium formation. a) Micrograph montage to show Vts1 localisation during a time series from germination to mature appressorium development (with 45 min intervals). Conidia were harvested from the *Δvts1*: *VTS1-GFP* strain at 10 dpi, inoculated onto glass coverslips and observed by confocal microscopy during 24h. Scale bar = 10 μm. Micrographs represent observations from three biological replicates. **b)** Schematic representation to show Vts1 localisation during appressorium morphogenesis. From 0 to 15h, Vts1 localises at the conidium septal pore, apical cell, germ tube and the growing appressorium. However, after 15 h, Vts1 localisation concentrates in the appressorium.

4.2.10 Vts1 is a cytoplasmic protein that accumulates at the septal pore and appressorium pore

Based on our transcriptomic and proteomic data, we found that *VTS1* is expressed early in appressorium formation. To determine the Vts1 localisation pattern, I decided to carry out a live-imaging analysis of *Δvts1:*Vts1-GFP. I evaluated Vts1 localisation during appressorium development from 0-24h on hydrophobic coverslips (with Alice Eseola). At 0h, Vts1-GFP fluorescence was homogeneously distributed in conidial cells (Figure 4.22). During the initial minutes of germination, we observed that GFP fluorescence accumulated

at the septal pore of the conidium and in the apical cell from where the germ tube emerges (Figure 4.22 and Figure 4.23). From 20min to 4h, the Vts1-GFP signal concentrated more in the growing germ tube (Figure 4.22). Finally, from 4h to 24 h, GFP fluorescence accumulated in the appressorium (Figure 4.23). Consistent with transcriptomic and proteomic data, these observations suggests that *VTS1* is expressed and translated during blast disease from fungus germination up to appressorium maturation.
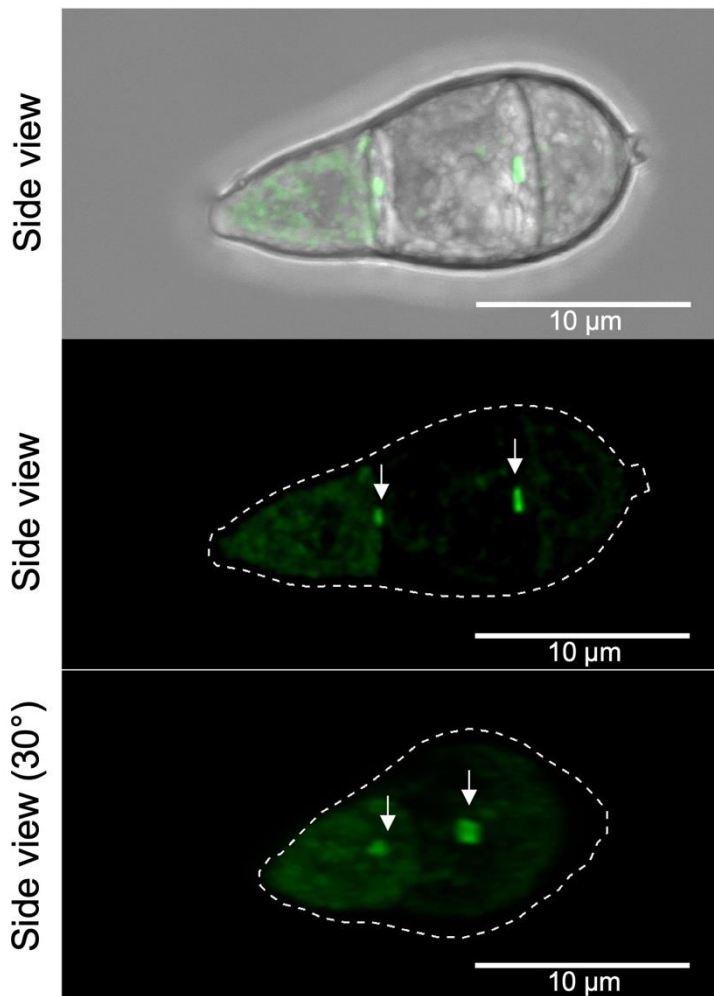
Figure 4.23. Vts1 localises to the septal pore. Micrographs to show Vts1 localisation in conidia. Conidia were harvested from *Δvts1*:*VTS1-GFP* strain 10 dpi and observed by laser confocal microscopy. White arrowheads point to septal pores of the conidium. Scale bar = 10 μm. Micrograph represent observations from three biological replicates.
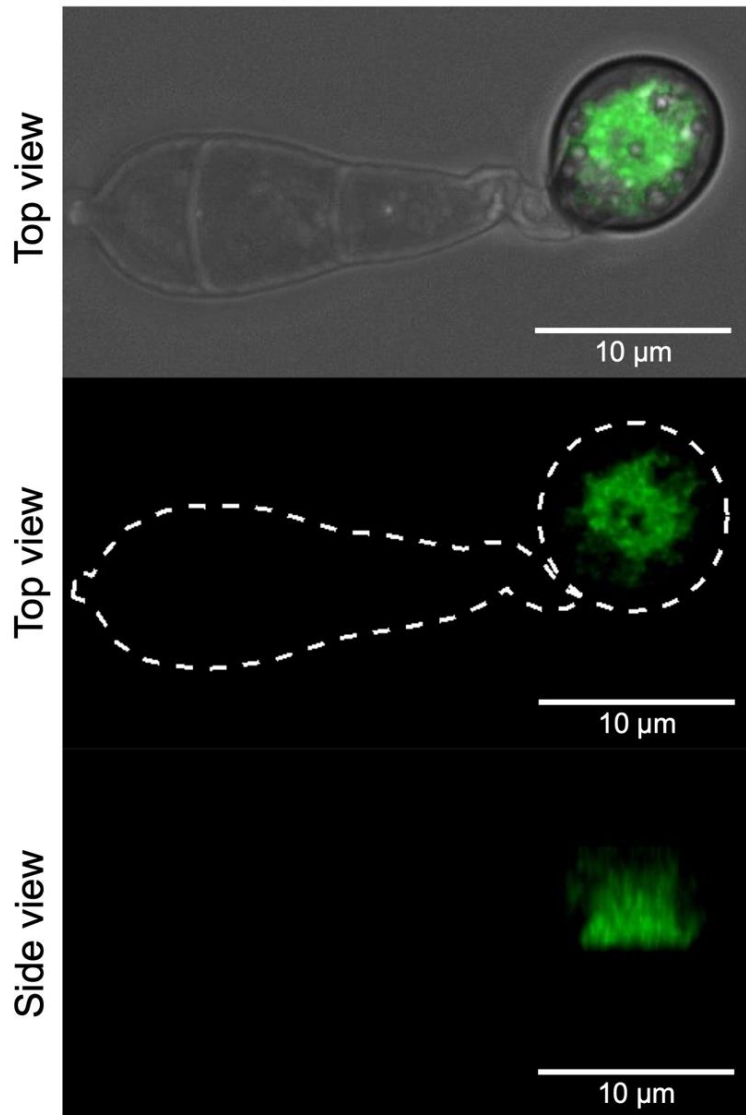
Figure 4.24. Vts1 localises to the appressorium. Micrographs to show Vts1 localisation in a mature appressorium. Conidia were harvested from *Δvts1*:*VTS1-GFP* strain 10 dpi, inoculated onto glass coverslips and observed by laser confocal microscopy at 24h. White dotted lines indicate conidium and appressorium position. Scale bar = 10 μm. Micrograph represent observations from three biological replicates.

Because *Δvts1* is affected in appressorium formation and Vts1 localises at the appressorium pore, I decided to investigate the role of Vts1 in appressorium development. To obtain insight into Vts1 function, we decided to carry out a 3D reconstruction of its sub-cellular localisation pattern in a mature appressorium. To this end, we acquired images of *Δvts1:*Vts1-GFP after 24h of germination on hydrophobic coverslips (with Alice Eseola). Then, we used those images to construct a 3D projection of the GFP fluorescence signal.

We observed that the GFP signal accumulated at the base of the appressorium, coincident with the position of the appressorium pore (Figure 4.24). Sub-cellular localisation experiments therefore showed that Vts1 has distinct patterns of cellular localisation during appressorium morphogenesis, including initial localisation to the conidium septal pore, the apical cell, the germ tube and then at the pore of the mature appressorium (Figure 4.24).

To confirm that Vts1 localised to the appressorium pore, I decided to carry out a colocalisation experiment using a fluorescent marker of the septin ring. For this purpose, we used a Septin5-RFP (*SUR* resistant) plasmid to transform the *Δvts1:*Vts1-GFP strain. After PCR and RFP signal screening, I selected two independent transformants to analyse Vts1 and Septin5 co-localisation. Interestingly, we observed that Vts1 has a similar spatial localisation to septin ring within the appressorium pore (Figure 4.25). These observations suggests that Vts1 is a septin proximal protein that accumulates in the appressorium pore from where the penetration peg is formed.

4.2.11 Spatial Vts1 localisation is affected when Pmk1 is inactivated during appressorium formation

To investigate the role of Vts1 in appressorium development further and in light of its Pmk1-dependent phosphorylation, I reasoned that if Vts1 phosphorylation is relevant for its biological function, then it might be possible to observe an effect on Vts1 localisation when Pmk1 is inactivated. I therefore transformed the Vts1-GFP vector in the *M. oryzae pmk1*[AS] mutant. I carried out PCR and GFP signal screening to select two independent transformants for further analysis. Additionally, I measured the plasmid copy number (Anglia iDNA). I then selected two independent *pmk1*[AS] transformants with a single copy of Vts1-GFP for further analysis.

To evaluate the effect of Pmk1 on Vts1 localisation, I first defined the time at which I could inhibit Pmk1 to study appressorium formation. I found that germlings were able to differentiate into melanised appressoria and conidial cells collapsed when the inhibitor was added after 4-8 h (Figure 4.26). By contrast, when 1Na-PP1 was added from 0-3 h, germlings did not differentiate into an appressorium. Consistent with previous research, these results show that Pmk1 function is abrogated during appressorium morphogenesis when its kinase activity is inhibited using a chemical genetic method (Sakulkoo et al., 2018). Although Pmk1 activity is essential for appressorium development, this confirmed the process can still proceed normally after the germ tube has committed to differentiate into an appressorium. I therefore concluded that inhibiting Pmk1 after 6-8 h of germination would allow me to study its effect on Vts1 localisation in the incipient appressorium.

I next performed a Vts1 localisation experiment following Pmk1 inactivation. I inhibited Pmk1 at 6 and 8 h after germination and then observed Vts1 GFP signal using the *pmk1^AS^:VTS1-GFP* strain at 24h (with Alice Eseola). When I added 1NA-PP1 at 6h, I found that 45% of treated germlings showed Vts1 accumulation in the apical cell and non-collapsed conidium (Figure 4.26). I observed a similar phenotype in 29% of germlings treated after 8h of germination. Conversely, in the control non-treated germlings Vts1 accumulated at the appressorium and conidium collapsed normally (Figure 4.26). Based on these experiments of Vts1 localisation in the complemented strain *Δvts1:*Vts1-GFP, we can conclude that inhibition of Pmk1 activity during appressorium morphogenesis impairs the correct spatial localisation of Vts1.
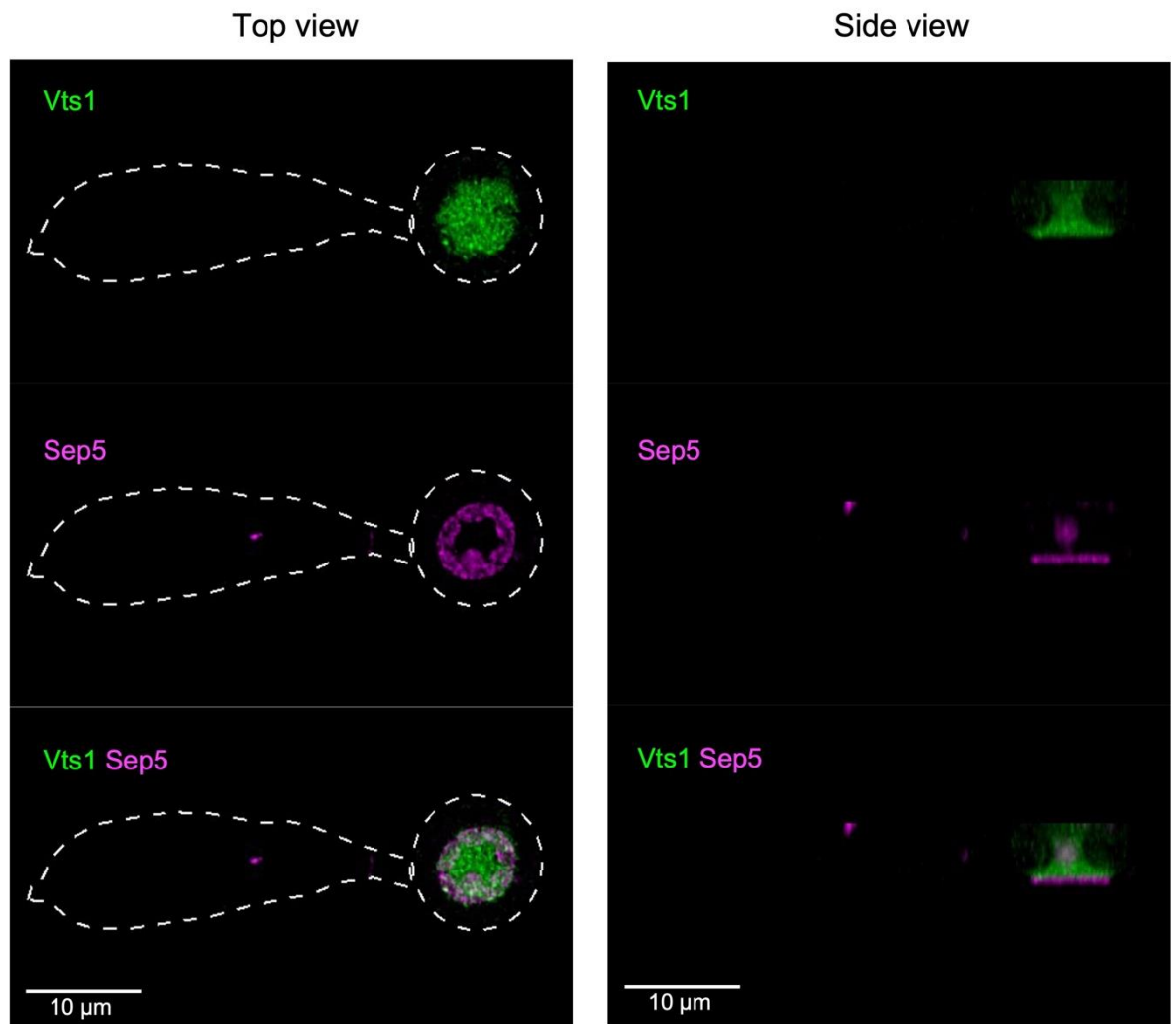
Figure 4.25. Vts1 has partially co-localises with the septin ring in the appressorium pore of *M. oryzae.* Micrographs to show Vts1-GFP and Sep5-RFP localisation in a mature appressorium at 24 h. Conidia were harvested from *Δvts1*: *VTS1-GFP/Sep5-RFP* strain 10 dpi, inoculated onto glass coverslips and observed by laser confocal microscopy at 24h.

White dotted lines indicate the conidium and appressorium position. Scale bar = 10 μm. Micrographs are representative observations from three biological replicates of the experiment.
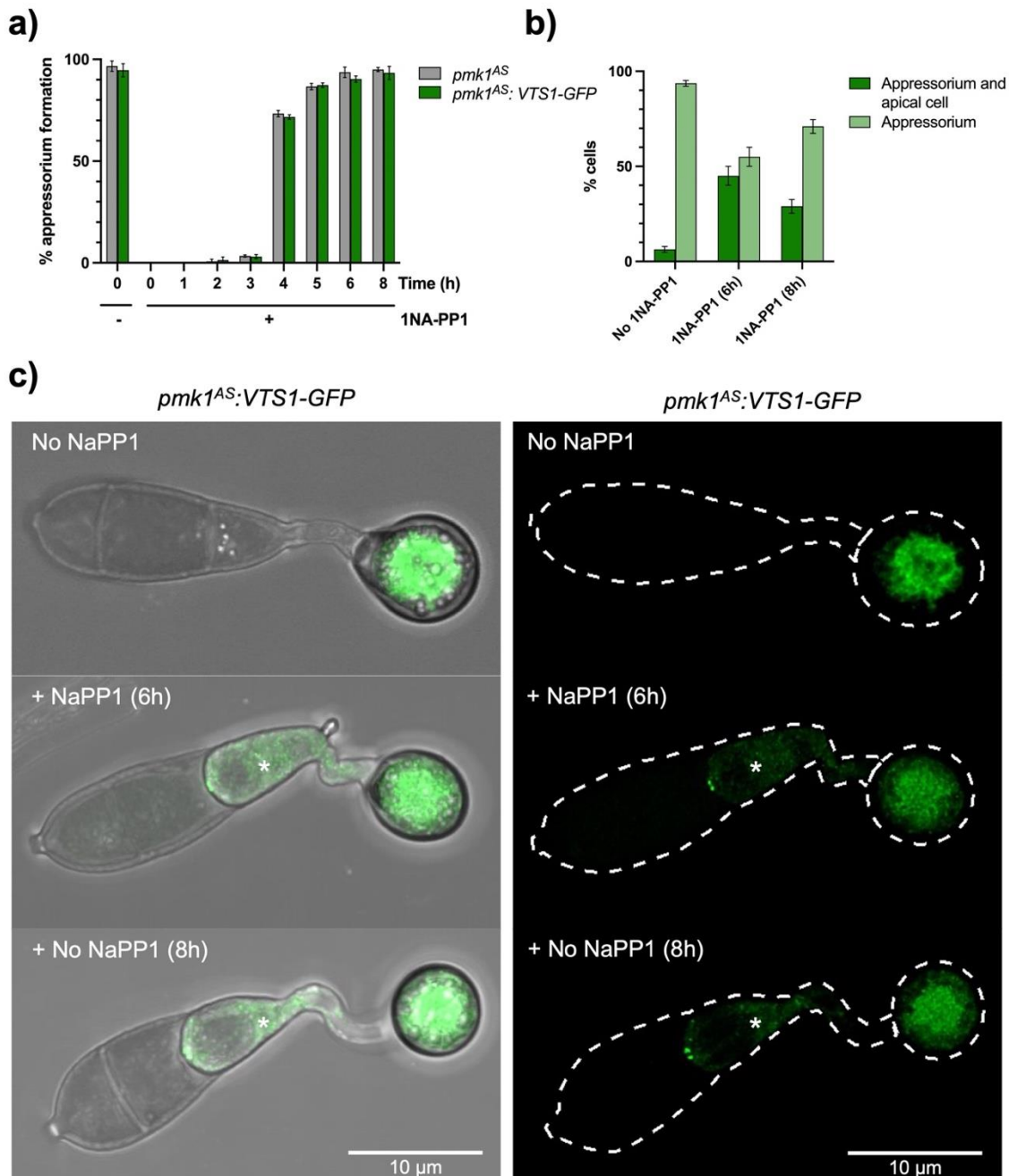
Figure 4.26. Vts1 localisation is impaired when Pmk1 is inactivated. a) Bar chart to show the frequency of appressorium development of $pmk1^{AS}$ and $pmk1^{AS}$: *VTS1-GFP* at 24 h when 1NaPP1 (5 μg) was added at different timepoints. Three biological replicates were carried out with 100 appressoria recorded per replicate. **b)** Bar chart to show frequency of

Vts1-GFP localisation when 5µg 1NaPP1 was added to appressoria at 6h and 8h. Counts were recorded at 24 hpi. Three biological replicates were carried out with 50 appressoria recorded for each replicate. **c)** Micrographs to show representative localisation of Vts1-GFP in appressoria of *pmk1^AS^: VTS1-GFP* treated +/- 5 µg 1NaPP1. Conidia were harvested from *pmk1^AS^: VTS1-GFP* strain 10 dpi, inoculated onto glass coverslips and observed by laser confocal microscopy at 24h. White dotted lines indicate position of the conidium and appressorium. Scale bar = 10 µm.

4.2.12 Generation of non-phosphorylatable and phosphomimetic alleles of the *VTS1* gene in *M. oryzae*

To understand the biological significance of Pmk1-dependent phosphorylation of Vts1, I decided to construct different alleles of *VTS1* carrying mutations to modulate the phosphorylation status of these serine and threonine phosphorylation residues. Non-phosphorylatable or phosphodead mutants require amino acid substitutions that avoid phosphorylation, typically an alanine substitution (Gratz et al., 2020). Conversely to create a phosphomimetic mutant, requires substitutions to either glutamate and aspartate residues because their charges are similar to that of phosphoserine (Shipston & Tian, 2016).
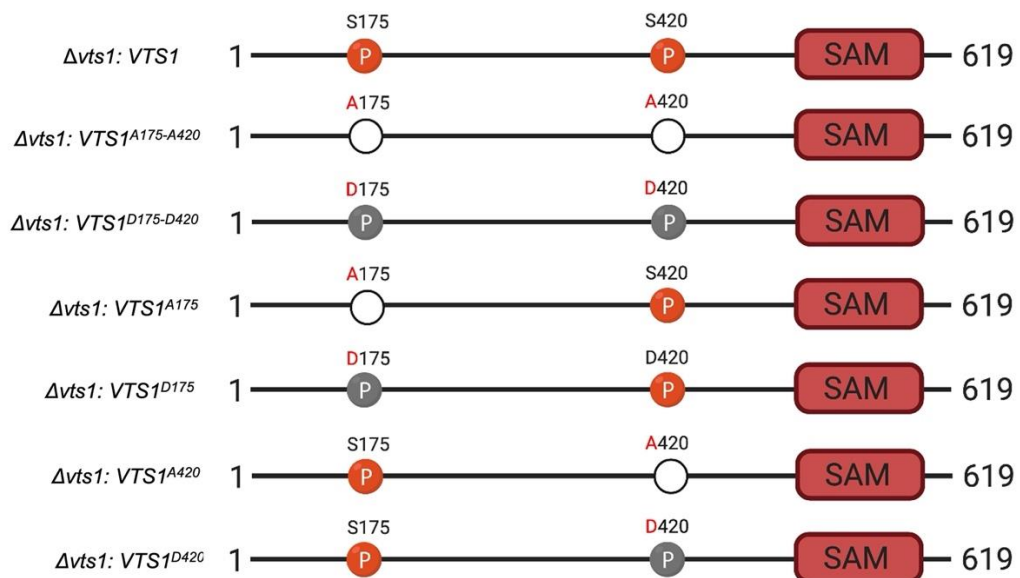
Figure 4.27. Design of Vts1 phosphorylation-directed mutants. Schematic representation to show Vts1 phosphorylation alleles created in this study. Amino acid substitutions are shown as a single letter code.

Based on our quantitative phosphoproteomic approach and *in vitro* phosphorylation assay, we have generated evidence that phosphorylation on serine 175 and serine 420 is dependent on Pmk1 MAPK activity. To understand the function of these Vts1 phosphorylation sites in *M. oryzae*, I decided to generate phosphorylation-directed mutants at these sites. For this purpose, I designed double and single Vts1 mutant alleles substituting the serine residues for alanine and aspartic acid to make phosphodead and phosphomimetic variants, respectively (Figure 4.27). For the design of these mutant variants, I also considered the *M. oryzae* optimal codon usage for alanine and aspartate. Using the RefSeq database (http://www.ncbi.nlm.nih.gov/refseq) (O'Leary et al., 2016), I found that the blast fungus uses the codon GCC for alanine and GAC for aspartate predominantly. To generate *VTS1* phosphoallele single mutants, I introduced point mutations using primers that amplified the *VTS1* promoter and coding sequence from pScBar-Vts1-GFP. To produce *VTS1* double mutants, I synthesised a DNA fragment using gBlocks™ by IDT technologies. I then cloned the amplicons and synthesised fragments containing point mutations by In-Fusion® cloning technology into pScBar. Positive plasmids containing the different Vts1 phosphoalleles were then confirmed by PCR and DNA sanger sequencing. I transformed the phosphodead pScBar-VTS1$^{A175-A420}$, pScBar-VTS1^{A175}, pScBar-VTS1^{A420} and phosphomimetic pScBar-VTS1$^{D175-D420}$, pScBar-VTS1^{D175}, pScBar-VTS1^{D420} variants into the *M. oryzae △vts1* strain with 8μg of plasmid DNA using the protoplast method of transformation.

Selection of Vts1 phosphorylation variants included additional steps. I screened putative positive transformants that were able to grow on selection media with 200 μg/mL of BASTA by PCR and GFP expression under the epifluorescence microscope. Then, I purified the PCR product and sequenced it to confirm the presence of the predicted point mutations. Additionally, I sent DNA from my positive transformants to Anglia iDNA for qPCR analysis to quantify plasmid copy number insertion. Finally, I verified Vts1 variant expression by western bot analysis to evaluate mutants with a similar level and pattern of expression. I selected two positive transformants for phenotyping experiments. In this way a series of Vts1 phosphorylation-modulated mutants were created in the blast fungus.

4.2.13 Phosphorylation of serine 175 of Vts1 is required for efficient mycelial growth, appressorium development and rice blast disease

In order to understand the relevance of Pmk1-dependent Vts1 phosphorylation, I decided to evaluate the phenotype of the Vts1 phosphorylation variants. Phenotypic analysis of

Δvts1 null mutant had shown that an effect on mycelial growth and pigmentation, conidiation, appressorium formation and plant infection. Interestingly, I observed that when *Δvts1* is transformed with Vts1-GFP then all these phenotypes were complemented (Figure 4.21). Therefore, I reasoned that complementation of *Δvts1* with each of the Vts1 phosphorylation mutants would provide a reliable system to study the role of phosphorylation in the biological function of Vts1.
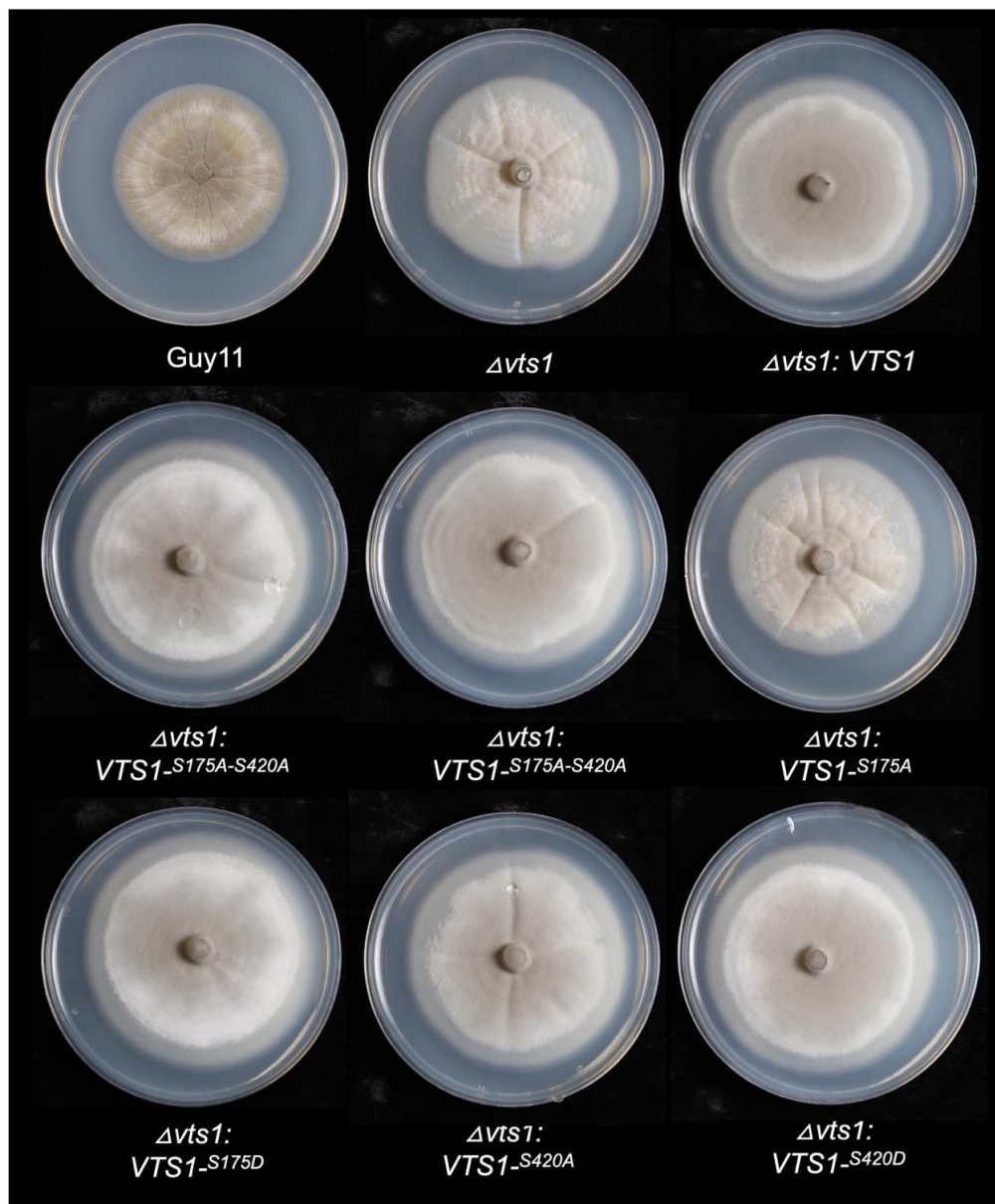
Figure 4.28. Phenotype of Vts1 phosphorylation variants in mycelium. Photographs to show the mycelial phenotype of colonies of the wild-type strain Guy11, *Δvts1* mutant and Vts1 phosphorylation alleles. Photographs were taken after incubating *M. oryzae* strains on CM at 26 °C for 10 days.

Table 4.3. Phenotypes of the Vts1 phosphorylation mutants in *M. oryzae*.

Strain	Growth rate (mm/d)	Conidiation (spores/cm^2)	Appressorium	
			1 cell	2 cells
Guy11	2.98 $\pm$ 0.08	34.69 $\pm$ 5.18	95.52 $\pm$ 3.05	3.77 $\pm$ 3.35
Δvts1	2.24 $\pm$ 0.06	2.34 $\pm$ 0.21	41.50 $\pm$ 19.27	58.11 $\pm$ 19.86
Δvts1: VTS1^{WT}	3.02 $\pm$ 0.18	30.37 $\pm$ 2.98	93.58 $\pm$ 4.38	5.54 $\pm$ 5.09
Δvts1: VTS1$^{A175-A420}$	3.10 $\pm$ 0.11	0.83 $\pm$ 0.41	60.12 $\pm$ 7.28	38.18 $\pm$ 8.12
Δvts1: VTS1$^{D175-D420}$	3.12 $\pm$ 0.06	0.94 $\pm$ 0.34	60.52 $\pm$ 2.25	38.24 $\pm$ 2.73
Δvts1: VTS1^{A175}	2.48 $\pm$ 0.05	3.38 $\pm$ 1.07	49.93 $\pm$ 2.70	47.41 $\pm$ 1.73
Δvts1: VTS1^{D175}	3.06 $\pm$ 0.06	0.40 $\pm$ 0.13	85.65 $\pm$ 6.99	12.41 $\pm$ 8.29
Δvts1: VTS1^{A420}	3.09 $\pm$ 0.04	1.01 $\pm$ 0.45	82.27 $\pm$ 0.82	16.07 $\pm$ 1.28
Δvts1: VTS1^{D420}	3.01 $\pm$ 0.03	0.47 $\pm$ 0.08	87.45 $\pm$ 3.39	10.77 $\pm$ 1.86

To study the impact of Vts1 phosphorylation in mycelium, I grew mutant strains containing *VTS1^{WT}*, *VTS1$^{A175-A420}$*, *VTS1$^{D175-D420}$*, *VTS1^{A175}*, *VTS1^{A420}*, *VTS1^{D175}* and *VTS1^{D420}* on CM agar plates for 10 dpi. As controls, I used Guy11 and the Δvts1 mutant. Apart from *VTS1^{A175}*, all mutant colonies had a similar morphology than wild-type and the complemented strain (Figure 4.28). However, *VTS1^{A175}*, was more similar to the Δvts1 mutant showing a smaller whitish colony (Figure 4.28). When I measured growth rate, I found that *VTS1^{A175}* and Δvts1 had the slowest rates of 2.24 mm/d and 2.48 mm/d, respectively, compared to the rest of the strains that all grew at more than 3 mm/d (Table 4.3) (Figure 4.28). The findings suggest that mutation of Ser-175 to Ala-175 of Vts1 influences vegetative growth.
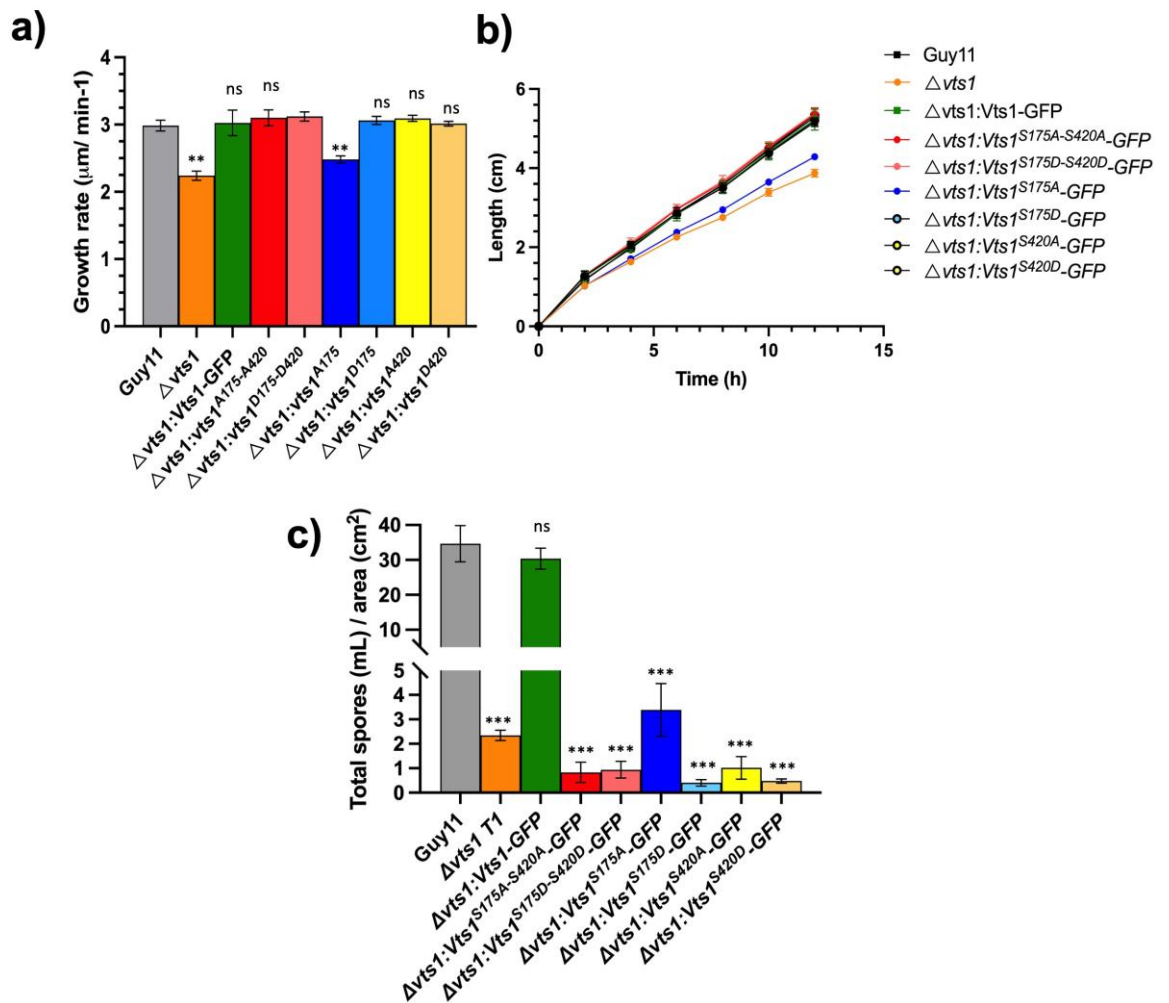
Figure 4.29. Phenotype of Vts1 phosphorylation variants during vegetative growth and conidiogenesis. a) Bar chart to show growth rate and **b)** Line graph of growth of colonies measured at 2, 4, 6, 8, 10 and 12 dpi on CM plates. **c)** Bar chart to show conidiogenesis. For sporulation assays CM plates were flooded with 5 mL dH_2O to harvest conidia. Spores were harvested, pelleted by centrifugation, resuspended in 1 mL, and counted. Calculations were then carried out to determine the number of conidia generated per cm^2 of mycelium. CM plates were inoculated with 8mm plugs of mycelium from Guy11, *Δvts1* and Vts1 phosphorylation mutants. Plates were incubated at 26 °C for a period of 12 days (growth rate experiments) and 10 days (sporulation assay experiment). Three biological replicates were carried out with 50 appressoria recorded for replicate. *$P < 0.05$: **$P < 0.01$; ***$P < 0.001$ represent significant differences using the ANOVA test. Error bars represent the standard deviation of three independent biological replicates of the experiment.

Because conidiogenesis is severely impaired in the mutant, I decided to investigate whether it was related to phosphorylation of S175 and S420. To this end, I tested conidia production in all different Vts1 alleles from mycelium grown in CM after 10 dpi. In all strains, conidium morphology was normal. As shown previously, $\Delta vts1$ has a 93.5% reduced conidiation compared to wild type (Figure 4.15). A similar effect is shown $VTS1^{A175}$, where I observed a 90.26% of reduction in spores. Interestingly, this phenotype was more pronounced for $VTS1^{A175-A420}$, $VTS1^{D175-D420}$, $VTS1^{D175}$, $VTS1^{A420}$ and $VTS1^{D420}$ where spore production was equally diminished, between 97-98.85% (Table 4.3) (Figure 4.29). These results demonstrate that none of the phosphorylation variants was able to complement the $\Delta vts1$ conidiation phenotype. Taken together, this provides evidence that phosphorylation of Vts1 residues S175 and S420 is not responsible for the conidiogenesis phenotype by absence of Vts1.

Because appressorium morphogenesis is impaired in $\Delta vts1,$ I investigated whether Vts1 phosphorylation variants were of physiological relevance in appressorium morphogenesis. For this purpose, I studied *in vitro* appressorium formation in each of the different phosphorylation mutants using Guy11, $VTS1^{WT}$ and $\Delta vts1$ as control strains. As shown in Figure 4.30, most of the three-celled conidia germinated in the different strains. As observed previously for $\Delta vts1$, all Vts1 variants presented a high number of germinated conidia forming two germ tubes: one differentiated into an appressorium and other that did not complete appressorium differentiation after 24h (Table 4.3) (Figure 4.30). We also observed conidia with two germ tubes emerging from either basal or apical cells as for the $\Delta vts1$ null mutant (Figure 4.30). These results, which are summarised in Table 4.3, show that there is no difference between double phosphodead ($VTS1^{A175-A420}$) or double phosphomimetic ($VTS1^{D175-D420}$) alleles, both of which exhibited phenotypes that were closer to those of the $\Delta vts1$ mutant. Strikingly, the mutation of serine 175 to aspartate (Vts1^{D175}), but not alanine (Vts1^{D175}) partially restores the wild-type phenotype. However, $VTS1^{A420}$ and $VTS1^{D420}$ displayed a similar phenotype to Guy11 and $VTS1^{WT}$. When considered together these data suggest that phosphorylation of residue S175 of Vts1, but not S420 is necessary for its role in appressorium morphogenesis.
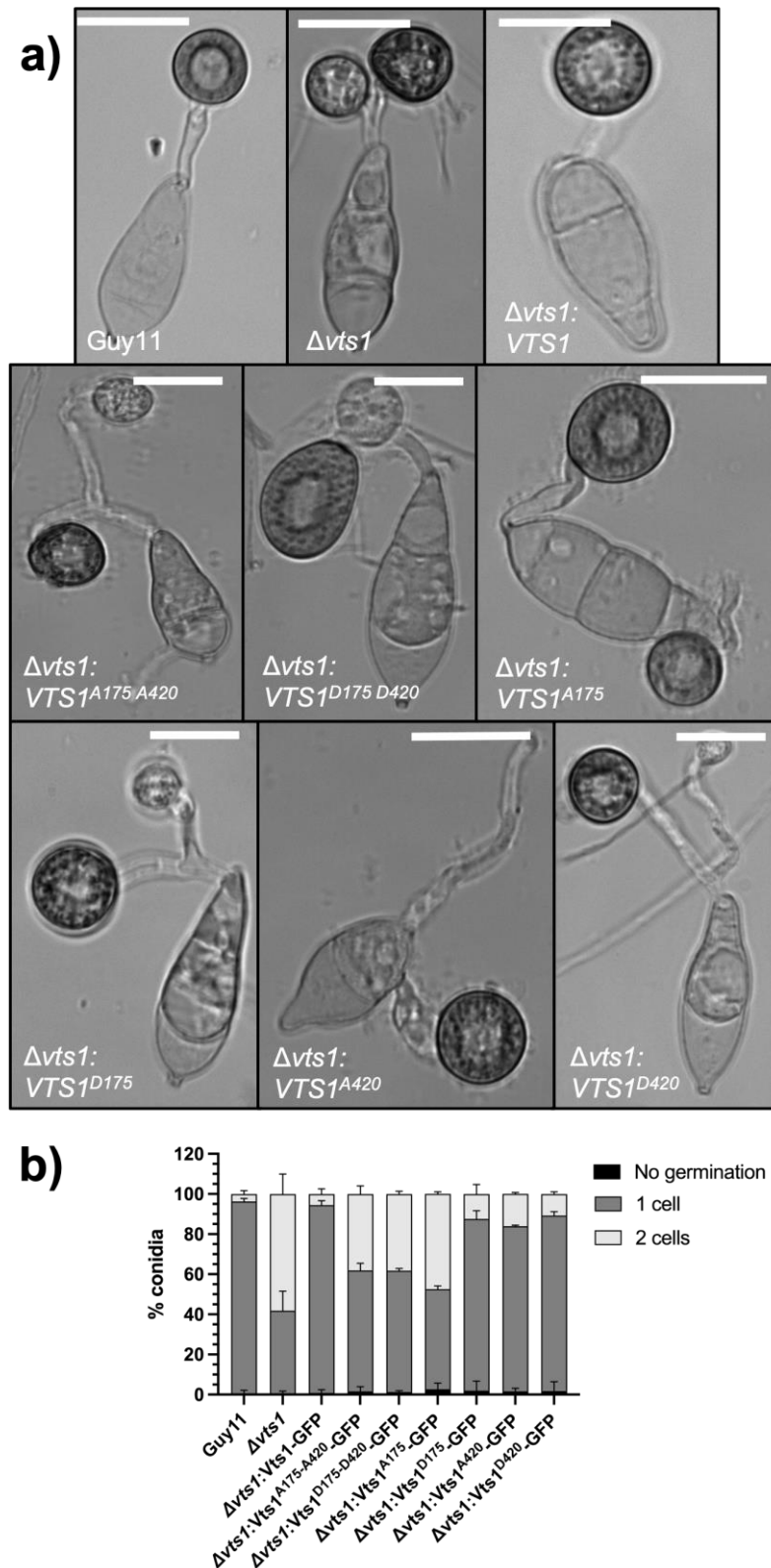
Figure 4.30. Phenotype of Vts1 phosphorylation variants in appressorium formation.
a) Micrographs to show appressorium development of Guy11, *Δvts1* and Vts1 phosphorylation mutant strains. Conidia were harvested from Guy11 and *Δvts1*, inoculated onto glass coverslips, and observed at 24h. Scale bar= 10μm. **b)** Bar chart showing

frequency of conidia germination from one and two cells. Three biological replicates were carried out with 50 appressoria recorded for replicate. *$P < 0.05$: **$P < 0.01$; ***$P < 0.001$ represent significance using unpaired two-tailed Student's *t*-test.

Figure 4.31. Phenotype of Vts1 phosphorylation variants during plant infection. Leaf drop assay using 3-week-old seedlings of rice cultivar C0-39 that were inoculated with equal amounts of conidial suspensions of Guy11, *Δvts1* and Vts1 phosphorylation mutant strains (10^5 conidia mL^{-1}) in 0.2% gelatine. Seedlings were incubated for 5 days to develop blast disease at 26 °C. Fully susceptible, sporulating disease lesions can be distinguished by their white centres.

To test weather Vts1 phosphorylation variants affect pathogenicity, I decided to infect rice leaves of 21-day-old seedlings cultivar CO-39. I carried out a leaf drop infection assay using 10^5 spores mL^{-1} from Vts1 phosphorylation variants and Guy11, *VTS1^{WT}* and *Δvts1* as control strains. After 5 dpi, Guy11, *VTS1^{WT}, VTS1$^{A175-A420}$, VTS1$^{D175-D420}$, VTS1^{D175}, VTS1^{A420}* and *VTS1^{D420}* produced lesions on the rice leaves where spores were inoculated (Figure 4.31). Lesions presented a normal phenotype with a greyish colour in the middle due to mycelial growth (Figure 4.31). By contrast, Vts1 null mutant and *VTS1^{A175}* showed significantly reduced or no lesions around the inoculation area (Figure 4.31). This result suggests that the phosphodead mutant *VTS1^{A175}* is as severely affected in plant infection as *Δvts1*. Taken together, we conclude that mutation of serine 175 to alanine (Vts1^{S175A}), but not aspartic acid (Vts1^{S175D}) is sufficient to significantly reduce plant infection by *M. oryzae*.

Phosphorylation of Vts1 in S175 and S420 occurs within different MAPK phosphorylation motifs, SP and PxSP respectively. Both phosphosites contain the presence of a proline at position +1 which is the minimal requirement for a MAPK phosphorylation site (Bigeard et

al., 2018). However, Vts1 S420 presents a proline at position -2 that has been suggested to indicate different target selectivity and, therefore, to function by another mechanism (Berriri et al., 2012; Sörensson et al., 2012). To gain further information regarding Vts1 S175 and S420 phosphosites, I looked at the conservation of these Vts1 sites in other filamentous fungi. For this analysis, I aligned Vts1 sequences from different fungi including *S. cerevisiae*. Interestingly, I found that Vts1 S175 and neighbouring amino acids are conserved among filamentous fungi (Figure 4.32). Conversely, the Vts1 S420 phosphosite is present in a non-conserved area (Figure 4.32). Vts1 phosphorylation at serine position 175 and serine position 420 therefore have different motif properties that is consistent with them serving a distinct function.
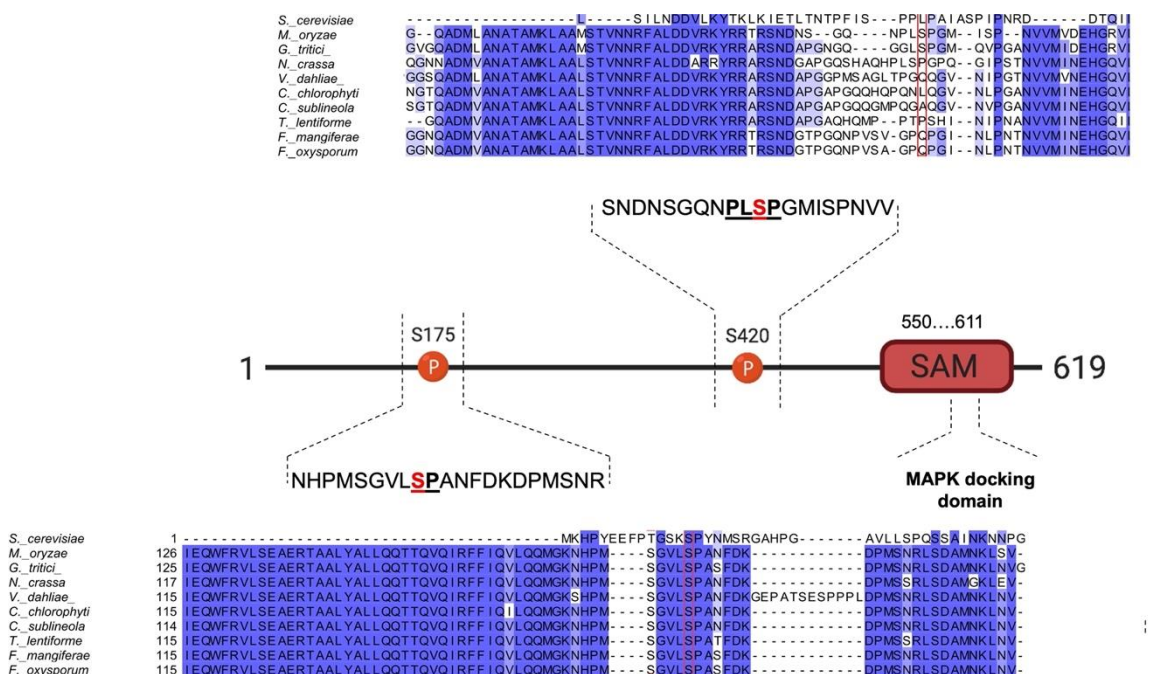
Figure 4.32. The Vts1 S175 residue is present in a conserved region among filamentous fungi. Schematic representation to show arrangement of each phosphorylation site identified for Vts1 and its conservation. Alignments of neighbouring regions surrounding Vts1 S175 and S420 from different filamentous fungi were carried out using ClustalX.

4.3 Discussion

Mitogen-activated protein kinases (MAPKs) translate extracellular signals to intracellular responses to regulate a wide variety of cellular programmes (Cargnello & Roux, 2011). For

this reason, they are important regulators of the response of cells to external changes in environment, such as osmotic or oxidative stress for example. MAPK signalling pathways are also important in development of multicellular organisms, including mammalian species and plants, where they also play role in plant immunity. In fungi where MAPK pathways have been extensively studied, they are key regulators of the response to external signals such as pheromones involved in mating, osmotic and cell wall stress. However, many of the functions of MAPKs, especially in filamentous fungi, are not yet clear. These include the identification of the signals that induce their activity, the means by which they are activated and, in particular, the mechanisms by which MAPK signal transduction pathways operate. In *M. oryzae,* the pathogenicity MAPK Pmk1 is a master regulator of appressorium morphogenesis and invasive growth (Xu & Hamer, 1996). Pmk1 influences the expression of more than 6000 genes during appressorium formation in the blast fungus (Osés-Ruiz et al., 2021) and is an absolute pre-requisite for formation of these cells. Furthermore, Pmk1 is required for transpressorium formation during cell-to-cell movement in rice tissue (Cruz-Mireles et al., 2021; Sakulkoo et al., 2018). The MAPK pathway is, therefore, pivotal to the ability of *M. oryzae* to cause blast disease. Despite its importance, very little is known about the range of proteins that are phosphorylated by Pmk1 or the biological functions of many of these target proteins. Understanding the function of the full repertoire of Pmk1 substrates is vital is the biology of appressorium formation is to be fully understood.

In this Chapter, I have presented results from an analysis of the SAM domain-containing protein Vts1, a putative Pmk1 target identified by quantitative phosphoproteomics. All previously described Pmk1 targets have been found using direct targeting methods such as co-immunoprecipitation (co-IP), yeast two hybrid (Y2H) experiments and/or using a candidate gene approach. Pmk1 interactors such as Pic1 and Pic5, for example, were discovered by Y2H analysis (Zhang et al., 2011) and the transcription factors Mst12 and Hox7 were defined as Pmk1 interactors based on a combination of transcriptional profile analysis and subsequent phosphoproteomic and *in vitro* MAPK assays (Osés-Ruiz et al., 2021). In this study I found that Vts1 interacts with, and is phosphorylated by, Pmk1, based on evidence from parallel reaction monitoring, co-IP and *in vitro* kinase assays. Given that MAPK substrate selectivity occurs via docking sites (Cargnello & Roux, 2011), it is possible that the Pmk1-Vts1 interaction is mediated by the predicted docking motif of Vts1 within its SAM domain.

Across the Eukaryotes, Vts1 appears to be a highly conserved protein (She et al., 2017). Its orthologues, for example, *VTS1* in *S. cerevisiae* or Smaug in metazoans, encode proteins known to bind RNA through the SAM domain (Lee et al., 2010; She et al., 2017). In yeast, *VTS1* was first discovered as a suppressor of vt1-2 mutant cells with growth and

vacuole transport defects (Dilcher et al., 2001). However, Vts1 has not yet been studied in filamentous fungi. It is also striking that *M. oryzae* Vts1 has only limited similarity to its orthologue in yeast that is restricted to the C-terminal part of the protein where the SAM domain is located. This restricted similarity might suggest that *M. oryzae* Vts1 (and orthologues predicted in other filamentous fungi), may play a different biological function. It is not clear, for example, if the SAM domain in *M. oryzae* Vts1 is required for protein-protein interactions or whether it also has an RNA-binding activity as in yeast.

I have also demonstrated that a *M. oryzae* Δ*vts1* mutant has severe phenotypes, affecting growth, conidiogenesis, appressorium development and virulence, all of which can be complemented by reintroduction of a wild-type *VTS1* allele into *M. oryzae.* Perhaps the most striking phenotype observed is that Δ*vts1* mutants often produce a second aberrant appressorium-like cell. This developmental phenotype suggests that without Vts1 appressorium maturation cannot be completed, consistent with the lack of septin ring formation at the appressorium pore. Instead, a second round of appressorium morphogenesis is initiated which then aborts before the cell can mature. Such a distinct developmental phenotype has not been previously observed in *M . oryzae.* However, it is somewhat reminiscent of the phenotype of Δ*hox7* mutants in which multiple swellings occur at the germ tube tip, but without appressorium formation. The difference is that appressorium formation is completed in Δ*vts1* mutants, but then appears to be re-initiated, compared to the arrest of Δ*hox7* mutants earlier in the process. Comparing these two mutants and the range of downstream genes that they potentially regulate will be critical in defining how the mutant phenotypes observed are associated with the precise timing of their action during appressorium morphogenesis. Interestingly, in yeast, Vts1 is a non-essential gene whose null mutant has normal growth but very poor ascospore generation (Deutschbauer et al., 2002; Itakura et al., 2020). Inter-species complementation analysis will be necessary to determine whether *M. oryzae* Vts1 is a functional homologue of the RNA-binding protein in yeast.

Localisation of Vts1 also revealed potential aspects of its biological function. Vts1 localises, for instance, at the conidium septal pore, apical cell, and in the growing germ tube and appressorium, suggesting that it serves a role throughout the early stages of appressorium development, as early as during spore germination and extension. The Pmk1-Vts1 interaction appears to occur in the appressorium and its localisation to this compartment is clearly Pmk1-dependant. Co-localisation studies with septin and gelsolin also demonstrated that Vts1 shares spatial localisation with the septin ring at the base of the appressorium, suggesting it may form part of a specific protein signalling complex during appressorium

maturation. In *Neurospora crassa*, the scaffold protein HAM-5 was identified as a component of the MAK-2 MAPK pathway using a phosphoproteomic approach (Jonkers et al., 2014). Similar to *M. oryzae* Vts1, HAM-5 localisation was observed in conidia, germlings, hyphae and septa. Based on the evidence that SAM-domain containing proteins are important scaffolds in diverse cascades, Vts1 might be playing such a role during appressorium morphogenesis in a Pmk1-dependent manner. In this context, it would be interesting to explore the interaction of Vts1 with other components of the Pmk1 signalling pathway that have also been shown to contain a SAM domain, such as Mst50 and Mst11. It is possible, for example, that Vts1 forms different complexes to regulate appressorium morphogenesis and may have multiple interactions within the signalling pathway.

Phosphorylation in a proline-directed site is a fundamental hallmark of MAPK targets during signal transduction (Cargnello & Roux, 2011). Our results provide both *in vivo* and *in vitro* evidence that Vts1 is phosphorylated at two proline-directed residues, S175 and S420, within a MAPK motif. There is little information regarding how Pmk1 regulates its previously described targets by phosphorylation. Recently, it has been reported that Mst12 and Hox7 have Pmk1-dependent phosphorylation at S133 and S158, respectively (Osés-Ruiz et al., 2021). In the case of Hox7, its phosphorylation is required for its biological function during appressorium morphogenesis (Osés-Ruiz et al., 2021). In the case of Pic1, Pic5 and Sfl1, however, there is no information about the mechanism by which they are phosphorylated by Pmk1 and, indeed, direct evidence that they are phosphorylated in this way is currently lacking. In this study, we discovered using phosphorylation-directed mutants that Vts1 phosphorylation at position S175, but not S420, is necessary for the role of Vts1 in vegetative growth, appressorium formation and plant infection. Interestingly, S175 phosphorylation of Vts1 was only detected upon contact with a hydrophobic surface whereas Vts1 S420 was already present from 0-6h during appressorium formation (Table 4.1). The different temporal phosphorylation patterns for Vts1 Ser-175 and Ser-420 might point to distinct functions for these two phosphosites in Vts1 activity. Potentially, Pmk1 may regulate this dual phosphorylation in response to different signals or to control different physiological processes in the blast fungus. Our data provide evidence of a complex regulatory network exerted on Vts1. This property raises the possibility that Vts1 might be necessary to integrate multiple signals in the Pmk1 signalling cascade.

Taken together, the set of *in vivo* and *in vitro* experiments described in this Chapter provides a new understanding of a novel Pmk1 target, Vts1, and shows that it is a critical regulator of appressorium morphogenesis and, therefore, rice blast disease.

Chapter 5:

5 Determining the role of Pmk1 in transpressorium-dependent invasive growth by *M. oryzae*

5.1 Introduction

After *M. oryzae* has established a functional appressorium, the fungus changes its growth direction to rupture the host cuticle. A rigid penetration peg ruptures the cuticle and then differentiates into bulbous hyphae to initiate invasive growth (Eseola et al., 2021). During primary cell colonisation, invasive hyphae develop by budding and undergo major modifications in primary metabolism (Fernandez & Wilson, 2014). At this stage, the pathogen differentiates a plant-derived membrane-rich structure called the Biotrophic Interfacial Complex (BIC) (Giraldo et al., 2013; Kankanala et al., 2007; Khang et al., 2010). Although the BIC is thought to be a focal plant defence reaction, there is a growing evidence that the blast fungus uses the BIC to transfer effector proteins into plant cells (Cruz-Mireles et al., 2021).

Effector proteins are critical for a successful plant colonisation. Pathogens secrete them into host cells to supress immune responses and control plant processes needed for infection (Kobayashi et al., 2022). In *M. oryzae*, evidence has been reported for two different secretion mechanisms. Effectors secreted into the cytoplasm appear to follow a different system than effectors secreted to the apoplast (Giraldo et al., 2013). Cytoplasmic effectors preferentially accumulate in the BIC, whereas apoplastic effectors are secreted from the invasive hyphae (Giraldo et al., 2013). After secretion, cytoplasmic effectors can be detected in the cytoplasm of both invaded and adjacent rice cells (Khang et al., 2010). It is believed that effectors can therefore move through plasmodesmata to prepare neighbouring cells for invasion (Khang et al., 2010; Oliveira-Garcia et al., 2021). In the case of apoplastic effectors, they do not enter host cells and accumulate instead in the apoplastic space enclosed within the extra-invasive hyphal membrane (EIHM) where they outline invasive hyphae (Giraldo et al., 2013). Although it is widely known that *M. oryzae* effectors are essential for tissue invasion, their delivery mechanisms into the living host cells remains unclear.

After the fungus has completely invaded the first epidermal cell, it subsequently spreads to neighbouring cells to colonise host tissue. In *M. oryzae*, as in many other plant and animal pathogens, the cellular mechanisms involved in the movement of the fungus from one cell

to the other are largely unknown (Cruz-Mireles et al., 2021). Using live cell imaging experiments, it has been reported that the blast fungus forms a swollen structure at rice cell junctions and then undergoes significant hyphal constriction from 5 µm to 0.6-1 µm diameter at pit field sites where plasmodesmata are located (Kankanala et al., 2007; Sakulkoo et al., 2018). This process resembles what occurs during primary cell host penetration because the penetration peg structure has a very similar diameter when visualised by light microscopy (Cruz-Mireles et al., 2021), and a similar role in cell wall rupture.

The Pmk1 pathway has a central role in *M. oryzae* cell-to-cell movement. Using a chemical genetic approach, it has been shown that inhibition of the Pmk1 kinase with the ATP analogue 1NaPP1 prevents the blast fungus from moving between rice cells (Sakulkoo et al., 2018). Interestingly, it has been suggested that hyphal constriction and invasion of neighbouring cells is regulated by Pmk1 in a septin-dependent manner (Sakulkoo et al., 2018). In addition, it has been also demonstrated that Pmk1 regulates the expression of a group of effector-encoding genes that might suppress plant immunity at plasmodesmata (Sakulkoo et al., 2018). According to this report, Pmk1 is involved in the morphogenetic transition from bulbous hyphae into the narrow invasive hyphae to physically traverse cell-wall crossing points in rice cells (Cruz-Mireles et al., 2021). These findings draw parallels between the appressorium and the transpressorium, an infection structure formed by fungi to move between cells (Cruz-Mireles et al., 2021; Liese & Schmid, 1964). However, it is unclear how the Pmk1 cascade regulates both morphogenetic processes and how their developmental biology differs.

In this Chapter, I report the role of Pmk1 cascade during transpressorium-dependent cell-to-cell movement using a chemical genetic strategy coupled to a comparative phosphoproteomic approach. I report the identification of 39 potential downstream targets of the Pmk1 pathway. Among them, are a group of Pmk1 Regulated Effectors (PREs), proteins from the secretory pathway, such as Sec31, and the SAM domain containing protein, Vts1. When considered together, this evidence provides insight in Pmk1 control of transpressorium formation and invasive growth.

5.2   Results

5.2.1   Pmk1 is required for cell-to-cell movement

Previous work in our research group, reported that Pmk1 activity is required to move from the primary rice cell to neighbouring cells (Sakulkoo et al., 2018). As a starting point for the project, I investigated the phenotype of Pmk1 mutants during cell-to-cell movement in the

blast fungus. For this, I prepared a leaf sheath infection assay to replicate Sakulkoo et al 2018, cell-to-cell movement experiment, using the Pmk1 analogue sensitive mutant (*pmk1*[AS]) using the same conditions. Consistent with previous observations, addition of the inhibitor 1Na-PP1 after 26h of infection resulted in entrapment of invasive hyphae in the first invaded rice cell (Figure 5.1). By contrast, non-treated *pmk1*[AS] resulted in a wild-type phenotype in which the blast fungus was able to spread into proximal rice cells (Figure 5.1). This result confirms that Pmk1 is necessary for transpressorium-dependent cell-to-cell movement during host tissue invasion.
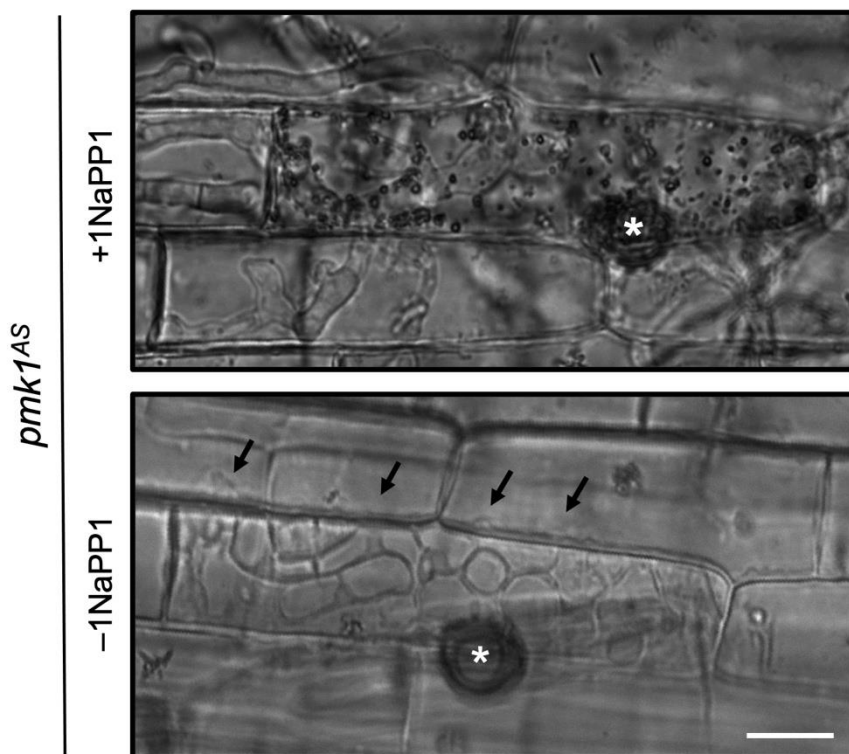
Figure 5.1. Pmk1 inhibition prevents *M. oryzae* transpressorium-dependent cell-to-cell movement. Micrographs to show the effect of *pmk1*[AS] growing in rice cells of susceptible cultivar CO-39 in the absence (on top) or presence (on the bottom) of 1Na-PP1. Asterisks indicate sites of appressorium-mediated penetration. Arrows indicate swollen invasive hyphal cells pressed against the cell wall. Scale bars are 20 µm.

5.2.2 Using discovery phosphoproteomics to investigate Pmk1 function during transpressorium-dependent cell-to-cell movement

As the role of Pmk1 during cell-to-cell movement has only been recently discovered, little is known regarding how this kinase controls the process. It has been demonstrated that Pmk1

is required for the differential expression of 1457 genes when the pathogen invades neighbouring cells (Sakulkoo et al., 2018). Interestingly, it was found that Pmk1 alters the expression of a subset of fungal effector genes involved in host immunity suppression and morphogenetic regulators at the crossing points (Sakulkoo et al., 2018). However, the precise mechanisms underlying invasive growth mediated by Pmk1 are largely unknown (Cruz-Mireles et al., 2021).

To gain insight into the phosphorylation cascade operating downstream of Pmk1, I decided to carry out a comparative phosphoproteomic approach during invasive growth to identify downstream components. To this end, I generated infected rice material using the *M. oryzae pmk1^{AS}* mutant in the same conditions reported previously (Figure 5.2). Because the amount of fungal biomass in infected tissue is minimal and phosphoproteomics does not include an amplification step in the same way as RNAseq analysis, I with Dr. Miriam Osés-Ruiz first produced a large amount of infected material using different methods to enrich fungal proteins prior to LC-MS analysis. I then processed all samples by mass-spectrophotometry with Dr. Frank Menke. For the first method, we infected 50 entire leaf sheaths per condition (+/- 1NaPP1) and processed the entire sample for protein extraction. I then separated the sample into soluble and microsomal fractions using ultracentrifugation, as specified in Chapter 2. For the second method, we infected 50 leaf sheaths per condition (+/- 1NaPP1) but separated the first epidermal layer of each leaf sheath for protein extraction. For the third method, we carried out a leaf drop assay and cut the infected area into disks. I then used 20 leaf disks per condition. As previously established, Pmk1 activity was inhibited with 1NaPP1 after 26 h and samples were harvested at 32h post infection (Figure 5.2). For each method, we used Guy11 +/- 1NaPP1 and non-infected leaf sheaths or leaf disk as controls. As shown in Table 5.1, the amount of fungal material in the three methods ranged between 5.68-10.1% of the total protein. While the overall fungal material detected by LC-MS was minimal compared to rice proteins, the most efficient method was sample fractionation. Even though the sample collection or processing was different among the methods employed to process infected samples, the conditions used to perform the experiment were the same. Additionally, most of the fungal proteins identified by LC-MS overlapped between the different methods. For those reasons, I merged the results obtained to facilitate downstream analysis.

Table 5.1. Experimental strategy to increase fungal biomass for Pmk1 comparative phosphoproteomic experiments of infected rice tissue.

Experiment		Percentage of fungal proteins in sample		Number of fungal proteins		Fungal proteins phosphorylated in a MAPK motif	
Leaf sheath	Soluble fraction	10.1 %	6.2 %	96	72	84	62
	Microsomal fraction		3.9 %		24		22
Leaf sheath (epidermis)		5.68 %		75		73	
Leaf drop		7.35 %		78		62	

To detect downstream targets of Pmk1 involved in tissue invasion, I analysed the phosphoproteomic profile of rice tissue containing *M. oryzae* colonising (- 1Na-PP1) and trapped (+ 1Na-PP1) rice cells. From all different LC-MS experiments, we detected a total of 2707 phosphorylated proteins. However, only 169 (6.7%) were fungal proteins and 142 of these were phosphorylated at a MAPK motif (Figure 5.3). To generate quantitative data, Dr. Paul Derbyshire applied Parallel Reaction Monitoring (PRM) to the phosphorylated fungal peptides in a MAPK motif, but this approach was not successful. Therefore, I used the semiquantitative discovery proteomics data to define the putative components of Pmk1 pathway during cell-to-cell movement. Using the proteomics software Scaffold, I found that 39 proteins contained differentially phosphorylated peptides when Pmk1 was inactivated (Figure 5.3). In total, using a comparative phosphoproteomic approach, we identified 39 putative components of Pmk1 cascade during invasive growth.
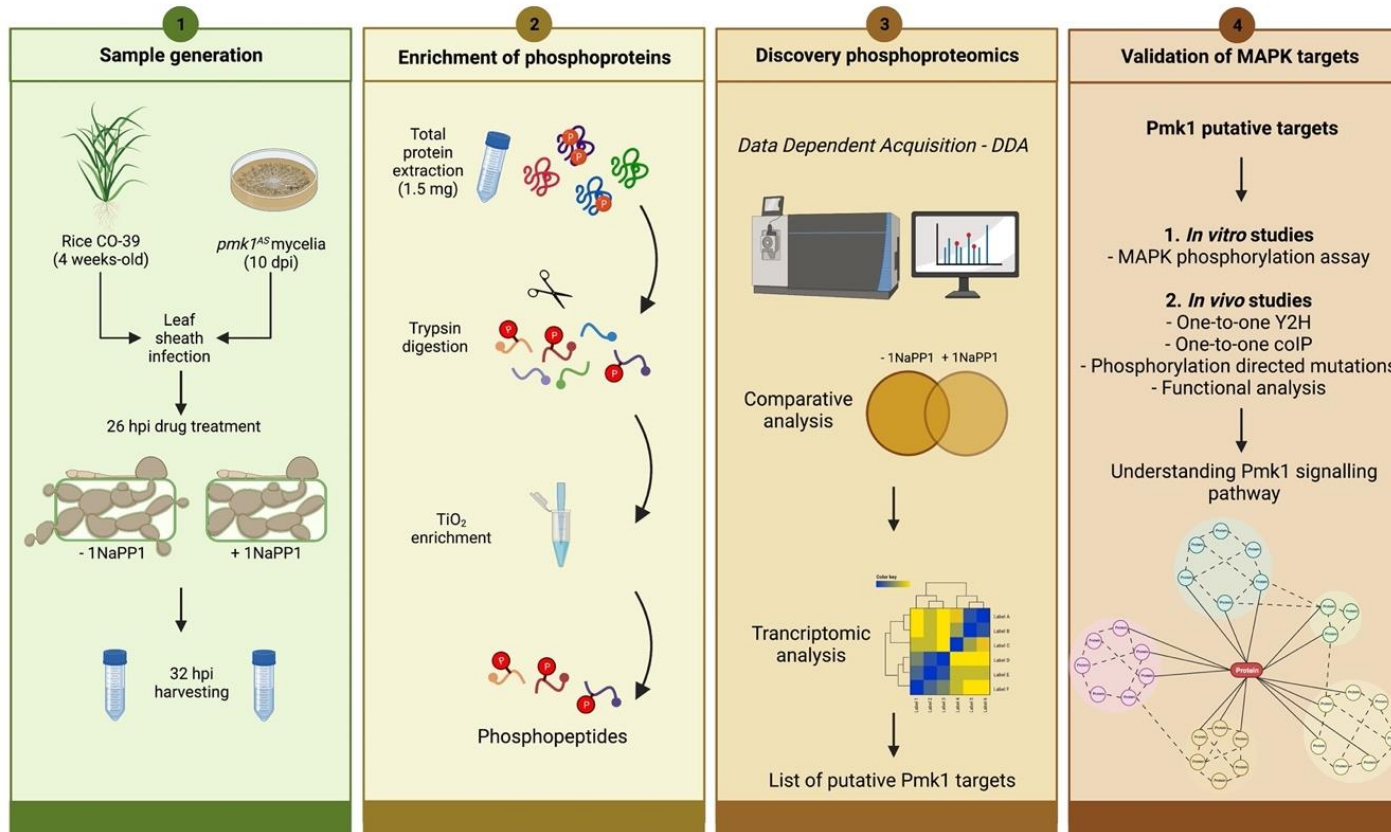
Figure 5.2. Phosphoproteomics experimental workflow and data analysis pipeline to identify Pmk1 targets during invasive growth of rice tissue by *M. oryzae*. Flowchart to show experimental strategy during 1) sample generation, 2) enrichment of phosphoproteins, 3) discovery phosphoproteomics and d) validation of targets to identify novel components of Pmk1 cascade during transpressorium-dependent cell-to-cell movement.

Determining the role of Pmk1 in transpressorium-dependent invasive growth by M. oryzae

Table 5.2. Pmk1 putative targets identified during invasive growth by discovery phosphoproteomics

Gene ID	Name	Description	Category
MGG_00124	Uncharacterised	Degradation factor Def1	Unknown function
MGG_00348	Uncharacterised	Splicing factor U2af large subunit	Protein synthesis
MGG_00432	Uncharacterised	Unknown	Unknown function
MGG_01108	Uncharacterised	Transport protein Sec31	Secretion
MGG_01378	Uncharacterised	Wd40 repeat-like-containing domain protein	Unknown function
MGG_01641	Uncharacterised	HMG box protein	DNA regulation
MGG_01656	Uncharacterised	Nucleotide excision repair protein Rad23	DNA regulation
MGG_01745	Uncharacterised	Zinc finger protein Gcs1	Cell division
MGG_02481	Uncharacterised	Unknown	Unknown function
MGG_02564	Uncharacterised	Unknown	Unknown function
MGG_04197	Uncharacterised	Cell lysis protein/Reticulon-like protein	Unknown function
MGG_04776	Uncharacterised	Unknown	Unknown function
MGG_04863	Uncharacterised	Cullin-associated Nedd8-dissociated protein 2	Ubiquitylation
MGG_04882	Uncharacterised	UBX domain-containing protein	Ubiquitylation
MGG_05264	Uncharacterised	Translation initiation factor 4b	Protein synthesis
MGG_05427	Uncharacterised	Microtubule-associated protein	Cytoskeleton-related
MGG_06318	Uncharacterised	Pumilio domain-containing protein	Protein synthesis
MGG_06396	Uncharacterised	Initiation factor 4f subunit	Protein synthesis
MGG_06419	Uncharacterised	Unknown	Unknown function
MGG_06719	Uncharacterised	ATP-citrate synthase subunit 1	Fatty acids synthesis
MGG_07008	Uncharacterised	Nucleolar protein nop-58	Nucleolar protein
MGG_07716	Uncharacterised	DnaJ domain-containing protein	Protein synthesis
MGG_09507	Uncharacterised	Universal stress protein	Unknown function
MGG_09629	Uncharacterised	Unknown	Unknown function
MGG_10538	Uncharacterised	Transcriptional activator Snf5	Protein synthesis
MGG_11061	Uncharacterised	Unknown	Unknown function
MGG_11737	Uncharacterised	Unknown	Unknown function
MGG_12141	Uncharacterised	Sec16/ Secretory pathway	Secretion
MGG_12370	Uncharacterised	FHA domain-interacting nucleolar phosphoprotein	Nucleolar protein
MGG_12671	Uncharacterised	Unknown	Unknown function
MGG_12809	Uncharacterised	KH domain-containing protein	Unknown function
MGG_13063	Uncharacterised	Unknown	Unknown function
MGG_18017	Uncharacterised	Carbonic anhydrase 2	Unknown function
MGG_03644	Sec61	Translocon protein/Secretory pathway	Secretion
MGG_04708	Som1	Transcription factor	Transcription factor
MGG_06334	Vts1	SAM-domain containing protein	Pmk1 pathway
MGG_09517	Vps1	Vacuolar sorting protein 1/Dynamin related protein	Vesicular trafficking
MGG_09560	Exp5	Nuclear import and export protein	Nuclear protein
MGG_13014	Chs5	Chitin synthase	Chitin synthesis

To understand the role of pmk1 during cell-to-cell movement, I carried out functional characterisation of potential targets. As described in Chapter 3 for the annotation of Pmk1 targets in the appressorium, I used GO database for *M. oryzae* (Osés-Ruiz et al., 2021;

Sakulkoo et al., 2018), and "MagnaGenes (v.1.0)" database in the current analysis (Foster et al., 2021). Thirty-three of the Pmk1 putative targets have not been studied previously in the blast fungus, so I annotated their function based on the Blast2GO predictions (Conesa & Götz, 2008) (Table 5.2). Among the uncharacterised proteins, there are 10 with no functional domain described in any organism. Interestingly, the most represented cellular processes were protein synthesis, secretion, DNA regulation, structural nuclear proteins and ubiquitylation (Table 5.2) (Figure 5.4).
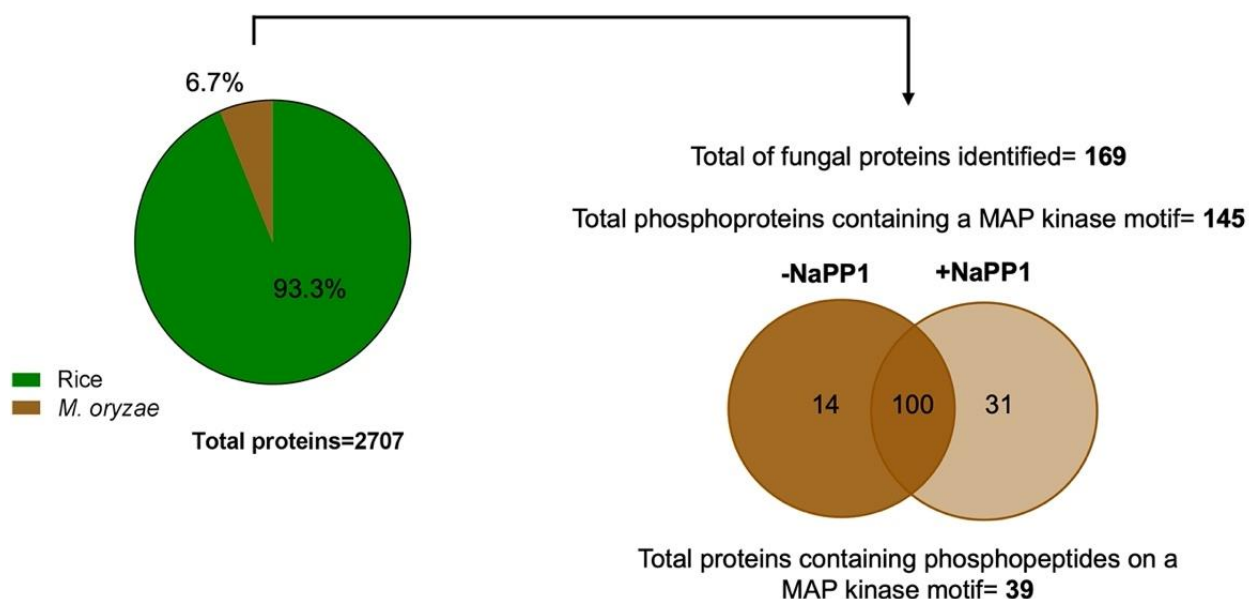
Figure 5.3. Identification of MAP kinase targets during *M. oryzae* transpressorium-dependent cell-to-cell movement by discovery phosphoproteomics. Flowchart to show *M. oryzae* genes enrichment and comparative analysis to identify Pmk1 targets during invasive growth using discovery phosphoproteomics.
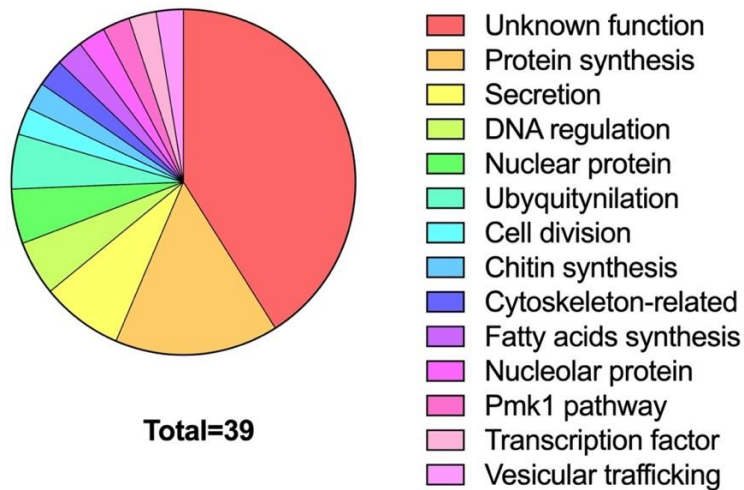
Figure 5.4. Functional analysis of putative Pmk1 targets identified by comparative discovery proteomics. Pie chart to show functional analysis using Blast2GO and MagnaGenes (v.1.0) of the 39 proteins identified by comparative discovery proteomics as putative interactors of Pmk1.
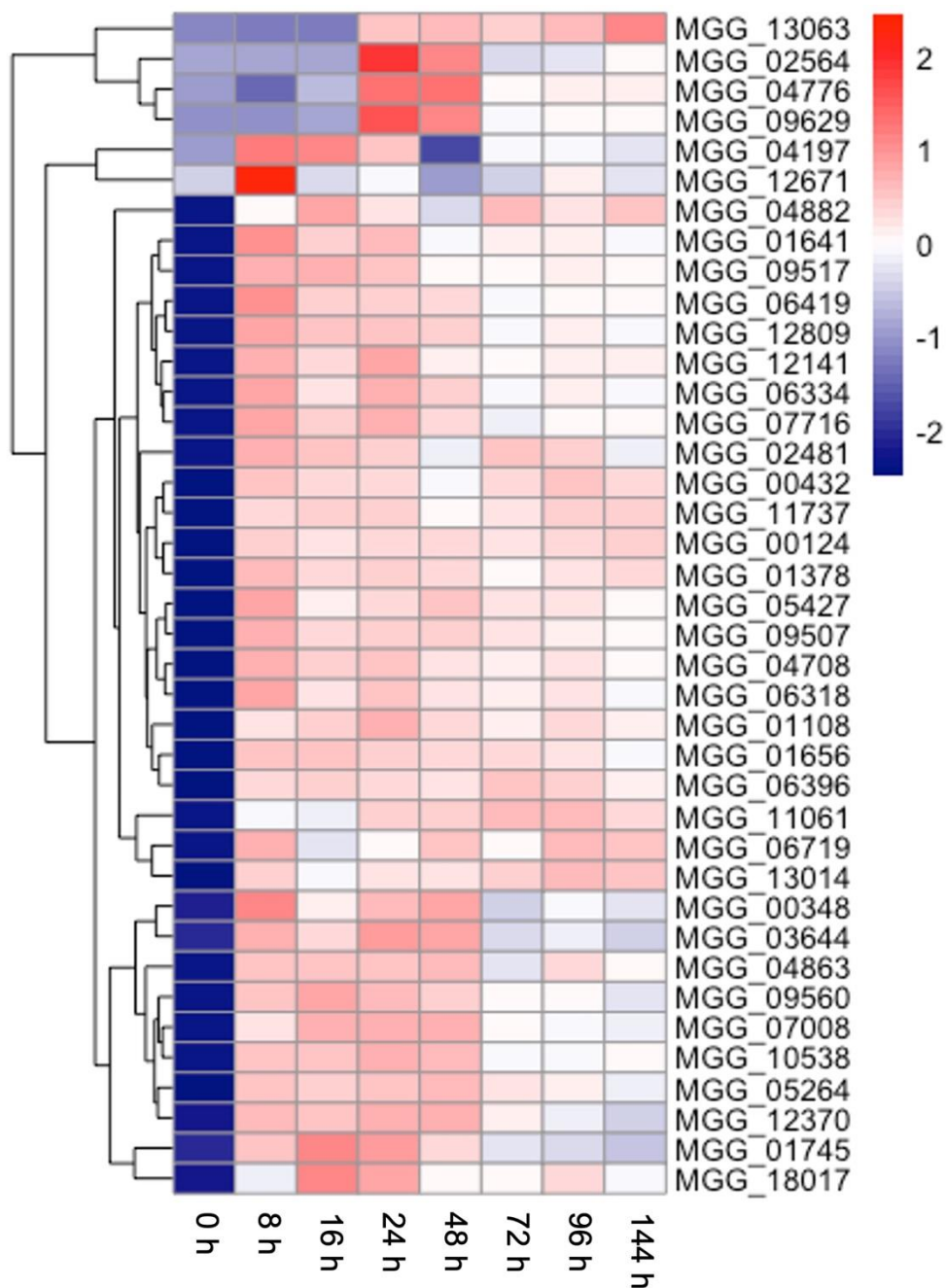
Figure 5.5. Relative transcript abundance of putative downstream targets of Pmk1 during a time course of rice infection by _M. oryzae_. Heatmap to show temporal pattern of relative transcript abundance of 39 proteins containing a MAPK motif during _M. oryzae_ cell-to-cell movement. These proteins were identified by discovery phosphoproteomics of _pmk1_[AS] in absence and presence of 1NaPP1.

5.2.3 Putative Pmk1 targets during cell-to-cell movement express during infection

To narrow down the list of possible targets of Pmk1 signalling involved in transpressorium function, I decided to use gene expression information. A time course transcriptomic data set of fungal genes during rice infection has been generated (Dr. Xia Yan, unpublished). Fungal genes expression profile has been studied in a time course dependent manner. I hypothesised that fungal genes that play a role during cell-to-cell movement would be expressed during infection. To test this idea, I generated a heat map with the expression profile of the 39 potential Pmk1 targets found by discovery proteomics with Dr. Bozeng Tang (Figure 5.5). This analysis confirmed that these proteins are expressed during plant infection and present different expression profiles.

5.2.4 Identification of a group of effector candidates preferentially regulated by Pmk1

From transcriptomic analysis, I identified a cluster of 3 non-characterised proteins that are exclusively expressing during transpressorium-mediated cell-to-cell movement. Invasive growth from the primary invaded cell to proximal rice cells occurs between 26-48 h of infection (Sakulkoo et al., 2018). During the infection time-course, we found that MGG_02564, MGG_04776 and MGG_09629 proteins are only expressed at 24 h and 48 h (Figure 5.6). Interestingly, in the RNAseq data previously reported (Sakulkoo et al., 2018), these proteins were expressed after 32h of infection but showed no expression when Pmk1 was inhibited from 26h to 32 h during invasive growth (Figure 5.7). Consistent with these observations, I found peptides of these proteins when Pmk1 was active (-1NaPP1) but no peptides when Pmk1 was inactive (+1NaPP1) in our comparative phosphoproteomic analysis (Figure 5.7). These data suggest that MGG_02564, MGG_04776 and MGG_09629 gene expression and their translation is dependent on Pmk1 function.

From the functional analysis I learned that MGG_02564, MGG_04776 and MGG_09629 have not been previously described in *M. oryzae*. Additionally, there is no orthologue studied for these proteins in any organism and they do not show similarity to any functionally characterised protein domain. Interestingly, using the software SignalP 6.0 and EffectorP (Teufel et al., 2022), I found that the three proteins have are putative effectors and contain predicted signal peptides in the N-terminal region suggesting that they can be secreted and translocated (Table 5.3). An independent transcriptomic analysis in our lab demonstrated that MGG_02564, MGG_04776 and MGG_09629 are candidate effector proteins with late expression in *M. oryzae* infection (Dr. Xia Yan, unpublished). For all the reasons above, I

decided to name these proteins *Pmk1 Regulated Effectors* (PREs). Taken together, I conclude that *PRE1* (MGG_02564), *PRE2* (MGG_04776) and *PRE3* (MGG_09629) are effector genes encoding proteins that are predicted to be secreted.
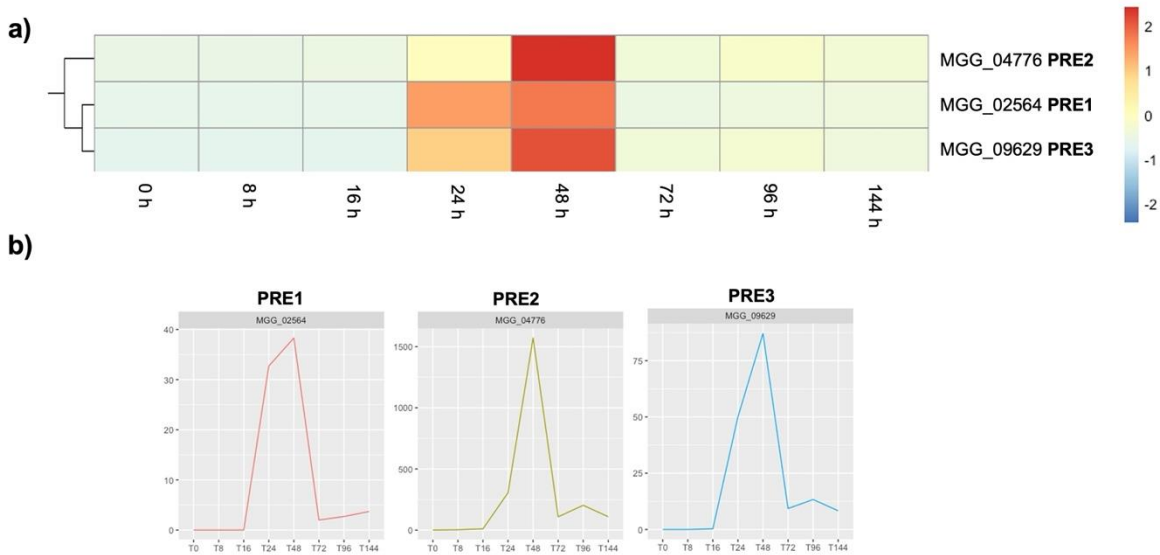
Figure 5.6. PREs are specifically expressed between 24-48 h during plant infection.
a) Heat map and b) plots to show transcript relative abundance of PREs during *M. oryzae* transpressorium-dependent cell-to-cell movement. Expression of *PREs* was specifically observed between 24 - 48 h of infection.
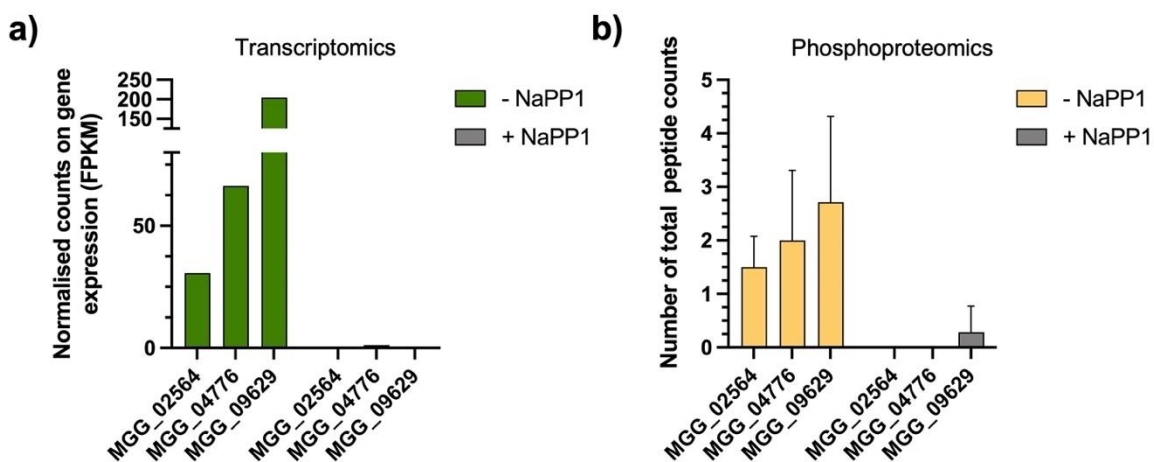
Figure 5.7. PRE expression is inhibited when Pmk1 is inactivated. Bar graphs to show a) transcriptomic and b) phosphoproteomic analysis of PRE accumulation upon Pmk1 inactivation after 26 h of infection. Transcriptomic analysis was previously reported by Sakulkoo et al., 2018 and phosphoproteomic analysis is from the current study.
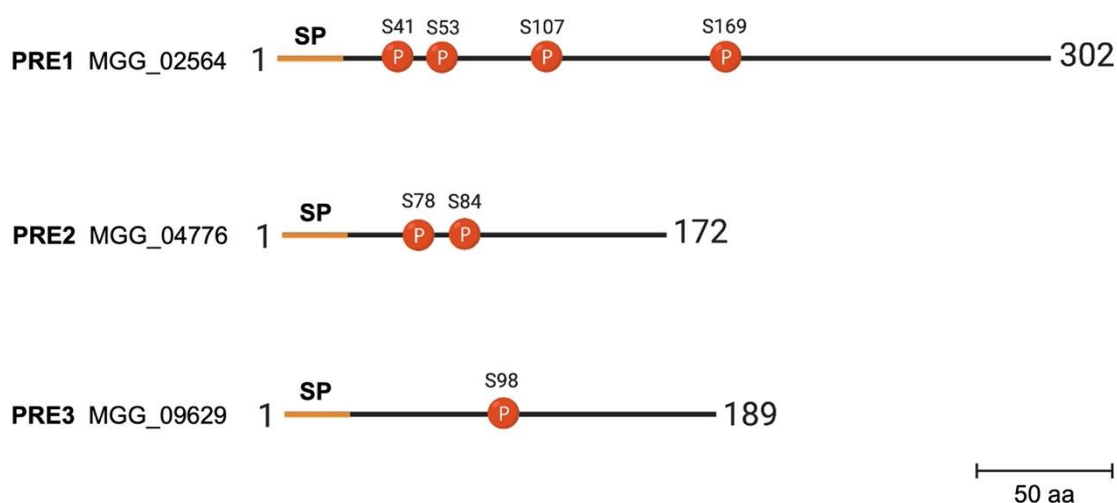
Figure 5.8. PREs are phosphorylated effector proteins. Diagram to show PRE phosphorylated sites during transpressorium-dependent cell-to-cell movement. Phosphorylation sites are represented in red; phosphoserine position is indicated using amino acid single letter code (S).

Table 5.3. Pmk1 Regulated Effectors analysed with SignalP 6.0

Gene ID	Name	Signal peptide?	SignalP score	EffectorP	Cleavage site
MGG_02564	PRE1	Yes	0.996	0.97/ Yes	Between aa position 22 and 23
MGG_04776	PRE2	Yes	0.998	0.78/Yes	Between aa position 21 and 22
MGG_09629	PRE3	Yes	0.966	0.87/Yes	Between aa position 17 and 18

Determining the role of Pmk1 in transpressorium-dependent invasive growth by M. oryzae
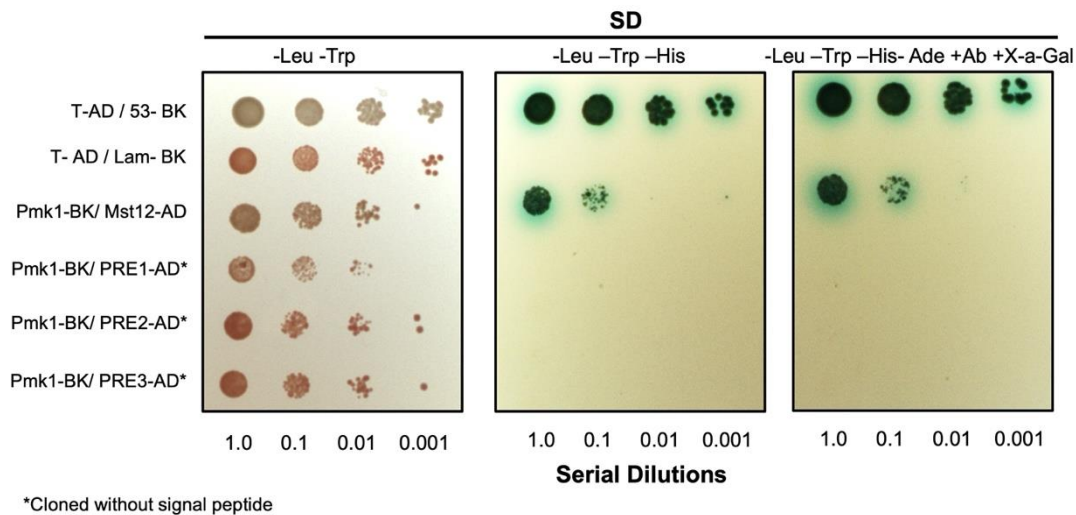
Figure 5.9. PREs do not interact with Pmk1. A Y2H assay was carried out and showed that Pmk1 and PREs effector proteins do not interact. Protein interactions were tested in yeast grown on SD medium -Trp -Leu -Ade -His +X gal +Au (right panels). Viability of all transformed yeast cells were demonstrated by growing them on SD medium -Trp -Leu (left panel). Yeast cells were spotted onto the media as tenfold dilution series. Mst12 was used as a positive control.

From our comparative phosphoproteomics analysis, I found that the PREs are phosphorylated proteins on at least one MAPK motif. We identified 4 phosphoserines linked to a proline in PRE1 (S41, S53, S107, S169), 2 in PRE2 (S78, S84) and 1 in PRE3 (S98) (Figure 5.8). As mentioned earlier, PRE expression, translation and, consequently, phosphorylation are dependent on Pmk1 activity. In order to investigate whether these effectors are directly regulated by Pmk1, I carried out a Y2H analysis to test for a direct interaction. For this experiment, I extracted DNA from Guy11 to clone each PRE coding sequence without the signal peptide to avoid secretion during analysis. It was possible to amplify by PCR the truncated version of each gene using genomic DNA as template because PREs do not have predicted introns. The PCR products were then cloned into the Y2H prey vector pGADT7. As previously reported, I used the known Pmk1 interactor Mst12 as a positive control (Osés-Ruiz et al., 2021). In both stringent media, yeast co-transformed with Pmk1 (prey) and Mst12 (bait) grew significantly. However, there was no yeast growth in selection media for co-transformants containing Pmk1 as prey and PREs as bait (Figure 5.9). This experiment suggests that Pmk1 do not interact directly with PREs. Therefore, PREs phosphorylation may not be directly regulated by Pmk1.

To elucidate PRE function during invasive growth, I decided to study their localisation. For this purpose, I fused PREs genes under their native promoters with GFP. Using a forward primer including *Eco*RI and a reverse primer having *Hind*III, I amplified PRE genes with its 1.5 Kb upstream promoter region from genomic Guy11 DNA. I cloned this amplicon into pScBar vector for GFP C-terminal fusion. This vector also contains the BAR gene for selection in *M. oryzae*. To investigate PREs regulation by Pmk1, I transformed 8 µg of each pScBar-PRE1-GFP, pScBar-PRE2-GFP and pScBar-PRE3-GFP into *M. oryzae pmk1^{AS}* strain. Positive transformants were selected based on PCR and GFP signal screening. To quantify the copy number of insertion, I used the qPCR analysis (Anglia iDNA). I selected two independent *pmk1^{AS}*:PRE1-GFP, *pmk1^{AS}*:PRE2-GFP and *pmk1^{AS}*:PRE3-GFP for downstream experiments.
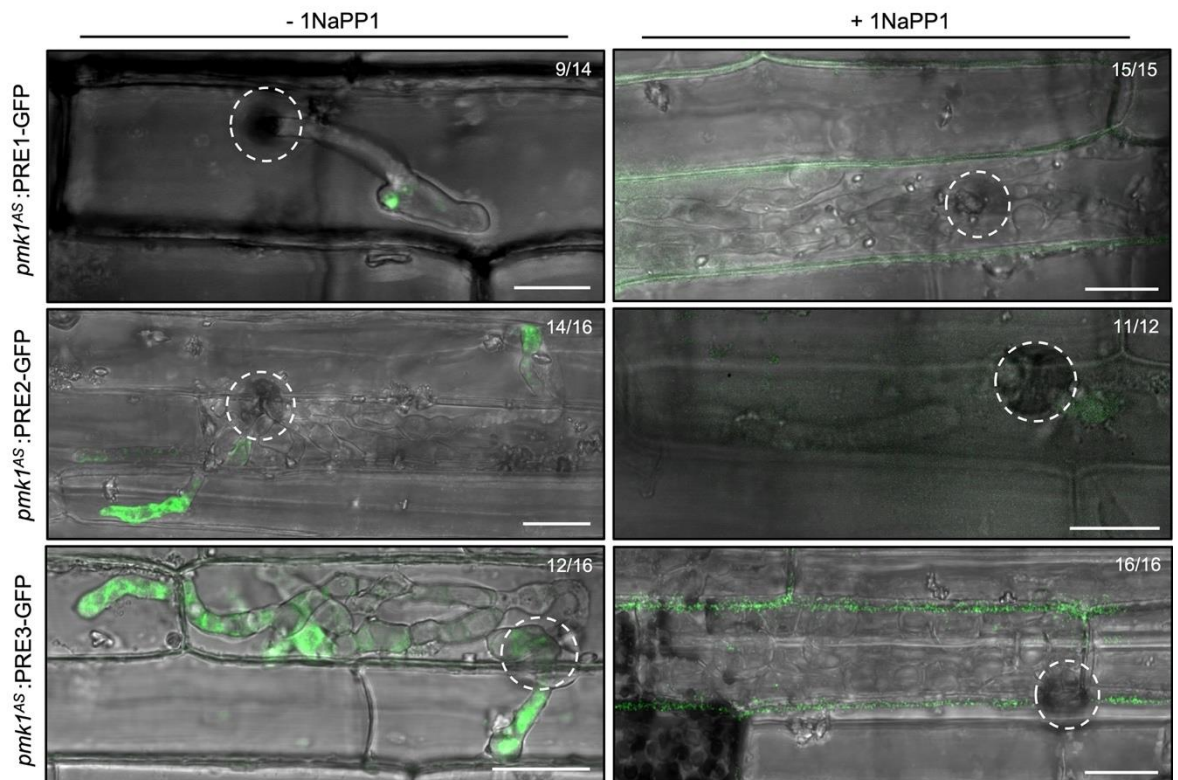
Figure 5.10. PRE localisation is affected when Pmk1 is inactivated. Micrographs to show representative localisation of PREs during cell-to-cell movement when *pmk1^{AS}*: *PRE1-GFP, pmk1^{AS}*: *PRE2-GFP and pmk1^{AS}*: *PRE3-GFP* were treated with +/- 5 µg of 1NaPP1. Conidia were harvested from *pmk1^{AS}*: *PRE(s)-GFP* strain 10 dpi, inoculated onto CO-39 leaf sheaths 4 weeks-old and observed by confocal microscopy at 48h. White dotted lines indicate position of appressorium. Scale bar = 10 µm.

Determining the role of Pmk1 in transpressorium-dependent invasive growth by M. oryzae

To evaluate PRE localisation, I performed the analysis under Pmk1 inactivation. For that I tracked the PREs GFP fluorescence signal during transpressorium-dependent cell-to-cell movement (with Alice Eseola). Similar to previous experiments, I inhibited Pmk1 at 26 h with 5 μM of 1NaPP1. The absence of 1NaPP1 was used as control. When Pmk1 was active, PRE2 and PRE3 GFP signal accumulated at the growing hyphal tip crossing the neighbouring cells (Figure 5.10). By contrast, PRE1 has a focal localisation at the _Biotrophic Interfacial Complex_ (BIC) (Figure 5.10). Interestingly, when I inhibited Pmk1 activity, we did not detect the GFP signal of the transformed fungus in the samples (Figure 5.10). Consistent with previous observations, these data indicates that Pmk1 inactivation affects PREs accumulation during invasive growth. Taken together, I conclude that PRE proteins localise to the growing hyphal tip or BIC in a Pmk1-dependent manner activity during transpressorium-dependent cell-to-cell movement.
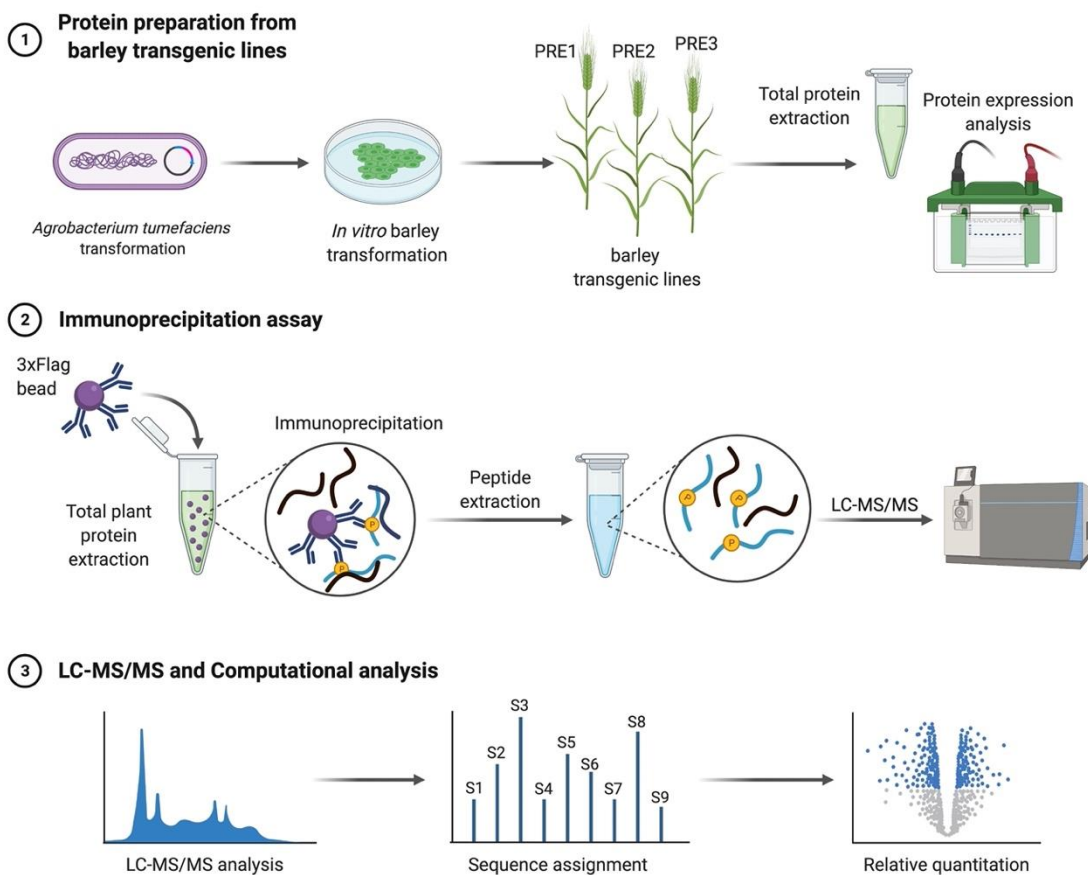
Figure 5.11. Experimental workflow and data analysis pipeline to PREs interactome _in planta_. Flowchart to show the 3 experimental stages for PREs interactome generation: a) Sample generation, b) immunoprecipitation assay and c) data analysis.

Pathogen effectors are excellent molecular probes to investigate cellular mechanisms with which they interfere. Several studies have, for example, used effectors as tools to reveal the processes they target within the host (Petre et al., 2021; Toruño et al., 2016; Win et al., 2012). From our transcriptomic and proteomic data, I learned that PREs are likely to be phosphorylated effectors indirectly controlled by the Pmk1 MAPK. To understand the mechanisms Pmk1 regulate PRE during invasive growth, I decided to study PRE protein-protein interactions. To this end, together with Dr. Juan Carlos De la Concepción, we designed a pipeline to identify PRE interactors using barley transgenic lines and immunoprecipitation coupled to mass-spectrometry (IP-MS) (Figure 5.11). We used barley to investigate PREs interactomes because its transformation is quicker than rice and we assumed the processes targeted by the effectors would likely be conserved. First, we cloned PREs into pICSL4723 as N-terminal 3xflag fusions. Then, we transformed *Hordeum vulgare* Golden Promise plants using a *Agrobacterium*-mediated transformation technique described for cereals (with the help of TSL Tissue Culture & Transformation platform lead by Matthew Smoker) (Hensel et al., 2009). Barley transgenic embryos were grown on hygromycin selection medium and positive seedlings screened by PCR and Western blot analysis to confirm plasmid insertion and protein expression. With this pipeline we obtained stable transgenic barley lines expressing PRE2-3xflag and PRE3-3xflag for IP-MS experiments (Figure 5.12). Together, using PREs as molecular probes, we are now able to dissect the cellular processes controlled by Pmk1 during cell-to-cell movement.
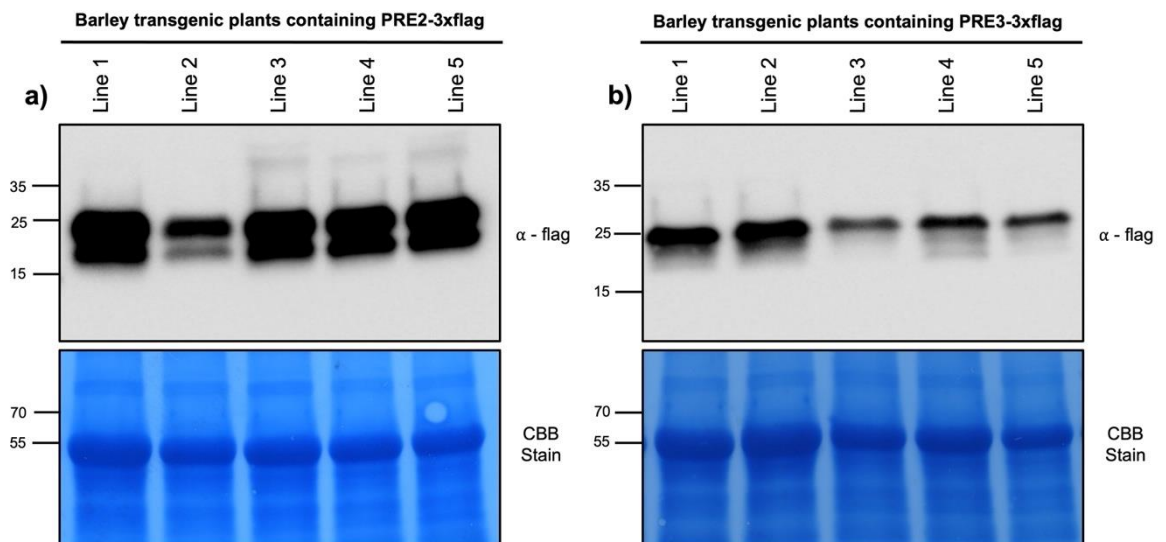
Figure 5.12. *PRE2* and *PRE3* expressed in barley transgenic lines. Western blot analysis to show a) *PRE2*-3xflag and b) *PRE3*-3xflag (C-terminally tagged with 3xflag) expression of candidate transgenic barley lines. Total proteins extract was immunoblotted with anti-flag antisera and blots were stained with Coomassie blue (CBB).

5.2.5 Investigating Vts1 role during transpressorium formation

In Chapter 3, I demonstrated that Vts1 was a potential target of Pmk1 using our quantitative phosphoproteomics method during early appressorium development. In Chapter 4, I functionally characterised Vts1 and demonstrated that it is a direct target of Pmk1 during early in infection. As I have confirmed that Vts1 is part of the Pmk1 pathway and have transcriptomics and proteomics evidence that this protein is also expressed during invasive growth, I decided to investigate its role during transpressorium-dependent cell-to-cell movement.

To gain insight into Vts1 function during invasive growth, I studied its localisation. In Chapter 4, I explained how I generated the *M. oryzae* strain *pmk1^AS: VTS1-GFP* to investigate Vts1 localisation upon Pmk1 inactivation during appressorium development. I tracked Vts1 GFP signal in the presence and absence of the drug 1NaPP1 during cell-to-cell movement (with Alice Eseola). As expected, when Pmk1 was active, the fungus was able to colonise neighbouring rice cells. At this stage, the Vts1 signal accumulated at the hyphal constriction (Figure 5.13). During entrapment, when Pmk1 was inhibited at 26 h, Vts1 localisation was also observed proximal to constrictions in hyphae (Figure 5.13). These observations suggest that although Pmk1 is expressed during cell-to-cell movement, its localisation do not change when Pmk1 is not functional.
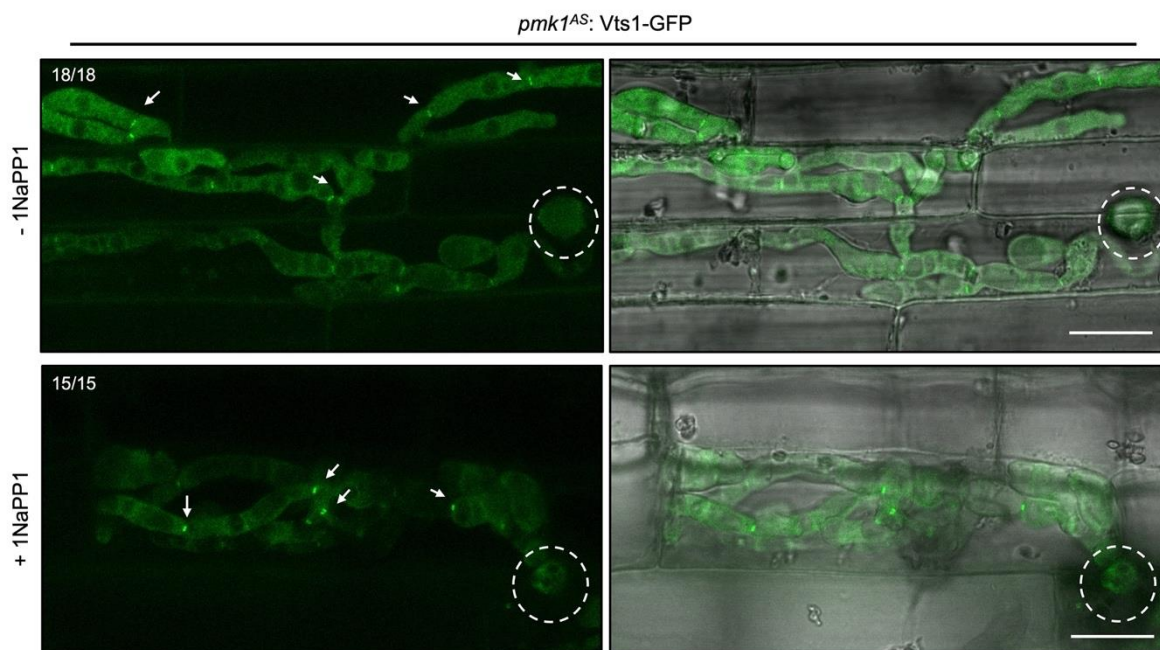
Figure 5.13. Vts1 localisation is not affected when Pmk1 is inactivated during cell-to-cell movement. Micrographs to show representative localisation of Vts1 during cell-to-cell movement when *pmk1^AS: VTS1-GFP* was treated with +/- 5 μg of 1NaPP1. Conidia were

harvested from *pmk1^AS*: *VTS1-GFP* strain 10 dpi, inoculated onto CO-39 leaf sheaths 4 weeks-old and observed by confocal microscopy at 48h. White dotted lines indicate appressorium position. Scale bar = 10 μm.

Based in our discovery proteomics semiquantitative method, I identified that Vts1 is differentially phosphorylated during cell-to-cell movement. At this stage of infection, we did not find any phosphorylated peptide in a MAPK motif for Vts1 when Pmk1 was active. Nevertheless, Vts1 threonine 14 was phosphorylated when Pmk1 was inhibited (Figure 5.13). Interestingly, Vts1 T14 was not a differential phosphorylation site when I studied Vts1 phosphorylation during early appressorium formation. Also, we did not detect this phosphothreonine in our *in vitro* MAPK phosphorylation assay. Possibly, this reflects that Vts1 regulation through phosphorylation is dynamic during different stages of infection.

5.2.6 Investigating Sec31 role during transpressorium formation

The secretory pathway has been largely studied in Eukaryotes and represents a major component of vesicular trafficking in the endomembrane system and Golgi apparatus (Shikano & Colley, 2013). Despite its relevance, it is not clear how it is regulated in the blast fungus in the context of infection. From our comparative phosphoproteomic approach, I found that the proteins Sec16, Sec31 and Sec61 from secretory pathways are differentially phosphorylated upon Pmk1 inactivation. In *M. oryzae*, Sec61 has been shown to have a role in protein translocation of apoplastic effectors (Wei et al., 2020). Whereas Sec16 and Sec31 have not yet been characterised, but their orthologues in yeast are part of the COPII vesicle coat complex that mediates transport of proteins from the endoplasmic reticulum (ER) to the Golgi apparatus (Bharucha et al., 2013; Salama et al., 1997). In *S. cerevisiae*, Sec31 was also reported to have a phenotype related to invasive growth (Shively et al., 2013). Therefore, I decided to study Sec31 function during cell-to-cell movement in the blast fungus.

In the current phosphoproteomic analysis, I found that Sec31 is a differentially phosphorylated protein. We identified that Sec31 threonine 973 is phosphorylated in our control samples when Pmk1 is active during invasive growth. However, we did not detect phosphorylation of this residue when Pmk1 was inactivated after 26 h. Interestingly, we also found Sec31 to be differentially phosphorylated in appressorium formation when we compared the genotypes Guy11 and *Δpmk1.* In this case, Sec31 serine 513 was not phosphorylated in Guy11 but highly phosphorylated in a *Δpmk1* mutant. Sec31 is therefore phosphorylated at different residues during appressorium morphogenesis and cell-to-cell movement.

To learn about Sec31 function, I decided to investigate its localisation during plant tissue colonisation. For this, I cloned the Sec31 gene with its 1.5 Kb promoter into pScBar as a GFP C-terminal fusion. I transformed 8 µg of pScBar-Sec31-GFP vector into protoplasts of *M. oryzae pmk1^{AS}* strain. Because pScBar has the BAR gene for hygromycin resistance, I selected positive transformants growing on selection media for PCR and GFP signal screenings. To study Sec31 role, I chose positive transformants containing a single copy insertion based on qPCR analysis (Anglia iDNA). We tracked Sec31 GFP signal in the Pmk1 chemical inhibition experiment at 26 h, together with Alice Eseola. In all experiments, we observed that Sec31 localised as puncta in the fungus. Images for quantification of punctate structures numbers were obtained from 50 Z stacks consisting of 1 µm depth field multi-layered images with similar settings for all samples. To detect and quantify punctate structures in green channel, the Z stacks were separated into individual images with the ImageJ (2.0) program and analysed. The counting procedure was based on a naked-eye detection of punctate structures to avoid cytoplasm noise. When Pmk1 was functional, Sec31 mostly accumulated in the invasive hyphae crossing to the neighbouring cells at the base of transpressorium (Figure 5.14). However, when Pmk1 was inhibited, Sec31 puncta localised everywhere in trapped hyphae (Figure 5.14). Interestingly, when I counted Sec31 puncta structures per fungal cell, there was a significant reduction upon Pmk1 inhibition and an increase in their size (Figure 5.14). These data suggest that Sec31 localisation may be dependent on Pmk1 activity.
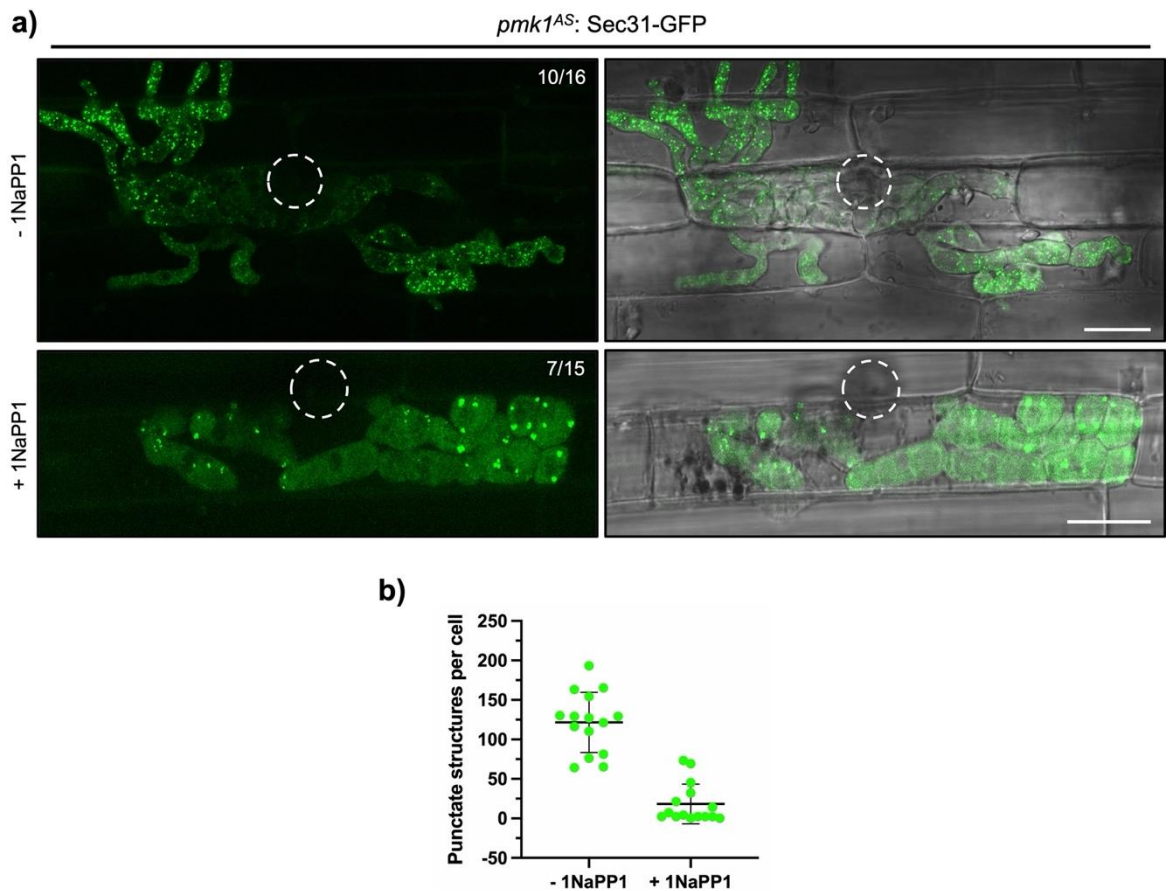
Figure 5.14. Sec31 localisation is impaired when Pmk1 is inactivated during transpressorium-dependent cell-to-cell movement. a) Micrographs to show representative localisation of Sec31 during cell-to-cell movement when *pmk1^AS^: SEC31-GFP* was treated with +/- 5 μg of 1NaPP1. Conidia were harvested from *pmk1^AS^: SEC31-GFP* strain 10 dpi, inoculated onto CO-39 leaf sheaths 4 weeks-old and observed by confocal microscopy at 48h. White dotted lines indicate appressorium position. Scale bar = 10 μm. b) Chart to show Sec31 puncta structures accumulation upon 1NaPP1 treatment. Dot plots were generated with mean of punctate numbers generated from stacks obtained in three independent biological experiments. Three biological replicates were carried out with 15 invaded cells recorded per replicate.

5.3 Discussion

Recently, the importance of the Pmk1 MAPK signalling pathway to regulation of *M. oryzae* transpressorium-dependent cell-to-cell movement has been reported. There are therefore clear parallels between appressorium and transpressorium development, and this

discovery provides many new questions regarding how the Pmk1 signalling regulate both morphogenetic transitions during plant infection and tissue colonisation. This provided the motivation to carry out a comparative phosphoproteomic analysis of transpressorium development.

In this Chapter, I have reported how we used a chemical genetic approach together with comparative phosphoproteomics to identify potential downstream components of Pmk1 during transpressorium-dependent cell-to-cell movement. With this pipeline, I was able to identify 39 proteins with at least one phosphosite differentially phosphorylated in a MAPK motif dependent on Pmk1 activity. Interestingly, I found that the proteins with orthologues were related to 13 different cellular functions including secretion, cell division, cytoskeleton remodelling and vesicular trafficking. However, the remaining proteins are of unknown function and have not been yet characterised. In this Chapter, I explored the function of some of the putative targets of the Pmk1 signalling pathway and identified a novel group of effector proteins (PREs), a new component of the cascade (Vts1) and an uncharacterised component of the secretory pathway (Sec31).

Using a comparative phosphoproteomic pipeline, I identified fungal proteins from rice leaf sheath material infected with *M. oryzae*. Unfortunately, we identified only a small number of proteins from the pathogen. The amount of rice phosphoproteins in the samples did not allow detection of many of fungal proteins. Because of the challenge of having so little biomass available, it is important, in future, to refine this method by setting up conditions where *M. oryzae* phosphoproteins are more abundant. For instance, increasing the concentration of the blast fungus during infections or using complementary proximity-labelling based methods such as TurboID. However, with the current approach we found 2707 total soluble phosphoproteins from which 145 contained a MAP kinase phosphorylation motif. We were, therefore, able to carry out a method to study phosphorylated proteins upon Pmk1 inactivation during transpressorium-dependent cell-to-cell movement.

In the current proteomic study and using a previous transcriptomic analysis, I identified a subset of three Pmk1-regulated putative effectors (PREs). Based on phosphoproteomics and cell imaging, I found that PRE1, PRE2 and PRE3 are phosphorylated candidate effectors that are only expressed when Pmk1 is functional. Interestingly, the role of Pmk1 regulating effector gene expression during cell-to-cell movement has been previously suggested. Using the same experimental pipeline but for a transcriptomic analysis, it was demonstrated that Pmk1 regulates expression of a subset of effector genes implicated in plant immunity suppression, such as Avr-Pita1, Slp1, Avr-Pik, Bas2 and Bas3 (Sakulkoo et

al., 2018). Although we did not find this characterised group of effectors in our analysis, the RNAseq experiment showed that *PRE1*, *PRE2* and *PRE3* are positively regulated by Pmk1 (Figure 5.6). Altogether, our transcriptomic and proteomic studies, therefore, suggest that Pmk1 regulates effector gene expression and, potentially, post-translationally regulates their activity during invasive growth. Possibly, as part of its own phosphorylation cascade.

An interesting finding is that PREs localisation is affected when Pmk1 function is inhibited. Interestingly, it has been previously observed that inactivation of Pmk1 also impairs localisation of Bas2 and Bas3 effectors (Sakulkoo et al., 2018). Bas2 and Bas3 are Cysteine-rich secreted effectors with a putative function at cell wall crossing sites (Mosquera et al., 2009). Therefore, in agreement with previous studies, Pmk1 appears to be required for the production and localisation of secreted effectors involved in cell wall crossing.

There is no current evidence that effectors are phosphorylated by a pathogen MAPK to cause disease. The role of MAPKs regulating effectors by phosphorylation has been poorly investigated in any pathosystems. Thus, it will be relevant to dissect the role of the PREs in the Pmk1 phosphorelay. To understand PRE functions in transpressorium-dependent cell-to-cell movement, it will be necessary to investigate their interactome. Large-scale interactor screenings, such as IP-MS using stable transgenic lines, might help to define missing gaps between Pmk1 function and PRE localisation. For this reason, I made stable transgenic lines expressing an effector gene and these will be analysed by IP-MS in future to identify putative targets.

Pathogen effectors can, however, be phosphorylated by plant kinases. In other pathosystems, it has been demonstrated that effectors rely on host phosphorylation to enhance their virulence (Bhattacharjee et al., 2015). The *Pseudomonas syringae* effectors AvrPto, AvrPtoB, AvrB and HopQ can, for example, be phosphorylated by the plant host (Anderson et al., 2006; Desveaux et al., 2007; Li et al., 2013; Marroquin-Guzman et al., 2017; Yeam et al., 2010). In the case of AvrPtoB, it has been also found that phosphorylation is caused by the conserved plant kinase SnRK2.8 (Lei et al., 2020). Similarly, the cys nematode effector 10A07 recruits its host phosphorylation machinery to promote disease in *Arabidopsis* (Hewezi et al., 2015). These cross-kingdom phosphorylation events are not limited to plant pathogens however because they have also been reported in symbiotic relationships (Skorpil et al., 2005; Zhang et al., 2011). Due to the conditions we used to carry out our phosphoproteomics analysis, I cannot exclude that PRE phosphorylation might be a plant dependent-process. Therefore, investigating the

function of the PRE effectors might lead to discovery of novel regulation mechanisms in *M. oryzae*-host interaction.

Another putative target of Pmk1 during cell-to-cell movement is the SAM domain containing protein Vts1. In Chapter 4, I described how we determined that Vts1 is a novel component of the Pmk1 cascade during early appressorium morphogenesis. Vts1 is, however, also a Pmk1 target during invasive growth. This finding reinforces the hypothesis that Vts1 may act as a scaffold protein in the cascade. MAPK protein scaffolds confer spatial and temporal regulation to the pathway bringing multiple components into close proximity to facilitate signal propagation (Brown & Sacks, 2009). Because Vts1 has a similar localisation to the MAPK scaffold protein Ham-5 in *N. crassa* (Jonkers et al., 2014), it possibly fulfils a similar role in assembling complexes at the correct cellular location. Future experiments studying SAM-domain interacting proteins will reveal if there are distinct Pmk1 complexes at different stages of infection. Surprisingly, the Vts1 differentially regulated phosphosite during invasive growth is threonine 14 which is distinct from residues identified in the early appressorium regulation. Vts1 differential phosphorylation, therefore, highlights the intricate level of control over MAPK signalling.

In the blast fungus, the role of secretory proteins during infection has been poorly investigated. In the current target validation analysis, I have studied the COPII vesicle coat complex orthologue Sec31. Interestingly, Sec31 localisation was impaired when Pmk1 was not functional during invasive growth. It will be interesting to define if this protein is a direct target of Pmk1 due to phosphorylation of T973. Possibly, Pmk1 regulates secretion of virulence determinants through the Sec31 pathway that help the pathogen to move from one cell to another.

Appressoria and transpressoria perform a very similar function in allowing a pathogen to overcome a physical obstacle in the plant. Interestingly, they also have some similarities such as the fact that they both precede a morphogenetic switch, both have a septin-mediated mechanism and both are regulated by the Pmk1 pathway (Cruz-Mireles et al., 2021). Our phosphoproteomic analysis has defined potentially new and novel determinants of transpressorium development. This information will be of value in understanding parallels and differences between these two infection structures.

Chapter 6:

6   General discussion

Pmk1 was identified as a major determinant of pathogenicity more than 25 years ago and the role of this kinase has been investigated in many diverse plant pathogens. However, despite its importance, little is known about the phosphorylation events governing the Pmk1 MAPK cascade. It has been demonstrated that the Pmk1 MAPK pathway controls morphogenetic transitions leading to appressorium and transpressorium formation (Osés-Ruiz et al., 2021; Sakulkoo et al., 2018; Xu & Hamer, 1996), but the molecular mechanisms that are needed to operate these two infection stages remain elusive (Cruz-Mireles et al., 2021). In this thesis, I have presented a comparative phosphoproteomic analysis during appressorium and transpressorium development. I have analysed early appressorium morphogenesis in the blast fungus with temporal resolution, allowing the delineation of phosphorylation changes of proteins expressed early in infection. By applying a comparative approach, I was able to identify changes in phosphorylation that are Pmk1-dependent and, therefore, to identify putative targets of Pmk1. As an example of how this dataset may be used to investigate components of Pmk1 pathway, I characterised in detail the SAM domain containing protein Vts1. Similarly, I used a combination of chemical genetics, phosphoproteomics and transcriptomics to define Pmk1-dependent determinants that mediate *M. oryzae* transpressorium-dependent cell-to-cell movement. The data generated led us to investigate the role of a subset of P̲mk1 R̲egulated E̲ffectors (PRE) and the secretory pathway protein Sec31 during invasive growth.

6.1   Phosphoproteomics as an approach to study Pmk1 during appressorium formation and cell-to-cell movement

It is well-known that the use of phosphoproteomics for functional studies provides new opportunities to identify phosphorylated targets but also challenges. A thoughtful study from an evolutionary perspective has estimated that 65 % of phosphosites in phosphoproteome are non-functional (Landry et al., 2009; Lienhard, 2008). Therefore, it is important to incorporate methods that allow the prioritisation of phosphorylation sites for subsequent functional studies (Landry et al., 2009; Xiao et al., 2016). In this study, I used a comparative approach that helped to filter putative targets of Pmk1 and select phosphosites to be studied in functional analysis. In our data from analysing early appressorium formation, the comparison of *M. oryzae* proteomes in mutants lacking activity of Pmk1 constituted a filtering layer. In the data obtained from cell-to-cell movement, comparing

phosphoproteomes of plant material infected with functional and non-functional Pmk1 was a vital criterion. In both datasets, phosphosites within a MAPK motif and in targets containing a MAPK docking domain were prioritised. Together, both phosphoproteomic datasets illustrate a robust repertoire of potential Pmk1 downstream targets. We anticipate that this information will be of value in investigating different aspects of infection-related development, including the temporal regulation of virulence determinants required for invasive growth by the blast fungus.

6.2 How can Vts1 regulate Pmk1 signalling?

The SAM domain containing protein Vts1 was identified as a putative target of Pmk1 in two different phosphoproteomic approaches to investigate Pmk1 MAPK signalling. I validated Vts1 as a direct target of Pmk1 with multiple approaches. Vts1 is a protein of unknown function that contains a SAM domain. SAM domains are present in most of the proteins involved in complex formation (Knight et al., 2011). For this reason, the SAM domain is one of the most versatile modules in Eukaryotes (Denay et al., 2017). Secondly, Vts1 showed different subcellular localisations, such as the appressorium pore during appressorium development and at hyphal constrictions during appressorium development. Vts1 is expressed during plant infection and differentially phosphorylated during appressorium morphogenesis and invasive growth. Differential localisation and regulation by phosphorylation are two of the most common features of scaffold proteins in MAPK signalling (Pan et al., 2012). Therefore, I forward the hypothesis that Vts1 is a scaffold protein in the Pmk1 pathway.

In Eukaryotes, scaffold proteins are thought to shape MAPK signalling and help determine signalling specificity (Dhanasekaran et al., 2007; Witzel et al., 2012). They often represent an additional level of complexity to the dynamics of signalling and contribute to specificity of pathways (Harris et al., 2001). In *S. cerevisiae*, the scaffold protein Ste5 for example binds to Ste11, Ste7, Fus3/ Kss1 MAPKs of the pheromone module and recruits them to the membrane to amplify the signal (Lamson et al., 2006; Pryciak & Huntress, 1998). In the filamentous fungus *N. crassa*, the scaffold protein Ham-5 and Ham-14, are components of the MEK-2 pathway, and involved in recruiting distinct complexes to regulate the role of the MAPK signalling in chemotropism and cell fusion, respectively (Jonkers et al., 2016; Jonkers et al., 2014). In the case of the blast fungus, Mst50 is a putative scaffold protein of the Pmk1 cascade (Li et al., 2017; Park et al., 2006; Zhao et al., 2005). Strikingly, Mst50 contains a SAM domain but does not interact with Pmk1 (Zhao et al., 2005). I demonstrated that Vts1 binds to Pmk1, and this raises the possibility that Vts1 forms complexes with Mst50 to bring together Pmk1 with upstream components of the pathway. Potentially, these

complexes may be important to mediate infection-related morphogenesis of the blast fungus.

6.3 Pmk1 controls effectors during cell-to-cell movement at transcriptional and potentially post-translational levels

During biotrophy, the blast fungus secretes an array of molecules for successful plant colonisation. It has been reported that effector proteins and secondary metabolites are secreted into host cells to perturb plant defence mechanisms and facilitate pathogen invasion (Giraldo et al., 2013; Kankanala et al., 2007; Khang et al., 2010; Mosquera et al., 2009; Patkar et al., 2015). The signalling mechanisms that orchestrate production and delivery of effectors is poorly understood. In *M. oryzae*, evidence demonstrates that the Pmk1 cascade controls the expression of a group of effector genes including Avr-Pita1, Slp1, Avr-Pik, Bas2 and Bas3 to perturb host immune responses (Sakulkoo et al., 2018). It has been proposed that these effectors play a role in suppressing plasmodesmata immunity preventing their closure to allow hyphal invasion while preserving host cell integrity (Sakulkoo et al., 2018). This is one of the very first studies illustrating how a fungal MAPK could mediate the infection strategy of successful host colonisation.

The current study provides further evidence that the blast fungus uses the Pmk1 MAPK phosphorylation cascade to regulate the function of effectors during cell-to-cell movement. Although transcriptomic and proteomic data suggests Pmk1 regulates part of the effector production during invasive growth, it is not clear how this operates. Here, I have found that Pmk1 may control PRE1, PRE2 and PRE3 function indirectly. Previous evidence suggests that MAPKs shape gene expression in a temporal manner via the regulation of TFs (Hazzalin & Mahadevan, 2002; Nadal-Ribelles et al., 2018). However, I hypothesise that Pmk1 may also induce effector production by phosphorylation of TFs. A previous study reported that the TF Slf1 is phosphorylated by Pmk1 and has a key role during invasive growth (Li et al., 2011) (Figure 6.1). In this thesis, I found that Som1 is a putative target of Pmk1 during invasive growth. Som1 is a transcriptional regulator associated with cellular differentiation and plant infection (Yan et al., 2011). Potentially, the study of Pmk1-regulated TFs involved in fungal host colonisation might reveal the signalling cascade that operates downstream to control effector production.

6.4 Can Pmk1 control the secretory pathway during rice blast infection?

During invasive growth, it is clear that the blast fungus secretes many molecules including proteins, such as effectors and hydrolytic enzymes, as well as secondary metabolites, to

facilitate the spread of disease (Cruz-Mireles et al., 2021; Valent, 2021). The mechanisms that underpin secretion during infection, however, remain elusive. The majority of the work to investigate secreted molecules in the blast fungus has been on the mechanism of effector delivery and translocation (Giraldo et al., 2013; Khang et al., 2010; Kim et al., 2020; Mosquera et al., 2009; Zhang & Xu, 2014). However, before exit, secreted molecules have to be synthesised and modified using the conserved secretory pathway in Eukaryotes (Farhan & Rabouille, 2011). This pathway involves organised transport between the rough endoplasmic reticulum (rough ER) and the Golgi complex to facilitate protein folding and post-translational modifications such as glycosylation (Spang, 2009). The secretory pathway comprises a large set of proteins and all the canonical components have been described in the model fungus *S. cerevisiae* (Delic et al., 2013).

Interestingly, in the current study, I identified components of the secretory pathway as putative targets of Pmk1 during appressorium morphogenesis and tissue colonisation. Sec16, Sec31 and Sec61 were identified as phosphoproteins that are differentially regulated upon inhibition of Pmk1 activity. In particular, Sec31 phosphorylation was affected in both appressorium and invasive growth (Chapter 3 and Chapter 5). Sec16 and Sec31 are subunits of the COPII vesicles that mediate anterograde transport (ER to *cis*-Golgi) before secretion (Delic et al., 2013). In yeast, Sec16 and Sec31 are encoded by single genes, and individual null mutants are affected in vegetative and invasive growth, respectively (Shively et al., 2013; Sopko et al., 2006). Conversely, in mammals, Sec16 and Sec31 have two paralogues suggesting that the COPII transport has evolved to increase complexity in multicellular organisms (Delic et al., 2013). These reports illustrate the conservation of proteins involved in anterograde transport in Eukaryotes.

Strikingly, it has been shown that anterograde protein transport can be regulated by phosphorylation of Sec31. In yeast, phosphorylation and dephosphorylation cycles of Sec31 are associated with the budding of COPII vesicles (Salama et al., 1997). In *Trypanosoma brucei*, the G_1 cyclin-dependant kinase CRK1 furthermore controls COPII trafficking through Sec31 phosphorylation (Hu et al., 2016). Whereas in mammals, Sec31 has been demonstrated to be phosphorylated by different kinases, including Casein Kinase II (CK2) and Protein Kinase D (PKD) (Dephoure et al., 2008; Farhan et al., 2010; Franz-Wachtel et al., 2012; Olsen et al., 2006). These data suggest that Sec31 is a conserved hub that controls secretion and is regulated by phosphorylation. It is intriguing to know why the blast regulates Sec31 via the Pmk1 cascade. Maybe, Pmk1 operates COPII trafficking to enable timely delivery of Pmk1-dependent effectors or morphogenetic determinants during invasive growth. Clearly, Pmk1, as a master regulator of pathogenesis, might play a role on regulating secretory processes during blast disease.

6.5 How the Pmk1 pathway regulates appressorium and transpressorium morphogenesis

Appressorium and transpressorium formation follow similar morphogenetic programmes. They are both initiated after recognition of physical and chemical cues encountered on the surface that leads to a morphogenetic switch from polarised growth to an isotopically expanded invasive structure (Whiteford & Spanu, 2002). These two specialised structures then form a polarised infection peg to rupture the host cell wall. Finally, the developing infection hypha is encircled by the host plasma membrane after passing through the physical barrier of the cell wall (Sakulkoo et al., 2018). Evidence suggests that both of these morphogenetic processes are septin-mediated events that are regulated by Pmk1 (Cruz-Mireles et al., 2021). Therefore, the parallels between appressorium and transpressorium raise questions regarding how the Pmk1 cascade operates in both developmental programmes. For instance, what are the environmental cues that trigger phosphorylation changes during appressorium and transpressorium morphogenesis? In the blast fungus potential sensors have been identified in the appressorium such as GPCRs and ion channel proteins (DeZwaan et al., 1999; Kou et al., 2017; Liu et al., 2011), but the role of these sensors is still poorly investigated.

Another intriguing question is how Pmk1 MAPK cascade specificity is determined during appressorium and transpressorium morphogenesis. There is little information regarding how fungal MAPK cascades are triggered and modulated across different developmental stages. Evidence from other eukaryotic systems suggests that regulation of MAPK pathways can be complex because they function as a network connected at various levels of the kinase cascade (Cargnello & Roux, 2011; Dóczi et al., 2012). Nevertheless, different hypotheses suggest that spatio-temporal activation, feedback loops, compartmentalisation of signalling by complex formation and signal magnitude can contribute to MAPK cascade specificity that switches the cellular programme (Bardwell, 2006; Pouysségur & Lenormand, 2003; Serrano et al., 2018; Shuaib et al., 2016). For example, a quantitative phosphorylation study has revealed that developmental changes in *Schizosaccharomyces pombe* depend on multiple sequential waves of phosphorylation regulated by polarised growth determinants and cell-cycle kinases (Swaffer et al., 2018). Potentially, the Pmk1 cascade is also regulated by phosphorylation waves, whose spatio-temporal activation phosphorylates specific downstream targets that then determine morphogenetic switches (Figure 6.6). Indeed, the blast fungus is an excellent system to study global MAPK cascade regulation in pathogenicity.

6.6 Understanding the Pmk1 pathway in the blast fungus can help us to dissect other pathogenicity mechanisms in filamentous fungi

The MAPK Pmk1 is orthologue of the MAPKs Fus3 and Kss1 in *S. cerevisiae*. In most filamentous ascomycetes, there is only one MAPK orthologue for Fus3 and Kss1 and this has been shown to be important for plant pathogenesis (Jiang et al., 2018). Because of this homology, the majority of the Pmk1 pathway components identified in pathogenic fungi have been compared to the pheromone response module in budding yeast. Although Fus3 and Kss1 are generally believed to possess redundant overlapping functions, recent findings make clearer that both kinases have specialised regulatory mechanisms in mating differentiation and invasive growth transitions, respectively (Errede et al., 2015). The Pmk1 pathway have been studied more intensely in the blast fungus than in any other pathogenic species. Evidence in *M. oryzae* indicates that Pmk1 controls morphogenetic transitions during infection. This function might therefore be more equivalent to the recently discovered roles of Kss1 signalling rather than Fus3 in *S. cerevisiae*. Potentially, the Kss1 function was co-opted to regulate pathogenicity related mechanisms in filamentous ascomycetes. Therefore, discoveries in Kss1 pathway might help us to dissect Pmk1 signalling in the blast fungus.

A significant proportion of the characterised Pmk1 putative targets identified in appressorium and invasive growth belong to highly conserved processes in Eukaryotes. For example, our findings on the secretory pathway proteins can help to understand the function of phosphorylation sites in other paralogues. Similarly, considering that Vts1 is conserved in filamentous fungi, it will be necessary to investigate its function in fungal pathogens. Theoretically, Vts1 orthologues might be undergoing similar regulatory mechanisms based on phosphorylation. Therefore, the list of pathogenic determinants we present here should be directly applicable to investigate infection-related phosphoregulatory processes across fungal pathogens.

6.7 Concluding remarks and future directions

This study aimed to broaden our understanding of Pmk1 MAPK signalling during *M. oryzae* infection by identifying novel components of the cascade and describing their function during rice blast disease. The findings presented in this thesis highlight the complexity of the Pmk1-dependent signalling mechanisms implicated in the appressorium and transpressorium development. Nevertheless, this work also raises many open questions. For example, what are the signals sensed by the fungus to activate the Pmk1 cascade? What is the nature of the spatio-temporal dynamics of Pmk1 activation during appressorium

and transpressorium morphogenesis? Is the Pmk1 activation complex conserved during appressorium and transpressorium formation, or distinct in early infection cell? How does the Pmk1 cascade maintain specificity across the different morphogenetic transitions? Is Vts1 a scaffold protein of the Pmk1 core complex? Do PRE effectors act to suppress plasmodesmatal-related immunity and to allow transpressorium-dependent cell-to-cell movement? How are PREs phosphorylated? Is this a fungal-driven process or does it happen after their delivery? Does Pmk1 control the secretory pathway to ensure exocytosis and delivery of virulence factors? Answering these fundamental questions will help advance our understanding of signalling mechanisms governed by Pmk1 during rice blast disease.
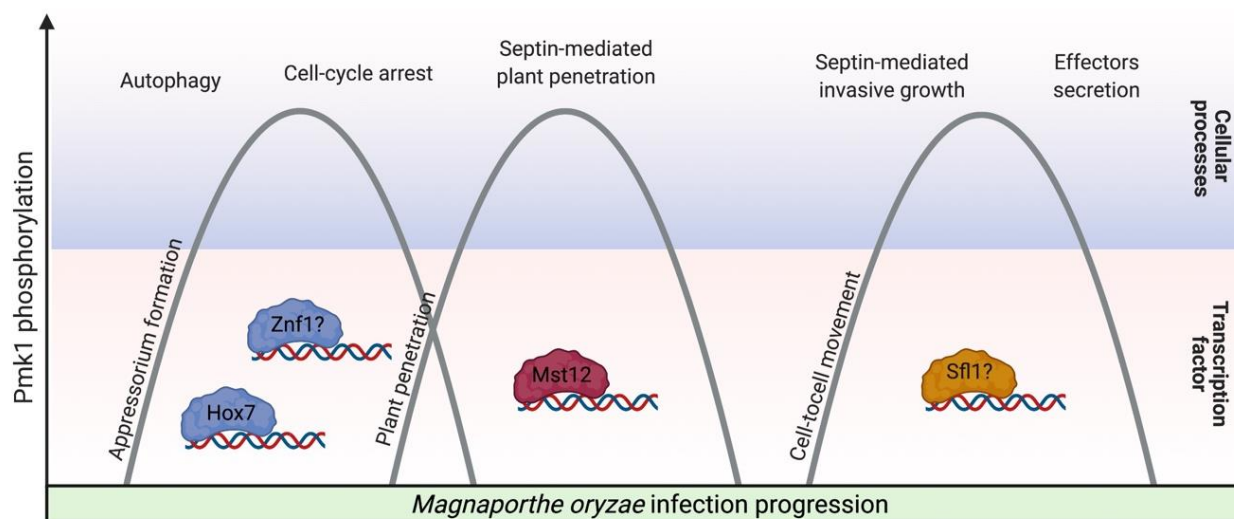
Figure 6.1. Model for MAPK Pmk1 spatio-temporal activation during *M. oryzae* infection. Schematic representation to illustrate the hypothesis that Pmk1 activation occurs in waves of phosphorylation during rice blast disease. The reported TFs identified as downstream Pmk1 are shown. During early infection, Pmk1 is phosphorylated to activate Hox7 and, possibly, Znf1. Hox7 regulates expression of genes implicated in autophagy and cell-cycle arrest (Osés-Ruiz et al., 2021). During plant penetration, Pmk1 controls morphogenetic transition to a re-polarised appressorium by activating Mst12 (Osés-Ruiz et al., 2021; Park et al., 2002). Finally, during cell-to-cell movement, Pmk1 regulates effector secretion and transpressorium formation through TFs involved in invasive growth, such as Sfl1 (Li et al., 2011). This hypothesis implies that the specificity of the cascade is determined by phosphorylation waves.

References

Alepuz, P. M., Jovanovic, A., Reiser, V., & Ammerer, G. (2001). Stress-induced MAP kinase Hog1 is part of transcription activation complexes. *Molecular Cell*, *7*(4), 767–777. https://doi.org/10.1016/S1097-2765(01)00221-0

Anderson, J. C., Pascuzzi, P. E., Xiao, F., Sessa, G., & Martin, G. B. (2006). Host-mediated phosphorylation of type III effector AvrPto promotes Pseudomonas virulence and avirulence in tomato. *The Plant Cell*, *18*(2), 502–514. https://doi.org/10.1105/TPC.105.036590

Ardito, F., Giuliani, M., Perrone, D., Troiano, G., & Muzio, L. Lo. (2017). The crucial role of protein phosphorylation in cell signaling and its use as targeted therapy. *International Journal of Molecular Medicine*, *40*(2), 271. https://doi.org/10.3892/IJMM.2017.3036

Asai, T., Tena, G., Plotnikova, J., Willmann, M. R., Chiu, W. L., Gomez-Gomez, L., … Sheen, J. (2002). MAP kinase signalling cascade in Arabidopsis innate immunity. *Nature 2002 415:6875*, *415*(6875), 977–983. https://doi.org/10.1038/415977a

Bardwell, L. (2006). Mechanisms of MAPK signalling specificity. *Biochemical Society Transactions*, *34*(Pt 5), 837–841. https://doi.org/10.1042/BST0340837

Bartoli, C., Roux, F., & Lamichhane, J. R. (2015). Molecular mechanisms underlying the emergence of bacterial pathogens: an ecological perspective. *Molecular Plant Pathology*, *17*(2):303-10. https://doi.org/10.1111/mpp.12284

Bekker-Jensen, D. B., Bernhardt, O. M., Hogrebe, A., Martinez-Val, A., Verbeke, L., Gandhi, T., … Olsen, J. V. (2020). Rapid and site-specific deep phosphoproteome profiling by data-independent acquisition without the need for spectral libraries. *Nature Communications*, *11*(1), 1–12. https://doi.org/10.1038/s41467-020-14609-1

Bensimon, A., Heck, A. J. R., & Aebersold, R. (2012). Mass spectrometry–based proteomics and network biology. *Annual Review of Biochemistry*, 81, 379–405. https://doi.org/10.1146/annurev-biochem-072909-100424

Bentham, A. R., de la Concepcion, J. C., Mukhi, N., Zdrzałek, R., Draeger, M., Gorenkin, D., … Banfield, M. J. (2020). A molecular roadmap to the plant immune system. *The Journal of Biological Chemistry*, *295*(44), 14916–14935. https://doi.org/10.1074/JBC.REV120.010852

Berriri, S., Garcia, A. V., dit Frey, N. F., Rozhon, W., Pateyron, S., Leonhardt, N., …

Colcombet, J. (2012). Constitutively active Mitogen-Activated Protein Kinase versions reveal functions of Arabidopsis MPK4 in pathogen defense signaling. *The Plant Cell*, *24*(10), 4281–4293. https://doi.org/10.1105/TPC.112.101253

Berrow, N. S., Alderton, D., Sainsbury, S., Nettleship, J., Assenberg, R., Rahman, N., … Owens, R. J. (2007). A versatile ligation-independent cloning method suitable for high-throughput expression screening applications. *Nucleic Acids Research*, *35*(6), e45–e45. https://doi.org/10.1093/nar/gkm047

Bharucha, N., Liu, Y., Papanikou, E., McMahon, C., Esaki, M., Jeffrey, P. D., … Glick, B. S. (2013). Sec16 influences transitional ER sites by regulating rather than organizing COPII. *Molecular Biology of the Cell*, *24*(21), 3406. https://doi.org/10.1091/MBC.E13-04-0185

Bhattacharjee, S., Noor, J. J., Gohain, B., Gulabani, H., Dnyaneshwar, I. K., & Singla, A. (2015). Post-translational modifications in regulation of pathogen surveillance and signaling in plants: The inside- (and perturbations from) outside story. *IUBMB Life*, *67*(7), 524–532. https://doi.org/10.1002/IUB.1398

Bigeard, J., & Hirt, H. (2018). Nuclear signaling of plant MAPKs. *Frontiers in Plant Science*, *9*, 469. https://doi.org/10.3389/FPLS.2018.00469/BIBTEX

Bin Yusof, M. T., Kershaw, M. J., Soanes, D. M., & Talbot, N. J. (2014). FAR1 and FAR2 regulate the expression of genes associated with lipid metabolism in the rice blast fungus Magnaporthe oryzae. *PloS One*, *9*(6). https://doi.org/10.1371/JOURNAL.PONE.0099760

Bishop, A. C., Ubersax, J. A., Pøtsch, D. T., Matheos, D. P., Gray, N. S., Blethrow, J., … Shokat, K. M. (2000). A chemical switch for inhibitor-sensitive alleles of any protein kinase. *Nature*, *407*(6802), 395–401. https://doi.org/10.1038/35030148

Blazek, M., Santisteban, T. S., Zengerle, R., & Meier, M. (2015). Analysis of fast protein phosphorylation kinetics in single cells on a microfluidic chip. *Lab on a Chip*, *15*(3), 726–734. https://doi.org/10.1039/C4LC00797B

Boulton, T. G., Nye, S. H., Robbins, D. J., Ip, N. Y., Radzlejewska, E., Morgenbesser, S. D., … Yancopoulos, G. D. (1991). ERKs: a family of protein-serine/threonine kinases that are activated and tyrosine phosphorylated in response to insulin and NGF. *Cell*, *65*(4), 663–675. https://doi.org/10.1016/0092-8674(91)90098-J

Bourett, T. M., & Howard, R. J. (1992). Actin in penetration pegs of the fungal rice blast pathogen,Magnaporthe grisea. *Protoplasma 1992 168:1*, *168*(1), 20–26.

https://doi.org/10.1007/BF01332647

Bourett, T. M., & Howard, R. J. (1990). *In vitro* development of penetration structures in the rice blast fungus Magnaporthe grisea. *Canadian Journal of Botany*, *68*(2), 329–342. https://doi.org/10.1139/b90-044

Brachmann, A., Schirawski, J., Müller, P., & Kahmann, R. (2003). An unusual MAP kinase is required for efficient penetration of the plant surface by Ustilago maydis. *The EMBO Journal*, *22*(9), 2199–2210. https://doi.org/10.1093/emboj/cdg198

Brown, M. D., & Sacks, D. B. (2009). Protein Scaffolds in MAP Kinase Signalling. *Cellular Signalling*, *21*(4), 462. https://doi.org/10.1016/j.cellsig.2008.11.013

Bruno, K. S., Tenjo, F., Li, L., Hamer, J. E., & Xu, J.-R. (2004). Cellular localization and role of kinase activity of PMK1 in Magnaporthe grisea. *Eukaryotic Cell*, *3*(6), 1525–1532. https://doi.org/10.1128/EC.3.6.1525-1532.2004

Cao, H., Huang, P., Zhang, L., Shi, Y., Sun, D., Yan, Y., … Lu, J. (2016). Characterization of 47 Cys2 -His2 zinc finger proteins required for the development and pathogenicity of the rice blast fungus Magnaporthe oryzae. *The New Phytologist*, *211*(3), 1035–1051. https://doi.org/10.1111/NPH.13948

Cargnello, M., & Roux, P. P. (2011). Activation and function of the MAPKs and their substrates, the MAPK-activated protein kinases. *Microbiology and Molecular Biology Reviews : MMBR*, *75*(1), 50. https://doi.org/10.1128/MMBR.00031-10

Catlett, N. L., Lee, B.-N., Yoder, O. C., Catlett, N. L., Lee, B., & Turgeon, B. G. (2003). Split-marker recombination for efficient targeted deletion of fungal genes. *Fungal Genetics Reports*, *50*(1), 9–11. https://doi.org/10.4148/1941-4765.1150

Chang, L., & Karin, M. (2001). Mammalian MAP kinase signalling cascades. *Nature*, *410*(6824), 37–40. https://doi.org/10.1038/35065000

Chen, C., Harel, A., Gorovoits, R., Yarden, O., & Dickman, M. B. (2007). MAPK regulation of sclerotial development in Sclerotinia sclerotiorum is linked with pH and cAMP sensing. *Molecular Plant-Microbe Interactions*, *17*(4), 404–413. https://doi.org/10.1094/MPMI.2004.17.4.404

Chen, R. E., & Thorner, J. (2007). Function and regulation in MAPK signaling pathways: Lessons learned from the yeast Saccharomyces cerevisiae. *Biochimica et Biophysica Acta (BBA) - Molecular Cell Research*, *1773*(8), 1311–1340. https://doi.org/10.1016/j.bbamcr.2007.05.003

Cho, Y., Cramer, R. A., Kim, K. H., Davis, J., Mitchell, T. K., Figuli, P., … Lawrence, C. B. (2007). The Fus3/Kss1 MAP kinase homolog Amk1 regulates the expression of genes encoding hydrolytic enzymes in Alternaria brassicicola. *Fungal Genetics and Biology : FG & B*, *44*(6), 543–553. https://doi.org/10.1016/J.FGB.2006.11.015

Choudhary, C., & Mann, M. (2010). Decoding signalling networks by mass spectrometry-based proteomics. *Nature Reviews Molecular Cell Biology 2010 11:6*, *11*(6), 427–439. https://doi.org/10.1038/nrm2900

Conesa, A., & Götz, S. (2008). Blast2GO: A comprehensive suite for functional analysis in plant genomics. *International Journal of Plant Genomics*, *2008*, 619832. https://doi.org/10.1155/2008/619832

Courchesne, W. E., Kunisawa, R., & Thorner, J. (1989). A putative protein kinase overcomes pheromone-induced arrest of cell cycling in S. cerevisiae. *Cell*, *58*(6), 1107–1119. https://doi.org/10.1016/0092-8674(89)90509-6

Cousin, A., Mehrabi, R., Guilleroux, M., Dufresne, M., Van Der Lee, T., Waalwijk, C., … Kema, G. H. J. (2006). The MAP kinase-encoding gene MgFus3 of the non-appressorium phytopathogen Mycosphaerella graminicola is required for penetration and in vitro pycnidia formation. *Molecular Plant Pathology*, *7*(4), 269–278. https://doi.org/10.1111/J.1364-3703.2006.00337.X

Cruz-Mireles, N., Eisermann, I., Garduño-Rosales, M., Molinari, C., Ryder, L. S., Tang, B., … Talbot, N. J. (2021). The biology of invasive growth by the rice blast fungus Magnaporthe oryzae. *Methods in Molecular Biology*, *2356*, 19–40. https://doi.org/10.1007/978-1-0716-1613-0_2

Cruz-Mireles, N., Eseola, A. B., Osés-Ruiz, M., Ryder, L. S., & Talbot, N. J. (2021). From appressorium to transpressorium—Defining the morphogenetic basis of host cell invasion by the rice blast fungus. *PLOS Pathogens*, *17*(7), e1009779. https://doi.org/10.1371/journal.ppat.1009779

Cruz, C. D., & Valent, B. (2017). Wheat blast disease: danger on the move. *Tropical Plant Pathology*, *42*(3), 210–222. https://doi.org/10.1007/S40858-017-0159-z/figures/4

Dagdas, Y. F., Yoshino, K., Dagdas, G., Ryder, L. S., Bielska, E., Steinberg, G., & Talbot, N. J. (2012). Septin-mediated plant cell invasion by the rice blast fungus, Magnaporthe oryzae. *Science*, *336*(6088), 1590–1595. https://doi.org/10.1126/science.1222934

De Godoy, L. M. F., Olsen, J. V., Cox, J., Nielsen, M. L., Hubner, N. C., Fröhlich, F., … Mann, M. (2008). Comprehensive mass-spectrometry-based proteome quantification

of haploid versus diploid yeast. *Nature*, *455*(7217), 1251–1254. https://doi.org/10.1038/nature07341

de Jong, J. C., McCormack, B. J., Smirnoff, N., & Talbot, N. J. (1997). Glycerol generates turgor in rice blast. *Nature*, *389*(6648), 244. https://doi.org/10.1038/38418

De la Concepcion, J. C., Maidment, J. H. R., Longya, A., Xiao, G., Franceschetti, M., & Banfieldi, M. J. (2021). The allelic rice immune receptor Pikh confers extended resistance to strains of the blast fungus through a single polymorphism in the effector binding interface. *PLOS Pathogens*, *17*(3), e1009368. https://doi.org/10.1371/JOURNAL.PPAT.1009368

De la Concepcion, J. C., Franceschetti, M., Maclean, D., Terauchi, R., Kamoun, S., & Banfield, M. J. (2019). Protein engineering expands the effector recognition profile of a rice NLR immune receptor. *ELife*, *8*. https://doi.org/10.7554/ELIFE.47713

Dean, R. A. (1997). Signal pathways and appressorium morphogenesis. *Annu. Rev. Phytopathol*, *35*, 211–245. https://doi.org/10.1146/annurev.phyto.35.1.211

Dean, R. A., Talbot, N. J., Ebbole, D. J., Farman, M. L., Mitchell, T. K., Orbach, M. J., … Dirren, B. W. (2005). The genome sequence of the rice blast fungus Magnaporthe grisea. *Nature*, *434*(7036), 980–986. https://doi.org/10.1038/nature03449

Dean, R., Van Kan, J. A. L., Pretorius, Z. A., Hammond-Kosack, K. E., Di Pietro, A., Spanu, P. D., … Foster, G. D. (2012). The top 10 fungal pathogens in molecular plant pathology. *Molecular Plant Pathology*, *13*(4), 414–430. https://doi.org/10.1111/j.1364-3703.2011.00783.x

Delic, M., Valli, M., Graf, A. B., Pfeffer, M., Mattanovich, D., & Gasser, B. (2013). The secretory pathway: exploring yeast diversity. *FEMS Microbiology Reviews*, *37*(6), 872–914. https://doi.org/10.1111/1574-6976.12020

Denay, G., Vachon, G., Dumas, R., Zubieta, C., & Parcy, F. (2017). Plant SAM-domain proteins start to reveal their roles. *Trends in Plant Science*, *22*(8), 718–725. https://doi.org/10.1016/J.TPLANTS.2017.06.006

Dephoure, N., Gould, K. L., Gygi, S. P., & Kellogg, D. R. (2013). Mapping and analysis of phosphorylation sites: A quick guide for cell biologists. *Molecular Biology of the Cell*, *24*(5), 535–542. https://doi.org/10.1091/mbc.e12-09-0677/asset/images/large/535fig2.jpeg

Dephoure, N., Zhou, C., Villén, J., Beausoleil, S. A., Bakalarski, C. E., Elledge, S. J., & Gygi,

S. P. (2008). A quantitative atlas of mitotic phosphorylation. *Proceedings of the National Academy of Sciences of the United States of America*, *105*(31), 10762–10767. https://doi.org/10.1073/PNAS.0805139105

Desveaux, D., Singer, A. U., Wu, A. J., McNulty, B. C., Musselwhite, L., Nimchuk, Z., … Dangl, J. L. (2007). Type III effector activation via nucleotide binding, phosphorylation, and host target interaction. *PLoS Pathogens*, *3*(3). https://doi.org/10.1371/JOURNAL.PPAT.0030048

Deutschbauer, A. M., Williams, R. M., Chu, A. M., & Davis, R. W. (2002). Parallel phenotypic analysis of sporulation and postgermination growth in Saccharomyces cerevisiae. *Proceedings of the National Academy of Sciences*, *99*(24), 15530–15535. https://doi.org/10.1073/PNAS.202604399

DeZwaan, T. M., Carroll, A. M., Valent, B., & Sweigard, J. A. (1999). Magnaporthe grisea Pth11p is a novel plasma membrane protein that mediates appressorium differentiation in response to inductive substrate cues. *Plant Cell*, *11*(10), 2013–2030. https://doi.org/10.1105/tpc.11.10.2013

Dhanasekaran, D. N., Kashef, K., Lee, C. M., Xu, H., & Reddy, E. P. (2007). Scaffold proteins of MAP-kinase modules. *Oncogene 2007 26:22*, *26*(22), 3185–3202. https://doi.org/10.1038/sj.onc.1210411

Di Pietro, A., García-MacEira, F. I., Méglecz, E., & Roncero, M. I. (2001). A MAP kinase of the vascular wilt fungus Fusarium oxysporum is essential for root penetration and pathogenesis. *Molecular Microbiology*, *39*(5), 1140–1152. Retrieved from http://www.ncbi.nlm.nih.gov/pubmed/11251832

Dilcher, M., Köhler, B., & Von Mollard, G. F. (2001). Genetic interactions with the yeast Q-SNARE VTI1 Reveal Novel Functions for the R-SNARE YKT6. *Journal of Biological Chemistry*, *276*(37), 34537–34544. https://doi.org/10.1074/JBC.M101551200

Dóczi, R., ökrész, L., Romero, A. E., Paccanaro, A., & Bögre, L. (2012). Exploring the evolutionary path of plant MAPK networks. *Trends in Plant Science*, *17*(9), 518–525. https://doi.org/10.1016/J.TPLANTS.2012.05.009

Doehlemann, G., Berndt, P., & Hahn, M. (2006). Different signalling pathways involving a Galpha protein, cAMP and a MAP kinase control germination of Botrytis cinerea conidia. *Molecular Microbiology*, *59*(3), 821–835. https://doi.org/10.1111/J.1365-2958.2005.04991.X

Dulal, N., Rogers, A., Wang, Y., & Egan, M. (2020). Dynamic assembly of a higher-order

septin structure during appressorium morphogenesis by the rice blast fungus. *Fungal Genetics and Biology : FG & B, 140*. https://doi.org/10.1016/J.FGB.2020.103385

Ebbole, D. J. (2007). Magnaporthe as a model for understanding host-pathogen interactions. *Annual Review of Phytopathology, 45*(1), 437–456. https://doi.org/10.1146/annurev.phyto.45.062806.094346

Elion, E.A. (2015). MAP kinase modules in signaling. *Reference Module in Biomedical Sciences.* https://doi.org/10.1016/B978-0-12-801238-3.98742-7

Elion, E. A., Brill, J. A., & Fink, G. R. (1991). FUS3 represses CLN1 and CLN2 and in concert with KSS1 promotes signal transduction. *Proceedings of the National Academy of Sciences of the United States of America, 88*(21), 9392–9396. https://doi.org/10.1073/PNAS.88.21.9392

Elion, E. A., Grisafi, P. L., & Fink, G. R. (1990). FUS3 encodes a cdc2+/CDC28-related kinase required for the transition from mitosis into conjugation. *Cell, 60*(4), 649–664. https://doi.org/10.1016/0092-8674(90)90668-5

Errede, B., Vered, L., Ford, E., Pena, M. I., & Elston, T. C. (2015). Pheromone-induced morphogenesis and gradient tracking are dependent on the MAPK Fus3 binding to Gα. *Molecular Biology of the Cell, 26*(18), 3343–3358. https://doi.org/10.1091/MBC.E15-03-0176/ASSET/IMAGES/LARGE/3343FIG10.JPEG

Eseola, A. B., Ryder, L. S., Osés-Ruiz, M., Findlay, K., Yan, X., Cruz-Mireles, N., … Talbot, N. J. (2021). Investigating the cell and developmental biology of plant infection by the rice blast fungus Magnaporthe oryzae. *Fungal Genetics and Biology, 154*, 103562. https://doi.org/10.1016/J.FGB.2021.103562

Farhan, H., & Rabouille, C. (2011). Signalling to and from the secretory pathway. *Journal of Cell Science, 124*(2), 171–180. https://doi.org/10.1242/JCS.076455

Farhan, H., Wendeler, M. W., Mitrovic, S., Fava, E., Silberberg, Y., Sharan, R., … Hauri, H. P. (2010). MAPK signaling to the early secretory pathway revealed by kinase/phosphatase functional screening. *The Journal of Cell Biology, 189*(6), 997–1011. https://doi.org/10.1083/JCB.200912082

Fausto, A., Rodrigues, M. L., & Coelho, C. (2019). The Still Underestimated Problem of Fungal Diseases Worldwide. *Frontiers in Microbiology, 10*(FEB). https://doi.org/10.3389/FMICB.2019.00214

Fernández-Niño, S. M. G., Smith-Moritz, A. M., Chan, L. J. G., Adams, P. D., Heazlewood,

J. L., & Petzold, C. J. (2015). Standard flow liquid chromatography for shotgun proteomics in bioenergy research. *Frontiers in Bioengineering and Biotechnology*, *3*(APR), 44. https://doi.org/10.3389/FBIOE.2015.00044/ABSTRACT

Fernandez, J., & Wilson, R. A. (2014). Cells in cells: morphogenetic and metabolic strategies conditioning rice infection by the blast fungus Magnaporthe oryzae. *Protoplasma*, *251*(1), 37–47. https://doi.org/10.1007/s00709-013-0541-8

Finn, R. D., Bateman, A., Clements, J., Coggill, P., Eberhardt, R. Y., Eddy, S. R., … Punta, M. (2014). Pfam: the protein families database. *Nucleic Acids Research*, *42*(D1), D222–D230. https://doi.org/10.1093/nar/gkt1223

Fisher, M. C., Henk, D. A., Briggs, C. J., Brownstein, J. S., Madoff, L. C., McCraw, S. L., & Gurr, S. J. (2012). Emerging fungal threats to animal, plant and ecosystem health. *Nature*, *484*(7393), 186–194. https://doi.org/10.1038/nature10947

Foster, A. J., Ryder, L. S., Kershaw, M. J., & Talbot, N. J. (2017). The role of glycerol in the pathogenic lifestyle of the rice blast fungus Magnaporthe oryzae. *Environmental Microbiology*, *19*(3), 1008–1016. https://doi.org/10.1111/1462-2920.13688

Foster, A. J., Were, V. M., Yan, X., Win, J., Harant, A., Langner, T., … Talbot, N. J. (2021). MagnaGenes (v.1.0): an open science database of gene function studies in the blast fungus Magnaporthe oryzae. https://doi.org/10.5281/ZENODO.4647766

Franz-Wachtel, M., Eisler, S. A., Krug, K., Wahl, S., Carpy, A., Nordheim, A., … Macek, B. (2012). Global detection of protein kinase D-dependent phosphorylation events in nocodazole-treated human cells. *Molecular & Cellular Proteomics : MCP*, *11*(5), 160–170. https://doi.org/10.1074/MCP.M111.016014

Frawley, D., & Bayram, Ö. (2020). The pheromone response module, a mitogen-activated protein kinase pathway implicated in the regulation of fungal development, secondary metabolism and pathogenicity. *Fungal Genetics and Biology*, *144*, 103469. https://doi.org/10.1016/J.FGB.2020.103469

Fu, T., Shin, J.-H., Lee, N.-H., Lee, K. H., & Kim, K. S. (2022). Mitogen-activated protein kinase CsPMK1 is essential for pepper fruit anthracnose by Colletotrichum scovillei. *Frontiers in Microbiology*, *13*. https://doi.org/10.3389/FMICB.2022.770119

Garrenton, L. S., Young, S. L., & Thorner, J. (2006). Function of the MAPK scaffold protein, Ste5, requires a cryptic PH domain. *Genes & Development*, *20*(14), 1946. https://doi.org/10.1101/GAD.1413706

Gartner, A., Nasmyth, K., & Ammerer, G. (1992). Signal transduction in Saccharomyces cerevisiae requires tyrosine and threonine phosphorylation of FUS3 and KSS1. *Genes & Development*, *6*(7), 1280–1292. https://doi.org/10.1101/GAD.6.7.1280

Ghosh, P. N., Fisher, M. C., & Bates, K. A. (2018). Diagnosing emerging fungal threats: a one health perspective. *Frontiers in Genetics*, *9*, 376. https://doi.org/10.3389/fgene.2018.00376

Gilbert, R. D., Johnson, A. M., & Dean, R. A. (1996). Chemical signals responsible for appressorium formation in the rice blast fungus Magnaporthe grisea. *Physiological and Molecular Plant Pathology*, *48*(5), 335–346. https://doi.org/10.1006/PMPP.1996.0027

Giraldo, M. C., Dagdas, Y. F., Gupta, Y. K., Mentlak, T. A., Yi, M., Martinez-Rocha, A. L., … Valent, B. (2013). Two distinct secretion systems facilitate tissue invasion by the rice blast fungus Magnaporthe oryzae. *Nature Communications*, *4*(1), 1–12. https://doi.org/10.1038/ncomms2996

Gnad, F., Doll, S., Song, K., Stokes, M. P., Moffat, J., Liu, B., … Belvin, M. (2016). Phosphoproteome analysis of the MAPK pathway reveals previously undetected feedback mechanisms. *Proteomics*, *16*(14), 1998–2004. https://doi.org/10.1002/PMIC.201600119

Gratz, R., Brumbarova, T., Ivanov, R., Trofimov, K., Tünnermann, L., Ochoa-Fernandez, R., … Bauer, P. (2020). Phospho-mutant activity assays provide evidence for alternative phospho-regulation pathways of the transcription factor FER-LIKE IRON DEFICIENCY-INDUCED TRANSCRIPTION FACTOR. *The New Phytologist*, *225*(1), 250–267. https://doi.org/10.1111/NPH.16168

Grimshaw, S., Mott, H. R., Stott, K. M., Nielsen, P. R., Evetts, K. A., Hopkins, L. J., ... Owen, D. (2004). Structure of the sterile α- motif (SAM) domain of the Saccharomyces cerevisiae mitogen-activated protein kinase pathway-modulating protein Ste50 and analysis of its interaction with the Ste11 SAM. Journal of Biological Chemistry. 279 (3) 2192-2201. https://doi.org/10.1074/jbc.M305605200

Gruhler, A., Olsen, J. V., Mohammed, S., Mortensen, P., Færgeman, N. J., Mann, M., & Jensen, O. N. (2005). Quantitative phosphoproteomics applied to the yeast pheromone signaling pathway. *Molecular & Cellular Proteomics : MCP*, *4*(3), 310–327. https://doi.org/10.1074/MCP.M400219-MCP200

Gu, S. qin, Yang, Y., Li, P., Zhang, C. zhi, Fan, Y., Zhang, X. yu, … Dong, J. gao. (2013). Stk2, a mitogen-activated protein kinase from setosphaeria turcica, specifically

complements the functions of the Fus3 and Kss1 of Saccharomyces cerevisiae in filamentation, invasive growth, and mating behavior. *Journal of Integrative Agriculture*, *12*(12), 2209–2216. https://doi.org/10.1016/S2095-3119(13)60296-8

Guo, H., Ahn, H. K., Sklenar, J., Huang, J., Ma, Y., Ding, P., … Jones, J. D. G. (2020). Phosphorylation-regulated activation of the Arabidopsis RRS1-R/RPS4 immune receptor complex reveals two distinct effector recognition mechanisms. *Cell Host & Microbe*, *27*(5), 769-781.e6. https://doi.org/10.1016/J.CHOM.2020.03.008

Guo, J., Dai, X., Xu, J. R., Wang, Y., Bai, P., Liu, F., … Kang, Z. (2011). Molecular characterization of a Fus3/Kss1 type MAPK from Puccinia striiformis f. sp. tritici, PsMAPK1. *PLoS ONE*, *6*(7). https://doi.org/10.1371/JOURNAL.PONE.0021895

Gupta, Y. K., Dagdas, Y. F., Martinez-Rocha, A.-L., Kershaw, M. J., Littlejohn, G. R., Ryder, L. S., … Talbot, N. J. (2015). Septin-dependent assembly of the exocyst is essential for plant infection by Magnaporthe oryzae. *The Plant Cell*, *27*(11), 3277–3289. https://doi.org/10.1105/tpc.15.00552

Gustin, M. C., Albertyn, J., Alexander, M., & Davenport, K. (1998). MAP kinase pathways in the yeast Saccharomyces cerevisiae. *Microbiology and Molecular Biology Reviews*, *62*(4), 1264. https://doi.org/10.1128/mmbr.62.4.1264-1300.1998

Hamel, L.-P., Nicole, M.-C., Duplessis, S., & Ellis, B. E. (2012). Mitogen-activated protein kinase signaling in plant-interacting fungi: distinct messages from conserved messengers. *The Plant Cell*, *24*(4), 1327–1351. https://doi.org/10.1105/tpc.112.096156

Hamer, J. E., Howard, R. J., Chumley, F. G., & Valent, B. (1988). A mechanism for surface attachment in spores of a plant pathogenic fungus. *Science*, *239*(4837), 288–290. https://doi.org/10.1126/science.239.4837.288

Harris, K., Lamson, R. E., Nelson, B., Hughes, T. R., Marton, M. J., Roberts, C. J., … Pryciak, P. M. (2001). Role of scaffolds in MAP kinase pathway specificity revealed by custom design of pathway-dedicated signaling proteins. *Current Biology*, *11*(23), 1815–1824. https://doi.org/10.1016/S0960-9822(01)00567-X/ATTACHMENT/6F146C29-DF6E-466D-B17D-685161AF2625/MMC1.PDF

Hazzalin, C. A., & Mahadevan, L. C. (2002). MAPK-regulated transcription: a continuously variable gene switch? *Nature Reviews Molecular Cell Biology 2002 3:1*, *3*(1), 30–40. https://doi.org/10.1038/nrm715

He, P., Wang, Y., Wang, X., Zhang, X., & Tian, C. (2017). The mitogen-activated protein

kinase CgMK1 governs appressorium formation, melanin synthesis, and plant infection of Colletotrichum gloeosporioides. *Frontiers in Microbiology*, *8*(NOV). https://doi.org/10.3389/FMICB.2017.02216

Hensel, G., Kastner, C., Oleszczuk, S., Riechen, J., & Kumlehn, J. (2009). Agrobacterium-mediated gene transfer to cereal crop plants: current protocols for barley, wheat, triticale, and maize. *International Journal of Plant Genomics*, *2009*. https://doi.org/10.1155/2009/835608

Hewezi, T., Juvale, P. S., Piya, S., Maier, T. R., Rambani, A., Rice, J. H., … Baum, T. J. (2015). The cyst nematode effector protein 10a07 targets and recruits host posttranslational machinery to mediate its nuclear trafficking and to promote parasitism in Arabidopsis. *The Plant Cell*, *27*(3), 891–907. https://doi.org/10.1105/TPC.114.135327

Hoehenwarter, W., Thomas, M., Nukarinen, E., Egelhofer, V., Rohrig, H., Weckwerth, W., … Beckers, G. J. M. (2013). Identification of novel *in vivo* MAP kinase substrates in Arabidopsis thaliana through use of tandem metal oxide affinity chromatography. *Molecular & Cellular Proteomics : MCP*, *12*(2), 369–380. https://doi.org/10.1074/MCP.M112.020560

Horbach, R., Navarro-Quesada, A. R., Knogge, W., & Deising, H. B. (2011). When and how to kill a plant cell: Infection strategies of plant pathogenic fungi. *Journal of Plant Physiology*, *168*(1), 51–62. https://doi.org/10.1016/J.JPLPH.2010.06.014

Howard, R. J., Ferrari, M. A., Roach, D. H., & Money, N. P. (1991). Penetration of hard substrates by a fungus employing enormous turgor pressures. *Proceedings of the National Academy of Sciences of the United States of America*, *88*(24), 11281. https://doi.org/10.1073/PNAS.88.24.11281

Howard, R. J., & Valent, B. (1996). Breaking and entering: Host penetration by the fungal rice blast pathogen Magnaporthe grisea. *Annual Review of Microbiology*, *50*(1), 491–512. https://doi.org/10.1146/annurev.micro.50.1.491

Hu, H., Gourguechon, S., Wang, C. C., & Li, Z. (2016). The G1 cyclin-dependent kinase CRK1 in Trypanosoma brucei regulates anterograde protein transport by phosphorylating the COPII subunit Sec31. *Journal of Biological Chemistry*, *291*(30), 15527–15539. https://doi.org/10.1074/JBC.M116.715185

Huang, J., Si, W., Deng, Q., Li, P., & Yang, S. (2014). Rapid evolution of avirulence genes in rice blast fungus Magnaporthe oryzae. *BMC Genetics*, *15*(1), 45.

https://doi.org/10.1186/1471-2156-15-45

Islam, M. T., Croll, D., Gladieux, P., Soanes, D. M., Persoons, A., Bhattacharjee, P., … Kamoun, S. (2016). Emergence of wheat blast in Bangladesh was caused by a South American lineage of *Magnaporthe oryzae*. *BMC Biology*, *14*(1), 84. https://doi.org/10.1186/s12915-016-0309-7

Islam, M. T., Kim, K.-H., & Choi, J. (2019). Wheat blast in Bangladesh: the current situation and future impacts. *The Plant Pathology Journal*, *35*(1), 1. https://doi.org/10.5423/PPJ.RW.08.2018.0168

Itakura, A. K., Chakravarty, A. K., Jakobson, C. M., & Jarosz, D. F. (2020). Widespread prion-based control of growth and differentiation strategies in Saccharomyces cerevisiae. *Molecular Cell*, *77*(2), 266. https://doi.org/10.1016/J.MOLCEL.2019.10.027

Jagodzik, P., Tajdel-Zielinska, M., Ciesla, A., Marczak, M., & Ludwikow, A. (2018). Mitogen-activated protein kinase cascades in plant hormone signaling. *Frontiers in Plant Science*, *9*, 1387. https://doi.org/10.3389/fpls.2018.01387

Jenczmionka, N. J., & Schäfer, W. (2005). The Gpmk1 MAP kinase of Fusarium graminearum regulates the induction of specific secreted enzymes. *Current Genetics*, *47*(1), 29–36. https://doi.org/10.1007/s00294-004-0547-z

Jiang, C., Zhang, X., Liu, H., & Xu, J.-R. (2018). Mitogen-activated protein kinase signaling in plant pathogenic fungi. *PLOS Pathogens*, *14*(3), e1006875. https://doi.org/10.1371/journal.ppat.1006875

Jones, J. D. G., & Dangl, J. L. (2006). The plant immune system. *Nature*, *444*(7117), 323–329. https://doi.org/10.1038/nature05286

Jonkers, W., Fischer, M. S., Do, H. P., Starr, T. L., & Louise Glass, N. (2016). Chemotropism and cell fusion in Neurospora crassa relies on the formation of distinct protein complexes by HAM-5 and a novel protein HAM-14. *Genetics*, *203*(1), 319. https://doi.org/10.1534/GENETICS.115.185348

Jonkers, W., Leeder, A. C., Ansong, C., Wang, Y., Yang, F., Starr, T. L., … Glass, N. L. (2014). HAM-5 functions as a MAP kinase scaffold during cell fusion in Neurospora crassa. *PLoS Genetics*, *10*(11). https://doi.org/10.1371/JOURNAL.PGEN.1004783

Jun, S. C., Kim, J. H., & Han, K. H. (2020). The conserved MAP kinase MpkB regulates development and sporulation without affecting aflatoxin biosynthesis in Aspergillus flavus. *Journal of Fungi (Basel, Switzerland)*, *6*(4), 1–16.

https://doi.org/10.3390/JOF6040289

Kankanala, P., Czymmek, K., & Valent, B. (2007). Roles for rice membrane dynamics and plasmodesmata during biotrophic invasion by the blast fungus. *The Plant Cell*, *19*(2), 706–724. https://doi.org/10.1105/tpc.106.046300

Kawamata, T., Kamada, Y., Kabeya, Y., Sekito, T., & Ohsumi, Y. (2008). Organization of the pre-autophagosomal structure responsible for autophagosome formation. *Molecular Biology of the Cell*, *19*(5), 2039. https://doi.org/10.1091/MBC.E07-10-1048

Kershaw, M. J., & Talbot, N. J. (2009). Genome-wide functional analysis reveals that infection-associated fungal autophagy is necessary for rice blast disease. *Proceedings of the National Academy of Sciences*, *106*(37), 15967–15972. https://doi.org/10.1073/PNAS.0901477106

Khang, C. H., Berruyer, R., Giraldo, M. C., Kankanala, P., Park, S. Y., Czymmek, K., … Valent, B. (2010). Translocation of Magnaporthe oryzae effectors into rice cells and their subsequent cell-to-cell movement. *Plant Cell*, *22*(4), 1388–1403. https://doi.org/10.1105/tpc.109.069666

Khoury, G. A., Baliban, R. C., & Floudas, C. A. (2011). Proteome-wide post-translational modification statistics: frequency analysis and curation of the swiss-prot database. *Scientific Reports 2011 1:1*, *1*(1), 1–5. https://doi.org/10.1038/srep00090

Khush, G. S. (2005). What it will take to Feed 5.0 Billion Rice consumers in 2030. *Plant Molecular Biology*, *59*(1), 1–6. https://doi.org/10.1007/s11103-005-2159-5

Kim, C. A., & Bowie, J. U. (2003). SAM domains: uniform structure, diversity of function. *Trends in Biochemical Sciences*, *28*(12), 625–628. https://doi.org/10.1016/J.TIBS.2003.11.001

Kim, K. Y., Truman, A. W., & Levin, D. E. (2008). Yeast Mpk1 mitogen-activated protein kinase activates transcription through Swi4/Swi6 by a noncatalytic mechanism that requires upstream signal. *Molecular and Cellular Biology*, *28*(8), 2579–2589. https://doi.org/10.1128/MCB.01795-07

Kim, S., Kim, C. Y., Park, S. Y., Kim, K. T., Jeon, J., Chung, H., … Lee, Y. H. (2020). Two nuclear effectors of the rice blast fungus modulate host immunity via transcriptional reprogramming. *Nature Communications 2020 11:1*, *11*(1), 1–11. https://doi.org/10.1038/s41467-020-19624-w

Kim, S., Park, S. Y., Kim, K. S., Rho, H. S., Chi, M. H., Choi, J., … Lee, Y. H. (2009).

Homeobox transcription factors are required for conidiation and appressorium development in the rice blast fungus Magnaporthe oryzae. *PLOS Genetics*, *5*(12), e1000757. https://doi.org/10.1371/JOURNAL.PGEN.1000757

Kim, Soonok, Ahn, I.-P., Rho, H.-S., & Lee, Y.-H. (2005). MHP1, a Magnaporthe grisea hydrophobin gene, is required for fungal development and plant colonization. *Molecular Microbiology*, *57*(5), 1224–1237. https://doi.org/10.1111/j.1365-2958.2005.04750.x

Knight, M. J., Leettola, C., Gingery, M., Li, H., & Bowie, J. U. (2011). A human sterile alpha motif domain polymerizome. *Protein Science : A Publication of the Protein Society*, *20*(10), 1697. https://doi.org/10.1002/PRO.703

Kobayashi, M., Utsushi, H., Fujisaki, K., Takeda, T., Yamashita, T., & Terauchi, R. (2022). A jacalin-like lectin domain-containing protein of Sclerospora graminicola acts as an apoplastic virulence effector in plant-oomycete interactions. *Molecular Plant Pathology*. https://doi.org/10.1111/MPP.13197

Koeck, M., Hardham, A. R., & Dodds, P. N. (2011). The role of effectors of biotrophic and hemibiotrophic fungi in infection. *Cellular Microbiology*, *13*(12), 1849–1857. https://doi.org/10.1111/j.1462-5822.2011.01665.x

Kong, S., Park, S. Y., & Lee, Y. H. (2015). Systematic characterization of the bZIP transcription factor gene family in the rice blast fungus, Magnaporthe oryzae. *Environmental Microbiology*, *17*(4), 1425–1443. https://doi.org/10.1111/1462-2920.12633

Kou, Y., Tan, Y. H., Ramanujam, R., & Naqvi, N. I. (2017). Structure-function analyses of the Pth11 receptor reveal an important role for CFEM motif and redox regulation in rice blast. *The New Phytologist*, *214*(1), 330–342. https://doi.org/10.1111/NPH.14347

Krisak, L., Strich, R., Winters, R. S., Hall, J. P., Mallory, M. J., Kreitzer, D., … Winter, E. (1994). SMK1, a developmentally regulated MAP kinase, is required for spore wall assembly in Saccharomyces cerevisiae. *Genes & Development*, *8*(18), 2151–2161. https://doi.org/10.1101/GAD.8.18.2151

Kumar, S., Stecher, G., Li, M., Knyaz, C., & Tamura, K. (2018). MEGA X: Molecular evolutionary genetics analysis across computing platforms. *Molecular Biology and Evolution*, *35*(6), 1547–1549. https://doi.org/10.1093/MOLBEV/MSY096

Kyriakis, J. M., & Avruch, J. (2012). Mammalian MAPK signal transduction pathways activated by stress and inflammation: A 10-year update. *Physiological Reviews*, *92*(2),

689–737.
https://doi.org/10.1152/PHYSREV.00028.2011/ASSET/IMAGES/LARGE/Z9J002122
6100012.JPEG

Lake, D., Corrêa, S. A. L., & Müller, J. (2016). Negative feedback regulation of the ERK1/2 MAPK pathway. *Cellular and Molecular Life Sciences*, *73*(23), 4397. https://doi.org/10.1007/S00018-016-2297-8

Lamson, R. E., Takahashi, S., Winters, M. J., & Pryciak, P. M. (2006). Dual role for membrane localization in yeast MAP kinase cascade activation and its contribution to signaling fidelity. *Current Biology : CB*, *16*(6), 618–623. https://doi.org/10.1016/J.CUB.2006.02.060

Landry, C. R., Levy, E. D., & Michnick, S. W. (2009). Weak functional constraints on phosphoproteomes. *Trends in Genetics*, *25*(5), 193–197. https://doi.org/10.1016/J.TIG.2009.03.003

Langner, T., Białas, A., & Kamoun, S. (2018). The blast fungus decoded: genomes in flux. *MBio*, *9*, e00571-18. https://doi.org/10.1128/mBio.00571-18

Lassowskat, I., Böttcher, C., Eschen-Lippold, L., Scheel, D., & Lee, J. (2014). Sustained mitogen-activated protein kinase activation reprograms defense metabolism and phosphoprotein profile in Arabidopsis thaliana. *Frontiers in Plant Science*, *5*, 554. https://doi.org/10.3389/fpls.2014.00554

Latorre, S. M., Reyes-Avila, C. S., Malmgren, A., Win, J., Kamoun, S., & Burbano, H. A. (2020). Differential loss of effector genes in three recently expanded pandemic clonal lineages of the rice blast fungus. *BMC Biology*, *18*(1). https://doi.org/10.1186/S12915-020-00818-Z

Lee, C. H., Shin, Y. K., Phung, T. T. H., Bae, J. S., Kang, Y. H., Nguyen, T. A., … Seo, Y. S. (2010). Involvement of Vts1, a structure-specific RNA-binding protein, in Okazaki fragment processing in yeast. *Nucleic Acids Research*, *38*(5), 1583. https://doi.org/10.1093/NAR/GKP1135

Lei, L., Stevens, D. M., & Coaker, G. (2020). Phosphorylation of the Pseudomonas effector AvrPtoB by Arabidopsis SnRK2.8 is required for bacterial virulence. *Molecular Plant*, *13*(10), 1513–1522. https://doi.org/10.1016/j.molp.2020.08.018/attachment/2c784e01-8dfb-471a-94e3-8f9a89091d95/mmc1.pdf

Leng, Y., & Zhong, S. (2015). The role of mitogen-activated protein (MAP) kinase signaling

components in the fungal development, stress response and virulence of the fungal cereal pathogen Bipolaris sorokiniana. *PLOS ONE, 10*(5), e0128291. https://doi.org/10.1371/JOURNAL.PONE.0128291

Lev, S, Sharon, A., Hadar, R., Ma, H., & Horwitz, B. A. (1999). A mitogen-activated protein kinase of the corn leaf pathogen Cochliobolus heterostrophus is involved in conidiation, appressorium formation, and pathogenicity: diverse roles for mitogen-activated protein kinase homologs in foliar pathogens. *Proceedings of the National Academy of Sciences of the United States of America, 96*(23), 13542–13547. https://doi.org/10.1073/pnas.96.23.13542

Lev, Sophie, & Horwitz, B. A. (2003). A mitogen-activated protein kinase pathway modulates the expression of two cellulase genes in Cochliobolus heterostrophus during plant infection. *The Plant Cell, 15*(4), 835–844. https://doi.org/10.1105/tpc.010546

Li, C., Sun, W., Cao, S., Hou, R., Li, X., Ming, L., … Liu, F. (2022). The CfMK1 gene regulates reproduction, appressorium formation, and pathogenesis in a pear anthracnose-causing fungus. *Journal of Fungi (Basel, Switzerland), 8*(1). https://doi.org/10.3390/JOF8010077

Li, G., Zhang, X., Tian, H., Choi, Y.-E., Tao, W. A., & Xu, J.-R. (2017). *MST50* is involved in multiple MAP kinase signaling pathways in *Magnaporthe oryzae. Environmental Microbiology, 19*(5), 1959–1974. https://doi.org/10.1111/1462-2920.13710

Li, G., Zhou, X., Kong, L., Wang, Y., Zhang, H., Zhu, H., … Xu, J.-R. (2011). MoSfl1 is important for virulence and heat tolerance in Magnaporthe oryzae. *PLoS ONE, 6*(5), e19951. https://doi.org/10.1371/journal.pone.0019951

Li, G., Zhou, X., & Xu, J.-R. (2012). Genetic control of infection-related development in Magnaporthe oryzae. *Current Opinion in Microbiology, 15*(6), 678–684. https://doi.org/10.1016/J.MIB.2012.09.004

Li, W., Yadeta, K. A., Elmore, J. M., & Coaker, G. (2013). The Pseudomonas syringae effector HopQ1 promotes bacterial virulence and interacts with tomato 14-3-3 proteins in a phosphorylation-dependent manner. *Plant Physiology, 161*(4), 2062–2074. https://doi.org/10.1104/PP.112.211748

Li, Y., & Wu, H. (2012). A clustering method based on k-means algorithm. *Physics Procedia, 25*, 1104–1109. https://doi.org/10.1016/J.PHPRO.2012.03.206

Liang, X., Wei, T., Cao, M., Zhang, X., Liu, W., Kong, Y., … Sun, G. (2019). The MAP kinase

CfPMK1 Is a Key regulator of pathogenesis, development, and stress tolerance of Colletotrichum fructicola. *Frontiers in Microbiology*, *10*, 1070. https://doi.org/10.3389/fmicb.2019.01070

Lienhard, G. E. (2008). Non-functional phosphorylations? *Trends in Biochemical Sciences*, *33*(8), 351–352. https://doi.org/10.1016/J.TIBS.2008.05.004

Liese, W., & Schmid, R. (1964). Über das Wachstum von Bläuepilzen durch verholzte Zellwände. *Journal of Phytopathology*, *51*(4), 385–393. https://doi.org/10.1111/j.1439-0434.1964.tb03445.x

Lilley, K. S., & Dupree, P. (2006). Methods of quantitative proteomics and their application to plant organelle characterization. *Journal of Experimental Botany*, *57*(7), 1493–1499. https://doi.org/10.1093/JXB/ERJ141

Lin, C. H., Yang, S. L., Wang, N. Y., & Chung, K. R. (2010). The FUS3 MAPK signaling pathway of the citrus pathogen Alternaria alternata functions independently or cooperatively with the fungal redox-responsive AP1 regulator for diverse developmental, physiological and pathogenic processes. *Fungal Genetics and Biology : FG & B*, *47*(4), 381–391. https://doi.org/10.1016/J.FGB.2009.12.009

Liu, W., Zhou, X., Li, G., Li, L., Kong, L., Wang, C., … Xu, J.-R. (2011). Multiple plant surface signals are sensed by different mechanisms in the rice blast fungus for appressorium formation. *PLoS Pathogens*, *7*(1), e1001261. https://doi.org/10.1371/journal.ppat.1001261

Liu, X., Zhou, Q., Guo, Z., Liu, P., Shen, L., Chai, N., … Zhang, Z. (2020). A self-balancing circuit centered on moosm1 kinase governs adaptive responses to host-derived ros in magnaporthe oryzae. *ELife*, *9*, 1–28. https://doi.org/10.7554/ELIFE.61605

Ma, B., Ning, Y. N., Li, C. X., Tian, D., Guo, H., Pang, X. M., … Feng, J. X. (2021). A mitogen-activated protein kinase PoxMK1 mediates regulation of the production of plant-biomass-degrading enzymes, vegetative growth, and pigment biosynthesis in Penicillium oxalicum. *Applied Microbiology and Biotechnology*, *105*(2). https://doi.org/10.1007/S00253-020-11020-0

MacLean, B., Tomazela, D. M., Shulman, N., Chambers, M., Finney, G. L., Frewen, B., … MacCoss, M. J. (2010). Skyline: an open source document editor for creating and analyzing targeted proteomics experiments. *Bioinformatics*, *26*(7), 966. https://doi.org/10.1093/BIOINFORMATICS/BTQ054

Marroquin-Guzman, M., Sun, G., & Wilson, R. A. (2017). Glucose-ABL1-TOR signaling

modulates cell cycle tuning to control terminal appressorial cell differentiation. *PLOS Genetics*, *13*(1), e1006557. https://doi.org/10.1371/journal.pgen.1006557

Mattila, P. K., Pykäläinen, A., Saarikangas, J., Paavilainen, V. O., Vihinen, H., Jokitalo, E., & Lappalainen, P. (2007). Missing-in-metastasis and IRSp53 deform PI(4,5)P2-rich membranes by an inverse BAR domain-like mechanism. *The Journal of Cell Biology*, *176*(7), 953–964. https://doi.org/10.1083/JCB.200609176

Mendgen, K., & Hahn, M. (2002). Plant infection and the establishment of fungal biotrophy. *Trends in Plant Science*, *7*(8), 352–356. https://doi.org/10.1016/S1360-1385(02)02297-5

Meng, Y., Zhang, X., Tang, D., Chen, X., Zhang, D., Chen, J., & Fang, W. (2021). A novel nitrogen and carbon metabolism regulatory cascade is implicated in entomopathogenicity of the fungus Metarhizium robertsii. *MSystems*, *6*(3). https://doi.org/10.1128/MSYSTEMS.00499-21

Menke, F. L. H., Kang, H.-G., Chen, Z., Park, J. M., Kumar, D., & Klessig, D. F. (2005). Tobacco transcription factor WRKY1 is phosphorylated by the MAP kinase SIPK and mediates HR-like cell death in tobacco. *Molecular Plant-Microbe Interactions*, *18*(10), 1027–1034. https://doi.org/10.1094/MPMI

Menke, F. L. H., Van Pelt, J. A., Pieterse, C. M. J., & Klessig, D. F. (2004). Silencing of the mitogen-activated protein kinase MPK6 compromises disease resistance in Arabidopsis. *The Plant Cell*, *16*(4), 897–907. https://doi.org/10.1105/TPC.015552

Mey, G., Oeser, B., Lebrun, M. H., & Tudzynski, P. (2002). The biotrophic, non-appressorium-forming grass pathogen Claviceps purpurea needs a Fus3/Pmk1 homologous mitogen-activated protein kinase for colonization of rye ovarian tissue. *Molecular Plant-Microbe Interactions : MPMI*, *15*(4), 303–312. https://doi.org/10.1094/MPMI.2002.15.4.303

Mithoe, S. C., Ludwig, C., Pel, M. J., Cucinotta, M., Casartelli, A., Mbengue, M., … Menke, F. L. (2016). Attenuation of pattern recognition receptor signaling is mediated by a MAP kinase kinase kinase. *EMBO Reports*, *17*(3), 441–454. https://doi.org/10.15252/embr.201540806

Mithoe, S. C., & Menke, F. L. H. (2011). Phosphoproteomics perspective on plant signal transduction and tyrosine phosphorylation. *Phytochemistry*, *72*(10), 997–1006. https://doi.org/10.1016/J.PHYTOCHEM.2010.12.009

Moriwaki, A., Kihara, J., Mori, C., & Arase, S. (2007). A MAP kinase gene, BMK1, is required

for conidiation and pathogenicity in the rice leaf spot pathogen Bipolaris oryzae. *Microbiological Research*, *162*(2), 108–114. https://doi.org/10.1016/J.MICRES.2006.01.014

Mosquera, G., Giraldo, M. C., Khang, C. H., Coughlan, S., & Valent, B. (2009). Interaction transcriptome analysis identifies Magnaporthe oryzae BAS1-4 as Biotrophy-associated secreted proteins in rice blast disease. *The Plant Cell, 21*(4), 1273–1290. https://doi.org/10.1105/tpc.107.055228

Müller, P., Aichinger, C., Feldbrügge, M., & Kahmann, R. (1999). The MAP kinase Kpp2 regulates mating and pathogenic development in Ustilago maydis. *Molecular Microbiology, 34*(5), 1007–1017. https://doi.org/10.1046/J.1365-2958.1999.01661.X

Müller, P., Weinzierl, G., Brachmann, A., Feldbrügge, M., & Kahmann, R. (2003). Mating and pathogenic development of the Smut fungus Ustilago maydis are regulated by one mitogen-activated protein kinase cascade. *Eukaryotic Cell, 2*(6), 1187–1199. https://doi.org/10.1128/EC.2.6.1187-1199.2003

Mutiga, S. K., Rotich, F., Were, V. M., Kimani, J. M., Mwongera, D. T., Mgonja, E., … Talbot, N. J. (2021). Integrated strategies for durable rice blast resistance in sub-saharan africa. *Plant Disease, 105*(10), 1–22. https://doi.org/10.1094/PDIS-03-21-0593-FE/ASSET/IMAGES/LARGE/PDIS-03-21-0593-FEF8.JPEG

Nadal-Ribelles, M., Solé, C., Martínez-Cebrián, G., Posas, F., & Nadal, E. de. (2018). Shaping the transcriptional landscape through MAPK signaling. *Gene Expression and Control.* https://doi.org/10.5772/INTECHOPEN.80634

Nakagami, H., Sugiyama, N., Mochida, K., Daudi, A., Yoshida, Y., Toyoda, T., … Shirasu, K. (2010). Large-scale comparative phosphoproteomics identifies conserved phosphorylation sites in plants. *Plant Physiology, 153*(3), 1161–1174. https://doi.org/10.1104/PP.110.157347

Nishi, H., Shaytan, A., & Panchenko, A. R. (2014). Physicochemical mechanisms of protein regulation by phosphorylation. *Frontiers in Genetics, 5*(AUG), 270. https://doi.org/10.3389/FGENE.2014.00270/BIBTEX

Nishimura, M., Park, G., & Xu, J.-R. (2003). The G-beta subunit MGB1 is involved in regulating multiple steps of infection-related morphogenesis in Magnaporthe grisea. *Molecular Microbiology, 50*(1), 231–243. Retrieved from http://www.ncbi.nlm.nih.gov/pubmed/14507377

O'Leary, N. A., Wright, M. W., Brister, J. R., Ciufo, S., Haddad, D., McVeigh, R., … Pruitt,

K. D. (2016). Reference sequence (RefSeq) database at NCBI: current status, taxonomic expansion, and functional annotation. *Nucleic Acids Research*, *44*(D1), D733–D745. https://doi.org/10.1093/NAR/GKV1189

Oliveira-Garcia, E., Tamang, T. M., Park, J., Dalby, M., Martin-Urdiroz, M., Herrero, C. R., … Valent, B. (2021). Clathrin-mediated endocytosis facilitates internalization of Magnaporthe oryzae effectors into rice cells. *BioRxiv*, 2021.12.28.474284. https://doi.org/10.1101/2021.12.28.474284

Olsen, J. V., Blagoev, B., Gnad, F., Macek, B., Kumar, C., Mortensen, P., & Mann, M. (2006). Global, *in vivo*, and site-specific phosphorylation dynamics in signaling networks. *Cell*, *127*(3), 635–648. https://doi.org/10.1016/J.CELL.2006.09.026

Olsen, J. V., & Mann, M. (2013). Status of large-scale analysis of post-translational modifications by mass spectrometry. *Molecular & Cellular Proteomics : MCP*, *12*(12), 3444. https://doi.org/10.1074/MCP.O113.034181

Osés-Ruiz, M., Cruz-Mireles, N., Martin-Urdiroz, M., Soanes, D. M., Eseola, A. B., Tang, B., … Talbot, N. J. (2021). Appressorium-mediated plant infection by Magnaporthe oryzae is regulated by a Pmk1-dependent hierarchical transcriptional network. *Nature Microbiology*, *6*(11), 1383–1397. https://doi.org/10.1038/S41564-021-00978-W

Osés-Ruiz, M., & Talbot, N. J. (2017). Cell cycle-dependent regulation of plant infection by the rice blast fungus Magnaporthe oryzae. *Communicative & Integrative Biology*, *10*(5–6), e1372067. https://doi.org/10.1080/19420889.2017.1372067

Pan, C. Q., Sudol, M., Sheetz, M., & Low, B. C. (2012). Modularity and functional plasticity of scaffold proteins as p(l)acemakers in cell signaling. *Cellular Signalling*, *24*(11), 2143–2165. https://doi.org/10.1016/J.CELLSIG.2012.06.002

Panwar, V., McCallum, B., & Bakkeren, G. (2013). Endogenous silencing of *Puccinia triticina* pathogenicity genes through *in planta* -expressed sequences leads to the suppression of rust diseases on wheat. *The Plant Journal*, *73*(3), 521–532. https://doi.org/10.1111/tpj.12047

Park, G., Xue, C., Zhao, X., Kim, Y., Orbach, M., & Xu, J.-R. (2006). Multiple upstream signals converge on the adaptor protein Mst50 in Magnaporthe grisea. *The Plant Cell*, *18*(10), 2822–2835. https://doi.org/10.1105/tpc.105.038422

Park, G., Xue, C., Zheng, L., Lam, S., & Xu, J.-R. (2002). MST12 regulates infectious growth but not appressorium formation in the rice blast fungus Magnaporthe grisea. *Molecular Plant-Microbe Interactions*, *15*(3), 183–192.

https://doi.org/10.1094/MPMI.2002.15.3.183

Park, J., Kong, S., Kim, S., Kang, S., & Lee, Y. H. (2014). Roles of forkhead-box transcription factors in controlling development, pathogenicity, and stress response in Magnaporthe oryzae. *The Plant Pathology Journal*, *30*(2), 136. https://doi.org/10.5423/PPJ.OA.02.2014.0018

Patkar, R. N., Benke, P. I., Qu, Z., Chen, Y. Y. C., Yang, F., Swarup, S., & Naqvi, N. I. (2015). A fungal monooxygenase-derived jasmonate attenuates host innate immunity. *Nature Chemical Biology*, *11*(9), 733–740. https://doi.org/10.1038/NCHEMBIO.1885

Pearson, G., Robinson, F., Beers Gibson, T., Xu, B., Karandikar, M., Berman, K., & Cobb, M. H. (2001). Mitogen-Activated Protein (MAP) kinase pathways:regulation and physiological functions. *Endocrine Reviews*, *22*(2), 153–183. https://doi.org/10.1210/EDRV.22.2.0428

Perez-Nadales, E., & Di Pietro, A. (2015). The transmembrane protein Sho1 cooperates with the mucin Msb2 to regulate invasive growth and plant infection in Fusarium oxysporum. *Molecular Plant Pathology*, *16*(6), 593–603. https://doi.org/10.1111/MPP.12217/SUPPINFO

Pérez-Nadales, E., & Di Pietro, A. (2011). The membrane mucin Msb2 regulates invasive growth and plant infection in Fusarium oxysporum. *The Plant Cell*, *23*(3), 1171–1185. https://doi.org/10.1105/tpc.110.075093

Peterson, A. C., Russell, J. D., Bailey, D. J., Westphall, M. S., & Coon, J. J. (2012). Parallel reaction monitoring for high resolution and high mass accuracy quantitative, targeted proteomics. *Molecular & Cellular Proteomics : MCP*, *11*(11), 1475. https://doi.org/10.1074/MCP.O112.020131

Petre, B., Contreras, M. P., Bozkurt, T. O., Schattat, M. H., Sklenar, J., Schornack, S., … Win, J. (2021). Host-interactor screens of Phytophthora infestans RXLR proteins reveal vesicle trafficking as a major effector-targeted process. *The Plant Cell*, *33*(5), 1447–1471. https://doi.org/10.1093/PLCELL/KOAB069

Pham, C. L. L., Rey, A., Lo, V., Soulès, M., Ren, Q., Meisl, G., … Sunde, M. (2016). Self-assembly of MPG1, a hydrophobin protein from the rice blast fungus that forms functional amyloid coatings, occurs by a surface-driven mechanism. *Scientific Reports*, *6*(1), 25288. https://doi.org/10.1038/srep25288

Pouysségur, J., & Lenormand, P. (2003). Fidelity and spatio-temporal control in MAP kinase (ERKs) signalling. *European Journal of Biochemistry*, *270*(16), 3291–3299.

https://doi.org/10.1046/J.1432-1033.2003.03707.X

Pryciak, P. M., & Huntress, F. A. (1998). Membrane recruitment of the kinase cascade scaffold protein Ste5 by the Gβγ complex underlies activation of the yeast pheromone response pathway. *Genes & Development*, *12*(17), 2684–2697. https://doi.org/10.1101/GAD.12.17.2684

Qi, L., Kim, Y., Jiang, C., Li, Y., Peng, Y., & Xu, J.-R. (2015). Activation of Mst11 and feedback inhibition of germ tube growth in Magnaporthe oryzae. *Molecular Plant-Microbe Interactions*, *28*(8), 881–891. https://doi.org/10.1094/MPMI-12-14-0391-R

Rajakulendran, T., Sahmi, M., Kurinov, I., Tyers, M., Therrien, M., & Sicheri, F. (2008). CNK and HYP form a discrete dimer by their SAM domains to mediate RAF kinase signaling. *Proceedings of the National Academy of Sciences*, *105*(8), 2836–2841. https://doi.org/10.1073/PNAS.0709705105

Ramachander, R., Kim, C.A., Phillips, M.L., Mackereth, C.D., Thanos, C.D., McIntosh, L.P. & Bowie, J.L. (2002). Oligomerization-dependent association of the SAM domains from Schizosaccharomyces pombe Byr2 and Ste4. *The Journal of Biological Chemistry*, 42 (18) 39585-39593. https://doi.org/10.1074/jbc.M207273200

Ramazi, S., & Zahiri, J. (2021). Post-translational modifications in proteins: resources, tools and prediction methods. *Database*, *2021*. https://doi.org/10.1093/DATABASE/BAAB012

Rauniyar, N. (2015). Parallel reaction monitoring: a targeted experiment performed using high resolution and high mass accuracy mass spectrometry. *International Journal of Molecular Sciences*, *16*(12), 28566. https://doi.org/10.3390/IJMS161226120

Rauyaree, P., Ospina-Giraldo, M. D., Kang, S., Bhat, R. G., Subbarao, K. V., Grant, S. J., & Dobinson, K. F. (2005). Mutations in VMK1, a mitogen-activated protein kinase gene, affect microsclerotia formation and pathogenicity in Verticillium dahliae. *Current Genetics*, *48*(2), 109–116. https://doi.org/10.1007/S00294-005-0586-0

Rispail, N., & Di Pietro, A. (2009). Fusarium oxysporum Ste12 controls invasive growth and virulence downstream of the Fmk1 MAPK cascade. *Molecular Plant-Microbe Interactions*, *22*(7), 830–839. https://doi.org/10.1094/MPMI-22-7-0830

Rispail, N., Soanes, D. M., Ant, C., Czajkowski, R., Grünler, A., Huguet, R., … Di Pietro, A. (2009). Comparative genomics of MAP kinase and calcium-calcineurin signalling components in plant and human pathogenic fungi. *Fungal Genetics and Biology : FG & B*, *46*(4), 287–298. https://doi.org/10.1016/J.FGB.2009.01.002

Rossomando, A. J., Payne, D. M., Weber, M. J., & Sturgill, T. W. (1989). Evidence that pp42, a major tyrosine kinase target protein, is a mitogen-activated serine/threonine protein kinase. *Proceedings of the National Academy of Sciences of the United States of America*, *86*(18), 6940–6943. https://doi.org/10.1073/PNAS.86.18.6940

Ruiz-Roldán, M. C., Maier, F. J., & Schäfer, W. (2001). PTK1 , a mitogen-activated-protein kinase gene, is required for conidiation, appressorium formation, and pathogenicity of Pyrenophora teres on barley. *Molecular Plant-Microbe Interactions*, *14*(2), 116–125. https://doi.org/10.1094/MPMI.2001.14.2.116

Rydén, M., Englund, M., & Ali, N. (2021). ProteoMill: efficient network-based functional analysis portal for proteomics data. *Bioinformatics*, *37*(20), 3491–3493. https://doi.org/10.1093/BIOINFORMATICS/BTAB373

Ryder, L. S., Cruz-Mireles, N., Molinari, C., Eisermann, I., Eseola, A., & Talbot, N. J. (2022). The appressorium at a glance. *Journal of Cell Science*, *In Press*

Ryder, L. S., Dagdas, Y. F., Mentlak, T. A., Kershaw, M. J., Thornton, C. R., Schuster, M., … Talbot, N. J. (2013). NADPH oxidases regulate septin-mediated cytoskeletal remodeling during plant infection by the rice blast fungus. *Proceedings of the National Academy of Sciences*, *110*(8), 3179–3184. https://doi.org/10.1073/pnas.1217470110

Ryder, L. S., & Talbot, N. J. (2015). Regulation of appressorium development in pathogenic fungi. *Current Opinion in Plant Biology*, *26*, 8–13. https://doi.org/10.1016/j.pbi.2015.05.013

Sakulkoo, W., Osés-Ruiz, M., Oliveira Garcia, E., Soanes, D. M., Littlejohn, G. R., Hacker, C., … Talbot, N. J. (2018). A single fungal MAP kinase controls plant cell-to-cell invasion by the rice blast fungus. *Science*, *359*(6382), 1399–1403. https://doi.org/10.1126/science.aaq0892

Salama, N. R., Chuang, J. S., & Schekman, R. W. (1997). Sec31 encodes an essential component of the COPII coat required for transport vesicle budding from the endoplasmic reticulum. *Molecular Biology of the Cell*, *8*(2), 205. https://doi.org/10.1091/MBC.8.2.205

Savage, S. R., & Zhang, B. (2020). Using phosphoproteomics data to understand cellular signaling: A comprehensive guide to bioinformatics resources. *Clinical Proteomics*, *17*(1), 1–18. https://doi.org/10.1186/S12014-020-09290-X/TABLES/7

Savary, S., Willocquet, L., Pethybridge, S. J., Esker, P., McRoberts, N., & Nelson, A. (2019). The global burden of pathogens and pests on major food crops. *Nature Ecology &*

Evolution, *3*(3), 430–439. https://doi.org/10.1038/s41559-018-0793-y

Schamber, A., Leroch, M., Diwo, J., Mendgen, K., & Hahn, M. (2010). The role of mitogen-activated protein (MAP) kinase signalling components and the Ste12 transcription factor in germination and pathogenicity of Botrytis cinerea. *Molecular Plant Pathology*, *11*(1), 105–119. https://doi.org/10.1111/J.1364-3703.2009.00579.X

Serrano, A., Illgen, J., Brandt, U., Thieme, N., Letz, A., Lichius, A., … Fleißner, A. (2018). Spatio-temporal MAPK dynamics mediate cell behavior coordination during fungal somatic cell fusion. *Journal of Cell Science*, *131*(9). https://doi.org/10.1242/JCS.213462

She, R., Chakravarty, A. K., Layton, C. J., Chircus, L. M., Andreasson, J. O. L., Damaraju, N., … Greenleaf, W. J. (2017). Comprehensive and quantitative mapping of RNA-protein interactions across a transcribed eukaryotic genome. *Proceedings of the National Academy of Sciences of the United States of America*, *114*(14), 3619–3624. https://doi.org/10.1073/PNAS.1618370114

Shi, Z., Christian, D., & Leung, H. (1998). Interactions between spore morphogenetic mutations affect cell types, sporulation, and pathogenesis in Magnaporthe grisea. *Molecular Plant-Microbe Interactions*, *11*(3), 199–207. https://doi.org/10.1094/MPMI.1998.11.3.199

Shikano, S., & Colley, K. J. (2013). Secretory pathway. *Encyclopedia of Biological Chemistry: Second Edition*, 203–209. https://doi.org/10.1016/B978-0-12-378630-2.00507-7

Shipston, M. J., & Tian, L. (2016). Posttranscriptional and posttranslational regulation of BK channels. *International Review of Neurobiology*, *128*, 91–126. https://doi.org/10.1016/BS.IRN.2016.02.012

Shively, C. A., Eckwahl, M. J., Dobry, C. J., Mellacheruvu, D., Nesvizhskii, A., & Kumar, A. (2013). Genetic networks inducing invasive growth in Saccharomyces cerevisiae identified through systematic genome-wide overexpression. *Genetics*, *193*(4), 1297–1310. https://doi.org/10.1534/GENETICS.112.147876/-/DC1/GENETICS.112.147876-3.PDF

Shuaib, A., Hartwell, A., Kiss-Toth, E., & Holcombe, M. (2016). Multi-compartmentalisation in the MAPK signalling pathway contributes to the emergence of oscillatory behaviour and to ultrasensitivity. *PLOS ONE*, *11*(5), e0156139. https://doi.org/10.1371/JOURNAL.PONE.0156139

Sievers, F., & Higgins, D. G. (2014). Clustal Omega, accurate alignment of very large numbers of sequences. *Methods in Molecular Biology (Clifton, N.J.), 1079*, 105–116. https://doi.org/10.1007/978-1-62703-646-7_6

Singh, P. K., Gahtyari, N. C., Roy, C., Roy, K. K., He, X., Tembo, B., … Chawade, A. (2021). Wheat blast: a disease spreading by intercontinental jumps and its management strategies. *Frontiers in Plant Science, 12,* 1467. https://doi.org/10.3389/FPLS.2021.710707/BIBTEX

Skamnioti, P., & Gurr, S. J. (2009, March). Against the grain: safeguarding rice from rice blast disease. *Trends in Biotechnology,* Vol. 27, pp. 141–150. https://doi.org/10.1016/j.tibtech.2008.12.002

Skorpil, P., Saad, M. M., Boukli, N. M., Kobayashi, H., Ares-Orpel, F., Broughton, W. J., & Deakin, W. J. (2005). NopP, a phosphorylated effector of Rhizobium sp. strain NGR234, is a major determinant of nodulation of the tropical legumes Flemingia congesta and Tephrosia vogelii. *Molecular Microbiology, 57*(5), 1304–1317. https://doi.org/10.1111/J.1365-2958.2005.04768.X

Soanes, D. M., Chakrabarti, A., Paszkiewicz, K. H., Dawe, A. L., & Talbot, N. J. (2012). Genome-wide transcriptional profiling of appressorium development by the rice blast fungus Magnaporthe oryzae. *PLoS Pathogens, 8*(2), e1002514. https://doi.org/10.1371/journal.ppat.1002514

Solomon, P. S., Waters, O. D. C., Simmonds, J., Cooper, R. M., & Oliver, R. P. (2005). The Mak2 MAP kinase signal transduction pathway is required for pathogenicity in Stagonospora nodorum. *Current Genetics, 48*(1), 60–68. https://doi.org/10.1007/S00294-005-0588-Y/FIGURES/5

Sopko, R., Huang, D., Preston, N., Chua, G., Papp, B., Kafadar, K., … Andrews, B. (2006). Mapping pathways and phenotypes by systematic gene overexpression. *Molecular Cell, 21*(3), 319–330. https://doi.org/10.1016/J.MOLCEL.2005.12.011

Sörensson, C., Lenman, M., Veide-Vilg, J., Schopper, S., Ljungdahl, T., Grøtli, M., … Andreasson, E. (2012). Determination of primary sequence specificity of Arabidopsis MAPKs MPK3 and MPK6 leads to identification of new substrates. *The Biochemical Journal, 446*(2), 271–278. https://doi.org/10.1042/BJ20111809

Spang, A. (2009). On vesicle formation and tethering in the ER–Golgi shuttle. *Current Opinion in Cell Biology, 21*(4), 531–536. https://doi.org/10.1016/J.CEB.2009.03.003

Strumillo, M. J., Oplová, M., Viéitez, C., Ochoa, D., Shahraz, M., Busby, B. P., … Beltrao,

P. (2019). Conserved phosphorylation hotspots in eukaryotic protein domain families. *Nature Communications 2019 10:1*, *10*(1), 1–11. https://doi.org/10.1038/s41467-019-09952-x

Swaffer, M. P., Jones, A. W., Flynn, H. R., Snijders, A. P., & Nurse, P. (2018). Quantitative phosphoproteomics reveals the signaling dynamics of cell-cycle kinases in the fission yeast Schizosaccharomyces pombe. *Cell Reports*, *24*(2), 503–514. https://doi.org/10.1016/J.CELREP.2018.06.036

Taj, G., Agarwal, P., Grant, M., & Kumar, A. (2010). MAPK machinery in plants: Recognition and response to different stresses through multiple signal transduction pathways. *Plant Signaling & Behavior*, *5*(11), 1370. https://doi.org/10.4161/PSB.5.11.13020

Takáč, T., & Šamaj, J. (2015). Advantages and limitations of shot-gun proteomic analyses on Arabidopsis plants with altered MAPK signaling. *Frontiers in Plant Science*, *6*(FEB), 107. https://doi.org/10.3389/FPLS.2015.00107/BIBTEX

Takano, Y., Kikuchi, T., Kubo, Y., Hamer, J. E., Mise, K., & Furusawa, I. (2000). The Colletotrichum lagenarium MAP kinase gene CMK1 regulates diverse aspects of fungal pathogenesis. *Molecular Plant-Microbe Interactions*, *13*(4), 374–383. https://doi.org/10.1094/MPMI.2000.13.4.374

Talbot, N J, Ebbole, D. J., & Hamer, J. E. (1993). Identification and characterization of MPG1, a gene involved in pathogenicity from the rice blast fungus Magnaporthe grisea. *The Plant Cell*, *5*(11), 1575–1590. https://doi.org/10.1105/tpc.5.11.1575

Talbot, N. J. (2003). On the trail of a cereal killer: exploring the biology of Magnaporthe grisea. *Annual Review of Microbiology*, *57*(1), 177–202. https://doi.org/10.1146/annurev.micro.57.030502.090957

Talbot, N. J. (2019). Appressoria. *Current Biology*, *29*(5), R144–R146. https://doi.org/10.1016/J.CUB.2018.12.050

Tang, J., Bai, J., Chen, X., Zheng, L., Liu, H., & Huang, J. (2020). Two protein kinases UvPmk1 and UvCDC2 with significant functions in conidiation, stress response and pathogenicity of rice false smut fungus Ustilaginoidea virens. *Current Genetics*, *66*(2), 409–420. https://doi.org/10.1007/S00294-019-01029-Y

Tembo, B., Mulenga, R. M., Sichilima, S., M'siska, K. K., Mwale, M., Chikoti, P. C., … Braun, H. J. (2020). Detection and characterization of fungus (Magnaporthe oryzae pathotype Triticum) causing wheat blast disease on rain-fed grown wheat (Triticum aestivum L.) in Zambia. *PLOS ONE*, *15*(9), e0238724.

https://doi.org/10.1371/journal.pone.0238724

Teufel, F., Almagro Armenteros, J. J., Johansen, A. R., Gíslason, M. H., Pihl, S. I., Tsirigos, K. D., … Nielsen, H. (2022). SignalP 6.0 predicts all five types of signal peptides using protein language models. *Nature Biotechnology 2022*, 1–3. https://doi.org/10.1038/s41587-021-01156-3

Theodosiou, A., & Ashworth, A. (2002). MAP kinase phosphatases. *Genome Biology*, *3*(7), reviews3009.1. https://doi.org/10.1186/GB-2002-3-7-REVIEWS3009

Toruño, T. Y., Stergiopoulos, I., & Coaker, G. (2016). Plant-pathogen effectors: cellular probes interfering with plant defenses in spatial and temporal manners. *Annual Review of Phytopathology*, *54*, 419–441. https://doi.org/10.1146/ANNUREV-PHYTO-080615-100204

Turjanski, A. G., Vaqué, J. P., & Gutkind, J. S. (2007). MAP kinases and the control of nuclear events. *Oncogene 2007 26:22*, *26*(22), 3240–3253. https://doi.org/10.1038/sj.onc.1210415

Turrà, D., Segorbe, D., & Di Pietro, A. (2014). Protein Kinases in plant-pathogenic fungi: conserved regulators of infection. *Annual Review of Phytopathology*, *52*(1), 267–288. https://doi.org/10.1146/annurev-phyto-102313-050143

Valent, B., Farrall, L., & Chumley, F. G. (1991). Magnaporthe grisea genes for pathogenicity and virulence identified through a series of backcrosses. *Genetics*, *127*(1), 87–101. https://doi.org/10.1093/GENETICS/127.1.87

Valent, B. (2021). The impact of blast disease: past, present, and future. *Methods in Molecular Biology (Clifton, N.J.)*, *2356*, 1–18. https://doi.org/10.1007/978-1-0716-1613-0_1

van Esse, H. P., Reuber, L., & van der Does, D. (2019). GM approaches to improve disease resistance in crops. *New Phytologist*, nph.15967. https://doi.org/10.1111/nph.15967

Van Ngo, H., & Mostowy, S. (2019). Role of septins in microbial infection. *Journal of Cell Science*, *132*(9). https://doi.org/10.1242/JCS.226266

Velásquez, A. C., Danve Castroverde, C. M., & Yang He, S. (2018). Review plant-pathogen warfare under changing climate conditions. *Current Biology*, *28*(10):R619-R634. https://doi.org/10.1016/j.cub.2018.03.054

Veneault-Fourrey, C., Barooah, M., Egan, M., Wakley, G., & Talbot, N. J. (2006). Autophagic fungal cell death is necessary for infection by the rice blast fungus.

Science, *312*(5773), 580–583. https://doi.org/10.1126/science.1124550

Wang, C., Zhang, S., Hou, R., Zhao, Z., Zheng, Q., Xu, Q., … Xu, J. R. (2011). Functional Analysis of the Kinome of the Wheat Scab Fungus Fusarium graminearum. *PLOS Pathogens*, *7*(12), e1002460. https://doi.org/10.1371/JOURNAL.PPAT.1002460

Wei, W., Xiong, Y., Zhu, W., Wang, N., Yang, G., & Peng, F. (2016). Colletotrichum higginsianum mitogen-activated protein kinase ChMK1: role in growth, cell wall integrity, colony melanization, and pathogenicity. *Frontiers in Microbiology*, *7*:1212. https://doi.org/10.3389/FMICB.2016.01212

Wei, Y. Y., Liang, S., Zhang, Y. R., Lu, J. P., Lin, F. C., & Liu, X. H. (2020). MoSec61β, the beta subunit of Sec61, is involved in fungal development and pathogenicity, plant immunity, and ER-phagy in Magnaporthe oryzae. *Virulence*, *11*(1), 1685. https://doi.org/10.1080/21505594.2020.1848983

Wei, Z., & Liu, H. T. (2002). MAPK signal pathways in the regulation of cell proliferation in mammalian cells. *Cell Research 2002 12:1*, *12*(1), 9–18. https://doi.org/10.1038/sj.cr.7290105

Whiteford, J., & Spanu, P. (2002). Hydrophobins and the interactions between fungi and plants. *Molecular Plant Pathology*, *3*(5), 391–400. Retrieved from http://www.ebi.ac.uk/clustalw/

Whitmarsh, A. J. (2007). Regulation of gene transcription by mitogen-activated protein kinase signaling pathways. *Biochimica et Biophysica Acta*, *1773*(8), 1285–1298. https://doi.org/10.1016/J.BBAMCR.2006.11.011

Widmann, C., Gibson, S., Jarpe, M. B., & Johnson, G. L. (1999). Mitogen-activated protein kinase: Conservation of a three-kinase module from yeast to human. *Physiological Reviews*, *79*(1), 143–180. https://doi.org/10.1152/PHYSREV.1999.79.1.143/ASSET/IMAGES/LARGE/JNP.JA04F13.JPEG

Wilson, R. A., & Talbot, N. J. (2009). Under pressure: investigating the biology of plant infection by Magnaporthe oryzae. *Nature Reviews Microbiology*, *7*(3), 185–195. https://doi.org/10.1038/nrmicro2032

Win, J., Chaparro-Garcia, A., Belhaj, K., Saunders, D. G. O., Yoshida, K., Dong, S., … Kamoun, S. (2012). Effector biology of plant-associated organisms: concepts and perspectives. *Cold Spring Harbor Symposia on Quantitative Biology*, *77*, 235–247. https://doi.org/10.1101/SQB.2012.77.015933

Witzel, F., Maddison, L., & Blüthgen, N. (2012). How scaffolds shape MAPK signaling: What we know and opportunities for systems approaches. *Frontiers in Physiology*, *3 DEC*, 475. https://doi.org/10.3389/FPHYS.2012.00475/BIBTEX

Wu, Y., Xu, L., Liu, J., Yin, Z., Gao, X., Feng, H., & Huang, L. (2017). A mitogen-activated protein kinase gene (VmPmk1) regulates virulence and cell wall degrading enzyme expression in Valsa mali. *Microbial Pathogenesis*, *111*, 298–306. https://doi.org/10.1016/J.MICPATH.2017.09.003

Xiao, Q., Miao, B., Bi, J., Wang, Z., & Li, Y. (2016). Prioritizing functional phosphorylation sites based on multiple feature integration. *Scientific Reports 2016 6:1*, *6*(1), 1–10. https://doi.org/10.1038/srep24735

Xiong, D., Yu, L., Shan, H., & Tian, C. (2021). CcPmk1 is a regulator of pathogenicity in Cytospora chrysosperma and can be used as a potential target for disease control. *Molecular Plant Pathology*, *22*(6), 710–726. https://doi.org/10.1111/MPP.13059

Xu, J. R., & Hamer, J. E. (1996). MAP kinase and cAMP signaling regulate infection structure formation and pathogenic growth in the rice blast fungus Magnaporthe grisea. *Genes & Development*, *10*(21), 2696–2706. Retrieved from http://www.ncbi.nlm.nih.gov/pubmed/8946911

Xu, J. R. (2000). MAP kinases in fungal pathogens. *Fungal Genetics and Biology*, *31*(3), 137–152. https://doi.org/10.1006/fgbi.2000.1237

Yamamoto, H., Fujioka, Y., Suzuki, S. W., Noshiro, D., Suzuki, H., Kondo-Kakuta, C., … Ohsumi, Y. (2016). The intrinsically disordered protein Atg13 mediates supramolecular assembly of autophagy initiation complexes. *Developmental Cell*, *38*(1), 86–99. https://doi.org/10.1016/J.DEVCEL.2016.06.015

Yan, X., Li, Y., Yue, X., Wang, C., Que, Y., Kong, D., … Wang, Z. (2011). Two novel transcriptional regulators are essential for infection-related morphogenesis and pathogenicity of the rice blast fungus Magnaporthe oryzae. *PLOS Pathogens*, *7*(12), e1002385. https://doi.org/10.1371/JOURNAL.PPAT.1002385

Yeam, I., Nguyen, H. P., & Martin, G. B. (2010). Phosphorylation of the Pseudomonas syringae effector AvrPto is required for FLS2/BAK1-independent virulence activity and recognition by tobacco. *The Plant Journal : For Cell and Molecular Biology*, *61*(1), 16–24. https://doi.org/10.1111/J.1365-313X.2009.04028.X

Yi, M., & Valent, B. (2013). Communication between filamentous pathogens and plants at the biotrophic interface. *Annual Review of Phytopathology*, *51*(1), 587–611.

https://doi.org/10.1146/annurev-phyto-081211-172916

Yue, X., Que, Y., Xu, L., Deng, S., Peng, Y., Talbot, N. J., & Wang, Z. (2016). ZNF1 encodes a putative C2H2 zinc-finger protein essential for appressorium differentiation by the rice blast fungus magnaporthe oryzae. *Molecular Plant-Microbe Interactions*, *29*(1), 22–35. https://doi.org/10.1094/MPMI-09-15-0201-R/ASSET/IMAGES/LARGE/MPMI-09-15-0201-R_F9.JPEG

Zhang, H., Xue, C., Kong, L., Li, G., & Xu, J.-R. (2011). A Pmk1-interacting gene is involved in appressorium differentiation and plant infection in Magnaporthe oryzae. *Eukaryotic Cell*, *10*(8), 1062–1070. https://doi.org/10.1128/EC.00007-11

Zhang, L., Chen, X. J., Lu, H. Bin, Xie, Z. P., & Staehelin, C. (2011). Functional analysis of the type 3 effector nodulation outer protein L (NopL) from Rhizobium sp. NGR234: symbiotic effects, phosphorylation, and interference with mitogen-activated protein kinase signaling. *The Journal of Biological Chemistry*, *286*(37), 32178–32187. https://doi.org/10.1074/JBC.M111.265942

Zhang, N., Luo, J., Rossman, A. Y., Aoki, T., Chuma, I., Crous, P. W., … Xu, J. R. (2016). Generic names in Magnaporthales. *IMA Fungus*, *7*(1), 155. https://doi.org/10.5598/IMAFUNGUS.2016.07.01.09

Zhang, S., Jiang, C., Zhang, Q., Qi, L., Li, C., & Xu, J. R. (2016). Thioredoxins are involved in the activation of the *PMK1* MAP kinase pathway during appressorium penetration and invasive growth in *Magnaporthe oryzae*. *Environmental Microbiology*, *18*(11), 3768–3784. https://doi.org/10.1111/1462-2920.13315

Zhang, S., & Xu, J. R. (2014). Effectors and Effector Delivery in Magnaporthe oryzae. *PLOS Pathogens*, *10*(1), e1003826. https://doi.org/10.1371/JOURNAL.PPAT.1003826

Zhang, S., & Klessig, D. F. (2001). MAPK cascades in plant defense signaling. *Trends in Plant Science*, *6*(11), 520–527. https://doi.org/10.1016/S1360-1385(01)02103-3

Zhang, T., Chen, S., & Harmon, A. C. (2016). Protein–protein interactions in plant mitogen-activated protein kinase cascades. *Journal of Experimental Botany*, *67*(3), 607–618. https://doi.org/10.1093/JXB/ERV508

Zhang, X., Bian, Z., & Xu, J. R. (2018). Assays for MAP kinase activation in Magnaporthe oryzae and other plant pathogenic Fungi. *Methods in Molecular Biology*, *1848*, 93–101. https://doi.org/10.1007/978-1-4939-8724-5_8

Zhang, Y., Choi, Y. E., Zou, X., & Xu, J. R. (2011). The FvMK1 mitogen-activated protein

kinase gene regulates conidiation, pathogenesis, and fumonisin production in Fusarium verticillioides. *Fungal Genetics and Biology : FG & B*, *48*(2), 71–79. https://doi.org/10.1016/J.FGB.2010.09.004

Zhang, Z., & Gurr, S. J. (2001). Expression and sequence analysis of the Blumeria graminis mitogen-activated protein kinase genes, Mpk1 and Mpk2. *Gene*, *266*(1–2), 57–65. https://doi.org/10.1016/S0378-1119(01)00381-X

Zhao, X., Kim, Y., Park, G., & Xu, J.-R. (2005). A Mitogen-activated protein kinase cascade regulating infection-related morphogenesis in Magnaporthe grisea. *The Plant Cell Online*, *17*(4), 1317–1329. https://doi.org/10.1105/tpc.104.029116

Zhao, X., Mehrabi, R., & Xu, J.-R. (2007). Mitogen-activated protein kinase pathways and fungal pathogenesis. *Eukaryotic Cell*, *6*(10), 1701–1714. https://doi.org/10.1128/EC.00216-07

Zhao, Xinhua, & Xu, J.-R. (2007). A highly conserved MAPK-docking site in Mst7 is essential for Pmk1 activation in Magnaporthe grisea. *Molecular Microbiology*, *63*(3), 881–894. https://doi.org/10.1111/j.1365-2958.2006.05548.x

Zheng, L., Campbell, M., Murphy, J., Lam, S., & Xu, J.-R. (2000). The BMP1 gene is essential for pathogenicity in the gray mold fungus Botrytis cinerea. *Molecular Plant-Microbe Interactions*, *13*(7), 724–732.

Zhou, X., Zhao, X., Xue, C., Dai, Y., & Xu, J.-R. (2014). Bypassing both surface attachment and surface recognition requirements for appressorium formation by overactive ras signaling in Magnaporthe oryzae. *Molecular Plant-Microbe Interactions*, *27*(9), 996–1004. https://doi.org/10.1094/MPMI-02-14-0052-R

Appendix I

Table I. List of strains.

Strain	Genotype description	Source
Guy11	Wild-type	Lab stock
Δpmk1	Pmk1 null mutant	Lab stock
PMK1-GFP	Pmk1 null mutant complement with PMK1-GFP	Lab stock
pmk1^AS	Pmk1 null mutant complement with Pmk1 analogue sensitive allele	Lab stock
ToxA:GFP	Wild-type strain Guy11 transformed with ToxA:GFP	Lab stock
VTS1-GFP	Wild-type strain Guy11 transformed with *VTS1-GFP*	This study
Δvts1	Vts1 null mutant	This study
SEP5-GFP	Wild-type strain Guy11 transformed with *SEP5-GFP*	Lab stock
Gelsolin-GFP	Wild-type strain Guy11 transformed with *Gelsolin-GFP*	Lab stock
Δvts1:SEP5-GFP	Vts1 null mutant transformed with *SEP5-GFP*	This study
Δvts1:SEP5-GFP	Vts1 null mutant transformed with *SEP5-GFP*	This study
Δvts1:VTS1-GFP	Vts1 null mutant complemented with *VTS1-GFP*	This study
SEP5-RFP	Wild-type strain Guy11 transformed with *SEP5-RFP*	Lab stock
Δvts1:VTS1-GFP/SEP5-RFP	Vts1 null mutant complemented with *VTS1-GFP* and *SEP5-RFP*	This study
pmk1AS:VTS1-GFP	Pmk1 null mutant complement with Pmk1 analogue sensitive allele transformed with *VTS1-GFP*	This study
Δvts1:VTS1-GFP^A175-A420	Vts1 null mutant complemented with VTS1 A175-A420 phosphodead allele	This study
Δvts1:VTS1-GFP^D175-D420	Vts1 null mutant complemented with VTS1 D175-D420 phosphomimetic allele	This study
Δvts1:VTS1-GFP^A175	Vts1 null mutant complemented with VTS1 A175 phosphodead allele	This study
Δvts1:VTS1-GFP^A420	Vts1 null mutant complemented with VTS1 A420 phosphodead allele	This study
Δvts1:VTS1-GFP^D175	Vts1 null mutant complemented with VTS1 D175 phosphomimetic allele	This study
Δvts1:VTS1-GFP^D420	Vts1 null mutant complemented with VTS1 D420 phosphomimetic allele	This study
pmk1^AS:PRE1-GFP	Pmk1 null mutant complement with Pmk1 analogue sensitive allele transformed with *PRE1-GFP*	This study
pmk1^AS:PRE2-GFP	Pmk1 null mutant complement with Pmk1 analogue sensitive allele transformed with *PRE2-GFP*	This study
pmk1^AS:PRE3-GFP	Pmk1 null mutant complement with Pmk1 analogue sensitive allele transformed with *PRE3-GFP*	This study
pmk1^AS:SEC31-GFP	Pmk1 null mutant complement with Pmk1 analogue sensitive allele transformed with *SEC31-GFP*	This study

Table II. List of plasmids.

Gene ID	Gene Name	Plasmid Name	Designed for	Source
MGG_09565	Pmk1	Pmk1 prey	Y2H	Lab stock
MGG_09566	Pmk1	Pmk1 bait	Y2H	Lab stock
MGG_12958	Mst12	Mst12 prey	Y2H	Lab stock
MGG_12958	Mst12	Mst12 bait	Y2H	Lab stock
MGG_06334	Vts1	Vts1 prey	Y2H	This study
MGG_06334	Vts1	Vts1 bait	Y2H	This study
MGG_01376	Tyrosine-phosphatase 1 (Ptp 3/2)	Phosphatase 1 prey	Y2H	This study
MGG_01376	Tyrosine-phosphatase 1 (Ptp 3/2)	Phosphatase 1 bait	Y2H	This study
MGG_00883	Ste11	Ste11 prey	Y2H	This study
MGG_00883	Ste11	Ste11 bait	Y2H	This study
MGG_09531	RhoGTPase 8	RhoGTPase prey	Y2H	This study
MGG_09531	RhoGTPase 8	RhoGTPase bait	Y2H	This study
MGG_11061	Hypothetical protein	MGG_11061 prey	Y2H	This study
MGG_11061	Hypothetical protein	MGG_11061 bait	Y2H	This study
MGG_06419	Hypothetical protein	MGG_06419 prey	Y2H	This study
MGG_06419	Hypothetical protein	MGG_06419 bait	Y2H	This study
MGG_12809	Hypothetical protein	MGG_12809 prey	Y2H	This study
MGG_12809	Hypothetical protein	MGG_12809 bait	Y2H	This study
MGG_07714	Phosphatidate phosphatase	Phosphatidate prey	Y2H	This study
MGG_07714	Phosphatidate phosphatase	Phosphatidate bait	Y2H	This study
MGG_05257	Ring finger protein	Ring finger prey	Y2H	This study
MGG_05257	Ring finger protein	Ring finger bait	Y2H	This study
MGG_06403	PH domain-containing	PHd-prey	Y2H	This study
MGG_06403	PH domain-containing	PHd-bait	Y2H	This study
MGG_09629	PRE3	NP PRE3-prey	Y2H	This study
MGG_04776	PRE2	NP PRE2-prey	Y2H	This study
MGG_02564	PRE1	NP PRE1-prey	Y2H	This study
MGG_01108	Sec31	Sec31 GFP	GFP localisation	This study
MGG_06334	Vts1	Vts1 GFP	GFP localisation	This study
MGG_09629	PRE3	PRE3 GFP	GFP localisation	This study
MGG_04776	PRE2	PRE2 GFP	GFP localisation	This study
MGG_02564	PRE1	PRE1 GFP	GFP localisation	This study

MGG_09565	Pmk1	GST-Pmk1	Protein purification	This study
MGG_06334	Vts1	6xHis-Vts1	Protein purification	This study
	MEK2DD	6xHis-MEK2DD	Protein purification	Lab stock
	MPK6	6xHis-MPK6	Protein purification	Lab stock
MGG_02564	PRE1	pICSL4723-PRE1	Barley transformation	This study
MGG_04776	PRE2	pICSL4723-PRE2	Barley transformation	This study
MGG_09629	PRE3	pICSL4723-PRE3	Barley transformation	This study
MGG_03087	Septin5	SEP5-GFP	GFP localisation	Lab stock
MGG_03087	Septin5	SEP5-RFP	RFP localisation	Lab stock
MGG_06334	VTS1$^{A175-A420}$ phosphodead allele	VTS1$^{A175-A420}$ phosphodead allele	Pathogenicity and GFP localisation	This study
MGG_06334	VTS1$^{D175-D420}$ phosphomimetic allele	VTS1$^{D175-D420}$ phosphomimetic allele	Pathogenicity and GFP localisation	This study
MGG_06334	VTS1^{A175} phosphodead allele	VTS1^{A175} phosphodead allele	Pathogenicity and GFP localisation	This study
MGG_06334	VVTS1^{A420} phosphodead allele	VVTS1^{A420} phosphodead allele	Pathogenicity and GFP localisation	This study
MGG_06334	VTS1^{D175} phosphomimetic allele	VTS1^{D175} phosphomimetic allele	Pathogenicity and GFP localisation	This study
MGG_06334	VTS1^{D420} phosphomimetic allele	VTS1^{D420} phosphomimetic allele	Pathogenicity and GFP localisation	This study

Table III. List of oligos.

Oligo	Sequence
GFP_F	ATGGTGAGCAAGGGCGAGGA
TrpC_GFP_R	TCGACGGTATCGATAAGCTTCTCGAGTGGAGATGTGGAGT
Fw 9629p	TGCAGCCCAATGTGGAATTCTACCCTTACCGCCATAGTAA
Rv9629_GFP	GCCCTTGCTCACCATTGCGGTAAACGTCCTTGTCC
1108p_F	TGCAGCCCAATGTGGAATTCGCCGATGCGCACAGCGAGGG
1108 Int_F	GTCGATCAAGGCTGGTGACTTG
1108 Int_R	CCAGCCTTGATCGACTCCTCAAACTTCTCAGTTGC
6334p_F	TGCAGCCCAATGTGGAATTCGGTTTGTAAGTACCGCACTC
6334_GFP_R	GCCCTTGCTCACCATAGTAGATAGACGTCCCTCAG
1108_GFP_R	GCCCTTGCTCACCATAGGAGTAGCCTTGCTCATGC
pGADT7_1108_F	GGAGGCCAGTGAATTCATGGTCCGACTTAGGGAGATC
pGADT7_1108_R	CGAGCTCGATGGATCCCTAAGGAGTAGCCTTGCTCAT
pGADT7_6334_F	GGAGGCCAGTGAATTCATGTCAGCTGCTCAGTCCACC
pGADT7_6334_R	CGAGCTCGATGGATCCTTAAGTAGATAGACGTCCCTC
pGADT7_11061_F	GGAGGCCAGTGAATTCATGGCGCTACAAGCCGCATAC
pGADT7_11061_R	CGAGCTCGATGGATCCCTAGAAATCCCAAAAGCTACC
pGADT7_12809_F	GGAGGCCAGTGAATTCATGCCATCGCAAAGGCCCGAA

pGADT7_12809_R	CGAGCTCGATGGATCCCTAAACTCCAGGGGGGCCGGT
2564p_F	TGCAGCCCAATGTGGAATTCACCGCTTGGGTCGAGTCCAG
2564_GFP_R	GCCCTTGCTCACCATCCTGGGCCCAACCTGCTTGG
4776p_F	TGCAGCCCAATGTGGAATTCATTTGTTTTTTTTCTTGCCG
4776_GFP_R	GCCCTTGCTCACCATGTTTTGGGCCAGGGGCGCAG
1376_BK_F	CATGGAGGCCGAATTCATGCCTCCAGAACAGCCGCAG
1376_BK_R	GCAGGTCGACGGATCCTTACGCAGCTTGCTTCGCTTC
1376_AD_F	GGAGGCCAGTGAATTCATGCCTCCAGAACAGCCGCAG
1376_AD_R	CGAGCTCGATGGATCCTTACGCAGCTTGCTTCGCTTC
6334_Int_R	CCTTATCAAAGTTGGCGGGTGAC
6334_Int_F	CCAACTTTGATAAGGATCCCATGTCAAACCGTCTC
6334_BK_F	CATGGAGGCCGAATTCATGTCAGCTGCTCAGTCCACC
6334_BK_R	GCAGGTCGACGGATCCTTAAGTAGATAGACGTCCCTC
1108_Int_E1_R	CTTGAATCCGCACTGATGCTTG
1108_Int_E2_F	CAGTGCGGATTCAAGGTTTTTTGATATTGCATGGG
1108_BK_F	CATGGAGGCCGAATTCATGGTCCGACTTAGGGAGATC
1108_BK_R	GCAGGTCGACGGATCCCTAAGGAGTAGCCTTGCTCAT
883_AD_F	GGAGGCCAGTGAATTCATGTATCCAGGAAGTAGCC
883_AD_R	CGAGCTCGATGGATCCTCAGTACGTCCCTCTGATCTTG
07714_AD_F	GGAGGCCAGTGAATTCATGCAATCGCAGTCGGCATG
07714_AD_R	CGAGCTCGATGGATCCCTATCTTTTCAGCTCTGCCATCGC
05257_AD_F	GGAGGCCAGTGAATTCATGTTCAGCCAACAACCGAG
05257_AD_R	CGAGCTCGATGGATCCCTAGGCTCTCGCTATGTCGTC
06403_AD_F	GGAGGCCAGTGAATTCATGCTTGAAACCATGGTTGACG
06403_AD_R	CGAGCTCGATGGATCCTCAAGCCGCAAGGTTGATGG
pGADT7_6419_F	GGAGGCCAGTGAATTCATGAGTGCAGCCATCGCCATG
pGADT7_6419_R	CGAGCTCGATGGATCCTCAAGAGTGGAACAGGTCCCA
883_BK_F	CATGGAGGCCGAATTCATGTATCCAGGAAGTAGCC
883_BK_R	GCAGGTCGACGGATCCTCAGTACGTCCCTCTGATCTTG
07714_BK_F	CATGGAGGCCGAATTCATGCAATCGCAGTCGGCATG
07714_BK_R	GCAGGTCGACGGATCCCTATCTTTTCAGCTCTGCCATCGC
05257_BK_F	CATGGAGGCCGAATTCATGTTCAGCCAACAACCGAG
05257_BK_F	GCAGGTCGACGGATCCCTAGGCTCTCGCTATGTCGTC
06403_BK_F	CATGGAGGCCGAATTCATGCTTGAAACCATGGTTGACG
06403_BK_R	GCAGGTCGACGGATCCTCAAGCCGCAAGGTTGATGG
2564_NoSP_AD_F	GGAGGCCAGTGAATTCAGTTCCTCCCCCGGCCAGTCTTT
04776_NoSP_AD_F	GGAGGCCAGTGAATTCCTGCAGGCCGCCGACGAGCC
09629_NoSP_AD_F	GGAGGCCAGTGAATTCATGCCTCCGATCGGCGAGGA
pOPIN_Pmk1_FL_F	AAGTTCTGTTTCAGGGCCCGATGTCTCGCGCCAATCCACC
pOPIN_Pmk1_FL_R	ATGGTCTAGAAAGCTTTACCGCATAATTTCCTGGTAGATG
Vts1_PD1_F	AGTTTTGGCCCCCGCCAACTTTGATAAGGGTCAGT
Vts1_PD1_R	AGTTGGCGGGGGGCCAAAACTCCTGAC
Vts1_PD2_F	CCCTCTAGCCCCGGGTATGATCTCCCCCAACGTCG
Vts1_PD2_R	TCATACCCGGGGCTAGAGGGTTCTGTC
Vts1_PM1_F	AGTTTTGGACCCCGCCAACTTTGATAAGGGTCAGT
Vts1_PM1_R	AGTTGGCGGGGTCCAAAACTCCTGAC
Vts1_PM2_F	CCCTCTAGACCCGGGTATGATCTCCCCCAACGTCG
Vts1_PM2_R	TCATACCCGGGTCTAGAGGGTTCTGTC
Vts1_LF5	TCCCCTGCCTGCGCATTGGCGTGG
Vts1_LF3	GTCGTGACTGGGAAAACCCTGGCGCTGGCGGCGTGAGTGTTGGAGGCC
Vts1_RF5	TCCTGTGTGAAATTGTTATCCGCTCAAGACTGAGGGACGTCTATCTAC
Vts1_RF3	CCTCTTTCGTCGATGCACATATGC
Vts1g_500 UP_F	TTTGTAAGTACCGCACTCATCCTG
Vts1_pOPINs_F	AAGTTCTGTTTCAGGGCCCGATGTCAGCTGCTCAGTCCACC
Vts1_pOPINs_R	ATGGTCTAGAAAGCTTTATTAAGTAGATAGACGTCCCTC
Vts1_LF1_F	CCTTGGGAAAGTCTCGAAACAGTTGC
Vts1_LF2_F	GCTGAGCTTGCACAACTCTAATCAAC

Vts1_ATG_F	ATGTCAGCTGCTCAGTCCACC
Vts1_RF1_R	AGCTTTCCAAGTCTGCAAGGGC
Vts1_RF2_R	TCGTAATGTCCATATGCGCCG
Vts1_Int_seq_R1	GCTGACTCTGCATCCCTTGCA
Vts1_Int_seq_R2	CTTGTCAGAAGCGGTCAGGGTT
MGG_09531_AD_F	GGAGGCCAGTGAATTCATGCCAGAATTCAGCGATTCTT
MGG_09531_AD_R	CGAGCTCGATGGATCCCTAGTCGTCCATGGGTTTGTCCA
MGG_09531_BK_F	CATGGAGGCCGAATTCATGCCAGAATTCAGCGATTCTT
MGG_09531_BK_R	GCAGGTCGACGGATCCTAGTCGTCCATGGGTTTGTCCA

Appendix II

Part of the work contained in this thesis has contributed to the following publications:

List of publications

Ryder LS, **Cruz-Mireles N**, Molinari C, Eisermann I, Eseola AB, & Talbot NJ. (2022). The appressorium at a glance. *Journal of Cell Science*, In Press

Osés-Ruiz M, **Cruz-Mireles N**, Martin-Urdiroz M, Soanes DM, Eseola AB… Menke FLH, Talbot NJ. (2021) Appressorium-mediated plant infection by Magnaporthe oryzae is regulated by a Pmk1-dependent hierarchical transcriptional network. *Nature Microbiology*, *6*(11):1383-1397. doi: 10.1038/s41564-021-00978-w.

Cruz-Mireles N, Eseola AB, Osés-Ruiz M, Ryder LS, Talbot NJ. (2021) From appressorium to transpressorium-Defining the morphogenetic basis of host cell invasion by the rice blast fungus. *PLoS Pathogens*, *17*(7):e1009779. doi: 10.1371/journal.ppat.1009779.

Cruz-Mireles N, Eisermann I, Garduño-Rosales M, Molinari C, Ryder LS, Tang B, Yan X, Talbot NJ. (2021) The biology of invasive growth by the rice blast fungus Magnaporthe oryzae. *Methods Molecular Biology*, 2356:19-40. doi: 10.1007/978-1-0716-1613-0_2.

Eseola AB, Ryder LS, Osés-Ruiz M, Findlay K, Yan X, **Cruz-Mireles N**, Molinari C, Garduño-Rosales M, Talbot NJ. (2021) Investigating the cell and developmental biology of plant infection by the rice blast fungus Magnaporthe oryzae. *Fungal Genetics Biology*, 154:103562. doi: 10.1016/j.fgb.2021.103562.

Ryder LS, Dagdas YF, Kershaw MJ, Venkataraman C, Madzvamuse A, Yan X, **Cruz-Mireles N** … Menke FLH, Talbot NJ. (2019) A sensor kinase controls turgor-driven plant infection by the rice blast fungus. *Nature*, 574(7778):423-427. doi: 10.1038/s41586-019-1637-x.

Check for updates

Appressorium-mediated plant infection by *Magnaporthe oryzae* is regulated by a Pmk1-dependent hierarchical transcriptional network

Míriam Osés-Ruiz [1 ✉], Neftaly Cruz-Mireles[1,7], Magdalena Martin-Urdiroz[2,7], Darren M. Soanes [2], Alice Bisola Eseola[1], Bozeng Tang[1], Paul Derbyshire[1], Mathias Nielsen [3], Jitender Cheema[3], Vincent Were[1], Iris Eisermann[1], Michael J. Kershaw[2], Xia Yan [1], Guadalupe Valdovinos-Ponce [4,5], Camilla Molinari [1], George R. Littlejohn [2,6], Barbara Valent [4], Frank L. H. Menke [1] and Nicholas J. Talbot [1 ✉]

Rice blast is a devastating disease caused by the fungal pathogen *Magnaporthe oryzae* that threatens rice production around the world. The fungus produces a specialized infection cell, called the appressorium, that enables penetration through the plant cell wall in response to surface signals from the rice leaf. The underlying biology of plant infection, including the regulation of appressorium formation, is not completely understood. Here we report the identification of a network of temporally coregulated transcription factors that act downstream of the Pmk1 mitogen-activated protein kinase pathway to regulate gene expression during appressorium-mediated plant infection. We show that this tiered regulatory mechanism involves Pmk1-dependent phosphorylation of the Hox7 homeobox transcription factor, which regulates genes associated with induction of major physiological changes required for appressorium development—including cell-cycle control, autophagic cell death, turgor generation and melanin biosynthesis—as well as controlling a additional set of virulence-associated transcription factor–encoding genes. Pmk1-dependent phosphorylation of Mst12 then regulates gene functions involved in septin-dependent cytoskeletal re-organization, polarized exocytosis and effector gene expression, which are necessary for plant tissue invasion. Identification of this regulatory cascade provides new potential targets for disease intervention.

Rice blast disease is an important threat to global food security[1]. The disease starts when asexual spores of *Magnaporthe oryzae*, called conidia, land on the hydrophobic surface of a rice leaf inducing differentiation of an infection cell called an appressorium[1–3]. The appressorium develops turgor of up to 8.0 MPa due to glycerol accumulation, which generates osmotic pressure[4]. Glycerol is maintained in the appressorium by melanin in the cell wall, which reduces its porosity[4,5]. Development of the appressorium is tightly linked to the cell cycle, autophagy[6–8] and metabolic checkpoint control mediated by TOR kinase and the cAMP-dependent protein kinase A (PKA) pathway[9–11]. Appressorium turgor is monitored by a sensor kinase, Sln1, and once a threshold is reached[12], septin GTPases in the appressorium pore form a hetero-oligomeric complex that scaffolds cortical F-actin at the base of the appressorium[13,14]. This leads to force generation to pierce the cuticle with a rigid penetration hypha. Once inside the leaf, invasive hyphae colonize the first epidermal cell before seeking out plasmodesmata-rich pit fields through which the fungus invades neighbouring cells[15]. *M. oryzae* actively suppresses plant immunity using fungal effector proteins delivered into plant cells[16]. After five days, disease lesions appear from which the fungus sporulates to colonize neighbouring plants.

Formation of an appressorium by *M. oryzae* requires a conserved pathogenicity mitogen-activated protein kinase (MAPK), called Pmk1 (ref. [17]). Pmk1 mutants cannot form appressoria or cause plant infection, even when plants are wounded[17]. Instead, Δ*pmk1* mutants produce undifferentiated germlings that undergo several rounds of mitosis and septation[17,18]. Pmk1 is also responsible for lipid and glycogen mobilization to the appressorium, autophagy in the conidium[4,8,19,20] and invasive cell-to-cell movement[15]. A set of pl surface sensors[21] that trigger cAMP–PKA signalling are required for Pmk1 activation[17], and a TOR-dependent nutrient sensing pathway is necessary for appressorium formation, acting upstream, or perhaps independently, of Pmk1 (refs. [9–11]). The mechanism by which Pmk1 exerts such an important role in plant infection has remained largely unknown and only one transcriptional regulator, Mst12, which may act downstream of Pmk1, has been characterized in detail. Mst12 mutants form appressoria normally but are non-functional and cannot cause disease[22].

In this study we set out to identify the mechanism by which major transcriptional changes are regulated during appressorium development by *M. oryzae*. We identified major temporal changes in gene expression in response to an appressorium-inductive hydrophobic

[1]The Sainsbury Laboratory, Norwich Research Park, University of East Anglia, Norwich, UK. [2]School of Biosciences, University of Exeter, Exeter, UK. [3]John Innes Centre, Norwich Research Park, Norwich, UK. [4]Department of Plant Pathology, Kansas State University, Manhattan, KS, USA. [5]Present address: Department of Plant Pathology, Colegio de Postgraduados, Montecillo, Texcoco, Mexico. [6]Present address: Department of Biological and Marine Sciences, University of Plymouth, Drakes Circus, Plymouth, UK. [7]These authors contributed equally: Neftaly Cruz-Mireles and Magdalena Martin-Urdiroz. ✉e-mail: miriam.oses-ruiz@tsl.ac.uk; nick.talbot@tsl.ac.uk

surface, which require Pmk1 or Mst12. We provide evidence that a hierarchical network of transcription factors (TFs), regulated by the Pmk1 MAPK, are necessary for the complex transcriptome changes associated with appressorium-mediated plant infection.

Results

The Pmk1 MAPK is necessary for appressorium development in response to surface hydrophobicity. *M. oryzae* develops appressoria when spores are incubated in water on hard hydrophobic surfaces. They form within 6 h and septins accumulate at the base of the incipient appressorium in a ring structure by 8 h (ref. [13]; Extended Data Fig. 1a). A single round of mitosis occurs and the conidium undergoes autophagy and degradation of its three nuclei[8], resulting in a single appressorium nucleus by 14 h (Extended Data Fig. 1a). By contrast, when *M. oryzae* conidia germinate on a hydrophilic surface, they do not undergo autophagy and develop undifferentiated germlings[11] (Extended Data Fig. 1a,b)[6]. Multiple rounds of mitosis occur and by 24 h approximately 50% of germlings contain >4 nuclei (Extended Data Fig. 1a,b). Similarly, Pmk1 mutants do not undergo autophagy or develop appressoria and instead form undifferentiated germlings (Fig. 1a and Extended Data Fig. 1c,d)[17,20]. The response of the fungus to a hydrophilic surface[10] therefore mirrors that of Pmk1 mutants.

We first determined the global transcriptional response of *M. oryzae* to surface hydrophobicity compared with that associated with loss of Pmk1. We isolated total RNA from a wild-type strain of *M. oryzae*, Guy11, at different time points during appressorium development on hydrophobic glass coverslips (hereafter referred to as HP) and hydrophilic Gelbond membranes (hereafter called HL), from 0–24 h after inoculation. In parallel, we incubated conidia of a Δ*pmk1* mutant on an HP surface for an identical time period and carried out RNA sequencing analysis (RNA-seq). Differentially expressed genes (DEGs) were defined using a *P* value adjusted for the false-discovery rate ($P_{adj} < 0.01$) and a moderated log$_2$-transformed fold change in gene expression (mod_lfc) > 1 to define upregulated genes and mod_lfc < −1 to define downregulated genes (Fig. 1b,c). We observed 3,917 *M. oryzae* DEGs in response to surface hydrophobicity (HP versus HL) and 6,333 DEGs in a Δ*pmk1* mutant compared with the isogenic wild-type Guy11 (Supplementary Tables 1 and 2). A comparison of these gene sets identified 3,555 DEGs in response to an HP surface and the presence of Pmk1, a small set of 362 Pmk1-independent DEGs in response to HP surfaces and 2,778 Pmk1-dependent genes not showing differential expression (Fig. 1d and Supplementary Table 3). We conclude that 90% of the DEGs in *M. oryzae* in response to surface hydrophobicity are Pmk1-dependent.

The set of 3,555 HP- and Pmk1-dependent genes identified functions associated with appressorium morphogenesis, such as autophagy[6,8]. Seven *ATG* genes, for example, were highly expressed during the early stages of appressorium development and downregulated from 8 h onwards (Supplementary Fig. 1). Similarly, cell cycle-related genes were differentially regulated in response to HP surfaces[23] and many were Pmk1-dependent (Supplementary Fig. 2). Genes encoding cyclins, the cyclin-dependent kinase *CDC28* and its positive and negative regulators *MIH1* and *SWE1*, respectively[24], all showed expression peaks at 4–6 h, coincident with appressorium morphogenesis (Supplementary Figs. 2 and 3). By contrast, cyclin-associated gene expression was delayed and CDK-related gene expression oscillated abnormally in the Δ*pmk1* mutants. Genes required for the DNA damage response pathway[25], such as *DUN1*, were mis-regulated in the Δ*pmk1* mutants. Fifty of the 79 known G protein-coupled receptors in *M. oryzae*[26] were differentially regulated in response to HP and 48 were Pmk1-dependent (Supplementary Fig. 4). Analysis of the DEGs additionally implicated 14 acetyltransferases, 13 ABC transporters, 2 Bin-amphiphysin-Rvs (BAR)-domain proteins, 95 major facilitator superfamily transporters, 24 protein kinases, 3 fas-

ciclins, 6 cutinases and 86 TFs with appressorium morphogenesis (Supplementary Table 3).

We next analysed 2,778 Pmk1-dependent, HP surface-independent genes. There was considerable overlap in predicted gene functions (Supplementary Table 3) but with changes associated with appressorium maturation, such as cytoskeletal remodelling genes encoding actin-binding proteins, cofilin, coronin, the F-actin capping protein Fes/CIP4 and EFC/F-BAR-domain proteins (Supplementary Fig. 5). Differential expression of septins and associated regulators was also observed (Supplementary Fig. 5b–d)[12,13]. Pmk1 therefore acts as a global regulator of the *M. oryzae* response to surface hydrophobicity, but its function clearly extends beyond initial development to appressorium maturation.

Defining the role of Mst12 in regulating appressorium gene expression. As Pmk1 is required for the expression of 6,333 genes during appressorium development, we identified downstream regulators to establish the hierarchy of genetic control. Mst12 has been reported to be regulated by Pmk1 (ref. [22]; Fig. 2a) but, unlike Δ*pmk1* mutants, Δ*mst12* mutants still form appressoria, although they cannot infect plants[22] (Extended Data Fig. 2a,b). To help define the function of Mst12, we carried out live-cell imaging and found the Δ*mst12* mutant impaired in its ability to undergo septin-dependent F-actin remodelling at the appressorium pore (Fig. 2b)[13]. Microtubules were disorganized in appressoria of the Δ*mst12* mutants (Fig. 2b) and, consistent with septin disorganization, the PAK-related kinase Chm1, ezrin/radixin/moesin protein Tea1, BAR domain-containing protein Rvs167, and staurosporine and temperature sensitive-4 (Stt4) lipid kinase (Fig. 2c)[12,13] were all mis-localized. Mst12 is therefore necessary for septin-dependent re-polarization of the appressorium and we thus performed comparative RNA-seq of the Δ*mst12* and Δ*pmk1* mutants (Supplementary Tables 4 and 5). This led to the identification of 2,512 DEGs in the Δ*mst12* mutant with significant changes in gene expression during conidial germination and, particularly after 8 h, during appressorium maturation (Fig. 2d). A set of 4,052 genes were also identified as Pmk1-dependent but Mst12-independent, with 2,281 genes regulated by both Pmk1 and Mst12 (Fig. 2e). Only 231 Mst12-dependent genes were Pmk1-independent (Fig. 2e). Appressorium-specific gene functions, such as melanin biosynthesis[27], were not expressed in the Δ*pmk1* mutants and delayed in expression in the Δ*mst12* mutants, consistent with delayed onset of appressorium formation compared with Guy11 (Extended Data Fig. 2c–f).

To investigate appressorium maturation, gene functions regulated by both Pmk1 and Mst12 were defined among the 2,281 DEGs. These included the cutinase gene family, implicated in plant infection[28] (Supplementary Fig. 6a–c), and a family of membrane-associated fasciclin glycoproteins involved in cell adhesion[29,30] (Supplementary Fig. 6d–g). Three fasciclins—Flp1 (MGG_02884), Flp2 (MGG_09372) and Flp3 (MGG_05483)—are present in *M. oryzae* and Flp1 plays a role in adhesion and pathogenicity[31]. A total of 436 genes predicted to encode secreted proteins[32] were also Pmk1- and Mst12-dependent, including seven known effector genes (Extended Data Fig. 3a–c), two of which, Bas2 and Bas3, have been reported to be Pmk1-dependent during invasive growth[15]. We therefore expressed Bas2p:green fluorescent protein (GFP) in a *pmk1*^AS mutant. This mutant allows conditional inactivation of the MAPK in the presence of the ATP analogue 1-naphthyl-PP1 (1NA-PP1; ref. [15]). When 1NA-PP1 was applied to the *pmk1*^AS mutant expressing Bas2pGFP, we observed a loss of Bas2–GFP fluorescence, suggesting that Pmk1 is necessary for its expression before plant infection (Extended Data Fig. 3d,e).

Given the significant effect of Mst12 on septin-dependent re-polarization—which is necessary for exocyst organization[25]—we reasoned that Δ*mst12* might be impaired in secretory functions. GFP fusion proteins of exocyst components were therefore expressed
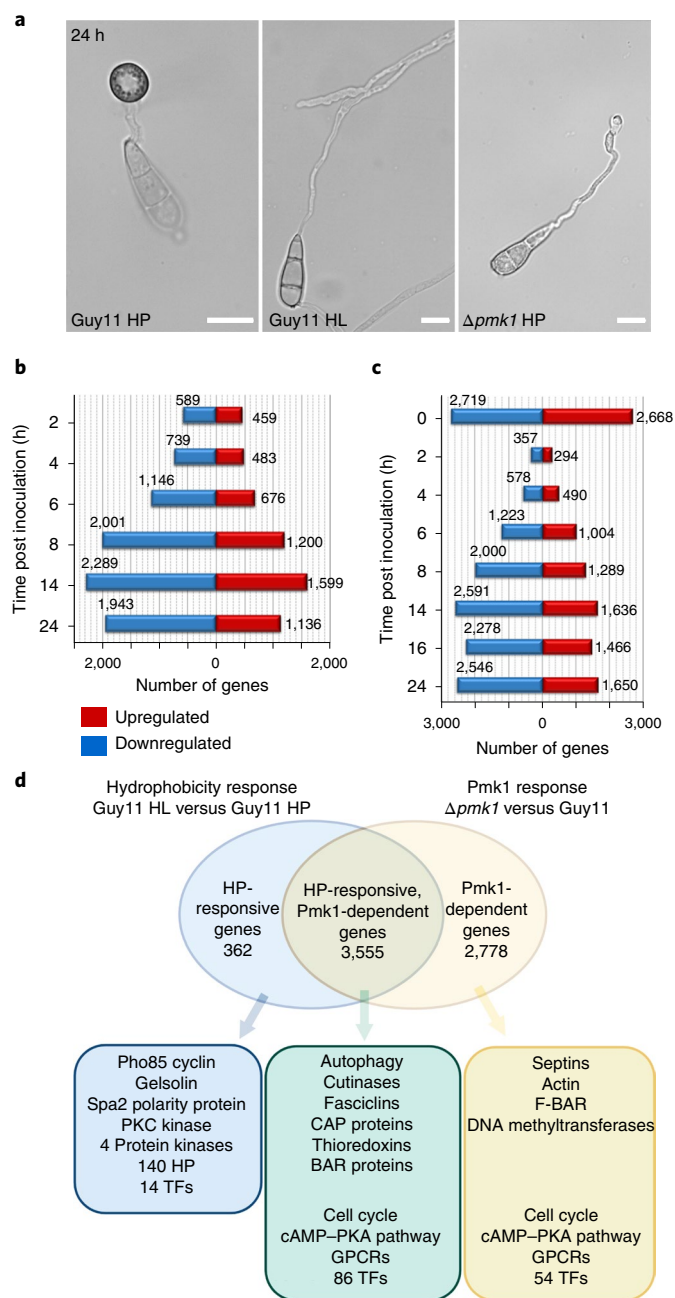
Fig. 1 | Global comparative transcriptional profile analysis to define the response of *M. oryzae* to surface hydrophobicity and the presence/absence of the Pmk1 MAPK. a, Bright-field microscopy to show germ-tube extension and appressorium formation of *M. oryzae* Guy11 on an HP (left) and an HL (middle) surface as well as a Δ*pmk1* mutant on an HP surface (right) 24 h after inoculation. Scale bars, 10 μm. **b**, Number of upregulated ($P_{adj} < 0.01$ and mod_lfc > 1) and downregulated ($P_{adj} < 0.01$ and mod_lfc < −1) genes in Guy11 in response to incubation on HL surfaces relative to HP surfaces between 2 and 24 h after inoculation. **c**, Number of upregulated ($P_{adj} < 0.01$ and mod_lfc > 1) and downregulated ($P_{adj} < 0.01$ and mod_lfc < −1) genes in a Δ*pmk1* mutant as compared with the wild-type Guy11 0–24 h after incubation on an HP surface. **d**, Venn diagram illustrating overlapping sets of genes with at least twofold differential expression in at least two time points ($P_{adj} < 0.01$ and mod_lfc > 1 or mod_lfc < −1) in Guy11 in response to incubation on HP or HL surfaces, or between the Δ*pmk1* mutant compared with Guy11 on an HP surface. Three distinct populations of genes were identified: HP-surface responsive only, HP-responsive and Pmk1-dependent, and Pmk1-dependent only. GPCRs, G protein–coupled receptors.

in Δ*mst12* and Guy11 *M. oryzae* (Extended Data Fig. 3f–k). In the Guy11 appressoria, exocyst components form a ring structure that is absent in the Δ*mst12* mutants (Extended Data Fig. 3f–k). We conclude that Pmk1 and Mst12 are necessary for the expression of genes involved in cytoskeleton reorientation, exocyst and effector functions during plant tissue invasion.

We used chromatin immunoprecipitation with sequencing (ChIP–seq) to identify direct targets of Mst12. A functional Mst12–GFP fusion protein was expressed in a Δ*mst12* strain, which complemented the mutant phenotype and localized to the appressorium nucleus (Extended Data Fig. 4a,b). Cross-linked chromatin was isolated from mycelium, followed by immunoprecipitation and sequencing of Mst12–GFP-bound genomic DNA. ChIP–seq identified 1,596 broad peaks within ±2 kb of 726 genes (Supplementary Table 6), which defined 113 downregulated and 65 upregulated genes (Fig. 2f and Extended Data Fig. 4c). We calculated the number of Mst12-dependent genes (based on RNA-seq analysis during appressorium development) that were direct ChIP–seq-defined targets of Mst12. This revealed a considerable overlap of 113 genes directly controlled by Mst12 (Fig. 2g). Among these, 25 genes encode putative secreted proteins, such as the SET domain (PF00856) containing the protein-encoding gene *MCG1* (MGG_00339)[33] and a secreted catalase (MGG_06442)[34] (Supplementary Table 6). We predicted consensus binding motifs from peak sequences obtained by ChIP–seq analysis identifying five over-represented motifs in these sequences (Fig. 2h). We found that Motifs 1–3 were over-represented ($P < 0.001$) in the promoters of the Mst12-dependent genes identified by RNA-seq. For example, Motif 1 was present in 609 of 1,848 genes (32.95%) downregulated in the Δ*mst12* mutants during appressorium development (Extended Data Fig. 4d). The Mst12 targets include genes reported to play roles in appressorium maturation and plant infection (Supplementary Table 6). Rvs167 (ref. [13]), for example, is an Mst12 target (Fig. 2i), consistent with its mis-localization in Δ*mst12* appressoria (Fig. 2c) and differential gene expression (Supplementary Table 6). Similarly, the 1,3,6,8-tetrahydroxynaphthalene reductase-encoding gene *4HNR*, involved in melanin biosynthesis[35], is an Mst12 target (Fig. 2i) and downregulated in Δ*mst12* mycelium (Supplementary Fig. 7). Comparative ChIP–seq and RNA-seq analysis therefore provided evidence that Mst12 regulates cellular functions associated with appressorium maturation.

Identification of the hierarchy of transcriptional regulation required for appressorium development by *M. oryzae*. As Mst12 regulates a subset of genes associated with appressorium re-polarization, we reasoned that Pmk1 must regulate additional TFs, including some acting earlier during development. We therefore determined the total number of putative TF-encoding genes that were differentially regulated by at least twofold ($P_{adj} < 0.01$ and mod_lfc > 1 or mod_lfc < −1) in at least two time points in the Δ*pmk1* and/or Δ*mst12* mutants compared with Guy11 *M. oryzae*. We found 140 such TF genes, of which 95 were expressed during appressorium morphogenesis and Pmk1-dependent, with 45 associated with the later stages of appressorium maturation and dependent on both Pmk1 and Mst12 (Fig. 3a). We plotted heatmaps for each gene set (Fig. 3b–d), which revealed a clade of 15 TF-encoding genes severely downregulated in the Δ*pmk1* mutant, which we called Clade 4 (Fig. 3c and Supplementary Table 7). This includes nine Zn₂Cys₆ TFs, some of which were previously implicated in stress responses (Fzc64, Fzc52, Fzc41 and Fzc30), conidial germination (Fzc50) and appressorium formation (Fzc75)[36]. Five Clade 4 TFs were uncharacterized and named *RPP* genes (for related to the Pmk1 pathway): *RPP1* (MGG_10212), *RPP2* (MGG_09276), *RPP3* (MGG_07218), *RPP4* (MGG_07368) and *RPP5* (MGG_08917). Clade 4 also includes the *PIG1* TF gene (MGG_07215), previously reported to regulate melanin biosynthesis[37], *ALCR* (MGG_02129),

a homologue of *AlcR* from *Aspergillus nidulans* responsible for the activation of ethanol utilization[38] and the homeobox-domain TF gene *HOX7* (MGG_12865), involved in appressorium formation[39]. These TF genes were downregulated in a Δ*pmk1* mutant from 4h (Fig. 3e)—the time when an appressorium first develops—and altered in expression in Δ*mst12* mutants at later time points, consistent with its delay in appressorium formation (Fig. 3f).

To test whether Clade 4 TF genes play important roles in appressorium development, we generated Δ*alcR*, Δ*rpp1*, Δ*rpp2*, Δ*rpp4*, Δ*rpp5*, Δ*rpp3*, Δ*rpp3*Δ*pig1* and Δ*hox7* mutants in either Δ*ku70* (a mutant of Guy11 lacking non-homologous DNA end-joining to facilitate homologous recombination[6]) or Guy11 (Supplementary Fig. 7). A double mutant of *RPP3* and *PIG1* was also made, because they are part of a gene cluster on chromosome 2 associated with melanin biosynthesis, including *BUF1* and *4HNR*[40], and we reasoned that the TFs might have overlapping functions. We inoculated 21-day-old seedlings of the blast-susceptible rice cultivar CO-39 with conidial suspensions of each mutant and quantified disease symptoms after 5d (Fig. 3g,h and Extended Data Fig. 5). Guy11 and Δ*ku70* were able to cause plant infection but, by contrast, the Δ*hox7* mutant was non-pathogenic[39] (Fig. 3g), while both the Δ*rpp3* and Δ*rpp3*Δ*pig1* mutants were reduced in virulence. Conversely, the Δ*aclR* mutant caused slightly more blast lesions than Guy11 (Fig. 3g,h).

The Hox7 homeobox TF is regulated by the Pmk1 MAP kinase.
To investigate the role of Clade 4 TFs in pathogenesis, we tested whether mutants could form appressoria (Extended Data Fig. 5b). All mutants made appressoria normally, except the Δ*hox7* mutants, which formed immature non-melanised terminal swellings that re-germinated into hypha-like structures (Fig. 4a and Extended Data Fig. 6a,b). Because the loss of *HOX7* affected appressorium development, we hypothesized it might act distinctly to Mst12 and other Clade 4 TFs. Hox7 is one of six homeobox-domain (PF00046) TFs and two homeobox KN domain (PF05920)-encoding genes previously identified, but its relationship to Pmk1 is unknown[39]. We therefore carried out comparative RNA-seq of Δ*hox7* with the Δ*pmk1* and Δ*mst12* mutants at 14h on HP surfaces (Fig. 4b and Supplementary Table 8,9). Hox7 controls the expression of 4,211 genes, of which 2,332 are downregulated ($P_{adj} < 0.01$ and mod_lfc < −1) and 1,879 upregulated ($P_{adj} < 0.01$ and mod_lfc > 1; Extended Data Fig. 6b). We then identified sets of overlapping genes in the Δ*hox7*, Δ*pmk1* and Δ*mst12* mutants showing differential expression compared with Guy11 (Fig. 4b). Pmk1 and Hox7 shared 1,942 DEGs, whereas Mst12 and Hox7 shared only 169 DEGs (Fig. 4b). Our analysis revealed 709 DGEs in the Δ*pmk1*, Δ*mst12* and Δ*hox7* mutants, with a very high level of similarity between the Δ*pmk1* and Δ*hox7* mutants, in contrast to Δ*mst12* (Extended Data Fig. 6c). We therefore reasoned that Hox7 might act downstream of Pmk1 to

regulate such a strongly overlapping set of genes. To test this idea, we investigated the expression of Clade 4 TFs and found that the gene expression patterns were similar between the Δ*pmk1* and Δ*hox7* mutants (Fig. 4c). Widening our analysis to the 1,942 genes that were differentially regulated by both Pmk1 and Hox7 revealed a strongly overlapping pattern of transcriptional regulation (Extended Data Fig. 6d). For example, Pmk1 and Hox7 are both required for the regulation of the RAM pathway, melanin biosynthesis, autophagy and cell-cycle control genes (Extended Data Fig. 6e). Expression of the cyclin genes *Cln3*, *Clb2* and *Clb3*; CDK-related genes *Mih1*, *Cdc28*, *Swe1* and *Cks1*; and the DNA damage response pathway-related genes *Cds1*, *Dun1* and *Chk1* (Extended Data Fig. 6f) as well as autophagy genes (Extended Data Fig. 6g) are mis-regulated in Δ*hox7* mutants. To investigate the role of Hox7 in cell-cycle control and autophagy, we introduced a Histone H1-red fluorescent protein (RFP) nuclear marker into Guy11 and Δ*pmk1* *M. oryzae* and a H1–GFP marker into the Δ*mst12* and Δ*hox7* mutants, and monitored the nuclear numbers for 24h following conidial germination (Fig. 4d). The Δ*hox7* mutant contained >4 nuclei by 24h, resembling Δ*pmk1*, whereas the Δ*mst12* mutant resembled Guy11 with a single nucleus in the appressorium. Hox7 may therefore be required for cell-cycle arrest in the apical cell of the conidium after mitosis and migration of daughter nuclei to the incipient appressorium and conidial cell, respectively[7]. Furthermore, conidia of both the Δ*hox7* and Δ*pmk1* mutants did not collapse due to autophagy by 24h, as observed in Guy11 and Δ*mst12*, consistent with the regulation of autophagy requiring both Pmk1 and Hox7.

A TOR kinase-dependent nutrient-sensing pathway has recently been shown to be required for appressorium morphogenesis, including cell-cycle arrest before infection, cell development and the onset of autophagy. This metabolic checkpoint is downstream of PKA but may act upstream of Pmk1 (refs. [9–11]). We decided to test whether the metabolic checkpoint affects the action of Pmk1 and Hox7. First, we tested whether the Δ*pmk1* and Δ*hox7* mutants were responsive to cAMP. The Δ*pmk1* mutant responded to exogenous cAMP treatment by undergoing increased hooking, as reported previously[17], as well as reduced conidial germination, whereas Δ*hox7* developed multiple aberrant non-melanised swellings and showed less hyphal-like growth. Pmk1 and Hox7 therefore seem to act downstream of cAMP–PKA signalling (Supplementary Fig. 8). We next tested whether inhibition of TOR might be compromised in the Δ*pmk1* and Δ*hox7* mutants, thereby explaining their inability to make appressoria and undergo autophagy. Spores of Guy11 *M. oryzae* and Δ*pmk1* and Δ*hox7* mutants were subject to forced inactivation of TOR with rapamycin. This treatment did not restore appressorium development or inhibit multiple nuclear divisions in the Δ*pmk1* mutants, consistent with previous observations[10], but also had no effect on the Δ*hox7* mutants, suggesting that

Fig. 2 | Functional analysis and comparative global transcriptional profile analysis in response to the presence/absence of the *M. oryzae* TF Mst12.
a, Schematic representation of the Pmk1 MAPK signalling pathway in *M. oryzae*. Dissociation of Mgb1 causes activation of Mst11 (MAPKKK), which activates Mst7 (MAPKK) and ultimately Pmk1 (MAPK). The MAPK signalling complex is scaffolded by Mst50. Mst7 activates Pmk1, which regulates a series of uncharacterized TFs as well as Mst12 (refs. [69,70]). **b**, Live-cell images showing the cellular localization of Lifeact–RFP, Sep3–GFP and β-tubulin–GFP in an appressorium pore of Guy11 and Δ*mst12* following incubation on an HP surface for 24h. **c**, Micrographs showing the cellular localization of Chm1–GFP, Tea1–GFP, Rvs167–GFP and Stt4–GFP in appressorium pores of Guy11 and Δ*mst12* following incubation on an HP surface for 24h. **b,c**, Scale bars, 10μm. **d**, Number of upregulated ($P_{adj} < 0.01$ and mod_lfc > 1) and downregulated ($P_{adj} < 0.01$ and mod_lfc < −1) genes in a Δ*mst12* mutant as compared with Guy11 at different time points (0–24h) following incubation on an HP surface. **e**, Venn diagram illustrating overlapping sets of DGEs with at least twofold differential expression in at least two time points ($P_{adj} < 0.01$ and mod_lfc > 1 or mod_lfc < −1) between a Δ*pmk1* mutant and Guy11 and a Δ*mst12* mutant versus Guy11, all incubated on an HP surface. Three distinct populations of genes were identified: Pmk1-dependent only, Pmk1- and Mst12-dependent, and Mst12-dependent only. **f**, Number of genes that were downregulated ($P_{adj} < 0.01$ and mod_lfc < -1), upregulated ($P_{adj} < 0.01$ and mod_lfc > 1) or bound by Mst12 during mycelium growth (determined by ChIP-seq; two biological replicates) **g**, Number of genes that were differentially regulated (downregulated ($P_{adj} < 0.01$ and mod_lfc < −1) and upregulated ($P_{adj} < 0.01$ and mod_lfc > 1)) or bound by Mst12 during appressorium development (determined by ChIP-seq; two biological replicates). **h**, Consensus DNA-binding motifs, predicted using MEME, for the TF Mst12 based on ChIP-seq. **i**, Representative raw ChIP-seq peaks and RNA-seq for the BAR domain–encoding gene (PF03114) *RVS167* (MGG_11497; left) and the tetrahydroxynaphthalene reductase–encoding gene *4HNR* (MGG_07216; right). The blue boxes indicate peaks identified by MACS2 using ChIP-seq analysis.

Pmk1 and Hox7 are not influenced by TOR activity (Supplementary Fig. 9). The TOR-dependent metabolic checkpoint has been reported to lead to a G2 arrest before appressorium morphogenesis[9,11]; we thus tested whether a forced G2 arrest in response to treatment with the microtubule polymerization inhibitor benomyl would restore appressorium development to the Δ*pmk1* and Δ*hox7* mutants. Benomyl treatment did not restore appressorium

formation or autophagy to either mutant or affect subsequent nuclear divisions (Supplementary Fig. 10a,b). Our results therefore indicate that Pmk1 and Hox7 act downstream of the cAMP–PKA pathway but are not dependent on the TOR-dependent metabolic checkpoint. This emphasises both the central role of Pmk1 as a global regulator of appressorium development by *M. oryzae*[15] and its close relationship to Hox7.
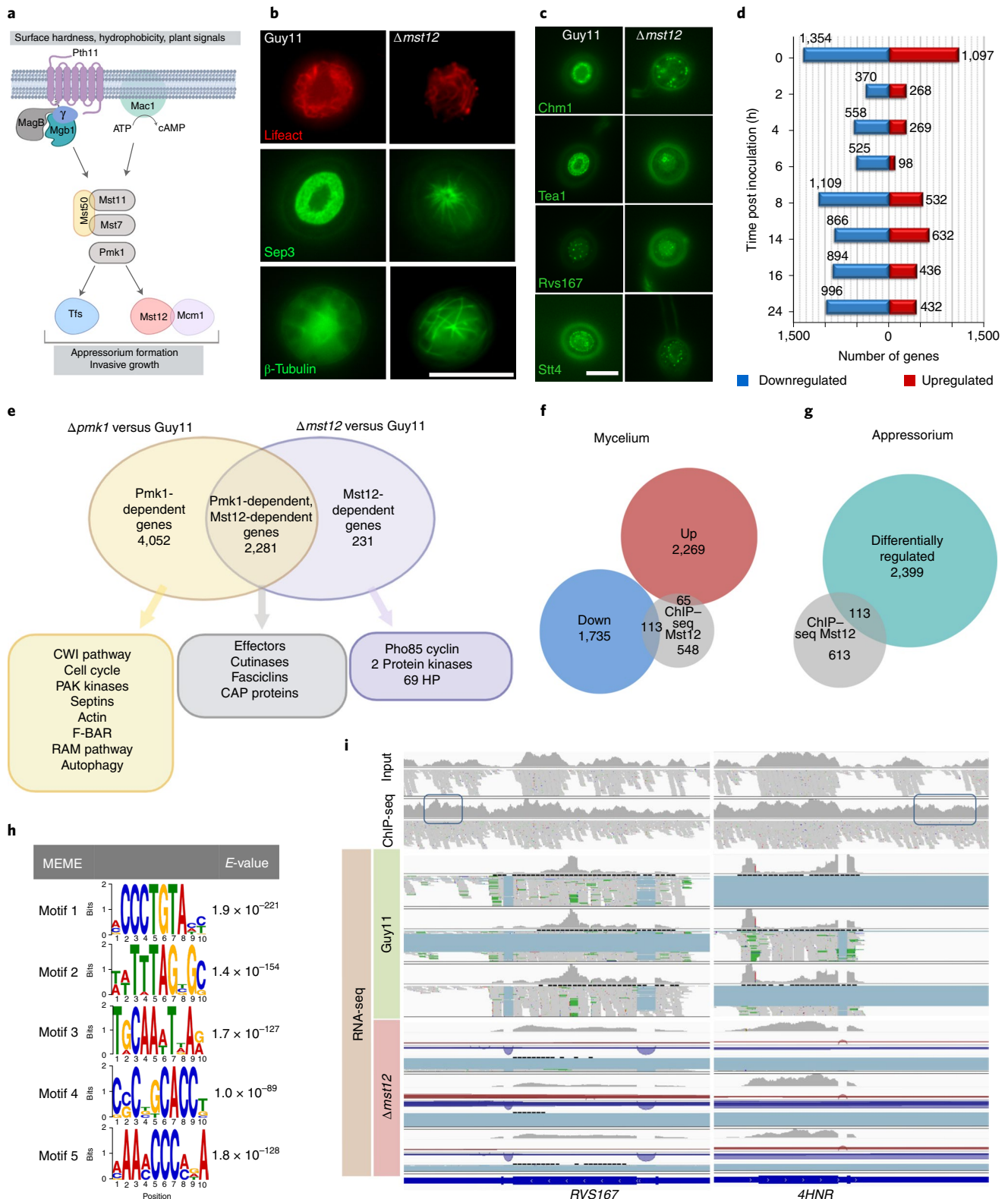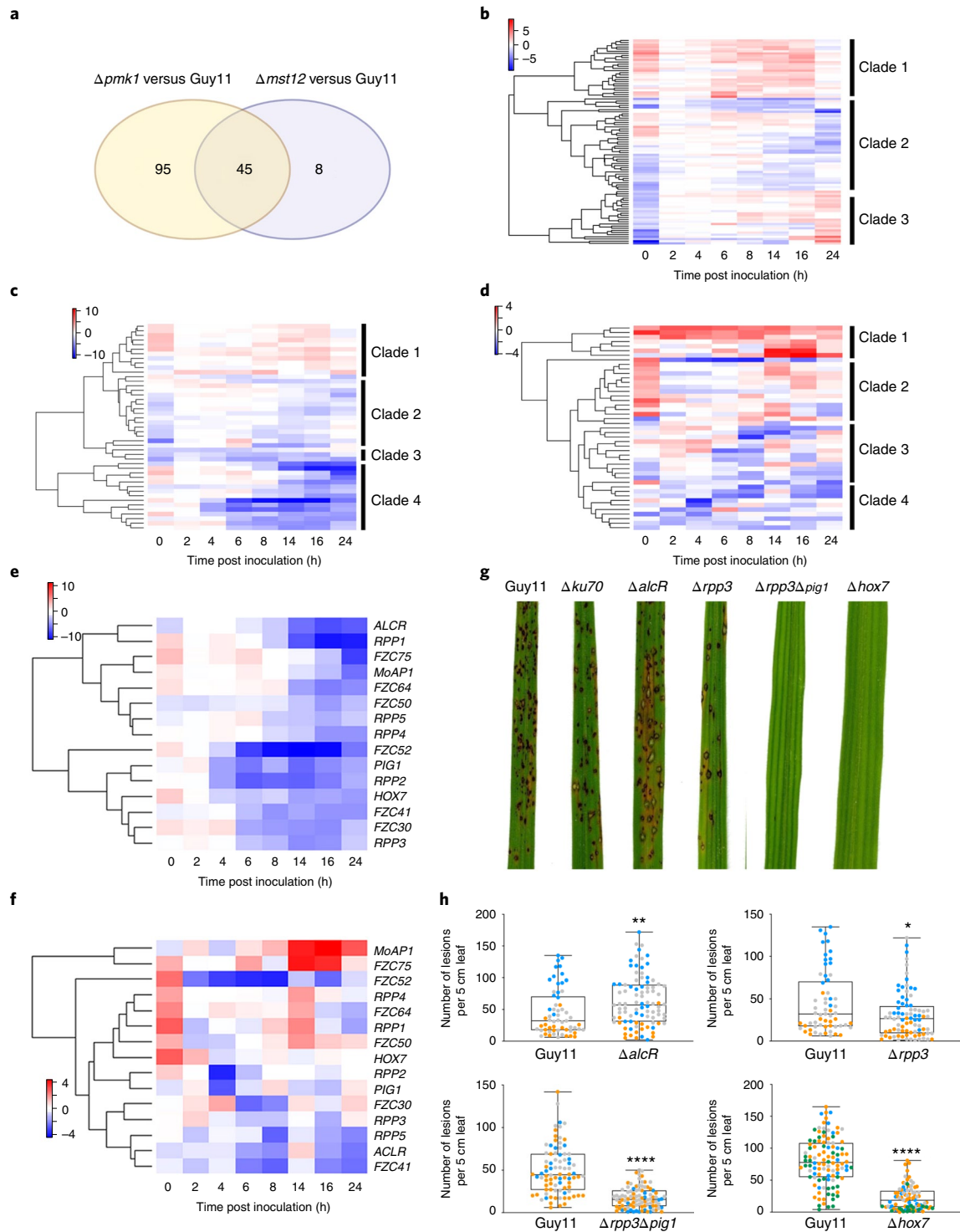
We carried out ChIP–seq analysis to identify targets of the TF Hox7. A functional Hox7–3×FLAG fusion protein was expressed in Δ*hox7*, which fully complemented its phenotype (Extended Data Fig. 7). Cross-linked chromatin was isolated from mycelium, followed by immunoprecipitation and sequencing of Hox7–3×FLAG-bound genomic DNA. ChIP–seq identified 242 broad peaks ±2 kb of 238 genes (Supplementary Table 10), which defined 15 downregulated and 66 upregulated genes during mycelium growth and 33 downregulated and 56 upregulated genes during appressorium development (Fig. 4e,f and Extended Data Fig. 7d). Among the Hox7 targets were three Clade 4 TFs—*FZC64* (MGG_00320) and *FZC52* (MGG_09676)[36],

and *RPP3* (MGG_07218)—consistent with Hox7 acting within a transcriptional hierarchy during appressorium morphogenesis. The melanin biosynthetic genes *RSY1* (MGG_05059), required for appressorium function[27], and *RTT109* encoding a H3K56 histone acetylation protein involved in pathogenicity[41] were also identified. Five over-represented consensus motifs within peak sequences were predicted by ChIP–seq (Fig. 4h). Motifs 1–5 were over-represented (*P* < 0.001) in Hox7-dependent DEGs, as identified by RNA-seq. Motif 2 was present in 1,989 of 2,332 Hox-dependent genes (85.29%) during appressorium development (Extended Data Fig. 7e). Targets of Hox7 included a basic Helix Loop Helix TF gene, MGG_10575,

Fig. 3 | Defining the hierarchy of transcriptional control during appressorium development by *M. oryzae*. a, Venn diagram showing overlapping sets of *M. oryzae* putative TF-encoding genes with at least twofold differential expression between Δ*pmk1* and Guy11; Δ*mst12* and Guy11; and Δ*pmk1*, Δ*mst12* and Guy11 in at least two time points ($P_{adj} < 0.01$ and mod_lfc > 1 or mod_lfc < −1). **b**, Heatmap showing the temporal pattern of the relative transcript abundance of 95 TF-encoding genes between Δ*pmk1* and Guy11. **c**, Heatmap showing the temporal pattern of the relative transcript abundance of 45 TF-encoding genes between Δ*pmk1* and Guy11. **d**, Heatmap showing the temporal pattern of the relative transcript abundance of 53 TF-encoding genes between Δ*mst12* and Guy11. **e**, Heatmap showing the temporal pattern of the transcript abundance of Clade 4 TF-encoding genes that are differentially regulated in Δ*pmk1* as compared with Guy11. **f**, Heatmap showing the temporal pattern of the transcript abundance of Clade 4 TF-encoding genes that are differentially regulated in Δ*mst12* as compared with Guy11. **b–f**, Genes that are downregulated in the mutant are shown in blue and those that are upregulated in red. **g**, Rice blast disease symptoms of the Δ*alcR*, Δ*rpp3*, Δ*rpp3*Δ*pig1* and Δ*hox7* mutants as compared with Guy11 and a Δ*ku70* mutant. Rice seedlings of cultivar CO-39 were spray-inoculated with conidial suspensions of equal concentrations of each *M. oryzae* strain and incubated for 5 d. **h**, Number of rice blast disease lesions generated per 5 cm leaf in pathogenicity assays. Box-and-whisker plots with individual data points (data points of different colours represent different biological replicates); the boxes show the 25th and 75th percentiles, the median is indicated by a horizontal line and the minimum and maximum values by the ends of the whiskers. A two-tailed non-parametric Mann–Whitney test was conducted; Δ*alcR* versus Guy11, **$P = 0.0017$, $n = 3$ biological replicates; Δ*rpp3* versus Guy11, *$P = 0.0131$, $n = 3$ biological replicates; Δ*rpp3*Δ*pig1* versus Guy11, ****$P < 0.0001$, $n = 3$ biological replicates; and Δ*hox7* versus Guy11, ****$P < 0.0001$, $n = 4$ biological replicates.

homologous to *Candida albicans CPH2* (4×10^{-22}), involved in hyper-filamentous growth and hyphae development[42] and a RAN1/PAT1 kinase gene (MGG_05074)-similar mammalian gene required for cell-cycle progression and meiotic development[43] (Fig. 4g).

Hox7 is a direct target of the Pmk1 MAP kinase in *M. oryzae*. To understand how Pmk1 regulates Hox7, we carried out exploratory and quantitative phosphoproteomic analyses. Phosphoproteins were purified from Δ*pmk1*, Δ*hox7* and Guy11 at 6 h following conidial germination and analysed by liquid chromatography with tandem mass spectrometry (LC–MS/MS). This revealed Pmk1-dependent phosphorylation of proteins associated with cell-cycle control—including Dun1 and Far1—the autophagy-related proteins Atg13 and Atg26, and eight components of the cAMP–PKA pathway[44,45]. A subset of phosphoproteins were also dependent on the presence of Hox7 (Fig. 5a).

Importantly, phosphorylation of Hox7 was detected at a proline-directed serine residue at position 158 within a PxSP MAP kinase motif, and two other residues, S126 and S254 (Fig. 5a and Extended Data Fig. 8). These serine residues, especially S158, were conserved among putative Hox7 orthologues in many filamentous fungi, but not yeast, species (Extended Data Fig. 8). To test whether phosphorylation of S126, S158 and S254 was Pmk1-dependent, parallel reaction monitoring (PRM) was performed in both Guy11 *M. oryzae* and Δ*pmk1* mutants (Supplementary Table 11). The PRM showed that the relative normalized intensity of peptides associated with S126 and S158 of Hox7 was reduced in Δ*pmk1* compared with Guy11 (Fig. 5b,c). We therefore decided to carry out PRM using the *pmk1*[AS] mutant in which MAPK activity could be inhibited with 1NA-PP1. Conidia of the *pmk1*[AS] mutant were germinated on an HP surface and treated with 1NA-PP1. Phosphoproteins were extracted at 2, 3 and 4 h following treatment with or without 1NA-PP1 (Fig. 5d) and the relative normalized intensity of peptides associated with S126 (Fig. 5f), S158 (Fig. 5g) and S254 (Fig. 5h) of Hox7 was

measured. There was a maximum intensity value at 3–4 h for the three peptides in the absence of NA-PP1 (Fig. 5f–h) but the relative normalized intensity of peptides was reduced ($P < 0.01$) in the presence of NA-PP1 (when Pmk1 is inactive), providing evidence that phosphorylation of S158 in particular depends on Pmk1, either directly or indirectly. We carried out an identical experiment in which 1NA-PP1 was added at later time points (4 h) to define the window of Pmk1-dependent phosphorylation of Hox7. The normalized intensity of phosphopeptides was reduced following Pmk1 inhibition (Extended Data Fig. 9) but less pronounced than in the original experiment (Fig. 5d–h), consistent with Pmk1-dependent phosphorylation of S158 of Hox7 occurring within the first 3–4 h of conidial germination.

To determine whether Pmk1 phosphorylates Hox7, we carried out an in vitro kinase assay, followed by LC–MS/MS. We expressed and purified 6×His–glutathione-*S*-transferase (GST)–Pmk1 (GST–Pmk1), 6×His–small ubiquitin-like modifier (SUMO)–Mst12 (SUMO–Mst12) and 6×His–maltose-binding protein (MBP)–Hox7t-342 proteins from *Escherichia coli* and incubated them in the presence of a recombinant, constitutively active MAPKK from tobacco (*Nicotiana tabacum*)[46] called MEK2[DD] (Fig. 6), which specifically activates Pmk1 in a pTEpY motif (see Extended Data Fig. 10b). When MEK2[DD]-activated GST–Pmk1 was incubated in the presence of SUMO–Mst12 we reproducibly detected phosphorylation at S133 of Mst12 within a MAP kinase motif PxSP (Fig. 6). Other phosphoproteins of Mst12 were also observed but consistent spectral counts were found for S133 (see Supplementary Table 12). This provides evidence that MEK2[DD] activates 6×His–GST–Pmk1, which enables Pmk1 to phosphorylate its targets, including Mst12. We were also able to detect phosphorylation of Hox7 and reproducibly identify a peptide associated with S158 (Fig. 6) as the clearest outcome of Pmk1-dependent phosphorylation, consistent with discovery phosphoproteomics and PRM experiments. We conclude that Pmk1 can phosphorylate Mst12 at S133 and Hox7 at S158, both of which occur within MAPK motifs .

Fig. 4 | Characterization of the Hox7 homeobox TF and its role in the regulation of gene expression during appressorium development by *M. oryzae*.
a, Bright-field microscopy of appressorium development by Guy11 and a Δ*hox7* mutant following incubation on an HP surface for 24 h. The arrow points to re-germination of an incipient appressorium and hyphal elongation. **b**, Venn diagram showing overlapping sets of genes with at least twofold difference ($P_{adj} < 0.01$ and mod_lfc > 1 or mod_lfc < −1) between Guy11 and the Δ*pmk1*, Δ*mst12* and Δ*hox7* mutants, respectively, during 14 h of appressorium development. **c**, Heatmap showing the relative transcript abundance of Clade 4–associated TF genes in the Δ*pmk1*, Δ*mst12* and Δ*hox7* mutants as compared with Guy11. **d**, Live-cell images showing nuclear dynamics in Guy11 and the Δ*pmk1*, Δ*hox7* and Δ*mst12* mutants, each expressing H1–RFP or H1–GFP, after 24 h germination on an HP surface. **a,d**, Scale bars, 10 μm. **e**, Number of genes that were downregulated ($P_{adj} < 0.01$ and mod_lfc < −1), upregulated ($P_{adj} < 0.01$ and mod_lfc > 1) or bound by Hox7 (grey) during mycelium growth (determined by ChIP–seq; three biological replicates). **f**, Number of genes that were downregulated ($P_{adj} < 0.01$ and mod_lfc < −1), upregulated ($P_{adj} < 0.01$ and mod_lfc > 1) or bound by Hox7 (grey) during appressorium development at 14 h (determined by ChIP–seq; three biological replicates). **g**, Representative raw ChIP–seq peaks and RNA-seq for the basic Helix Loop Helix TF gene (*bHLH*; MGG_10575) homologous to *C. albicans HMS1* and the *RAN1/PAT1* kinase gene (MGG_05074). The blue boxes represent the peaks identified by MACS2 using ChIP–seq analysis. **h**, Consensus DNA-binding motifs, predicted using MEME, for the TF Hox7 based on ChIP–seq analysis.

Pmk1-dependent Hox7 phosphorylation is necessary for appressorium development. To determine the physiological relevance of Hox7 phosphorylation, alleles of Hox7 were generated with serine–alanine substitutions to prevent phosphorylation and serine–aspartate substitutions to mimic phosphorylation. These

were expressed in a $\Delta hox7$ mutant. Conidia of Guy11, $\Delta hox7$, a $\Delta hox7$:TrpC-Hox7 strain complemented with the wild-type *HOX7* allele, the phospho-dead $\Delta hox7$:$TrpCp$-$Hox7^{S126A\text{-}S158A\text{-}S254A}$ mutant and the phosphomimetic $\Delta hox7$:$TrpCp$-$Hox7^{S126D\text{-}S158D\text{-}S254D}$ mutant were inoculated on HP surfaces. We then evaluated their ability to
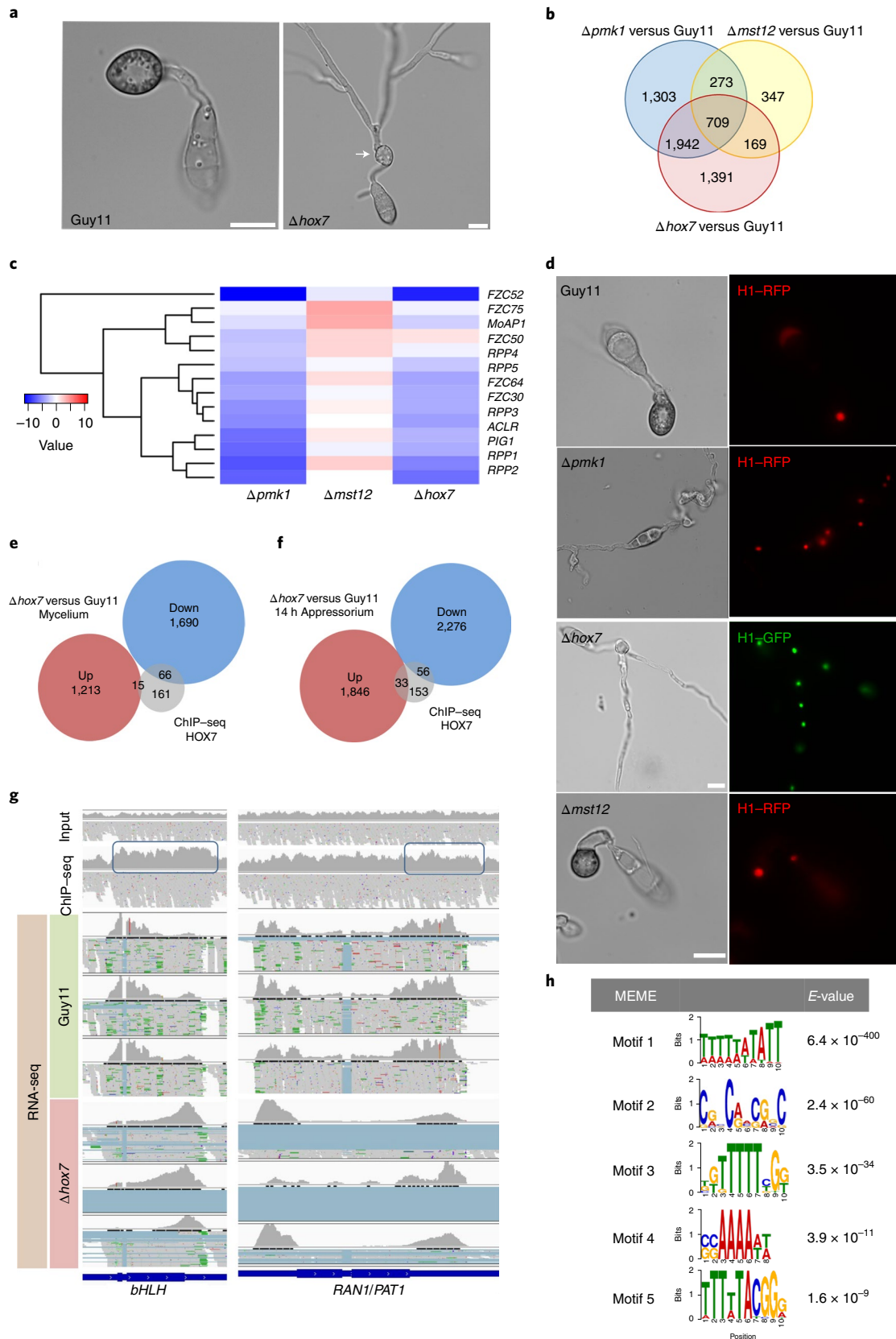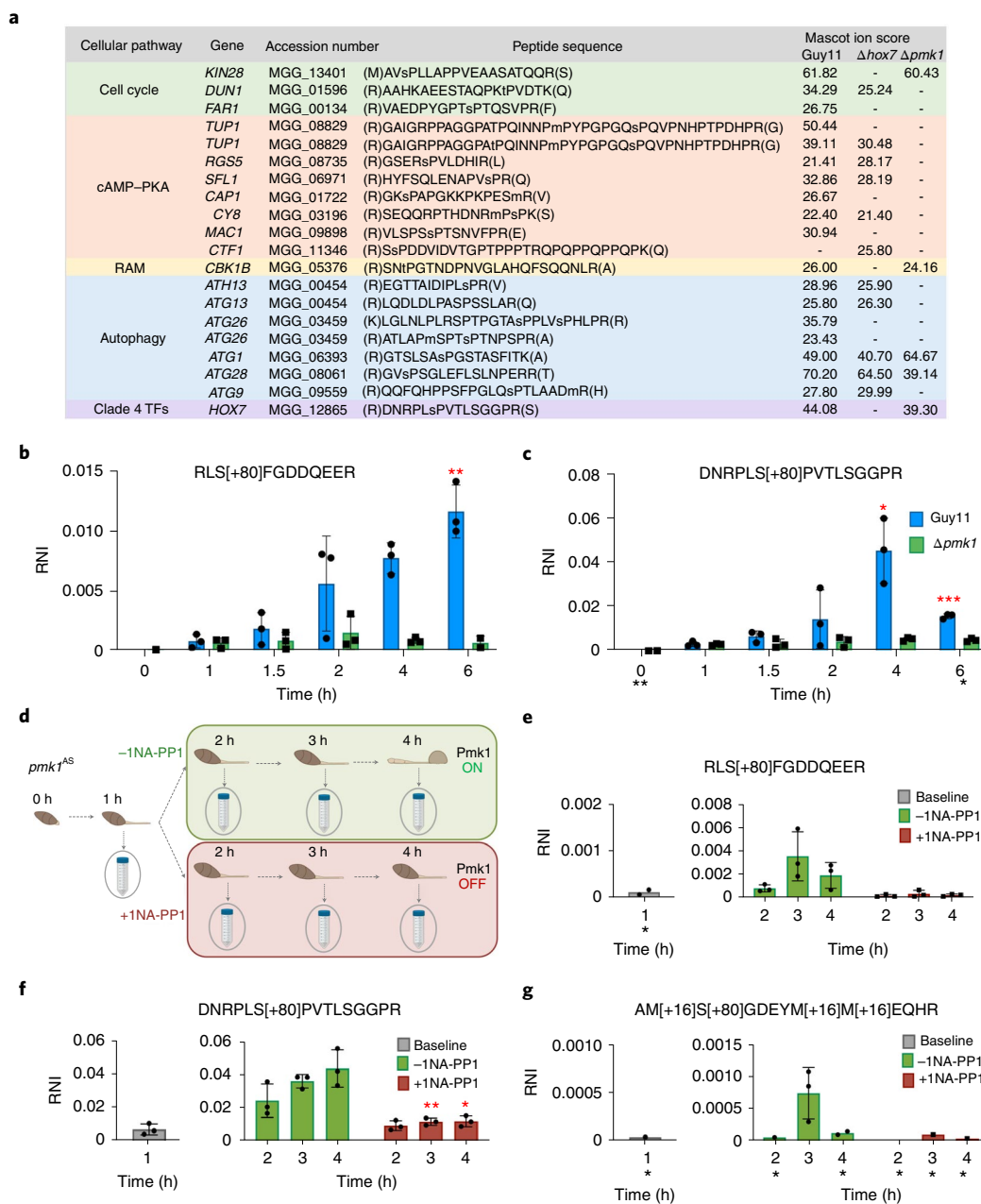
Fig. 5 | Phosphoproteomic analysis reveals Pmk1-dependent phosphorylation of Hox7 in *M. oryzae*. a, Classification of phosphoproteins identified by discovery phosphoproteomics in Guy11 and the Δ*pmk1* and Δ*hox7* mutants at 6 h of appressorium development on an HP surface. The specific peptide sequence containing proline-directed phosphorylation either at a serine or threonine residue (lowercase 's' and 't') for each accession number is shown with the corresponding Mascot ion score. **b**, Relative normalized intensity (RNI), determined by PRM, of the peptide associated with phosphorylated S126 of Hox7 during appressorium development up to 6 h after conidial germination in Guy11 *M. oryzae* and the Δ*pmk1* mutant. **P = 0.0088 (6 h). **c**, RNI of the peptide associated with phosphorylated S158 of Hox7 during appressorium development up to 6 h after conidial germination in Guy11 and Δ*pmk1*, determined by PRM. *P = 0.0418 (4 h) and ***P = 0.0004 (6 h). **d**, Experimental design for PRM to measure the RNI of peptides associated with the S126, S158 and S254 residues in Hox7. The *pmk1*^AS conditional mutant was incubated on an HP surface for 1 (baseline), 2, 3 and 4 h in the presence or absence of the ATP analogue 1NA-PP1 (+1NA-PP1 and −1NA-PP1, respectively). Falcon tubes represent sample collection. **e**, RNI of the peptide associated with phosphorylated S126 of Hox7 during appressorium development in *pmk1*^AS conditional mutant ±1NA-PP1, determined by PRM. **f**, RNI of peptide associated with phosphorylated S158 of Hox7 during appressorium development in *pmk1*^AS conditional mutant in ±1NA-PP1, determined by PRM. **P = 0.0027 (3 h) and *P = 0.0315 (4 h). **g**, RNI of the peptide associated with phosphorylated S254 of Hox7 during appressorium development in the *pmk1*^AS conditional mutant ±1NA-PP1, determined by PRM. **b,c,e–g**, Data are the mean ± s.d.; *n* = 3 biological replicates with one (**b,e–g**) or two (**c**) technical replicates per biological replicate. Black asterisks indicate that some peptides could not be detected in one or more biological replicates; red asterisks indicate significant *P* values.

form appressoria after 24 h. The phospho-dead Δ*hox7:TrpCp-Hox7*^S126A-S158A-S254A mutant was unable to develop appressoria and instead formed re-germinated terminal swellings. By contrast, the phosphomimetic Δ*hox7:TrpCp-Hox7*^S126D-S158D-S254D mutant was able to develop melanised appressoria but also exhibited a diverse set of other morphologies, which also varied among individual transformants

	Hox7								Mst12							
	MBP–Hox7t–342		MEK2DD and MBP–Hox7t–342		GST–Pmk1 and MBP–Hox7t–342		MEK2DD and GST–Pmk1 and MBP–Hox7t–342		SUMO–Mst12		MEK2DD and SUMO–Mst12		GST–Pmk1 and SUMO–Mst12		MEK2DD and GST–Pmk1 and SUMO–Mst12	
	Rep1	Rep2	Rep1	Rep2	Rep1	Rep2	Rep1	Rep2	Rep1	Rep2	Rep1	Rep2	Rep1	Rep2	Rep1	Rep2
SUMO–Hox7t-342																
(R)DNRPL[pS]PVTLSGGPR (S158)																
S6/7: phospho (+79.97)					2	2	6	7								
(R)DNRPLSPV[pT]LSGGPR																
T9/10: phospho (+79.97)							2	1								
LRVIPQDGQTSTPSSTTSPISGPPG[pT]L[pT]PPE[pY]VHSP[pTS]QNK(R)																
T26: phospho (+79.97)							1									
T28: phospho (+79.97)							1									
Y32: phospho (+79.97)								2								
S38: phospho (+79.97)								1								
T37: phospho (+79.97)								1								
LYTSQSQA[pY]QR																
Y9: phospho (+79.97)					1											
SNSPTMSTLAMAAP[pS]PHAPFKK																
S15: phospho (+79.97)								1								
SSTSDSWAGS[pS]RT[pS]PFLPGTSTSTLR																
S11: phospho (+79.97)								2								
S14: phospho (+79.97)								1								
TSPFLPGTSTSTLR[pS]PAAIEQNDPMDR																
S15: phospho (+79.97)								1								
S15: phospho (+79.97), m25: oxidation (+15.99)							2									
VIPQDGQTSTPSSTTSPISGPPGTLTPPEYVHSPT[pS]QNKR																
S36: phospho (+79.97)								1								
MBP–Mst12																
SGTDASLEEPK[pS]PFLDFLYK (S133)																
S12: phospho (+79.97)															4	2
HAS**M**PAYGLEYSPAP[pS]FVSSHYDDYGNR																
M4: oxidation (+15.99), s16: phospho (+79.97)															1	
[pS]A[pT]VMGSEVGPYPQK																
S1: phospho (+79.97)											1					
S1: phospho (+79.97), m5: oxidation (+15.99)											1				1	
T3: phospho (+79.97)											1					
T3: phospho (+79.97), m5: oxidation (+15.99)											1				1	

Fig. 6 | Purified recombinant GST–Pmk1 phosphorylates MBP–Hox7 and SUMO–Mst12 in vitro. MBP–Hox7 and SUMO–Mst12 were incubated with or without GST–Pmk1 and 6×His-tagged MEK2DD in the presence of 1 µM ATP for 30 min, as indicated in each column. Phosphorylated peptides were identified by LC–MS/MS and the spectra were manually inspected. MEK2DD phosphorylates the activation loop of Pmk1 in vitro, activating the Pmk1 kinase activity (see Supplementary Table 13). Activated purified GST–Pmk1 phosphorylates multiple residues on MBP–Hox7t-342 and SUMO–Mst12 TFs, including sites in the PxSP motifs identified in vivo. Phosphopeptides are shown with modified residues in red, and phosphorylation is shown as pS or pT in brackets (+79.97 Da) and oxidized methionine by M (+15.99 Da). Spectral counts are shown from two technical replicates (Rep1 and Rep2), with the position of the modified residue indicated. MBP–Hox7t-342, His-tagged MBP–Hox7 truncated (Met1-Q342) fusion protein.

(Extended Data Fig. 10). Hox7 phosphorylation by Pmk1 is therefore necessary for its function during appressorium development by *M. oryzae*.

Discussion
In this study we have identified the global transcriptional signature associated with appressorium development by *M. oryzae* in response to surface hydrophobicity and used comparative transcriptome analysis to define a hierarchy of Pmk1-dependent TFs necessary for appressorium morphogenesis. Collectively, this has enabled formulation of the model presented in Fig. 7c.

The TF Hox7 emerges from this study as an important regulator of appressorium development. Hox7 was previously reported to be necessary for plant infection[39] but its function was unknown. Based on phosphoproteomic analysis of a Δ*pmk1* mutant, PRM of a conditional *pmk1*[AS] mutant and an in vitro kinase assay, we can conclude that Hox7 is phosphorylated at S158 in a Pmk1-dependent manner within a MAP kinase phosphorylation motif (Fig. 5). We have also demonstrated that Pmk1-dependent Hox7 phosphorylation is required for its biological function because a Δ*hox7* mutant cannot be complemented by a non-phosphorylatable Hox7 protein, while expression of a phosphomimetic allele of *HOX7* is
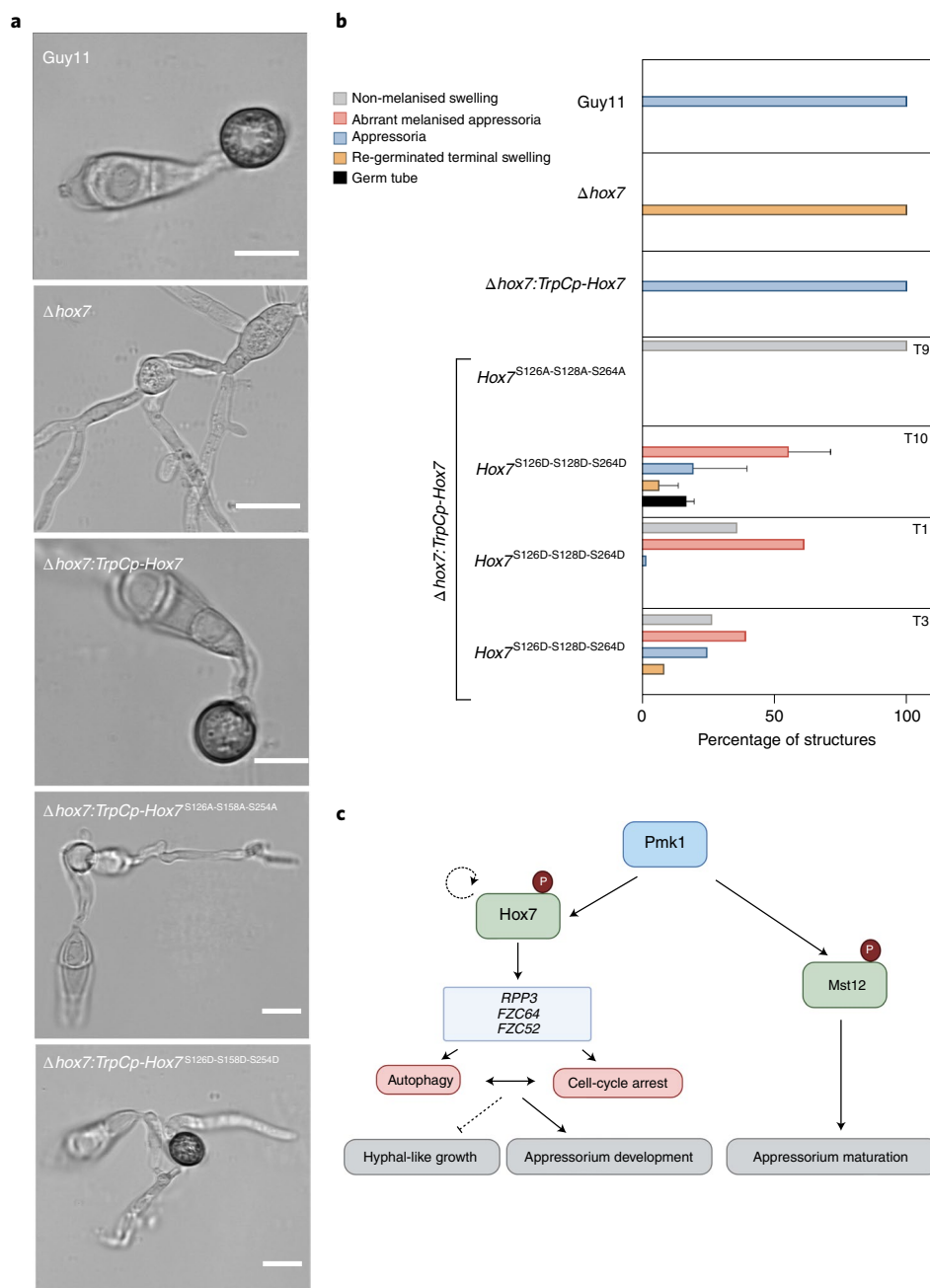
Fig. 7 | Pmk1-dependent phosphorylation of Hox7 is required for appressorium development. a, Micrographs showing appressorium development of Guy11, the Δ*hox7* null mutant, complemented strain Δ*hox7:TrpC-Hox7*, Δ*hox7* null mutant expressing a phospho-dead allele of *Hox7* (Δ*hox7:TrpCp-Hox7*[S126A-S158A-S254A]; Transformant 9, T9) and Δ*hox7* null mutant expressing a phosphomimetic allele of *Hox7* (Δ*hox7:TrpCp-Hox7*[S126D-S158D-S254D]). Micrographs were obtained following conidial incubation on an HP surface for 24 h. Scale bars, 10 μm. Expression of a *Hox7* phosphomimetic allele can restore appressorium formation, whereas the *Hox7* phospho-dead allele fails to complement Δ*hox7*. **b**, Frequency of infection structure formation by Guy11; Δ*hox7*; and the Δ*hox7:TrpC-Hox7*, Δ*hox7:TrpCp-Hox7*[S126A-S158A-S254A] and Δ*hox7:TrpCp-Hox7*[S126D-S158D-S254D] transformants (T10, T1 and T3 are three independent fungal transformants from three independent fungal transformation experiments). Three biological replicates of the experiment were performed. A total of 476 structures were counted for the entire experiment; data are the mean ± s.e.m. **c**, Model illustrating hierarchical control of gene expression by the Pmk1 MAPK and associated TFs Hox7 and Mst12 in *M. oryzae*. Hox7 is directly phosphorylated by Pmk1 at S158, which may also exert a positive effect on *HOX7* gene expression (dotted line). Hox7 directly regulates expression of Clade 4–associated TF-encoding genes *RPP3*, *FZC64* and *FZC52*, as well as targets to regulate autophagy and cell cycle arrest following the initial round of mitosis, following conidial germination. Hox7 induces appressorium development and represses hyphal growth. Pmk1 also phosphorylates Mst12 at S133 to regulate the expression of genes associated with maturation of the appressorium, including septin-dependent cytoskeletal re-organization and, re-polarization, exocytosis and effector expression.

sufficient to restore appressorium development. The range of phenotypes observed in mutants expressing a phosphomimetic allele of *HOX7* also provides evidence for the fundamental role of this TF in germ-tube development and appressorium morphogenesis, including a potential inhibitory effect on hyphal growth. As a direct target of Pmk1, Hox7 seems to be positioned at the top of a hierarchy of TFs associated with appressorium morphogenesis, which is consistent with the significant overlap in DEGs of both the Δ*pmk1*

and Δ*hox7* mutants. ChIP–seq furthermore revealed three of the Clade 4 TFs—*FZC64*, *FZC52* (ref. [36]) and *RPP3*—to be targets of Hox7, suggesting that they may constitute the next layer of a hierarchy of transcriptional regulators.

Homeobox TFs act both as activators and repressors of gene expression during multicellular development[47]. They were first described as developmental-switch genes in *Drosophila melanogaster* and subsequently in many other eukaryotes[48,49]. Homeobox TFs have also been extensively studied in cancer biology, where they are implicated in the control of autophagy and cell-cycle regulation. In glioblastomas, for example, HoxC9 acts as a negative regulator of autophagy by controlling activation of beclin1, by regulating transcription of death-associated protein kinase1 (ref. [50]), whereas in neuroblastomas, HoxC9 interacts directly with cyclins to promote G1 arrest by downregulating the transcription of cyclin and CDK genes[51]. Here we have shown how Pmk1 and Hox7 are both essential for the expression of autophagy-related and cell cycle-control genes during appressorium morphogenesis. Hox7 may therefore be essential for G1 arrest in the appressorium nucleus, which follows the initial round of mitosis in the germ tube after conidial germination, given its regulation of genes potentially involved in G1 regulation—such as *Dun1*, *Cds1* and *Chk1*—and the multiple rounds of mitosis observed in the Δ*hox7* mutants[7,25]. This is consistent with Pmk1-dependent phosphorylation of Dun1 and Far1. Cell-cycle arrest may be necessary to repress hyphal-like growth and trigger conidial cell death, but the mechanism by which this occurs and precise interplay with the initiation of autophagy in the conidium require further study. One possibility is that Hox7 is influenced by starvation stress because appressorium development is repressed by exogenous nutrients[1,23,52]. However, the TOR-dependent metabolic checkpoint, reported to lead to a G2 arrest in the conidial nucleus before mitosis[9–11], is not necessary for the action of Pmk1 or Hox7, because TOR inactivation by rapamycin or induction of G2 arrest with benomyl have no effect on the mutant phenotypes of either regulator. How nutrient-sensing affects Hox7 is therefore unclear but interplay with the Snf1 kinase pathway may occur. In yeast[53], Snf1 regulates Atg1 and Atg13, acting antagonistically to the cyclin protein kinase Pho85, which in turn is a negative regulator of autophagy[54]. Moreover, Pho85 regulates infection-associated morphogenesis and virulence in pathogenic fungi such as *Ustilago maydis* and *C. albicans*[55–57]. In *M. oryzae*, Snf1 mutants are impaired in appressorium development, lipid mobilization and turgor generation[58], but the role of Snf1 in the control of autophagy, cell-cycle progression and its relationship to the TOR-dependent metabolic checkpoint[9–11] are unknown. Investigating the interplay of Snf1 and Pho85 with Hox7 may therefore prove valuable in future.

The role of Mst12 is also more clearly defined by this study. Mst12 is directly phosphorylated by Pmk1 at S133 within a MAPK phosphorylation motif but acts in a very distinct way to Hox7, controlling expression of more than 2,000 genes involved in appressorium function. For example, *RVS167*, which is implicated in septin-dependent appressorium re-polarization[15], is a direct target of Mst12. However, Mst12 also regulates an additional 53 TFs as well as genes associated with plant tissue colonization, including a subset of effectors involved in suppression of host immunity. Together, our observations suggest that the Mst12 TF regulates a wide range of functions associated with fungal invasive growth.

In summary, we have provided evidence that Pmk1 MAPK acts as a global regulator of appressorium development and fungal invasive growth by controlling a hierarchical network of transcriptional regulators, including Hox7 and Mst12. In this way appressorium morphogenesis can be seen to be orchestrated by a small number of master regulators acting directly downstream of Pmk1 that are responsible for direct regulation of a set of target genes, including a large family of TF-encoding genes, collectively necessary for the

rapid elicitation of the extensive transcriptome changes required for appressorium development.

Methods

Fungal strains, growth conditions and plant infection assays. All of the *M. oryzae* isolates used and generated in this study are stored in the laboratory of N.J.T. (The Sainsbury Laboratory). Fungal strains were routinely incubated at 26 °C with a 12 h photoperiod on complete medium[1]. Rice infections were performed using the blast-susceptible rice (*Oryza sativa*) cultivar CO-39 (ref. [59]). For plant infections, conidial suspensions (5×10^4 conidia ml^{-1} in 0.1% gelatin) were spray-inoculated onto three-week-old seedlings and incubated for 5 d in a controlled-environment chamber at 24 °C with a 12 h photoperiod and 90% relative humidity. The disease-lesion density was recorded 5 d post inoculation, as described previously[60]. Fungal transformations were carried out as previously described[60]. For leaf spot infection experiments, one-week-old leaves of the barley cultivar Golden Promise were spot-inoculated with 20 µl of a 1×10^4 conidia ml^{-1} suspension in 0.2% gelatin in unwounded and needle-wounded leaves. The leaves were incubated on humidity chambers, and lesions were harvested after 5 d and transferred to 2 ml tubes with 300 µl of double-distilled water. Spores from the lesions were recovered by vortex mixing and quantified. The experiments were repeated at least three times.

Generation of GFP fusion plasmids and strains expressing GFP and RFP fusions. The corresponding DNA sequences were retrieved from the *M. oryzae* database (http://fungi.ensembl.org/Magnaporthe_oryzae/Info/Index). In-Fusion cloning (In-Fusion cloning kit, Clontech Laboratories) was used to generate Flp1–GFP and Flp2–GFP. The sequences of the primers used are provided in Supplementary Table 13. Amplified fragments were cloned into HindIII-digested 1284 pNEB-Nat-Yeast vector with the *BAR* gene conferring bialophos (BASTA) resistance. Plasmids expressing GFP and RFP fusions were transformed into Guy11, and Δ*pmk1*, Δ*mst12* and Δ*hox7* mutants and *M. oryzae* transformants with single insertions were selected by Southern blot analysis. Independent *M. oryzae* transformants were used for screening and selected for consistency of fluorescence localization.

Generation of complementation, phosphomimetic and phospho-dead strains. In-Fusion cloning (Clontech Laboratories) was used to generate Mst12–GFP, TrpCp-Hox7, TrpCp-Hox7$^{S126A-S158A-S254A}$, TrpCp-Hox7$^{S126D-S158D-S254D}$ and hox7p:Hox7 (2, 1.5 and 1 kb) using the primers in Supplementary Table 13. Mst12 amplified fragments were cloned into 1284 pNEB-Nat-Yeast cloning vector with the *BAR* gene conferring bialophos (BASTA) resistance. Hox7 fragments were cloned into pCB1532 containing a sulfonylurea-resistant allele of the *ILV2* gene encoding acetolactate synthase under the *A. nidulans* TrpC promoter or Hox7 native promoter. The plasmid constructs were introduced ectopically into fungal strains via PEG-mediated transformation[60]. Presence of the phosphomimetic and phospho-dead alleles was confirmed by Phusion PCR, cleaned enzymatically using ExoSAP-IT PCR product cleanup reagent (Thermo Fisher Scientific) and sequenced. Transformants with single insertions of Mst12–GFP plasmid were confirmed by quantitative PCR by iDna Genetics Ltd.

Generation of *M. oryzae* targeted gene deletion mutants. Targeted gene replacement mutants of *M. oryzae*[60] were generated using the split marker technique[6]. Gene-specific, split marker constructs were amplified using the primers in Supplementary Table 13 and fused with the bialophos (BASTA)-resistance cassette or hygromycin-resistance gene cassette transformed either into Guy11 or Δ*ku70*. Transformants were selected on glufosinate (30 µg ml^{-1}) or hygromycin (200 µg ml^{-1}) and assessed by Southern blot analysis to verify complete deletion of each gene.

In vitro appressorium development assays and live-cell imaging. Appressorium development was induced on borosilicate 18 mm × 18 mm glass coverslips, termed the HP surface in all experiments (Fisher Scientific). Conidial suspensions were prepared at 5×10^4 conidia ml^{-1} in double-distilled water, and 50 µl of the conidial suspension was placed on the coverslip surface and incubated in a controlled-environment chamber at 24 °C. For incubation on non-inductive surfaces, the hydrophilic surface of Gelbond (Sigma) was used (the HL surface). Epifluorescence and differential interference contrast microscopy were carried out using an IX81 motorized inverted microscope (Olympus) and images were captured using a Photometrics CoolSNAP HQ2 camera (Roper Scientific) under control of the MetaMorph v7.8 software (MDS Analytical Technologies). Datasets were compared using an unpaired Student's *t*-test. For the rapamycin exposure experiment, conidia were harvested from nine-day-old cultures and resuspended in 1 µg ml^{-1} rapamycin (Sigma). The spore suspensions were inoculated onto HP coverslips for 24 h. For the benomyl exposure experiment, conidia were harvested from nine-day-old cultures and spore solutions were prepared. Conidial suspensions were prepared at 5×10^4 conidia ml^{-1} in double-distilled water incubated on HP coverslips. At 2.5 h, 50 µM benomyl (Sigma) was added to the conidial suspensions. After 3 h, benomyl was removed with sterile double-distilled water. Images were acquired at 24 h to determine the frequency of appressorium

formation. Solvent-only (dimethylsulfoxide) control experiments were carried out for all drug treatments.

RNA extraction and RNA-seq analysis. For time-series appressorial RNA-seq analysis, conidia were harvested from ten-day-old complete medium agar plates, washed and conidial suspensions (7.5×10^5 conidia ml^{-1}) were prepared in the presence of 50 ng μl^{-1} 1,16-hexadecanediol (Sigma). This spore suspension was poured into square Petri dishes (Greiner Bio One), to which ten glass coverslips (Cole-Parmer) were attached with adhesive. Appressorium formation was monitored using a Will-Wetzlar light inverted microscope (Wilovert, Hund Wetzlar) for each time point, ensuring homogeneous, synchronized infection structure formation. Samples were collected and total RNA was extracted using the Qiagen RNeasy plant mini kit according to manufacturer's instructions. RNA-seq libraries were prepared using 5 μg total RNA with a True-Seq RNA sample preparation kit from Illumina (Agilent) according to the manufacturer's instructions and sequenced using an Illumina 2000 Sequencer. Output short reads were aligned against *M. oryzae* genome sequence version 8.0 using the TopHat software[61]. Data analysis was performed using DESeq, which determines differential gene expression using the mod_lfc value[62]. Transcript abundances for each gene and P_{adj} values were generated. To determine the significant differences of the pairwise comparisons, the *P* value was adjusted to $P \leq 0.01$.

For mycelial RNA-seq, two-day-old *M. oryzae* mycelium liquid cultures were grown at 24 °C with shaking at 125 r.p.m. Samples were collected and total RNA extracted using RNeasy Plant Mini kit (Qiagen) according to the manufacturer's instructions. Samples were sent to Novogene for library preparation and sequencing using the HiSeq 2500 Illumina technology. Raw reads were aligned to the reference genome 70-15 version 8 transcript FASTA file using a pseudo aligner Kallisto to obtain transcript abundance as transcripts per million[63]. The R package DESeq was used to determine log$_2$-transformed fold change values to identify DEGs. To analyse ChIP–seq results using IGV viewer, raw reads were cleaned and trimmed using fastp v. 0.20.1 and reads were mapped using hisat2 v. 2.1.0. The mapping parameters used were '–dta -t–no-softclip -k 10–score-min L,0,–0.6–reorder–no-unal'. The mapped reads were stored in the BAM format and were sorted and indexed using Samtools v. 1.5.

Protein extraction, phosphoprotein-enrichment, mass-spectrometry analysis for discovery phosphoproteomics, PRM and phosphopeptide quantification. Total protein was extracted from lyophilized *M. oryzae* appressoria from Guy11 and germlings of Δ*pmk1* mutants generated on borosilicate glass coverslips (18 mm × 18 mm; Thermo Fisher Scientific) at 0, 1, 1.5 and 2 h for the PRM experiment. For discovery phosphoproteomics, total protein was extracted from lyophilized *M. oryzae* appressoria from Guy11 and the Δ*pmk1* and Δ*hox7* mutants generated on borosilicate 18 mm × 18 mm glass coverslips (HP; Thermo Fisher Scientific) at 6 h, as performed for the RNA-seq experiments. Lyophilized appressoria were resuspended in extraction buffer (8 M urea, 150 mM NaCl, 100 mM Tris, pH 8, 5 Mm EDTA, 1 μg ml^{-1} aprotinin and 2 μg ml^{-1} leupeptin), mechanically disrupted in a 2010 GenoGrinder tissue homogenizer (1 min at 1,300 r.p.m.) and centrifuged for 10 min at 16,000*g* at 4 °C (Eppendorf Micro-centrifuge 5418). The supernatant was removed and used to determine the total protein concentration using the Bradford assay. For phosphopeptide enrichment, sample preparation started from 1–3 mg of total protein extract dissolved in ammonium bicarbonate buffer containing 8 M urea. First, the protein extracts were reduced with 5 mM Tris (2-carboxyethyl) phosphine (TCEP) for 30 min at 30 °C with gentle shaking, followed by alkylation of cysteine residues with 40 mM iodoacetamide at room temperature for 1 h. The samples were diluted to a final concentration of 1.6 M urea with 50 mM ammonium bicarbonate and digested overnight with trypsin (Promega; enzyme-to-substrate ratio of 1:100). Peptide digests were purified using C18 SepPak columns (Waters), as described previously[64]. Phosphopeptides were enriched using titanium dioxide (GL Science) with phthalic acid as a modifier[64]. Finally, the phosphopeptides were eluted by a pH shift to 10.5 and immediately purified using C18 microspin columns (The Nest Group Inc.; 5–60 μg loading capacity). After purification, all of the samples were desiccated in a SpeedVac, stored at −80 °C and resuspended in 2% acetonitrile with 0.1% trifluoroacetic acid before mass-spectrometry analysis. LC–MS/MS analysis was performed using an Orbitrap Fusion trihybrid mass spectrometer (Thermo Scientific) and nanoflow ultra-high-performance liquid chromatography (UHPLC) system (Dionex Ultimate3000, Thermo Scientific). Peptides were trapped to a reverse phase trap column (Acclaim PepMap, C18, 5 μm, 100 μm × 2 cm; Thermo Scientific). The peptides were eluted in a gradient of 3–40% acetonitrile in 0.1% formic acid (solvent B) over 120 min, followed by a gradient of 40–80% solvent B over 6 min at a flow rate of 200 nl min^{-1} at 40 °C. The mass spectrometer was operated in positive-ion mode with nano-electrospray ion source with a fused silica emitter with an inner diameter of 0.02 mm (New Objective). A voltage of 2,200 V was applied via platinum wire held in PEEK T-shaped coupling union, with the transfer capillary temperature set to 275 °C. The Orbitrap mass-spectrometry scan resolution of 120,000 at 400 *m/z*, range of 300–1,800 *m/z*, was used, and the automatic gain control was set to 2×10^5 and maximum injection time to 50 ms. In the linear ion trap, MS/MS spectra were triggered using a data-dependent acquisition method, with 'top speed' and 'most intense ion' settings. Selected

precursor ions were fragmented sequentially in both the ion trap using collision-induced dissociation and in the higher-energy collisional dissociation cell. The dynamic exclusion was set to 15 s. The charge state allowed between +2 and +7 charge states to be selected for MS/MS fragmentation.

Peak lists in Mascot generic file format (.mgf files) were prepared from raw data using the MSConvert package (Matrix Science). Peak lists were searched on Mascot server v. 2.4.1 (Matrix Science) against either *M. oryzae* (isolate 70-15, version 8) database or an in-house contaminants database. The MS/MS peak lists were exported using Discoverer v2.2 (Thermo Scientific). Tryptic peptides with up to two possible mis-cleavages and charge states +2, +3 and +4 were allowed in the search. The following modifications were included in the search: oxidized methionine, phosphorylation on serine, threonine, tyrosine as variable modification and carbamidomethylated cysteine as static modification. Data were searched with a monoisotopic precursor and fragment ion mass tolerance of 10 ppm and 0.6 Da, respectively. The Mascot results were combined in Scaffold v. 4 (Proteome Software) to validate the MS/MS-based peptide and protein identifications, and annotate spectra. The position of the modified residue and the quality of spectra for individual phosphopeptides were manually inspected and validated.

Peptide quantitation was performed using PRM, as described previously[65]. The phosphopeptides RLS[+80]FGDDQEER, DNRPLS[+80]PVTLSGGPR and AM[+16]S[+80]GDEYM[+16]M[+16]EQHR were targeted to measure Hox7 phosphorylation at S126, S158 and S254, respectively. The PRM assay also included a selection of control peptides (Supplementary Table 11) with similar relative intensities in each sample and used to measure the relative phosphopeptide content. Target peptide intensities were normalized to the summed control peptide intensities to correct for differences in phosphopeptide yield. The assays were performed for two or three biological replicates with one or two technical replicates and results are provided as the mean ± s.d.

ChIP–seq assays. Two-day-old *M. oryzae* mycelium liquid cultures were grown at 24 °C with shaking at 125 r.p.m. The mycelium (2 g) was cross-linked with 1% formaldehyde for 15 min, followed by a 5 min incubation with 125 mM glycine. The cross-linked mycelium samples were ground to fine powder and resuspended in Honda buffer (20 mM HEPES, 0.44 M sucrose, 1.25% (wt/vol) Ficoll, 2.5% (wt/vol) dextran T40, 10 mM MgCl$_2$, 0.5% Triton X-100, 5 mM dithiothreitol and 1×protease inhibitor mixture (Roche)). The suspension was filtered through sterile Miracloth (Calbiochem), washed twice with sterile distilled water and centrifuged at 3,500*g* for 5 min. The nuclear pellets were resuspended in four volumes of Nuclei lysis buffer (50 mM Tris–HCl, pH 8.0, 10 mM EDTA, 1% SDS and 1×protease inhibitor mixture) and sonicated with 15 pulses of 30 s (30 s intervals) using a Diagenode Bioruptor (high setting). Immunoprecipitation was carried out overnight at 4 °C using GFP-trap beads (Chromotek) and anti-FLAG M2 beads (Invitrogen). Reverse cross-linking was carried out overnight with 5 M NaCl at 65 °C and 600 r.p.m., followed by treatment with 40 μg proteinase K for 1–2 h at 45 °C. The samples were treated with a ChIP DNA kit concentrator kit (Zymogen) and finally eluted in a volume of 15–20 μl. The samples were sent to BGI Genomics for library preparation and 50 bp single-end sequencing using HiSeq 2500 (Illumina). The reads were mapped, cleaned and aligned to *M. oryzae* genome version 8 using BWA aligner v. 0.5.7. Peaks were identified by MACS2 version 2.1.1 (ref. [66]) with the following parameters: -g 41027733 -q 0.1–bdg—nomodel–extsize 180–broad–broad-cutoff 0.1. Sequences under the peaks were predicted for ±2 kb flanks and analysed using Python bespoke scripts. Motif discovery was carried out using MEME and MEME-ChIP (https://meme-suite.org/meme/index.html). Data visualization was carried out using Integrative Genome Viewer[67]. Motif abundance was tested in ±2 kb regions of DEGs (mod_lfc < −1 or mod_lfc > 1 and P_{adj} < 0.01) of the RNA datasets of mycelium and appressorium development of Δ*hox7* versus Guy11 and Δ*mst12* versus Guy11 using FIMO (https://meme-suite.org/meme/index.html).

Cloning for heterologous protein purification and in vitro kinase phosphorylation assay. For protein expression, complementary DNA encoding full-length Pmk1, full-length Mst12 and Hox7 containing MAPK docking domain and MAPK phosphorylation motif (Met1-Q342) were amplified and cloned into the pOPINM, pOPINS3C and pOPINM vectors, respectively[68], using the In-Fusion cloning technique (Takara Bio) and the primers in Supplementary Table 13. The pOPINM constructs encoding Pmk1, Mst12 and Hox7 fused to the amino-terminal solubility tags 6×His–GST–Pmk1, 6×His–SUMO–Mst12 and 6×His–MBP–Hox7 were transformed into *E. coli* Rosetta (DE3) pLysS. The cells were cultured in LB medium at 37 °C for 6 h, followed by induction with 1 mM isopropyl β-D-1-thiogalactopyranoside at 16 °C overnight. The cells were harvested by centrifugation and resuspended in 50 mM Tris–HCl, pH 7.5, 500 mM NaCl, 50 mM glycine, 5% (vol/vol) glycerol and 20 mM imidazole supplemented with EDTA-free protease inhibitor tablets (cOmplete Roche). The cells were lysed by sonication and the cell debris were removed by centrifugation. The clarified lysate was purified by immobilized metal affinity Natchromatography using a HisTrap column (GE Life Sciences) connected to a Superdex 75 16/60 or Superdex 200 16/60 gel filtration column pre-equilibrated in 20 mM HEPES, pH 7.5 and 150 mM NaCl using an AKTA Xpress purification system (GE Life Sciences). Fractions

containing His-tagged proteins were pooled and concentrated to 1–3 mg ml^{-1}. The purified protein was confirmed by SDS–PAGE analysis and mass spectrometry. Heterologous production and purification of MEK2^{DD} was performed as previously described[46].

For in vitro phosphorylation assays, 6×His–GST-tagged Pmk1 (250 ng) was activated by incubation with recombinant MEK2^{DD} (250 ng). Recombinant 6×His–SUMO-tagged Mst12 (500 ng) and 6×His–MBP-tagged Hox7 (500 ng) were incubated with active Pmk1 in kinase buffer (25 mM Tris, pH 7.5, 10 mM MnCl$_2$, 1 mM EGTA and 1 mM dithiothreitol) in the presence of 1 mM ATP at 30 °C for 30 min. Proteins were separated by SDS–PAGE and transferred to polyvinylidene difluoride membrane using a Trans-Blot turbo transfer system (Bio-Rad). The polyvinylidene difluoride membrane was blocked with 2% BSA in Tris-buffered saline and 1% Tween 20. His-tag detection was carried using polyclonal anti-6×His horseradish peroxidase-conjugated antibody (Abcam). Activated Pmk1 was detected using Phospho-p44/42 MAPK (Erk1/2) (Thr202/Tyr204) (Santa Cruz Biotechnology) and anti-rabbit horseradish peroxidase-conjugated antibodies. Pierce ECL western blotting substrate (Thermo Fisher Scientific) was used for detection. The membranes were imaged using an ImageQuant LAS 4000 luminescent imager (GE Life Sciences). Phosphorylated residues were analysed by LC–MS/MS in data-dependent mode as described earlier.

Statistics and reproducibility. All experiments were conducted with at least two biological replicates and technical replicates of an appropriate sample size, estimated based on what is established in the field. The sample sizes, number of biological and technical replicates, and the statistical tests used in each experiment are specified in the figure legends. No statistical methods were used to pre-determine the sample size and blinding was applied on the disease symptoms of the spray inoculation experiments. For the appressorial development assays, data were analysed using an unpaired two-tailed Student's t-test. $P < 0.05$ was considered significant; $*P < 0.05$, $**P < 0.01$, $***P < 0.001$ and $****P < 0.0001$. $P > 0.05$ was considered non-significant and exact values are shown where appropriate. The micrographs where no n is specified in the figure legend represent at least 90 cells over three independent biological replicates. Dot plots were routinely used to show individual data points and generated using Prism7 (GraphPad). Bar graphs of appressorial assays show the mean ± s.e.m. (unless stated otherwise) and were generated using Prism7 (GraphPad). In pathogenicity assays, datasets were tested before comparison for normal distribution using the Shapiro–Wilk normality test. In all cases where at least one dataset was non-normally distributed ($P > 0.05$ in Shapiro–Wilk tests), we used non-parametric Mann–Whitney testing. Analysis of non-normal datasets are represented by box-and-whisker plots that show the 25th and 75th percentiles, the median, and the minimum and maximum values by the ends of the whiskers. A two-tailed Welch's unpaired t-test of three biological replicates with two technical replicates per biological replicate, unless otherwise stated, was applied to the PRM experiments. The DESeq package was used to call differential gene expression (P_{adj}) and the P value was corrected for multiple testing using the Benjamini–Hochberg adjustment. Over-representation of motifs identified by ChIP–seq analysis was verified using the Fisher's exact test.

Reporting Summary. Further information on research design is available in the Nature Research Reporting Summary linked to this article.

Data availability
The RNA-seq data described in this study have been submitted to the European Nucleotide Archive (ENA): appressorial RNA-seq data under the accession number PRJEB36580 and mycelial RNA-seq data under the accession number PRJEB44745. The ChIP–seq data described in this study have been submitted to Gene Expression Omnibus under the accession number GSE182534. The proteomic data described in this study have been deposited into the ProteomeXchange Consortium via PRIDE (Perez-Riverol et al., 2019) partner repository with the dataset identifier PXD025700. The PRM data have been made publicly available through PanoramaWeb (https://panoramaweb.org/84ne1U.url) and the corresponding ProteomeXchange ID for the data is PXD028052. The *M. oryzae* genome database used in this study was http://fungi.ensembl.org/Magnaporthe_oryzae/Info/Index. All *M. oryzae* strains generated in this study are freely available on request from the corresponding authors. Source data are provided with this paper.

Code availability
Scripts for the analysis and prediction of the peaks of ChIP–seq experiments have been publicly deposited in GitHub at https://github.com/threadmapper/sequence-under-peaks.

References
1. Talbot, N. J. On the trail of a cereal killer: exploring the biology of *Magnaporthe grisea*. *Annu. Rev. Microbiol.* **57**, 177–202 (2003).
2. DeZwaan, T. M., Carroll, A. M., Valent, B. & Sweigard, J. A. *Magnaporthe grisea* Pth11p is a novel plasma membrane protein that mediates appressorium differentiation in response to inductive substrate cues. *Plant Cell* **11**, 2013–2030 (1999).
3. Hamer, J. E., Howard, R. J., Chumley, F. G. & Valent, B. A mechanism for surface attachment in spores of a plant pathogenic fungus. *Science* **239**, 288–190 (1988).
4. de Jong, J. C., McCormack, B. J., Smirnoff, N. & Talbot, N. J. Glycerol generates turgor in rice blast. *Nature* **389**, 244–244 (1997).
5. Howard, R. J., Ferrari, M. A., Roach, D. H. & Money, N. P. Penetration of hard substrates by a fungus employing enormous turgor pressures. *Proc. Natl Acad. Sci. USA* **88**, 11281–11284 (1991).
6. Kershaw, M. J. & Talbot, N. J. Genome-wide functional analysis reveals that infection-associated fungal autophagy is necessary for rice blast disease. *Proc. Natl Acad. Sci. USA* **106**, 15967–15972 (2009).
7. Saunders, D. G., Aves, S. J. & Talbot, N. J. Cell cycle-mediated regulation of plant infection by the rice blast fungus. *Plant Cell* **22**, 497–507 (2010).
8. Veneault-Fourrey, C., Barooah, M., Egan, M., Wakley, G. & Talbot, N. J. Autophagic fungal cell death is necessary for infection by the rice blast fungus. *Science* **312**, 580–583 (2006).
9. Marroquin-Guzman, M., Sun, G. & Wilson, R. A. Glucose-ABL1-TOR signaling modulates cell cycle tuning to control terminal appressorial cell differentiation. *PLoS Genet.* **13**, e1006557 (2017).
10. Marroquin-Guzman, M. & Wilson, R. A. GATA-dependent glutaminolysis drives appressorium formation in *Magnaporthe oryzae* by suppressing TOR inhibition of cAMP/PKA signaling. *PLoS Pathog.* **11**, e1004851 (2015).
11. Sun, G., Qi, X. & Wilson, R. A. A feed-forward subnetwork emerging from integrated TOR- and cAMP/PKA-signaling architecture reinforces *Magnaporthe oryzae* appressorium morphogenesis. *Mol. Plant Microbe Interact.* **32**, 593–607 (2019).
12. Ryder, L. S. et al. NADPH oxidases regulate septin-mediated cytoskeletal remodeling during plant infection by the rice blast fungus. *Proc. Natl Acad. Sci. USA* **110**, 3179–3184 (2013).
13. Dagdas, Y. F. et al. Septin-mediated plant cell invasion by the rice blast fungus, *Magnaporthe oryzae*. *Science* **336**, 1590–1595 (2012).
14. Rocha, R. O., Elowsky, C., Pham, N. T. T. & Wilson, R. A. Spermine-mediated tight sealing of the *Magnaporthe oryzae* appressorial pore-rice leaf surface interface. *Nat. Microbiol.* **5**, 1472–1480 (2020).
15. Sakulkoo, W. et al. A single fungal MAP kinase controls plant cell-to-cell invasion by the rice blast fungus. *Science* **359**, 1399–1403 (2018).
16. Giraldo, M. C. et al. Two distinct secretion systems facilitate tissue invasion by the rice blast fungus *Magnaporthe oryzae*. *Nat. Commun.* **4**, 1996 (2013).
17. Xu, J. R. & Hamer, J. E. MAP kinase and cAMP signaling regulate infection structure formation and pathogenic growth in the rice blast fungus *Magnaporthe grisea*. *Genes Dev.* **10**, 2696–2706 (1996).
18. Saunders, D. G., Dagdas, Y. F. & Talbot, N. J. Spatial uncoupling of mitosis and cytokinesis during appressorium-mediated plant infection by the rice blast fungus *Magnaporthe oryzae*. *Plant Cell* **22**, 2417–2428 (2010).
19. Dean, R. A. et al. The genome sequence of the rice blast fungus *Magnaporthe grisea*. *Nature* **434**, 980–986 (2005).
20. Thines, E., Weber, R. W. & Talbot, N. J. MAP kinase and protein kinase A-dependent mobilization of triacylglycerol and glycogen during appressorium turgor generation by *Magnaporthe grisea*. *Plant Cell* **12**, 1703–1718 (2000).
21. Becker, J., Liermann, J. C., Opatz, T., Anke, H. & Thines, E. GKK1032A$_2$, a secondary metabolite from *Penicillium* sp. IBWF-029-96, inhibits conidial germination in the rice blast fungus *Magnaporthe oryzae*. *J. Antibiot.* **65**, 99–102 (2012).
22. Park, G., Xue, C., Zheng, L., Lam, S. & Xu, J. R. MST12 regulates infectious growth but not appressorium formation in the rice blast fungus *Magnaporthe grisea*. *Mol. Plant Microbe Interact.* **15**, 183–192 (2002).
23. Soanes, D. M., Chakrabarti, A., Paszkiewicz, K. H., Dawe, A. L. & Talbot, N. J. Genome-wide transcriptional profiling of appressorium development by the rice blast fungus *Magnaporthe oryzae*. *PLoS Pathog.* **8**, e1002514 (2012).
24. Oses-Ruiz, M. & Talbot, N. J. Cell cycle-dependent regulation of plant infection by the rice blast fungus Magnaporthe oryzae. *Commun. Integr. Biol.* **10**, e1372067 (2017).
25. Oses-Ruiz, M., Sakulkoo, W., Littlejohn, G. R., Martin-Urdiroz, M. & Talbot, N. J. Two independent S-phase checkpoints regulate appressorium-mediated plant infection by the rice blast fungus *Magnaporthe oryzae*. *Proc. Natl Acad. Sci. USA* **114**, E237–E244 (2017).
26. Kulkarni, R. D., Thon, M. R., Pan, H. & Dean, R. A. Novel G-protein-coupled receptor-like proteins in the plant pathogenic fungus *Magnaporthe grisea*. *Genome Biol.* **6**, R24 (2005).
27. Chumley, F. G. & Valent, B. Genetic analysis of melanin deficient, nonpathogenic mutants of *Magnaporthe grisea*. *Mol. Plant Microbe Interact.* **3**, 135–143 (1990).

28. Skamnioti, P. & Gurr, S. J. *Magnaporthe grisea* Cutinase2 mediates appressorium differentiation and host penetration and is required for full virulence. *Plant Cell* **19**, 2674–2689 (2007).

29. Johnson, K. L., Jones, B. J., Bacic, A. & Schultz, C. J. The fasciclin-like arabinogalactan proteins of *Arabidopsis*. A multigene family of putative cell adhesion molecules. *Plant Physiol.* **133**, 1911–1925 (2003).

30. Seifert, G. J. Fascinating fasciclins: A surprisingly widespread family of proteins that mediate interactions between the cell exterior and the cell surface. *Int. J. Mol. Sci.* https://doi.org/10.3390/ijms19061628 (2018).

31. Dong, B. et al. MgAtg9 trafficking in *Magnaporthe oryzae*. *Autophagy* **5**, 946–953 (2009).

32. Petersen, T. N., Brunak, S., von Heijne, G. & Nielsen, H. SignalP 4.0: discriminating signal peptides from transmembrane regions. *Nat. Methods* **8**, 785–786 (2011).

33. Haijiao, L. et al. A novel *Magnaporthe oryzae* gene *MCG1*, encoding an extracellular globular protein, affects conidial germination and appressorial formation. *Int. J. Agric. Technol.* **7**, 1647–1660 (2011).

34. Skamnioti, P., Henderson, C., Zhang, Z., Robinson, Z. & Gurr, S. J. A novel role for catalase B in the maintenance of fungal cell-wall integrity during host invasion in the rice blast fungus *Magnaporthe grisea*. *Mol. Plant Microbe Interact.* **20**, 568–580 (2007).

35. Mosquera, G., Giraldo, M. C., Khang, C. H., Coughlan, S. & Valent, B. Interaction transcriptome analysis identifies *Magnaporthe oryzae* BAS1-4 as biotrophy-associated secreted proteins in rice blast disease. *Plant Cell* **21**, 1273–1290 (2009).

36. Lu, J., Cao, H., Zhang, L., Huang, P. & Lin, F. Systematic analysis of Zn2Cys6 transcription factors required for development and pathogenicity by high-throughput gene knockout in the rice blast fungus. *PLoS Pathog.* **10**, e1004432 (2014).

37. Sweigard, J. A., Carroll, A. M., Farrall, L., Chumley, F. G. & Valent, B. *Magnaporthe grisea* pathogenicity genes obtained through insertional mutagenesis. *Mol. Plant Microbe Interact.* **11**, 404–412 (1998).

38. Felenbok, B. The ethanol utilization regulon of *Aspergillus nidulans*: the alcA–alcR system as a tool for the expression of recombinant proteins. *J. Biotechnol.* **17**, 11–17 (1991).

39. Kim, S. et al. Homeobox transcription factors are required for conidiation and appressorium development in the rice blast fungus *Magnaporthe oryzae*. *PLoS Genet.* **5**, e1000757 (2009).

40. Howard, R. J. & Valent, B. Breaking and entering: host penetration by the fungal rice blast pathogen *Magnaporthe grisea*. *Annu. Rev. Microbiol.* **50**, 491–512 (1996).

41. Kwon, S. et al. Role of the histone acetyltransferase Rtt109 in development and pathogenicity of the rice blast fungus. *Mol. Plant Microbe Interact.* **31**, 1200–1210 (2018).

42. Lane, S., Zhou, S., Pan, T., Dai, Q. & Liu, H. The basic helix-loop-helix transcription factor Cph2 regulates hyphal development in *Candida albicans* partly via Tec1. *Mol. Cell. Biol.* **21**, 6418–6428 (2001).

43. McLeod, M. et al. Cpc2, a fission yeast homologue of mammalian RACK1 protein, interacts with Ran1 (Pat1) kinase to regulate cell cycle progression and meiotic development. *Mol. Cell. Biol.* **20**, 4016–4027 (2000).

44. Mitchell, T. K. & Dean, R. A. The cAMP-dependent protein kinase catalytic subunit is required for appressorium formation and pathogenesis by the rice blast pathogen *Magnaporthe grisea*. *Plant Cell* **7**, 1869–1878 (1995).

45. Xu, J.-R., Urban, M., Sweigard, J. A. & Hamer, J. E. The *CPKA* gene of *Magnaporthe grisea* is essential for appressorial penetration. *Mol. Plant Microbe Interact.* **10**, 187–194 (1997).

46. Menke, F. L. et al. Tobacco transcription factor WRKY1 is phosphorylated by the MAP kinase SIPK and mediates HR-like cell death in tobacco. *Mol. Plant Microbe Interact.* **18**, 1027–1034 (2005).

47. Pearson, J. C., Lemons, D. & McGinnis, W. Modulating Hox gene functions during animal body patterning. *Nat. Rev. Genet.* **6**, 893–904 (2005).

48. McGinnis, W., Garber, R. L., Wirz, J., Kuroiwa, A. & Gehring, W. J. A homologous protein-coding sequence in *Drosophila* homeotic genes and its conservation in other metazoans. *Cell* **37**, 403–408 (1984).

49. Bürglin, T. R. & Affolter, M. Homeodomain proteins: an update. *Chromosoma* **125**, 497–521 (2016).

50. Xuan, F. et al. Homeobox C9 suppresses Beclin1-mediated autophagy in glioblastoma by directly inhibiting the transcription of death-associated protein kinase 1. *Neuro Oncol.* **18**, 819–829 (2016).

51. Mao, L. et al. HOXC9 links cell-cycle exit and neuronal differentiation and is a prognostic marker in neuroblastoma. *Cancer Res.* **71**, 4314–4324 (2011).

52. Wilson, R. A., Gibson, R. P., Quispe, C. F., Littlechild, J. A. & Talbot, N. J. An NADPH-dependent genetic switch regulates plant infection by the rice blast fungus. *Proc. Natl Acad. Sci. USA* **107**, 21902–21907 (2010).

53. Celenza, J. L. & Carlson, M. Mutational analysis of the *Saccharomyces cerevisiae* SNF1 protein kinase and evidence for functional interaction with the SNF4 protein. *Mol. Cell. Biol.* **9**, 5034–5044 (1989).

54. Wang, Z., Wilson, W. A., Fujino, M. A. & Roach, P. J. Antagonistic controls of autophagy and glycogen accumulation by Snf1p, the yeast homolog of AMP-activated protein kinase, and the cyclin-dependent kinase Pho85p. *Mol. Cell. Biol.* **21**, 5742–5752 (2001).

55. Castillo-Lluva, S., Alvarez-Tabarés, I., Weber, I., Steinberg, G. & Pérez-Martin, J. Sustained cell polarity and virulence in the phytopathogenic fungus *Ustilago maydis* depends on an essential cyclin-dependent kinase from the Cdk5/Pho85 family. *J. Cell Sci.* **120**, 1584–1595 (2007).

56. Huang, D., Friesen, H. & Andrews, B. Pho85, a multifunctional cyclin-dependent protein kinase in budding yeast. *Mol. Microbiol.* **66**, 303–314 (2007).

57. Shapiro, R. S. et al. Pho85, Pcl1, and Hms1 signaling governs *Candida albicans* morphogenesis induced by high temperature or Hsp90 compromise. *Curr. Biol.* **22**, 461–470 (2012).

58. Zeng, X.-Q. et al. Crosstalk between SNF1 pathway and the peroxisome-mediated lipid metabolism in *Magnaporthe oryzae*. *PLoS ONE* **9**, e103124 (2014).

59. Valent, B. & Chumley, F. G. Molecular genetic analysis of the rice blast fungus, *Magnaporthe grisea*. *Annu. Rev. Phytopathol.* **29**, 443–467 (1991).

60. Talbot, N. J., Ebbole, D. J. & Hamer, J. E. Identification and characterization of *MPG1*, a gene involved in pathogenicity from the rice blast fungus *Magnaporthe grisea*. *Plant Cell* **5**, 1575–1590 (1993).

61. Trapnell, C. et al. Transcript assembly and quantification by RNA-Seq reveals unannotated transcripts and isoform switching during cell differentiation. *Nat. Biotechnol.* **28**, 511–515 (2010).

62. Anders, S. & Huber, W. Differential expression analysis for sequence count data. *Genome Biol.* **11**, 106 (2010).

63. Bray, N. L., Pimentel, H., Melsted, P. & Pachter, L. Near-optimal probabilistic RNA-seq quantification. *Nat. Biotechnol.* **34**, 525–527 (2016).

64. Mithoe, S. C. et al. Attenuation of pattern recognition receptor signaling is mediated by a MAP kinase kinase kinase. *EMBO Rep.* **17**, 441–454 (2016).

65. Guo, H. et al. Phosphorylation-regulated activation of the *Arabidopsis* RRS1-R/RPS4 immune receptor complex reveals two distinct effector recognition mechanisms. *Cell Host Microbe* **27**, 769–781.

66. Zhang, Y. et al. Model-based analysis of ChIP-Seq (MACS). *Genome Biol.* **9**, R137 (2008).

67. Robinson, J. T. et al. Integrative genomics viewer. *Nat. Biotechnol.* **29**, 24–26 (2011).

68. Berrow, N. S. et al. A versatile ligation-independent cloning method suitable for high-throughput expression screening applications. *Nucleic Acids Res.* **35**, e45 (2007).

69. Turra, D., Segorbe, D. & Di Pietro, A. Protein kinases in plant-pathogenic fungi: conserved regulators of infection. *Annu. Rev. Phytopathol.* **52**, 267–288 (2014).

70. Zhao, X. & Xu, J. R. A highly conserved MAPK-docking site in Mst7 is essential for Pmk1 activation in *Magnaporthe grisea*. *Mol. Microbiol.* **63**, 881–894 (2007).

Author contributions

M.O.-R. and N.J.T. conceptualized the project. Experimental analyses were carried out by M.O.-R., N.C.-M., M.M.-U., A.B.E., M.N., I.E., X.Y., M.J.K., X.Y., C.M. and G.R.L. F.L.H.M designed, and P.D. and F.L.H.M. carried out, the phosphoproteomic analysis. G.V.-P. and B.V. generated the Δ*rpp3* mutant. Bioinformatic analysis was performed by M.O.-R., D.M.S., B.T., J.C. and V.W. The paper was written by M.O.-R. and N.J.T., with contributions from all authors.

Competing interests

The authors declare no competing interests.

Additional information

Extended data is available for this paper at https://doi.org/10.1038/s41564-021-00978-w.

Supplementary information The online version contains supplementary material available at https://doi.org/10.1038/s41564-021-00978-w.

Correspondence and requests for materials should be addressed to Míriam Osés-Ruiz or Nicholas J. Talbot.

Peer review information *Nature Microbiology* thanks Lászlo Nagy, Antonio Di Pietro and the other, anonymous, reviewer(s) for their contribution to the peer review of this work. Peer reviewer reports are available.

Reprints and permissions information is available at www.nature.com/reprints.

Publisher's note Springer Nature remains neutral with regard to jurisdictional claims in published maps and institutional affiliations.

PLOS PATHOGENS

From appressorium to transpressorium— Defining the morphogenetic basis of host cell invasion by the rice blast fungus

Neftaly Cruz-Mireles⬡, **Alice Bisola Eseola**⬡, **Míriam Osés-Ruiz**⬡, **Lauren S. Ryder**, **Nicholas J. Talbot**⬡*

The Sainsbury Laboratory, University of East Anglia, Norwich Research Park, Norwich, United Kingdom

* nick.talbot@tsl.ac.uk

Introduction

To cause disease, many fungal pathogens develop specialised structures to rupture the tough outer layers of their plant or animal hosts. These infection cells, called appressoria, have been extensively studied in many fungal species [1]. However, once inside host tissue, pathogens must also invade new cells and traverse host cell junctions. How they do this has received much less attention, but recent evidence from the rice blast fungus suggests that cell invasion within a host plant may also require the development of a specialised infection structure. Here, we compare the developmental biology of invasive growth during different stages of plant infection by the rice blast fungus. We identify the remarkable parallels between the biology of appressorium development and cell-to-cell movement. Finally, we evaluate evidence suggesting that a specialised infection cell—the transpressorium—is necessary for invasive growth.

How does the rice blast fungus puncture an intact leaf?

Rice blast disease is one of the world's most important crop diseases, each year destroying enough rice to feed 60 million people [2]. Given that rice is the staple food for almost 3.7 billion of the world's population—many of them in low-income countries—blast disease represents a clear and present danger to global food security. The blast fungus *Magnaporthe oryzae* can, however, infect more than 50 different grass species, including other major cereals such as barley, oats, finger millet, and wheat. Significant outbreaks of wheat blast have occurred in Brazil, Bangladesh [3,4], and, most recently, in Zambia [5]—now threatening wheat production on 3 continents. Understanding the biology of blast diseases is therefore important if new disease control strategies are to be developed.

To gain entry to a plant, *M. oryzae* uses a dome-shaped, melanin-pigmented appressorium [1]. A conidium germinates on the leaf surface to form a polarised germ tube, which differentiates into an appressorium within 4 to 6 hours. There are 3 important prerequisites for appressorium morphogenesis. First of all, a hard hydrophobic surface [6] must be recognised by *M. oryzae*, which requires the Pmk1 mitogen-activated protein kinase (MAPK) signalling pathway. Upstream sensory proteins trigger a phosphorylation cascade that involves Mst11 (mitogen-activated protein kinase kinase kinase, MAPKKK), Mst7 (mitogen-activated protein kinase kinase, MAPKK), and Pmk1 (MAPK). In the absence of Pmk1, the fungus is unable to form an appressorium, and, therefore, incapable of causing disease [7]. The second prerequisite is that the germinating cell of the 3-celled conidium must undergo mitosis. An S phase checkpoint is necessary for the initiation of appressorium development, and the nucleus must then pass through G2-M to enable appressorium maturation to progress [8]. Finally, the

3-celled conidium undergoes autophagy and an iron-dependent programmed cell death process, called ferroptosis, before its contents are trafficked to the appressorium [9,10]. If this process is impaired by mutation of genes required for autophagy, then the fungus is unable to cause disease because appressoria cannot repolarise. The initiation of autophagy requires both Pmk1 and cell cycle progression, but is also linked to starvation stress and a target of rapamycin (TOR) kinase–dependent metabolic checkpoint [11], because appressoria only develop in the absence of exogenous nutrients.

How does the appressorium function?

Once formed, the appressorium adheres tightly to the leaf cuticle and develops enormous turgor of up to 8.0 MPa (approximately 80 atmospheres of pressure). This huge pressure is generated by accumulating high concentrations of glycerol and other polyols [12,13], which draw water into the cell by osmosis. The appressorium has a differentiated cell wall rich in melanin, which reduces cell wall porosity, thereby preventing exodus of polyols but allowing water entry to continue. Melanisation of the appressorium is essential for turgor generation, and mutants that cannot synthesise dihydroxynaphthalene melanin are unable to cause blast disease [14]. Turgor is applied at the base of the appressorium as mechanical force, enabling a narrow, rigid penetration hypha to rupture the rice leaf cuticle [13]. This requires cytoskeletal reorientation, followed by rapid actin polymerisation [15–17]. Filamentous actin forms a toroidal network around the appressorium pore, a region at the base of the appressorium lacking melanin, which marks the points from which the penetration peg emerges [15,18]. Septin guanosine triphosphatases (GTPases) are necessary for actin remodelling, forming a ring structure around the appressorium pore, which provides cortical rigidity and acts as a lateral diffusion barrier. This facilitates the organisation of polarity determinants and proteins involved in membrane deformation and exocytosis [15,17]. In the absence of any of the 4 core septins that form the hetero-oligomeric septin ring at the appressorium pore, the cell is unable to repolarise and puncture the leaf cuticle. Penetration peg emergence therefore involves a switch from isotropic to polarised, anisotropic growth at the appressorium pore [19]. It is also clear that these changes in cytoskeletal conformation only occur once a critical threshold of appressorium turgor has been achieved [20]. A turgor-sensing histidine-aspartate kinase, Sln1, is necessary for sensing when maximal turgor has been reached, modulating further pressure generation. Mutants lacking the Sln1 kinase generate excess appressorial turgor, but cannot repolarise and are thus unable to apply the pressure generated as protrusive force [20]. Sln1 is necessary to down-regulate both glycerol synthesis, likely regulated by the cAMP-dependent protein kinase A pathway, and melanisation. As a consequence, *sln1* mutants form hypermelanised nonfunctional appressoria [20]. In addition, a pressure-dependent cell cycle S phase checkpoint in the appressorium is essential for septin-dependent repolarisation [21].

How is rice tissue colonised by the blast fungus?

Once inside a plant cell, the penetration hypha differentiates into bulbous, branched hyphae that rapidly fill the interior of the cell. These invasive hyphae grow by budding, and the fungus undergoes significant changes in primary metabolism [22] during initial cell colonisation. Soon after its entry into a plant cell, a plant membrane–rich cap is also observed at the tip of the penetration peg. The fungus buds at this point and differentiates into an invasive hypha, but the membrane-rich structure remains and is known as the biotrophic interfacial complex (BIC) [23,24]. The BIC might originate as a focal plant defence reaction, but an increasing body of evidence suggests that *M. oryzae* utilises this structure to deliver effector proteins into plant cells. Effectors are secreted pathogen proteins necessary for suppression of plant immune
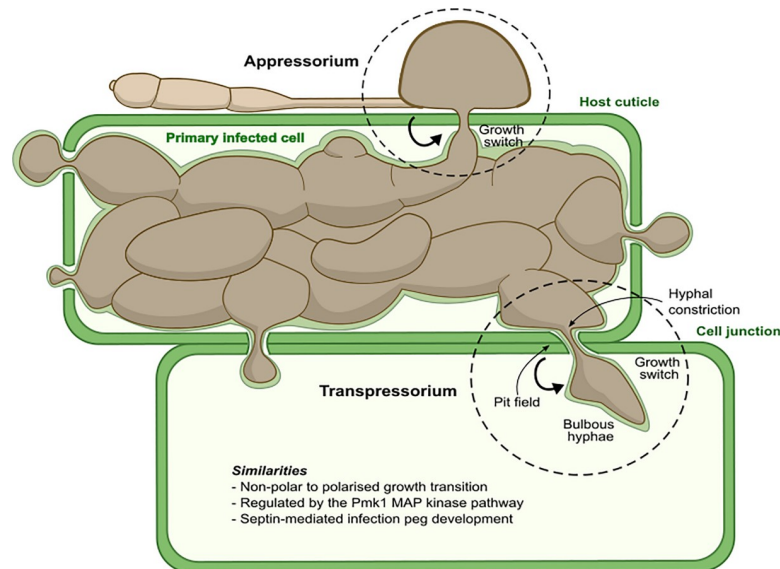
Fig 1. Infection structures of the rice blast fungus: The appressorium and transpressorium. A schematic figure describing the characteristics and developmental biology of appressoria and transpressoria—specialised infection structures formed by *Magnaporthe oryzae* to penetrate the host cuticle and traverse cell junctions, respectively. MAP, mitogen-activated protein.

responses. Secretion of effectors into the cytoplasm involves a distinct secretory pathway to conventional hyphal tip–mediated secretion of extracellular effectors [24]. Only once the fungus has fully occupied the initial epidermal cell does it invade adjacent cells, normally in a highly synchronous manner, spreading from cell to cell and rapidly occupying host tissue (Fig 1).

What is a transpressorium?

How fungal pathogens spread from cell to cell in host tissue is largely unstudied in either plant or animal pathogenic fungi. In *M. oryzae*, severe hyphal constrictions were observed during invasive growth and appeared to correlate with pit fields where plasmodesmata accumulate [23]. Plasmodesmata are cytoplasmic conduits that link together plant cells [25]. Live-cell imaging of cell-to-cell movement by *M. oryzae* has shown that invasive hyphae become swollen (approximately 5.0 μm in diameter) at rice cell junctions and then undergo severe hyphal constriction to a diameter of 0.6 to 0.8 μm (measured by electron microscopy) [26]. This is very similar to the process that occurs when an appressorium forms a penetration peg, with both structures having a similar diameter when visualised by light microscopy (0.8 to 0.9 μm), as shown in Fig 2. Hyphal constriction is accompanied by actomyosin ring formation at the cell junctions. Interestingly, it has been reported that the Pmk1 MAPK cascade, which regulates appressorium morphogenesis, is also necessary for hyphal constriction and cell-to-cell invasion in a septin-dependent mechanism [26]. Using a conditional analogue–sensitive mutant of Pmk1, it was shown that the inhibition of the Pmk1 MAPK with the ATP analogue Napthyl-PP1 prevents *M. oryzae* from moving between rice cells [26]. This suggests that the Pmk1 pathway is involved in the morphogenetic switch of bulbous hyphae into narrow infection pegs that traverse rice cells. Interestingly, Pmk1 also regulates the expression of a subset of fungal effector genes that may be required for suppression of plasmodesmatal immunity. During initial infection, plasmodesmatal conductance is maintained to enable effectors to move
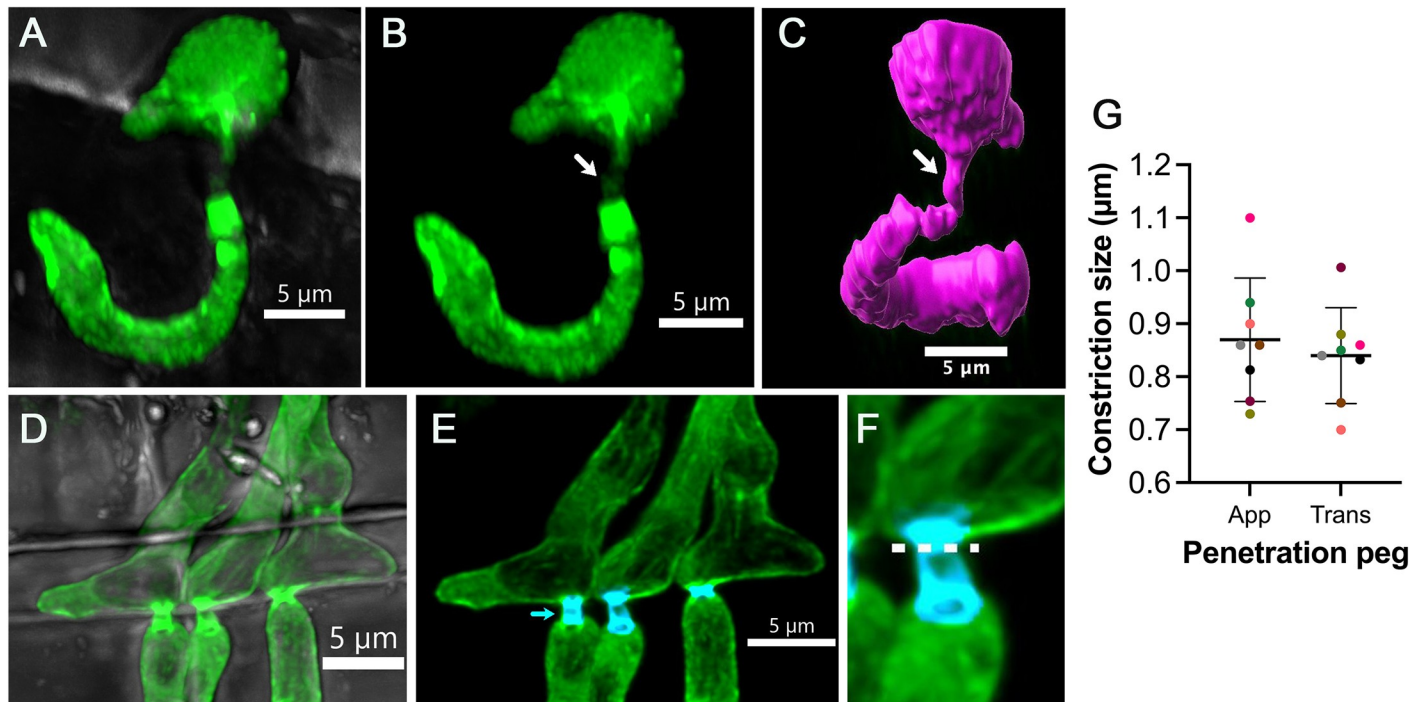
Fig 2. Cell-to-cell movement during the rice blast infection. Live-cell imaging of *Magnaporthe oryzae* strain expressing gelsolin–GFP during rice infection. **(A, B)** Three-dimensional projection micrographs showing the appressorium entry site into rice leaf sheath. The arrow indicates the penetration peg, which subsequently differentiates into a primary invasive hypha at 24 hpi. **(C)** Three-dimensional rendering of the base of the *M. oryzae* appressorium with a penetration peg (arrowed) and primary invasive hypha within an epidermal rice cell. **(D, E)** Three-dimensional projection micrographs to show the specialised transpressorium required for cell-to-cell invasion by *M. oryzae*. The cyan colour indicates the constriction site when the fungus passes through a plasmodesmata-rich pit field. **(F)** Enlarged image of the transpressorium crossing point. The dotted line indicates the region selected for measurement of the diameter of the hyphal constriction point. **(G)** Plot showing the mean diameter of the App and Trans. Data were collected from 3 different rice seedling infections (*n* = 8 pegs measured in each experiment), with data points colour coded for each biological replication of the experiment. App, appressorium penetration peg; Trans, transpressorium penetration peg.

into adjacent unoccupied plant cells, which may involve manipulation of plasmodesmata by fungal effectors to prevent their closure. However, it is also clear that even when plant immune responses are suppressed or host tissue is killed, the fungus still needs to undergo pit field location and hyphal constriction in order to traverse cell junctions [26].

Appressorium development and cell-to-cell movement therefore appear to be morphogenetically related processes. Both involve isotropic expansion of a swollen germ tube or a hyphal tip, followed by the generation of a much narrower infection peg, to rupture either the cuticle or plant cell wall at pit fields. This similarity has been noted previously by careful observers of plant–fungal interactions, who coined the term "transpressorium" to describe *in planta* infection structures formed by fungi to move between host cells. Liese and Schmid were the first to describe transpressoria when they studied *Ceratocystis* sp. infection of *Pinus strobus* [27,28]. They reported how swollen structures underwent severe constriction to form hyphae of much smaller diameter involved in the penetration of the cell wall of neighbouring cells [27]. Once the transpressorium peg reached the lumen of the adjacent cell, it then expanded to the normal diameter of an invasive hypha [27]. Liese suggested that the transpressorium penetrates the cell wall using a combination of localised enzymatic activity and mechanical pressure [29]. Appressoria and transpressoria therefore fulfil a very similar function, enabling traversal of a physical obstacle [27,30]. Although these findings were reported more than 55 years ago, there have not been further reports of transpressorium morphogenesis. Recent observations in *M. oryzae* of its Pmk1-dependent, septin-mediated cell-to-cell movement mechanisms, however,

are completely consistent with the experiments of Liese and Schmid [27] and thoughtful reviewers of appressorium biology [28].

Transpressorium-like structures have also been reported in other filamentous fungi. Hyphal morphogenetic reprogramming into specialised structures has been largely studied in model fungal species, such as *Neurospora crassa* and *Aspergillus nidulans* [31]. Recent studies in *Podospora anserina* have, for example, shown that narrow hyphae are developed during fungal growth in order to breach cellulosic substrates such as cellophane [32]. Additionally, recent elegant studies of hyphal morphological adaptation to occupy extremely narrow channels suggest that a trade-off may exist between plasticity and velocity in hyphal growth [33]. These observations provide evidence that generation of specialised hyphae-derived structure for invasive growth may be a conserved mechanism in filamentous fungi. Elucidating the common morphological components of transpressorium and transpressorium-like invasive hyphae will be an exciting future challenge.

What are the parallels between appressoria and transpressoria?

Many common features are shared between appressoria and transpressoria. First, their development involves departure from polarised growth and formation of an isotropically expanded hyphal/germ tube tip. Both types of infection cell also form following recognition of physical cues of the surfaces they encounter [34]. A symmetry breaking process then occurs, whereby a polarised infection peg is formed to rupture the host cell wall, either at the leaf surface or at pit fields between host cells. Finally, after passing through the structural barrier, the emerging infection hypha is surrounded by the invaginated plant plasma membrane. This occurs not only upon initial infection, but also, remarkably, every time the fungus enters a new host cell [26]. A separate extra-invasive hyphal membrane compartment is always formed as well as a BIC [23,26]. These morphogenetic processes during both appressorium and transpressorium development require the Pmk1 MAPK—acting downstream of the thigmotropic perception of the cell/cuticle surface—which regulates septin-dependent cytoskeletal remodelling.

What do we not understand about invasive growth by the blast fungus?

The obvious parallels between appressorium and transpressorium development raise many questions. What are the thigmotropic signals, for example, perceived by hyphal tips, which lead to appressorium and transpressorium morphogenesis, and which sensory proteins are necessary for their perception? While some putative sensors have been identified for appressorium development [35,36], this process is far from well understood. Does perception of these surface cues lead to membrane curvature generation in the fungus, acting as a signal for septin aggregation during development of infection cells [37,38]? This might, for example, explain how pit fields are recognised as indentations in the cell wall surface. Is there a cell cycle dependency for transpressorium development, as there is for appressorium formation? Mitosis occurs at cell junctions [39], but is this a prerequisite for transpressorium formation, and, if so, does a similar S phase checkpoint mechanism act at this time [21]? Is there a quorum sensing or nutritional dependency for transpressorium development? Invasive hyphae appear to fill epidermal cells completely before invasion of neighbouring cells, suggesting that such a signal might exist, while it is also clear that transpressorium function and biotrophic growth may be linked to metabolic control and TOR kinase regulation [40]. Finally, and perhaps most intriguing of all, does transpressorium function require pressure generation and application of mechanical force in the same way as an appressorium, and, if so, are transpressoria ever melanised? Or, alternatively, does cell wall crossing occur exclusively via enzymatic activity?

We have much to learn about the mechanisms of invasive growth by pathogenic fungi, but the role of the transpressorium—which has hitherto been largely unrecognised—may prove to be as significant to fungal pathogenesis as that of the appressorium.

References

1. Talbot NJ. Appressoria. Curr Biol. 2019; 29:R144–6. https://doi.org/10.1016/j.cub.2018.12.050 PMID: 30836078

2. Skamnioti P, Gurr SJ. Against the grain: safeguarding rice from rice blast disease. Trends Biotechnol. 2009; 27:141–50. https://doi.org/10.1016/j.tibtech.2008.12.002 PMID: 19187990

3. Islam MT, Croll D, Gladieux P, Soanes DM, Persoons A, Bhattacharjee P, et al. Emergence of wheat blast in Bangladesh was caused by a South American lineage of *Magnaporthe oryzae*. BMC Biol. 2016; 14:84. https://doi.org/10.1186/s12915-016-0309-7 PMID: 27716181

4. Islam MT, Kim K-H, Choi J. Wheat blast in Bangladesh: the current situation and future impacts. Plant Pathol J. 2019; 35:1. https://doi.org/10.5423/PPJ.RW.08.2018.0168 PMID: 30828274

5. Tembo B, Mulenga RM, Sichilima S, M'siska KK, Mwale M, Chikoti PC, et al. Detection and characterization of fungus (Magnaporthe oryzae *pathotype Triticum*) causing wheat blast disease on rain-fed grown wheat (Triticum aestivum L.) in Zambia. Wang Z, editor. PLoS ONE. 2020;e0238724:15. https://doi.org/10.1371/journal.pone.0238724 PMID: 32956369

6. Dean RA. Signal pathways and appressorium morphogenesis. Annu Rev Phytopathol. 1997; 35:211–45. https://doi.org/10.1146/annurev.phyto.35.1.211 PMID: 15012522

7. Xu JR. MAP kinases in fungal pathogens. Fungal Genet Biol. 2000; 31:137–52. https://doi.org/10.1006/fgbi.2000.1237 PMID: 11273677

8. Saunders DGO, Aves SJ, Talbot NJ. Cell cycle-mediated regulation of plant infection by the rice blast fungus. Plant Cell. 2010; 22:497–507. https://doi.org/10.1105/tpc.109.072447 PMID: 20190078

9. Veneault-Fourrey C, Barooah M, Egan M, Wakley G, Talbot NJ. Autophagic fungal cell death is necessary for infection by the rice blast fungus. Science. 2006; 312:580–3. https://doi.org/10.1126/science.1124550 PMID: 16645096

10. Shen Q, Liang M, Yang F, Deng YZ, Naqvi NI. Ferroptosis contributes to developmental cell death in rice blast. New Phytol. 2020; 227:1831–46. https://doi.org/10.1111/nph.16636 PMID: 32367535

11. Marroquin-Guzman M, Sun G, Wilson RA. Glucose-ABL1-TOR signaling modulates cell cycle tuning to control terminal appressorial cell differentiation. Copenhaver GP, editor. PLoS Genet. 2017; e1006557:13. https://doi.org/10.1371/journal.pgen.1006557 PMID: 28072818

12. de Jong JC, McCormack BJ, Smirnoff N, Talbot NJ. Glycerol generates turgor in rice blast. Nature. 1997; 389:244–4. https://doi.org/10.1038/38418

13. Foster AJ, Ryder LS, Kershaw MJ, Talbot NJ. The role of glycerol in the pathogenic lifestyle of the rice blast fungus *Magnaporthe oryzae*. Environ Microbiol. 2017; 19:1008–16. https://doi.org/10.1111/1462-2920.13688 PMID: 28165657

14. Chumley FG, Valent B. Genetic analysis of melanin-deficient, nonpathogenic mutants of Magnaporthe grisea. Mol Plant Microbe Interact. 1990; 3:135–43.

15. Dagdas YF, Yoshino K, Dagdas G, Ryder LS, Bielska E, Steinberg G, et al. Septin-mediated plant cell invasion by the rice blast fungus, Magnaporthe oryzae. Science. 2012; 336:1590–5. https://doi.org/10.1126/science.1222934 PMID: 22723425

16. Osés-Ruiz M, Talbot NJ. Cell cycle-dependent regulation of plant infection by the rice blast fungus Magnaporthe oryzae. Commun Integr Biol. 2017; 10:e1372067. https://doi.org/10.1080/19420889.2017.1372067 PMID: 29259729

17. Ryder LS, Dagdas YF, Mentlak TA, Kershaw MJ, Thornton CR, Schuster M, et al. NADPH oxidases regulate septin-mediated cytoskeletal remodeling during plant infection by the rice blast fungus. Proc Natl Acad Sci U S A. 2013; 110:3179–84. https://doi.org/10.1073/pnas.1217470110 PMID: 23382235

18. Gupta YK, Dagdas YF, Martinez-Rocha A-L, Kershaw MJ, Littlejohn GR, Ryder LS, et al. Septin-dependent assembly of the exocyst is essential for plant infection by Magnaporthe oryzae. Plant Cell. 2015; 27:3277–89. https://doi.org/10.1105/tpc.15.00552 PMID: 26566920

19. Bourett TM, Howard RJ. *In vitro* development of penetration structures in the rice blast fungus *Magnaporthe grisea*. Can J Bot. 1990; 68:329–42. https://doi.org/10.1139/b90-044

20. Ryder LS, Dagdas YF, Kershaw MJ, Venkataraman C, Madzvamuse A, Yan X, et al. A sensor kinase controls turgor-driven plant infection by the rice blast fungus. Nature. 2019; 574:423–7. https://doi.org/10.1038/s41586-019-1637-x PMID: 31597961

21. Oses-Ruiz M, Sakulkoo W, Ittlejohn GR, Martin-Urdiroz M, Talbot NJ. Two independent S-phase checkpoints regulate appressorium-mediated plant infection by the rice blast fungus *Magnaporthe oryzae*. Proc Natl Acad Sci U S A. 2017; 114:E237–44. https://doi.org/10.1073/pnas.1611307114 PMID: 28028232

22. Fernandez J, Wilson RA. Cells in cells: morphogenetic and metabolic strategies conditioning rice infection by the blast fungus *Magnaporthe oryzae*. Protoplasma. 2014; 251:37–47. https://doi.org/10.1007/s00709-013-0541-8 PMID: 23990109

23. Kankanala P, Czymmek K, Valent B. Roles for rice membrane dynamics and plasmodesmata during biotrophic invasion by the blast fungus. Plant Cell. 2007; 19:706–24. https://doi.org/10.1105/tpc.106.046300 PMID: 17322409

24. Khang CH, Berruyer R, Giraldo MC, Kankanala P, Park SY, Czymmek K, et al. Translocation of *Magnaporthe oryzae* effectors into rice cells and their subsequent cell-to-cell movement. Plant Cell. 2010; 22:1388–403. https://doi.org/10.1105/tpc.109.069666 PMID: 20435900

25. Faulkner C, Akman OE, Bell K, Jeffree C, Oparka K. Peeking into pit fields: A multiple twinning model of secondary plasmodesmata formation in tobacco. Plant Cell. 2008; 20:1504–18. https://doi.org/10.1105/tpc.107.056903 PMID: 18667640

26. Sakulkoo W, Osés-Ruiz M, Oliveira Garcia E, Soanes DM, Littlejohn GR, Hacker C, et al. A single fungal MAP kinase controls plant cell-to-cell invasion by the rice blast fungus. Science. 2018; 359:1399–403. https://doi.org/10.1126/science.aaq0892 PMID: 29567712

27. Liese W, Schmid R. Über das Wachstum von Bläuepilzen durch verholzte Zellwände. J Phytopathol. 1964; 51:385–93. https://doi.org/10.1111/j.1439-0434.1964.tb03445.x

28. Emmett RW, Parberry DG. Appressoria. Annu Rev Phytopathol. 1975; 13:147–67.

29. Liese W. Ultrastructural aspects of woody tissue disintegration. Annu Rev Phytopathol. 1970; 8:231–58. https://doi.org/10.1146/annurev.py.08.090170.001311

30. Jones EBG. Fungal adhesion. Mycol Res. 1994; 98:961–81. https://doi.org/10.1016/S0953-7562(09)80421-8

31. Riquelme M, Aguirre J, Bartnicki-García S, Braus GH, Feldbrügge M, Fleig U, et al. Fungal Morphogenesis, from the Polarized Growth of Hyphae to Complex Reproduction and Infection Structures. Microbiol Mol Biol Rev. 2018: 82. https://doi.org/10.1128/MMBR.00068-17 PMID: 29643171

32. Brun S, Malagnac F, Bidard F, Lalucque H, Silar P. Functions and regulation of the nox family in the filamentous fungus podospora anserina: A new role in cellulose degradation. Mol Microbiol. 2009; 74:480–96. https://doi.org/10.1111/j.1365-2958.2009.06878.x PMID: 19775249

33. Fukuda S, Yamamoto R, Yanagisawa N, Takaya N, Sato Y, Riquelme M, et al. Trade-off between plasticity and velocity in mycelial growth. MBio. 2021; 12:1–11. https://doi.org/10.1128/mBio.03196-20 PMID: 33727355

34. Whiteford J, Spanu P. Hydrophobins and the interactions between fungi and plants. Mol Plant Pathol. 2002; 3:391–400. Available from: http://www.ebi.ac.uk/clustalw/ https://doi.org/10.1046/j.1364-3703.2002.00129.x PMID: 20569345

35. DeZwaan TM, Carroll AM, Valent B, Sweigard JA. *Magnaporthe grisea* Pth11p is a novel plasma membrane protein that mediates appressorium differentiation in response to inductive substrate cues. Plant Cell. 1999; 11:2013–30. https://doi.org/10.1105/tpc.11.10.2013 PMID: 10521529

36. Liu W, Zhou X, Li G, Li L, Kong L, Wang C, et al. Multiple plant surface signals are sensed by different mechanisms in the rice blast fungus for appressorium formation. PLoS Pathog. 2011; 7:e1001261. https://doi.org/10.1371/journal.ppat.1001261 PMID: 21283781

37. Bridges AA, Jentzsch MS, Oakes PW, Occhipinti P, Gladfelter AS. Micron-scale plasma membrane curvature is recognized by the septin cytoskeleton. J Cell Biol. 2016; 213:23–32. https://doi.org/10.1083/jcb.201512029 PMID: 27044896

38. Cannon KS, Woods BL, Crutchley JM, Gladfelter AS. An amphipathic helix enables septins to sense micrometer-scale membrane curvature. J Cell Biol. 2019; 218:1128–37. https://doi.org/10.1083/jcb.201807211 PMID: 30659102

39. Pfeifer MA, Khang CH. A nuclear contortionist: the mitotic migration of *Magnaporthe oryzae* nuclei during plant infection. Mycology. 2018; 9:202–10. https://doi.org/10.1080/21501203.2018.1482966 PMID: 30181926

40. Sun G, Elowsky C, Li G, Wilson RA. TOR-autophagy branch signaling via Imp1 dictates plant-microbe biotrophic interface longevity. PLoS Genet. 2018; 14:e1007814. https://doi.org/10.1371/journal.pgen.1007814 PMID: 30462633

Chapter 2

The Biology of Invasive Growth by the Rice Blast Fungus *Magnaporthe oryzae*

Neftaly Cruz-Mireles, Iris Eisermann, Marisela Garduño-Rosales, Camilla Molinari, Lauren S. Ryder, Bozeng Tang, Xia Yan, and Nicholas J. Talbot

Abstract

This introductory chapter describes the life cycle of *Magnaporthe oryzae*, the causal agent of rice blast disease. During plant infection, *M. oryzae* forms a specialized infection structure called an appressorium, which generates enormous turgor, applied as a mechanical force to breach the rice cuticle. Appressoria form in response to physical cues from the hydrophobic rice leaf cuticle and nutrient availability. The signaling pathways involved in perception of surface signals are described and the mechanism by which appressoria function is also introduced. Re-polarization of the appressorium requires a septin complex to organize a toroidal F-actin network at the base of the cell. Septin aggregation requires a turgor-dependent sensor kinase, Sln1, necessary for re-polarization of the appressorium and development of a rigid penetration hypha to rupture the leaf cuticle. Once inside the plant, the fungus undergoes secretion of a large set of effector proteins, many of which are directed into plant cells using a specific secretory pathway. Here they suppress plant immunity, but can also be perceived by rice immune receptors, triggering resistances. *M. oryzae* then manipulates pit field sites, containing plasmodesmata, to facilitate rapid spread from cell to cell in plant tissue, leading to disease symptom development.

Key words Appressorium, Fungus, *Pyricularia*, Septins, Autophagy, Cell cycle, MAP kinase, Virulence, Plasmodesmata, Rice, Wheat, Pathogenesis

1 Introduction

The rice blast fungus has emerged as a major model system for understanding the molecular basis of fungal pathogenesis and the biology of plant immunity. Insights made from studying the fungus include a detailed understanding of the biology of infection structure development and the critical role of specific signal transduction pathways that regulate the initial stages of plant infection. These signaling functions are associated with broader physiological processes—such as starvation stress adaptation, surface perception, and autophagy—as well as fundamental cellular mechanisms involved in

asymmetry generation, polarization, and cell cycle control. Definition of fungal effector proteins in the rice blast fungus has, meanwhile, led to new insight into the suppression of plant immunity and the specific recognition processes involved in immune receptor perception and disease resistance. When considered together, these discoveries have provided a platform for generating the most detailed understanding of a plant-fungal interaction. Such developments require the generation of new and specific methods, and this volume is significant in collecting the full spectrum of cell biological, biochemical, and physiological methods developed for studying this devastating pathogen. Here, we describe the life cycle of the fungus, highlighting what is understood about the biology of rice blast and where the methods described in the chapters that follow have been (or will be) pivotal to new understanding.

2 The Early Events of Plant Infection

2.1 The Life Cycle of Magnaporthe Oryzae

To cause infection, the rice blast fungus *Magnaporthe oryzae* (syn. *Pyricularia oryzae*) forms three-celled, teardrop-shaped (pyriform) conidia which develop under humid conditions, erupting at the tips of aerial conidiophores that emerge from disease lesions [1]. *M. oryzae* sporulates at dawn, at the maximum dew point, allowing dewdrop splash and wind to carry spores to neighboring plants and fields. This process is regulated by circadian clock control (*see* Chapter 13 by Griffin and Littlejohn). Conidia initially attach to the hydrophobic, waxy surface of a rice leaf using an adhesive called spore tip mucilage, released from an apical compartment in the spore [2]. In the presence of water, conidial germination occurs within 2 h and a narrow-polarized germ tube emerges from the apical cell of the conidium [3]. The germ tube tip begins to flatten at the leaf surface and swells in a process known as "hooking" [3]. The swollen tip of the germ tube then morphologically differentiates into a specialized single-celled infection structure called an "appressorium" (*see* Fig. 1a).

The dome-shaped appressorium is a prerequisite for plant infection and enables the fungus to physically rupture the plant host cuticle [1]. As the appressorium matures, it generates a melanin layer located between the appressorium plasma membrane and the cell wall [3] (for ultrastructural analysis of appressoria, *see* Chapter 6 by Rocha and Wilson). The melanin layer is porous, allowing water to be taken up by the appressorium while at the same time retaining larger molecules such as glycerol and other polyols to accumulate in the cell [4, 5]. When water enters the appressorium, against the high concentration gradient of glycerol, this generates hydrostatic turgor pressure that is rapidly translated into mechanical force to drive a narrow rigid penetration hypha from the base of the appressorium to rupture the rice leaf cuticle
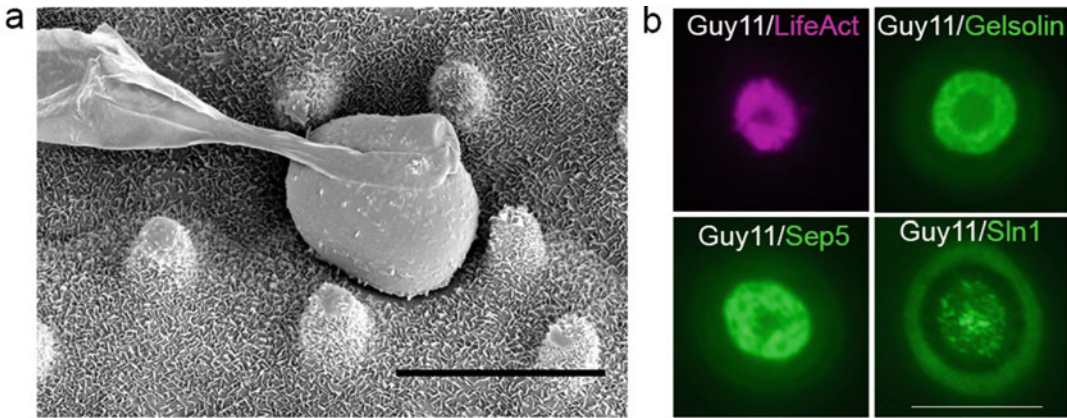
Fig. 1 Appressorium morphogenesis in the rice blast fungus. (**a**) Scanning electron micrograph showing an appressorium on the rice leaf surface. The conidium has already collapsed due to autophagic cell death. Bar = 10 μm. Micrograph by Kim Findlay, John Innes Centre Bio-Imaging. (**b**) Reorganization of the fungal cytoskeleton at the appressorium pore. An F-actin toroidal network can be visualized by expression of LifeAct-mCherry and Gelsolin-GFP. This is scaffolded by a septin ring, shown here by expression of Sep5-GFP. The turgor sensor kinase Sln1-GFP localizes to the appressorium pore. Bar = 10 μm

[5, 6]. The fungus invaginates the host plant plasma membrane and rapidly fills the epidermal cells, secreting effectors to suppress the host immunity [7, 8]. Once the bulbous invasive hyphae fill the first infected host cell, the fungus accesses the neighboring plant cells through pit field sites where plasmodesmata accumulate [9]. Disease lesions then become visible 96 h after infection, and sporulation occurs under the conditions of high humidity. Conidia spread to neighboring plants and fields and the *M. oryzae* life cycle is complete [10, 11].

Although seldom observed in the field, *M. oryzae* also has the capacity to undergo sexual reproduction, in which two individuals of different mating type (Mat1-1 and Mat1-2) form a flask-shaped perithecium, which contains numerous asci, each of which carries eight ascospores—with each pair of spores representing one of the four products of meiosis. Sexual reproduction is common in some host-limited forms of *M. oryzae*, such as finger millet pathogens, for instance, but most rice-infecting strains of the fungus have lost fertility [10].

To initiate appressorium development, the fungus responds to physiological and biochemical cues, which include surface hardness, hydrophobicity, and rice leaf waxes [1]. These signals are translated through signaling pathways to trigger appressorium formation on an appropriate host cell surface [12]. The secreted class I hydrophobin gene *MPG1* is highly expressed during germination, appressorium formation, and plant infection [13]. The hydrophobin is secreted into the space between the fungal cell wall and plant tissue surface, self-assembling to form an amyloid structure which

increases the wettability of the leaf surface, aiding the action of cutinases and triggering appressorium development [13, 14]. Perception of the hydrophobic cuticle involves integral G-protein-coupled receptors (GPCRs), such as Pth11, composed of seven transmembrane domains and an extracellular cysteine-rich domain [15]. Pth11 detects external physical cues from the rice leaf surface, leading to adenylate cyclase activation. Targeted gene replacement of *PTH11* in *M. oryzae* generates mutants unable to form appressoria, which are consequently non-pathogenic [16]. It has been suggested that the G-protein signal pathway also acts as an upstream signaling pathway for response to the hardness of the leaf surface [17]. The Gα subunit MagB suppresses appressorium formation on non-inductive surfaces and maintains adenylate cyclase in an inactive state [18]. The regulator of G-protein signaling proteins (RGSs) also controls MagB and cAMP levels during appressorium morphogenesis [19]. Rgs1 interacts with MagA, MagB, and MagC subunits in *M. oryzae* [1, 18, 20] and deletion of *RGS1* causes elevated cAMP levels [18], consistent with Rgs1 negatively regulating G-protein signaling through interaction with MagB and MagA. It is thought that upon activation from surface cues, these receptors transduce information to the protein kinase A-dependent cAMP response pathway and other signaling pathways [18, 21]. Cyclic AMP signaling transmits signals to downstream effectors that induce appressorium development [22–24]. *MAC1*, encoding adenylate cyclase, catalyzes production of cAMP from ATP, while cAMP phosphodiesterases hydrolyze cAMP [10, 19, 25]. Null mutants of *MAC1* cannot elaborate appressoria, but this phenotype can be remediated by exogenous cAMP [26]. Formation of appressoria on non-inductive hydrophilic surfaces can be induced by exogenous cAMP [27], and this ultimately activates the cAMP-dependent protein kinase A [28], a tetrameric holoenzyme which phosphorylates target proteins associated with appressorium maturation and turgor generation [24]. Cyclic AMP signaling is repressed by the target of rapamycin (TOR) [29] kinase and glutamine levels, regulated by the Asd4 transcription factor, which are key to the progression of appressorium development [30]. The precise control of sugar sensing and nitrogen source utilization are critical components of the regulation of appressorium function, which only occurs under starvation conditions [31, 32]. The analysis of cell signaling in *M. oryzae* has been greatly facilitated by methods to purify protein complexes, as described in Chapter 8 by Li and Wilson.

2.2 The Role of the Pmk1 MAP Kinase in Appressorium Development

The pathogenicity MAP kinase 1 (Pmk1) signaling pathway is a conserved signaling cascade in pathogenic fungi and has been reported to be crucial for plant infection in more than 20 plant pathogenic species [33, 34]. Many components of the pathway were identified initially by homology to the Fus3/Kss1 MAPK

cascade in the model fungus *Saccharomyces cerevisiae* and, subsequently, by using *M. oryzae* as a guide.

In *M. oryzae*, it has long been known that the Pmk1 MAPK is required for appressorium morphogenesis. The absence of Pmk1 by generation of a Δ*pmk1* null mutant is sufficient to render the fungus non-pathogenic [23, 35], and Δ*pmk1* mutants fail to form appressoria, but are non-pathogenic even when spores are inoculated into wounded leaves. Recently, it has been shown that a conditionally inactive *pmk1^{AS}* analogue-sensitive mutant of *M. oryzae* fails to move from rice cell-to-rice cell during invasive growth, implicating the MAPK in formation of specialized structures required to traverse the host cells [32]. A Δ*pmk1* mutant still responds to hydrophobic surfaces or exposure to exogenous cAMP by forming swollen germ tube tips [23]. The Pmk1 MAPK is expressed throughout vegetative growth of *M. oryzae*, and it has been reported that during appressorium maturation, GFP-Pmk1 localizes to the appressorium nucleus, consistent with the observations in other filamentous fungi that MAPKs can be translocated to the nucleus in response to specific stimuli [36].

During appressorium development, the Pmk1 MAP kinase is activated by its upstream MAPKK Mst7 and MAPKKK Mst11 [37]. Mst7 and Mst11 deletion mutants also fail to form appressoria and are non-pathogenic [37]. The Mst7 MAPKK appears to activate Pmk1 by phosphorylation of threonine and tyrosine residues in the well-conserved MAP kinase TXY motif [33, 37]. It has been reported that the interaction between Mst7 and Pmk1 occurs via a Mst7 MAPK-docking domain [38, 39]. Moreover, Mst7 forms homodimers and requires the action of thioredoxins to activate Pmk1 during ROS signaling [40]. The MAPKKK Mst11 can also be regulated by its self-inhibitory binding and through interaction with Ras proteins, via a Ras association domain [41, 42]. Both Mst11 and Mst7 form a complex with a scaffold protein, Mst50, that works as an adaptor [38, 43, 44]. Mst50 deletion mutants are defective in appressorium formation and non-pathogenic [44]. The Mst50 interaction with Mst7 and Mst11 is predicted to be direct, and the interaction between Mst50 and Mst11 occurs through its sterile α-motif (SAM) domain, although detailed in vivo binding assays are still necessary to confirm all of the Pmk1 signaling pathway interactions [44]. Ordering signaling pathways benefits from experimental methods such as bypass suppressor analysis, as described using the example of the osmosensing pathway (HOG pathway) by Jacob and Bersching in Chapter 18.

Upstream of the Mst50-Mst11-Mst7 complex, the G-beta subunit Mgb1 [45], the plasma membrane protein Pth11 [16, 46], and the sensing surface proteins Msb2 and Sho1 are necessary for initiation of appressorium morphogenesis [38]. Mgb1 is predicted to interact directly with Mst50, suggesting

that Mst50 may integrate multiple upstream signals to activate the Pmk1 MAPK cascade [44]. Mgb1, Pth11, Msb2, and Sho1 also play a role in the surface recognition pathway and activation of cyclic AMP-protein kinase A (cAMP-PKA) [38]. There is undoubtedly a link between cAMP-PKA and Pmk1 pathways, but the exact mechanism by which this occurs remains unclear [47]. It is clear, however, that TOR kinase must remain inactive in order for appressorium development to proceed [29].

Little is known regarding the downstream targets of Pmk1, which regulate appressorium development. By yeast two-hybrid analysis, two Pmk1-interacting clones (PICs) were identified that serve roles in conidiation and appressorium differentiation [48]. PIC5 mutants are defective in germ tube growth and appressorium formation [48]. Transcription factors, such as the homeobox protein Hox7 and the C2/H2 Zn finger-domain protein Znf1, may operate downstream of the Pmk1 cascade and are also indispensable for appressorium formation [49, 50]. A comparative transcriptomics analysis of Δ*pmk1* mutants showed that 481 genes appear to be positively regulated by Pmk1 during germination, including known pathogenic components such as the GAS proteins and Pth11 [51]. Phosphoproteomic approaches will be necessary to understand the phosphorylation-dependent signal transduction events of the pathway, as detailed in Chapter 9 by Michna and Tenzer. These studies have benefited enormously from the ability to generate mutants very rapidly using targeted gene replacement methods and, more recently, the generation of CRISPR-Cas9-mediated genome editing, as described by Arazoe in Chapter 12.

2.3   Cell Cycle Control of Appressorium Development and Autophagic Cell Death

M. oryzae appressorium morphogenesis is tightly regulated by cell cycle progression [1, 52–54]. Cell cycle regulation, for example, is necessary to initiate the appearance of the fungal germ tube from the three-celled conidium. At this stage, one of the nuclei migrates into the germ tube, where it undergoes a single round of mitosis. The daughter nucleus then migrates to the tip of the germ tube, before isotropic swelling begins that leads to the formation of the appressorium. The other daughter nucleus returns to the conidium where it is degraded [1, 55]. Evidence implicating cell cycle control has been reported, for example, by generating temperature-sensitive mutations of the *NIMA* gene [52]. This gene is fundamental to mitosis and involved in the conserved DNA damage repair checkpoint pathway [52, 56]. When tested, together with a DNA synthesis inhibitor (hydroxyurea, HU), it was verified that successful execution of DNA replication (S-phase) is required for initiation of appressorium development [52]. Additionally, to ensure successful DNA duplication and segregation, cells arrest the cell cycle when DNA damage occurs [57]. This happens through inhibitory phosphorylation of the B-cyclin-CDK1 complex by two serine-threonine protein kinases of the DNA damage

response (DDR) pathway [57]. Identification and mutant generation of the corresponding *M. oryzae* serine-threonine kinases involved revealed that they were both involved in the S-phase checkpoint during the early stages of the appressorium development [54]. However, this cell cycle checkpoint is not the only one that has been reported. There may also be a TOR-dependent G2 delay that is essential for appressorium autophagy to occur [29]. After the first round of mitosis, a threshold of turgor must also be reached in the appressorium, for its nucleus to transition from G1 to S-phase [53, 54]. This was tested using turgor-deficient mutants which are arrested in G1 and do not continue with infection [54]. This second cell cycle checkpoint appears to be controlled in a novel DDR-independent manner [53, 54]. These studies have benefited very significantly from live-cell imaging techniques, as detailed by Rogers et al. in Chapter 7.

Degradation of the remaining three conidial nuclei and collapse of the three-celled conidium (Fig. 1a) are also necessary for appressorium maturation and mediated by cell cycle control [1, 29, 53]. When mitosis is blocked, for example, appressorium formation is prevented, as well as conidial autophagy [1, 52]. Targeted deletion of *M. oryzae* autophagy-associated genes showed that the collapse of the three-celled conidium requires autophagy [1]. Two independent studies of the function of Atg1 and Atg8 demonstrated the requirement for autophagy in appressorium maturation [58, 59]. Autophagy mutants produce appressoria normally, but conidia fail to collapse, and, as a consequence, appressoria cannot re-polarize and are therefore not in a position to cause plant infection [4, 53, 58, 59]. Recent evidence has been presented that suggests that the final collapse and death of conidia requires a form of iron-dependent cell death, called ferroptosis, to occur [60]. Methods to study the onset of autophagy in *M. oryzae* are described by Li et al. in Chapter 14.

3   Appressorium Maturation

3.1   Turgor Generation and Turgor Sensing in *M. oryzae*

Appressoria in *M. oryzae* are simple unicellular structures, but they can be intricate multicellular structures, such as "infection cushions" in other pathogenic species [61–63]. Once mature the appressorium develops enormous turgor of up to 8.0 MPa, accumulating up to 3.0 M glycerol and other polyols to draw water into the cell by osmosis (Fig. 1a) [5]. The appressoria adhere tightly to the host surface aided by the action of mucilage, related to the spore tip mucilage that attaches conidia to the leaf surface, and the action of cutinases [64]. The appressorium develops a differentiated cell wall rich in melanin that is impermeable to glycerol which is also necessary for turgor generation. The melanin barrier allows water to enter the cell against the osmotic gradient and to

retain glycerol, generating enormous hydrostatic pressure [2, 5]. Rusts and powdery mildews can form functional appressoria in the absence of water, suggesting the mechanism for turgor generation is distinct [47]. In fact, as we begin to evaluate the important criteria essential for successful appressorium turgor generation, it is apparent that not all appressoria generating fungi have the same requirements. Studies have, for example, revealed that appressorium turgor can be generated in the absence of melanin; in the soybean rust fungus *Phakopsora pachyrhizi*, for instance, non-melanized appressoria are still able to generate 5.13 MPa of pressure [65, 66]. Similarly, in the anthracnose pathogen of corn, *Colletotrichum graminicola*, turgor is still generated even when melanin biosynthesis is inhibited. Furthermore, cytorrhysis assay analysis of the osmolyte content using a method called Mach-Zehnder interferometry showed melanin is not required for solute accumulation and turgor generation [67]. This suggests that melanin does not provide the barrier for osmolytes in *C. graminicola* in the way it does in *M. oryzae* [47]. It is likely there are other components of the appressorium cell wall that can compensate for the function of melanin to achieve high turgor. A detailed biochemical and ultrastructural analysis of different appressoria cell walls is therefore vital in our understanding of how such extraordinary turgor pressures can be achieved.

Determining the precise mechanism for how the appressorium monitors turgor has been a long-standing conundrum. Previous work showed *M. oryzae* does not regulate appressorium turgor generation as cellular turgor is regulated in *S. cerevisiae*. In yeast, glycerol synthesis is regulated by the MAPK high-osmolarity glycerol response signaling pathway (HOG pathway), but in *M. oryzae*, the *HOG* homologue *OSM1* is dispensable for pathogenicity and glycerol production [68]. It is likely therefore that distinct biochemical routes for glycerol synthesis exist with different form of regulation. Conidia, for example, contain significant amounts of lipid, glycogen, trehalose, mannitol, and other storage products. Methods to study carbohydrate accumulation in *M. oryzae* are described by Grünewald et al., in Chapter 4. Considering conidia germinate in water droplets, glycerol must originate de novo from one or more of these sources (for a detailed review, *see* [6]).

Recent evidence has suggested that Sln1, a histidine-aspartate kinase, enables the appressorium to sense when a critical threshold of turgor has been reached, and thereby regulate host penetration [69]. Sln1 is an osmosensor in yeast that regulates hyperosmotic adaptation through the Hog1 MAPK pathway [70], and a previous study revealed *M. oryzae SLN1* to be necessary for pathogenicity [71]. A combination of cell biology, molecular genetics, discovery phosphoproteomics, and mathematical modeling demonstrated that the Sln1 sensor kinase responds to appressorium turgor by interacting with a set of upstream proteins that monitor cell

expansion, including stretch-activated ion channel proteins, Mic1, Mic2, and Mic3, that maintain osmotic homeostasis within the cell. Once the required threshold of turgor is reached, it is maintained through the action of Sln1 by negatively regulating melanin biosynthesis and the cAMP/PKA pathway. Pkc1, the central regulator of the cell-integrity pathway, likely phosphorylates the phosphodiesterase PdeH to modulate cAMP levels and, as a consequence, will control lipolysis and glycerol production. Pkc1 may also target NoxR, a key regulator of the NADPH oxidase complex for regulated synthesis of ROS, which is necessary for septin-mediated cytoskeletal reorganization (Fig. 1b) [69, 72].

3.2 Cytoskeletal Remodeling During Appressorium Development

Experiments performed in the last decade began to explain the mechanism by which the re-establishment of the polarized growth occurs at the contact interface between the blast fungus and the plant host [73]. These morphogenetic phenomena ultimately lead to the generation and protrusion of the penetration peg into the host cuticle [73]. The penetration hypha emerges from the appressorium pore, which is the site of remodeling of the actin cytoskeleton [73, 74]. Filamentous actin (F-actin) is actively studied in filamentous fungi, due to its importance in polarized growth and morphogenesis [75–78]. F-actin interacts with associated proteins to confer stability to the different arrangements and organization of the cytoskeleton. F-actin can form high-order structures like patches, cables, and actomyosin contractile rings; these arrays have different functions and are responsible for distinct processes [75–77, 79–81]. A practical tool to visualize F-actin in live cells is the reporter LifeAct, which consists of the first 17 amino acids (M GVADLIKKFESISKEE) of the actin-binding protein Abp140 of budding yeast *Saccharomyces cerevisiae* [82]. Live-cell imaging of the actin cytoskeleton during appressorium development in *M. oryzae* has been carried out by expressing LifeAct-RFP (red fluorescent protein), which revealed an extensive toroidal F-actin network surrounding the appressorium pore at the base of the infection cell [73]. Assembly of the F-actin network during the generation of turgor in the appressorium indicates that specific reorientation of the cytoskeleton occurs at the base of the infection cell to achieve plant infection [73, 74]. It is here that septin GTPases play such an essential role by remodeling actin, forming a ring of 5.9 μm that colocalizes with the F-actin network at the appressorium pore [72, 73]. The septin ring also acts as a lateral diffusion barrier for specific actin-associated proteins, such as Las17, which polymerizes F-actin via the arp2/3 complex, and gelsolin, a key protein in the assembly and disassembly of the actin filaments [69, 73].

F-actin provides cortical rigidity prior to penetration peg emergence, as demonstrated in experiments performed in the *M. oryzae* mutants, Δ*cdc42* and Δ*chm1*, where the septin and F-actin

networks are unable to form successfully [73]. Tea1, an ERM (ezrin, radixin, moesin) protein, tagged with GFP (green fluorescent protein), colocalizes with the F-actin and septin networks [73]. Interestingly, ERM proteins may link F-actin to the plasma membrane through an actin-binding domain in their C-terminus and an ERM domain that binds transmembrane proteins in their N-terminus [83], which supports the idea that ERM protein-actin linkages occur at the appressorium pore [73].

3.3 Septin-Dependent Plant Infection

Septins are guanosine triphosphatases (GTPases) [84] that were originally reported to play an essential role during cell division in *S. cerevisiae* [85] and are now recognized as key components of the cytoskeleton, like actin and microtubules. Septins are expressed in all eukaryotic organisms, with the exception of plants, and implicated in many cellular processes [28, 84, 86]. Septins consist of a highly conserved central GTP-binding domain, flanked by N- and C-terminal regions, and between the N-terminus and the GTP-binding domain is a short polybasic region (PBR). This region binds to negatively charged phospholipids and is responsible for interacting with membranes. A septin unique element [87] overlaps with the GTP-binding domain and is located toward the C-terminus. It is assumed that this region takes part in septin polymerization. The C-terminus itself is indispensable for septin-protein interactions [84, 88, 89]. Septins interact in a specific way with themselves and/or other septins at which they form dynamic hetero-oligomeric complexes [73, 90]. In *M. oryzae* the four core septin genes *SEP3*, *SEP4*, *SEP5*, and *SEP6* are homologues of the *S. cerevisiae* genes *CDC3*, *CDC10*, *CDC11*, and *CDC12*. During rice infection the hetero-oligomeric septin ring forms at the base of the appressorium (*see* Fig. 1b), and its formation and the dynamic recruitment of the F-actin have been visualized by quantitative 4D widefield fluorescence imaging [91]. The septin ring can only assemble after Sln1-dependent turgor sensing [69, 72] and progression of the appressorium nucleus through S-phase [54]. Sln1 acts through the Pkc1-dependent cell-integrity pathway to activate the Nox2-NoxR complex [69, 72] to regulate septin recruitment. The transcription factor Tpc1 regulates expression of the NADPH oxidase p22phox subunit Nox-D [92], and activation of the NADPH oxidase leads to regulated synthesis of ROS. The Ras-GTPase activating protein, Smo1, is also indispensable for septin recruitment and organization at the appressorium pore and negatively regulates the Ras2 signaling complex, while also directly interacting with the four core septins and components of the exocyst complex [93]. Additionally, assembly of the septin ring requires Cdc42 (a small GTPase of the Rho family) and Chm1 (a p21-activated kinase) which phosphorylates septins [73, 89]. The Mps1 MAPK and Mst12 are furthermore involved in septin assembly [94, 95]. In this context, sumoylation plays an

additional role because attachment of a small ubiquitin-like modifier (SUMO) to septins is necessary for correct septin ring localization [96]. In this way septins recruit and organize the F-actin network at the appressorium pore, making phosphoinositide linkages between septins and the plasma membrane and facilitating F-actin plasma membrane linkages via ezrin, radixin, moesin (ERM) proteins, such as Tea1. The lateral diffusion barrier function of septins also secures the correct positioning of Las17 and Rvs167 [73], as well as the exocyst complex to the appressorium pore [97]. When considered together, septin-dependent functions are crucial for appressorium-mediated penetration to invade the leaf tissue.

4   Invasive Growth

4.1   BIC Formation and Translocation of Effectors

After successfully breaching the host plant cuticle, *M. oryzae* rapidly adapts to its new host environment [98, 99]. The fungus forms primary invasive hyphae after penetration of the rice epidermis [100]. Invasive hyphae develop as bulbous, branching structures that fill the epidermal cells [101–103]. Invasive hyphae are encased by the host extra-invasive hyphal membrane (EIHM), which provides a compartment to seal fungal invasive hyphae inside the host cell [101, 103]. During the biotrophic infection, the fungus secretes effector proteins and secondary metabolites into the host cells, which interfere with plant immunity response and physiology, thereby facilitating invasion and expansion [101, 102, 104]. This includes the modulation of host jasmonate signaling by a fungal monooxygenase to suppress immunity responses [105]. Methods to analyze secondary metabolism in *M. oryzae* are described in Chapter 3 by Skellam. Manipulation of the host environment includes suppressing the oxidative burst by oxidative denitrification of nitroalkanes using nitronate monooxygenase, encoded by the *NMO2* gene [106].

In the early stage of the infection, a structure is formed at the tip of the primary infecting hyphae, called the biotrophic interfacial complex (BIC) (*see* Fig. 2) [103, 104, 107]. Once the invasive hypha differentiates into bulbous branched structure, the BIC is positioned sub-apically and is a site where fungal effector proteins accumulate [108]. Formation of the BIC recurs when the fungus invades each new neighboring cell and requires *NMO2* [106]. Evidence has been reported which suggests that two distinct secretion pathways exist for the delivery of fungal effectors by *M. oryzae* [102]. Apoplastic effectors are secreted by a Golgi-dependent, brefeldin A-sensitive pathway, while effectors secreted into the host cells are secreted by a Golgi-independent, exocyst-dependent but brefeldin A-insensitive pathway. Cytoplasmic effectors also accumulate in the BIC, which appears to be the predominant
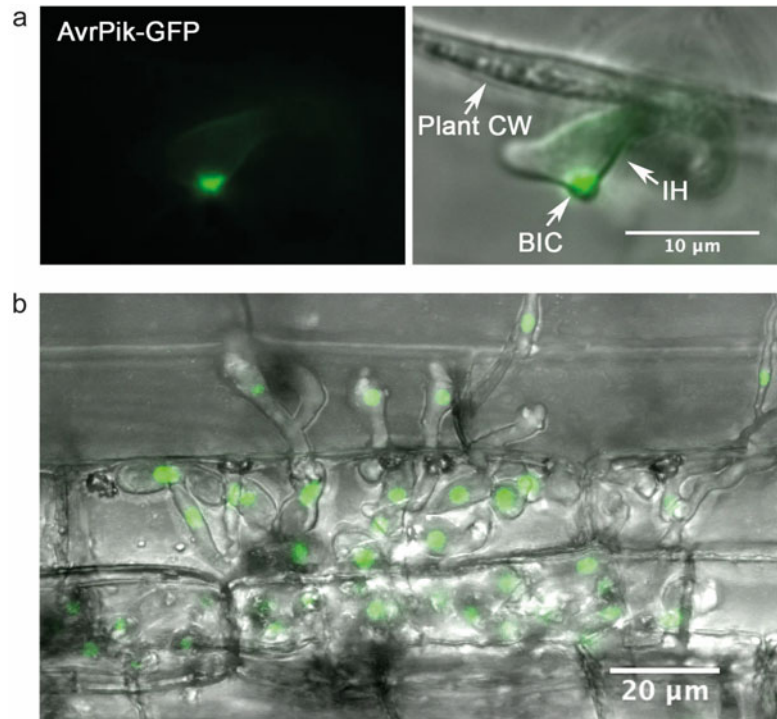
Fig. 2 Laser confocal imaging of invasive growth of the rice blast fungus. (**a**) The biotrophic interfacial complex (BIC) formed in the first invaded cell, as visualized by the expression of AvrPik-GFP. Bar = 10 μm. (**b**) Invasive hyphae spreading throughout the rice tissue. Hyphae are expressing H1-GFP to show nuclei. Bar = 20 μm

route for their delivery, based on photobleaching experiments [102]. To obtain these detailed results was made possible through the methods to study the effector secretion systems of *M. oryzae* described by Oliveira-Garcia and Valent in Chapter 5. Recently, a gene involved in BIC formation, called *RBF1*, has been reported [108]. An *rbf1* mutant shows reduced virulence and triggers plant immunity in epidermal cells, consistent with the importance of the BIC in immune suppression mechanisms during invasive growth [108].

After 32–36 h *M. oryzae* invasive hyphae constrict and move through the pit fields to neighboring cells [35]. This process is regulated by the Pmk1 MAPK, which when conditionally inactivated prevents cell-to-cell spread by the fungus [32]. By contrast, the Mps1 MAPK is not required for cell-to-cell movement, but is involved in invasive hypha differentiation by coordinating the accumulation of α-1,3-glucans which may protect the fungus by avoiding degradation from plant-derived chitinases [94, 109]. The transcription factor Mig1, regulated by Mps1, is also necessary for invasive growth [110], while the Swi6 transcription factor is

involved in cell wall integrity and the response to oxidative stress during invasive growth of *M. oryzae* [111]. It is also clear that the tight regulation of fungal metabolism is key to these morphogenetic transitions [112–114]. The maintenance of EIHM integrity, for example, requires *IMP1* and is tightly linked to the TOR-dependent regulation of autophagy, which must be tightly controlled during biotrophic growth [115].

Rice blast effectors have now been identified in significant numbers and their functions are beginning to be understood [116–118]. Methods to functionally analyze effectors are reported in Chapter 16 by Liu. Studies have shown diverse cytoplasmic effectors in *M. oryzae* accumulate BICs [104], including almost all the effector molecules known to be recognized by the immune receptor products of rice blast resistance genes, such as Avr-Pita, Avr-Pizt, Pwl1, Pwl2, and Bas1 [103], and the exocrine protein MC69 [103, 119, 120]. Pwl2 is not only secreted at the BIC, but has also been observed in adjacent uninfected rice cells, when these are plasmolyzed to concentrate the cytoplasmic signal [100]. Conversely, apoplastic effectors are secreted into the extracellular space between the hyphae and the EIHM, such as Bas4 and Slp1 [7, 104]. In the early stage of infection, Slp1, a LysM protein, aggregates at the interface between the plant and the fungus and can bind to chitin oligomers, released from the growing fungus, thereby inhibiting their perception by chitin receptors, such as CEBiP [7].

In many pathogens, effectors have been characterized based on their specific expression profiles in plants [121–125]. For instance, it has been shown that AvrE1 and HopM1 effectors secreted by phytopathogenic bacteria are essential bacterial proliferation in the apoplast of *Arabidopsis* [126]. In general, effectors are defined as virulence components which promote infection and manipulate plant immunity [127]. However, pathogen effectors can also be recognized by immune receptors [128–130]. In many species of plants and animals, intracellular receptors containing nucleotide-binding (NB) domains and leucine-rich repeat (LRR) proteins can detect effectors, either directly or indirectly [131, 132]. There are about 500 NB-LRRs known in rice, which are considered to act against *M. oryzae*, although only 33 discrete R-genes have been described in detail [133]. The first reported interaction was between Pi-ta and the fungal effector AVR-Pita, in which the rice immune receptor Pi-ta may bind to the AVR-Pita effector and lead to a hypersensitive reaction [134]. This also, however, allows the pathogen to conquer effector-triggered immunity by frequent mutation of effector-encoding genes that disrupt the specific interaction between effectors and the corresponding immune receptors in rice. The *Avr-Pik* alleles (*Pik/km/kp*) in *M. oryzae*, for example, show high levels of selection polymorphism [135, 136]. Similarly, the function of *Avr-CO39* has been abolished by transposon

insertions in some isolates, leading to the gain of virulence in rice lines containing *CO39* [87]. Frequent mutations and transposon insertions therefore provide allelic diversity in avirulence genes in *M. oryzae*. For example, *Avr-Pita* is very unstable with a high level of translocation in the genome [137], and *Avr-Pi9* in *M. oryzae* has been subject to Mg-SINE insertion that has led to virulence on *Pi9*-containing rice cultivars [138]. A similar situation has occurred to drive the recent evolution of *M. oryzae* wheat blast isolates [139].

4.2 Effector Function in M. oryzae

It is clear that *M. oryzae* secretes a very large battery of effector proteins into the plant cells during invasive growth to facilitate disease development, although the virulence functions of relatively few effectors have been determined [107, 140].

The majority of cytoplasmic effectors are small secreted proteins, with little homology outside of *M. oryzae*, although often well conserved among rice pathogens and other host-limited forms of the fungus [141]. Relatively few show clear homologies to proteins of known function; *AVR-Pita*, however, does encode a protein that contains a zinc-dependent metalloprotease domain, suggesting that it may cleave its cognate virulence target, although this has not been shown, and it is reported to bind directly to its cognate immune receptor Pi-ta [142]. The *ACE1* gene encodes a non-ribosomal peptide synthetase (NRPS)-polyketide synthase (PKS) hybrid enzyme. *ACE1* may therefore catalyze production of a secondary metabolite required for virulence that can be perceived by an immune receptor [143, 144]. The corresponding R gene *Pi33*, however, has not yet been identified [145]. A significant number of fungal effectors await characterization, including the family of fungal biotrophy associated secreted (BAS) effectors identified based on their expression profiles and localization during biotrophic growth [105]. Their function is still unknown because the generated mutants for these effectors failed to show clear phenotypes. However, further analysis has determined distinct cellular localizations—BAS1 shows accumulation at the BIC and cytoplasm, BAS2 and BAS3 localize to the BIC and the plant cell wall crossing points, and BAS4 accumulates in the outer space of the invasive hyphae, highlighting the potential diversity in their function.

Significant insight into the precise perception events leading to plant immunity has recently been gained using the rice blast pathosystem. Many NLR (nucleotide-binding, leucine-rich repeat) immune receptor proteins operate in pairs in a synergistic manner, where one NLR acts as a "sensor" and the second as a "helper" [146]. In *M. oryzae*, this organization is found, for example, in *Pii-1/Pii-2*, *Pik-1/Pik-2*, and *Pi-CO39/Pia* (Rga4/Rga5) gene pairs [147]. Recognition of the cognate Avr effector therefore requires a combination of two NLR proteins, which work together. Avr-Pia and Avr1-CO39 are both recognized by the RGA4/RGA5 pair of

NLRs, and this occurs by direct binding to a heavy metal-associated domain (HMA or RATX1), integrated into RGA5 [148]. This integrated domain may mimic the virulence target of these effectors because HMAs are implicated in host defense-associated ROS generation. The physical interaction of RGA4 and RGA5 prevents cell death that is mediated by RGA4, and the presence of AVR-Pia relieves that suppression, resulting in hypersensitive cell death [147]. The rice NLR, Pik-1, has also been shown to contain an integrated HMA domain, although inserted between the coiled domain and nucleotide-binding site (NB-ARC), and acts together with the helper NLR, Pik-2, in the recognition of AVR-Pik [135]. Multiple alleles of *Pik-1* can recognize different allelic forms of AVR-Pik. For example, *Pikp* rice lines are resistant to isolates carrying *AVR-Pik-D*, but susceptible to those expressing *AVR-Pik-E*, *AVR-Pik-A*, and *AVR-Pik-C* [135]. Structural analysis of the Pikp-HMA/AVR-PikD complex has revealed specific interactions leading to immunity [149], and this has led to further structure-function studies that have used protein engineering of the HMA domain of Pikp-1 to extend its recognition profile to different allelic variants of AVR-Pik [150, 151].

The concerted action of the battery of effectors secreted into the host cells leads to the suppression of plant defense and rapid proliferation of *M. oryzae* in rice tissue. Necrotic lesions then form, and host cell death is elicited. Conidiation occurs from disease lesions and the fungus spreads to new host plants. Methods to detect fungal colonization of seeds are described by Chadha in Chapter 15, and methods to identify novel fungicides for rice blast control are reported by Bohnert et al., in Chapter 10.

In summary, the life cycle of *M. oryzae* is exemplified by specific, highly orchestrated developmental transitions and precise adaptations to biotrophic growth in plant tissue, such as the evolution of a large family of effector proteins that can suppress immunity and overwhelm plant defenses, allowing the fungus to grow very rapidly in host tissue and cause blast disease. It is for these reasons that the rice blast fungus constitutes such a difficult pathogen to control. The methods in this volume do, however, provide the tools to make very rapid progress in understanding rice blast disease, which will be pivotal to its durable control.

References

1. Wilson RA, Talbot NJ (2009) Under pressure: investigating the biology of plant infection by Magnaporthe oryzae. Nat Rev Microbiol 7:185–195

2. Hamer JE, Howard RJ, Chumley FG, Valent B (1988) A mechanism for surface attachment in spores of a plant pathogenic fungus. Science 239:288

3. Bourett TM, Howard RJ (1990) In vitro development of penetration structures in the rice blast fungus Magnaporthe grisea. Can J Bot 68:329–342

4. Kershaw MJ, Talbot NJ (2009) Genome-wide functional analysis reveals that infection-associated fungal autophagy is necessary for rice blast disease. Proc Natl Acad Sci U S A 106:15967–15972

5. de Jong JC, McCormack BJ, Smirnoff N, Talbot NJ (1997) Glycerol generates turgor in rice blast. Nature 389:244–244

6. Foster AJ, Ryder LS, Kershaw MJ, Talbot NJ (2017) The role of glycerol in the pathogenic lifestyle of the rice blast fungus Magnaporthe oryzae. Environ Microbiol 19(3):1008–1016

7. Mentlak TA, Kombrink A, Shinya T, Ryder LS, Otomo I, Saitoh H, Terauchi R, Nishizawa Y, Shibuya N, Thomma BP, Talbot NJ (2012) Effector-mediated suppression of chitin-triggered immunity by Magnaporthe oryzae is necessary for rice blast disease. Plant Cell 24:322–335

8. Yan X, Talbot NJ (2016) Investigating the cell biology of plant infection by the rice blast fungus Magnaporthe oryzae. Curr Opin Microbiol 34:147–153

9. Martin-Urdiroz M, Oses-Ruiz M, Ryder LS, Talbot NJ (2016) Investigating the biology of plant infection by the rice blast fungus Magnaporthe oryzae. Fungal Genet Biol 90:61–68

10. Talbot NJ (2003) On the trail of a cereal killer: exploring the biology of Magnaporthe grisea. Ann Rev Microbiol 57:177–202

11. Wang X, Valent B (2009) Advances in genetics, genomics and control of rice blast disease. Springer Science & Business Media, Berlin/Heidelberg

12. Liu W, Zhou X, Li G, Li L, Kong L, Wang C, Zhang H, Xu J-R (2011) Multiple plant surface signals are sensed by different mechanisms in the rice blast fungus for appressorium formation. PLoS Pathog 7:e1001261

13. Talbot NJ, Ebbole DJ, Hamer JE (1993) Identification and characterization of MPG1, a gene involved in pathogenicity from the rice blast fungus Magnaporthe grisea. Plant Cell 5:1575–1590

14. Pham CL, Rey A, Lo V, Soules M, Ren Q, Meisl G, Knowles TP, Kwan AH, Sunde M (2016) Self-assembly of MPG1, a hydrophobin protein from the rice blast fungus that forms functional amyloid coatings, occurs by a surface-driven mechanism. Sci Rep 6:25288

15. Kulkarni RD, Thon MR, Pan H, Dean RA (2005) Novel G-protein-coupled receptor-like proteins in the plant pathogenic fungus Magnaporthe grisea. Genome Biol 6:R24

16. DeZwaan TM, Carroll AM, Valent B, Sweigard JA (1999) Magnaporthe grisea pth11p is a novel plasma membrane protein that mediates appressorium differentiation in response to inductive substrate cues. Plant Cell 11:2013–2030

17. Liu S, Dean RA (1997) G protein α subunit genes control growth, development, and pathogenicity of Magnaporthe grisea. Mol Plant-Microbe Interact 10:1075–1086

18. Liu H, Suresh A, Willard FS, Siderovski DP, Lu S, Naqvi NI (2007) Rgs1 regulates multiple Gα subunits in Magnaporthe pathogenesis, asexual growth and thigmotropism. EMBO J 26:690–700

19. Fang EG, Dean RA (2000) Site-directed mutagenesis of the magB gene affects growth and development in Magnaporthe grisea. Mol Plant-Microbe Interact 13:1214–1227

20. Ramanujam R, Yishi X, Liu H, Naqvi NI (2012) Structure-function analysis of Rgs1 in Magnaporthe oryzae: role of DEP domains in subcellular targeting. PLoS One 7:e41084

21. Bölker M (1998) Sex and crime: heterotrimeric G proteins in fungal mating and pathogenesis. Fungal Genet Biol 25:143–156

22. Kang SH, Khang CH, Lee Y-H (1999) Regulation of cAMP-dependent protein kinase during appressorium formation in Magnaporthe grisea. FEMS Microbiol Lett 170:419–423

23. Xu J-R, Hamer JE (1996) MAP kinase and cAMP signaling regulate infection structure formation and pathogenic growth in the rice blast fungus Magnaporthe grisea. Genes Dev 10:2696–2706

24. Adachi K, Hamer JE (1998) Divergent cAMP signaling pathways regulate growth and pathogenesis in the rice blast fungus Magnaporthe grisea. Plant Cell 10:1361–1373

25. Dean RA, Talbot NJ, Ebbole DJ, Farman ML, Mitchell TK, Orbach MJ, Thon M, Kulkarni R, Xu J-R, Pan H, Read ND, Lee Y-H, Carbone I, Brown D, Oh YY, Donofrio N, Jeong JS, Soanes DM, Djonovic S, Kolomiets E, Rehmeyer C, Li W, Harding M, Kim S, Lebrun M-H, Bohnert H, Coughlan S, Butler J, Calvo S, Ma L-J, Nicol R, Purcell S, Nusbaum C, Galagan JE, Birren BW (2005) The genome sequence of the rice blast fungus Magnaporthe grisea. Nature 434:980–986

26. Choi W, Dean RA (1997) The adenylate cyclase gene MAC1 of Magnaporthe grisea controls appressorium formation and other aspects of growth and development. Plant Cell 9:1973–1983

27. Gilbert RD, Johnson AM, Dean RA (1996) Chemical signals responsible for appressorium

formation in the rice blast fungus Magnaporthe grisea. Physiol Mol Plant Pathol 48:335–346

28. Douglas LM, Alvarez FJ, McCreary C, Konopka JB (2005) Septin function in yeast model systems and pathogenic fungi. Eukaryot Cell 4:1503–1512

29. Dean R, Van Kan JA, Pretorius ZA, Hammond-Kosack KE, Di Pietro A, Spanu PD, Rudd JJ, Dickman M, Kahmann R, Ellis J, Foster GD (2012) The top 10 fungal pathogens in molecular plant pathology. Mol Plant Pathol 13:414–430

30. Marroquin-Guzman M, Wilson RA (2015) GATA-dependent glutaminolysis drives appressorium formation in Magnaporthe oryzae by suppressing TOR inhibition of cAMP/PKA signaling. PLoS Pathog 11:e1004851

31. Wilson RA, Gibson RP, Quispe CF, Littlechild JA, Talbot NJ (2010) An NADPH-dependent genetic switch regulates plant infection by the rice blast fungus. Proc Natl Acad Sci U S A 107:21902–21907

32. Fernandez J, Wright JD, Hartline D, Quispe CF, Madayiputhiya N, Wilson RA (2012) Principles of carbon catabolite repression in the rice blast fungus: Tps1, Nmr1-3, and a MATE-family pump regulate glucose metabolism during infection. PLoS Genet 8: e1002673

33. Jiang C, Zhang X, Liu H, Xu J-R (2018) Mitogen-activated protein kinase signaling in plant pathogenic fungi. PLoS Pathog 14: e1006875

34. Turrà D, Segorbe D, Di Pietro A (2014) Protein kinases in plant-pathogenic fungi: conserved regulators of infection. Annu Rev Phytopathol 52:267–288

35. Sakulkoo W, Osés-Ruiz M, Oliveira Garcia E, Soanes DM, Littlejohn GR, Hacker C, Correia A, Valent B, Talbot NJ (2018) A single fungal MAP kinase controls plant cell-to-cell invasion by the rice blast fungus. Science 359:1399–1403

36. Bruno KS, Tenjo F, Li L, Hamer JE, Xu JR (2004) Cellular localization and role of kinase activity of PMK1 in Magnaporthe grisea. Eukaryot Cell 3:1525–1532

37. Zhao X, Kim Y, Park G, Xu J-R (2005) A mitogen-activated protein kinase Cascade regulating infection-related morphogenesis in Magnaporthe grisea. Plant Cell Online 17:1317–1329

38. Li G, Zhou X, Xu J-R (2012) Genetic control of infection-related development in Magnaporthe oryzae. Curr Opin Microbiol 15:678–684

39. Zhao X, Xu J-R (2007) A highly conserved MAPK-docking site in Mst7 is essential for Pmk1 activation in Magnaporthe grisea. Mol Microbiol 63:881–894

40. Zhang S, Jiang C, Zhang Q, Qi L, Li C, Xu J-R (2016) Thioredoxins are involved in the activation of the PMK1 MAP kinase pathway during appressorium penetration and invasive growth in Magnaporthe oryzae. Environ Microbiol 18:3768–3784

41. Qi L, Kim Y, Jiang C, Li Y, Peng Y, Xu J-R (2015) Activation of Mst11 and feedback inhibition of germ tube growth in Magnaporthe oryzae. Mol Plant-Microbe Interact 28:881–891

42. Zhou X, Zhao X, Xue C, Dai Y, Xu J-R (2014) Bypassing both surface attachment and surface recognition requirements for Appressorium formation by overactive Ras signaling in Magnaporthe oryzae. Mol Plant-Microbe Interact 27:996–1004

43. Li G, Zhang X, Tian H, Choi Y-E, Tao WA, Xu J-R (2017) MST50 is involved in multiple MAP kinase signaling pathways in Magnaporthe oryzae. Environ Microbiol 19:1959–1974

44. Park G, Xue C, Zhao X, Kim Y, Orbach M, Xu JR (2006) Multiple upstream signals converge on the adaptor protein Mst50 in Magnaporthe grisea. Plant Cell 18:2822–2835

45. Nishimura M, Park G, Xu J-R (2003) The G-beta subunit MGB1 is involved in regulating multiple steps of infection-related morphogenesis in Magnaporthe grisea. Mol Microbiol 50:231–243

46. Kou Y, Tan YH, Ramanujam R, Naqvi NI (2017) Structure-function analyses of the Pth11 receptor reveal an important role for CFEM motif and redox regulation in rice blast. New Phytol 214:330–342

47. Ryder LS, Talbot NJ (2015) Regulation of appressorium development in pathogenic fungi. Curr Opin Plant Biol 26:8–13

48. Zhang H, Xue C, Kong L, Li G, Xu J-R (2011) A Pmk1-interacting gene is involved in appressorium differentiation and plant infection in Magnaporthe oryzae. Eukaryot Cell 10:1062–1070

49. Kim S, Park SY, Kim KS, Rho HS, Chi MH, Choi J, Park J, Kong S, Park J, Goh J, Lee YH (2009) Homeobox transcription factors are required for conidiation and appressorium development in the rice blast fungus Magnaporthe oryzae. PLoS Genet 5:e1000757

50. Yue X, Que Y, Xu L, Deng S, Peng Y, Talbot NJ, Wang Z (2016) ZNF1 encodes a putative C2H2 zinc-finger protein essential for

appressorium differentiation by the Rice blast fungus Magnaporthe oryzae. Mol Plant-Microbe Interact 29:22–35

51. Soanes DM, Chakrabarti A, Paszkiewicz KH, Dawe AL, Talbot NJ (2012) Genome-wide transcriptional profiling of appressorium development by the Rice blast fungus Magnaporthe oryzae. PLoS Pathog 8:e1002514

52. Saunders DG, Aves SJ, Talbot NJ (2010) Cell cycle-mediated regulation of plant infection by the rice blast fungus. Plant Cell 22:497–507

53. Oses-Ruiz M, Talbot NJ (2017) Cell cycle-dependent regulation of plant infection by the rice blast fungus Magnaporthe oryzae. Commun Integr Biol 10:e1372067

54. Oses-Ruiz M, Sakulkoo W, Littlejohn GR, Martin-Urdiroz M, Talbot NJ (2017) Two independent S-phase checkpoints regulate appressorium-mediated plant infection by the rice blast fungus Magnaporthe oryzae. Proc Natl Acad Sci U S A 114:E237–E244

55. Saunders DG, Dagdas YF, Talbot NJ (2010) Spatial uncoupling of mitosis and cytokinesis during appressorium-mediated plant infection by the rice blast fungus Magnaporthe oryzae. Plant Cell 22:2417–2428

56. Osmani AH, O'Donnell K, Pu RT, Osmani SA (1991) Activation of the nimA protein kinase plays a unique role during mitosis that cannot be bypassed by absence of the bimE checkpoint. EMBO J 10:2669–2679

57. Rhind N, Russell P (1998) Mitotic DNA damage and replication checkpoints in yeast. Curr Opin Cell Biol 10:749–758

58. Veneault-Fourrey C, Barooah M, Egan M, Wakley G, Talbot NJ (2006) Autophagic fungal cell death is necessary for infection by the rice blast fungus. Science 312:580–583

59. Liu XH, Lu JP, Zhang L, Dong B, Min H, Lin FC (2007) Involvement of a Magnaporthe grisea serine/threonine kinase gene, MgATG1, in appressorium turgor and pathogenesis. Eukaryot Cell 6:997–1005

60. Shen Q, Liang M, Yang F, Deng YZ, Naqvi NI (2020) Ferroptosis contributes to developmental cell death in rice blast. New Phytol 227(6):1831–1846

61. Armentrout V, Downer A (1987) Infection cushion development by Rhizoctonia solani on cotton. Phytopathology 77:619–623

62. Mendgen K, Hahn M, Deising H (1996) Morphogenesis and mechanisms of penetration by plant pathogenic fungi. Annu Rev Phytopathol 34:367–386

63. Talbot NJ (2019) Appressoria. Curr Biol 29:R144–r146

64. Skamnioti P, Gurr SJ (2007) Magnaporthe grisea Cutinase2 mediates appressorium differentiation and host penetration and is required for full virulence. Plant Cell 19:2674

65. Chang HX, Miller LA, Hartman GL (2014) Melanin-independent accumulation of turgor pressure in appressoria of Phakopsora pachyrhizi. Phytopathology 104:977–984

66. Loehrer M, Botterweck J, Jahnke J, Mahlmann DM, Gaetgens J, Oldiges M, Horbach R, Deising H, Schaffrath U (2014) In vivo assessment by Mach–Zehnder double-beam interferometry of the invasive force exerted by the Asian soybean rust fungus (Phakopsora pachyrhizi). New Phytol 203:620–631

67. Ludwig N, Löhrer M, Hempel M, Mathea S, Schliebner I, Menzel M, Kiesow A, Schaffrath U, Deising HB, Horbach R (2013) Melanin is not required for turgor generation but enhances cell-wall rigidity in appressoria of the corn pathogen Colletotrichum graminicola. Mol Plant-Microbe Interact 27:315–327

68. Dixon KP, Xu JR, Smirnoff N, Talbot NJ (1999) Independent signaling pathways regulate cellular turgor during hyperosmotic stress and appressorium-mediated plant infection by Magnaporthe grisea. Plant Cell 11:2045

69. Ryder LS, Dagdas YF, Kershaw MJ, Venkataraman C, Madzvamuse A, Yan X, Cruz-Mireles N, Soanes DM, Oses-Ruiz M, Styles V, Sklenar J, Menke FLH, Talbot NJ (2019) A sensor kinase controls turgor-driven plant infection by the rice blast fungus. Nature 574:423–427

70. Tao W, Deschenes RJ, Fassler JS (1999) Intracellular glycerol levels modulate the activity of Sln1p, a Saccharomyces cerevisiae two-component regulator. J Biol Chem 274:360–367

71. Zhang H, Liu K, Zhang X, Song W, Zhao Q, Dong Y, Guo M, Zheng X, Zhang Z (2010) A two-component histidine kinase, MoSLN1, is required for cell wall integrity and pathogenicity of the rice blast fungus, Magnaporthe oryzae. Curr Genet 56(6):517–528

72. Ryder LS, Dagdas YF, Mentlak TA, Kershaw MJ, Thornton CR, Schuster M, Chen J, Wang Z, Talbot NJ (2013) NADPH oxidases regulate septin-mediated cytoskeletal remodeling during plant infection by the rice blast fungus. Proc Natl Acad Sci 110:3179

73. Dagdas YF, Yoshino K, Dagdas G, Ryder LS, Bielska E, Steinberg G, Talbot NJ (2012) Septin-mediated plant cell invasion by the rice blast fungus, Magnaporthe oryzae. Science 336:1590–1595

74. Bourett TM, Howard RJ (1992) Actin in penetration pegs of the fungal rice blast pathogen, Magnaporthe grisea. Protoplasma 168:20–26

75. Delgado-Álvarez DL, Callejas-Negrete OA, Gomez N, Freitag M, Roberson RW, Smith LG, Mouriño-Pérez RR (2010) Visualization of F-actin localization and dynamics with live cell markers in Neurospora crassa. Fungal Genet Biol 47:573–586

76. Delgado-Álvarez DL, Bartnicki-García S, Seiler S, Mouriño-Pérez RR (2014) Septum development in Neurospora crassa: the septal actomyosin tangle. PLoS One 9:e96744

77. Upadhyay S, Shaw BD (2008) The role of actin, fimbrin and endocytosis in growth of hyphae in aspergillus nidulans. Mol Microbiol 68:690–705

78. Berepiki A, Lichius A, Shoji JY, Tilsner J, Read ND (2010) F-actin dynamics in Neurospora crassa. Eukaryot Cell 9:547–557

79. Roberson RW (1992) The actin cytoskeleton in hyphal cells of Sclerotium rolfsii. Mycologia 84:41–51

80. Taheri-Talesh N, Horio T, Araujo-Bazán L, Dou X, Espeso EA, Peñalva MA, Osmani SA, Oakley BR (2008) The tip growth apparatus of aspergillus nidulans. Mol Biol Cell 19:1439–1449

81. Berepiki A, Lichius A, Read ND (2011) Actin organization and dynamics in filamentous fungi. Nat Rev Microbiol 9:876–887

82. Riedl J, Crevenna AH, Kessenbrock K, Yu JH, Neukirchen D, Bista M, Bradke F, Jenne D, Holak TA, Werb Z, Sixt M, Wedlich-Soldner R (2008) Lifeact: a versatile marker to visualize F-actin. Nat Methods 5:605–607

83. Gilden J, Krummel MF (2010) Control of cortical rigidity by the cytoskeleton: emerging roles for septins. Cytoskeleton (Hoboken) 67:477–486. https://doi.org/10.1002/cm.20461

84. Van Ngo H, Mostowy S (2019) Role of septins in microbial infection. J Cell Sci 132: jcs226266. https://journals.biologists.com/jcs/article/132/9/jcs226266/57414/Role-of-septins-in-microbial-infection

85. Hartwell LH (1971) Genetic control of the cell division cycle in yeast IV. Genes controlling bud emergence and cytokinesis. Exp Cell Res 69:265–276

86. Spiliotis ET, Nelson WJ (2006) Here come the septins: novel polymers that coordinate intracellular functions and organization. J Cell Sci 119:4–10

87. Tosa Y, Osue J, Eto Y, Oh H-S, Nakayashiki H, Mayama S, Leong SA (2005) Evolution of an Avirulence gene, AVR1-CO39, concomitant with the evolution and differentiation of Magnaporthe oryzae. Mol Plant-Microbe Interact 18:1148–1160

88. Sirajuddin M, Farkasovsky M, Zent E, Wittinghofer A (2009) GTP-induced conformational changes in septins and implications for function. Proc Natl Acad Sci U S A 106:16592–16597

89. Versele M, Thorner J (2004) Septin collar formation in budding yeast requires GTP binding and direct phosphorylation by the PAK, Cla4. J Cell Biol 164:701–715

90. Sirajuddin M, Farkasovsky M, Hauer F, Kuhlmann D, Macara IG, Weyand M, Stark H, Wittinghofer A (2007) Structural insight into filament formation by mammalian septins. Nature 449:311–315

91. Dulal N, Rogers A, Wang Y, Egan M (2020) Dynamic assembly of a higher-order septin structure during appressorium morphogenesis by the rice blast fungus. Fungal Genet Biol 140:103385

92. Galhano R, Illana A, Ryder LS, Rodriguez-Romero J, Demuez M, Badaruddin M, Martinez-Rocha AL, Soanes DM, Studholme DJ, Talbot NJ, Sesma A (2017) Tpc1 is an important Zn(II)2Cys6 transcriptional regulator required for polarized growth and virulence in the rice blast fungus. PLoS Pathog 13:e1006516

93. Kershaw MJ, Basiewicz M, Soanes DM, Yan X, Ryder LS, Csukai M, Oses-Ruiz M, Valent B, Talbot NJ (2019) Conidial morphogenesis and Septin-mediated plant infection require Smo1, a Ras GTPase-activating protein in Magnaporthe oryzae. Genetics 211:151–167

94. Xu JR, Staiger CJ, Hamer JE (1998) Inactivation of the mitogen-activated protein kinase Mps1 from the rice blast fungus prevents penetration of host cells but allows activation of plant defense responses. Proc Natl Acad Sci U S A 95:12713–12718

95. Park G, Xue C, Zheng L, Lam S, Xu JR (2002) MST12 regulates infectious growth but not appressorium formation in the rice blast fungus Magnaporthe grisea. Mol Plant-Microbe Interact 15:183–192

96. Liu C, Li Z, Xing J, Yang J, Wang Z, Zhang H, Chen D, Peng YL, Chen XL (2018) Global analysis of sumoylation function reveals novel insights into development

and appressorium-mediated infection of the rice blast fungus. New Phytol 219:1031–1047

97. Gupta YK, Dagdas YF, Martinez-Rocha A-L, Kershaw MJ, Littlejohn GR, Ryder LS, Sklenar J, Menke F, Talbot NJ (2015) Septin-dependent assembly of the exocyst is essential for plant infection by Magnaporthe oryzae. Plant Cell 27:3277

98. Armijo G, Schlechter R, Agurto M, Muñoz D, Nuñez C, Arce-Johnson P (2016) Grapevine pathogenic microorganisms: understanding infection strategies and host response scenarios. Front Plant Sci 7:382

99. Fernandez J, Orth K (2018) Rise of a cereal killer: the biology of Magnaporthe oryzae biotrophic growth. Trends Microbiol 26:582–597

100. Yi M, Valent B (2013) Communication between filamentous pathogens and plants at the biotrophic interface. Annu Rev Phytopathol 51:587–611

101. Kankanala P, Czymmek K, Valent B (2007) Roles for rice membrane dynamics and plasmodesmata during biotrophic invasion by the blast fungus. Plant Cell 19:706–724

102. Giraldo MC, Dagdas YF, Gupta YK, Mentlak TA, Yi M, Martinez-Rocha AL, Saitoh H, Terauchi R, Talbot NJ, Valent B (2013) Two distinct secretion systems facilitate tissue invasion by the rice blast fungus Magnaporthe oryzae. Nat Commun 4:1996

103. Khang CH, Berruyer R, Giraldo MC, Kankanala P, Park SY, Czymmek K, Kang S, Valent B (2010) Translocation of Magnaporthe oryzae effectors into rice cells and their subsequent cell-to-cell movement. Plant Cell 22:1388–1403

104. Mosquera G, Giraldo MC, Khang CH, Coughlan S, Valent B (2009) Interaction transcriptome analysis identifies Magnaporthe oryzae BAS1-4 as biotrophy-associated secreted proteins in rice blast disease. Plant Cell 21:1273–1290

105. Patkar RN, Benke PI, Qu Z, Chen YY, Yang F, Swarup S, Naqvi NI (2015) A fungal monooxygenase-derived jasmonate attenuates host innate immunity. Nat Chem Biol 11:733–740

106. Marroquin-Guzman M, Hartline D, Wright JD, Elowsky C, Bourret TJ, Wilson RA (2017) The Magnaporthe oryzae nitrooxidative stress response suppresses rice innate immunity during blast disease. Nat Microbiol 2:17054

107. Valent B, Khang CH (2010) Recent advances in rice blast effector research. Curr Opin Plant Biol 13:434–441

108. Nishimura T, Mochizuki S, Ishii-Minami N, Fujisawa Y, Kawahara Y, Yoshida Y, Okada K, Ando S, Matsumura H, Terauchi R, Minami E, Nishizawa Y (2016) Magnaporthe oryzae glycine-rich secretion protein, Rbf1 critically participates in pathogenicity through the focal formation of the biotrophic interfacial complex. PLoS Pathog 12:e1005921

109. Fujikawa T, Kuga Y, Yano S, Yoshimi A, Tachiki T, Abe K, Nishimura M (2009) Dynamics of cell wall components of Magnaporthe grisea during infectious structure development. Mol Microbiol 73:553–570

110. Mehrabi R, Ding S, Xu J-R (2008) MADS-box transcription factor Mig1 is required for infectious growth in Magnaporthe grisea. Eukaryot Cell 7:791

111. Qi Z, Wang QI, Dou X, Wang WEI, Zhao Q, Lv R, Zhang H, Zheng X, Wang P, Zhang Z (2012) MoSwi6, an APSES family transcription factor, interacts with MoMps1 and is required for hyphal and conidial morphogenesis, appressorial function and pathogenicity of Magnaporthe oryzae. Mol Plant Pathol 13:677–689

112. Fernandez J, Wilson RA (2012) Why no feeding frenzy? Mechanisms of nutrient acquisition and utilization during infection by the rice blast fungus Magnaporthe oryzae. Mol Plant-Microbe Interact 25:1286–1293

113. Fernandez J, Marroquin-Guzman M, Wilson RA (2014) Mechanisms of nutrient acquisition and utilization during fungal infections of leaves. Annu Rev Phytopathol 52:155–174

114. Fernandez J, Marroquin-Guzman M, Wilson RA (2014) Evidence for a transketolase-mediated metabolic checkpoint governing biotrophic growth in rice cells by the blast fungus Magnaporthe oryzae. PLoS Pathog 10:e1004354

115. Sun G, Elowsky C, Li G, Wilson RA (2018) TOR-autophagy branch signaling via Imp1 dictates plant-microbe biotrophic interface longevity. PLoS Genet 14:e1007814

116. Molloy S (2010) Fungal biology: Magnaporthe effectors on the move. Nat Rev Microbiol 8:466–467

117. Kamoun S (2006) A catalogue of the effector secretome of plant pathogenic oomycetes. Annu Rev Phytopathol 44:41–60

118. Govers F, Bouwmeester K (2008) Effector trafficking: RXLR-dEER as extra gear for delivery into plant cells. Plant Cell 20:1728–1730

119. Saitoh H, Fujisawa S, Mitsuoka C, Ito A, Hirabuchi A, Ikeda K, Irieda H, Yoshino K, Yoshida K, Matsumura H, Tosa Y, Win J, Kamoun S, Takano Y, Terauchi R (2012)

Magnaporthe oryzae and related species. PLoS Pathog 7:e1002147

138. Zhang S, Wang L, Wu W, He L, Yang X, Pan Q (2015) Function and evolution of Magnaporthe oryzae avirulence gene AvrPib responding to the rice blast resistance gene Pib. Sci Rep 5:11642

139. Inoue Y, Vy TTP, Yoshida K, Asano H, Mitsuoka C, Asuke S, Anh VL, Cumagun CJR, Chuma I, Terauchi R, Kato K, Mitchell T, Valent B, Farman M, Tosa Y (2017) Evolution of the wheat blast fungus through functional losses in a host specificity determinant. Science 357:80

140. De Wit PJ, Mehrabi R, Van den Burg HA, Stergiopoulos I (2009) Fungal effector proteins: past, present and future. Mol Plant Pathol 10:735–747

141. Wang B-H, Ebbole DJ, Wang Z-h (2017) The arms race between Magnaporthe oryzae and rice: diversity and interaction of Avr and R genes. J Integr Agric 16:2746–2760

142. Orbach MJ, Farrall L, Sweigard JA, Chumley FG, Valent B (2000) A telomeric avirulence gene determines efficacy for the rice blast resistance gene pi-ta. Plant Cell 12:2019–2032

143. Bohnert HU, Fudal I, Dioh W, Tharreau D, Notteghem JL, Lebrun MH (2004) A putative polyketide synthase/peptide synthetase from Magnaporthe grisea signals pathogen attack to resistant rice. Plant Cell 16:2499–2513

144. Wolpert TJ, Dunkle LD, Ciuffetti LM (2002) Host-selective toxins and avirulence determinants: what's in a name? Annu Rev Phytopathol 40:251–285

145. Berruyer R, Adreit H, Milazzo J, Gaillard S, Berger A, Dioh W, Lebrun MH, Tharreau D (2003) Identification and fine mapping of

Pi33, the rice resistance gene corresponding to the Magnaporthe grisea avirulence gene ACE1. Theor Appl Genet 107:1139–1147

146. Wu CH, Abd-El-Haliem A, Bozkurt TO, Belhaj K, Terauchi R, Vossen JH, Kamoun S (2017) NLR network mediates immunity to diverse plant pathogens. Proc Natl Acad Sci U S A 114:8113–8118

147. Cesari S, Kanzaki H, Fujiwara T, Bernoux M, Chalvon V, Kawano Y, Shimamoto K, Dodds P, Terauchi R, Kroj T (2014) The NB-LRR proteins RGA4 and RGA5 interact functionally and physically to confer disease resistance. EMBO J 33:1941–1959

148. Cesari S, Thilliez G, Ribot C, Chalvon V, Michel C, Jauneau A, Rivas S, Alaux L, Kanzaki H, Okuyama Y, Morel JB, Fournier E, Tharreau D, Terauchi R, Kroj T (2013) The rice resistance protein pair RGA4/RGA5 recognizes the Magnaporthe oryzae effectors AVR-pia and AVR1-CO39 by direct binding. Plant Cell 25:1463–1481

149. Maqbool A, Saitoh H, Franceschetti M, Stevenson CEM, Uemura A, Kanzaki H, Kamoun S, Terauchi R, Banfield MJ (2015) Structural basis of pathogen recognition by an integrated HMA domain in a plant NLR immune receptor. elife 4:e08709

150. De la Concepcion JC, Franceschetti M, Maqbool A, Saitoh H, Terauchi R, Kamoun S, Banfield MJ (2018) Polymorphic residues in rice NLRs expand binding and response to effectors of the blast pathogen. Nat Plants 4:576–585

151. De la Concepcion JC, Franceschetti M, MacLean D, Terauchi R, Kamoun S, Banfield MJ (2019) Protein engineering expands the effector recognition profile of a rice NLR immune receptor. elife 8:e47713

Investigating the cell and developmental biology of plant infection by the rice blast fungus *Magnaporthe oryzae*

Alice Bisola Eseola [a],[1], Lauren S. Ryder [a],[1], Míriam Osés-Ruiz [a], Kim Findlay [b], Xia Yan [a], Neftaly Cruz-Mireles [a], Camilla Molinari [a], Marisela Garduño-Rosales [a],[2], Nicholas J. Talbot [a],[*]

[a] *The Sainsbury Laboratory, University of East Anglia, Norwich Research Park, Norwich NR47UH, United Kingdom*
[b] *The John Innes Centre, Norwich Research Park, NR47UH, United Kingdom*

ABSTRACT

Magnaporthe oryzae is the causal agent of rice blast disease, the most widespread and serious disease of cultivated rice. Live cell imaging and quantitative 4D image analysis have provided new insight into the mechanisms by which the fungus infects host cells and spreads rapidly in plant tissue. In this video review article, we apply live cell imaging approaches to understanding the cell and developmental biology of rice blast disease. To gain entry to host plants, *M. oryzae* develops a specialised infection structure called an appressorium, a unicellular dome-shaped cell which generates enormous turgor, translated into mechanical force to rupture the leaf cuticle. Appressorium development is induced by perception of the hydrophobic leaf surface and nutrient deprivation. Cargo-independent autophagy in the three-celled conidium, controlled by cell cycle regulation, is essential for appressorium morphogenesis. Appressorium maturation involves turgor generation and melanin pigment deposition in the appressorial cell wall. Once a threshold of turgor has been reached, this triggers re-polarisation which requires regulated generation of reactive oxygen species, to facilitate septin GTPase-dependent cytoskeletal re-organisation and re-polarisation of the appressorium to form a narrow, rigid penetration peg. Infection of host tissue requires a further morphogenetic transition to a pseudohyphal-type of growth within colonised rice cells. At the same time the fungus secretes an arsenal of effector proteins to suppress plant immunity. Many effectors are secreted into host cells directly, which involves a specific secretory pathway and a specialised structure called the biotrophic interfacial complex. Cell-to-cell spread of the fungus then requires development of a specialised structure, the transpressorium, that is used to traverse pit field sites, allowing the fungus to maintain host cell membrane integrity as new living plant cells are invaded. Thereafter, the fungus rapidly moves through plant tissue and host cells begin to die, as the fungus switches to necrotrophic growth and disease symptoms develop. These morphogenetic transitions are reviewed in the context of live cell imaging studies.

1. Introduction

The blast fungus *Magnaporthe oryzae* (synonym of *Pyricularia oryzae*) (Dean et al., 2012) is able to infect more than 50 different grass species, including staple crops such as rice, millets and barley (Langner et al., 2018). It is estimated that rice blast disease causes losses of around 6% of the global rice harvest every year (Savary et al., 2019) across all rice-growing regions of the world, but epidemics routinely cause up to 30% yield losses (Wilson and Talbot, 2009). Rice blast therefore represents a severe problem in the 85 countries where rice is grown (Skamnioti and Gurr, 2007) and to 50% of the world's population who depend on rice as their main source of calories (Khush et al., 2005).

M. oryzae furthermore has the capacity to jump from one host to another. Wheat blast, for example, first appeared in 1985 in Brazil following a likely host jump from a grass-infecting isolate of the fungus (Inoue et al., 2017). Increases in global trade since that time, have

allowed the disease to spread, emerging in 2016 in Bangladesh, where it now threatens wheat production (Islam et al., 2016), with potential to spread to India, the world's second largest wheat producer (Islam et al., 2019), and most recently to Zambia (Tembo et al., 2020). When considered together with the ongoing rice blast disease pressures world-wide, *M. oryzae* represents a very significant threat to global food security. Learning about the basic biology of blast disease is therefore important if new disease-control strategies are to be developed.

The blast fungus has been extensively studied over the past three decades, facilitated by its genetic tractability and development of a suite of molecular genetic tools and genomic resources (Ebbole et al., 2007). Indeed, *M. oryzae* is now a model system that has revealed important concepts associated with fungal-plant interactions (Dean et al., 2012; Ebbole et al., 2007), such as the molecular basis of appressorium morphogenesis (Xu et al., 2000; Talbot et al., 2019) appressorium function (Wilson and Talbot, 2009; Fernandez and Orth, 2018), secretory processes associated with effector proteins (Giraldo et al., 2013),
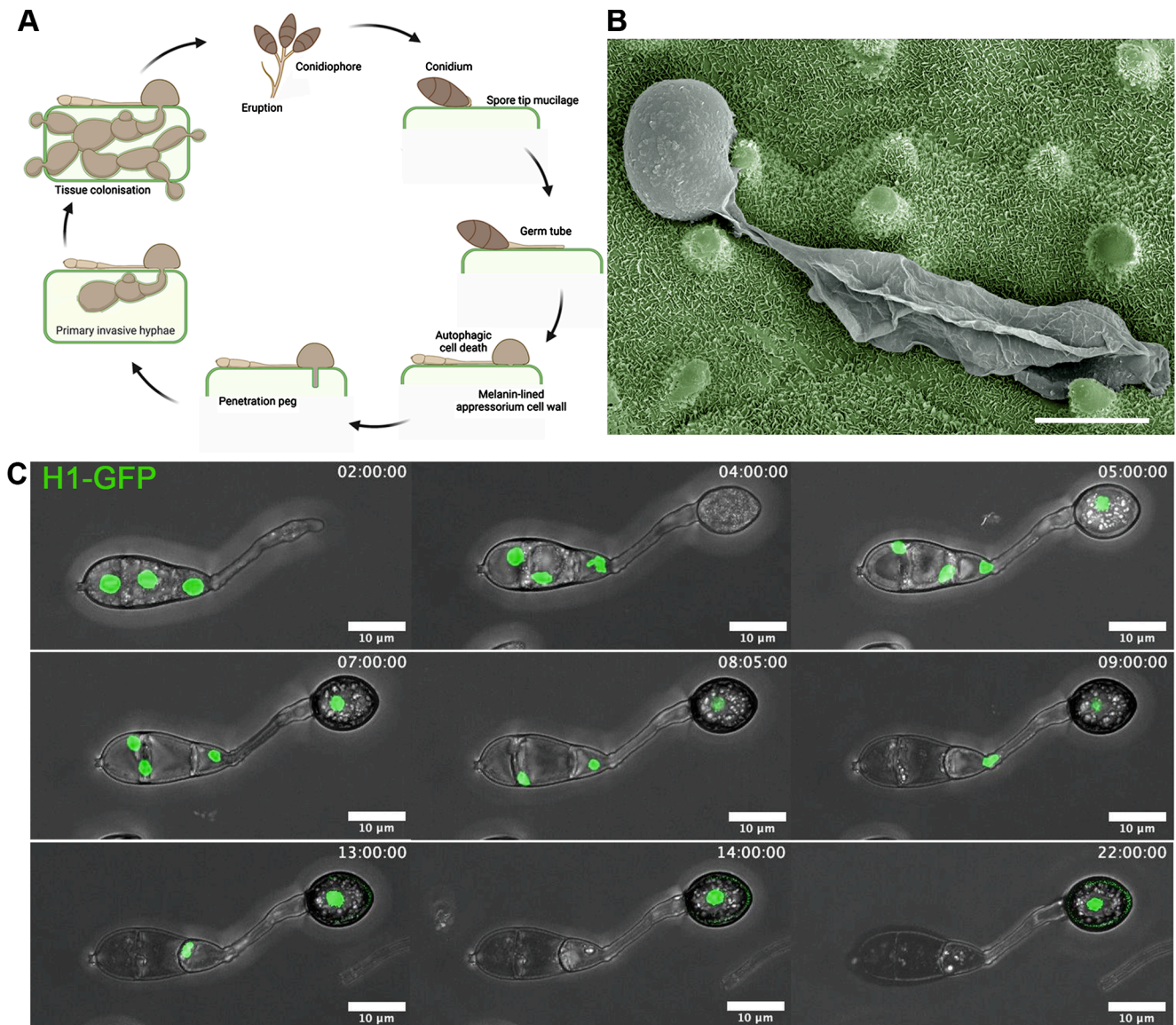

Fig. 1. Infection related morphogenesis in the rice blast fungus *Magnaporthe oryzae*. (A) Life cycle of *M. oryzae*. Infection begins when a three-celled conidium lands and attaches to the hydrophobic surface of a rice leaf. The spore germinates producing a long narrow germ tube that differentiates into an appressorium. The single celled appressorium matures, and the three celled conidium collapses and dies in a programmed process requiring autophagy and ferroptosis. The appressorium melanises and generates enormous cellular turgor pressure. This is translated into mechanical force leading to rupture of the rice leaf cuticle. Plant tissue invasion occurs by means of bulbous invasive hyphae that invaginate the rice plasma membrane and spread to neighbouring epidermal cells via pit fields containing plasmodesmata. Disease lesions develop after 72-96hpi, and sporulation occurs under humid conditions. Emergence of new infections occurs once spores are delivered to new host plants by dewdrop splash. (B) Scanning electron micrograph with false colouring, of a dome-shaped appressorium (grey) on the rice leaf surface (green). The contents of the spore are degraded by autophagy and trafficked to the appressorium resulting in enormous turgor that is translated into a mechanical force to rupture the waxy rice leaf cuticle. (C) Time-lapse confocal fluorescence images of nuclear division and cell-cycle progression during appressorium development in *M. oryzae*. Images show Guy11 expressing H1-GFP germinated on glass coverslips 2-19hpi. Scale bar = 10 μm. (For interpretation of the references to colour in this figure legend, the reader is referred to the web version of this article.)

structure–function relationships governing pathogen recognition by host immune receptors (Bentham et al., 2020; De la Concepcion et al., 2020) and pathogen genome organisation (Langner et al., 2021; Dean et al., 2005).

This video article focuses on a series of investigations that have provided new insight into the manner in which the fungus is able to infect rice plants. We start by reviewing the morphogenetic changes associated with development of an appressorium on the rice leaf surface. We highlight cellular changes accompanying appressorium development and how infection-related morphogenesis is controlled by cell cycle progression. We then describe the manner in which *M. oryzae* re-models its cytoskeleton during appressorium maturation, leading to formation of the rigid penetration peg, which ruptures the leaf cuticle. Next, we outline the biology of plant infection by the rice blast fungus, revealing the extraordinary capacity of this pathogen to proliferate within living host tissue and overwhelm plant defences. The use of quantitative 4D imaging and high-resolution video microscopy has provided unparalleled insights into the biology of this devastating plant pathogen and allows new studies to take place with far greater resolution than was previously possible.

1.1. Cell cycle control and regulated autophagy are necessary for appressorium formation

Conidia of *M. oryzae* germinate rapidly on the leaf surface, forming a polarised germ tube within two hours of contact with a hydrophobic surface. The spore sticks tightly to the leaf surface by means of spore tip mucilage, released from an apical compartment upon hydration (Hamer et al., 1988). The germ tube usually emerges from the apical cell of the conidium, extending for a short distance (15–30 μm see Video 1 from 2:00), while adhering tightly to the underlying surface, before swelling and hooking at its tip to form a specialised infection structure, the appressorium (Fig. 1A, B, Video 1 from 2:15 to 3:35) (Talbot et al., 2003). Appressorium differentiation requires S-phase to have been completed by the nucleus within the germinating conidial cell (Osés-Ruiz et al., 2017). A single round of mitosis is then necessary to enable maturation of the appressorium (Osés-Ruiz et al., 2017; Kershaw and Talbot, 2009). As the appressorium matures, its cell wall becomes lined with a thick layer of melanin necessary for the development of turgor by the appressorium (Video 1, 4:00–7:50). At the same time, glycerol accumulates to molar concentrations to generate hydrostatic turgor due to rapid influx of water into the cell. The conidium undergoes an autophagy-dependent process leading to cell death, trafficking the contents of all three conidial cells into the appressorium (Video 1, conidial cell death is achieved by 10:00), which is necessary for infection (Kershaw and Talbot, 2009). Conidial collapse has been reported to involve ferroptosis as the ultimate mechanism leading to cell death (Shen et al., 2020). To investigate nuclear division, a strain of the fungus expressing a Histone H1: green fluorescent protein (GFP) gene fusion (Kershaw and Talbot, 2009) was imaged during appressorium differentiation over a period of 24 h. After the first round of mitosis (Video 2, 4:00–4:10), one daughter nucleus from the germinating conidial cell migrates into the incipient appressorium, leaving the remaining nuclei to be degraded by autophagy-mediated conidial cell death. (Fig. 1C, Fig. 2A, B), as shown in Video 2 (conidial nuclei degraded by 13:45) (Kershaw and Talbot, 2009; Veneault-Fourrey et al., 2006). During appressorium maturation, the nucleus in the appressorium then arrests in G1 before progression through S-phase, which is a necessary pre-requisite to re-polarisation (Saunders et al., 2010a, 2010b). Mutants impaired in melanin accumulation do not mature or trigger the S-phase checkpoint. A turgor-dependent cell cycle checkpoint therefore regulates appressorium function, leading to cytoskeletal re-organization and

penetration peg emergence (Fig. 2C) (Osés-Ruiz et al., 2017). After re-polarisation and plant infection, the appressorium remains mitotically active (Jenkinson et al., 2017), providing nuclei into nascent invasive hyphae (Pfeifer and Khang, 2018).
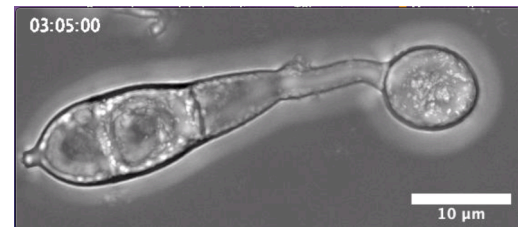
Video 1. Live cell imaging of appressorium development and maturation. Conidia were harvested from wild type strain Guy11 and inoculated onto glass coverslips. The movie was captured using a Leica SP8 laser confocal microscope 2-15hpi. The movie is a maximum projection of Z-stack, frames were taken every 5 min and are displayed at 15 frames per sec. Time scale is in hours: mins. Scale bar =10 μm.
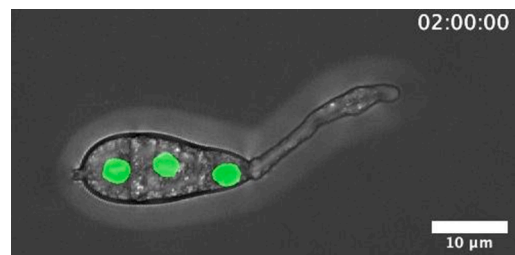

Video 2. Live cell imaging of cell-cycle progression during appressorium development. Conidia were harvested from Guy11 expressing H1-GFP and inoculated onto glass coverslips. The white arrow indicates the point at which the nucleus inside the incipient cell undergoes a single round of mitosis. The movie was captured using a Leica SP8 laser confocal microscope 0-24 hpi. The movie is a maximum projection of Z-stack Frames were taken every 5 min and are displayed at 15 frames per sec . Time scale is in hour: min: sec . Scale bar =10 μm.

1.2. The Pmk1 MAP kinase signalling pathway regulates appressorium morphogenesis

The development of appressoria in response to the hard, hydrophobic leaf surface and absence of exogenous nutrients also requires the Pmk1 MAP kinase signalling pathway, which is critical to invasive growth by *M. oryzae* (Zhao and Xu, 2007), a function conserved in many diverse pathogenic fungal species (Turrà et al., 2014). Pmk1 is a homologue of the *Saccharomyces cerevisiae* Fus3 kinase associated with pheromone signalling (Xu and Hamer, 1996) and the wider pathway links cell surface perception with appressorium morphogenesis (Xu et al., 2000; Turrà et al., 2014). As a consequence, Δ*pmk1* mutants fail to form appressoria, and do not undergo autophagic conidial cell death, as shown in Fig. 2D, E. Pmk1 also, however, plays a role subsequent to appressorium-mediated infection. A conditional, analogue-sensitive mutant of Pmk1 (*pmk1*[AS]) is, for example, unable to move from cell-to-cell at pit field sites, containing plasmodesmata, during rice tissue invasion when inactivated by the specific kinase inhibitor 1 napthyl-PP1 (Fig. 2F) (Xu and Hamer, 1996; Sakulkoo et al., 2018). Pmk1 is activated by a MAPKK (Mst7) and a MAPKKK (Mst11) (Zhao et al., 2005), which in turn are regulated by a putative scaffold protein Mst50 (Park et al., 2006). The Pmk1 MAPK cascade controls the activity of a very large number of downstream targets involved in development and pathogenesis. The transcription factors Hox7 and Znf1, for example, are essential for appressorium formation while Mst12 is required for

A

B

C

D

E

F
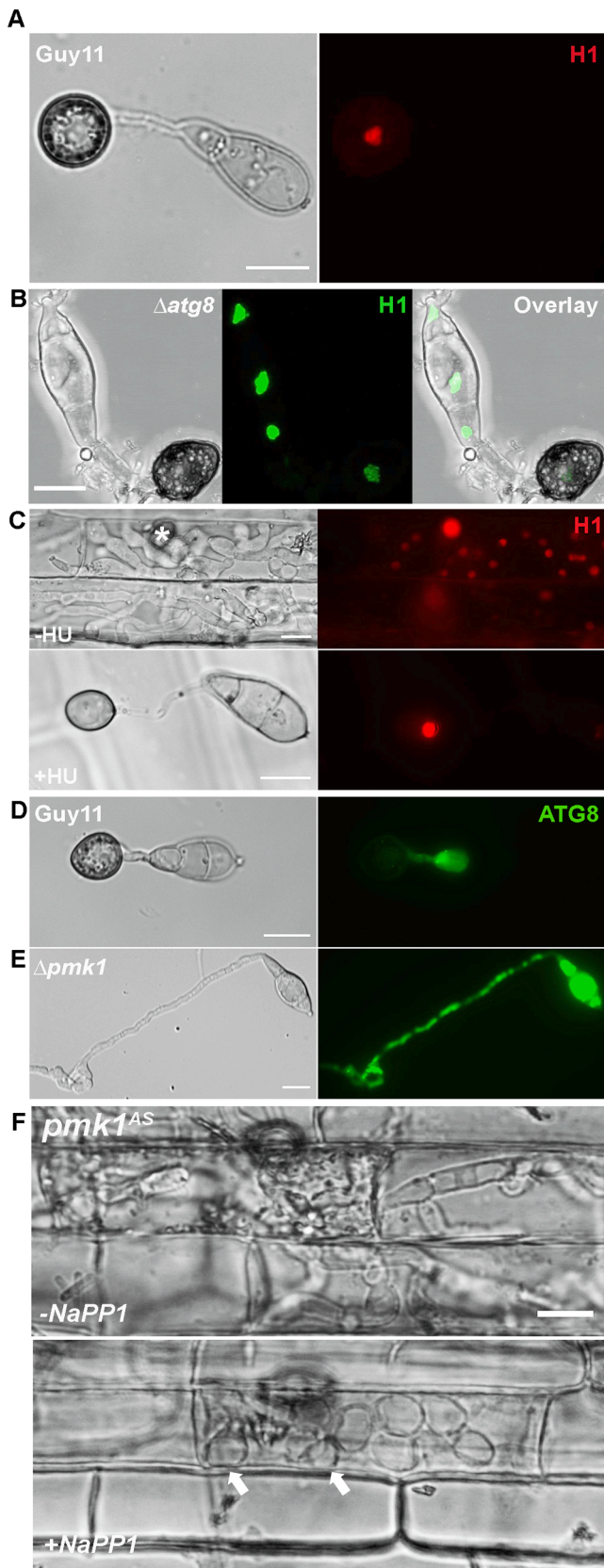
(caption on next column)

Fig. 2. Cell cycle control and autophagy are tightly linked processes to appressorium development and invasive growth. (A) Micrograph to show appressorium formation of Guy11 expressing H1-RFP at 24 hpi on hydrophobic glass coverslips. At this time, just one daughter nucleus remains in the appressorium, as the original three nuclei have been degraded by autophagy-mediated conidial cell death. **(B)** Confocal micrograph of the autophagy-deficient null mutant, Δ *atg8*, expressing H1-GFP at 24 hpi on hydrophobic coverslips. **(C)** Micrographs showing completion of DNA replication is necessary for plant infection. Rice leaf sheath observed 48 hpi after inoculation with Guy11 expressing H1-RFP after exposure to 1 M of the DNA replication inhibitor hydroxyurea (HU) at 10 hpi. Asterisk indicates appressorium penetration site. **(D)** Micrographs showing the effect of Pmk1 inhibition on appressorium development 24 hpi. Spores treated with 5 μM 1NA-PP1 at 1 hpi. Asterisks indicate appressorium penetration sites. **(E)** Micrographs to show autophagosome localization in Guy11 and Δ*pmk1* mutant expressing GFP-Atg8 at 24 hpi on glass coverslips. **(F)** Pmk1 MAP kinase is required for cell-to-cell movement during invasive growth. Micrographs at 48 hpi of infected CO39 rice leaf sheath tissue treated with 5 μM of NA-PP1 inhibitor at 26 hpi. Arrows indicate attempts to cross to neighbouring cells. Scale bar = 10 μm.

penetration and invasive growth (Park et al., 2002; Kim et al., 2009; Yue et al., 2015). Consequently, the Pmk1 MAPK pathway is fundamental to development of appressoria, although how it is activated by cell surface signals, in particular, is still not well understood.

1.3. Septin-dependent re-polarisation of the appressorium

Once formed, appressoria develop enormous turgor of up to 8.0 MPa, by developing a melanin-rich cell wall (Video 1) that is able to retain glycerol and other polyols. (de Jong et al., 1997) A critical threshold of turgor allows the fungus to re-orientate its cytoskeleton, and transition from isotropic expansion to anisotropic, polarised, growth during plant infection. A turgor-sensing histidine aspartate kinase, Sln1, is necessary for modulation of turgor, and acts as a regulator of the downstream pathways required for appressorium repolarisation (Ryder et al., 2019). These include, most notably, the aggregation of a hetero-oligomeric complex of septin GTPases which form a toroidal structure at the base of the appressorium. Septins re-organise F-actin to the precise point of plant infection (Dagdas et al., 2012). A *M. oryzae* strain expressing Sep5-GFP under control of the native Sep5 promotor allows visualisation of septin ring dynamics during a period of 0–24 h, when conidia are incubated on hydrophobic glass coverslips (Video 3; Fig. 3A). Septin recruitment to the appressorium pore begins to occur markedly from 7:00 (Video 3) and the ring then becomes apparent by 9:48, showing some constriction by 16:00. The ring is then maintained in appressoria incubated on a non-yielding surface. By contrast, on rice leaf sheath which can be penetrated by appressoria, the ring forms in the same manner but then undergoes further constriction to a diameter of approximately 0.9–1.1 μm after 28 hpi when the penetration peg is formed (Fig. 3A, Fig. 4, Video 3 and Video 4). A recent study using quantitative 4D widefield fluorescence imaging has revealed the spatiotemporal dynamics of F-actin and septin ring recruitment and organisation at the appressorium pore (Dulal et al., 2021). The septin ring provides cortical rigidification and acts as a diffusion barrier for the action of polarity determinants, endocytic proteins, the exocyst complex, and actin-binding proteins (Dagdas et al., 2012; Gupta et al., 2015). In addition to F-actin, the microtubule cytoskeleton is re-oriented in the direction of cuticle penetration (Dulal et al., 2021). Organisation of septins in the appressorium involves very long chain fatty acids (VLCFAs), that act as mediators of septin interactions at membrane interfaces. Inhibiting VLCFA biosynthesis therefore prevents rice infection by *M. oryzae* providing a new potential fungicidal target (He et al., 2020). Assembly of the septin appressorium pore complex is also controlled by the Nox2/NoxR complex which regulates septin-mediated cytoskeletal dynamics. The actin-binding protein gelsolin, for instance, which regulates actin dynamics by uncapping free barbed ends to promote actin polymerisation, is a likely target for regulation by ROS
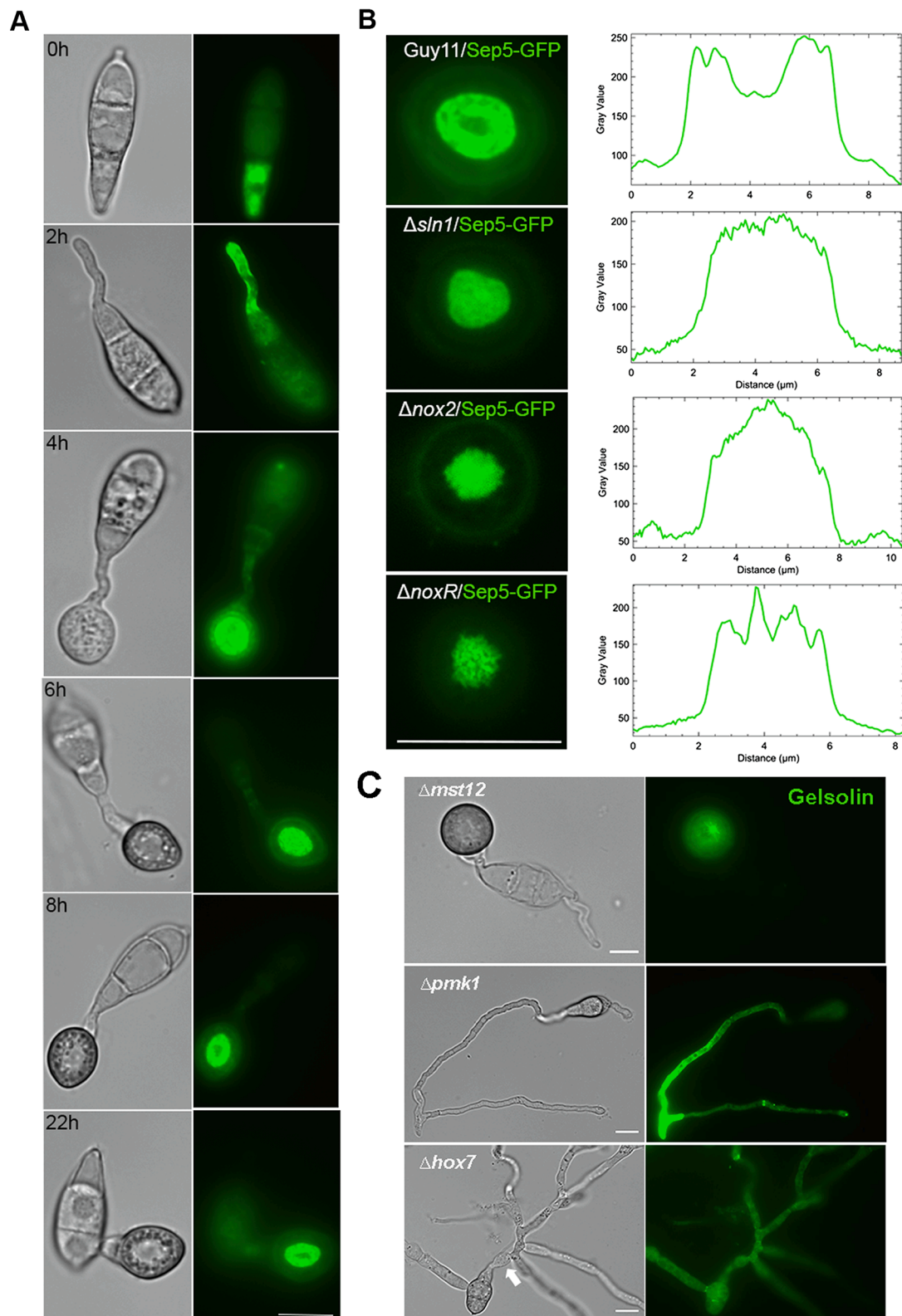
Fig. 3. Septin dependent network organisation in *M. oryzae* appressoria. (A) Time course of cortical septin ring formation during appressorium morphogenesis in *M. oryzae*. Micrographs of septin ring organisation visualised by expression of Sep5-GFP in the wild type strain Guy11. Conidial suspensions at 5×10^4 mL^{-1} were inoculated onto glass coverslips and images were captured at different time intervals during infection-related-development (0–22 h). **(B)** *M. oryzae* mutants displaying aberrant septin ring aggregation. Micrographs and corresponding linescan graphs to show organisation of Sep5-GFP expressed in appressoria of Guy11, Δsln1, Δnox2, and ΔnoxR mutants after 20-24hpi. Scale bar = 10 μm. **(C)** Live cell imaging to show cellular localization of Gelsolin-GFP in the appressorium pore of Δmst12, Δpmk1 and Δhox7 mutants at 24 hpi on glass coverslips. Arrow indicates an incipient appressorium. Scale bar = 10 μm.
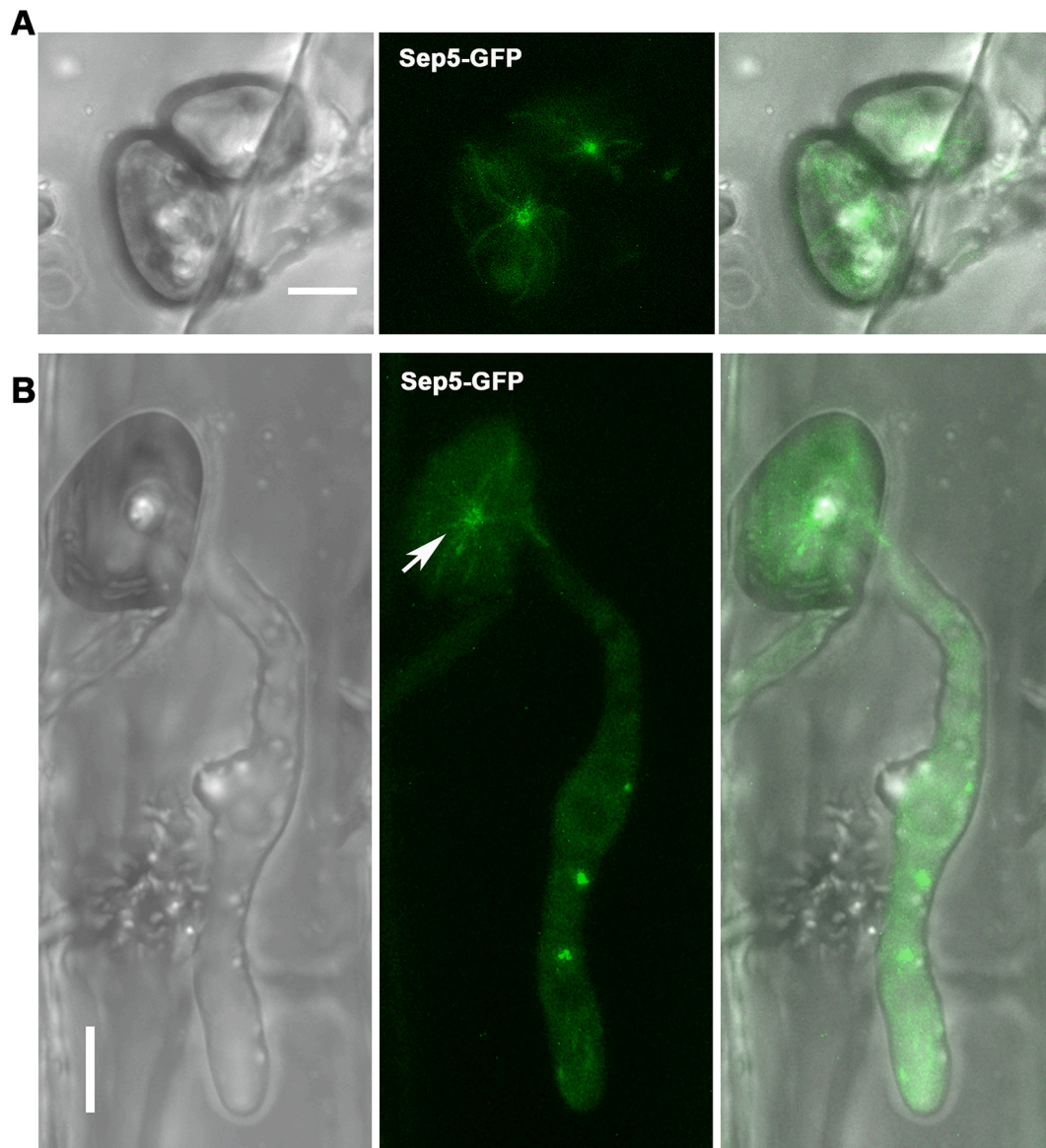
Fig. 4. A toroidal septin network assembles at the appressorium pore on a plant surface. (A) Micrographs of septin ring organisation visualised by expression of Sep5-GFP in wild type strain Guy11. Conidial suspensions at 5×10^4 mL^{-1} were inoculated onto rice leaf sheath and images captured at 16hpi. On a rice leaf surface, the septin ring assembles in the same manner as when appressoria form on hydrophobic glass coverslips, but undergoes further constriction for penetration peg emergence. **(B)** Micrographs of Sep5-GFP expressed in primary invasive as small dynamic puncta, after constriction of the septin ring in appressoria. Images were captured after 28hpi. Scale bar = 10 μm.

(Ryder et al., 2013) and an important component of the appressorium pore. We generated a *M. oryzae* strain expressing Gelsolin-GFP under control of the native Gelsolin promotor. Using 3D maximum projection, Z-stack images were captured at 24hpi (Fig. 3B, Video 5) (Ryder et al., 2013). Gelsolin forms a highly organised toroidal structure situated at the base of the appressorium (Video 5) in a septin-dependent manner (Veneault-Fourrey, 2006). Septin and F-actin ring formation also requires the Pmk1 MAP kinase pathway and the putative downstream transcription factors, such as Mst12 (Dagdas et al., 2012) and Hox7 (Kim et al., 2009), as shown in Fig. 3C. The turgor sensing Sln1 kinase is necessary for determining when a threshold of hydrostatic pressure has been reached in the appressorium to enable re-polarisation. As a consequence, Δ*sln1* mutants are unable to organise septins at the site of

penetration and a clear ring structure does not form (Fig. 3B). Sln1 acts in parallel with the protein kinase C cell integrity pathway to suppress melanin biosynthesis and the cAMP-dependent signalling protein kinase A pathway, thereby modulating turgor generation (Ryder et al., 2019). In addition, the turgor-dependent S-phase checkpoint is triggered enabling septin mediated plant infection (Fig. 5) (Osés-Ruiz et al., 2017; Ryder et al., 2019). Another significant factor in enabling the appressorium to function is its attachment to the leaf surface. Critically, the force of fungal attachment must exceed the force of penetration at the peg, otherwise the cell would simply lift off the surface. It has been shown that spermine synthase (*SPS1*) is important for surface attachment by buffering reactive oxygen species generation in the endoplasmic reticulum, thereby facilitating efficient mucilage secretion that
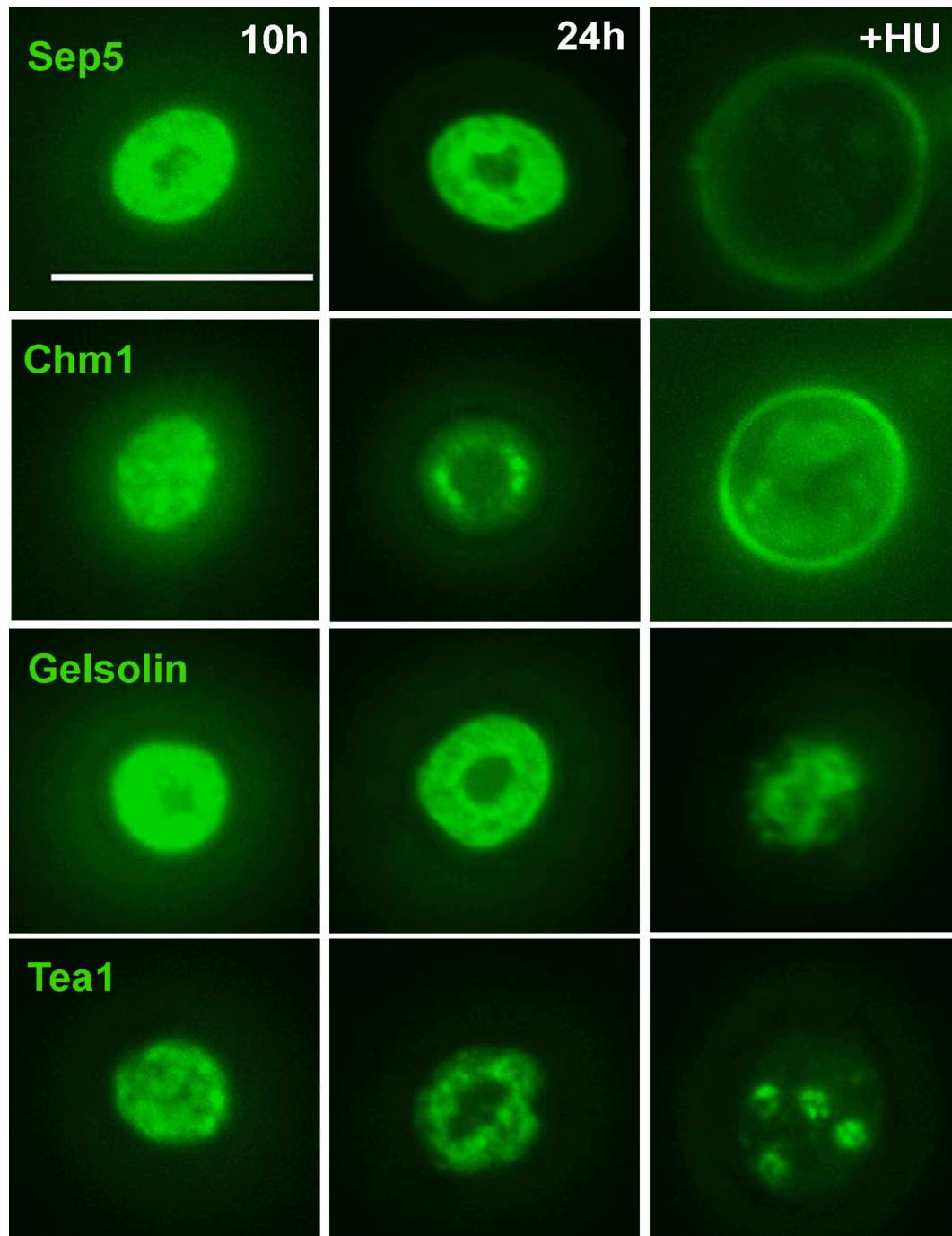
Fig. 5. Completion of S-phase affects localization of septin-associated proteins at the appressorium pore. Micrographs to show the localization of Sep5-GFP, Chm1-GFP, Gelsolin-GFP and Tea1–GFP during appressorium development at 10 hpi, 24 hpi, and 24 hpi with addition of 200 mM of Hydroxyurea (HU) at 10 hpi. Inhibiting DNA replication with HU disrupts septin-mediated cytoskeletal reorganisation. Scale bar = 10 μm.
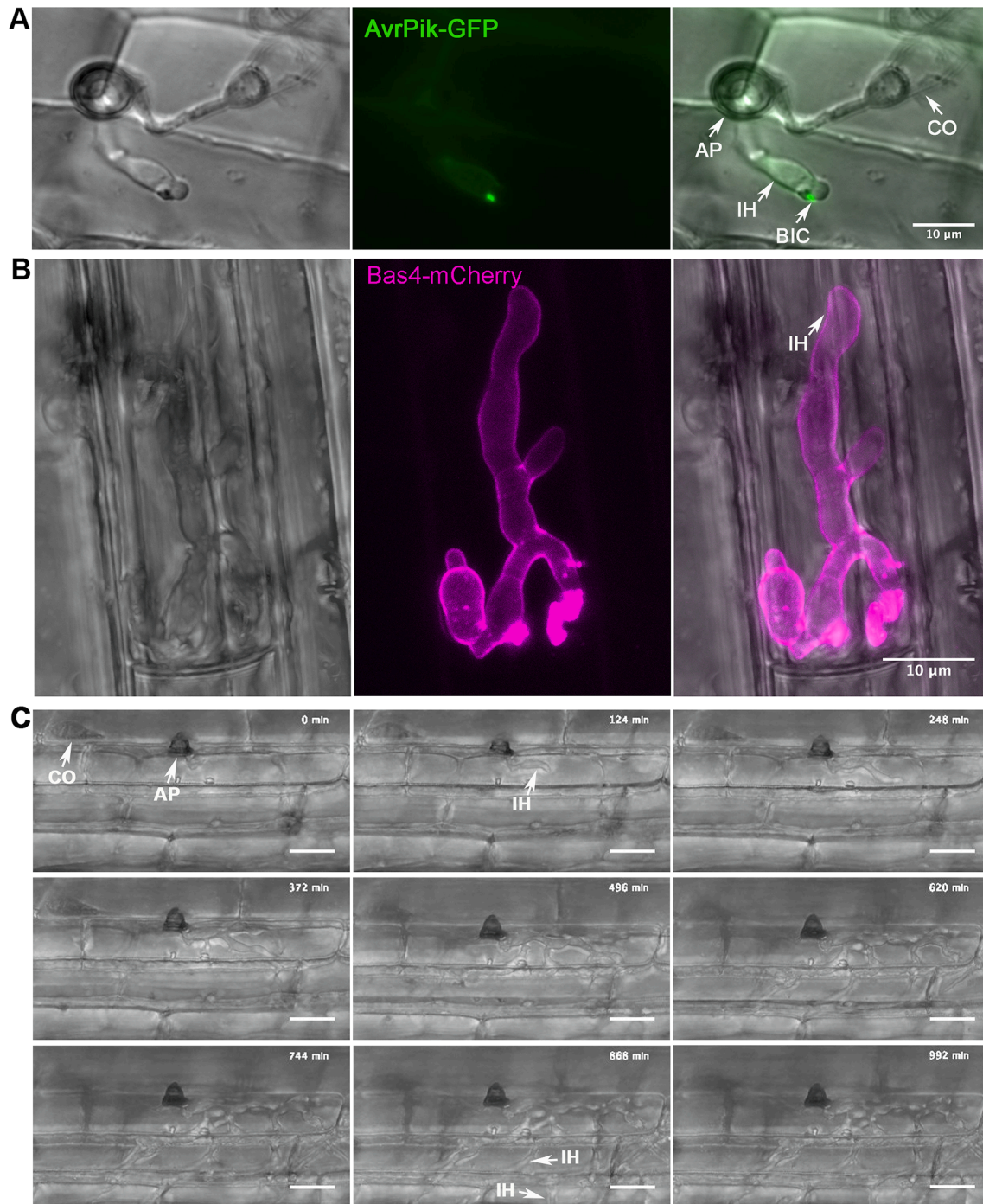
Fig. 6. Visualisation of the expression of cytoplasmic and apoplastic effectors during invasive growth. (A) Micrograph of Guy11 expressing cytoplasmic effector Avrpik-GFP 28 h post inoculation. Avrpik accumulates predominantly at the biotrophic interfacial complex (BIC). Scale bar = 10 μm. **(B)** Micrograph of Guy11 expressing apoplastic effector Bas4-mCherry, accumulating in the apoplast 28hpi. **(C)** A time course of invasive hyphal growth. Conidial suspensions of Guy11 were inoculated onto rice leaf sheath and images were captured every 10 min from the point of penetration (24hpi) for 16 h. Scale bar = 20 μm.

provides the tight seal necessary for the appressorium to function. In the absence of Sps1, appressoria do not adhere tightly to the plant surface, impairing infection (Rocha et al., 2020)

Video 3. Dynamic assembly of a septin ring in *M. oryzae* appressoria. Live cell imaging of septin dynamics during appressorium development in *M. oryzae*. Movie shows Guy11 expressing Sep5-GFP during appressorium development on glass coverslips. The movie was captured using a Leica SP8 laser confocal microscope 0-24 hpi. The movie is a maximum project ion of Z-stack. Frames were taken every 5 min and are displayed at 15 frames per sec . Time scale is in hour: min: secScale bar= 10 μm.
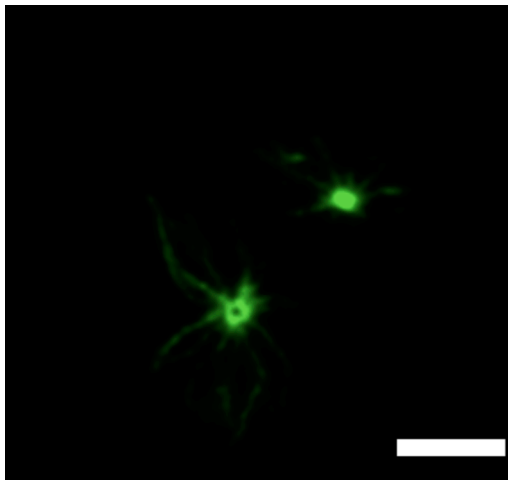
Video 4. Septin ring formation on a rice leaf surface. Conidia were harvested from a *M. oryzae* transformant expressing a Sep5-GFP gene fusion and inoculated onto rice leaf sheath. The animation is a Z-stack captured at 28 hpi using a Leica SP8 laser confocal microscope and displayed at 1 frame per sec. Scale bar= 5 μm.
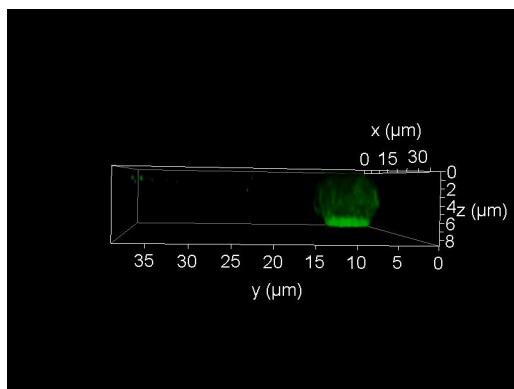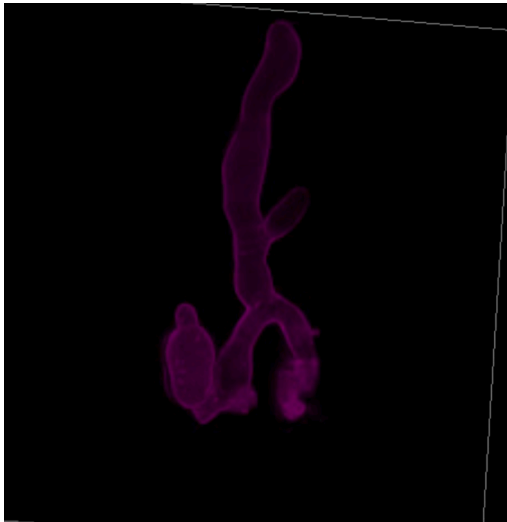

Video 5. Gelsolin ring formation in *M. oryzae*. Conidia were harvested from a *M. oryzae* transformant expressing a Gelsolin-GFP gene fusion and inoculated

onto glass coverslips. Three-dimensional maximum projection Z-stack images were captured at 24 hpi using a Leica SP8 laser confocal microscope and displayed at 15 frames per sec. Scale bar= 10 μm.

1.4. The cell biology of invasive growth by M. oryzae

Once the fungus has penetrated the leaf, it develops primary invasive hyphae (IH) that invaginate the plant plasma membrane within the first epidermal cell colonized. The membrane around the invasive hyphae is known as the extra-invasive hyphal membrane (EIHM), but is entirely a plant-derived membrane which tightly surrounds the fungal cell wall (Kankanala et al., 2007; Mentlak et al., 2012). The fungus secretes a battery of effectors proteins during this time, which are either directed to the apoplast– the space between the fungal cell wall and the EIHM –or the cytoplasm of the host cell. Fungal effectors suppress plant host immunity to facilitate colonisation of plant tissue (Fig. 6A, B) (Kankanala et al., 2007; Yan and Talbot, 2016). A membrane-rich structure forms at the tip of the primary IH and the fungus appears to then bud from this point, whereby the membrane-rich structure forms the biotrophic interfacial complex (BIC), a plant derived membrane-rich body located outside the fungal cell wall (Giraldo et al., 2013; Shipman et al., 2017). Cytoplasmic effectors, such as AVR-Pik and Pwl2, accumulate at the BIC and are also translocated into plant cells. A bright single punctum of AvrPik-GFP is, for example, observed defining the BIC structure, as shown in Fig. 6A. By contrast, apoplastic effectors such as Bas4 outline the invasive hyphae contained within the EIHM (Fig. 6B) when expressed as a Bas4:mCherry fusion protein, although the BIC is also visible (Video 6). Secretion of effectors to these distinct destinations is directed by different secretory pathways. Apoplastic effectors are secreted in a Golgi-dependent, brefeldin A-sensitive manner to the invasive hyphal tip. By contrast, cytoplasmic effectors are secreted from the BIC-adjacent cell into the BIC in an exocyst-dependent pathway that is brefeldin A-insensitive (Giraldo et al., 2013). It has been shown that the TOR (Target-Of Rapamycin) nutrient-signaling pathway is important in mediating membrane integrity at the plant-fungal biotrophic interface. Deletion of a novel vacuolar protein gene *IMP1*, led to mutants impaired in BIC formation which released apoplastic effectors into the plant host cytoplasm (Sun et al., 2018). The deployment of a large battery of effector proteins enables *M. oryzae* to overcome plant immunity and rapidly move from the first invaded cell to neighbouring cells, through pit fields. Interestingly, this involves a specific morphogenetic transition in which the hyphal tip swells when it makes contact with a pit field, followed by severe hyphal constriction to around 360 nm in diameter (equivalent to a pit field) and then emergence of a new invasive hypha in the neighbouring cell. This morphological transition is regulated by the Pmk1 MAP kinase (Sakulkoo et al., 2018; Kankanala et al., 2007) (Fig. 6C, and Video 7). When an analogue-sensitive *pmk1^{AS}* mutant is allowed to infect a host cell and then treated with the 1NA-PP1 inhibitor, it becomes trapped within the epidermal cell (Giraldo et al., 2013). The Pmk1 MAPK pathway is therefore required for septin-dependent constriction of invasive hyphae at cell wall crossing points in the same way as it is necessary for appressorium morphogenesis. Each crossing point can be clearly seen as being preceded by pronounced swelling of the invasive hypha (Video 7, 517 min), followed by severe constriction as the hypha moves into the next cell (Video 7, 641–713 min). Often mitosis is seen to occur just after the time of cell-to-cell movement (Pfeifer and Khang, 2018; Pfeifer et al., 2019), which can be visualised by observing tissue invasion in a *M. oryzae* strain expressing H1-GFP (see Video 8, from 34 min, in which the arrow shows cell crossing point, with mitosis occurring shortly afterwards by 36 min). Appressorium formation and cell wall crossing therefore have many common features requiring swelling into a yeast-like hemispherical cell, followed by re-polarisation and emergence of a narrow penetration peg or IH peg, respectively. The cell wall crossing structure has been termed the 'transpressorium', because of the resemblance to appressorium formation (see Video 9 in which the terminal swelling and infection peg formation can be seen in the 3D image.) (Emmett and Parbery, 1975). The regulation of

transpressorium formation by Pmk1 and the requirement for septin-mediated invasion (Giraldo et al., 2013) are consistent with the morphological conservation.
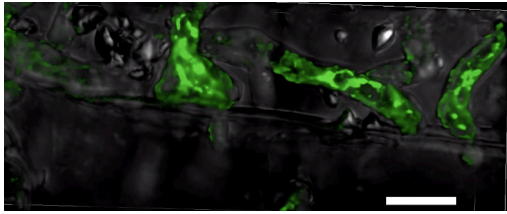

Video 6. Localisation of apoplastic effector Bas4. Conidia were harvested from a *M. oryzae* transformant expressing a Bas4-mCherry gene fusion and inoculated onto rice leaf sheath. Three-dimensional maximum projection Z-stack images were captured at 28 hpi using a Leica SP8 laser confocal microscope. Scale bar= 10 μm.
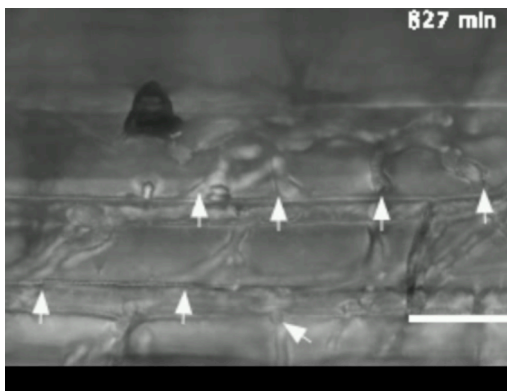
Video 7. Tissue colonisation by *M. oryzae*. Conidia were harvested from wild strain Guy11 and inoculated onto rice leaf sheath. Invasive growth was imaged every 10 minutes for a duration of 16 hours using a Leica SP8 laser confocal microscope. Arrows indicate the crossing points of invasive hyphae into neighbouring cells. The movie is a maximum projected Z-stack, frames were taken every 10 min and are displayed at 7 frames per sec. Time scale is in mins. Scale bar= 20 μm.
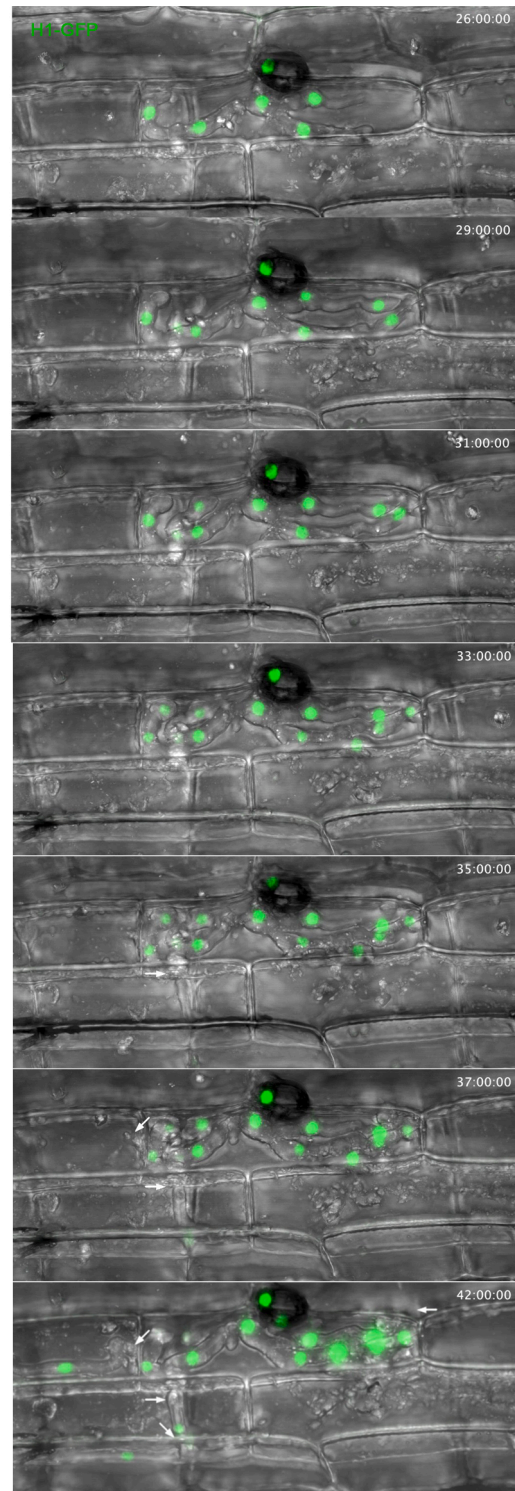
Video 8. Nuclear division during invasive growth by *M. oryzae*. Rice leaf sheath tissue inoculated with Guy11 expressing H1-GFP showing nuclear division during cell-to-cell movement by the fungus. Arrow indicates cell crossing point where transpressorium forms, which is shortly followed by mitosis and nuclear movement to the adjacent cell where it appears close to junction with the next cell (arrowed). The movie is a maximum projected Z-stack, with images recorded every 10 min, displayed at 15 frames per sec. Scale bar = 10 μm

**Video 9. High resolution imaging of the *M. oryzae* transpressorium.** Conidia were harvested from a *M. oryzae* transformant expressing a GFP-HDEL gene fusion and inoculated onto rice leaf sheath. 3D visualization of *M. oryzae* within an infected rice cell showed the specialised swollen hyphae termed the 'transpressorium', generated prior to movement into neighbouring cells. The 3D movie is displayed at 15 frames per sec.

The suppression of immunity responses by *M. oryzae* enables the fungus to colonise leaf tissue very efficiently. This is illustrated by Video 10 in which a strain expressing a nucleolar marker Fib1-GFP is seen to rapidly colonise plant tissue between 24 and 38 h after inoculation. During this period the number of fungal nuclei observed increases from
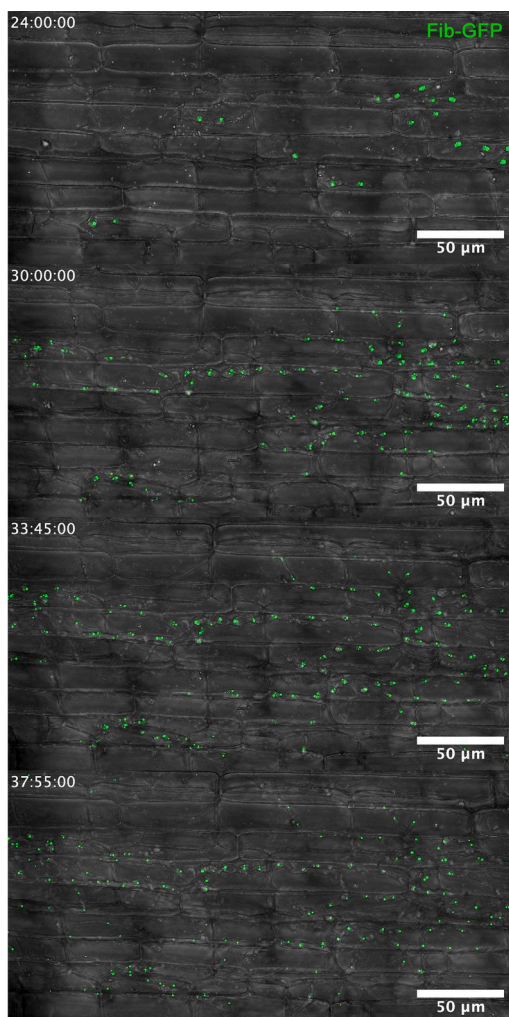
Video 10. Large field of view of rice tissue invasion by *M. oryzae*. Time lapse movie showing the colonisation of rice tissue by *M. oryzae* Guy11 strain expressing the nucleolar marker Fib-GFP. Invasive growth was imaged from 24 hpi to 38 hpi using a Leica SP8 laser confocal microscope. The movie is a maximum projected Z-stack displayed at 8 frames per sec. Scale bar = 50 μm. Still image shows four frames from the video which demonstrate the rapid cycles of nuclear division that occur during invasive growth.

18 to 85 in the field of view shown, highlighting the speed of cell division that accompanies fungal invasive growth in this 14 h period. A three-dimensional reconstruction of invasive hyphae demonstrates the extent of host colonization, as shown in Video 11. Here, fungal invasive hyphae are visualised using fluorescent wheat germ agglutinin, within propidium iodide-labelled plant tissue. Invasive hyphae are large bulbous and branched as they spread within epidermal and mesophyll cells, but more elongated as they move into vascular tissue. The colonisation of tissue is extremely rapid, with plant cells losing viability at the centre of a fungal colony as the fungus continually moves into viable cells, maintaining EIHM integrity as it does so. The central part of the colonies, which becomes visible as a disease lesion, will then produce aerial hyphae that develop into conidiophores bearing sympodial arrays of conidia.
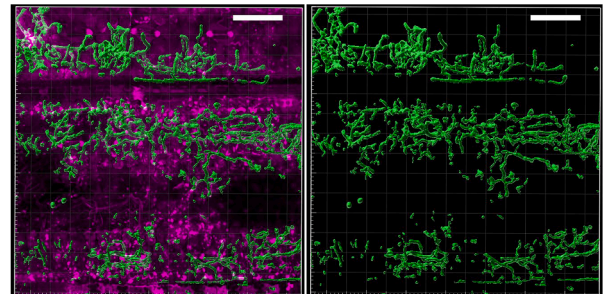
Video 11. Three-dimensional rendering of invasive hyphae colonising rice tissue. Fluorescence images highlighting the organisation of WGA-AF488-stained hyphae of *M. oryzae* Guy11 within infected rice tissue stained with propidium iodide. Scale bar = 50 μm.

2. Conclusions

In summary, live cell imaging studies have dramatically expanded our understanding of how rice plants are infected by the blast fungus *M. oryzae* (Osés-Ruiz et al., 2017; Ryder et al., 2019; Dagdas et al., 2012; Gupta et al., 2015; Ryder et al., 2013). Generation of functional appressoria provides the gateway for establishing rice blast disease, and it is now clear that this is a highly orchestrated developmental process, requiring several important prerequisites– such as perception of the hard-hydrophobic leaf surface, and response to cutin monomers or components of plant epicuticular waxes (Talbot et al., 2003). Next, the fungus utilises two key signalling pathways, the cAMP protein kinase A pathway and the highly conserved Pmk1 MAP kinase signalling pathway, regulated by G- protein signalling in the developing germ tube tip. The Pmk1 signalling pathway regulates appressorium formation, maturation, invasive growth and infection of plant tissue (Xu and Hamer, 1996). Pmk1, for instance, regulates expression of many genes encoding secreted fungal effectors proteins implicated in the suppression of host immunity, in addition to its better known role in symmetry-breaking and morphogenesis (Sakulkoo et al., 2018). Appressorium development is, however, also tightly coupled to cell cycle progression (Wilson and Talbot, 2009; Osés-Ruiz et al., 2017; Saunders et al., 2010), which is itself linked to nutrient availability and the critical role of TOR kinase as a growth regulator that is fundamental to the control of autophagy (Fernandez and Orth, 2018; Marroquin-Guzman et al., 2017; Marroquin-Guzman and Wilson, 2015). Once formed, the appressorium undergoes further changes and the role of glycerol and melanin biosynthesis in turgor generation are well established, but still lacking in specific details, particularly regarding gene regulation and the precise enzymatic activities necessary at each step in these pathways. A turgor-sensing mechanism has also now been reported for appressoria, linking turgor control to re-polarisation of the infection cell.

Many questions, however, remain to be answered regarding operation of an appressorium. How does the turgor-sensing complex work in

M. oryzae and what are its components? How precisely does Sln1 negatively regulate melanin biosynthesis, interact with the Pkc1 cell integrity pathway and negatively regulate glycerol production via the cAMP/PKA pathway? What is the precise trigger for septin aggregation at the appressorium pore and how does this differ from septin recruitment in well-studied processes, such as bud formation in *S. cerevisiae* (Ghose and Lew, 2020).

Following leaf infection, the biology of tissue colonisation by *M. oryzae* and the highly effective strategies deployed by the fungus to suppress host immunity, both metabolic and effector-driven, are becoming clearer (Marroquin-Guzman et al., 2017; Kim et al., 2020; Liu et al., 2021). The developmental transitions involved in traversing cell junctions within a rice leaf are just as striking and developmentally complex, as those on the leaf surface. The transpressorium has significant developmental parallels to the appressorium, having evolved to traverse the same type of structural barrier. Many components are conserved, such as the Pmk1 MAP pathway and septins, for example. However, there are clear differences, such as need to move from one viable cell to another, all the time maintaining EIHM integrity (Sakulkoo et al., 2018; Kankanala et al., 2007) and the requirement for host immunity to be suppressed at plasmodesmata, where such responses are often focused (Faulkner and Oparka). Critical questions include, how does the fungus identify plasmodesmata-rich pit fields as potential crossing points and suppress host immune response at these cell junctions? How are effectors secreted by invasive hyphae and delivered across the plant plasma? And what is the precise role of each effector protein and why is such a large arsenal of effectors necessary to establish blast disease (Yan and Talbot, 2016)?

Rapid advances in live cell imaging have therefore revealed the temporal and spatial dynamic of plant infection in unparalleled resolution, allowing a much more holistic understanding of nature of fungal pathogenesis by fungi such as *M. oryzae* to emerge.

Declaration of Competing Interest

The authors declare that they have no known competing financial interests or personal relationships that could have appeared to influence the work reported in this paper.

References

Bentham, A., et al., 2020. A molecular roadmap to the plant immune system. J. Biol. Chem. 295.

Dagdas, Y.F., et al., 2012. Septin-mediated plant cell invasion by the rice blast fungus, *Magnaporthe oryzae*. Science 336 (6088), 1590–1595.

de Jong, J.C., et al., 1997. Glycerol generates turgor in rice blast. Nature 389 (6648), 244–244.

De la Concepcion, J., et al., 2020. The allelic rice immune receptor Pikh confers extended resistance to strains of the blast fungus through a single polymorphism in the effector binding interface. PLoS Pathogens 17 (3), e1009368. https://doi.org/10.1371/journal.ppat.1009368.

Dean, R.A., et al., 2005. The genome sequence of the rice blast fungus Magnaporthe grisea. Nature 434 (7036), 980–986.

Dean, R., et al., 2012. The Top 10 fungal pathogens in molecular plant pathology. Mol. Plant Pathol 13 (4), 414–430.

Dulal, N., et al., 2021. Turgor-dependent and coronin-mediated F-actin dynamics drive septin disc-to-ring remodeling in the blast fungus Magnaporthe oryzae. J. Cell. Sci. 134 (5).

Ebbole, D.J., 2007. Magnaporthe as a Model for Understanding Host-Pathogen Interactions. Annu. Rev. Phytopathol. 45 (1), 437–456.

Emmett, R.W., Parbery, D.G., 1975. Appressoria. Annu. Rev. Phytopathol. 13 (1), 147–165.

Faulkner, C., Oparka, K.J. Plasmodesmata, in eLS. p. 1–7. https://doi.org/10.1002/9780470015902.a0001681.pub3.

Fernandez, J., Orth, K., 2018. Rise of a Cereal Killer: The Biology of Magnaporthe oryzae Biotrophic Growth. Trends Microbiol 26 (7), 582–597.

Ghose, C., Lew, D., 2020. Mechanistic insights into actin-driven polarity site movement in yeast. Mol. Biol. Cell 31 (10), 1085–1102.

Giraldo, M.C., et al., 2013. Two distinct secretion systems facilitate tissue invasion by the rice blast fungus Magnaporthe oryzae. Nat. Commun. 4 (1), 1996.

Gupta, Y.K., et al., 2015. Septin-Dependent Assembly of the Exocyst Is Essential for Plant Infection by *Magnaporthe oryzae*. Plant Cell 27 (11), 3277.

Hamer, J.E., et al., 1988. A Mechanism for Surface Attachment in Spores of a Plant Pathogenic Fungus. Science 239 (4837), 288.

He, M., et al., 2020. Discovery of broad-spectrum fungicides that block septin-dependent infection processes of pathogenic fungi. Nat. Microbiol. 5 (12), 1565–1575.

Inoue, Y., et al., 2017. Evolution of the wheat blast fungus through functional losses in a host specificity determinant. Science 357 (6346), 80.

Islam, M.T., et al., 2016. Emergence of wheat blast in Bangladesh was caused by a South American lineage of Magnaporthe oryzae. BMC Biol. 14 (1), 84.

Islam, M.T., Kim, K.-H., Choi, J., 2019. Wheat Blast in Bangladesh: The Current Situation and Future Impacts. Plant Pathol. J. 35 (1), 1–10.

Jenkinson, C.B., et al., 2017. The appressorium of the rice blast fungus Magnaporthe oryzae remains mitotically active during post-penetration hyphal growth. Fungal Genet. Biol. 98, 35–38.

Kankanala, P., Czymmek, K., Valent, B., 2007. Roles for Rice Membrane Dynamics and Plasmodesmata during Biotrophic Invasion by the Blast Fungus. Plant Cell 19 (2), 706.

Kershaw, M.J., Talbot, N.J., 2009. Genome-wide functional analysis reveals that infection-associated fungal autophagy is necessary for rice blast disease. Proc. Natl. Acad. Sci. 106 (37), 15967.

Khush, G.S., 2005. What it will take to Feed 5.0 Billion Rice consumers in 2030. Plant Mol. Biol. 59 (1), 1–6.

Kim, S., et al., 2009. Homeobox transcription factors are required for conidiation and appressorium development in the rice blast fungus *Magnaporthe oryzae*. PLoS Genet. 5 (12) e1000757–e1000757.

Kim, S., et al., 2020. Two nuclear effectors of the rice blast fungus modulate host immunity via transcriptional reprogramming. Nat. Commun. 11 (1), 5845.

Langner, T., et al., 2021. Genomic rearrangements generate hypervariable mini-chromosomes in host-specific isolates of the blast fungus. PLoS Genet. 17 (2), e1009386.

Langner, T., Białas, A., Kamoun, S., 2018. The blast fungus decoded: genomes in flux. mBio 9 (2), e00571–e618.

Liu, M., et al., 2021. Auxilin-like protein MoSwa2 promotes effector secretion and virulence as a clathrin uncoating factor in the rice blast fungus Magnaporthe oryzae. New Phytol.

Marroquin-Guzman, M., et al., 2017. The Magnaporthe oryzae nitrooxidative stress response suppresses rice innate immunity during blast disease. Nat. Microbiol. 2, 17054.

Marroquin-Guzman, M., Sun, G., Wilson, R.A., 2017. Glucose-ABL1-TOR signaling modulates cell cycle tuning to control terminal appressorial cell differentiation. PLoS Genet. 13 (1), e1006557.

Marroquin-Guzman, M., Wilson, R.A., 2015. GATA-dependent glutaminolysis drives appressorium formation in *Magnaporthe oryzae* by suppressing TOR inhibition of cAMP/PKA signaling. PLoS Pathog. 11 (4), e1004851.

Mentlak, T.A., et al., 2012. Effector-mediated suppression of chitin-triggered immunity by magnaporthe oryzae is necessary for rice blast disease. Plant Cell 24 (1), 322–335.

Osés-Ruiz, M., et al., 2017. Two independent S-phase checkpoints regulate appressorium-mediated plant infection by the rice blast fungus *Magnaporthe oryzae*. Proc. Natl. Acad. Sci 114 (2), E237.

Park, G., et al., 2002. MST12 Regulates Infectious Growth But Not Appressorium Formation in the Rice Blast Fungus Magnaporthe grisea. Molecular Plant-Microbe Interactions® 15 (3), 183–192.

Park, G., et al., 2006. Multiple upstream signals converge on the adaptor protein Mst50 in Magnaporthe grisea. Plant Cell 18 (10), 2822–2835.

Pfeifer, M.A., Khang, C.H., 2018. A nuclear contortionist: the mitotic migration of Magnaporthe oryzae nuclei during plant infection. Mycology 9 (3), 202–210.

Pfeifer, M.A., Jones, K., Khang, C.H., 2019. A strikingly-angled spindle mediates nuclear migration during colonization of rice cells infected by Magnaporthe oryzae. Fungal Genet. Biol. 126, 56–60.

Rocha, R.O., et al., 2020. Spermine-mediated tight sealing of the Magnaporthe oryzae appressorial pore–rice leaf surface interface. Nat. Microbiol. 5 (12), 1472–1480.

Ryder, L.S., et al., 2013. NADPH oxidases regulate septin-mediated cytoskeletal remodeling during plant infection by the rice blast fungus. Proc. Natl. Acad. Sci. 110 (8), 3179.

Ryder, L.S., et al., 2019. A sensor kinase controls turgor-driven plant infection by the rice blast fungus. Nature 574 (7778), 423–427.

Sakulkoo, W., et al., 2018. A single fungal MAP kinase controls plant cell-to-cell invasion by the rice blast fungus. Science 359 (6382), 1399.

Saunders, D.G.O., Aves, S.J., Talbot, N.J., 2010. Cell cycle-mediated regulation of plant infection by the rice blast fungus. Plant Cell 22 (2), 497.

Saunders, D.G.O., Dagdas, Y.F., Talbot, N.J., 2010. Spatial Uncoupling of Mitosis and Cytokinesis during Appressorium-Mediated Plant Infection by the Rice Blast Fungus *Magnaporthe oryzae*. Plant Cell 22 (7), 2417.

Savary, S., et al., 2019. The global burden of pathogens and pests on major food crops. Nat. Ecol. Evol. 3 (3), 430–439.

Shen, Q., et al., 2020. Ferroptosis contributes to developmental cell death in rice blast. New Phytol. 227 (6), 1831–1846.

Shipman, E.N., et al., 2017. Nuclear and structural dynamics during the establishment of a specialized effector-secreting cell by Magnaporthe oryzae in living rice cells. BMC Cell Biol. 18 (1), 11.

Skamnioti, P., Gurr, S.J., 2007. *Magnaporthe grisea* Cutinase2 Mediates Appressorium Differentiation and Host Penetration and Is Required for Full Virulence. Plant Cell 19 (8), 2674.

Sun, G., et al., 2018. TOR-autophagy branch signaling via Imp1 dictates plant-microbe biotrophic interface longevity. PLoS Genet. 14 (11) e1007814–e1007814.

Talbot, N.J., 2003. On the Trail of a Cereal Killer: Exploring the Biology of Magnaporthe grisea. Annu. Rev. Microbiol. 57 (1), 177–202.

Talbot, N.J., 2019. Appressoria. Curr. Biol. 29 (5), R144–R146.

Tembo, B., et al., 2020. Detection and characterization of fungus (Magnaporthe oryzae pathotype Triticum) causing wheat blast disease on rain-fed grown wheat (Triticum aestivum L.) in Zambia. PLoS ONE 15 (9), e0238724.

Turrà, D., Segorbe, D., Di Pietro, A., 2014. Protein kinases in plant-pathogenic fungi: conserved regulators of infection. Annu. Rev. Phytopathol. 52, 267–288.

Veneault-Fourrey, C., et al., 2006. Autophagic fungal cell death is necessary for infection by the rice blast fungus. Science 312 (5773), 580.

Wilson, R.A., Talbot, N.J., 2009. Under pressure: investigating the biology of plant infection by Magnaporthe oryzae. Nat. Rev. Microbiol. 7, 185.

Xu, J.-R., 2000. MAP Kinases in Fungal Pathogens. Fungal Genet. Biol. 31 (3), 137–152.

Xu, J.R., Hamer, J.E., 1996. MAP kinase and cAMP signaling regulate infection structure formation and pathogenic growth in the rice blast fungus Magnaporthe grisea. Genes Dev. 10 (21), 2696–2706.

Yan, X., Talbot, N.J., 2016. Investigating the cell biology of plant infection by the rice blast fungus Magnaporthe oryzae. Curr. Opin. Microbiol. 34, 147–153.

Yue, X., et al., 2015. ZNF1 Encodes a Putative C2H2 Zinc-Finger Protein Essential for Appressorium Differentiation by the Rice Blast Fungus Magnaporthe oryzae. Molecular Plant-Microbe Interactions® 29 (1), 22–35.

Zhao, X., et al., 2005. A Mitogen-Activated Protein Kinase Cascade Regulating Infection-Related Morphogenesis in *Magnaporthe grisea*. Plant Cell 17 (4), 1317.

Zhao, X., Xu, J.-R., 2007. A highly conserved MAPK-docking site in Mst7 is essential for Pmk1 activation in Magnaporthe grisea. Mol. Microbiol. 63 (3), 881–894.

LETTER

A sensor kinase controls turgor–driven plant infection by the rice blast fungus

Lauren S. Ryder[1,2], Yasin F. Dagdas[1,2,3], Michael J. Kershaw[1], Chandrasekhar Venkataraman[4], Anotida Madzvamuse[4], Xia Yan[1,2], Neftaly Cruz-Mireles[2], Darren M. Soanes[1], Miriam Oses-Ruiz[1,2], Vanessa Styles[4], Jan Sklenar[2], Frank L. H. Menke[2] & Nicholas J. Talbot[1,2]*

The blast fungus *Magnaporthe oryzae* gains entry to its host plant by means of a specialized pressure-generating infection cell called an appressorium, which physically ruptures the leaf cuticle[1,2]. Turgor is applied as an enormous invasive force by septin-mediated reorganization of the cytoskeleton and actin-dependent protrusion of a rigid penetration hypha[3]. However, the molecular mechanisms that regulate the generation of turgor pressure during appressorium-mediated infection of plants remain poorly understood. Here we show that a turgor-sensing histidine–aspartate kinase, Sln1, enables the appressorium to sense when a critical turgor threshold has been reached and thereby facilitates host penetration. We found that the Sln1 sensor localizes to the appressorium pore in a pressure-dependent manner, which is consistent with the predictions of a mathematical model for plant infection. A Δ*sln1* mutant generates excess intracellular appressorium turgor, produces hyper-melanized non-functional appressoria and does not organize the septins and polarity determinants that are required for leaf infection. Sln1 acts in parallel with the protein kinase C cell-integrity pathway as a regulator of cAMP-dependent signalling by protein kinase A. Pkc1 phosphorylates the NADPH oxidase regulator NoxR and, collectively, these signalling pathways modulate appressorium turgor and trigger the generation of invasive force to cause blast disease.

Plant pathogenic fungi cause many of the world's most devastating crop diseases, and pose a constant threat to global food security[4,5]. The fungus *Magnaporthe oryzae* causes rice blast—the most widespread and serious disease of rice[1]—as well as wheat blast, which recently spread from South America to Bangladesh, threatening wheat production across South Asia[6,7].

To infect plants, *M. oryzae* develops a specialized infection cell called an appressorium[2] that ruptures the leaf cuticle using huge invasive force. The appressorium generates turgor of up to 8.0 MPa by accumulating high concentrations of glycerol and other polyols[8]. A differentiated cell wall that is rich in melanin is essential for the generation of turgor, acting as a rigid structural barrier to prevent the efflux of solutes[8,9]. The translation of appressorium turgor into mechanical force causes a narrow penetration hypha to emerge from the base of the appressorium and breach the cuticle of the rice leaf[1]. Septin GTPases form a toroidal, hetero-oligomeric complex at the appressorium pore, and this complex scaffolds cortical F-actin at the point of plant infection. Septins provide cortical rigidity and act as a diffusion barrier for polarity determinants that mediate membrane curvature and protrusion of the penetration hypha[3]. Septin-mediated reorientation of F-actin also requires the regulated synthesis of reactive oxygen species by NADPH oxidases (NOX)[10].

We set out to investigate how the internal pressure of the appressorium is modulated to control repolarization. We reasoned that the appressorium must reach a critical turgor threshold to trigger septin-mediated reorganization of the cytoskeleton. To test this idea,

we first artificially lowered the turgor of the appressorium, and quantified the frequency of assembly of septin rings and the resulting disease lesions (Fig. 1). We observed fewer lesions when high concentrations of glycerol were applied to rice seedlings, demonstrating a relationship between appressorium turgor and infection (Fig. 1a, b). By contrast, application of glycerol to intact rice leaves had no effect (Extended Data Fig. 1). Septin organization was also impaired after treatment of appressoria with glycerol, and by treatment with the melanin biosynthesis inhibitor tricyclazole when applied before 16 hours post-inoculation (h.p.i.) (Fig. 1c, Extended Data Fig. 2a). Furthermore, septins and F-actin were mislocalized in the melanin-deficient mutants Δ*alb1*, Δ*rsy1* and Δ*buf1*, which fail to generate sufficient turgor for plant infection[9,11] (Fig. 1d, Extended Data Fig. 2b). We conclude that septin organization at the appressorium pore requires a critical threshold of cellular turgor and that this is essential for plant infection.

We postulated that a turgor sensor in appressoria must be necessary for the modulation of turgor pressure. To test this idea, we developed a mathematical model that couples geometric evolution laws for motion of the fungus and leaf surface with equations for the biosynthesis of melanin at the appressorium cortex, recruitment of septins and reorganization of F-actin (see Supplementary Information for a description and critical analysis of both the utility and the limitations of the mathematical model). A simulation of the model shows dynamics of appressorium repolarization that are consistent with experimental observations, and predicts that a mutant that lacks the turgor sensor will develop non-functional, hyper-melanized appressoria with excess turgor and aberrant deposition of septin and actin (Extended Data Fig. 3a, b; Supplementary Videos 1 and 2).

We next set out to identify the potential turgor sensor in *M. oryzae*. We noted that among potential candidates, *M. oryzae* possesses a homologue of the Sln1 histidine–aspartate sensor kinase—a known yeast osmosensor that modulates hyperosmotic adaptation through the high osmolarity glycerol (HOG) MAPK pathway[12]. The *HOG1* homologue in *M. oryzae*, *OSM1*, is dispensable for pathogenicity and glycerol production, suggesting that regulation of turgor is *OSM1*-independent[13]. *SLN1* was previously shown to be necessary for virulence in *M. oryzae*, but its function is unknown[14] (Fig. 2a, b, Extended Data Fig. 3c). Appressoria of a Δ*sln1* mutant generate extremely high turgor, as measured by incipient cytorrhysis[14] (Fig. 2c), but are non-functional. Live-cell imaging of *M. oryzae* that express a functional Sln1–GFP fusion showed that Sln1 localizes to the appressorium pore as infection cells generate pressure (Extended Data Fig. 3d, Supplementary Video 3). Localization of Sln1 was also sensitive to changes in turgor, and exposure to hyperosmotic glycerol led to Sln1 mislocalization (Fig. 2d) whereas the nuclear marker histone H1–GFP was unaffected (Extended Data Fig. 3e). The Δ*sln1* mutant also formed hyper-melanized appressoria (Fig. 2e)—a phenotype that was partially reversed by exposure to tricyclazole (Fig. 2e). Applying hyperosmotic stress to appressoria also enhanced the deposition of melanin in the

[1]Department of Biosciences, University of Exeter, Exeter, UK. [2]The Sainsbury Laboratory, University of East Anglia, Norwich, UK. [3]Gregor Mendel Institute of Molecular Plant Biology, Vienna, Austria. [4]School of Mathematical and Physical Sciences, Department of Mathematics, University of Sussex, Brighton, UK. *e-mail: nick.talbot@tsl.ac.uk
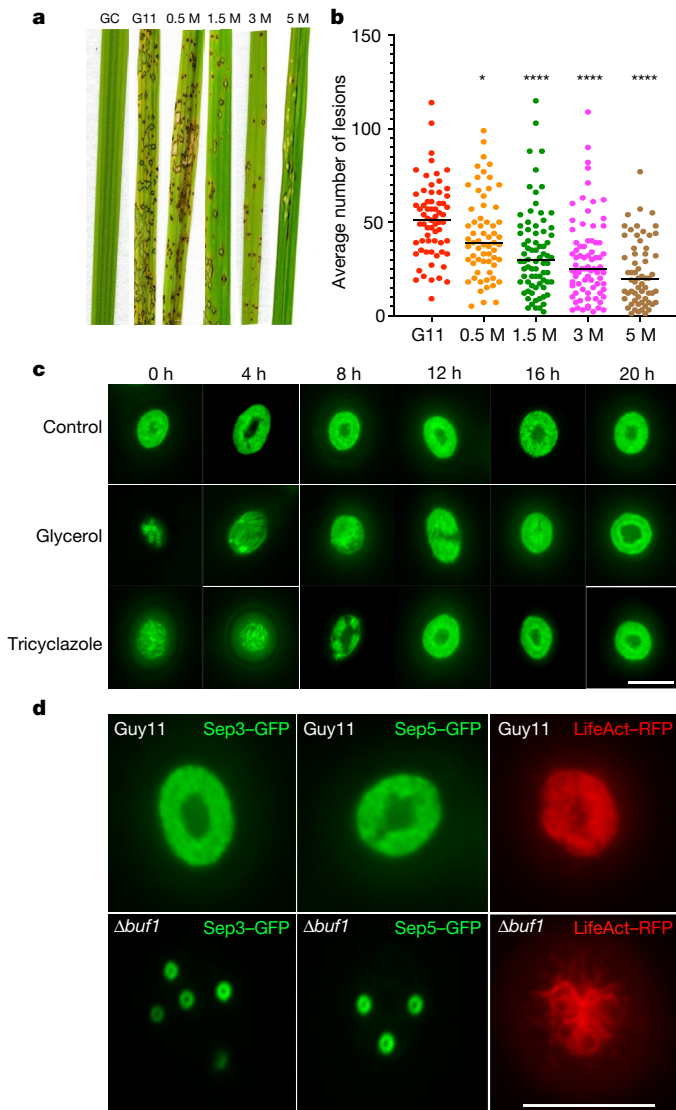
Fig. 1 | Reducing appressorium turgor prevents septin-ring formation and impairs blast infection. a, Seedlings of rice cultivar CO-39 were inoculated with a suspension of spores of *M. oryzae* (1×10^5 conidia per ml in an aqueous solution of 0.2% gelatin) of the wild-type strain Guy11. At 5 h.p.i., seedlings were sprayed with glycerol solutions of 0.5 M, 1.5 M, 3 M and 5 M, respectively. GC, glycerol control; G11, Guy11 control. Seedlings were incubated for 5 d to observe the symptoms of blast disease. **b,** Dot plot showing the frequency of disease lesions observed in a 5-cm zone from each individual leaf harvested (60 leaves were harvested per treatment). Data are the mean and individual data points for $n = 3$ independent biological replicates. A two-tailed, unpaired Student's *t*-test with Welch correction was used for comparisons with the Guy11 control (*$P = 0.0312$, ****$P < 0.0001$). **c,** Cellular localization of Sep5–GFP at the appressorium pore of Guy11 after treatment with 1.5 M glycerol or 100 μM tricyclazole between 0 and 20 h.p.i., imaged at 24 h.p.i. Images are representative of $n = 3$ independent biological replicates. **d,** Organization of Sep3–GFP, Sep5–GFP and LifeAct–RFP in the appressorium pore of the melanin-deficient mutant Δ*buf1*. Images represent $n = 3$ independent biological replicates. Scale bars, 10 μm (**c**, **d**).

wild-type Guy11 strain of *M. oryzae* (Extended Data Fig. 4), suggesting that Sln1 modulates melanization of the appressorium once sufficient turgor has been generated.

To identify cellular functions that are controlled by Sln1, we used RNA sequencing (RNA-seq) to compare global changes in gene expression in a Δ*sln1* mutant to wild-type Guy11 during appressorium development. Among 1,982 genes that were affected in expression by loss of *SLN1* at 16 h.p.i., the melanin biosynthetic genes *RSY1*

and *BUF1* were significantly upregulated in the Δ*sln1* mutant—consistent with increased melanization (Fig. 2e, Extended Data Fig. 5a). Furthermore, Sln1–GFP was mislocalized in Δ*alb1*, Δ*rsy1* and Δ*buf1* mutants (Fig. 2f). Notably, the *M. oryzae* response regulator mutants Δ*ssk1* and Δ*skn7* also display enhanced melanization[15] and in *Cryptococcus neoformans*, Δ*skn7*, Δ*ssk1* and Δ*tco1* mutants show similar phenotypes[16]. We reasoned that Sln1 negatively regulates melanin biosynthesis and turgor generation, and triggers repolarization of the appressorium. We therefore tested whether the organization of the septin ring and toroidal F-actin network in appressoria was affected in Δ*sln1* mutants Sep5–GFP and LifeAct–RFP (a marker of F-actin) were both mislocalized in Δ*sln1* mutants (Fig. 2g, Extended Data Fig. 5b). Septin organization was also impaired in Δ*alb1* mutants (Extended Data Fig. 5c), and disrupted in Δ*buf1* mutants, which are blocked at a later stage in production of 1, 8-dihydroxynaphthalene (DHN)-melanin (Fig. 1d). The Δ*sln1* mutant therefore continues to generate turgor in the appressorium, but reorganization of septins and formation of the penetration peg do not occur.

To investigate the putative Sln1 turgor-sensing complex, we immunoprecipitated Sln1–GFP from appressorium protein extracts at 16 h.p.i. and performed liquid chromatography–tandem mass spectrometry (LC–MS/MS) (Fig. 3a). Sln1 putatively interacts with two mechanosensitive ion-channel proteins, Mic1 and Mic3—similarly to previously described yeast proteins that respond to osmotic shock[17]. Blocking mechanosensitive ion channels with gadolinium and verapamil prevented appressorium formation (Extended Data Fig. 6), and although Mic1, Mic2 and Mic3 were individually dispensable for virulence, Mic2–GFP localized to the centre of the appressorium pore in an *SLN1*-dependent manner (Extended Data Fig. 7a–c). Sln1 also putatively interacts with two chitin synthases that are required for biosynthesis of the fungal cell wall, Chs4 and Chs5, and staining Δ*sln1* with calcofluor white revealed aberrant deposition of chitin within the cell wall of the appressorium (Extended Data Fig. 8a). This mirrors a previous study in *Arabidopsis thaliana*, which showed that *TOD1*—an alkaline ceramidase that regulates the turgor of guard cells and pollen tubes—acts by regulating cell-wall remodelling[18]. In addition, Sln1 interacts with Sum1, the regulatory subunit of cAMP-dependent protein kinase A (PKA), in both co-immunoprecipitation and yeast two-hybrid analyses (Fig. 3a, Extended Data Fig. 8b). PKA regulates the mobilization of lipid bodies and lipolysis, which leads to glycerol-dependent generation of turgor in *M. oryzae*[19]. The expression of *SUM1* is increased in a Δ*sln1* mutant, suggesting that Sln1 negatively regulates the PKA pathway to modulate the biosynthesis of glycerol (Fig. 3b). Consistent with this idea, the PKA drug inhibitor H-89 disrupts the organization of the appressorium pore in a dose-dependent manner, and localization of Sep5–GFP, gelsolin–GFP and Sln1–GFP is also impaired in a Δ*cpka* mutant (GenBank accession Q01143; Fig. 3c, Extended Data Fig. 9a–c). CpkA–GFP localizes to the appressorium pore (Fig. 3d) during the onset of turgor, consistent with its increased gene expression at this time (Fig. 3e).

Sln1 can also interact with protein kinase C (Pkc1), the central regulator of the cell-integrity pathway (Fig. 3b, Extended Data Fig. 8b). *PKC1* is an essential gene in *M. oryzae*, so to test its function in appressorium repolarization we used an allelic replacement mutant, *PKC1^AS*, which expresses an analogue-sensitive (Shokat) version of the kinase that is specifically sensitive to the ATP analogue 1NA-PP1[20]. Inhibition of Pkc1 by 1NA-PP1 disrupted the organization of Sep3–GFP, LifeAct–RFP and gelsolin–GFP at the appressorium pore (Fig. 3f), which was reversed by removal of 1Na-PP1 (Extended Data Fig. 10a). RNA-seq analysis of the *PKC1^AS* mutant in the presence or absence of 1NA-PP1 also showed a significant reduction in the expression of *NOX1, NOX2* and *NOXR* after 24 h[20] (Extended Data Fig. 10b). Furthermore, yeast two-hybrid analysis revealed transient interactions between Nox1, Nox2, NoxR and Pkc1 (Extended Data Fig. 10c). This is consistent with studies in humans that have demonstrated that PKC is required for phosphorylation of gp91phox (Nox2), and that this phosphorylation enhances the diaphorase activity of gp91phox and its binding to
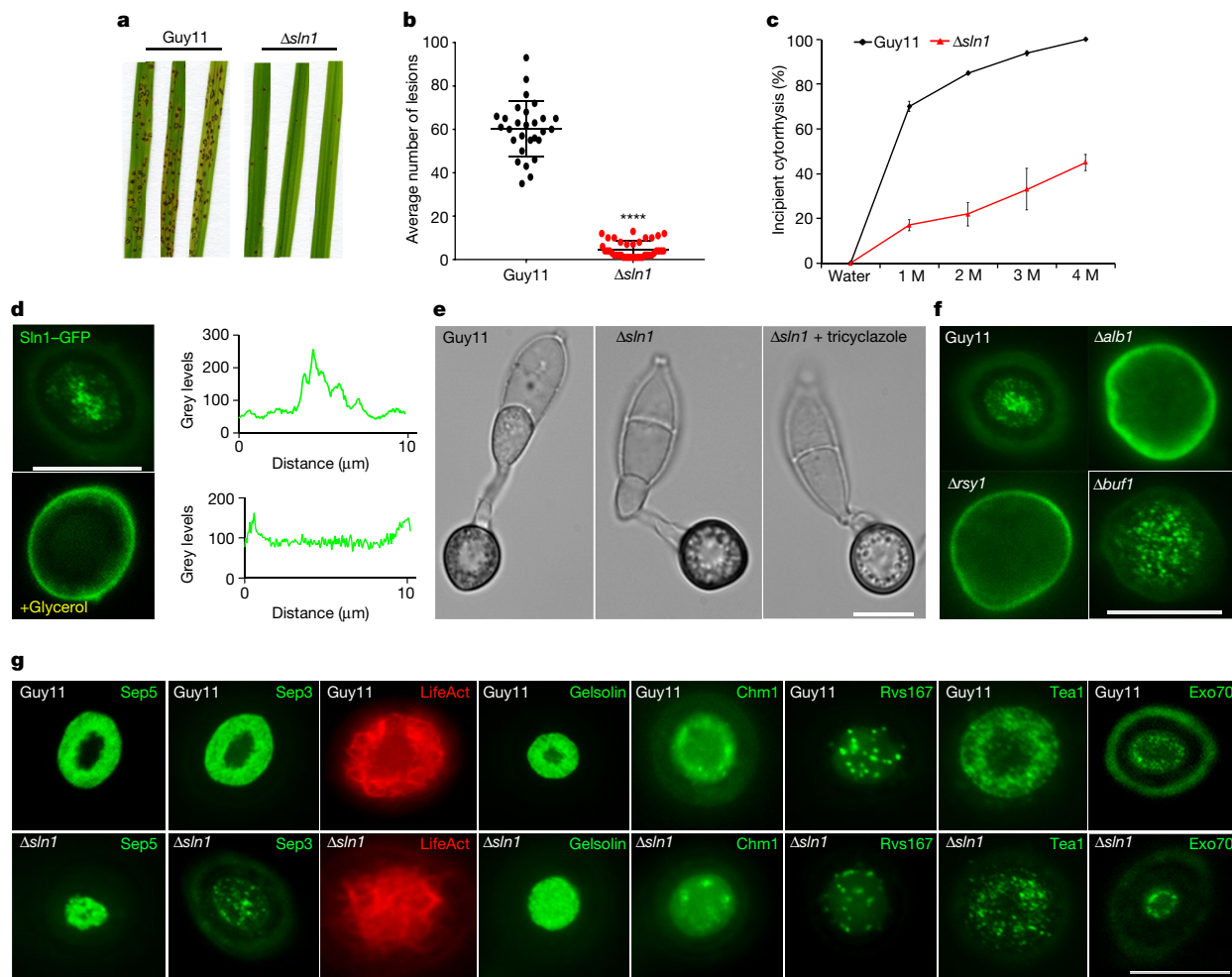
Fig. 2 | Identification of the Sln1 turgor-sensing kinase in *M. oryzae*.
a, Rice blast assay of a Δ*sln1* kinase mutant. Rice cultivar CO-39 was inoculated with a 0.2% gelatin suspension of 1×10^5 conidia per ml of wild-type Guy11 or the isogenic Δ*sln1* mutant, and incubated for 120 h to allow development of the symptoms of blast disease. **b**, Dot plot showing the frequency of disease lesions observed in a 5-cm zone from each individual leaf harvested (28 individual leaves were harvested per strain). Data are mean ± s.e.m. and individual data points for $n = 2$ independent biological replicates. ****$P < 0.0001$ (two-tailed, unpaired Student's *t*-test with Welch correction). **c**, Percentage of Guy11 and Δ*sln1*-mutant appressoria that undergo incipient cytorrhysis after treatment with glycerol solutions of 1.0–4.0 M. Data are mean ± s.e.m. for $n = 3$ independent experiments; 50 appressoria were counted per experiment. $P < 0.01$ for Guy11 versus 0.5 M glycerol; $P < 0.0001$ for Guy11 versus 1.5 M, 3 M and 4 M glycerol (two-tailed unpaired Student's *t*-test). **d**, Left,

epifluorescence micrographs showing the cellular distribution of Sln1–GFP in appressoria at 24 h.p.i., after exposure of appressoria to 1.5 M glycerol at 5 h.p.i. Right, line-scan graphs showing Sln1–GFP fluorescence in transverse sections of individual appressoria. Images are representative of $n = 3$ independent repeats of the experiment.
e, Micrographs of appressoria of Guy11 and a Δ*sln1* mutant to show the melanin layer. Hyper-melanization of Δ*sln1* could be reversed by exposure to tricyclazole. Images are representative of $n = 3$ independent repeats of the experiment. **f**, Sln1–GFP expression and localization in appressoria of Δ*alb1*, Δ*rsy1* and Δ*buf1* mutants at 24 h.p.i. Images are representative of $n = 3$ independent repeats of the experiment. **g**, Localization patterns of Sep3–GFP, Sep5–GFP, LifeAct–RFP, gelsolin–GFP, Chm1–GFP, Tea1–GFP and Exo70–GFP in appressorium pores of Guy11 and a Δ*sln1* mutant. Images are representative of $n = 3$ independent repeats of the experiment. Scale bars, 10 μm (**d**–**g**).

Rac2, p67phox (NoxR) and p47phox (Bem1)[21]. By phosphoproteomic analysis, we observed that Pkc1 phosphorylates NoxR at serine 321 (Extended Data Fig. 10d, Supplementary Table 2), consistent with activation of the NADPH oxidase complex[10,22] (which is necessary for septin-dependent plant infection) by Pkc1. Notably, Pkc1 also phosphorylates the phosphodiesterase PdeH—which regulates the PKA pathway—at serine 883, in addition to phosphorylating other proteins that are predicted to be involved in the sensing of turgor (Supplementary Table 2). Incipient cytorrhysis of a Δ*pdeH* mutant shows that it generates excess appressorium turgor, suggesting that PdeH is regulated by Sln1 (Extended Data Fig. 10e). PdeH in *M. oryzae* was previously shown to mediate cross-talk between the PKA, HOG and cell-integrity pathways[23]—consistent with a role in turgor sensing.

Finally, a cell-cycle checkpoint, triggered by the generation of appressorium turgor and by melanization, is known to regulate septin-dependent infection[24]. We therefore blocked the progression of cells

into S phase by treatment with hydroxyurea, which prevented Sln1 recruitment to the appressorium pore (Extended Data Fig. 10f). Operation of this cell-cycle checkpoint is thus critical to the sensing of turgor in appressoria.

When considered together with our mathematical modelling, the experimental data presented here provide evidence that turgor-driven infection of plants by *M. oryzae* is controlled by a sensor kinase, Sln1 (Fig. 4). Once a threshold of turgor is reached, Sln1 negatively regulates the biosynthesis of melanin and production of glycerol as the appressorium nucleus enters S-phase[24]. Isotropic expansion of the pressurized appressorium ceases, and Sln1 acts through the Pkc1-dependent cell-integrity pathway to activate the Nox2–NoxR NADPH oxidase—thereby recruiting septins to the appressorium pore and reorganizing F-actin to facilitate force generation and polarized growth. Sln1 also inhibits the cAMP/PKA pathway; Pkc1 acts directly on PdeH to modulate levels of cAMP, and may induce
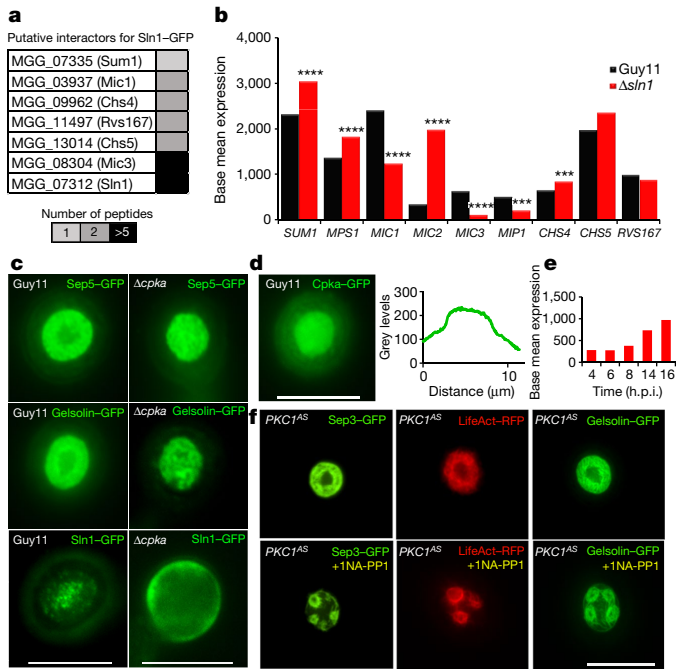
Fig. 3 | Characterization of the Sln1 turgor-sensing complex in *M. oryzae*. a, Putative Sln1-interacting peptides were immunoprecipitated from appressorium protein extracts at 16 h.p.i. from *M. oryzae* expressing Sln1–GFP or free cytoplasmic GFP using anti-GFP antibodies, and LC–MS/MS was performed to identify unique putatively interacting peptides. Colours represent the number of identified peptides for each selected protein. **b**, Differential expression of *SUM1*, *MPS1*, *MIC1*, *MIC2*, *MIC3*, *MIP1*, *CHS4*, *CHS5* and *RVS167* in Δ*sln1*-mutant appressoria compared to Guy11 appressoria at 16 h.p.i. by RNA-seq analysis. $n = 3$ independent biological repeats of the experiment for each strain. ***$P < 0.001$, ****$P < 0.0001$ (from multiple testing using the Benjamini–Hochberg method to estimate false discovery rate). **c**, Cellular localization of Sep5–GFP, gelsolin–GFP and Sln1–GFP in appressorium pores of Guy11 and a Δ*cpka* mutant at 24 h.p.i. Images are representative of $n = 3$ independent repeats of the experiment. **d**, Left, cellular distribution of Cpka–GFP in appressorium pores at 24 h.p.i. Right, line-scan graph showing Cpka–GFP fluorescence in a transverse section of an individual appressorium. Images are representative of $n = 3$ independent repeats of the experiment. **e**, Relative expression of *CPKA* from 4–16 h.p.i. during appressorium development. Data are from SuperSAGE analysis[26]. **f**, Localization of Sep3–GFP, LifeAct–RFP and gelsolin–GFP in appressorium pores of *PKC1^AS^* mutants in the presence or absence of 1NA-PP1. Images are representative of $n = 3$ independent repeats of the experiment.

glycerol efflux through the channel protein Mip1 (Fig. 3b). The septin ring acts as a diffusion barrier to ensure the localization of polarity determinants and regulate the polymerization of F-actin[3], recruitment of the exocyst complex[25] and activity of associated chitin and glucan synthases. Collectively, these processes lead to protrusion of a rigid penetration hypha, rupture of the rice leaf cuticle and onset of rice blast disease.

Online content

Any methods, additional references, Nature Research reporting summaries, source data, extended data, supplementary information, acknowledgements, peer review information; details of author contributions and competing interests; and statements of data and code availability are available at https://doi.org/10.1038/s41586-019-1637-x.

Fig. 4 | Model of turgor-driven invasion of a plant cell by the rice blast fungus. The Sln1 sensor kinase responds to appressorium turgor by interaction with a set of upstream monitors of cell expansion, including the stretch-activated ion-channel proteins Mic1, Mic2 and Mic3. Once a threshold of turgor is reached, Sln1 negatively regulates melanin biosynthesis and the cAMP/PKA pathway. Pkc1 acts directly on the PdeH phosphodiesterase to modulate levels of cAMP, and also acts to control lipolysis and glycerol production. Sln1 is then necessary for recruitment of septins to the appressorium pore, which requires Pkc1 and the NADPH oxidase Nox2. Septins tether cortical F-actin to the membrane, facilitating the formation of a toroidal network of F-actin, and organizing the exocyst complex and a large family of endocytic proteins at the pore. The septin ring acts as a diffusion barrier to ensure repolarization of the penetration peg, which involves the focused polymerization of F-actin and the activity of chitin and glucan synthases. A pressure-dependent S-phase checkpoint is also triggered[22] and is necessary for the action of Sln1. Collectively, these processes lead to breaching of the rice leaf cuticle.

1. Talbot, N. J. On the trail of a cereal killer: exploring the biology of *Magnaporthe grisea*. *Annu. Rev. Microbiol.* **57**, 177–202 (2003).
2. Ryder, L. S. & Talbot, N. J. Regulation of appressorium development in pathogenic fungi. *Curr. Opin. Plant Biol.* **26**, 8–13 (2015).
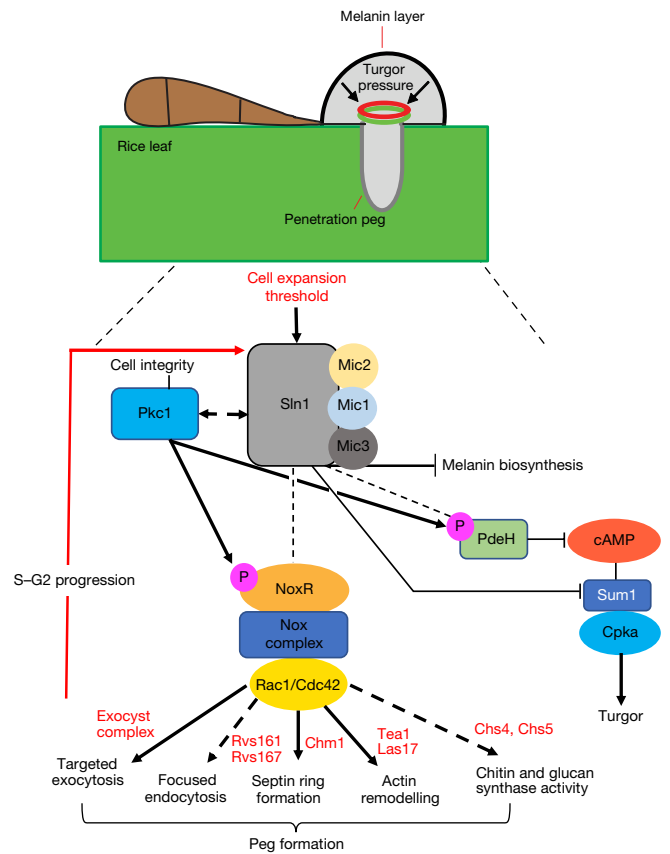3. Dagdas, Y. F. et al. Septin-mediated plant cell invasion by the rice blast fungus, *Magnaporthe oryzae*. *Science* **336**, 1590–1595 (2012).
4. Pennisi, E. Sowing the seeds for the ideal crop. *Science* **327**, 802–803 (2010).
5. Fisher, M. C. et al. Emerging fungal threats to animal, plant and ecosystem health. *Nature* **484**, 186–194 (2012).
6. Islam, M. T. et al. Emergence of wheat blast in Bangladesh was caused by a South American lineage of *Magnaporthe oryzae*. *BMC Biol.* **14**, 84 (2016).
7. Inoue, Y. et al. Evolution of the wheat blast fungus through functional losses in a host specificity determinant. *Science* **357**, 80–83 (2017).
8. de Jong, J. C. MCCormack, B. J., Smirnoff, N. & Talbot, N. J. Glycerol generates turgor in rice blast. *Nature* **389**, 244–245 (1997).
9. Chumley, F. G. & Valent, B. Genetic-analysis of melanin-deficient, nonpathogenic mutants of *Magnaporthe grisea*. *Mol. Plant Microbe Interact.* **3**, 135–143 (1990).
10. Ryder, L. S. et al. NADPH oxidases regulate septin-mediated cytoskeletal remodeling during plant infection by the rice blast fungus. *Proc. Natl Acad. Sci. USA* **110**, 3179–3184 (2013).
11. Wilson, R. A. & Talbot, N. J. Under pressure: investigating the biology of plant infection by *Magnaporthe oryzae*. *Nat. Rev. Microbiol.* **7**, 185–195 (2009).
12. Tao, W., Deschenes, R. J. & Fassler, J. S. Intracellular glycerol levels modulate the activity of Sln1p, a *Saccharomyces cerevisiae* two-component regulator. *J. Biol. Chem.* **274**, 360–367 (1999).
13. Dixon, K. P., Xu, J.-R., Smirnoff, N. & Talbot, N. J. Independent signaling pathways regulate cellular turgor during hyperosmotic stress and appressorium-mediated plant infection by *Magnaporthe grisea*. *Plant Cell* **11**, 2045–2058 (1999).

14. Zhang, H. et al. A two-component histidine kinase, *MoSLN1*, is required for cell wall integrity and pathogenicity of the rice blast fungus, *Magnaporthe oryzae*. *Curr. Genet.* **56**, 517–528 (2010).
15. Motoyama, T. et al. Involvement of putative response regulator genes of the rice blast fungus *Magnaporthe oryzae* in osmotic stress response, fungicide action, and pathogenicity. *Curr. Genet.* **54**, 185–195 (2008).
16. Bahn, Y. S., Kojima, K., Cox, G. M. & Heitman, J. A unique fungal two-component system regulates stress responses, drug sensitivity, sexual development, and virulence of *Cryptococcus neoformans*. *Mol. Biol. Cell* **17**, 3122–3135 (2006).
17. Nakayama, Y., Hirata, A. & Iida, H. Mechanosensitive channels Msy1 and Msy2 are required for maintaining organelle integrity upon hypoosmotic shock in *Schizosaccharomyces pombe*. *FEMS Yeast Res.* **14**, 992–994 (2014).
18. Chen, L. Y. et al. The *Arabidopsis* alkaline ceramidase TOD1 is a key turgor pressure regulator in plant cells. *Nat. Commun.* **6**, 6030 (2015).
19. Thines, E., Weber, R. W. S. & Talbot, N. J. MAP kinase and protein kinase A-dependent mobilization of triacylglycerol and glycogen during appressorium turgor generation by *Magnaporthe grisea*. *Plant Cell* **12**, 1703–1718 (2000).
20. Penn, T. J. et al. Protein kinase C is essential for viability of the rice blast fungus *Magnaporthe oryzae*. *Mol. Microbiol.* **98**, 403–419 (2015).
21. Raad, H. et al. Regulation of the phagocyte NADPH oxidase activity: phosphorylation of gp91[phox]/NOX2 by protein kinase C enhances its diaphorase activity and binding to Rac2, p67[phox], and p47[phox]. *FASEB J.* **23**, 1011–1022 (2009).
22. Mithoe, S. C. et al. Attenuation of pattern recognition receptor signaling is mediated by a MAP kinase kinase kinase. *EMBO Rep.* **17**, 441–454 (2016).
23. Yin, Z. et al. Phosphodiesterase MoPdeH targets MoMck1 of the conserved mitogen-activated protein (MAP) kinase signalling pathway to regulate cell wall integrity in rice blast fungus *Magnaporthe oryzae*. *Mol. Plant Pathol.* **17**, 654–668 (2016).
24. Osés-Ruiz, M., Sakulkoo, W., Littlejohn, G. R., Martin-Urdiroz, M. & Talbot, N. J. Two independent S-phase checkpoints regulate appressorium-mediated plant infection by the rice blast fungus *Magnaporthe oryzae*. *Proc. Natl Acad. Sci. USA* **114**, E237–E244 (2017).
25. Gupta, Y. K. et al. Septin-dependent assembly of the exocyst is essential for plant infection by *Magnaporthe oryzae*. *Plant Cell* **27**, 3277–3289 (2015).
26. Soanes, D. M., Chakrabarti, A., Paszkiewicz, K. H., Dawe, A. L. & Talbot, N. J. Genome-wide transcriptional profiling of appressorium development by the rice blast fungus *Magnaporthe oryzae*. *PLoS Pathog.* **8**, e1002514 (2012).

METHODS

Fungal strains, growth conditions and DNA analysis. Growth, maintenance and storage of *M. oryzae* isolates, medium composition, nucleic acid extraction and transformation were all as previously described[27]. Gel electrophoresis, restriction enzyme digestion, gel blots and sequencing were performed using standard procedures[28].

Assays of appressorium development and plant infection, quantification of melanin thickness and live cell imaging of cytoskeletal components of *M. oryzae*. Appressorium development was induced in vitro on borosilicate 18×18-mm glass coverslips (Thermo Fisher Scientific), adapted from a previous study[29]. A total of 50 μl of conidial suspension (5×10^4 ml^{-1}) was placed on a coverslip and incubated at 24 °C. Rice leaf sheaths were inoculated[30] to observe the development of invasive hyphae. The transgenic line expressing LTi6B was used to observe plant cell viability[31]. At the desired time points, tricyclazole (100 μM), an agent that inhibits melanin biosynthesis, was added to *M. oryzae* and infection-related development assayed. Glycerol was used at a final concentration of 1.5 M for coverslip assays unless otherwise stated, and 1–5 M for plant spraying, and samples were incubated at 24 °C. Gadolinium (100 μM) and verapamil (100 μM) were added at the indicated times to evaluate their effect on infection-related development (0–20 h). To determine the thickness of the melanin layer of the appressorium, appressoria were sampled at random intervals at the cell cortex. Development of appressoria was observed using an IX81 motorized inverted microscope (Olympus) and images were captured using a Photometrics CoolSNAP HQ2 camera (Roper Scientific), under control of the Metamorph software package (MDS Analytical Technologies). Datasets were compared using an unpaired Student's *t*-test.

Generation of GFP fusion plasmids. DNA sequences were retrieved from the *M. oryzae* database (http://fungi.ensembl.org/Magnaporthe_oryzae/Info/Index) and used to design primers (Supplementary Table 1). In-Fusion cloning based on in vitro homologous recombination was performed to generate Sln1–GFP and Cpka–GFP, using a commercial kit (In-Fusion Cloning kit; Clontech Laboratories). The primers used are shown in Supplementary Table 1. Sln1–GFP, Cpka–GFP and Mic2–GFP were inserted as EcoRI/HindIII fragments into a modified Strataclone (Stratagene) vector containing the *BAR* gene that confers bialophos (BASTA) resistance[32]. In all cases, several independent *M. oryzae* transformants were first screened for consistency of the fluorescent signal and a representative transformant was then selected for further analysis. Three independent experiments were performed in each case unless otherwise stated.

Targeted gene deletion of *MIC1*, *MIC2* and *MIC3* in *M. oryzae*. Targeted gene replacement of *M. oryzae MIC1*, *MIC2* and *MIC3* was performed using the split marker strategy[6]. To amplify the split *HPH*, *IVL1* or *BAR* templates, the primers used were M13 (forward) with HY/ VL/BA and M13 (reverse) with YG/IV/AR, as described[33]. *M. oryzae* mechanosensitive-ion-channel genes that contain the pfam domain (PF00924) were aligned with *Schizosaccharomyces pombe*, *Aspergillus nidulans* and *Neurospora crassa* (*Saccharomyces cerevisiae* and *Candida albicans* do not have genes with this domain). The sequence data for each mechanosensitive-ion-channel gene in *M. oryzae* were retrieved from the *M. oryzae* genome database at https://fungi.ensembl.org/Magnaporthe_oryzae/Info/Annotation/) and used to design specific primers (see Supplementary Table 1). Either Guy11 or the Δ*ku70* (*KU70* is also known as *YKU70*) mutant[33] was transformed with the deletion cassette for each gene fusion; *Mic1:hph*, *Mic2:ivl1* and *Mic3:bar* (2 μg of DNA for each flank). Transformants were selected in the presence of either hygromycin B (200 μg ml^{-1}), sulfonylurea (50 μg ml^{-1}) or bialophos (50 μg ml^{-1}) and were routinely screened and assessed using Southern blotting.

Co-immunoprecipitation experiments and LC–MS/MS analysis. Total protein was extracted from lyophilized *M. oryzae* appressoria (generated on borosilicate 18×18-mm glass coverslips (Thermo Fisher Scientific)) at 16 h.p.i., collected using a razor blade and snap-frozen in liquid nitrogen. *M. oryzae* strains that express Sln1–GFP and ToxA–GFP (control) were co-immunoprecipitated using the GFP-Trap protocol according to the manufacturer's instructions (ChromoTek). Preparation of peptides for LC–MS/MS was performed as follows. Proteins were separated by SDS–PAGE. Gels were cut into slices (5–10 mm) and proteins contained within gel slices were prepared for LC–MS/MS as described previously[34]. LC–MS/MS analysis was performed with an Orbitrap Fusion trihybrid mass spectrometer (Thermo Fisher Scientific) and a nanoflow high-performance liquid chromatography (HPLC) system (Dionex Ultimate3000, Thermo Fisher Scientific), as described previously[35] but with the following differences: MS/MS peak lists were exported in the Mascot generic file format using Discoverer v2.2 (Thermo Fisher Scientific). The database was searched with Mascot v.2.3 (Matrix Science), with the following differences: (1) the database searched with Mascot v.2.3 (Matrix Science) was the *M. oryzae* protein database with the inclusion of sequences of common contaminants such as keratins and trypsin; (2) carbamidomethylation of cysteine residues was specified as a fixed modification, and oxidized methionine was allowed as a variable modification. The other Mascot parameters used were as follows: (1) mass values were monoisotopic and the protein mass was unrestricted; (2) the peptide mass tolerance was 5 ppm and the fragment mass

tolerance was 0.6 Da; (3) two missed cleavages were allowed with trypsin. All Mascot searches were collated and verified with Scaffold (Proteome Software), and the subset database was searched with the Mascot server v.2.4.1 (Matrix Science). Accepted proteins passed the following threshold in Scaffold: 95% confidence for protein match and minimum of two unique peptide matches with 95% confidence.

Yeast two-hybrid analysis. In-Fusion Cloning based on in vitro homologous recombination was performed to generate vectors that express Sln1, Nox1, Nox2 and NoxR in the pGADT7 prey vector, and Mps1, Pkc1[20] and Sum1 in the pGBKT7 bait vector. Genes were amplified from *M. oryzae* cDNA derived from mycelium grown on liquid Complete Medium (CM) using primers with a 15-bp overhang and a restriction site complementary to the target vector (Supplementary Table 1). Fragments were cloned into pGBKT7 and pGADT7 plasmids and linearized by digestion with BamHI and EcoRI. Yeast two-hybrid assays using pGADT7- or pGBKT7-based constructs (Clontech) were performed according to the manufacturer's instructions (MATCHMAKER Gold Yeast Two-Hybrid System).

Comparative RNA-seq analysis. Total RNA was extracted from appressoria of the wild-type strain Guy11 and Δ*sln1* null mutant at 16 h.p.i., which were developed on hydrophobic coverslips using the RNeasy Plant Mini Kit for Total RNA extraction (Qiagen). RNA-seq libraries were then prepared from 5 μg of total RNA with the Illumina TruSeq RNA Sample Preparation Kit (Agilent) according to the manufacturer's instructions. Libraries were sequenced using the Illumina HiSeq 2500 platform. Reads were aligned against version 8.0 of the *M. oryzae* genome using TopHat software and analysis of the data was performed using DESeq through moderated log$_2$-transformed fold-change values (mod_lfc)[36,37]. Transcript abundances for each gene and adjusted *P* values and transcript abundance were determined as previously described[38].

Protein extraction and phosphoproteomic enrichment. Mycelium of the *M. oryzae PKC1^{AS}* mutant and Guy11 was prepared from CM shake cultures (125 r.p.m.) at 24 °C for 48 h. Mycelium was filtered through miracloth (Calbiochem), divided and treated with 1NA-PP1 at a final concentration of 500 nM for 4 h. An untreated control was also prepared at the same time point. Mycelium was then filtered, washed in distilled water and frozen in liquid nitrogen.

Frozen tissue was ground to a fine powder in liquid nitrogen, resuspended in extraction buffer (8 M urea, 150 mM NaCl, 100 mM Tris pH 8, 5 mM EDTA, 1 μg ml^{-1} aprotinin, 2 μg ml^{-1} leupeptin) and mechanically disrupted (8 min, 1,000 r.p.m.) in a 30-ml Potter-Elvehjem homogenizer incubated on ice[22]. The homogenate was then fractionated by centrifugation for 30 min at 10,000g (Sorvall SW34 rotor). The supernatant was removed and then centrifuged for 60 min at 100,000g (Sorvall T-647.5 rotor) to separate the cytosolic (supernatant) and microsomal (pellet) fractions. The microsomal pellet was then resuspended in extraction buffer. For phosphopeptide enrichment, sample preparation started with 1–3 mg of cytosolic or microsomal protein extract (confirmed by Bradford assay) dissolved in bicarbonate buffer containing 8 M urea. First, protein extracts were reduced with 5 mM tris(2-carboxyethyl)phosphine (TCEP) for 30 min at 30 °C with gentle shaking, followed by alkylation of cysteine residues with 40 mM iodoacetamide at room temperature for 1 h. Samples were diluted to a final concentration of 1.6 M urea with 50 mM ammonium bicarbonate and digested overnight with trypsin (Promega; 1:100 enzyme to substrate ratio). Peptide digests were purified using C18 SepPak columns (Waters) as described[39]. Phosphopeptides were enriched using titanium dioxide (TiO$_2$; GL Science) with phthalic acid as a modifier[22]. Finally, phosphopeptides were eluted by a pH shift to 10.5 and immediately purified using C18 microspin columns (The Nest Group; loading capacity of 5–60 μg). After purification, all samples were desiccated in a speed-vac, stored at −80 °C and resuspended in 2% acetonitrile with 0.1% trifluoroacetic acid before mass-spectrometry analysis[22].

Mass-spectrometry analysis of phosphopeptide-enriched samples. LC–MS/MS analysis was performed using an Orbitrap Fusion trihybrid mass spectrometer (Thermo Fisher Scientific) and a nanoflow ultra-high-performance liquid chromatography (UHPLC) system (Dionex Ultimate 3000, Thermo Fisher Scientific). Peptides were trapped on a reverse-phase trap column (Acclaim PepMap, C18 5 μm, 100 μm × 2 cm, Thermo Fisher Scientific). Peptides were eluted in a gradient of 3–40% acetonitrile in 0.1% formic (solvent B) acid over 120 min, followed by a gradient of 40–80% B over 6 min at a flow rate of 200 nl min^{-1} at 40 °C. The mass spectrometer was operated in positive-ion mode with a nano-electrospray ion source with ID 0.02-mm fused silica emitter (New Objective). A voltage of 2,200 V was applied via platinum wire held in PEEK T-shaped coupling union with the transfer capillary temperature set to 275 °C. The Orbitrap mass spectrometry scan resolution of 120,000 at 400 m/z, range 300–1,800 m/z was used, and the automatic gain control was set to 2×10^5 and the maximum injection time to 50 ms. In the linear ion trap, MS/MS spectra were triggered using a data-dependent acquisition method, with 'top speed' and 'most intense ion' settings. The selected precursor ions were fragmented sequentially both in the ion trap using collision-induced dissociation (CID) and in the higher-energy collisional dissociation (HCD) cell. Dynamic exclusion was set to 15 s. The charge state allowed between 2+ and 7+ charge states to be selected for MS/MS fragmentation.

Peak lists in the format of Mascot generic files (.mgf files) were prepared from raw data using the MSConvert package (Matrix Science). Peak lists were searched on Mascot server v.2.4.1 (Matrix Science) against either the *Magnaporthe oryzae* (isolate 70-15, v.8) database, or an in-house contaminants database. Tryptic peptides with up to two possible miscleavages and the charge states +2, +3, +4 were allowed in the search. The following modifications were included in the search: oxidized methionine; phosphorylation on serine, threonine, or tyrosine as a variable modification; and carbamidomethylated cysteine as a static modification. Data were searched with a monoisotopic precursor and fragment-ions mass tolerance set at 10 ppm and 0.6 Da, respectively. Mascot results were combined in Scaffold v.4 (Proteome Software) and exported in Excel (Microsoft Office)[22].

Statistical analysis. All experiments were conducted with technical and biological replicates at an appropriate sample size that was estimated on the basis of our previous experience. No statistical methods were used to predetermine sample size. No methods of randomization were applied but blinding was applied to the data on disease symptoms, which are shown in Fig. 1b. All experiments were replicated independently at least once, as indicated in each figure legend. Dot plots were routinely used to show individual data points for each experimental observation, and bar graphs, where shown, also contained individual data points for each experimental replicate. Statistical analyses were performed using GraphPad Prism 8 or Microsoft Excel. P values <0.05 were considered significant; *$P < 0.05$, **$P < 0.01$, ***$P < 0.001$, ****$P < 0.0001$. P values >0.05 were considered non-significant and exact values are shown where appropriate. The sample sizes and statistical tests used are stated in each figure legend.

Reporting summary. Further information on research design is available in the Nature Research Reporting Summary linked to this paper.

Data availability

All strains generated and datasets analysed during the current study, including codes and algorithms, are available either in public repositories as stated, or from the corresponding author on reasonable request.

27. Talbot, N. J., Salch, Y. P., Ma, M. & Hamer, J. E. Karyotypic variation within clonal lineages of the rice blast fungus, *Magnaporthe grisea*. *Appl. Environ. Microbiol.* **59**, 585–593 (1993).
28. Sambrook, J., Fritsch, E. F. & Maniatis, T. *Molecular Cloning: a Laboratory Manual* 2nd edn (Cold Spring Harbor Laboratory Press, New York, 1989).
29. Hamer, J. E. et al. A mechanism for surface attachment in spores of a plant pathogenic fungus. *Science* **239**, 288–290 (1988).
30. Kankanala, P., Czymmek, K. & Valent, B. Roles for rice membrane dynamics and plasmodesmata during biotrophic invasion by the blast fungus. *Plant Cell* **19**, 706–724 (2007).
31. Mentlak, T. A. et al. Effector-mediated suppression of chitin-triggered immunity by *Magnaporthe oryzae* is necessary for rice blast disease. *Plant Cell* **24**, 322–335 (2012).
32. Lindsay, R. J., Kershaw, M. J., Pawlowska, B. J., Talbot, N. J. & Gudelj, I. Harbouring public good mutants within a pathogen population can increase both fitness and virulence. *eLife* **5**, e18678 (2016).
33. Kershaw, M. J. & Talbot, N. J. Genome-wide functional analysis reveals that infection-associated fungal autophagy is necessary for rice blast disease. *Proc. Natl Acad. Sci. USA* **106**, 15967–15972 (2009).
34. Petre, B., Win, J., Menke, F. L. H. & Kamoun, S. Protein–protein interaction assays with effector–GFP fusions in *Nicotiana benthamiana*. *Methods Mol. Biol.* **1659**, 85–98 (2017).
35. Bender, K. W. et al. Autophosphorylation-based calcium (Ca^{2+}) sensitivity priming and Ca^{2+}/calmodulin inhibition of *Arabidopsis thaliana* Ca^{2+}-dependent protein kinase 28 (CPK28). *J. Biol. Chem.* **292**, 3988–4002 (2017).
36. Anders, S. & Huber, W. Differential expression analysis for sequence count data. *Genome Biol.* **11**, R106 (2010).
37. Trapnell, C. et al. Transcript assembly and quantification by RNA-seq reveals unannotated transcripts and isoform switching during cell differentiation. *Nat. Biotechnol.* **28**, 511–515 (2010).
38. Soanes, D. M., Chakrabarti, A., Paszkiewicz, K. H., Dawe, A. L. & Talbot, N. J. Genome-wide transcriptional profiling of appressorium development by the rice blast fungus *Magnaporthe oryzae*. *PLoS Pathog.* **8**, e1002514 (2012).
39. Ludwig, C., Claassen, M., Schmidt, A. & Aebersold, R. Estimation of absolute protein quantities of unlabeled samples by selected reaction monitoring mass spectrometry. *Mol. Cell. Proteomics* **11**, M111.013987 (2012).
40. Chojnacki, S., Cowley, A., Lee, J., Foix, A. & Lopez, R. Programmatic access to bioinformatics tools from EMBL–EBI update: 2017. *Nucleic Acids Res.* **45**, W550–W553 (2017).